T. Schanz

(Ed.)

Unsaturated Soils: Experimental Studies

Proceedings of the International Conference
"From Experimental Evidence towards
Numerical Modeling of Unsaturated Soils,"
Weimar, Germany, September 18–19, 2003

Volume I

Springer

SPRINGER PROCEEDINGS IN PHYSICS

T. Schanz (Ed.)

Unsaturated Soils: Experimental Studies

Proceedings of the International Conference
"From Experimental Evidence towards Numerical Modeling
of Unsaturated Soils," Weimar, Germany, September 18–19, 2003

Volume I

With 212 Figures and 44 Tables

Springer

Professor Dr. Ing. habil. Tom Schanz
Bauhaus-Universität Weimar
Professur Bodenmechanik
Coudraystraße 11c
99421 Weimar, Germany
E-mail: tom.schanz@bauing.uni-weimar.de

The use of general descriptive names, registered names, trademarks, etc. in this publication does not imply,
even in the absence of a specific statement, that such names are exempt from the relevant protective laws and
regulations and therefore free for general use.

Foreword

These proceedings document the various papers delivered and partially presented at the International Conference "From experimental evidence towards numerical modeling of unsaturated soils," which was held in Weimar (Germany) during 18-19 September 2003. The conference was organized under the auspices of the International Society of Soil Mechanics and Geotechnical Engineering (ISSMGE) and the National German Geotechnical Society (DGGT).

The need to understand the behavior of unsaturated soils is becoming exclusively essential for the geotechnical engineers and designers. In the last three decades many researchers have made significant contribution to the understanding of the unsaturated soil mechanics. Nevertheless, application of the subject to variety of new problems still requires our attention. This International conference is a mere attempt to unite researchers and engineers in geotechnical engineering and to discuss about the problems associated with the unsaturated soils. Doing so the objectives of these lecture notes are as follows:

- to promote unsaturated soil mechanics for practical application,
- to exchange experiences in experimental unsaturated soil mechanics and numerical modeling,
- to discuss application of unsaturated soil mechanics to variety of problems.

In other words, we could also name these two volumes as "From theory to daily practice".

I would like to extend my deep sense of appreciation as the editor and the Head of the organizing committee, to many persons who have contributed either directly or indirectly to organize the International conference and to finalize these proceedings. Firstly, I acknowledge the support provided by the German National research fund. I would like to mention specifically the involvement of the TC 6 ("Unsaturated Soils") Committee of the International Society. Secondly, I appreciate the effort of the members of the Technical committee, who have spent their valuable time to suggest the changes, improvement to the papers submitted. Finally I wish to convey my thanks to all the keynote and invited speakers, authors and delegates attending the conference.

I would like to express my deep sense of gratitude for the outstanding work performed by those involved in the technical and administrative organization of these proceedings. Special thanks go to my co-workers Ms. Yvonne Lins, Mr. S. S. Agus and Dr. S. Tripathy, who helped in guaranteeing the international standard of the scientific program and shaping the proceedings itself.

I would like to congratulate the authors for their very interesting presentations and the reported results and advances in the topics of this conference. Ms. Sandra Michael did significant contributions while incorporating the corrections in the papers as suggested by the Editor. Special thanks go to Dr. Thomas Ditzinger at Springer Publisher for the fruitful and personal co-operation so guaranteeing the high quality of these two volumes. I myself believe that this conference has meant another significant step towards the advancement and understanding of unsaturated soils. Studying the presented papers carefully we will learn about current international work in the field of: experimental unsaturated geotechnics, constitutive modeling in unsaturated geotechnics, the microstructure and its importance to soil behavior and further about environmental issues.

Weimar, January 2004   Tom Schanz

International Conference Weimar 2003
From experimental evidence towards numerical modelling of unsaturated soils

Introduction

The field of unsaturated soil mechanics has been propelled forward by a variety of concerns brought to the fore by societal demands. In the 1960s, a series of international conferences was convened to better understand the behavior of expansive soils. As a result of these conferences, geotechnical engineers became aware of the significant role played by soil suction. Consequently, the volume change behavior of expansive soils began to be viewed in terms of changes in soil suction. Later, there was considerable interest in studying landslides precipitated by a reduction in soil suction as a result of excessive rainfall over a period of time. In the 1980s, society began to demand greater accountability with regard to our stewardship of the environment. The need for accountability provided a great Impetus for research into the movement of water and chemicals through the unsaturated portion of the soil profile. Another application that provided an incentive to better understand unsaturated soil behavior was the need for adequate handling of radioactive wastes from nuclear power plants.

Over a period of about 30 years, the theories and formulations for unsaturated soil mechanics have been put forth and verified through numerous research studies. Unsaturated soil mechanics is now sometimes referred to as "Nonlinear Soil Mechanics" and it is interested that our understanding of unsaturated soil behavior has paralleled the development of computational ability to make numerical solutions available for geotechnical engineering practice.

In the frame of the International Conference "From experimental evidence towards numerical modeling of unsaturated soils", which was held in Weimar, Germany, autumn 2003, I would like to provide a few comments in response to 4 questions that have been placed before me by the Organizing Chairman, Dr. Tom Schanz. I will attempt to answer these questions by taking into consideration research studies around the world over the past few years. These questions are as follows.

1. What are the major landmark contributions in the last five years relative to the field of Unsaturated Soil Mechanics?

The past few years have indeed bore witness to a number of significant major landmark contributions in the area of unsaturated soil mechanics. I couldn't help thinking back to the time when Dr. Harianto Rahardjo and I completed the writing of the book entitled, "Soil Mechanics for Unsaturated Soils" in 1993. No sooner was the book completed than we realized that it had some shortcomings. It had shortcomings because some significant landmark developments were emerging in unsaturated soil mechanics. Our book attempted to take the classic areas of *saturated soil mechanics* and extend these areas to embrace *unsaturated soil behavior*. The book focused primarily on the areas of i.) seepage, ii.) volume change and iii.) shear strength. For each of those areas, the book presented, i.) theory, ii.) methods

of measuring the soil properties and iii.) application of the theory to engineering practice, for unsaturated soils. While the book provided an extension of the classic theories into the unsaturated soil range, implementation of unsaturated soil mechanics proved to be difficult due mainly to the cost of measuring unsaturated soil properties. However, engineers are problem-solvers and geotechnical engineers began to find ways whereby unsaturated soil mechanics could be implemented into routine geotechnical engineering.

As a result of extensive research in unsaturated soil mechanics, the soil-water characteristic curve, SWCC, emerged as a means for estimating unsaturated soil property functions. I would say that research into techniques for estimating unsaturated soil property functions has been one of the most significant research contributions in the last 5 to 10 years.

There are also other significant landmark contributions that have also been made. Significant progress has been made in developing elasto-plastic models for unsaturated soils; however, we need to realize that there is still need for more research on comprehensive elasto-plastic models that incorporate wetting and drying paths along all total stress loading paths. The models should be verified for a wide range of soils (e.g., sands, silts and clays) prepared as either initially remolded materials (e.g., compacted) or initially undisturbed. Consideration also needs to be given to the variations in soil model behavior that might occur in the occluded air bubble stage (near saturation), the desaturation phase between the air entry value and the residual suction stage, as well as the stage beyond residual suction conditions.

Significant contributions have been made by geotechnical engineers in the measurement of soil suction. There is great need for both "direct" and "indirect" means of measuring soil suction *in situ* and in the laboratory. The advances in the direct measurement of matric suctions beyond one atmosphere are to be hailed as a significant breakthrough. At the same time, it is important to be transparent regarding the limitations of this technology. Further research should be undertaken to more fully understand the factors that affect the longevity of such suction measurements. The advances in the use of "indirect" methods such as TDR and TC (i.e., Thermal Conductivity) are also worthy of mention particularly because of their ongoing functionality with limited maintenance over long-term monitoring.

2. What are the deficiencies we are facing today?

I believe that one of the primary deficiencies in unsaturated soil mechanics is the lack of comprehensive case histories where sufficient state variables have been measured in the field in order that an assessment can be made regarding the accuracy of the proposed theories for unsaturated soil behavior. We need to see the "Observational Method" used over and over again relative to the assessment of unsaturated soil behavior. It is interesting to note that the present Chairman of the TC6 Committee on Unsaturated Soils (Professor E. Alonso) has made a special plea for detailed case histories involving unsaturated soils.

I also believe that there is still need for more research into the measurement of matric suction *in situ* and in the laboratory. Limitations in the measurement of soil suction result in a deficiency to the overall implementation of unsaturated soil mechanics.

There have been numerous formulations that have been proposed in the research literature associated with elasto-plastic type soil models. While these formulations are encouraging to see, it is advantageous to have the models eventually formulated on a sound continuum mechanics basis, if at all possible. In other words, it is preferable that there be a clear distinction when using empiricism in the description of state variables for the models, as opposed to following the requirements of classical continuum mechanics. I would note that reference was made at this conference to a "constitutive stress" for an unsaturated soil. Such a reference is an oxymoron in the sense that "stress" is a state variable and the word, "constitutive" must link together state variables. The use of the word "effective stress" for unsaturated soils is also "constitutive" in character and therefore interjects empiricism at the onset of subsequent formulations. Researchers may choose to deviate from all the classical concepts of continuum mechanics in some of their formulations but it should be realized that these constitute deficiencies that we face as researchers in unsaturated soil mechanics.

3. Which major questions are still open ended?

I believe that models for unsaturated soil behavior need to be more clearly developed in relation to their position along the soil-water characteristic curve, SWCC. Just as there is a soil behavior models for a saturated soil; likewise there may need to be separate models (or at least, somewhat differing models) developed for soils in the desaturation zone (i.e., between the air entry value and the residual suction value) and the residual zone. In other words, there is evidence that the behavior of an unsaturated soil in the residual zone may be significantly different from its behavior in the desaturation zone between the air entry value and the residual value.

The fundamental physical characteristics of an unsaturated soil in the "residual suction" range need to be further studied with respect to volume change, shear and seepage behavior. For example, liquid water flow most likely ceases in the residual zone and only water vapor flow is of consequence. Therefore, the permeability function (or hydraulic conductivity function) should not be mathematically extended into the residual soil range when using empirical estimation techniques. This subject requires further research. Likewise, research is also required for the volume change and shear strength behavior of unsaturated soils in the residual soil range.

Research needs to be done regarding the required accuracy for the assessment of unsaturated soil property functions for various types of problems. In other words, estimation techniques may be suitable for certain types of problems but may be unsuitable for other problems. There needs to be guidelines made available to practicing geotechnical engineers.

4. Which are the goals for the next 5 years

I believe that one of the primary goals of the researcher engineers should be studies related to the implementation of unsaturated soil mechanics into routine engineering practice. There is a need to demonstrate in detail the implementation procedures that are to be used by practicing geotechnical engineers. There needs to be protocols (or standards of practice) established for acceptable engineering practice in order that engineers can be protected from excessive litigation associated with unsaturated soils problems.

There should be a review of all near-ground-surface geotechnical problems in order to develop engineering protocols for numerous types of problems. In so doing, it may be possible for some empirical practice procedures to be put onto a more reliable and theoretical basis.

Further attention needs to be given to the quantification of climatic conditions at specific engineering sites. In particular, more research is required on soil-atmosphere models that predict the actual evaporation at a site. As well, there is need for procedures for assessing runoff and infiltration into highly fractured, near-ground-surface soils. These procedures should be somewhat standardized to produce consistency and reliability in engineering practice.

In closing, I want to express my gratitude to Professor Tom Schanz and all his co-workers for the excellent conference that has been held. The organizers have drawn upon research from a variety of disciplines and geographic locations. In so doing, these conference proceedings provide a valuable addition to the unsaturated soil mechanics literature.

Saskatchewan, October 2003   Delwyn G. Fredlund

Contents

APPLICATIONS

HYDRAULIC BEHAVIOUR

Laboratory Experiments and Simulations on the Significance of Non-Equilibrium Effect in the Capillary Pressure-Saturation Relationship

[1]S. Majid Hassanizadeh

[2]Oubol Oung

[3]Sabine Manthey

[1]Section of Hydrology; Faculty of Civil Engineering and Geosciences; Delft
[2]University of Technology; P.O. Box 5048; 2600GA Delft; The Netherlands
Environmental Department, GeoDelft, Delft, The Netherlands
[3]Department of Hydromechanics and Modeling of Hydrosystems, Institute of
Hydraulic Engineering, University of Stuttgart, Pfaffenwaldring 61, 70569
Stuttgart, Germany

Abstract. Recent theories indicate that capillary pressure is perhaps not only a function of saturation but may also depend on the time rate of change of saturation. This is known as the dynamic or non-equilibrium effect. There is compelling experimental evidence reported in the literature that the non-equilibrium effect is observable, quantifiable, and significant. However, almost all reported experiments relate to unsaturated systems. In this work, we report on a recent series of experiments involving water and PCE. Quasi-static as well as dynamic capillary pressure curves for primary drainage, main drainage, and main imbibition, are measured. The data are used to estimate the non-equilibrium capillary pressure coefficient. Finally, a continuum-scale two-phase flow model has been employed to simulate the experiments. Variations of average pressures and average water saturation with time are calculated and compared with measured curves. It is found that the displacement process takes place much faster in simulations than in experiments. This is believed to be due to presence of dynamic effects not captured with the numerical model.

1. Introduction

In this paper, we study the significance of dynamic effects in capillary pressure – saturation relationship. A linear form of such a relationship has been suggested as (Hassanizadeh and Gray, 1993):

$$\left(p^n - p^w\right) - p^c\left(S\right) = -\tau\left(S\right)\frac{\partial S}{\partial t} \tag{1}$$

where p^n and p^w designate the average pressures of nonwetting and wetting phases, respectively, S is the wetting phase saturation, p^c is the traditional (quasi-static) capillary pressure, and τ is the dynamic capillary pressure coefficient.

We present results of laboratory experiments involving displacement of water and PCE in a soil sample. Both drainage and imbibition experiments have been carried out. The experimental results are analyzed and values of the dynamic coefficient τ under various conditions are determined.

In the second part of this work, the experiments are simulated by means of a numerical model. However, there is a clear discrepancy between experimental and model results when average saturation and capillary pressure is plotted as a function of time. The possible causes of this discrepancy are discussed.

2. Laboratory Experiments

A series of two-phase flow experiments involving water and PCE have been carried out. A schematic representation of the experimental setup is shown in Figure 1.

The experimental setup consisted of four main compartments: the upper chamber, soil sample chamber, the lower chamber, and water reservoir. The upper chamber served as the PCE inflow reservoir during drainage and as PCE collection reservoir during imbibition experiments. Conversely, the water reservoir served as the water collection reservoir during drainage and as the water supply reservoir during imbibition experiments. The lower chamber acted as a water flow-through reservoir.

The upper chamber contained air and PCE. Only PCE was in contact with the soil sample. Pressurized air was used to regulate the pressure of PCE. The pressure of PCE at the level of contact with the soil sample was measured with the aid of a hydrophobic pressure transducer. The soil sample chamber was cylindrical with a length of 3 cm and diameter of 6 cm.

The soil sample was placed between two glass filters. The upper filter was hydrophobic and, thus, it prevented water from leaving the soil at the top. The lower filter was hydrophilic and prevented PCE from leaving the sample at the bottom. The two filters were each supported by a membrane. One hydrophobic and one hydrophilic pressure transducer were inserted into the opposing sides of the sample holder in the middle. They served to measure the pressure of PCE and water, respectively, which were then used to compute capillary pressure. Water leaving or entering the soil sample passed through the lower chamber. The water pressure was monitored by means of a pressure transducer.

The water leaving the sample and passing through the lower chamber was collected in the water reservoir. The volume of water as a function of time was

determined from measurement of pressure of the water reservoir. This same information was used to determine the change of saturation of the soil sample as a function of time.

Different curves were obtained for different imposed air pressures. In quasi-static drainage experiments, the air pressure was increased incrementally, each time waiting until equilibrium was reached, i.e. no changes in pressure or saturation were observed. The equilibrium values of capillary pressure and saturation were plotted to obtain quasi-static $p^c - S$ curves. The final pressure had to be large enough to ensure full drainage of the sample but smaller than the entry pressure of the hydrophilic filter underlying the soil sample. Quasi-static capillary pressure curves are shown in Figure 2. As seen, for drainage, we have determined both primary and main curves whereas only main imbibition curve has been obtained.
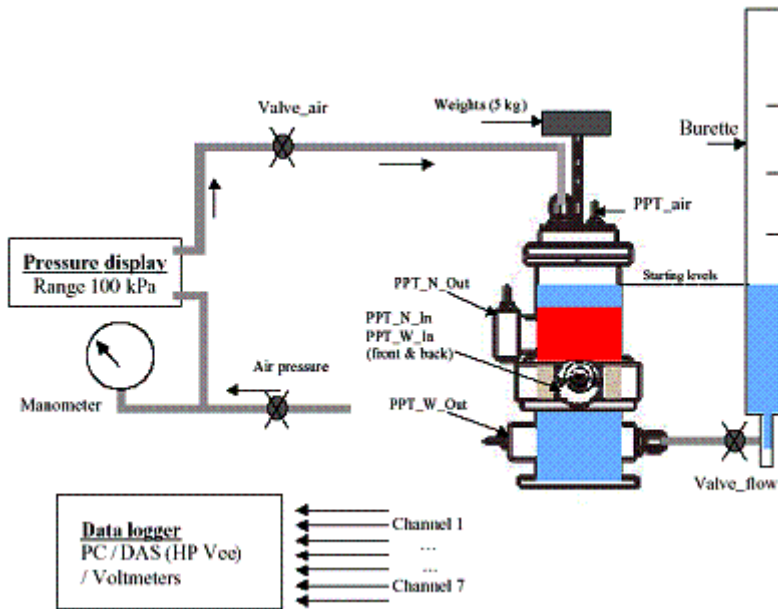
Fig. 1. Schematic representation of the experimental set up.

In dynamic experiments, the air pressure was increased to a large value, in one step. Continuous measurement of pressure of the two fluids and saturation resulted in the primary drainage dynamic capillary pressure-saturation curve. Obviously, higher air pressures resulted in a faster drainage of the sample, corresponding to a different dynamic drainage condition. The dynamic capillary pressure curves obtained for three different air pressures are shown in Figure 2.

3. Analysis of Experimental Data

In this section, we briefly describe the analysis of experimental data with the purpose of estimating the value of the transient capillary pressure coefficient τ. Let's, for convenience, denote $p^n - p^w$ by p^c_{dyn}. Thus, equations [2] may be written as

$$p^c_{dyn} - p^c = -\tau(S)\frac{\partial S}{\partial t} \tag{2}$$

This equation suggests that if we plot the difference $\Delta p^c = p^c_{dyn} - p^c$ vs $\partial S/\partial t$ for a given saturation value, we should get a straight line whose slope equals τ. Thus, each dynamic capillary pressure curve contributes only one point to the Δp^c vs $\partial S/\partial t$ plot for a given saturation. The resulting plots for various saturation values are given in Figure 3.
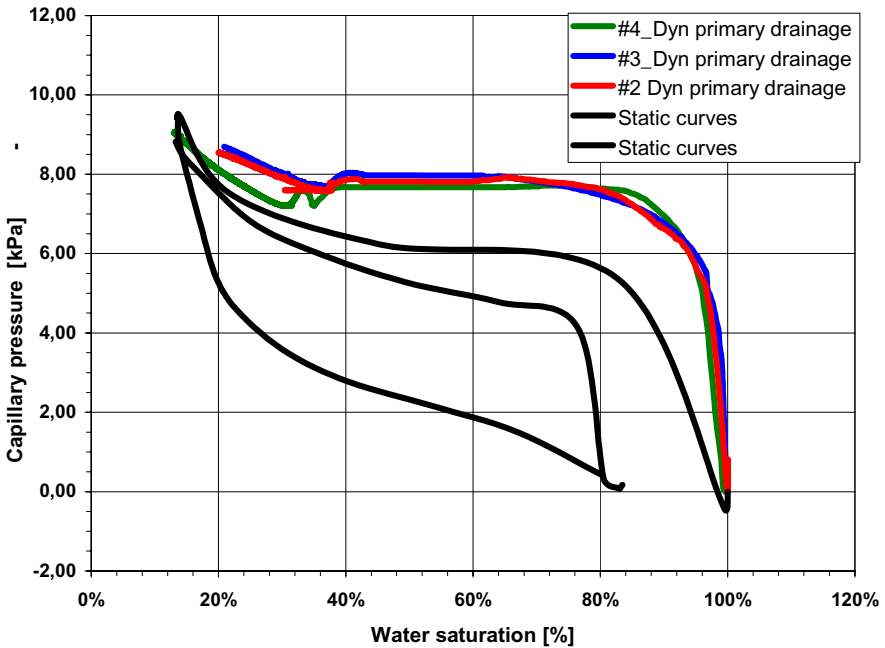
Fig. 2. Capillary pressure-saturation curves for quasi-static and dynamic experiments
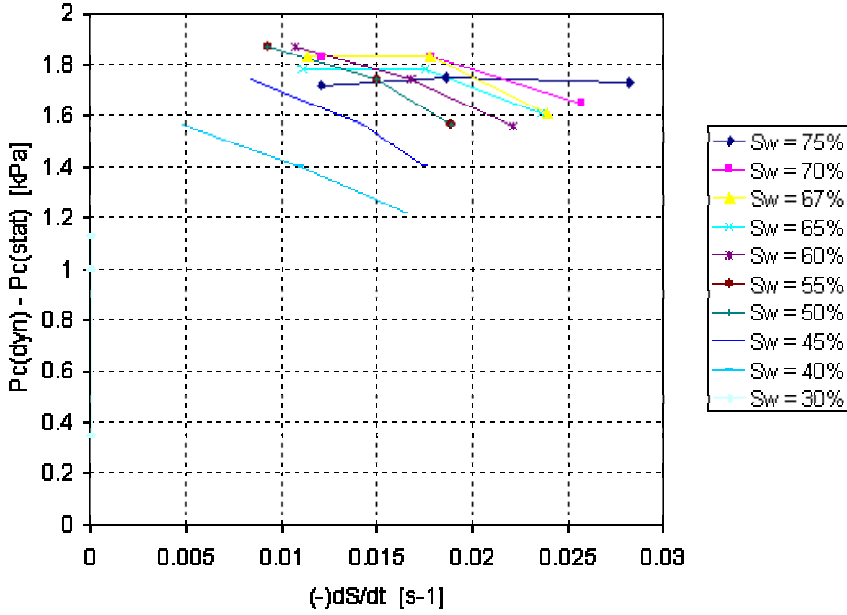
Fig. 3. Plot of Δp^c vs ∂S/∂t at various saturations.

It appears that the plotted points do not fall on a straight line. Moreover, contrary to equation [3] where the function runs through the origin, the fitted functions do not go through the origin. This means that the linear approximation [2] is not valid for the whole range of saturation. In other words, for small values of ∂S/∂t, a nonlinear relationship may be needed. Small values of ∂S/∂t occur near residual saturation. The calculated values of τ range between 5×10^5 to 6×10^5 kg/ms.

4. Simulation of the Experiments

In order to test the validity of classical two-phase flow equations, the laboratory experiments were simulated by means of a numerical model. In this section, the numerical model and the initial and boundary conditions are described. Experimental and numerical results for the averaged water saturation and local capillary pressure as a function of time and the transient capillary pressure-saturation relationship are compared and analyzed.

4.1 Description of the numerical model

The multiphase flow simulator MUFTE-UG (Bastian 1999) has been used for the simulation of the laboratory experiment. Basically, in this model, balance equations for two incompressible fluid phases. The numerical procedure is based on a node-centered Finite-Volume discretisation in space, the so-called BOX-scheme (Helmig 1997, Huber & Helmig 1999), and a backward-difference Euler-scheme for the time discretisation. A quasi Newton-Raphson scheme is employed to solve the nonlinear system of equations. The linear system of equations produced by the Newton-Rhapson algorithm is handled with a BiCGStab (stabilized biconjugate gradient) scheme applying a V-multigrid cycle as pre- and postsmoother.

In this set of simulations, primary variable are chosen to be the pressure of the wetting phase (subscript w) and the saturation of the non-wetting phase (subscript n). The governing equations are as follows if source/sink terms are neglected:

$$-\phi\rho_w\frac{\partial S_n}{\partial t}-\nabla\cdot\left\{\rho_w\frac{k_{rw}}{\mu_w}K\big(\nabla p_w-\rho_w g\big)\right\}=0 \tag{3}$$

$$\phi\rho_n\frac{\partial S_n}{\partial t}-\nabla\cdot\left\{\rho_n\frac{k_m}{\mu_n}K\big(\nabla p_w+\nabla p_c-\rho_n g\big)\right\}=0 \tag{4}$$

where ϕ is porosity, ρ is mass density, μ is dynamic viscosity, k_r is relative permeability, K is intrinsic permeability tensor, and g is gravity vector. These equations must satisfy the following restrictions:

$$S_n+S_w=1 \tag{5}$$

$$\nabla p_n=\nabla p_w+\nabla p_c \text{ with } p_c=p_c(S_w) \tag{6}$$

The dynamic capillary pressure effect at the grid scale is neglected; i.e., the capillary pressure is assumed to be a unique function of the water saturation. Brooks-Corey formula for the capillary pressure-saturation relationship (Brooks-Corey, 1964) is used. Furthermore, it is assumed that the k_r-S-relationships can be prescribed based on the P_c - S_w relationship (using Burdine formula; Burdine, 1953) and, thus, they do not need to be determined independently.

$$P_c(S_e)=\frac{S_w-S_{wr}}{1-S_{wr}-S_{nr}}=P_d S_e^{-1/\lambda} \tag{7}$$

$$k_{rw}=S_e^{2+3/\lambda},\ k_m=(1-S_e)^2\Big[1-S_e^{2+/\lambda}\Big] \tag{8}$$

where S_e denotes the effective water saturation.

4.2 Medium properties

The simulation domain consists of a hydrophobic membrane plus a membrane holder on the top, the sand sample, and a hydrophilic membrane and a membrane holder at the bottom. This corresponds directly to the experimental set-up described in the previous section. In Table 1, the parameters of the constitutive relationships for the Zeijen sand (column ZS), for the hydrophobic top membrane and its holder (column TM) and the hydrophilic bottom membrane and its holder (column BM) are given. The parameters for the Zeijen sand are based on a fit to the measured static primary drainage Pc-Sw curve (data points 1 and curve 2 in Figure 5), for the membranes corresponding values had to be assumed. The intrinsic permeability K was measured independently for all three media. Also, the porosity ϕ of the Zeijen sand was determined in the laboratory, but, porosity values for membranes were assumed based on manufacturer's data. Relevant parameters for the two fluid phases are given in Table 2.

Table 1. Parameters for the Zeijen sand (ZS), the hydrophobic top membrane including the holder (MT) and the hydrophilic bottom membrane including the holder (BM)

Parameter	ZS	TM	BM
porosity ϕ [-]	0.35	0.4	0.45
intrinsic permeability K [m^2]	$3.06 \cdot 10^{-12}$	$3.1 \cdot 10^{-12}$	$3.06 \cdot 10^{-13}$
entry pressure P_d [Pa]	5587	1000	$2.0 \cdot 10^4$
pore volume distribution index λ [-]	6.11	2.0	2.0
irreducible water saturation S_{wr} [-]	0.104	0.0	0.0
residual DNAPL saturation S_{nr} [-]	0.0	0.2	0.0

Table 2. Fluid parameters of water and DNAPL

Parameter	water	DNAPL
dynamic viscosity μ [kg/(m s)]	0.001	0.0009
density ρ [kg/m^3]	1000	1630

4.3 Initial and boundary conditions

In our primary drainage experiments, the soil sample and the bottom membrane are initially fully saturated with water. At the start of the experiment, the pressure of DNAPL at the top is increased from zero to 20.000 Pa. For the wetting phase, a no-flux boundary is imposed to account for the presence of the hydrophobic membrane. At the bottom of the domain a constant water pressure relating to a head of 0.03 m is imposed in accordance with the height of water in the water collection reservoir. A no-flow boundary at the bottom represents the presence of a hydrophilic membrane. Of course, the high entry pressure of the bottom

membrane prevents the DNAPL from reaching the lower boundary, as it was the case in the laboratory set-up. The sides of the domain are no-flux boundaries for both fluid phases.

4.4 Local and average variables

During the laboratory experiments pressure transducers measured the phase pressures in the middle of the sample. The contact area of pressure transducers with soil has a diameter of 6 mm. Thus, the measured pressures correspond to average values over a finite area in the middle of the sample. The average water saturation was determined from the changes in the water level in the burette. For numerical simulations the average water saturation and the phase-volume-weighted pressures were calculated for a given time step tn, considering only the part of the domain that represents the sand sample, using the following formulas:

$$\overline{S}_w^{tn} = \sum_{i=1}^{m} S_{wi}^{tn} \cdot w_i \ \text{ with } w_i = \frac{V_i^{node}}{V_{dom}} \tag{9}$$

$$\overline{p}_\alpha^{tn} = \frac{\sum_{i=1}^{m} p_{\alpha i}^{tn} \cdot V_i^{node} \cdot S_{\alpha i}^{tn} \cdot \varphi_i}{\sum_{i=1}^{m} V_i^{node} \cdot S_{\alpha i}^{tn} \cdot \varphi_i} \ \text{ with } \alpha = w, n \tag{10}$$

In these equations, V^{node} is the finite volume that belongs to a node in the grid, which consists of m nodes, and V_{dom} is the volume of the soil sample.

In order to be able to compare numerical and experimental results, also the average capillary pressure for a finite area in the middle of the sand sample, corresponding to the pressure transducer size, is tracked with time. This capillary pressure will be denoted as local pc in the following.

5. Simulation Results

The increase of the pressure of the non-wetting phase from zero to 20,000 Pa at the top of the domain causes the DNAPL to infiltrate the domain. A comparison of the development of the average water saturation with time between the experiment and the simulation reveals a significant difference in the transient behavior (see Figure 5).
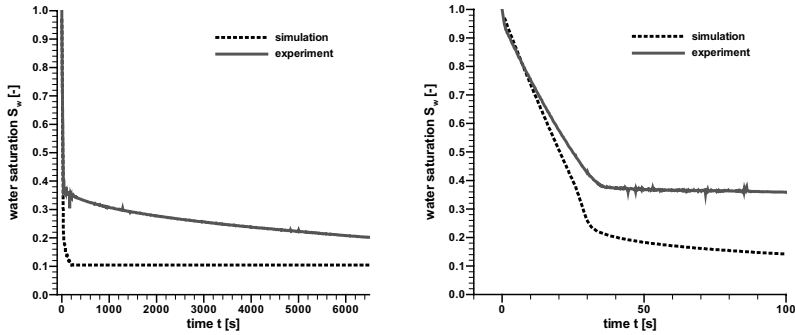
Fig. 4. Average water saturation as a function of time as measured in the laboratory experiment and as calculated from the simulation, for the whole duration (left) and zoomed in for the first 100 s (right) (primary drainage experiment with pn=20.000 Pa at the top)

Initially, both curves show a high outflow rate, which in the case of the laboratory experiment is followed by a slow approach to equilibrium starting at a water saturation of $\overline{S}_w \cong 0,36$ at time $t \cong 35s$. After that, the two curves exhibit different behaviors. The simulated curve shows that drainage continues (at somewhat smaller rate) and the residual saturation is reached rather quickly (at t = 250 s) and after that it remains constant. The experimental curve, however, shows a very long tail, with drainage continuing at a very small rate. At the end of the drainage experiment ($t \cong 6500s$), the irreducible water saturation, determined from the quasi-static experiment (see Figure 4) was not reached yet and the saturation was still changing.

The laboratory experiments yield quantifications of the damping coefficient τ, which can be determined based on the static and dynamic P_c-S_w-relationships and the saturation rates (see Eqn. 4). A dynamic P_c-S_w relationship can also be determined from the simulations although of course we still have local equilibriums. If we determine the dynamic P_c-S_w-relationship as done in the experiment (local measurement of the capillary pressure as a function of average water saturation) the dynamic primary drainage curve (curve 4 in Figure 5) does not always lie above the static primary drainage curve (curve 2 in Figure 5). However, this is to be expected for a drainage experiment where the difference between the dynamic and static P_c should always be positive. If the difference between the phase-volume-weighted pressures of the non-wetting and wetting phase is plotted as a function of average water saturation (curve 5 in Figure 5) the difference to the static curve is positive for all water saturations. However, the thus determined dynamic P_c is much higher than the one determined locally during the laboratory experiment (curve 3 in Figure 5).
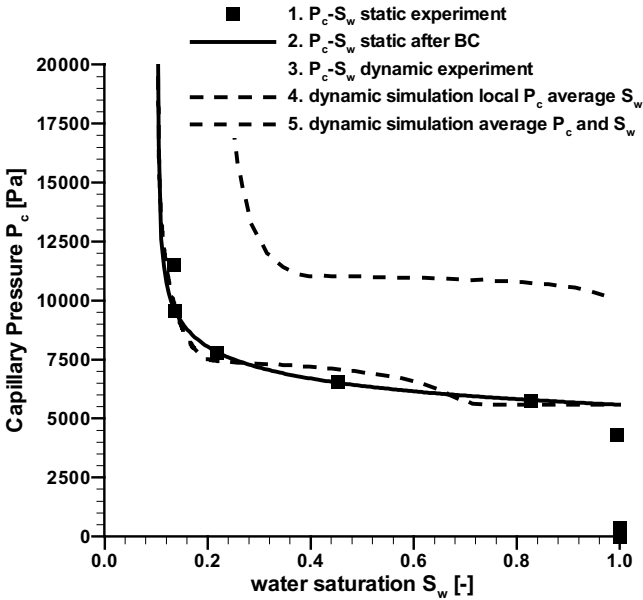
Fig. 5. Static and dynamic capillary pressure-saturation curves as determined in the laboratory and the simulations with differently determined capillary pressure (primary drainage experiment with Pn=20.000 Pa at the top)

6. Discussion and Conclusion

Displacement experiments reported in this paper have clearly shown that the traditional quasi-static capillary pressure curves for two-phase flow do correctly represent the relationship between the two phase pressures under flow conditions. The experiments were used to test an extended non-equilibrium the relationship between the two phase pressures and saturation. The experimental results were analyzed and values of the dynamic capillary pressure coefficient that appears in the extended theory were determined. The values of 5×10^5 to 6×10^5 kg/ms found here are in agreement with the range that is obtained in other laboratory experiments (see Hassanizadeh et al., 2002).

   The experiments have been simulated numerically. There is a reasonable agreement between measured and simulated capillary pressure curves. However, there is a marked difference between simulated and measured results for the change of saturation and capillary pressure in the sample with time. The differences between the measurement and the simulation could be attributed to the following reasons:

1. The relative permeability-saturation relationship should be determined independently and not deduced from the capillary pressure-saturation relationship.
2. The effective parameters of the Zeijen sand are not determined correctly.
3. The lower boundary condition does not represent the laboratory conditions well enough.
4. The assumptions underlying the physical-mathematical model (see Eqns. 5-8) do not apply to the dynamics of this experiment. These assumptions include neglecting of inertial terms or coupling terms due to friction effects between the two moving fluids. Moreover, it is implicitly assumed that the unique P_c-S_w relationship which was determined under quasi-static conditions can be applied to transient flow processes.

In order to test the first possible cause mentioned above, one would have to determine the k_r-S-relationships independently for which we do not have the means at the moment. However, this would mean again determining a constitutive relationship under steady-state conditions and applying it to transient flow processes. The second possible cause can be discarded with the justification that the intrinsic permeability and the P_c-S_w-relationship were determined independently several times. The third cause was tested with a kind of free-flow boundary at the lower end, which did not alter the numerical results perceptively. Regarding the fourth possible cause, we have calculated Reynold's number and it is found to be smaller than one throughout the experiment and, thus, neglecting of inertial terms is justified. Also, viscous coupling is found by other researchers not to be significant under such conditions. So, the only probable cause relates to the use of quasi-static capillary pressure curves under flow conditions. We plan to implement the extended relationship for the P_c-S_w function in our model and investigate its ability to simulate experimental results.

Acknowledgments

References

Bastian, P., 1999 : Numerical computation of multiphase flows in porous media. Habilitation thesis. Christian-Albrechts-Universität Kiel, Germany.
Brooks, R. H. and A. T. Corey, 1964: Hydraulic properties of porous media. Hydrology Papers. Colorado State University.

Burdine, N. T. 1953: Relative permeability calculations from pore size distribution data. *Petroleum Trans.*, 198: 71-77.

Helmig, R., 1997 : Multiphase flow and transport processes in the subsurface. Springer, Berlin, Heidelberg.

Hassanizadeh, S.M., M.A. Celia, and H.K. Dahle, "Dynamic effects in the capillary pressure-saturation relationship and their impacts on unsaturated flow," *Vadose Zone Journal*, **1**, pp. 38-57, 2002.

Huber, R. U. and R. Helmig, 1999: Multiphase Flow in Heterogeneous Porous Media: A Classical Finite Element Method Versus an IMPES-based Mixed FE/FV Approach *International Journal for Numerical Methods in Fluids*. 1(29): 899-920

Determination of hydro-mechanical Properties of Sand

Yvonne Lins[1] and Tom Schanz[1]

Laboratory of Soil Mechanics, Bauhaus-Universität Weimar, Coudraystr. 11 C, Weimar 99432, Germany (`yvonne.lins/tom.schanz@bauing.uni-weimar.de`)

Summary. In this study the behavior of an unsaturated sand is examined. The sand used is Hostun sand from France. The Soil-Water-Characteristic Curves (SWCCs) of loose and dense specimen were determined by using the suction mode and pressure mode axis translation technique under various vertical net stresses. One dimensional compression and rebound behavior was studied for specimens at different initial matric suction values. During these tests the matric suction was maintained constant during loading and unloading processes. To study the wetting induced collapse of the sand, specimens with a known matric suction and water content were prepared and then saturated at several vertical net stresses during loading. The study showed that the SWCC is not significantly influenced by vertical net stress. However there is a influence of initial suction on the compression behavior of the material which is manifested on the stiffness moduli, compression index and collapse potential of the sand used in this study. In comparison to these results, results from one dimensional compression and rebound tests, where water content was kept constant, for Quartz sand Weferlingen were added. Results from collapse potential test for Quartz sand Weferlingen are given, too.

Keywords: Hydro-mechanical behavior, unsaturated granular frictional materials, one dimensional compression rebound test, SWCC, collapse

1 Introduction

It is generally known that the presence of moisture in granular materials can drastically change their constitutive behavior. In literature results concerned with change of shear strength due to water content or matric suction [3] [16] and hydraulic conductivity [2] are given. In [20] experimental results are given on the SWCC for Hostun sand. Results of former investigations at Bauhaus University Weimar on the hydraulic conductivity are given in [9, 17, 15]. For determination of the effect of degree of saturation on the mechanical behavior of granular materials this experimental work was carried out. Observations of the coupled hydro-mechanical behavior were correlated with application and measurement of the negative pore water pressure. In this paper we concentrate on the determination of the capillary pressure saturation relationship (soil-water characteristic curve SWCC) and the constitutive behavior for confined compression.

Table 1. Properties of sand used

	Hostun Sand
Specific gravity ρ_s	2.65
Coefficient of uniformity C_u	1.50
Coefficient of curvature C_c	1.11
Classification (USCS)	SP

Experimental results of this work will be used to estimate constitutive parameters for numerical models and statistical approach. A statistical approach for SWCC is presented in [13, 12] and a theoretical approach to model unsaturated behavior of granular materials in the frame of the theory of plasticity is presented in [5].

2 Material used

The material used in this study is Hostun Sand [6, 18] from France. The properties of the sand are summarized in Table 1 and the grain size distribution curve is given in Figure 1. As can be seen from the grain size distribution curve it is a uniform graded medium sand. According to USCS classification the sand is described as a sand SP.
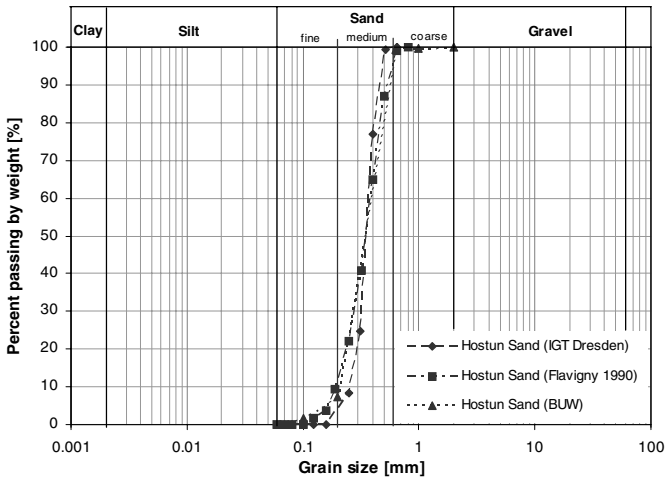
Fig. 1: Grain size distribution curves of sand tested by different laboratories
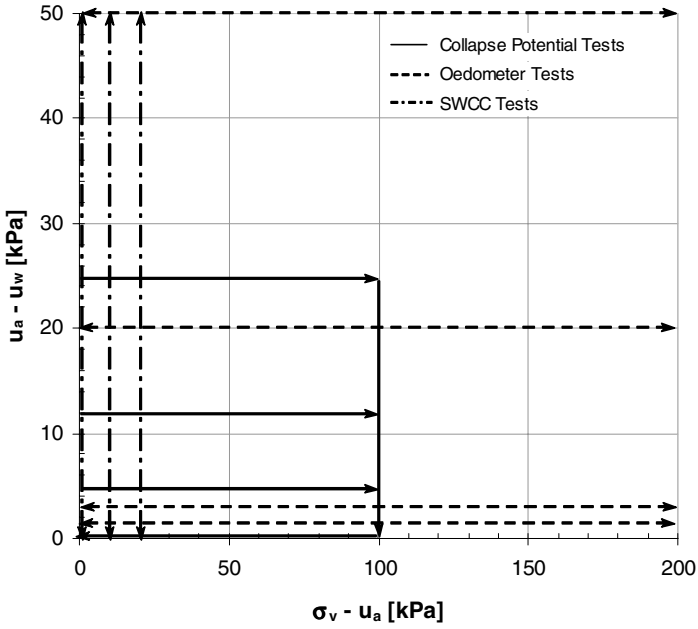
Fig. 2: Loading history of different laboratory tests

3 Experimental Program

The experimental program consists of determination of SWCC (Soil-Water-Characteristic Curves) as well as one dimensional compression rebound tests under different initial conditions. Detailed information on the different loading pathes are given in Fig. 2.

For determining Soil-Water-Characteristic Curves of the sand a modified pressure plate apparatus was used. This apparatus allows to apply vertical stress to the top of the specimen. One dimensional compression and rebound test were performed in a UPC Controlled-Suction Oedometer Cell [1]. Both cells are equipped with a porous stone on the top of the cell and a ceramic disc on the bottom of the cell. The ceramic discs used in this investigation have an air entry value of 1 bar. The used apparats are additionally equipped with a burette attached to the water reservoir below the ceramic disc and an air pressure control system connected to the top of the cell. Tests were carried out for loose specimen with an initial void ratio of $e_0 = 0.89 \pm 0.005$ and dense specimen with an initial void ratio of $e_0 = 0.66 \pm 0.005$. The precision for measured deformation is 0.001 mm and 0.6% of the absolute value for stresses (both vertical stress and air pressure).

3.1 Determination of Soil-Water-Characteristic Curve

SWCCs were determined for loose as well as for dense specimen. To examine the influence of net stress on the SWCC loose specimen were applied by a net stress of $\sigma^\star = 10$ and 20 kPa. Additionally SWCC for dense and loose specimen with net stress $\sigma^\star = 0$ kPa were performed. The SWCC for the sand were obtained by using pressure mode test and suction mode test.

The testing procedure consists of preparing a dry specimen directly into the fixed ring of the cell. By using the attached burette the specimen was saturated. From this condition the determination of SWCC started with a drying cycle followed by one wetting cycle.

SWCC of the sand was determined by both suction mode test and pressure mode test. By using the attached burette with a capacity of 25 cc and a least count of 0.05 cc the suction mode test was carried out for low suction values up to 3.0 kPa. Suctions of 0.1 kPa, 0.2 kPa, 0.5 kPa, 1.0 kPa, 1.5 kPa, 2.0 kPa and 3.0 kPa were induced by lowering down the burette with reference to the top of the ceramic disc. Higher suctions up to 50.0 kPa were applied by the pressure mode test. Therefore the connected air pressure control system was used. After finishing one drying and one wetting curve, wich are also called desorption curve and adsorption curve, the specimen was dismantled and the gravimetric water content was measured by oven drying method. By back calculation the volumetric water content Θ, the degree of saturation S_r and the gravimetric water content w corresponding to each matric suction applied were computed.

3.2 One dimensional compression and rebound tests

One dimensional compression and rebound tests with different initial conditions were carried out in this study:

– One dimensional compression and rebound test with constant suction.
– One dimensional compression and rebound test with constant water content.

Special attention was given to the error estimation related to the vertical net load. Correction was applied to the measured vertical net stresses due to shear stresses between the oedometer ring and the soil sample. Both frictional (fixed ring, triangular distribution of horizontal stress: $\sigma_h^{max} = (1-\sin\varphi_p)\sigma_v^\star$, loose: $\varphi_p = 34^o$, dense: $\varphi_p = 42^o$ [19]) and cohesional effects (derivation of capillary cohesion from SWCC) were taken into account following [8].

One dimensional compression rebound test with constant suction

Loose and dense dry specimen were prepared directly in the fixed oedoemter ring, followed by the saturation process. Suctions induced by suction mode test for $s = 1.5$ kPa and $s = 3.0$ kPa and pressure mode test for $s = 20$ kPa

and $s = 50.0$ kPa were applied to the sand samples and kept constant during the loading and unloading path. Specimen were loaded up to 200 kPa and then unloaded to 2 kPa.

One dimensional compression rebound test with constant water content

For comparison of the results from our actual study, test results from earlier work with Quartz sand Weferlingen were taken into account [14]. During this study specimen with different water contents were prepared. In difference to the tests carried out with constant suction values for this type of tests a porous stone was placed on the bottom as well as on the top of the specimen similar to standard one dimensional compression and rebound test equipment. Tests were run under undrained conditions.

3.3 Collapse potential tests

For different initial conditions the collapse potential of Hostun sand was studied. All specimen were prepared for loose conditions ($e_0 = 0.89 \pm 0.005$). During loading the specimens with constant suction or water content were saturated from the bottom of the cell by the attached burette at certain vertical net stress. The saturated specimen was loaded up to 100 kPa and unloaded. Saturation process was carried out at vertical net stresses of 5 kPa, 12 kPa and 25 kPa.

Method 1

For this method dry specimen were prepared in the oedometer cell, saturated and a suction of $s = 5.0$ kPa was induced by pressure mode. For the initial loading the specimen was saturated by net stress of $\sigma^\star = 5$ kPa and $\sigma^\star = 12$ kPa.

Method 2

Method 2 includes the preparation of a wet sand sample with a water content of $w = 5\%$. From the SWCC for loose specimen one can find out that a water content of $w = 5\%$ corresponds to a suction less than $s = 5$ kPa. By applying 5 kPa air pressure (pressure mode test) from the top of the specimen suction was applied. Samples were saturated at $\sigma^\star = 5$ kPa, 12 kPa and 25 kPa.

Method 3

Specimen with a water content of $w = 3\%$, which correlates to a suction of $s = 5.0$ kPa were prepared and loaded for undrained test conditions up to $\sigma^\star = 5$ kPa 12 kPa and 25 kPa, saturated, further loaded up to 100 kPa and unloaded. In difference to the first methods the ceramic disc on the bottom was replaced by a porous stone.

4 Experimental results

4.1 Soil-Water-Characteristic Curves for Hostun Sand

To study the influence of initial void ratio we display in Fig. 3 the results from SWCC test for one loose sample in comparison with one dense sample. The volumetric water content is plotted against matric suction for one drying cycle and one wetting cycle. According to [7] typical ranges of the SWCC are included into the diagram exemplary for the dense drying curve. By using the following equation [7] the data points were fitted (see also Fig 4)

$$\Theta_w = \frac{\Theta_s}{\left\{ ln \left[e + \left(\frac{\Psi}{a} \right)^n \right] \right\}^m}$$

(1)

where Θ_w is volumetric water content, Θ_s is the saturated water content, Ψ is the suction value and a, n, m are constants, e is the natural base of the logarithm. As can bee seen from Fig. 3 an air-entry value (AEV) of $\psi_{AEV} = 2.0$ kPa for dense specimen and an air-entry value of $\psi_{AEV} = 1.5$ kPa for loose specimen for drying path were found. When reaching the air-entry value the water content of both samples decreases rapidly for a small range of suction. This zone, the transition zone, is between 2.0 kPa to 4.0 kPa for the dense
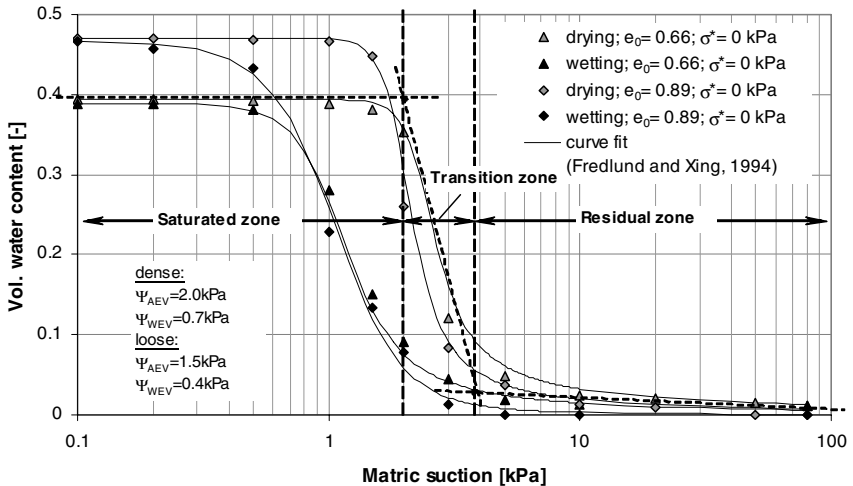
Fig. 3: Volumetric water content versus matric suction for loose and dense samples and $\sigma^\star = 0$

specimen and between 1.5 kPa to 4.0 kPa for the loose specimen. Residual zone starts at low suction values for the drying curve for loose as well as for the dense sand specimen. During wetting no significant changes in water content in a range of 50 kPa to 3 kPa were observed for the loose and dense specimen. For the wetting curve the transition zone starts at matric suction of 0.5 kPa for loose and dense samples. It ends at a matric suction of 3 kPa. Water-entry values (WEV) of $\psi_{WEV} = 0.7$ kPa for dense sand specimen and of $\psi_{WEV} = 0.3$ kPa for loose sand specimen were determined graphically. The saturated zone falls in a very narrow range from 0 kPa to 0.5 kPa.

From Fig. 3 it can be seen that after reaching the air-entry value the curves rapidly falling down to low values of volumetric water content. The slopes of the curves are steep, which is also reflected in the calculated value n (value describing the slope of the curve) during curve fitting. The following values were found for the loose specimen and dense specimen: $n = 8.5$ (drying curve,
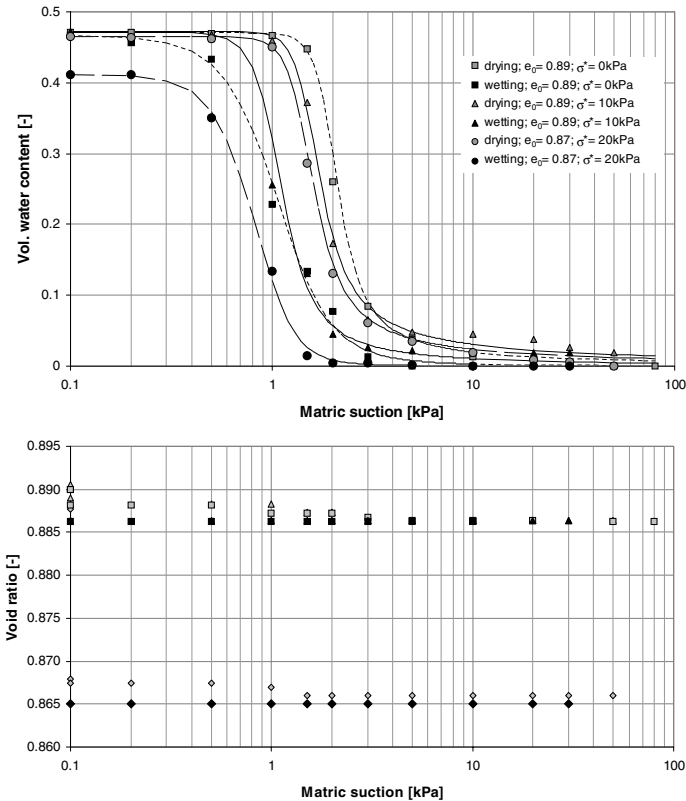
Fig. 4: SWCC - drying and wetting cycle for loose specimen under different vertical net stress and volumetric behaviour

loose), $n = 8.3$ (drying curve, dense), $n = 3.0$ (wetting curve, loose) and $n = 4.5$ (wetting path, dense). During drying the slope of the loose specimen is slightly steeper. Caused by the larger voids the loose specimen desaturates slightly faster. Because of larger voids the volumetric water content of the loose specimen is after reaching the air-entry value slightly smaller than for the dense one. Since void ratio decreases the pore sizes become smaller and as assumed the air-entry value with $\psi_{AEV} = 2.0$ for the dense specimen is slightly higher than for the loose specimen, where $\psi_{AEV} = 1.5$ was found. In opposite of the drying curve for the wetting curve the dense specimen is steeper. In this case the smaller voids absorb the water slightly faster.

Water content versus matric suction is plotted in Fig. 5. In Fig. 5it can be seen, that the water content of the dense specimen for saturated condition $S_r = 1.0$ is lower than for the loose one, because of smaller voids. Finally hysteresis is significant for both specimen.

In Fig. 4 the SWCCs for the loose specimens with different applied net stresses $\sigma^\star$ are presented. For these tests in Fig. 4 the matric suction s is plotted against the void ratio e, too. It can be seen that in contrast to cohesive soils, the SWCC is not significantly influenced by the level of net stress. SWCCs for all specimen fall in the same range. Due to applied suction there is no significant change in void ratio. Changes in void ratio were only measured during saturation process and after applying net stresses. The curves are characterized by the values given in Tab. 2.

Water content plotted against the matric suction for the loose and dense specimen are presented in Fig. 5, where experimental results from [20] are
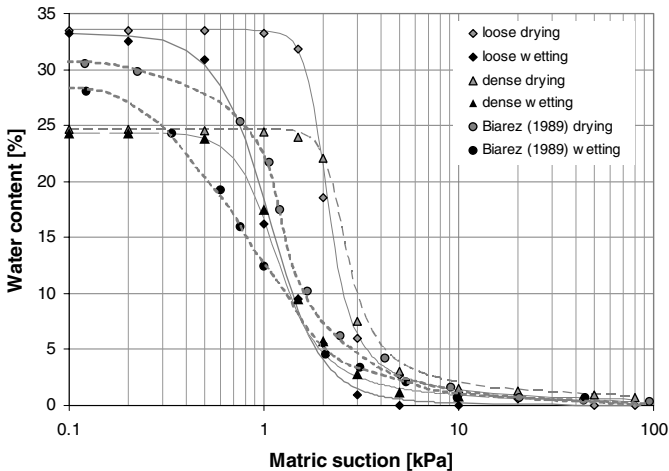
Fig. 5: SWCC for Hostun Sand: comparison with results from Biarez (1999)

Table 2. Calculated and measured parameters of SWCC with applied net stress

Applied net stress $\sigma^\star$ [kPa]	0	10	20
Matric suction s [kPa] for $S_r = 0.5$	2.00	1.80	1.60
Air-entry value [kPa]	1.50	1.20	1.10
Water-entry value [kPa]	0.40	0.70	0.35

included additionally. It can be seen that current results are in a good agreement with results taken from [20].

4.2 Results from one dimensional compression rebound tests

One dimensional compression rebound test with constant suction

Test results from one dimensional compression rebound tests are presented in Fig. 6. Applied vertical net stress is plotted versus volumetric strain and void ratio. For better understanding 3D plots of the oedometer results for loose and dense sand specimen are added in Fig. 7. From Fig. 6 and Fig. 7 one can see that as anticipated the stiffness for dense specimen is higher then for loose
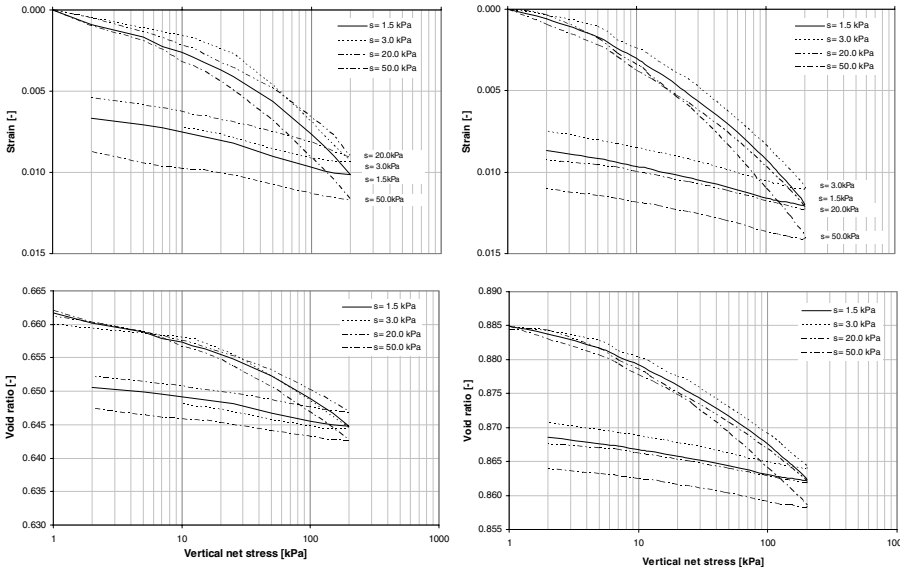
Fig. 6: Vertical stress versus strain and void ratio of dense (left) and loose (right) specimen in the oedometer cell for constant suction conditions
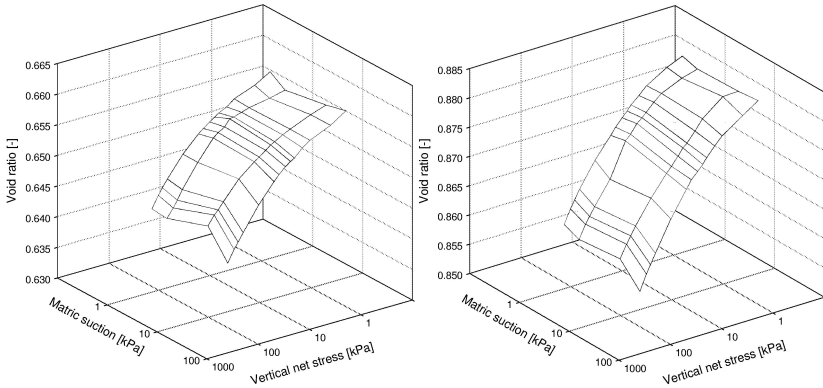
Fig. 7: 3D plots of oedometer test results for dense (left) and loose (right) sand samples

specimen. For the loose specimens a change in void ratio of approximately $\Delta e = 0.025$ and $\Delta e = 0.015$ for the dense specimens was calculated, which indicates a higher stiffness for the dense one.

The stiffness increases with matric suction from $s = 1.5$ kPa, 3.0 kPa and 20.0 kPa for the tests carried out for dense specimen. Lowest stiffness results from the test with a matric suction of $s = 50.0$ kPa. Similarly to the dense specimens for the loose one the lowest stiffness was calculated for the specimen with matric suction $s = 50.0$ kPa. With increase in matric suction from $s = 1.5$ kPa to 20.0 kPa the stiffness is slightly increasing. Comparing the unloading path of all tests one can state that, there is a similar behavior for all the specimens. To further underline the observed behavior we display the compression index $C_c^\star$ and the swelling index $C_s^\star$ in Fig 8. Compression index decreases first for suction less then about $3 kPa$ and increases again for higher suction values. As expected compression index of the dense specimen is less then the compression index of the loose one, which indicates a higher stiffness. No influence of the suction on the swelling index can be observed. According to Eqs. 2 the stress dependent stiffness moduli E_{oed} and E_{ur} were calculated for vertical net stress $\sigma^\star = 12 kPa$ as well as for $\sigma^\star = 100 kPa$, where E_{oed}^{ref} is the normalized stiffness modulus for initial loading and E_{ur}^{ref} is the normalized stiffness modulus for un-/reloading path. Results are given in Table 3. For the constant m we calculated for the dense specimen $m = 0.62$ to 0.81 and the loose specimen $m = 0.53$ to 0.73. For detailed information of determination of E_{oed} and E_{ur} see [11, 19].

$$E_{oed} = E_{oed}^{ref} \left(\frac{\sigma^\star}{\sigma_{ref}^\star} \right)^m \qquad E_{ur} = E_{ur}^{ref} \left(\frac{\sigma^\star}{\sigma_{ref}^\star} \right)^m \quad \sigma_{ref}^\star = 100 kPa \quad (2)$$
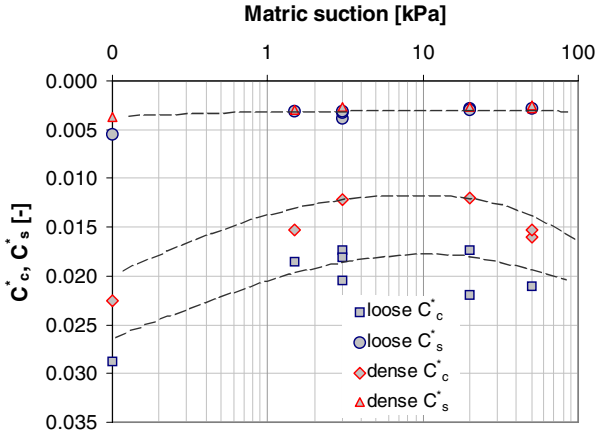
Fig. 8: Compression and swelling index versus suction

Table 3. Results for stiffness modulus in MPa for dense and loose specimen

Matric suction [kPa]	dry	1.5	3.0	20.0	50.0
dense					
$E_{oed}\ \sigma^\star = 100$	23.3	30.3	29.4	35.6	27.8
$E_{oed}\ \sigma^\star = 12$	10.4	6.9	8.2	8.1	5.7
$E_{ur}\ \sigma^\star = 100$	175.2	131.5	258.0	141.3	167.8
$E_{ur}\ \sigma^\star = 12$	8.0	14.8	10.4	15.9	16.3
loose					
$E_{oed}\ \sigma^\star = 100$	15.1	24.4	24.7	24.6	22.8
$E_{oed}\ \sigma^\star = 12$	6.7	6.6	7.1	5.4	4.9
$E_{ur}\ \sigma^\star = 100$	102.9	154.9	138.3	125.7	153.8
$E_{ur}\ \sigma^\star = 12$	7.6	15.0	12.0	17.2	17.0

One dimensional compression rebound test with constant water content

To compare the current results, results for $C_c^\star$ and $C_s^\star$ from previous investigations (constant water content tests) [14] are shown in Fig. 9. The results for $C_s^\star$ are similar to that shown in Fig. 8. In opposite to the current results on Hostun sand no influence of matric suction on $C_c^\star$ and thus on the stiffness can be observed. The results are very much scattered and no tendency is apparent.
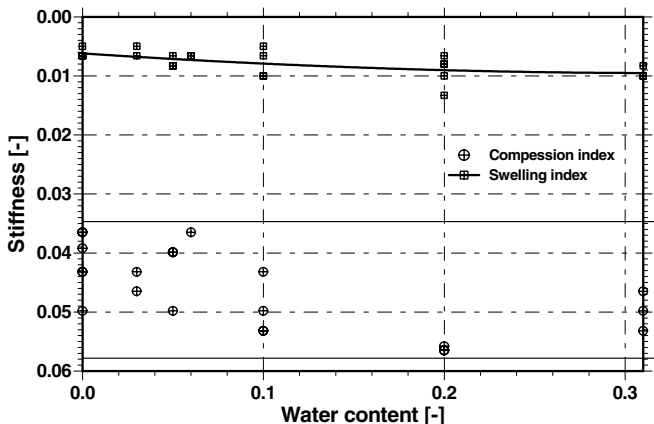
Fig. 9: Compression and swelling index versus water content, quartz sand Weferlingen ($e_0 \approx 0.84$, $(w_0 - w_{end})_{max} = \pm 0.03$)

Collapse potential

Results of oedometer tests for estimation of collapse potential are presented in Fig. 10 (Method 1), Fig 11 (Method 2) and Fig. 12 (Method 3) for loose samples. All diagrams show, that the collapse potential of Hostun Sand is very small. It seems that Method 1 is not a suitable procedure for estimation of collapse potential. Even during saturation at small net stress of $\sigma^\star = 5$ kPa a difference in void ratio of $\Delta e = 0.0016$ was measured. Reason for this behavior is, that macrostructure is already destroyed after first saturation process, before applying higher suction of 5 kPa.

Results from Method 2 show differences in void ratio of $\Delta e = 0.0033$ for saturation at $\sigma^\star = 5$ kPa, $\Delta e = 0.0022$ for saturation at $\sigma^\star = 12$ kPa and difference in void ratio of $\Delta e = 0.0020$ for saturation at $\sigma^\star = 25$ kPa. Comparing the compression index for loading path before and after saturation one can find that stiffness of the sand decreases with saturation process. The compression index $C_c^\star = 0.0108$ for first loading path with matric suction of $s = 5.0$ kPa in comparison with $C_c^\star = 0.0204$ for the second loading path with $S_r = 1.00$ is smaller and indicates higher stiffness.

The same behavior was found during Method 3, where we calculated $C_c^\star = 0.0094$ for first loading path and $C_c^\star = 0.0226$ for second loading path.

Fig. 13 presents results concerning the collapse potential of quartz sand Weferlingen. By using Method 3 this test was carried out ($w = 5\%$). Saturation was started at a vertical net stress of $\sigma^\star = 100$ kPa. The sand sample collapsed from void ratio of $e = 0.813$ to $e = 0.806$.
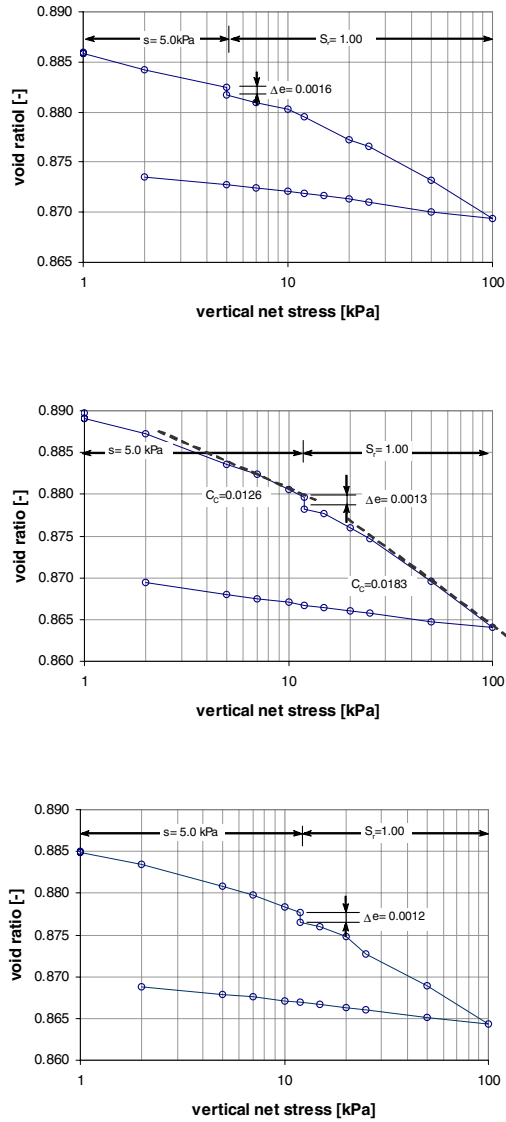
Fig. 10: Estimation of collapse for vertical net stress at (top) $\sigma^\star = 5.0$ kPa and (middle),(bottom) $\sigma^\star = 12.0$ kPa, loose Hostun Sand, Method 1
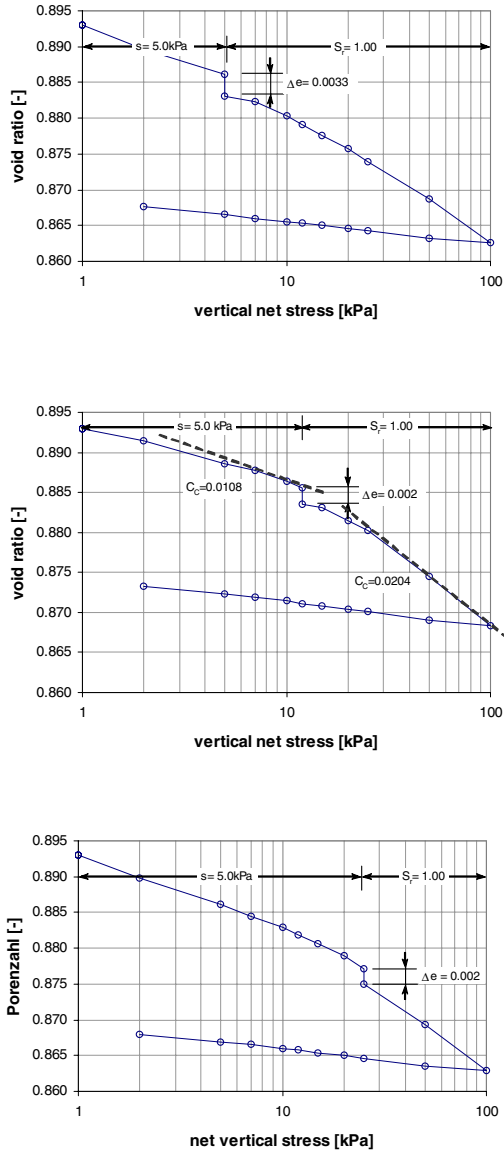
Fig. 11: Estimation of collapse for vertical net stress at (top) $\sigma^\star = 5.0$ kPa; (middle) $\sigma^\star = 12.0$ kPa and (bottom) $\sigma^\star = 25.0$ kPa, loose Hostun sand, Method 2
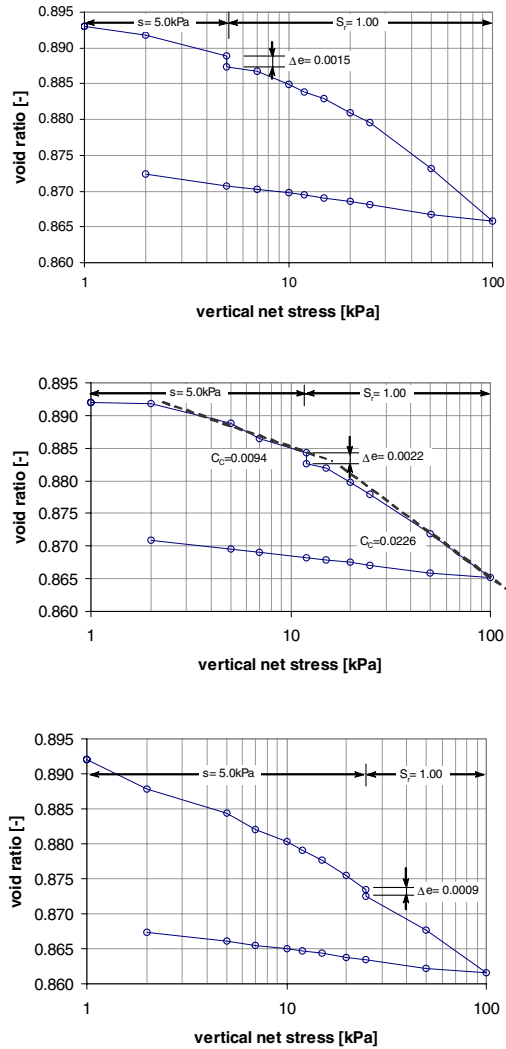
Fig. 12: Estimation of collapse for vertical net stress at (top) $\sigma^\star = 5.0$ kPa; (middle) $\sigma^\star = 12.0$ kPa and (bottom) $\sigma^\star = 25.0$ kPa, loose Hostun sand, Method 3

In comparison to the results of the Hostun Sand a distinct collapse behavior was established for quartz sand Weferlingen. In Fig. 13 oedometer results of two further tests with constant water content are shown. The compression
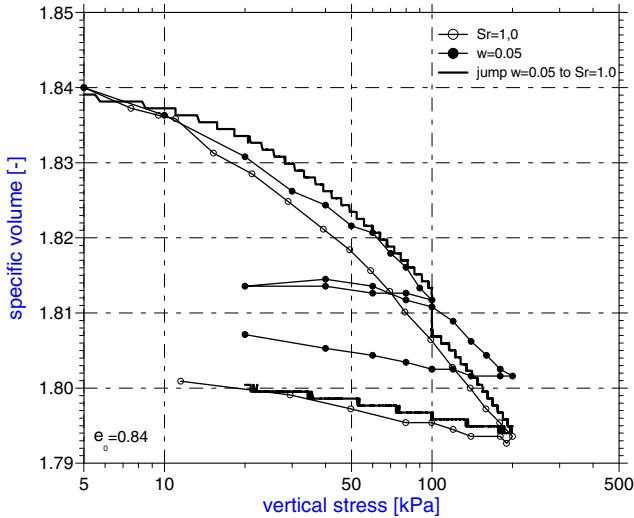
Fig. 13: Collapse potential of quartz sand Weferlingen: two oedometer tests with constant water content (w=5% and S_r=1.0) and one test with jump at 100 kPa from w=5% to S_r=1.0

curve for the sand sample with water content of $w = 5\%$ is close to the first part of the jump-test. After saturation process the compression curve of the jump-test follows the test with $S_r = 1.0$.

5 Conclusions

Summarizing the presented results we can draw the following conclusions:
The SWCC of Hostun sand displays a significant hysteretic behaviour. Compared to cohesive soils the effective range of suctions up to about 20 kPa requires special care for the testing procedure. No influence of the net stress could be observed. A change of void ratio during the tests was not measured. Changes in initial void ratio influence both hysteresis and air entry value.
Stiffness for one dimensional compression is clearly influenced by suction for the case initial loading. No influence was found for unloading.
Collapse potential was studied for loose conditions. Three different methods of sample preparation related to variation of initial conditions are described. Collapse potential is very small for the stress paths analysed.
Further studies will be related to the unsaturated hydraulic conductivity and the shear strength under biaxial and triaxial conditions for partially saturated states.

Acknowledgement

References

1. E. Romero: Chracterisation and thermo-hydromechanical behaviour of unsaturated boom clay: an experimental study. PhD Thesis, Universitat Politcnica de Catalunya, Barcelona (1999)
2. H.G. Gülzow: Dreidimensionale Berechnung des Zweiphasenströmungsfeldes beim Tunnelvortrieb in wassergesättigten Böden. PhD Thesis, RWHT Aachen, Aachen, (1994)
3. A.W. Bishop and I.B. Donald: The experimental study of partially saturated soil in the triaxial apparatus. In: *Proceedings of the 5th Int. Conf. Soil Mech.*, Paris, France, pp 13–22 (1961)
4. D. Croney and J.D. Coleman: Soil structure in relation to soil suction (pf). Journal of Soil Science **5**, 1, pp 75–84 (1954)
5. M. Datcheva and T. Schanz: Anisotropic bounding surface plasiticity with rotational hardening for unsaturated frictional materials. J. Phys. IV **105**, pp 305–312 (2003)
6. E. Flavigny and J. Desrues and B. Palayer: Note technique: Le sable d'Hostun RF. Rev. France. Géotech. **53**, pp 67–70 (1990)
7. D.G. Fredlund and A. Xing: Equations for the soil-water characteristic curve. Can. Ceotech. J. **31**, 4, pp 521–532 (1994)
8. D.G. Fredlund and A. Xing and M.D. Fredlund and S.L. Barbour: The relationship of the unsaturated soil shear strength to the soil-water characteristic curve. Can. Geotech. J. **33**, 4, pp 440–448 (1996)
9. S.S. Agus and E. C. Leong and T. Schanz: Assessment of statistical models for indirect determination of permeability functions from soil-water characteristic curves. Géotechnique, Vol. 53, No. 2, pp 279–282 (2003)
10. M. Th. van Genuchten: A closed-form equation for predicting the hydraulic conductivity of unsaturated soils. Soil Sci. Soc. Am. J., Vol. 44, pp 892–898 (1980)
11. J. Ohde: Zur Theorie der Druckverteilung im Baugrund. Bauingenieur, No. 20, pp 451–459 (1939)
12. E. Stoimenova and M. Datcheva and T. Schanz: Statistical modeling of the soil water characteristic curve for geotechnical data. In: *Proceedings of the First International Conference for Mathematics and Informatics for Industry*, Thessaloniki, Greece, pp 356–366 (2003)

13. E. Stoimenova and M. Datcheva and T. Schanz: Statistical approach in soil water characteristic curve modelling. In: *Proceedings of the International Conference From experimental evidence towards numerical modelling of unsaturated soils*, Weimar, Germany, (2003)
14. T. Schanz and V. Mikulitsch and Y. Lins: Untersuchungen an teilgesättigten granularen Reibungsmaterialien. In: *3. Workshop - Teilgesättigte Böden*, Weimar, Germany, pp 145–159 (2001)
15. Y. Lins and S.S. Agus and S. Tripathy and T. Schanz: Determination of unsaturated hydraulic conductivity for sands . In: *4. Workshop - Teilgesättigte Böden*, Weimar, Germany, pp 93–99 (2002)
16. I.B. Donald: Shear strength measurements in unsaturated non-cohesive soils with negative pore pressures. In: *2nd Australia-New Zealand Conf. Soil Mech. Found. Eng.*, Christchurch, New Zealand, pp 200–205 (1956)
17. T. Schanz and Y. Lins and S. Tripathy and S.S. Agus: Model test for determination of permeability and collapse potential of a partially saturated sand. In: *Paramentre de calcul geotéchnique*, Paris, France, pp 111–121 (2002)
18. E. Flavigny: Compilation des essais traiaxiauk de r/'evolution sur le sable d'Hostun RF. In: *International Report IMG*, (2002)
19. T. Schanz: Zur Modellierung des mechanischen Verhaltens von reibungsmaterialien. In: *Mitteilung 45*, Stuttgart, Germany, (2002)
20. J. Biarez and J.M. Fleureau and Indarto and S. Taibi and M.I. Zerhouni: Influence of negative pore pressure on the flow of granular materials in silos. In: *Powders and grains*, Rotterdam, Netherlands, pp 385–392 (1999)

Column test apparatus for the inverse estimation of soil hydraulic parameters under defined stress condition

A. Scheuermann, H. Montenegro, and A. Bieberstein

University of Karlsruhe, Institute of Soil Mechanics and Rock Mechanics and Federal Waterways Engineering and Research Institute (BAW), Karlsruhe

The experimental determination of soil hydraulic properties (soil water characteristic curve and unsaturated conductivity) over a large range of saturation is of utmost importance for any prediction of soil water dynamics and for evaluation of soil mechanical behaviour of unsaturated soils. However the hydraulic properties are expected to vary under stress, since inter alia they are mainly determined by the pore structure, which itself depends on the density of the soil and thus on the stress condition. A column test apparatus was developed to carry out multi-step outflow and inflow experiments under defined stress conditions on samples 45 cm in height and with a diameter of 19 cm. The simultaneous recording of pressure and changes in water content within the soil column at a reasonable temporal and spatial resolution is of crucial importance for the inverse parameter estimation process. A new measuring technique based on the method of Time-Domain-Reflectometry (TDR) permits the recording of continuos water profiles over the sample at a high temporal resolution. Transient in/outflow rates, water content profiles as well as tensiometer readings allow a detailed inspection of the hydraulic processes and yield a suitable data set for a more unique inverse parameter estimation. In the following paper the test apparatus will be introduced and results of an experiment will be presented.

Introduction

In many cases dynamic hydraulic processes in earth structures are of crucial importance for the stability evaluation of slopes of for example dikes, dams or hills (Lim et al.,1996, Ng et al., 2000). Here not only the seepage under almost saturated condition is of interest, also the unsaturated hydraulic processes may play a major role for the stability evaluation. One of the main hydraulic properties for such processes is the unsaturated conductivity of the soil, which depends largely on the suction of the soil. And the suction itself affects the soil mechanical behaviour of the corresponding earth material. The ability of a soil to absorb and store water in the pore structure is described by the soil water characteristic curve, which is considered commonly as a characteristic property. Actually suction de-

pends on different factors like the physical properties of the pore water – surface tension, viscosity and its all influencing factors like pH-value, temperature and others – as well as on the composition of the earth material (content of organic material, grain shape and grain size distribution). However the crucial property of a soil for the ability to store and release water is the pore structure, which is characterised by the pore sizes and their distribution as well as the interaction between the pores (Watabe et al., 2000, Kawai et al., 1999).

The established procedure to determine the unsaturated conductivity is to measure the soil water characteristic curve. By means of parameterisation of the soil water characteristic curve e.g. with the method of van Genuchten (1980) it is finally possible to estimate the unsaturated permeability using the analytical method of Mualem (1976). However, the main difficulty in this procedure is the adequate experimental determination of the soil water characteristic curve on representative samples under realistic mechanical and hydraulic boundary conditions.

Experimental setup

At the Institute of Soil Mechanics and Rock Mechanics at the University of Karlsruhe, in collaboration with the Federal Waterways and Research Institute in Karlsruhe, a column test apparatus was developed to carry out multi-step outflow and inflow experiments under defined stress conditions on samples 45 cm in height and with a diameter of 19 cm . Figure 1 shows the schematic description of the column test apparatus with appertaining measurement devices.
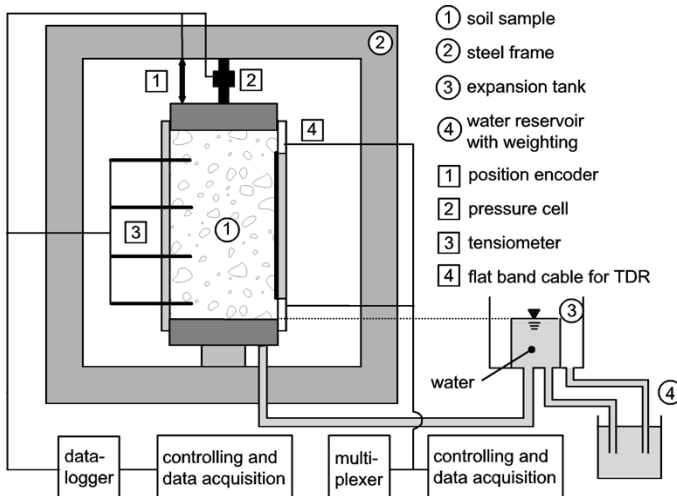
Fig. 1. Schematic description of the column test apparatus with appertaining measurement devices

The soil sample is located in a durex-bag, which is embedded in a pipe of fibre glass. On both ends the durex-bag is locked up with closing plates. In order to induce a hydraulic load on the sample – pressure as well as vacuum – a filter of sintered porous glass is installed in the lower plate. With this set up the pipe of fibre glass has no abutment and it floats, only held by the friction between the durex-bag and the pipe. The interface between durex-bag and pipe is greased with Vaseline in order to reduce the friction and to allow the sample to deform axial as unhindered as possible.

The apparatus is equipped with different measurement devices. In order to measure suction at different elevations four tensiometers are installed along the sample. For this, small windows are located in the pipe. A steel frame is used as an abutment for the mechanical load and with a pressure cell it is possible to measure the load. In order to acquire the deformation a position encoder is installed between the steel frame and the closing plate at the upper end of the column. For earth materials with higher permeability (e.g. sand) the hydraulic load is imposed by a hanging column of water and an expansion tank (cf. Figure 1 and 2). For materials of a small conductivity one has to apply the load on the sample over the gas phase through a variation of the air pressure. Figure 2 shows the column test apparatus during an experiment with sand.
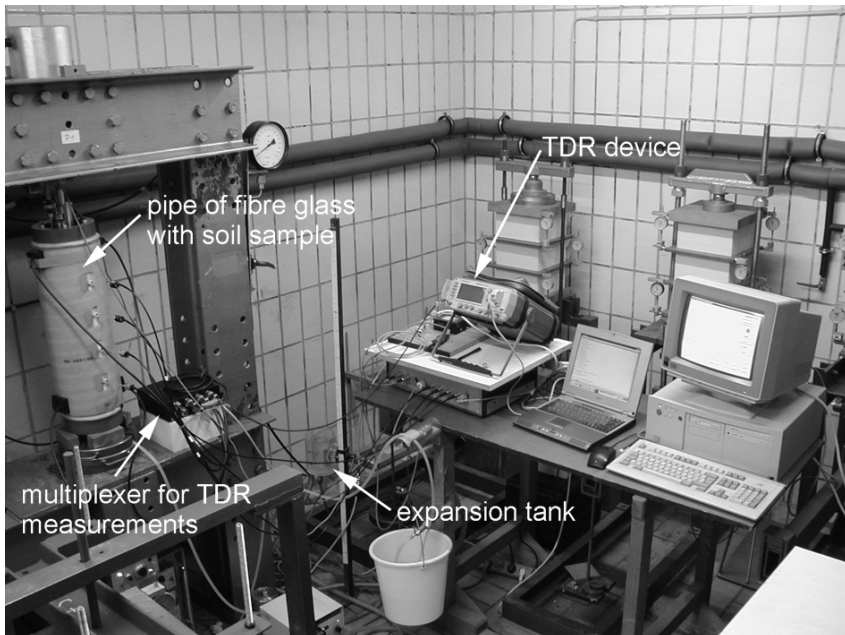
Fig. 2. Column test apparatus during an experiment with sand in April 2003

Measurement of water content using Time-Domain-Reflectometry (TDR)

TDR sensor

At two opposing positions in the column cross-section two flat band cables are installed as transmission lines between durex-bag and pipe for the measurements using the TDR-method (see Figure 3). The flat band cable used in the experiments is shown in Figure 3. The cable consists of three flat band copper wires covered with ployethylene insulation. The electrical field concentrates around the conductors and defines a sensitive area up to 5 cm around the cable. Normally this electrical field is axial-symmetric in two directions, but installed between pipe and durex-bag the electrical field will be deformed as it is shown in Figure 3.
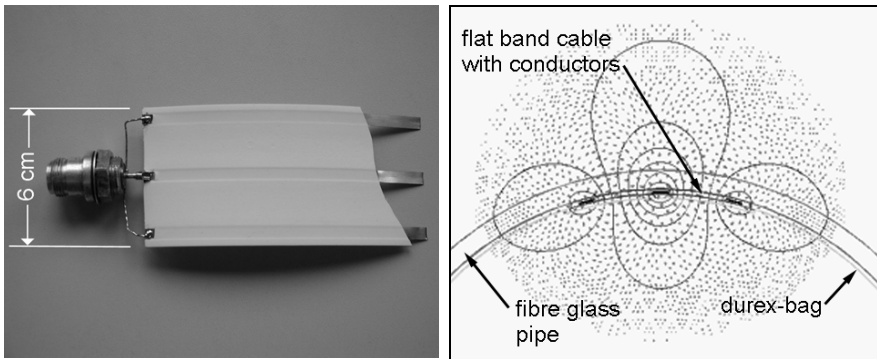
Fig. 3. Flat band cable and electrical field distribution for air inside the durex-bag (result of a numerical calculation)

The electrical properties of the flat band cable can be measured and calculated using a simple capacitance model. However for the installed flat band cable in the column test apparatus it was necessary to make a calibration using different materials with known or easy to measure dielectric coefficients. On one hand measurements with air (1), water (circa 80), glass-beads (circa 3) and water saturated glass-beads (circa 30) were used. On the other hand it was necessary to use further materials, because the range of values of the materials mentioned above are mostly out of the range in which the measurements with soils are located (between 5 and 40). Hence oil-water mixtures were used to spread out the range of values for the calibration and the measurements of water and air were neglected. The calibration – means correlation between capacitance C of the transmission line (sensor plus surrounding materials) and the dielectric coefficient of the material inside the durex-bag – of the column test apparatus for the TDR measurements is shown in Figure 4.
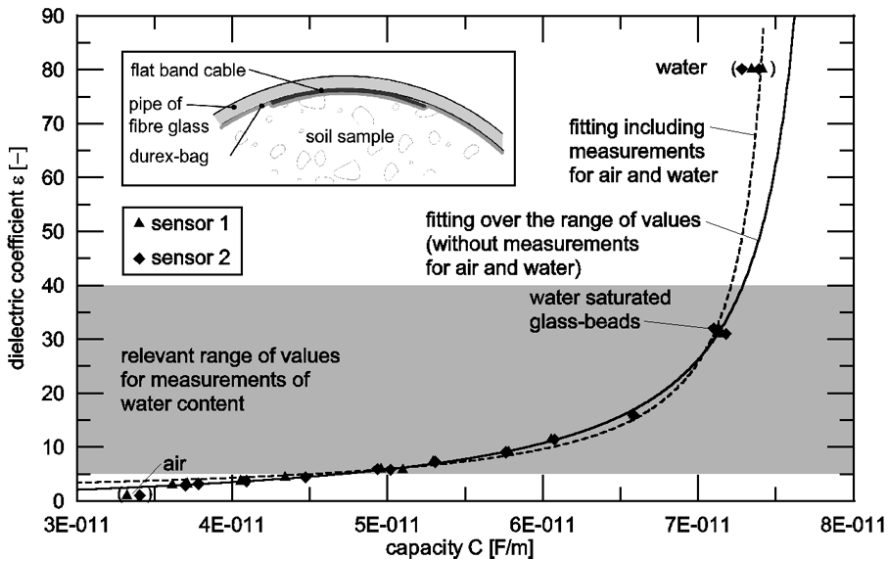
Fig. 4. Calibration of the transmission line in the column test apparatus

Reconstruction algorithm

For TDR measurements a fast rise time (about 200 ps) voltage step is launched into a coaxial cable and propagates through the system. At the transition between coaxial cable and transmission line (flat band cable plus surrounded material) a part of the pulse is reflected due to impedance mismatch. The remaining pulse travels along the transmission line until it is totally reflected at the open end or partially reflected at an end with a connected second coaxial cable. An oscillo-scope records the sum of incident signal and reflected signal, from which the travel time respectively the mean wave velocity in the transmission line can be de-termined. The dielectric coefficient of the surrounding soil can be calculated from the wave velocity and is related to the mean water content.

In order to use the whole amount of information of the measured signal a three step algorithm for reconstructing the water content profile along a transmission line was developed (Becker et al., 2003). In the first step the transmission line pa-rameters capacitance C(x) and conductance G(x) were reconstructed with two in-dependent time domain measurements from both sides of the flat band cable using the telegraph equation. In the second step C(x) was transformed into dielectric co-efficient ε(x). In the third step ε(x) was converted into a water content profile by standard transformations e.g. Topp et al. (1980) or by material specific calibration function.

Example of a multi-step inflow and outflow experiment

Material
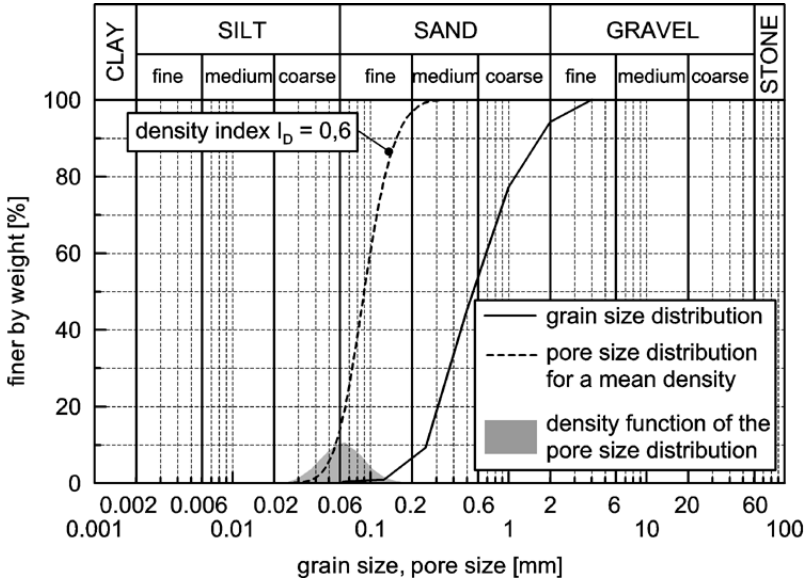
Fig. 5. Grain size and pore size distribution of the used sand material
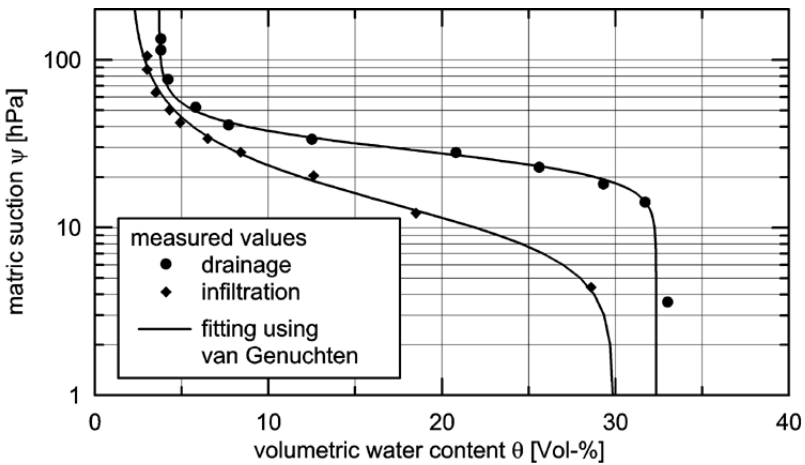
Fig. 6. Soil water characteristic curve of the used sand material

Considering the hydraulic properties a well known uniform sand was used for the first experiment with the column test apparatus. With grain sizes between 0.2 mm and 2 mm the sand shows a soil water characteristic curve with a distinctive transition from saturated to unsaturated condition (Figure 6). The air entry value of the material is about 10 hPa and the hydraulic conductivity is $2 \cdot 10^{-4}$ m/s. Figure 5 shows the grain size distribution as well as the pore size distribution and Figure 6 the soil water characteristic curve of the used material. The material specific calibration for the correlation between dielectric coefficient and water content is shown in Figure 7.
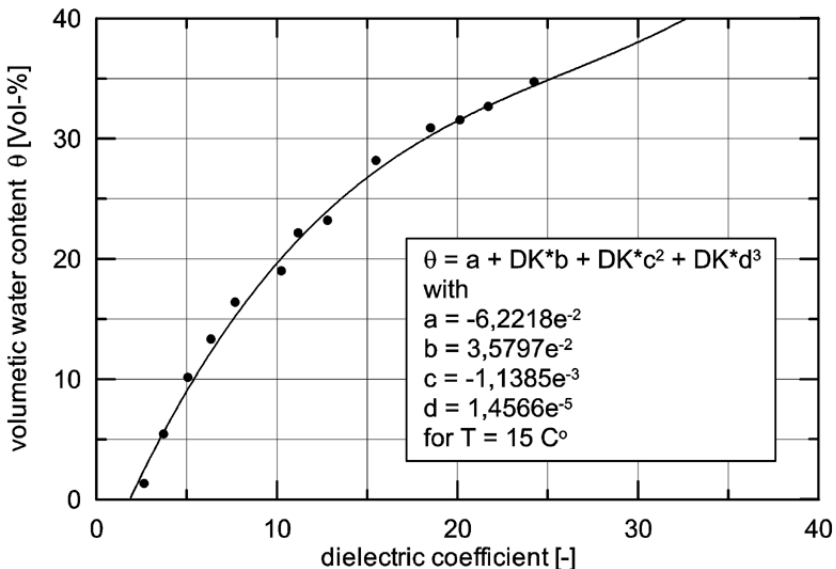
Fig. 7. Material specific calibration for the used sand material

Experiment

For a multi-step inflow and outflow experiment a soil sample is loaded sequentially and the arising pressure an saturation changes are recorded. A new hydraulic load has to be set before the state of equilibrium is reached. In this way the sample will be infiltrated and drained stepwise. In the presented experiment with the sand material the hydraulic load is imposed at the lower closing plate with a hanging column of water and an expansion tank (cf. Figure 1 and 2). At the upper closing plate atmospheric condition was set. Thus one can assume constant boundary condition at the upper end of the sample. For the first time a multi-step inflow and outflow experiment was carried out at the column test apparatus with different mechanical loads in April 2003.
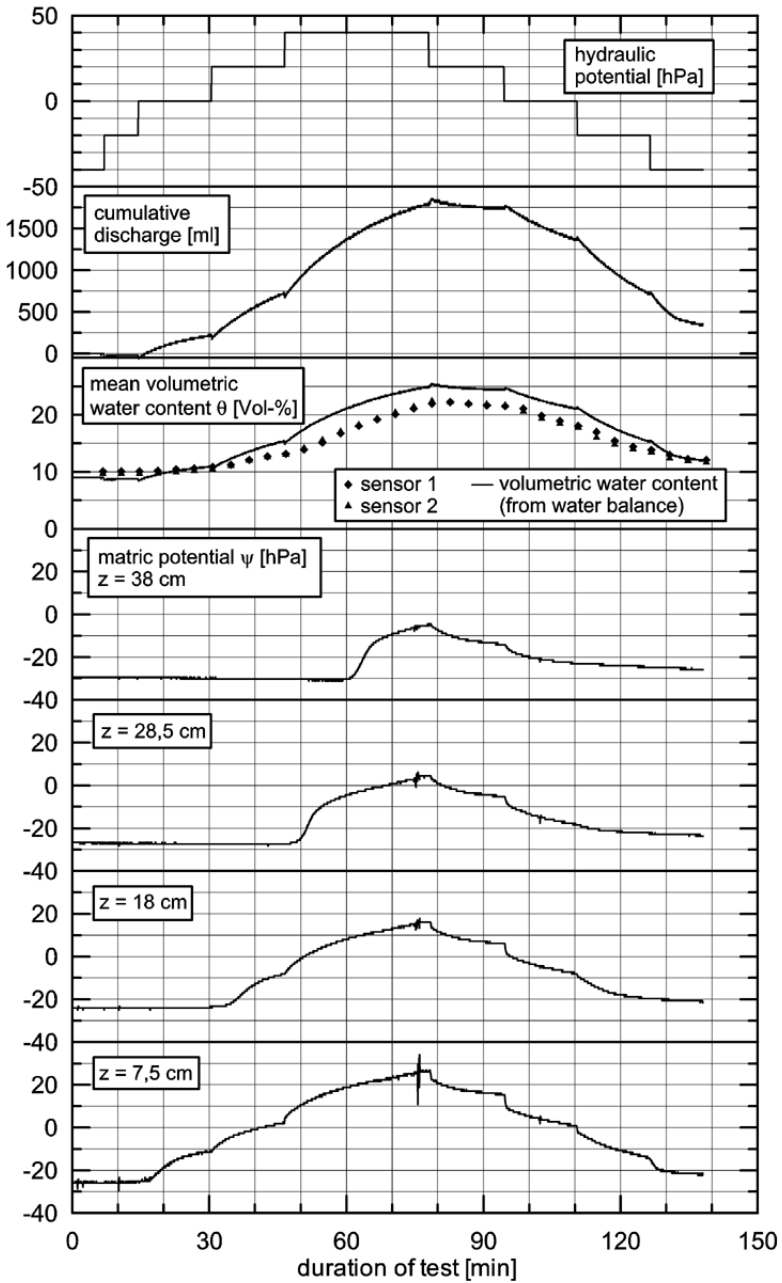
Fig. 8. Time series of the measured values of the experiment under a mechanical load of 300 kN/m^2

Figure 8 shows the time series of the measured hydraulic values of the experiment for a mechanical load of 300 kN/m^2. In the upper diagram the imposed hydraulic potential variation is shown with the reference level in the top edge of the lower closing plate. As one can see the inflow experiment as well as the outflow experiment were carried out in four steps each consisting of 20 hPa beginning at a initial suction of – 40 hPa. In the second graph the cumulative discharge is shown in ml. On the curve it can be seen that the adjustment of a new hydraulic load leads to small irrigation in the evolution of the discharge, but they remain small enough to be neglected in the evaluation. Under the cumulative discharge the mean volumetric water content measured with the TDR sensors (symbols) as well as calculated from the discharge (line) is plotted.

As it can be seen on the calculated curve for the mean volumetric water content and the measured values a difference in the values of up to 3 Vol-% appears. The reason for this discrepancy has to be search in the calibration of the transmission line. Sample drawing after the experiment along the transmission line should improve the calibration procedure in future.

The last four graphs show the time series of the measurements with the tensiometers. The positions of each tensiometer is shown in the figure. It is obvious that the tensiometer at the lowest location ($z = 7,5$ cm) shows the highest response on the stepwise changed hydraulic load. The rest of the tensiometers react later to the changes of the hydraulic load. The final condition of each tensiometers shows a lower suction than at the beginning of the experiment. This observation is verified by the higher mean volumetric water content what means that water was stored inside the sample.

Results of TDR-measurements

Subsequent only the results of the TDR measurements are discussed in detail. Figure 10 shows the temporal evolution of the mean volumetric water content for all experiments carried out at different mechanical loads. Each of the individual experiments was carried out with the same hydraulic loads. Every day two experiments were carried out, thus there was a break between the experiment with 100 kN/m^2 and 200 kN/m^2. The deformations between the experiments were 6 mm (0 to 100 kN/m^2), 2 mm (100 to 200 kN/m^2) and 1 mm (200 to 300 kN/m^2). As it can be seen from the graph more and more water was stored after each experiment (cf. Figure 10 b)). The final condition of the experiment at a load of 0 kN/m^2 was the initial condition for the experiment at a load of 100 kN/m^2 as it was also for the experiments at 200 kN/m^2 and 300 kN/m^2. Only for the initial condition of the experiment with 200 kN/m^2 there was no match with the final condition of the former experiment with 100 kN/m^2. The reason for that lies in the overnight break. During the night the sample had enough time to drain and thus to change the distribution of water.
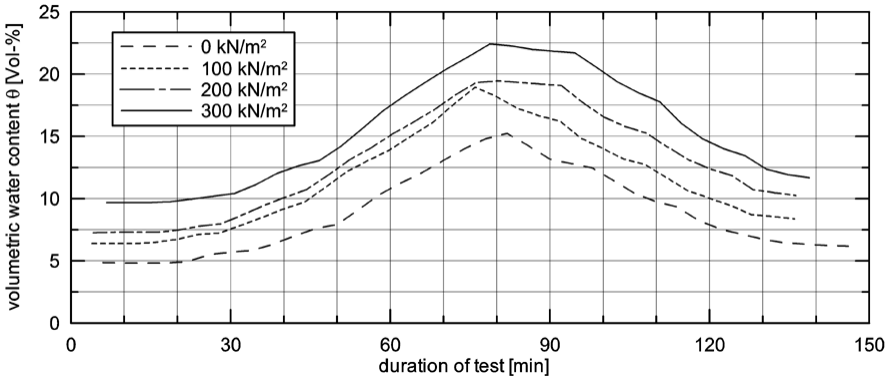
Fig. 9. Hydrograph of the mean volumetric water content measured at different mechanical loads
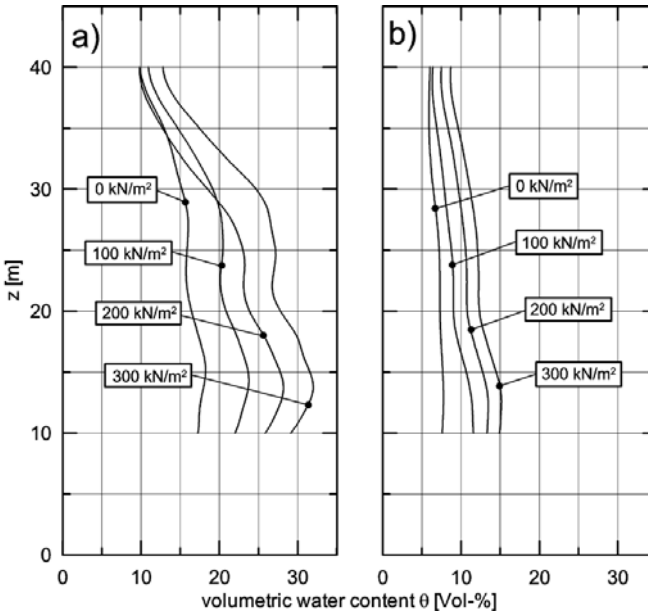
Fig. 10. Profiles of water content a) for the highest mean volumetric water content and b) at the end of each experiment

Figure 10 shows the spatial distribution of volumetric water content measured by TDR for the different mechanical loads a) for the highest measured mean water content and b) for the final condition. Also in this graphs one can recognise the stepwise accumulation of water after each hydraulic experiment. It is remarkable that the experiment at a load of 0 kN/m² at the highest mean volumetric water content showed no complete saturation even in the basis of the sample. From experi-

ment to experiment the water content rises over the whole sample. This observation is verified by measurements of the cumulative discharges.
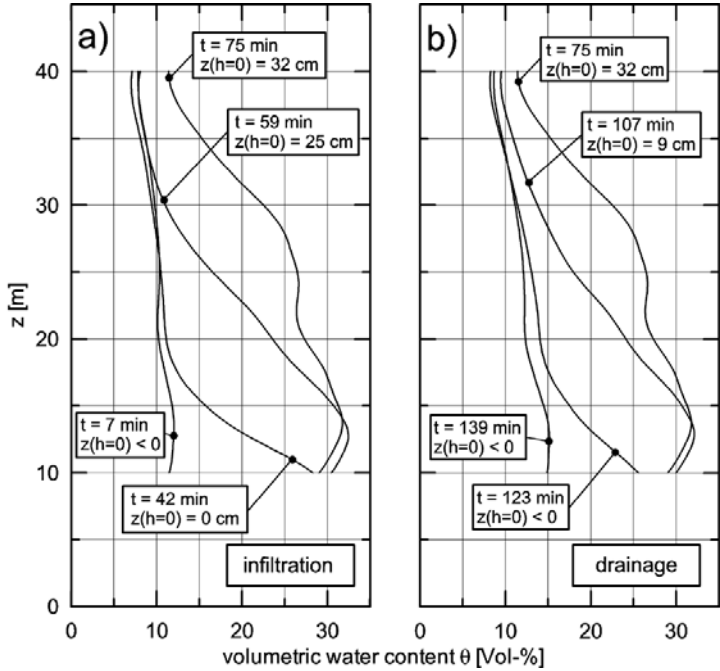
Fig. 11. Profiles of volumetric water content measured at different time steps with 300 kN/m^2 a) for the phase of infiltration and b) for the phase of drainage

Thus the question, which has to go into is if this storage patterns stem from the deformations or if this observation would be the same without any mechanical load. An explanation has to be search in the hysteresis of the material and the composite of the pore strcture. But this must be verified by future experiments with the same material.

Figure 11 shows profiles of volumetric water content for different time steps (cf. Figure 8) a) during the experiment with 300 kN/m^2 for the phase of infiltration and b) for the phase of drainage. The time of measurement and the appropriate level (z-coordinate) of the hydraulic zero potential is marked in the individual legends. The comparison of the water content profiles for the infiltration and the drainage in combination with the hydraulic zero potential shows, that during the infiltration a zero potential can be measured even for small volumetric water contents (cf. water content profile for t = 59 min.) Whereas for the phase of drainage we have above the level of hydraulic zero potential an area with still quite high volumetric water content. Even if the absolute values of water content might be imprecise, the measurements are significant.

Summary and conclusion

A new column test apparatus to carry out multi-step inflow and outflow experiments under defined stress condition was presented. The sample for this apparatus has a height of 45 cm with a diameter of 19 cm. A new measuring technique based on the Time-Domain-Reflectometry (TDR) permits the recording of continuos water content profiles over the height of the sample at a high temporal resolution. The presented results of water content measurements have shown, that such water content measurements can offer additional information about the processes inside a soil sample during a hydraulic experiment. The simultaneous recording of the hydraulic changes – like pressure respectively suction, water content and discharge – in a reasonable temporal and spatial resolution offers the opportunity of more unique inverse parameter estimation. A second aim is the attempt to estimate the unsaturated hydraulic conductivity direct from these measurements.

Reference

Becker, R., Bieberstein, A., Hübner, C., Nüesch, R., Schädel, W., Scheuermann, A., Schlaeger, S., Schuhmann, R. (2003): Nondestructive in situ and online measurments of soilphysical parameters. In: 12th Panamerican Conference on Soil Mechanics and Geotechnical Engineering and 39th U.S. Rock Mechanics Symposium, Cambridge, Massachusetts, USA, June 22-26, 2003, S. 277-285.

Van Genuchten, M. Th. (1980): A closed-form equation for predicting the hydraulic conductivity of unsaturated soils. Soil. Sci. Soc. Am. J. 44:892-898.

Kawai, K., Karube, D., Seguchi, H. (1999): Factors affecting on water retention characteristic of soils. In: Yagi, Yamagami & Jiang, Slope Stability Engineering, Balkema, Rotterdam, 381-386, ISBN 90 5809 079 5.

Lim, T. T., Rahardio, H., Chang, M. F., Fredlung, D. G. (1996): Effect of rainfall on matric suctions in a residual soil slope. Can. Geotech. J. 33: 618-628.

Mualem Y. (1976): A new model for predicting the hydraulic conductivity of unsatureated porous media. Water Resour. Res. 12:513-522.

Ng, C. W. W., Pang, Y. W. (2000): Influence of stress state on soil-water characteristic and slope stability. Journal of geotechnical and geoenvironmental engineering, february 2000, 157-165.

Topp, G.C., Davies, J. L., Annan, A. P. (1980): Electromagnetic determination of soil water content: Measurements in coaxial transmission lines. Water Resour. Res. 16:579-582.

Watabe, Y., Leroueil, S., Le Bihan, J.-P. (2000): Influence of compaction conditions on pore-size distribution and saturated hydraulic conductivity of galcial till. Can. Geotech. J. 37: 1184-1194.

Water permeability of unsaturated compacted kaolin

N. Peroni[1], E. Fratalocchi[2], and A. Tarantino[3]

[1] Dipartimento di Fisica e Ingegneria dei Materiali e del Territorio, Università Politecnica delle Marche, Via Brecce Bianche, 60131 Ancona, Italy, nicoletta_p@yahoo.it (✆)

[2] Dipartimento di Fisica e Ingegneria dei Materiali e del Territorio, Università Politecnica delle Marche, Via Brecce Bianche, 60131 Ancona, Italy, fratalocchi@univpm.it

[3] Dipartimento di Ingegneria Meccanica e Strutturale, Università degli Studi di Trento, via Mesiano 77, 38050 Trento, Italy, tarantin@ing.unitn.it

ABSTRACT: The paper presents an experimental investigation into the permeability of compacted kaolin. Tests were performed in a suction-controlled oedometer using the air overpressure technique: ambient air pressure (raised above the atmospheric pressure) was kept constant and pore water pressure was modified. Permeability was measured by monitoring water inflow in response to a suction decrease and interpolating experimental data using a simplified solution of Richards' equation (unsteady-state method). Corrections were made to account for the impedance of the high air-entry ceramic disc, the water lost by evaporation into the air pressure line and the air diffusing through the ceramic. The experimental results have shown that axis-translation technique may be problematic at high degrees of saturation and that permeability can be significantly underestimated.

INTRODUCTION

Hydraulic conductivity of unsaturated compacted soils is a key variable in many geotechnical and geoenvironmental problems. These include waste management structures (soil liners and covers), clay barriers for containment of contaminated soils, pollutant migration in the vadose zone, stability of road and railway embankments, and earth dams.

Soil permeability depends on the amount of pore space available for water. The available pore space reduces as the soil desaturates and, hence, hydraulic conductivity decreases with suction. Hydraulic conductivity can vary several orders of magnitude in the suction range of practical interest to engineers. This makes hy-

draulic conductivity a very critical variable in geotechnical and geoenvironmental design.

Despite the great relevance to engineering practice, unsaturated soil permeability is rarely measured in the laboratory or in the field. Experimental procedures are time consuming, require sophisticated equipment and necessitate considerable expertise. In addition, several experimental methods proposed in the literature (e.g. Vicol, 1990; Fredlund & Rahardjo, 1993; Jucà & Frydman 1996) are difficult to implement as they involve extremely low flow rates, especially at high suctions. As a result, many researchers have focused on procedures for indirectly predicting unsaturated hydraulic conductivity, most of them based on water retention data.

There are three approaches for estimating unsaturated permeability: macroscopic, statistical and empirical. The macroscopic and statistical models are based on the relationship between the water retention curve and the pore size distribution. Macroscopic models assume that each pore is connected only to pores of the same size (capillary model). The equation proposed by Brooks & Corey (1964) belongs to this class of models. In contrast, statistical models assume, more realistically, that pores of different size are interconnected. The Van Genuchten's equation (1980) is an example of statistical model. Empirical models are mathematical functions used to interpolate experimental data and often expressed in terms of non-dimensional variables (Richards, 1952; Gardner, 1958).

Several empirical equations have been proposed in the literature to correlate the unsaturated hydraulic conductivity to the degree of saturation. Nonetheless, the reliability of these relationships remains doubtful. In particular, correlation between measured and predicted unsaturated hydraulic conductivity may be poor in fine-grained soils such as compacted clays (Chiu & Shackelford, 1998).

This paper presents an experimental investigation on the permeability of compacted kaolin. Tests were carried out in an oedometer, where suction was controlled through the application of the axis translation technique. Ambient air pressure was kept constant and suction was changed by modifying pore water pressure (air overpressure technique). Permeability was measured by monitoring water inflow/outflow in response to a suction change.

EXPERIMENTAL APPARATUS

Unsaturated permeability was investigated using the controlled-suction oedometer designed and constructed at the Geotechnical Laboratory of the Universitat Politècnica de Catalunya, Barcelona, Spain (UPC) (Figure 1).

The oedometer cell is made of stainless steel and consists of four parts: the base, the oedometer ring, the air pressure chamber and the loading system. Vertical load was applied with compressed air. Two different pistons can be used with the oedometer. One allows the application of a net vertical stress equal to the difference between the air pressure over the piston and the pore air pressure. The other one makes it possible to double the net vertical stress without changing the air pressure over the piston. The two loading pistons are made of brass and end

with a rigid bronze coarse porous disc, which is in contact with the upper base of the sample.

Pore air pressure is supplied through the upper coarse porous disc. A 1 mm thick rubber membrane divides the loading chamber from the lower compartment containing the sample. The soil specimen is placed on a high air entry value (HAEV) ceramic disc (1.5 MPa), mounted recessed into the base plate. The ceramic disc allows the control of pore water pressure and it is connected to the water pressure line.
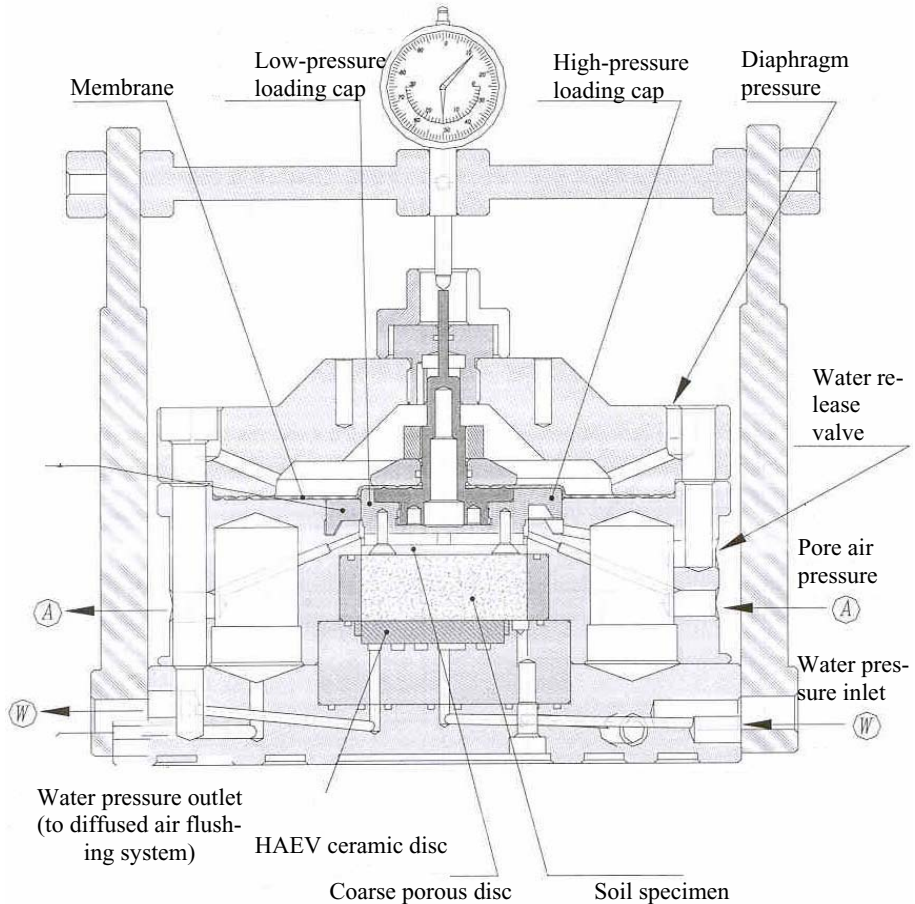
Fig. 1. Layout of the suction controlled oedometer (Di Mariano, 2000)

Water volume changes were measured using a graduated glass burette (resolution 0.02 ml) enclosed in a Perspex cylinder. The inner burette was connected to the specimen to monitor water inflow/outflow. Two immiscible liquids were present in the inner burette (de-aired water and a yellow coloured liquid) to form a

visible interface. It was verified that burette readings did not depend on water pressure. Room temperature was controlled in the range 22°C ± 1°C. Limiting temperature fluctuations is essential to obtain accurate readings of water volume change during the oedometer tests. Vertical displacements were measured with a mechanical micrometer having a resolution of 2 μm.

TEST MATERIAL AND SPECIMEN PREPARATION

Commercial processed kaolin (Rotoclay HB Goonvean, St.Austen, UK) was used in the present research work (Table 1).

Table 1. Properties of Rotoclay kaolin

Property	Reference	Value
Principal mineral	Product information	kaolinite
Specific gravity (G_s)	ASTM D854	2.65
Liquid Limit (LL)	ASTM D4318	52%
Plastic Limit (PL)	ASTM D4318	35%
Plastic Index (PI)	ASTM D4318	17%
Activity (A)	-	0.68
Particle Sizes:		
Silt (0.002÷0.074 mm)	ASTM D422	75%
Clay (<0.002 mm)	ASTM D422	25%
Maximum dry unit weight (γ_{dmax})	ASTM D698	14.3 kN/m^3
Optimum water content (w_{opt})	ASTM D698	28.5%

Distilled water ($EC < 20$ μS/cm) was used to moisten the kaolin prior to compaction to achieve the predetermined water content of 22.8% ± 0.4%. After moisture equalisation (about 24 hours), samples were dynamically compacted (Proctor Standard procedure) at the same initial dry unit weight ($\gamma_{dmax} = 13.97$ kN/m^3 ± 0.17 kN/m^3). The initial degree of saturation of the samples was $S_r \approx 68\%$. This value was sufficiently low to ensure that all pore filled with air were interconnected (continuous air phase). A specimen having diameter of 50 mm and height of 20 mm was finally cut from each compacted sample.

EXPERIMENTAL PROCEDURE

Saturation of the high air-entry ceramic

To achieve the desired bubbling pressure and to ensure continuity between the pore water and the water in the measuring system, the high air-entry ceramic disc was saturated prior to testing. To this end, the oedometer cell was filled with

deaired water and pressurised at 2 MPa. Then, the reservoir underneath the high air-entry ceramic was vented to the atmosphere to let water flow downwards under a pressure differential of 2 MPa. Saturation of the ceramic was therefore achieved by two mechanisms, dissolution of air bubbles due to the high water pressure and flushing out of undissolved bubbles due to the high pressure gradient (Romero 1999).

Steady state water outflow from the ceramic disc was used to calculate the permeability of the ceramic disc. This value was used to determine the impedance of the ceramic disc and, hence, to interpret the subsequent permeability tests. Monitoring water flow through the ceramic under steady state conditions made also it possible to detect possible cracks in the ceramic.

Mechanical and hydraulic paths

After flushing the drainage lines with deaired water, the specimen was placed inside the oedometer, the loading cap was rested on the specimen and the cell was finally assembled.

In the first stage, air pressure around the sample was increased to a target value of 0.5 MPa while keeping constant the water content of the specimen (undrained conditions with respect to water phase). The pore air pressure was raised to 0.5 MPa in steps by alternatively increasing the air pressure in the loading chamber (total stress) and the air pressure in the specimen chamber (pore air pressure). Air pressures were increased in such a way that the net vertical stress always remained greater than zero (but significantly less than the final target value). After raising the pore air pressure, the net stress was increased to its final value. This procedure is similar to the one suggested by Di Mariano (2000).

At the end of the loading path, a water pressure of 0.10 MPa was applied to the base of the specimen in order to impose an initial matric suction of 0.40 MPa. The pore water was then allowed to come to equilibrium with the applied matric suction.

Once equilibrium was attained, the specimen was wetted under constant net vertical stress using the air over-pressure technique as proposed by Romero (1999). This technique consists in keeping constant the pore air pressure (raised above the atmospheric value) and modifying the pore water pressure, in contrast to the more traditional water sub-pressure technique, where matric suction is controlled by modifying the air pressure and keeping constant the water pressure (usually at atmospheric value). The air over-pressure technique is preferable to the water sub-pressure technique, especially when testing fine-grained soils at high degrees of saturation (Romero, 1999; Gens & Romero, 2000). The variation of air pressure can induce irreversible arrangements in the soil skeleton, especially in unsaturated soils near saturation. Another advantage of the air over-pressure technique is that water pressure is maintained to values greater than atmospheric. This considerably reduces the volume of diffused air that accumulates underneath the high air-entry ceramic disc.

Measurement of water volume change

In order to accurately measure water volume changes, it was necessary to account for pore water losses due to evaporation into the pore air pressure line (open to atmosphere) and air diffusion through the high air-entry ceramic. Evaporation of pore water is driven by the relative humidity gradient between the air in the pore voids and the air in the specimen chamber, which is vented to atmosphere through the pore air pressure line. According to Romero (1999), evaporative fluxes reduce with increasing matric suction, with increasing relative humidity in the specimen chamber and with lower soil porosity.

Periodical flushing underneath the ceramic allowed the removal of diffused air from the water pressure line. This procedure was aimed at avoiding progressive cavitation and the consequent loss of continuity between the pore water and the water in the measuring system. Between two flushing procedures, air cavities slowly accumulated underneath the high air-entry ceramic, thus causing an error in the measurement of water volume change.

The measurement of the volume of water that crosses the high air-entry value disc was corrected to account for water evaporation and air diffusion. At the end of the transient process, the level of the meniscus in the inner graduated burette did not remain constant, as would be expected, but changed linearly with time. In particular, it registered pore water outflow at higher suctions ($s>0.3$ MPa), indicating that air diffusion was predominant over water evaporation and registered pore water inflow at low suctions ($s<0.3$ MPa), as water evaporation was the controlling factor. The constant rate of water volume change at the end of the transient process was used to correct water volume measurements.

DETERMINATION OF WATER PERMEABILITY

Water permeability was determined under transient conditions by analysing the corrected inflow data (wetting paths). This approach is an unsteady-state method, initially developed by Gardner (1956) for outflow.

For every single step of matric suction decrease, transient inflow data were interpolated using the following simplified solution of Richards' equation that takes into account the ceramic disc impedance (Miller & Elrick, 1958; Kunze & Kirham, 1962; Romero, 1999):

$$\frac{Q(t)}{Q_0} = 1 - \sum_{n=1}^{\infty} \frac{2 \exp\left(\alpha_n^2 D_w t / L^2\right)}{\alpha_n^2 \left(a + \cos ec^2 \alpha_n\right)} \tag{1}$$

where $Q(t)$ is the volume of intruded/extracted water at time t, Q_0 is the total volume of inflow/outflow for a suction decrement/increment, L is the specimen height, D_w is the capillary diffusivity that is dependent on water hydraulic conductivity, a is the ratio of impedance of the ceramic disc to the impedance of the soil $a = k_w e / k_d L$ (e is the ceramic disc thickness and k_d is the ceramic water coefficient

of permeability) and α_n is the nth solution of the equation $\alpha_n\,a = cot\alpha_n$ (for $n = 1,2,\ldots$). This equation is based on a number of simplifications: the soil skeleton is incompressible, the liquid is homogeneous and incompressible, the water flow is isothermal and the air flow in the porous medium is negligible or assumed to take place instantaneously. A non-linear, least-squares optimisation procedure was used to approximate test readings to the model prediction, in order to derive the D_w parameter. Water hydraulic conductivity was calculated from the following relationship:

$$k_w = \frac{D_w \gamma_w Q_0}{V \Delta u_w} \tag{2}$$

where Δu_w is the water pressure increment, V is the volume of the sample and γ_w is the water unit weight.

EXPERIMENTAL RESULTS AND INTERPRETATION

As a preliminary test, the saturated permeability was measured on a specimen 35 mm height and 102 mm diameter. Permeability test was carried out with flexible wall permeameter according to ASTM D5084. The specimen was first compacted at the same water content and dry density as the unsaturated samples and then consolidated at confining effective stress of 100 kPa and back-pressure of 310 kPa to ensure full saturation. Permeability was measured under steady state conditions applying hydraulic gradients ranging between 11 and 13. The saturated permeability was found equal to 2.3×10^{-9} m/s. A very similar value was measured by Mazzieri & Van Impe (2001), testing the same soil.

To investigate the unsaturated permeability, three oedometer tests were performed on unsaturated compacted specimens at net vertical stress of 0.04 MPa, 0.2 MPa and 0.5 MPa. The stress paths followed in these tests are shown in Fig. 2.

An example of the variations of gravimetric water content with time during the different wetting stages is shown in Figure 3 for the test run at 0.04 MPa net vertical stress. As matric suction decreases (i.e. water pressure increases), the gravimetric water content of the sample increases.
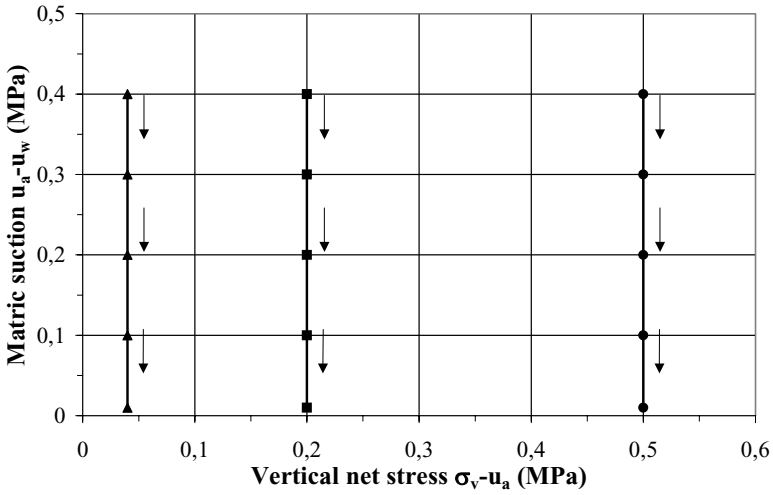
Fig. 2. Stress paths followed during oedometer tests
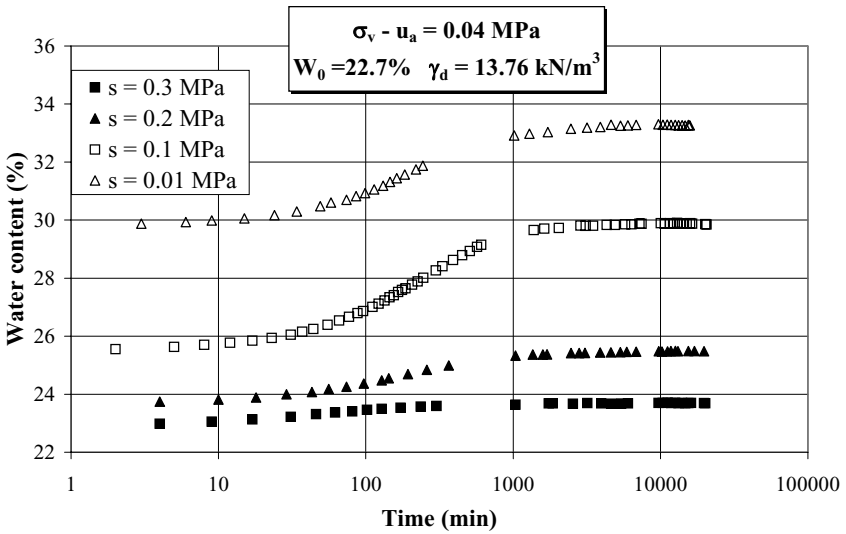
Fig. 3. Gravimetric water content versus time recorded during wetting stages at 0.04 MPa vertical net stress (Peroni, 2002)

For every single step of matric suction decrease, measured water inflows were interpolated using the simplified solution of Richards' equation, in order to determine water soil permeability at different degrees of saturation.

The values of water permeability obtained from the three oedometer tests are shown in Figure 4. As would be expected, the water permeability increases with the degree of saturation. It is also interesting to note that water permeability is not significantly influenced by the applied vertical net stress and, hence, by the variation of void ratio. This can be explained considering the Kozeny-Carman equation for permeability of porous media (Kozeny, 1927; Carman, 1956; quoted in Mitchell, 1992). At given temperature and degree of saturation, the water permeability k_w depends on void ratio e through the following relationship:

$$k_w\big|_{S_r,T} \propto \frac{e^3}{1+e} \tag{3}$$

In the three oedometer tests, the void ratio for given degree of saturation did not vary significantly $(\Delta e_{max} = 0.05)$. As a result, the change in water permeability associated with a change in void ratio was anticipated to be small $(k_w(e+\Delta e)/\,k_w(e)\big|_{Sr,T} \geq 0.87)$.
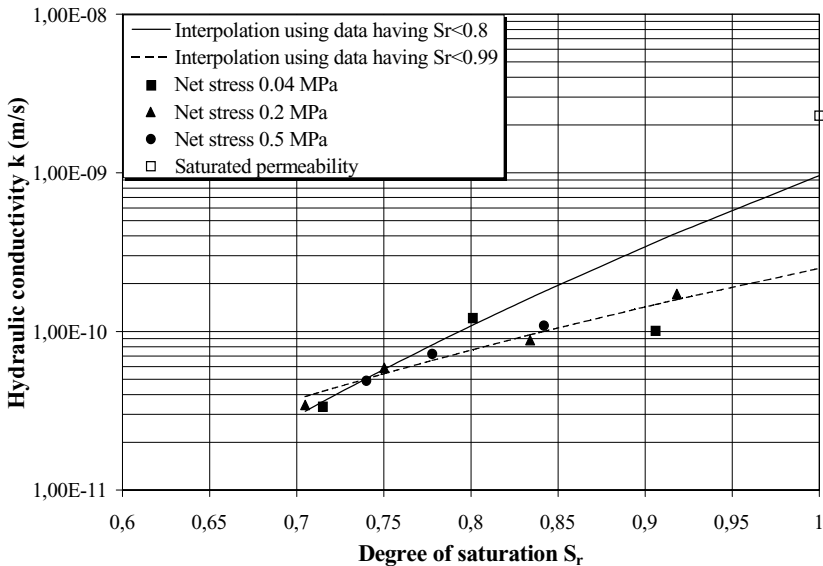
Fig. 4. Variation of water permeability with degree of saturation for different vertical net stresses (Peroni, 2002)

The most striking aspect of the data shown in Figure 4 is the discrepancy between the permeability measured on the saturated sample ($S_r = 1$) and the permeability at saturation obtained by extrapolating the unsaturated permeability data. If

these data are fitted using a power function as suggested by Brooks and Corey (1964), the following equation can be obtained:

$$k_w = 2.5 \times 10^{-10} S_r^{5.3} \, m/s \tag{4}$$

The difference between the measured and extrapolated permeability would therefore be about one order of magnitude. However, a closer inspection of the figure reveals that the saturated permeability is consistent with unsaturated data having $S_r < 0.8$. If these data are interpolated using a power function, the following equation is obtained:

$$k_w = 9.6 \times 10^{-10} S_r^{9.8} \, m/s \tag{5}$$

which gives a saturated permeability of 9.6×10^{-10} m/s, very close to the measured value (Figure 4). This result seems to suggest that the permeability is underestimated in the range of degrees of saturation from 0.8 to 1. This is not surprising, as air phase is likely to be in occluded form in this range of degrees of saturation. Here, the validity of the axis-translation technique is controversial. The exponent of the degree of saturation S_r in equation 5 is associated with the pore size distribution and falls within the range of observed values as reported by Mualem (1976).

Experimental results were then used to validate an empirical relation proposed by Vanapalli and Lobbezoo (2002) relating relative water permeability k_r (unsaturated permeability to permeability at saturation ratio) to the effective saturation ratio S_{re}:

$$S_{re} = \frac{w - w_{res}}{w_{sat} - w_{res}} \tag{6}$$

where w_{res} is the residual gravimetric water content, often associated to the hygroscopic water content, and w_{sat} is the saturated gravimetric water content. For the material tested, the residual water content was negligible and the effective degree of saturation was approximately equal to the degree of saturation. The equation proposed by Vanapalli and Lobbezoo (2002) is:

$$k_r = S_r^{7.9\gamma} \tag{7}$$

where γ is a parameter related to the plastic index PI of the soil $[\gamma = 14.08 \, (PI)^2 + 9.4 \, (PI) + 0.75]$. This relationship has some practical interest, as it would allow the estimate of the unsaturated permeability on the basis of an easy-to-determine parameter. These authors found that this relationship is in good agreement with experimental data for sandy and silty soils. For soils having plastic index greater than 0.20, experimental data were more scattered. They attributed such behaviour to the influence of soil structure on the coefficient of permeability or to the limited set of data analysed. For the material used in this experimental program, $PI = 0.17$ and then $\gamma = 2.75$. The equation proposed Vanapalli and Lobbezoo (2002) is then plotted in Fig. 5 together with the experimental data. It can

be observed that errors can be greater than one order of magnitude. This result confirms the difficulty in applying the proposed relationship to fine-grained soils.
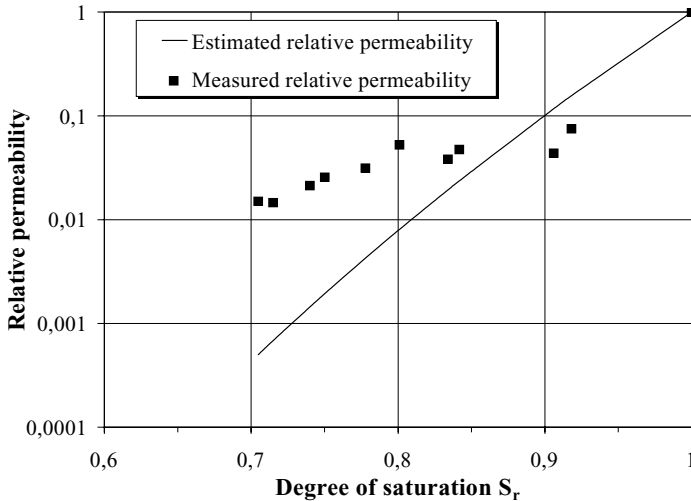
Fig. 5. Variation of relative water permeability with degree of saturation: experimental data and theoretical prediction.

CONCLUSIONS

A suction controlled oedometer was used to investigate unsaturated water permeability of compacted non-active clay (kaolin). Water permeability was measured using an unsteady-state method. Water inflow in response to a suction decrease was monitored and the experimental data were interpolated using a simplified solution of Richards' equation. Tests were conducted at different vertical net stresses (0.04, 0.2 and 0.5 MPa) and exploring degrees of saturation in the range from 0.7 to 1.

Experimental results indicate that unsaturated permeability can be underestimated at high degrees of saturation when using the axis-translation technique. At high degrees of saturation, the air phase becomes occluded within the pore water and unsaturated permeability becomes difficult to measure.

The empirical equation proposed by Vanapalli and Lobbezoo (2002) was used to estimate the relative water permeability as a function of the degree of saturation. This relationship proved very inaccurate for the clayey soil tested, confirming that this relationship is only applicable to silty and sandy soils.

Acknowledgements

REFERENCES

Brooks, R.H. & Corey, A.T. (1964) "Hydraulic properties of porous media" *Colorado State University Hydrology Paper, n. 3.*

Carman P. C.(1956) "Flow of gases through porous media", *Academic Press, New York.*

Chiu, T.F. & Shackelford, C.D. (1998) "Unsaturated Hydraulic Conductivity of Compacted Sand-Kaolin Mixtures", *Journal of Geotechnical and Geoenvironmental Engineering, Vol. 124, n. 2, pp. 160-170*

Di Mariano, A. (2000) "Le argille a scaglie ed il ruolo della suzione sulla loro deformabilità", *PhD Thesis, Università di Catania e di Palermo, Italy*

Fredlund, D.G. & Rahardjo, H. (1993) "Soil mechanics for unsaturated soils" *John Wiley & Sons, Inc. New York.*

Gardner, W.R. (1956) "Calculation of capillary conductivity from pressure plate outflow data" *Soil Science Soc. Am. Proc.*, *20, pp. 317-320.*

Gardner, W.R. (1958) "Some steady state solutions of the unsaturated moisture flow equation with application to evaporation from a water table" *Soil Science*, *85(4), pp. 228-232.*

Gens, A. & Romero, E. (2000) "Ensayos de Laboratorio" *Simposio sobre Geotecnica de las Infraestructuras del Trasporte, Barcellona, 27-29 June 2000*

Jucà, J.F.T. & Frydman, S. (1996) "Experimental techniques. States of the art report. " *In Proceeding 1st International Conference on Unsaturated Soils, Paris. E.E. Alonso and P. Delage (eds.), Balkema / Presses des Ponts et Chaussées, 3: 1257-1292.*

Kozeny J. (1927). ″Ueber kapillare leitung des wassers im boden", *Akad. Wiss., Wien, n.2a, 136.*

Kunze, R.J. & Kirkham, D. (1962) "Simplified accounting for membrane impedance in capillary conductivity determinations", *Soil Science Soc. Am. Proc.*, *26, pp. 421-426.*

Mazzieri, F., Van Impe, W. (2001) "Influence of preparation procedures on properties of compacted kaolin", *Proceedings XVth International Conference on Soil Mechanics and Geotechnical Engineering, Istanbul, 27-31 August 2001, Balkema, Rotterdam*

Mitchell, J.K. (1992) "Fundamentals of soil behavior", *John Wiley & Sons, New York.*

Miller, E.E. & Elrick, D.E. (1958) " Dynamic determination of capillary conductivity extended for non-negligible membrane impedance" *Soil Science Soc. Am. Proc.*, *22, pp. 483-486*

Mualem Y. (1976) "A new model for predicting the hydraulic conductivity of unsaturated porous media", *Water Resour. Res., 12*

Peroni, N. (2002) "Contributo allo studio delle proprietà idrauliche e della deformabilità di un terreno insaturo" *PhD Thesis, Università degli Studi di Ancona, Italy*

Richards, L.A. (1952) "Water conducting and retaining properties of soils in relation to irrigation" *In Proceeding of an International Symposium on Desert Research, Jerusalem, pp.523-546.*

Romero, E. (1999) "Characterisation and thermo-hydromechanical behaviour of unsaturated Boom Clay: an experimental study", *PhD Thesis, Universitat Politècnica de Catalunya*

Van Genuchten, M.Th, (1980) "A closed-form equation for predicting the hydraulic conductivity of unsaturated soils", *Soil Science Soc. Am. J. 44, pp. 892-898.*

Vanapalli, S.K. & Lobbezoo J.P., (2002) "A normalized function for predicting the coefficient of permeability of unsaturated soils" *3rd International Conference on Unsaturated Soils, Recife, Brazil, 2002*

Vicol, T. (1990) "Comportment hydraulique et mecanique d'un sol fin non saturé. Application à la modélisation", *PhD Thesis, Ecole Nationale des Ponts et Chaussées, Paris.*

Moisture retention curve in landfilled waste

Y.K. Kazimoglu, J.R. McDougall, and I.C. Pyrah

School of the Built Environment, Napier University, 10 Colinton Rd. Edinburgh Scotland, EH10 5DT, UK

Abstract. Moisture content and moisture movement are key factors in controlling the progress and rate of biodegradation within a landfill as it is the aqueous environment that facilitates the transport of nutrients and microbes. The modelling of infiltration and water movement requires information on the moisture retention and hydraulic conductivity properties, usually in the form of empirical functions such as those proposed by van Genuchten (1980). In waste however, the particle and pore size distribution, heterogeneity of waste composition and leachate chemistry complicate the determination of moisture retention and hydraulic conductivity. In this paper we describe the modification and use of a standard pressure plate apparatus to establish moisture retention properties of samples of 250 mm in diameter and the difficulties of using this method. Some initial results are presented.

Introduction

Despite legislative changes, landfill is, and continues to be, the main waste disposal option in many European countries. However, organic and inorganic materials are solubilised from the waste to form leachate, which may then migrate into the surrounding hydrogeology. The usual approach to leachate control is by designing and operating the landfill as a containment system. Liners and covers minimise the amount of water infiltrating the waste so that the mobilisation of the pollutant materials is prevented and contain any leachate generated and gas emissions. This type of landfill is known as dry containment but in such an environment, the waste remains largely unchanged and the containment system needs a long design life.

More recently there has been a move from dry storage to accelerated stabilisation of waste by operating landfills as flushing bioreactors. Accelerated stabilisa-

tion reduces the need for long-term containment and is usually promoted by the recirculation of leachate to maintain the moisture content of the solid waste at levels favourable for biodegradation. Regardless of the type of landfill system, modelling of landfill hydraulics is a useful input into the design of leachate collection and removal systems, and for predicting the amount and first appearance of leachate production. However, it is particularly relevant for the analysis of leachate recirculation systems, which must ensure an adequate distribution of moisture and biochemical entities.

Moisture contents and flow components in relation to surface infiltration and absorptive capacity of the waste can be determined using unsaturated flow models: a more detailed description of the use of such models for landfill hydraulics can be found in McDougall et al. (1996) and El-Fadel et al. (1997).

However, successful modelling of moisture movement within a landfill is constrained by a lack of understanding of the nature of moisture retention in landfilled waste. One aim of this paper is to highlight the role of the water retention curve in landfill hydraulics. A second aim is to present some simple modifications to standard pressure plate apparatus, by which the water retention properties of municipal solid waste (MSW) can be measured, and which takes account of the complications due to the pore and particle size range and leachate chemistry.

Absorption in MSW

The absorptive capacity of MSW is often characterised using the term field water capacity. Field water capacity refers to the amount of moisture that a porous medium can retain, against gravity, before discharge. In waste, the difference between the initial moisture content and its field water capacity is referred to as the absorptive capacity. Leachate is discharged when the moisture content in waste exceeds its field-water capacity, or when the amount of infiltration exceeds its absorptive capacity. However, the absorptive capacity of waste is often quoted as a single-valued parameter, which is a function of physical properties such as waste composition, density, porosity and age (El-Fadel, 1997; Yuen, 1999).

In fact, the absorptive capacity in landfill will vary in both time and space. Over time, moisture contents are modified by precipitation during infilling phase and leachate recirculation. In space, the fundamental nature of the moisture retention curve dictates that there will be a predictable variation in the vertical direction, i.e. with depth or equilibrium water pressure. Vorster (2001) has shown that water retention in waste is a function of its position relative to the phreatic surface, in other words, the hydraulic boundary conditions and the age of the material. So, field water capacity is more properly defined as the moisture content in hydrostatic equilibrium with the current hydraulic boundary conditions, which will vary with elevation; similarly, absorptive capacity is the difference between the current and equilibrium moisture content, which also varies with elevation. Consider Fig.1, which shows a typical water retention curve. Elements of waste deposited

near to the base of a site (close to a sump) will have a higher equilibrium moisture content than waste deposited at a higher elevation. If waste arrives on site with a uniform initial moisture content, moisture redistribution will be towards the equilibrium moisture profile and may result in a combination of both drainage and absorption (as shown in Fig.1). With a uniform field-water capacity, no such variation in moisture can be accommodated.

Unsaturated flow models, which are based on a non-uniform water retention curve, have been used with some success for the analysis of landfill hydraulics (Straub and Lynch, 1982; Korfiatis et al., 1984; and Ahmed et al., 1992).
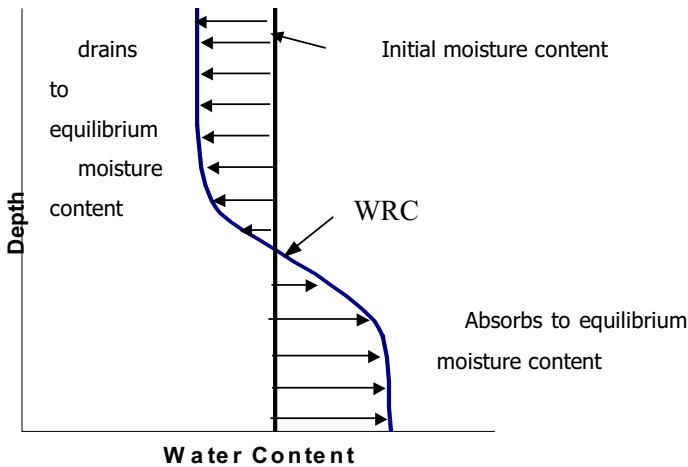
Fig. 1. Illustration of moisture storage over the depth of landfill

Experimental determination of water retention curve for MSW

The water retention curve defines the non-linear relationship between the water content (usually volumetric) and suction. The term suction refers to the negative pore-water pressure (relative to pore-air pressure) and is the field variable controlling water movement in unsaturated soils. The unsaturated hydraulic conductivity is defined using a coefficient (sometimes referred to as the relative permeability) which modifies the saturated hydraulic conductivity to account for the reduced pore volume available for liquid flow as a porous medium desaturates. Direct measurement of the unsaturated hydraulic conductivity is expensive, time consuming and a difficult task (Lam et al., 1987) so the relative permeability is usually deduced from the more easily measured water retention curve e.g. Clapp and Hornberger (1978) and van Genuchten (1980). Various equations exist for the

definition of the water retention curve and hydraulic conductivity; Straub and Lynch (1982), Korfiatis et al. (1984), and Ahmed et al. (1992), in their landfill simulations used the power equations suggested by Clapp and Hornberger (1978) with estimated parameter values rather than values based on experimental observations.

A number of instruments and techniques are available for the measurement of suction in soils; these can be classified as direct or indirect measurement techniques. Direct measurement techniques include tensiometers and pressure plate apparatus; indirect measurement techniques include the filter paper method, psychrometers, and osmotic dessicators (Fredlund and Rahardjo, 1993). The principles of operation, advantages and disadvantages of the above methods used for measuring water retention curves have been discussed in detail by Lee and Wray (1995) and Ridley et al. (2003).

In MSW, wide pore and particle size ranges complicate the measurement of suction; large volume samples are required. Furthermore, a complex and changing leachate chemistry will, through changes in osmotic soil water potential, undermine the calibration of indirect suction measurement techniques. The determination of moisture retention in MSW should therefore use a direct suction measurement technique – the presence of organic ions appears to have little effect on the suction measurements made using high air-entry value ceramic discs (Ridley et al, 2003) – and allow for as large a sample as possible. The following sections describe the modification of a commercially available pressure plate extractor, which goes some way to meet these requirements.

Modified pressure plate test

A commercially available pressure-plate extractor has been modified to establish the water retention curve of a large sample over suction ranges of 0-500 kPa. This suction range is particularly relevant for the simulation of leachate recirculation in MSW. In the pressure-plate apparatus, a pressure difference is maintained between the pore-air pressure, u_a, controlled using a compressor, and the pore-water pressure, u_w, which is at atmospheric pressure, by the surface-water interface in a saturated high air-entry ceramic disc. The suction imposed on the specimen is equal to the difference between applied air and pore-water pressures, and as long as the suction does not exceed the air-entry value of the plate (500 kPa) the high air-entry ceramic should remain saturated. It is believed that dissolved chemical salt molecules are small enough to pass through the ceramic plate so no osmotic potential develops between the sample and the water volume change measuring system.

Conventionally, in the pressure plate apparatus, the sample is removed and the volume of the water expelled at each suction increment is measured by weighing. Since a good hydraulic contact between the porous plate and the specimen is difficult to make when the specimen is replaced on the plate, a number of identical specimens are used with one being removed for each weighing and then discarded.

The particle and pore size distribution of MSW means that multiple specimens in a standard pressure plate apparatus are out of the question, however, the pressure plate test can be modified to make volumetric measurements of the expelled water on one large (250mm diameter) specimen. The water volume change in the specimen with each pressure increment is measured continuously using a burette connected to the pipe which carries water discharge from the ceramic disc. There is an advantage with this technique, that is, equilibrium of water content in the specimen with the applied matric suction can be visually confirmed. However, this method has a shortcoming. Gas can dissolve and diffuse through the liquid in the ceramic and come out of solution in the water volume measuring system. The presence of the gas in the measuring system will distort measurements of the volume of water expelled from the sample.

A further modification to the basic set-up can be made to allow the volume of diffused air to be removed and measured by attaching an air trap between the pressure chamber and the graduated burette. The layout of the experimental set-up is shown in Figure 2(a) and (b). A liquid circulation system, driven by a peristaltic pump, is used to move pockets of air, which accumulate adjacent to the ceramic plate, to the air trap. Liquid free of bulk air then flows back into the pressure plate cell where it re-joins the liquid discharge pipe through a y-piece mounted inside the pressure plate adjacent to the ceramic plate. To remove the diffused air in the air-trap, the valve on the air-trap is opened until the air is flushed out by the water from the burette. The difference of burette readings before and after the air removal is equal to the volume of the diffused air.

Initial results

Although the experimental set-up described in section 3.1 will be used to establish the water retention properties of MSW, a number of initial tests have been run to investigate the problem of air diffusion through a high air-entry value porous plate and the performance of the modified water and air volume measuring system. These tests were performed on a compacted silty-sand specimen of 98 mm diameter and 35 mm height. The water retention curve obtained for this specimen is shown in Figure 3. The volume of water expelled from the specimen and diffused air at various matric suctions during this test are presented in Figure 4. The air-trap was used to remove the air from the measuring system regularly every 24-48 hours to determine the change of volume of water in the specimen between the two successive suctions. Equilibrium is assumed to have been established when the level of water in the burette drops to the same point after allowing air to diffuse for 24 hours. This indicates that the movement of water expelled from the specimen at the applied matric suction has ceased. It may be noted that the volume of diffused air collected in the air-trap became significant only after the air pressure was elevated to 90 kPa. The level of the water expelled from the specimen with the increased matric suction after removal of diffused air is shown by the dashed line in Figure 3.
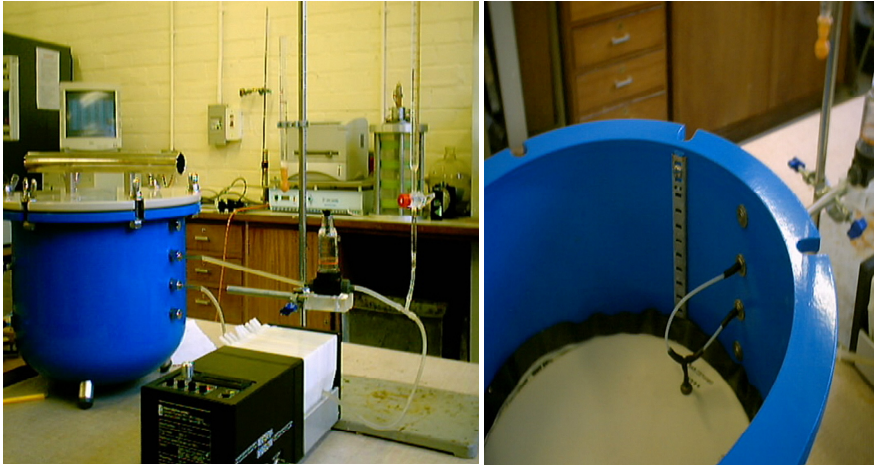
Fig. 2. a) The layout of the experimental set-up and b) detail of the circulation device in the pressure cell.
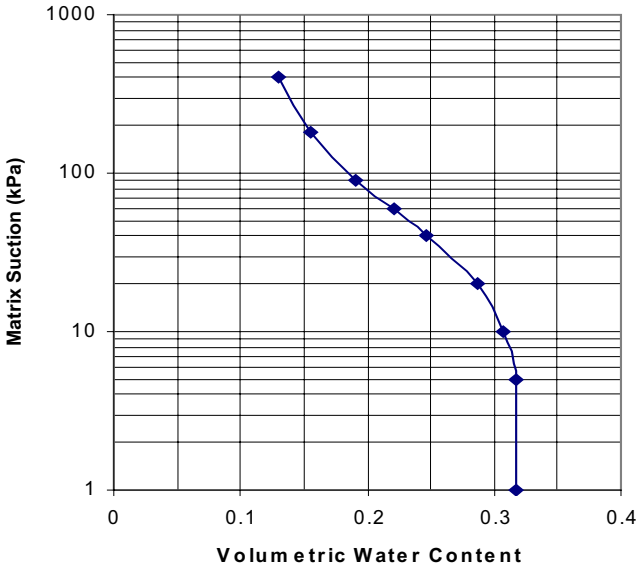
Fig. 3. Water Retention Curve of Compacted Silty-Sand Specimen.

Diffused air measurements from a different test (Figure 5) are consistent with a Fickian diffusion process, and the coefficient of air permeability constant over the pressure gradient range in question, i.e. there is a linear relationship between the volume rate of diffused air and the air pressure gradient applied.
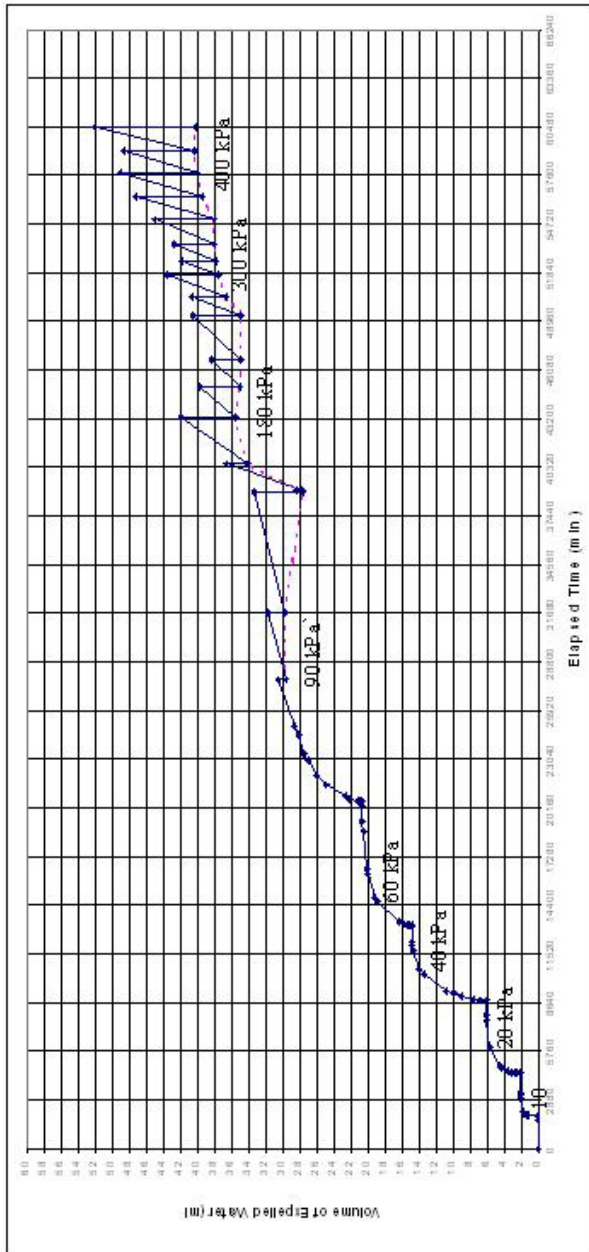
Fig. 4. The volume of water expelled from a silty sand specimen and gas diffusing through the ceramic disc during measurement of the water retention curve of a silty sand
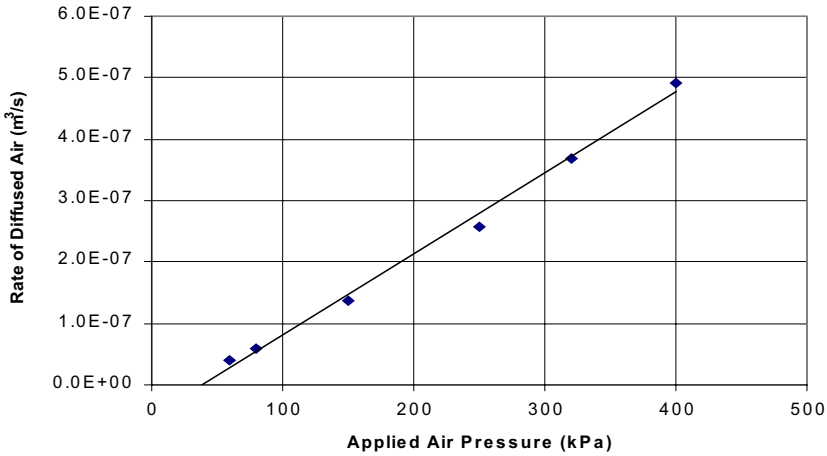
Fig. 5. Rate of Diffused Air through High Air-Entry Value Porous Plate

Concluding Remarks

This paper has highlighted the role of the water retention curve in relation to absorptive capacity in MSW. It has also described a simple modification to a commercial pressure plate apparatus for measuring the water retention curve of large specimens (250mm diameter). One of the advantages of the pressure plate, particularly in the case of waste refuse, is that complications due to leachate chemistry are minimised. An initial test on an inert material was carried out to check on equipment performance, and particularly to investigate air diffusion through the high air-entry value ceramic disc. The results of this test indicate that there is no significant volume of diffused gas at applied suctions of less than 90 kPa and confirm that the diffused gas volume varies linearly with the applied pressure gradient.

References

Ahmed, S., Khanbilvardi, R. M., Fillos, J., and Gleason, P. J. (1992). Two-Dimensional Leachate Estimation through Landfills. Journal of Hydraulic Engineering, 118(2), p306-322.

Clapp, R. B. and Hornberger, G.M. (1978). Empirical Equations for Some Soil Hydraulic Properties. Water Resources Research, 14(4), p601-604.

El-Fadel, M., Findikakis, A. N., and Leckie, J. O. (1997). Modelling Leachate Generation and Transport in Solid Waste Landfills. Environmental Technology, 18, p669-686.

Fredlund, D. G. and Rahardjo, H. (1993). Soil Mechanics for Unsaturated Soils. John Wiley and Sons. p70-76.

Korfiatis, G. P., Demetracopoulos, A. C., Bourodimas, E. L., and Nawy, E.G. (1984). Moisture Transport in a Solid Waste Column. Journal of Environmental Engrg. Div., ASCE, 110, p780-794.

Lam, L., Fredlund, D. G., and Barbour, S. L., (1987). Transient Model for Saturated-Unsaturated Soil Systems: A Geotechnical Engineering Approach. Can. Goetechnical J. 24, p565-580.

Lee, H. C. and Wray, W. K. (1995). Techniques to Evaluate Soil Suction-A Vital Unsaturated Soil Water Variable. Proceedings of the First International Conference on Unsaturated Soils. Paris, p615-622.

McDougall, J. R., Sarsby, R., W., and Hill, J. N. (1996). A Numerical Investigation of Landfill Hydraulics Using Variably Saturated Flow Theory. Geotechnique, 46(2), p329-341.

Ridley, A. M., Dineen, K., Burland, J. B., and Vaughan P. R. (2003). Soil Matrix Suction: Some Examples of Its Measurement and Application in Geotechnical Engineering. Geotechnique 53, No 2., p241-253

Straub, W. A., and Lynch, D. R. (1982). Models of Landfill Leaching: Organic Strength. Journal of Environmental Engrg. Div., ASCE, 108, p251-268.

van Genuchten, M. T. (1980). A Closed Form Equation for Predicting the Hydraulic Conductivity of Unsaturated Soils,. Soil Sci. Soc. Of Am. J. 44, p892-898.

Yuen S.T.S., Wang Q.J, Styles J.R., McMahon T.A (1997). The Role of Water in landfills : A Full-Scale Hydrological Study, AWWA 17th Federal Convention , Water in the Balance, Melbourne , Australia

Yuen S.T.S. (1999).Bioreactor Landfills Promoted by Leachate Recirculation: A Full_scale Study, Doctor of Philosophy Thesis, University of Melbourne.

The pF-curve of fine-grained soils at high pore water suction

Dr.-Ing. Peter Schick

Institute of Soil Mechanics and Foundation Engineering, University of the Federal Armed Forces, Munich, 85577 Neubiberg

Abstract. A recently developed two-component model for the relationship between saturation and pore water suction (pF-curve) is used, whose frame consists of simple, physically meaningful values. The main purpose in this paper is to describe the amount of pore water in soils at high suction. Relative air humidity may be regulated by salt solutions of defined concentration or by sulfuric acid of varying concentrations, which leads to a steady-state water content in soil specimen. In the range of high suction values, data achieved in this way are fitted by the two-component model with high accuracy. The comprehension of many phenomena such as drying and cracking, apparent overconsolidation near the surface or strength loss of cuttings in overconsolidated soils by weathering depends on the understanding of water binding behavior in soils, which is improved by this quantitative model.

1 Basic principles

The formulation of pF-curves by fitting suitable functions to measured values of suction and the degree of saturation remains unsatisfying as long as there is no plausible soil-mechanical reason – which is the case for some popular pF-curve models. However, it is not to be expected that pF-curves of fine- and mixed-grained soils may be forecast without any fitting parameters, because

- the mineralogical composition of grain material,
- the chemical composition of pore water solution and
- the geometry of pore space

affect the water-binding forces strongly and in manifold ways so that predictions with global averaged index and state variables (grain-size curve and porosity) have to remain a rough estimate. The proposed two-component model improves forecasting quality on the one hand and engineering comprehension of related geotechnical problems on the other hand. It is based upon physical facts which are valid for all soils and uses standardized classification and state variables as well as mineralogical indicators ([1], [2]). Due to the already implied information there are only two free parameters with physical meaning, which are necessary to fit the test data. Even if they are roughly estimated without a test, it is not possible to forecast physically invalid pF-curves with the two-component model.

The derivation of model equations has been shown in detail in [1], some helpful equations for model parameters followed in [3]. The most important aspects are given below. Two water components of different binding strength are distinguished:

- "Adsorption water", which is bound in the near surface of mineral grains by physical adsorption (degree of saturation part S_A)
- "Capillary water", which is fixed in the pore space by surface tension (degree of saturation part S_C).

The total degree of saturation is:

$$S(\psi) = S_A(\psi) + S_C(\psi) \tag{1}$$

The volume of adsorption water may be calculated from the thickness of adsorption water layer d_{wA} and the corresponding specific surface O. The latter may be calculated from the grain size number (fraction A_k of gravel/sand/silt/clay: $A_G/A_S/A_U/A_T$), three different constant grain shape factors and two index values for the mineralogical composition [1]. These are:

- clay mineral content in silt fraction $A_{TU} = A_{\text{Clay minerals in silt}}/A_U$
- montmorillonite content in total clay minerals $A_{MT} = A_{\text{Montmorill.}}/A_{\text{Clay minerals in total}}$

Among other factors, plasticity depends on A_{TU} and A_{MT}. If there is no clay-mineralogical analysis, the following empiric equations are useful [3]:

$$A_{TU} = 0.127 \cdot \ln\left(I_{P(A<0.4mm)}\right) + 0.729 \tag{2}$$

$$A_{MT} = 0.136 \cdot \ln\left(I_{P(A<0.4mm)}\right) + 0.393 \tag{3}$$
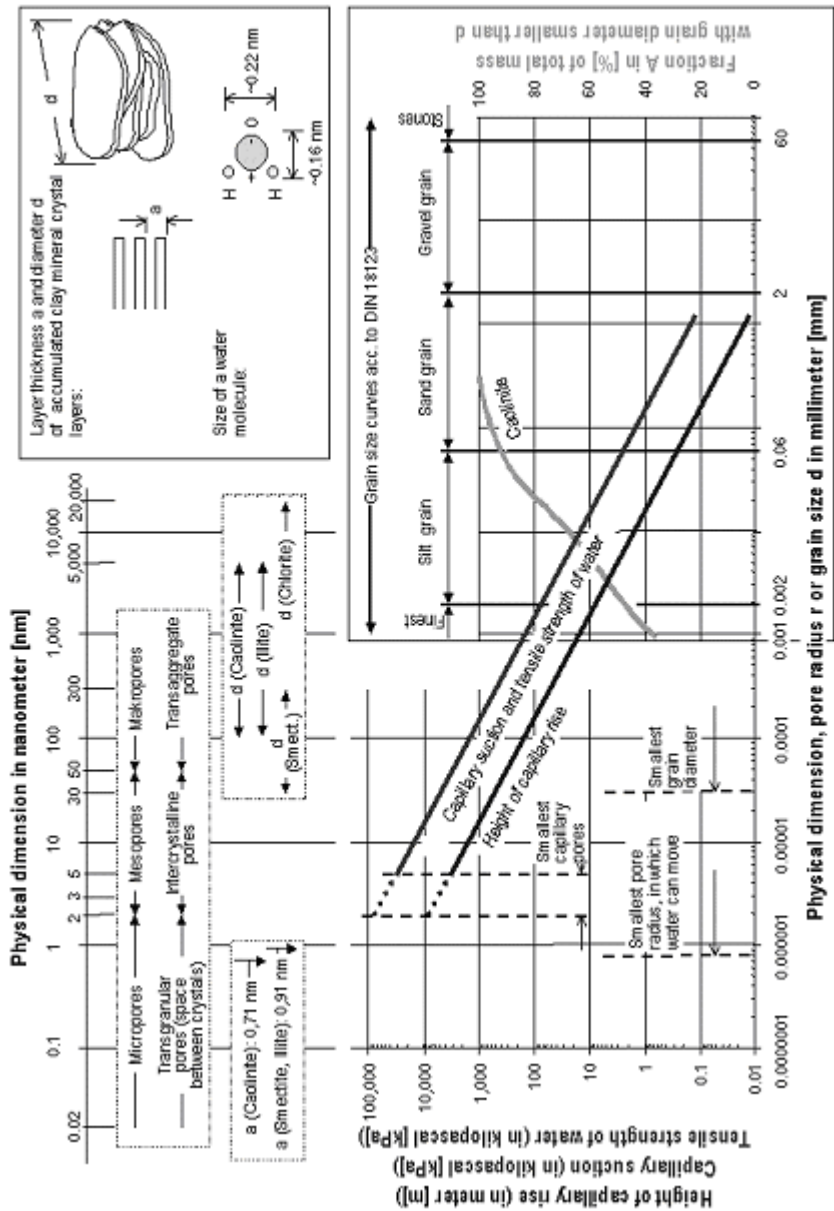
Fig. 1. Relevant orders of magnitude for dealing with pore water suction in fine-grained soils [1],[12]
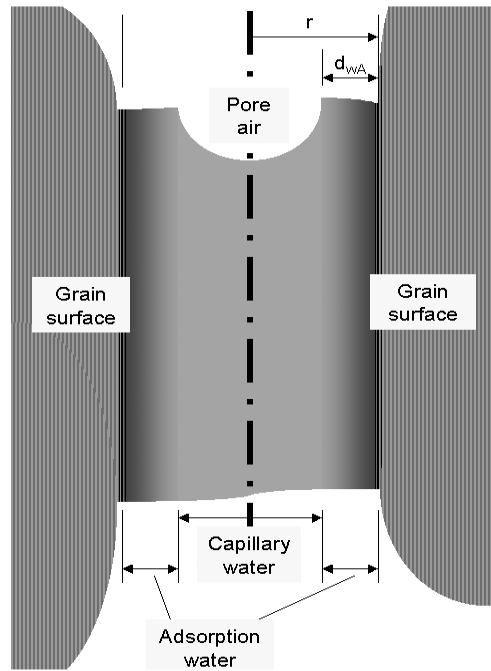
Fig. 2. Schematic sketch of water bound in the surrounding of grain surfaces

The adsorption water layer in compacted or natural soils is made up of hydration water – an ice-like layer with a thickness of a few molecules ($d = d_{hyd}$) – and a layer of water which is bound to the grain surface ever more loosely as the distance increases ($d = 1/\kappa$). Often:

$$d_{wA}(\psi \to 0) = d_{hyd} + \frac{1}{\kappa} \approx 2..5nm \qquad (4)$$

[4], it depends on the mineralogical and chemical composition of the grains and the pore water [13]. With a unified value of $d_{wA} = 4$ nm all test results evaluated up to now could be fitted easily ([1], [2], [3]). Pore space filled with adsorption water in the saturated state is:

$$n_{wA}(\psi = 0) = d_{wA}(\psi = 0) \cdot O \cdot \rho_d \qquad (5)$$

International literature deals with a usual value of ψ_{0A} = pF 7 (= 1,000,000 kN/m²) for maximum suction with a vanishing degree of saturation (e.g. [5]). Back-calculated values are smaller, as will be shown. The two-component model contains a correction function similar to [8] to force the pF-curve through the point ($S = 0$; ψ_{0A}) with increasing suction (Fig. 3a):

$$C_{pA} = 1 - \frac{\ln\left(1 + \dfrac{\psi}{\psi_{kap}}\right)}{\ln\left(1 + \dfrac{\psi_{0A}}{\psi_{kap}}\right)} \tag{6}$$

Therefore the degree of saturation due to adsorption water is:

$$S_A(\psi) = C_{pA} \cdot \frac{n_{wA}(\psi = 0)}{n} \tag{7}$$

The capillary water may be calculated by (1) afterwards. Like in the case of the adsorption water, the capillary water fraction of the total degree of saturation is being forced through the point ($S_C = 0$; ψ_{kap}) by a correction function (Fig. 3a):

$$C_{pC} = 1 - \frac{\ln\left(1 + \dfrac{\psi}{\psi_{kap}}\right)}{\ln(2)} \tag{8}$$

Thus, the capillary water content fraction is (according to [5], where it has been used for the whole pF-curve neglecting the difference between adsorption and capillary water):

$$S_C(\psi) = \left(1 - S_A(\psi = 0)\right) \cdot C_{pC} \cdot \left(\frac{1}{\ln\left(2.718.. + \left(\dfrac{\psi}{a}\right)^q\right)}\right)^m \tag{9}$$

The pF-curves from (1) and (4)-(9) show a sharp bend at $\psi = \psi_{kap} \approx$ 50,000 kN/m², where capillary water vanishes (Fig. 3b). Due to the almost complete lack of adsorption water, pF-curves of coarse grained soils are ending in ($S_C = 0$; ψ_{kap}). Because of $S_A = $ const., at low suction the form of the pF-curve is dominated by the capillary water curve (9).

a)

b)
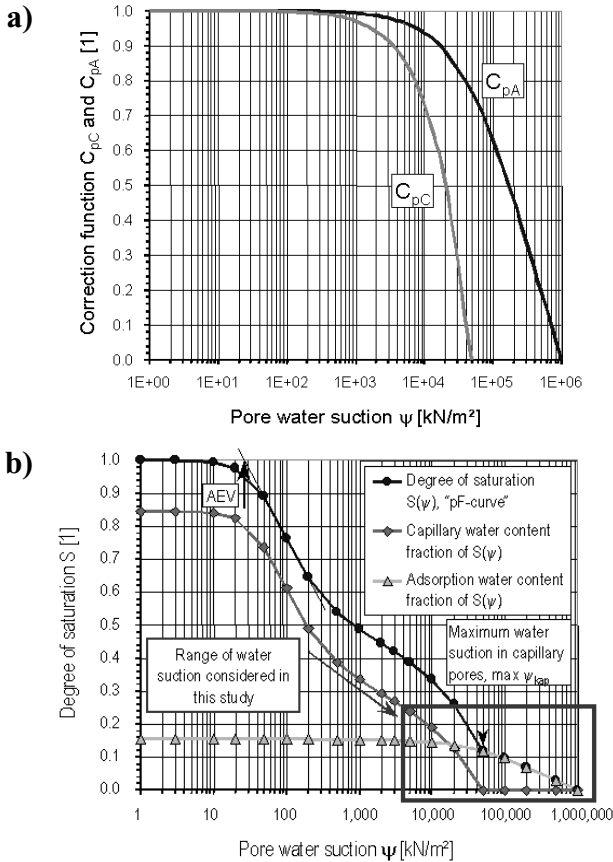
Fig. 3. Principle of two-component model. a): Correction functions (eqs. 6 and 8), b): pF-curve and its two components (eqs. 7 and 9)

2 Capillary water content

The capillary water $S_C(\psi)$ is fully determined by the amount of adsorption water and the three parameters a, q and m. With (9) the distribution function of equal radii of a capillary bundle may be calculated, if suction is transformed into an equal radius by the well-known equation for the height of capillary rise. Their sum-line (capillary pore radius curve) runs roughly parallel to the grain-size curve, but shifted to the left (Fig. 4b).

a)   **b)**
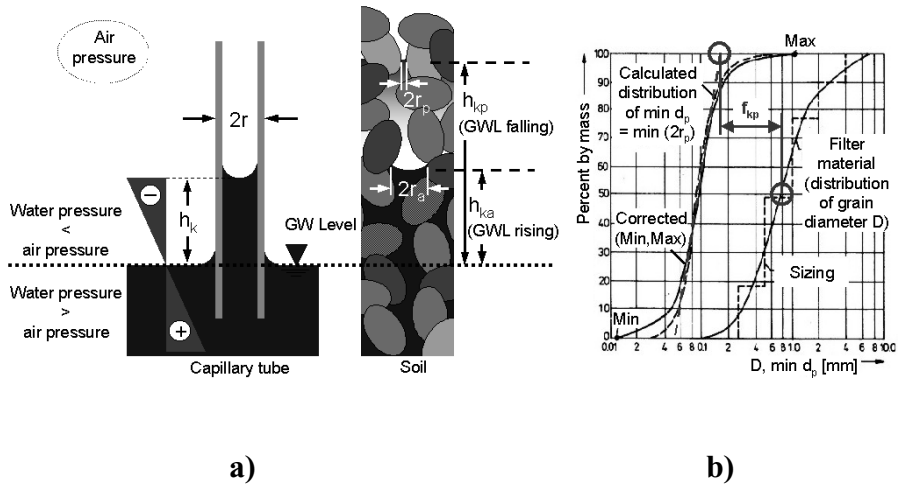
Fig. 4. a) Maximum capillary suction ψ_{kap} calculated from minimal capillary pore-radius min r_{kap}, b) Porosity and pore-size distribution of coarse-grained soils [9]

Parameter a in (9) shifts the upper part of the pF-curve nearly parallelly and therefore affects AEV (air-entry value) directly. A parameter study showed that $a \approx 2$ AEV. For coarse-grained soils, parameter a may be evaluated by AEV and the latter from the beginning of dewatering starting from the fully saturated state. Pore radii may be estimated from the grain-size curve. The assumption that the average minimal pore radius is about a tenth of median grain size (Fig. 4b) or a general distance factor f_{kp} leads to:

$$\min r_P = 0{,}1 \cdot d_{50} \qquad bzw. \qquad \min r_P = f_{kp} \cdot d_{50} \qquad (10a,b)$$

Then, suction at the beginning of dewatering is:

$$h_{k,p} \cdot \gamma_w = \frac{2 \cdot T_w \cdot \cos \alpha}{\min r_P} = \dots \qquad (11)$$

$$\dots = \frac{2 \cdot 7.5 \cdot 10^{-5} \left[\dfrac{kN}{m}\right] \cdot 1}{f_{kp} \cdot d_{50}[mm] \cdot 10^{-3}\left[\dfrac{m}{mm}\right]} = \frac{0.15}{f_{kp} \cdot d_{50}[mm]} \qquad \left[\dfrac{kN}{m^2}\right]$$

For gravels and sands within a range $d_{50} \approx 0.1..20$ mm and $f_{kp} = 0.1$, this leads to:

$$a \approx 2 \cdot \mathrm{AE}V = 2 \cdot h_{k,p} \cdot \gamma_w = \frac{0.30}{f_{kp} \cdot d_{50}[mm]} = 30..0.15 \tag{12}$$

(Fig. 5a). Only in soils with a steep grain-size curve is $f_{kp} > 0.1$. Single-grained soil fractions may have about $f_{kp} = 0.5$ due to large free-water pores and little density.

The situation at AEV corresponds to the water content at shrinkage limit LS in fine- and mixed-grained soils. Because suction acts like a one-dimensional load, AEV may be calculated as the stress on the normal consolidation line NCL, which determines the water content at the shrinkage limit: $\mathrm{AEV} \approx \sigma'(\mathrm{SL})$. Choosing LL and SL as reference points and assuming that the compression index C_C as well as the stress at liquid limit $\sigma'(\mathrm{LL})$ are linear functions of LL leads to the following equation as shown in [3]:

$$a = (a_1 - a_2 \cdot LL) \cdot \exp\left(\frac{(LL - SL) \cdot \dfrac{\rho_S}{\rho_W}}{a_3 \cdot LL - a_4}\right) \quad \left[\frac{kN}{m^2}\right] \tag{13}$$

with $a_1 = 8$ kN/m², $a_2 = 3$ kN/m², $a_3 = 0.8$ and $a_4 = 0.08$ (Fig. 5b).

Both parameters q and m are free parameters of the two-component model and can be used for fine adjustment between model and test results. They describe the form of the pF-curve. While q rotates the pF-curve around a fixed point, m changes the slope of the capillary curve in the range of $\psi = \max \psi_{kap}$. Suitable starting values are $q = 0.7$ and $m = 1.5$.

b)
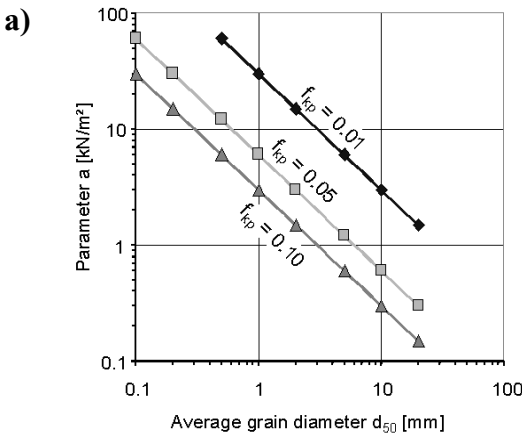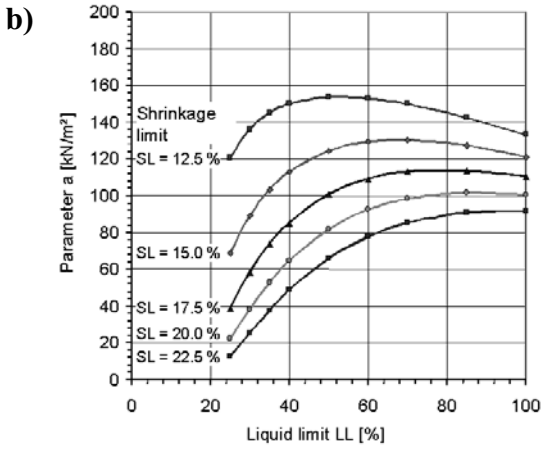
Fig. 5. Parameter a resp. Air-Entry Value (AEV): a) Coarse-grained soils (eq. 12), b) Fine-grained soils (eq. 13)
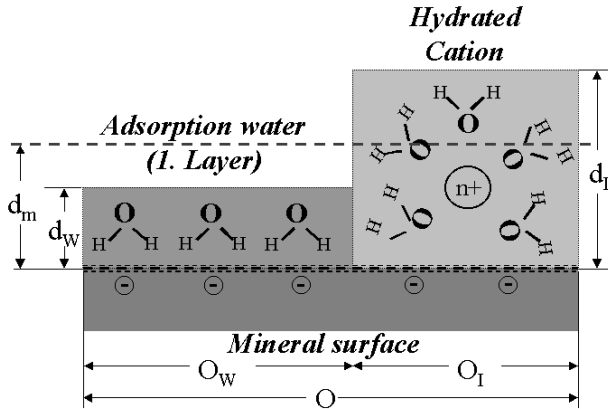
Fig. 6. Mineral surface model for calculation of maximum water binding energy ψ_{0A} (compare with Fig. 2)

3 Adsorption water content

The two-component model shall be applied to the test data from [6] and [7] by way of example. The principle of these tests is a constant water vapor pressure or humidity in a desiccator, which contains the soil sample. A salt solution dehumidifies the air due to its osmotic potential. By and by, a dynamic equilibrium is generated and equal numbers of water molecules are condensing and vaporizing. The higher the salt concentration, the lower the vapor pressure over the solution. A similiar equilibrium water content will exist in the soil sample, which depends on the surface ions on the clay mineral surfaces and the adjusted humidity. The same test may be carried out with sulfuric acid of different concentrations. Relative humidity of the air is:

$$\phi = \frac{c}{c_s(T)} = \frac{p_{WD}}{p_{WD,s}(T)} \qquad [1] \tag{14}$$

Pore water suction is the energy density (per volume) of the bound water in the transition zone from the fluid to the vapor phase. The equalization of the water vapor pressure potential according to the barometric height formula with the potential of water in the soil solution [10] leads to (15), if osmotic part of suction may be neglected due to small ion concentration:

$$\psi = \frac{1,000 \cdot R \cdot T}{V_{mol\,H_2O\,fl}} \cdot \ln\phi \qquad \left[\frac{kNm}{m^3} = \frac{kN}{m^2}\right] \tag{15}$$

(Conversion factor 1,000: [J/cm³] = [100³ Nm / m³] = [1,000 kN/m²]). Suction values in the range of 5,000 kN/m² < ψ < 450,000 kN/m² were created by this test method, which extends the measurable suction range to the highest possible values.

The energy of the first adsorbed water layer on a mineral surface is influenced by the strength of Van-der-Waals forces and hydrogen bonds between them as well as by the hydration energy for the ions on the mineral surface. The magnitude of this maximal suction ψ_{0A} may be estimated with a simple thermodynamic model (Fig. 7a, 7b) and the well-known energy of the involved physical or chemical bonds, expressed as G [kJ/mol]. Also the size of water molecules and hydrated ions is relevant as it rules the coating density B [mol/m²]. The total surface (Fig. 6) is divided into two parts:

$$O = O_W + O_I \qquad \left[\frac{m^2}{g}\right] \tag{16}$$

The binding energy per volume of each component has to be weighted by area:

$$\psi_{0A} = G_{WM} \cdot B_W \cdot \frac{1}{d_W} \cdot \frac{O_W}{O} + G_{WI} \cdot B_I \cdot \frac{1}{d_I} \cdot \frac{O_I}{O} \qquad \left[\frac{kJ}{m^3} = \frac{kN}{m^2} \right] \tag{17}$$

Evaluation of test data with the two-component-model is advantageous in this case because a separation into adsorption and capillary water is already contained in the model equations and no more artificial criteria are necessary for this purpose. The number of tests and the tested suction values, given by the used salt or sulfur solution concentrations, become irrelevant.

Except for the smallest values, generated suctions are larger than $\psi > 50,000$ kN/m², so that almost only adsorption water exists. The capillary curve with its parameters a, q and m is of little relevance in this case. For the evaluation of test data (Fig. 8), a = 150 kN/m² and m = 1.5 were kept constant and only q was used for fitting, which was fully sufficient. Especially for fitting the adsorption water content, four parameters are required:

- the montmorillonite content in the total clay mineral content A_{MT},
- the porosity n,
- the maximal suction at S→0, ψ_{0A}, and
- the thickness of adsorption water layer d_{wA}.

The water suction ψ_{0A} where saturation vanishes completely is between 600,000..800,000 kN/m² according to test data from [6] (Fig. 8) and between 500,000..600,000 kN/m² according to test data from [7] (Fig. 8). Estimations in the range of $\psi \approx 1,500$ kN/m² or less are not affected by the difference to the usual value of $\psi_{0A} = 1,000,000$ kN/m² (Fig. 3b). Calculation with a constant value of $\psi_{0A} = 700,000$ kN/m² is recommended, which will lead to a satisfying result in most cases.

Tab. 1: Parametric variation for estimation of ψ_{0A} with eq. (17)

Case	ΔG_{WM} [kJ/mol]	ρ_W [g/cm³]	ΔG_{WI} [kJ/mol]	l_I [nm]	O_W/O [1]	ψ_{0A} [kN/m²]
1 Basic case	10	1.4	250	0.78	0.90	787,510
2 Min ΔG_{WM}	5					437,510
3 Max ΔG_{WM}	20					1,487,510
4 Min ρ_W		1.0				587,510
5 Max ρ_W		1.5				837,510
6 Min ΔG_{WI}			40			714,002
7 Max ΔG_{WI}			1000			1,050,042
8 Min r_I				0.62		874,248
9 Max r_I				0.94		749,999
10 Min O_W/O					0.50	826,441
11 Max O_W/O					0.99	778,751

4 Applications

With the aforementioned model, real class A predictions of the pF-curve are now possible, without the need of measured values. Uncertainty is limited to the form of the capillary water curve between AEV and ψ_{kap}, that means to the parameters m und q. They have to be fitted.

As an example, a mixed-grained mineral sealing material called "Bentokies" was chosen (Fig. 8). All classification and state parameters are well known for this material [11]. The pF-curves were predicted for gravel with two maximal grain sizes (lab: max d = 16 mm, field: max d = 60 mm) and two porosities (lab: n = 18 / 22 %, field: n = 16 / 20 %). Because coarse grains don't affect capillary pore-size curve, distance to grain-size curve is larger than for fine-grained soils. Parameter a was calculated by (13), parameter q and m were assumed taking the experience from other soils into account.

Like the pF-curve, the water permeability of fine-grained soils must not be calculated from the geometry of pore space alone. An empiric equation for many soil types, especially for the fines content (A< 0.4 mm) of Bentokies, is:

$$\log\left(\frac{k}{k^*}\right) = m_k \cdot \log\left(\frac{n}{n^*}\right) \tag{18}$$

In this case, reference values are $n^*=n_{100}$ and $k^*=k_{100}$ with $\sigma'_V = 100$ kN/m² [11], where:

$$n_{100} = 18 \cdot I_P^{0,255} \quad and \quad \log k_{100} = -8.64 - 0.88 \cdot \log I_P \tag{19a,b}$$

The value m_k is between 1.5..2.5 and is influenced by many factors which cannot simply be quantified, like the model parameters q and m. (18) describes the change of permeability of a saturated sample with porosity reduced by mechanical one-dimensional compression. Because dewatering reduces the amount of pore space for water flow in a similiar way at least at high degrees of saturation, (18) may be used for unsaturated soils in the case of $S \gg S_A$. The additional assumption that only capillary water participates in the water flow but not the adsorption water leads to:

$$\frac{k}{k_{100}} = \left(S_C^*\right)^{m_k} \tag{20}$$

because $S_C^* = n_{wC}/n_{100}$, so that $k \to 0$ for $S \to S_A$, and $k_{100} = k(S_A+S_C=100\%)$. For typical values of a silt-clay-mixture ($I_P = 30\%$) chosen as an example a predicted pF-curve with its both components as well as (20) is shown in Fig. 9a, 9b. The proposed procedure determines the point ($S = S_A$) and the slope adjacent to $S = 1$ while the intermediate range has got the assumed form of a power function. Relations of this type are well known and confirm the usability of this method. Determination of m_k may be carried out by an oedometric permeability test.
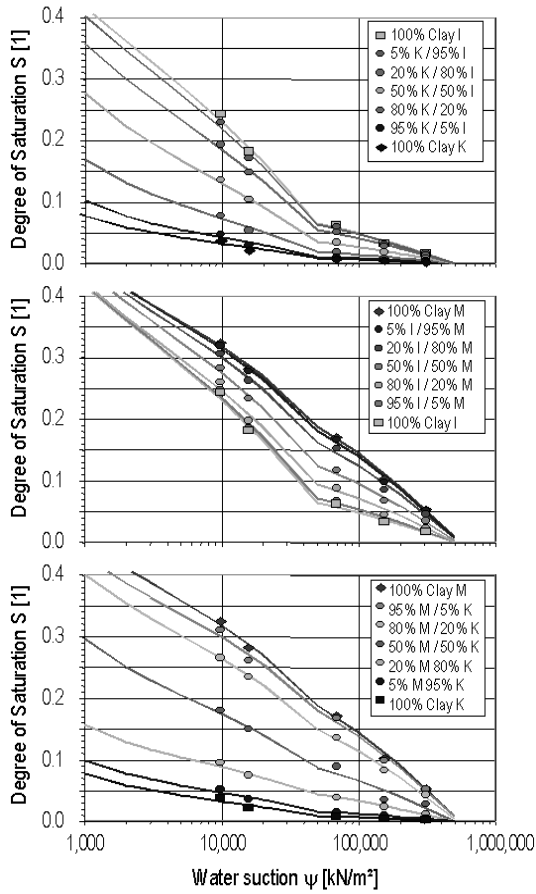
Fig. 7a. Back-calculation of pF-tests in the highest pore water suction range [2]. Mixtures of caolinitic/illitic clay, illitic/montmorillonitic clay and montmorillonitic/caolinitic clay
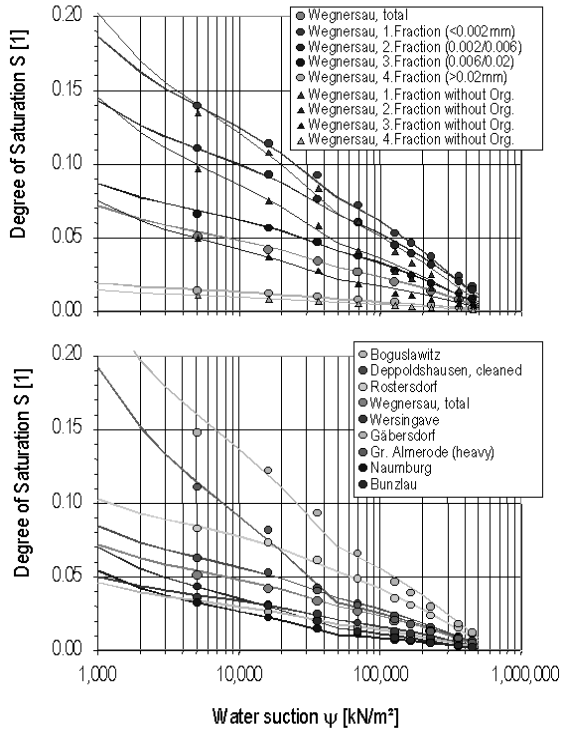
Fig. 7b. Back-calculation of pF-tests in the highest pore water suction range [2]. Several fractions of a fine-grained soil with and without organic content and several natural soils
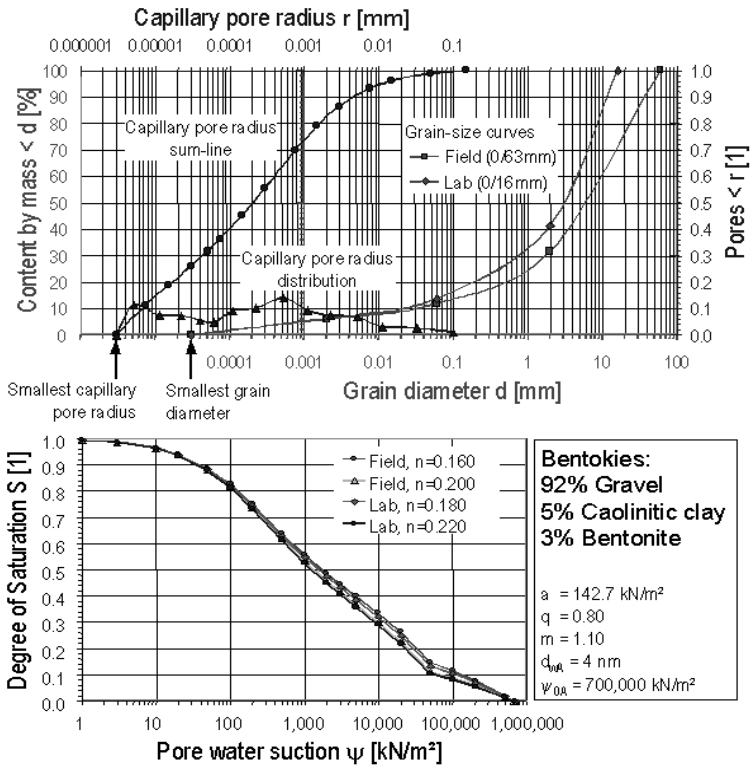
Fig. 8. Class A prediction of pF-curves for the mixed-grained sealing material "Bentokies" ([1], [11]]
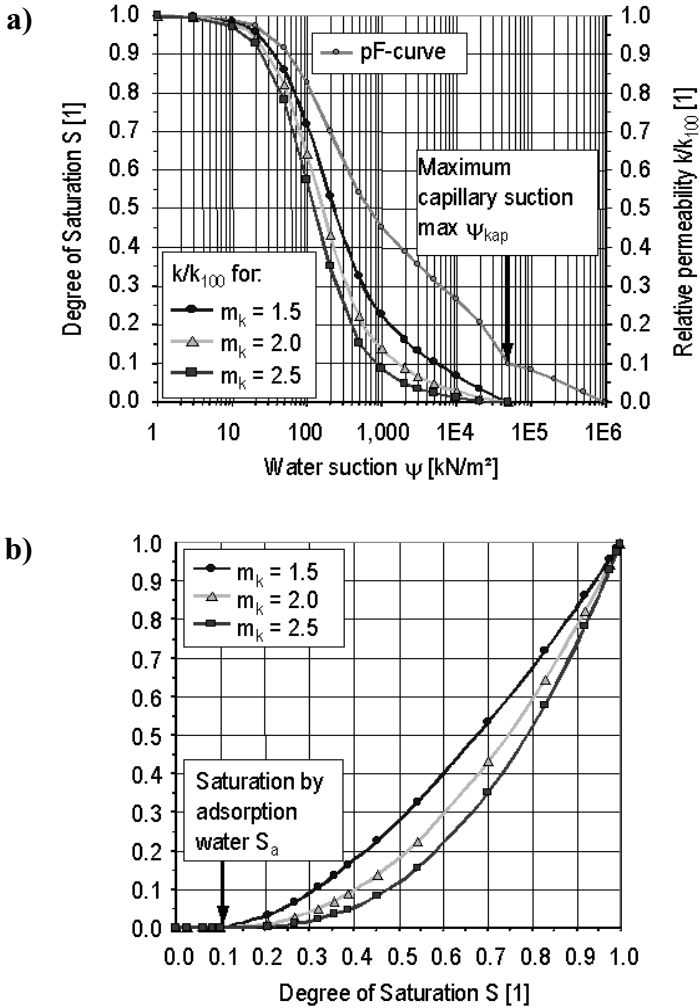
Fig. 9. Water permeability of unsaturated soils [1]. a) pF-curve and relative permeability dependent on water suction, b) relative permeability dependent on degree of saturation (eq. 20).

Notations

a [kN/m²], q [1], m [1]: *Model parameter for capillary water content.*
a_1 = 8 kN/m², a_2 = 3 kN/m², a_3 = 0.8, a_4 = 0.08: *Constants in (13)*
B_W, B_I [mol/m²]: *Coating density of water molecules or ions on grain surface*
c, c_s(T) [g/m³]: *Absolute humidity, index s: maximum humidity (saturation)*
d_{wA} = 4 nm: *Thickness of adsorption water layer*
G_{WM}, G_{WI} [kJ/mol]: *Binding energy between water molecules and grain surface or between water molecules and ions on the surface*
k, k* [m/s]: *Permeability or reference value of permeability*
LL [1], SL [1]: *Water content at liquid limit or shrinkage limit*
m_k [1]: *Slope in log-log-diagram of k = f(n) (eq. 18)*
n, n* [1]: *Porosity, reference value of porosity*
O [cm²/g]: *Specific surface of the soil (eq. 5), calculation acc. to Ref. [1]*
p_{WD}, $p_{WD,s}$(T) [kN/m²]: *Water vapor pressure, index s: maximum vapor pressure (saturation)*
min r_{kap} = 3E-06 mm: *Smallest radius of capillary pores*
R [J/(mol*K)] = 8.314: *General gas constant*
S [1]: *Degree of saturation, index A: Adsorption water, index C: Capillary water*
T_w = 7.5E-08 kN/mm: *Surface tension of water at 10°C*
T [K]: *Absolute temperature*
$V_{mol\ H2O\ fl}$ = 18 cm³/mol H_2O_{fl}: *Mol volume of liquid water (ρ_W= 1 g/cm³, M_W=18 g/mol)*
α = 0°: *Wetting angle of contact between water and mineral surface*
σ'(LL) [kN/m²]: *One-dimensional stress on NCL for w = LL*
ψ_{0A} = ψ(S→0) ≈ 700,000 kN/m²: *Max. water suction when S vanishes*
ψ_{kap} = 2 T_w cos α / min r_{kap} ≈ 50,000 kN/m²: *Max. water suction in capillary pores*

References

[1] SCHICK, P. (2002): Anwendung eines Zwei-Komponenten-Modells der pF-Kurve auf Strukturänderungen in Böden (*Application of a two-component model of the pF-curve to structure changes in soils*). Bautechnik 79 (2002), Heft 2

[2] SCHICK, P. (2002): Die pF-Kurve bindiger Böden bei großen Wasserspannungen (*The pF-curve of fine-grained soils at high water suction*). Bautechnik 79 (2002), Heft 12, S. 842-849

[3] SCHICK, P., SCHMID, J. (2003): Kenngrößen zur Wasserhaushaltsmodellierung der Baustoffe von Deponieoberflächenabdichtungssystemen (*Index values of soils for modeling the water balance of landfill capping systems*) Bauingenieur Band 78, Heft 4, April 2003, S. 203-214

[4] SHANG, J.Q., LO, K.Y., QUIGLEY, R.M. (1994): Quantitative determination of potential distribution in Stern - Gouy double-layer model. Can. Geotech. J. 31, pp 624-636.

[5] FREDLUND, D.G., RAHARDJO, H. (1993): Soil Mechanics for Unsaturated Soils. Wiley, New York.

[6] KURON, H. (1930): Versuche zur Feststellung der Gesamtoberfläche von Erdböden, Tonen und verwandten Stoffen *(Measurements on the evaluation of the total inner surface of soils, clays and similiar materials)*. Z. Pflanzenernährung u. Düngung A 18, S. 179-203

[7] LANGER, M. (1964): Untersuchungen zur Theorie der Wasseraufnahmefähigkeit von Tonen *(Evaluation of the theory of water uptake of soils)*. Vorträge der Baugrundtagung, 1964, S. 1-56

[8] FREDLUND, XING (1994): Equations for the soil-water characteristic curve. Can. Geotech. J 31: 521-532 (1994)

[9] SILVEIRA, A. (1965): An Analysis of the Problem of Washing Through in Protective Filters. Proc. 6th ICSMFE, Montreal

[10] HARTGE, HORN: Einführung in die Bodenphysik. 3. Auflage 1999

[11] SCHICK, P. (1997): Bodenmechanische und bautechnische Eigenschaften von Bentokiesdichtungen - Nachweis der Gebrauchstauglichkeit *(Properties of Bentokies-sealings for waste deposits – proof of security and serviceability)*. Bautechnik 74 (1997), H.5, S.320-330

[12] SCHICK, P. (2000): Zum Einfluss negativer Porenwasserspannungen auf die Standsicherheit von Einschnittsböschungen in überkonsolidierten Böden (*On the influence of negative pore water pressure on the safety of cutting slopes in overconsolidated soils*). In: Mitteilungen des Instituts für Bodenmechanik und Grundbau, UniBw München, H. 14, 2000.

[13] MITCHELL, J.K. (1993): Fundamentals of Soil Behaviour. Second Edition. John Wiley & Sons, New York.

References   of   the   author   are   available   as   pdf-document   on http://www.bauv.unibw-muenchen.de/institute/inst5
or contact peter.schick@unibw-muenchen.de

STRUCTURAL CHARACTERIZATION - MEASUREMENT OF SUCTION

Influence of microstructure on geotechnical properties of clays

R.M. Schmitz[1,2], C. Schroeder[1], and R. Charlier[1]

[1]Geomecanics and Engineering Geology - Géomac - Université de Liège, Belgium
[2] National Scientific Research Fund (F.N.R.S.)

Abstract. Clays are geomaterials, which are used in various applications in our society. The more common geotechnical applications are: waterproof cores of dams, barriers to contain waste, slurry walls etc. But even if clays are not used as construction materials the geotechnical engineer encounters them frequently during construction of e.g. foundations and tunnels. Within the group of clay minerals we find individual clay species that possess geotechnical properties that vary enormously. These differences in geotechnical properties can be related directly to the differences in microstructure of the clay minerals. In this contribution it is shown how the knowledge of clay microstructure from X ray diffraction analysis, thus knowledge of the clay mineralogy, can be used to assess the geotechnical behaviour of the clay. When mineralogical alteration processes of the clay are know from appropriate geological analogues, the geotechnical characteristics of the engineered clay structure can be estimated on the basis of these processes (e.g. containment of hazardous waste, infiltration of permeates in dams etc.). This implies however that the clay used as construction material is well characterised. A method to prepare such a clay atlas and how to use it is presented in this contribution.

1 Introduction

In environmental engineering clays are the most important construction materials used to seal hazardous waste from the biosphere until fossilisation of the waste occurs. The required technical life of the clay seal ranges from hundreds of years if domestic waste is concerned, to tens of thousands of years in the case of radwaste. During this period the clay barrier is exposed to varying environmental conditions, like changes in pore fluid chemistry or heat. This variation provokes microstructural changes, reflected in clay mineral alteration processes. These processes can be analysed relying on x ray diffraction techniques. The link between x ray diffraction techniques and geotechnical properties is provided by the equivalent basal spacing concept. The mineral alterations likely to occur were

simulated in the laboratory in the framework of a multidisciplinary research project funded by the Walloon region. Some of the alteration processes that were observed, will be discussed, referring to tests performed with natural clayey soils having a complex mineralogy representative of the clay reserves in Belgium on one hand and monomineral clays used for demonstration purposes on the other.

Materials

The materials that were used were natural Tertiary clays obtained in Soignies and Tournai (Ypresian) and in Kruibeke (Rupelian). Analysis revealed that the clays consist of illlite, neoformed volcanogenic illite-montmorillonite mixed layers (10-14m), illite-chlorite random mixed layers (10-14c), chlorite and kaolinite, and only in the Tournai clay some natural pillared smectite with Al hydroxyls in the interlayers (Sm_{Al}). The average composition of the clay minerals in the natural materials is given in Table 1. Next to these natural clays a reference smectite and kaolinite were used.

Methods

Geotechnical tests

The Atterberg test results of the natural clays were obtained using the Casagrande cup according to NF P94-051. The cone parameters give liquid limits that reasonably correspond with Casagrande liquid limits. However the very different procedures of the falling cone test and the Casagrande cup must lead to different values of liquid limits for extreme soils (Muir-Wood 1990). Above a liquid limit of 100% (Head 1992) the cone method tends to give slightly lower values. Although the cone method is preferred to the Casagrande method (Muir-Wood 1990) the data for the clay determined using the Casagrande cup were used because it is the most widespread method used in Belgium (Table 2). The average liquid limit and plasticity index values of the three natural clays (after gentle drying at 30°C and grinding) are given in Table 1.

Table 1. Average Atterberg properties and clay mineral composition

	LLcasa (%)	PI (%)	CF_{Illite}^{FOA} (%)	$CF_{(10-14c)}^{FOA}$ (%)	$CF_{(10-14m)}^{FOA}$ (%)	CF_{SmAl}^{FOA} (%)	$CF_{Kaolinite}^{FOA}$ (%)	$CF_{Chlorite}^{FOA}$ (%)	TCF^{TRP} (%)
Reference Kaolinite	59	25	10	0	0	0	90	0	95
Kruibeke average	63	34	28	18	17	5	13	19	71
Tournai average	1.2e2	76	16	7.0	68	9.0	0	0	81
Soignies average	35	11	33	15	16	6.0	20	10	49
Reference smectite	6.6e2	6.1e2	0	0	1.0e2	0	0	0	95

Table 2. Methods currently used to determine the liquid limit at Belgian Universities

University	Tool for Atterberg test	Standard
VU-Brussel	Casagrande cup	ASTM D4318
UL-Bruxelles	Casagrande cup	ASTM
FA-Gembloux	Casagrande cup	LCPC M.O. S.I.-4-1963
RU-Gent	Casagrande cup	BS 1377
	Cone penetrometer[1]	
U-Liège	Casagrande cup	NF P94-051
U-Louvain la Neuve	Casagrande cup	BS 1377 NF P94-051

[1] A cone penetrometer is present but used only if explicitly demanded by client

Clay mineralogy analysis

The mineralogy was determined using the Liège Clay Laboratory sample preparation as described in (ManWal 2001) and (Schmitz et al. 2001). The total clay fraction was analysed and not only the fraction smaller than 2 microns in order to take into account all clay minerals present.

The equivalent basal spacing

To relate the interlayer space and the basal spacing of a polymineral clay to the liquid limit the concept of equivalent basal spacing was previously introduced (Schmitz et al. 2002):

$$EBS = TCF^{TRP} \cdot \sum_{i=1}^{n} CF_i^{FOA} \cdot BS_i^{(001)FOA} \tag{1}$$

The relative amount of a clay mineral is multiplied with the basal spacing (Å) of this mineral known from literature. This step is repeated for all measured clay fractions. Then these values are summed. This sum is then corrected for the total amount of clay minerals in the sample.

An example: if the sample only consists of smectite; the $TCF^{TRP} = 1$, the $CF_{Smectite}^{FOA} = 1$ and the $BS_{Smectite}^{(001)FOA} = 14Å$. Therefore the EBS will be 14Å as well. If the sample only consists of sand: the EBS=0 Å

In Fig. 1 the EBS is plotted versus the liquid limit of the same samples (Casagrande cup). If a Boltzmann distribution of data is assumed (coefficient of determination is equal to 0.98) then

$$EBS = \frac{A_1 - A_2}{1 + e^{(LL_{Casa} - x_0)/x_d}} + A_2 \tag{2}$$

$$LL = x_d \cdot LN\left(\frac{A_1 - A_2}{EID - A_2} - 1\right) + x_0 \tag{3}$$

with: $A_1 = -1.268E2$; $A_2 = 1.315E1$; $x_0 = -1.528E2$ and $x_d = 6.571E1$
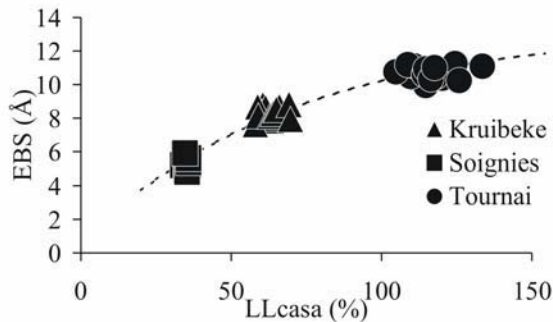
Fig. 1. The equivalent basal spacing versus the liquid limit of three natural clays (exposed to landfill leachates).
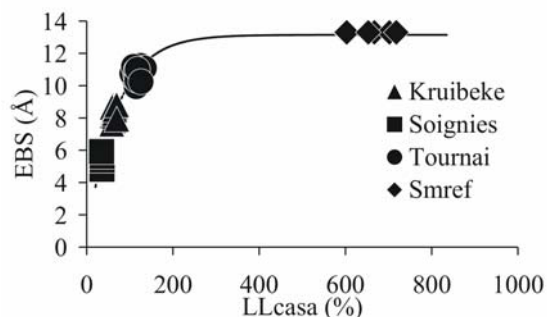
Fig. 2. The equivalent basal spacing versus the liquid limit of three natural clays and a reference smectite (Smref).

How the correlation between the EBS and the LL can be used to predict the behaviour of clay in engineering terms is shown in the examples in the next sections. Therefore reference is made to the following well known correlations between the Atterberg test results and other geotechnical properties:

Using the expression by (Terzaghi and Peck 1967) a link can be made between the liquid limit and the compression index:

$$C_C = 0.009 \cdot (LL - 10) \tag{4}$$

Using the expression by (Wetzel 1990) a link can be made between the specific surface of the clay and the liquid limit (if LL>50%):

$$S_a = \frac{(LL - 46.5)}{1.01} \tag{5}$$

If the results of index tests on a number of samples of related soils are plotted on a plasticity chart the points tend to lie on a straight line which is often approximately parallel to the A line (Muir-Wood 1990):

$$PI = A \cdot LL + B \tag{6}$$

The parameters A and B were determined for the three natural clays and the reference smectite:

Table 3. Relationship between LL and PL for different clay families. All samples were carefully dried, exposed to demineralised water and different landfill leachates. Results are the average of a total of 188 tests.

	A	B
Kruibeke average	0.94	-25.7
Tournai average	0.71	-6.55
Soignies average	1.97	-57.3
Reference smectite average	1.02	-62.3

With the relationship between the LL and the PI for each group, the change in PI can be estimated if a change in EBS is known. The PI of a clay can be related to the undrained shear strength as shown by (Mitchel 1993):

$$\phi = -6.6 \cdot Ln(PI) + 50.4 \tag{7}$$

Application EBS: Clay exposed to heat

What will happen to the clay barrier once it is exposed to heat, like in the case of storage of radioactive waste? From clay mineralogy it is known that heating to e.g. 500°C during several hours causes a collapse of smectite to 10 Å and the disappearance of the kaolinite peak. How these processes can be described in terms of EBS is shown below.

For the reference smectite the initial EBS = 0.95*14 = 13.3Å according to (1). This value corresponds using relationships (3) - (6) to:

LL >> 300%
PI >> 300%
Cc >> 3.2
Sa > 300 m²/g.

These values were validated as is evidenced by the following measured values: LL = 660%, PI = 610%, Cc = 5.3 (van Paassen 2002) and Sa = 556m²/g (Keijzer 2000).

After heating to 500°: EBS = 0.95*10 = 9.5 Å, corresponding using relationship (3), (4), (6) to:

LL=85%, PI=25% and Cc~0.7.

The clay has changed enormously but still, its properties are those of a high plastic clay (type: TA DIN18196 or CH BS1377). The liquid limit value is thus be representative of a smectite after collapse of the interlayer space without rehydration.

Atterberg tests cannot, however, be performed without re-exposure of the sample to water. Tests were performed to analyse the reversibility of the collapse of the interlayer space. After renewed exposure to water part of the collapsed smectite (43%) reopens while another part remains at 10 Å (57%). This corresponds to an EBS = 0.95*(0.57*10+0.43*14)= 11.7 Å and using relationships (3), (4) to a LL near 1.5E2% and Cc near 1.2.

The measured liquid limit varied between 1.6E2 and 1.9E2 % which is close to the predicted value. The variability is due the difficulty of rehydrating the clay after heating. The same observation is valid for the PI. Due to the heating the Cc also decreased, from 5.3 to 1.9, an order of magnitude predicted correctly by the EBS concept.

Fig. 3. The equivalent basal spacing versus the liquid limit of the reference smectite (Smref) and the same clay after heating to 500°C (Smref 500°C). **Fig. 4.** The equivalent basal spacing versus the liquid limit of the Tournai clay versus the Tournai clay after heating to 500°C (Taverage 500°C).

Tournai clay has an initial EBS = 0.81*(0.16*10+0.07*12+0.68*14+0.09*14) = 10.7 corresponding using relationship (3), (4), (6), (7) to:

LL near 1.1E2%, PI near 7.3E1%, Cc near 0.9, Sa = 65 m²/g and ϕ' near 22°.

The measured values are close:

LL = 1.2e2%, PI = 7.6e1%, Cc = 0.9 and a Sa = 66 m²/g only the ϕ' was higher than expected being equal to 27°.

When Tournai clay was exposed to 500°C heat it was impossible to determine the liquid limit afterwards. The clay did not rehydrate, and did not show the typical clayey stickiness. If it is assumed that this material had a liquid limit just below the test limit of about 28% (Wendehorst 1996). If it is assumed that the loss of its "plasticity" indicates destruction of the smectite clay minerals, this fraction has to be added to the fraction of non-clay minerals. This results in an EBS = 0.26*(0.49*10+0.23*12+0.28*14) = 3.0 Å and a LL = 15 %, indeed a value below the test limit of the liquid limit test. This indicates that our assumption was cor-

rect. The transition of the EBS and LL properties of the Tournai clay due to heating are shown in Fig. 4.

These examples show that although heating has a tremendous effect on the liquid limit, the impact is different depending on the relative composition of the clay minerals. The reference smectite could resist the effect of heating fairly good and can still be classified as a plastic clay (type TA DIN18196 or CH BS1377) after heating, whereas the Tournai clay changes from an plastic clay (TA or CH) a clay-silt mixture (ST). This behaviour was predicted for different clays using the EBS concept types and validated afterwards by performing the test.

Application EBS: Clay exposed to salt solutions

Background

Salts tend to change the behaviour of clays (Schmitz and van Paassen 2003) by the following processes:

- Osmotic effects

    - on a large scale: if the clay is considered as a semi-permeable membrane the presence of salts causes fluids to migrate from the clay outwards, producing a decrease of volume, increase of shear strength, etc.

    - on a small scale: if salts enter the clay by advection or diffusion, the thickness of the double layer is decreased, the clay particles approach each other, resulting in a decrease of the liquid limit, decrease of volume, increase of permeability, etc.

- Mineral alteration:

    - cations, like potassium, can enter the pseudohexagonal voids of Smectite. This causes to some degree an irreversible collapse of the interlayer space. The properties of this collapsed material will correspond to that of an illitic clay or illite-smectite mixed-layer, which generally have a lower liquid limit and higher shear strength.

- Crystallisation of salt crystals

    By increasing the concentrations of ions in the pore fluid by e.g. evaporation salts start to crystallise. This modifies the clay in two ways:

    - due to the hygroscopic nature of salt, water is drawn from the clays; this loss of water is accompanied by a decrease of volume, reorientation of clay particles, etc.

    - the presence of salt crystals in solid form increases the grain size of the total sample; the silt-sized fraction increases with respect to the clay fraction which results in a decrease of the liquid and plastic limit, an increase in internal angle of friction, etc.

Reference smectite

These processes can be described for the reference smectite in terms of EBS as follows:

initial EBS = 0.95*14 = 13.3 Å corresponding to a LL >> 300% and a Cc >> 3.2.

After addition of a KCl solution and air-drying the samples during only one cycle, the basal spacing collapsed to 12 Å. The EBS becomes:

EBS = 0.95*12 = 11.4 Å corresponding to a LL = 135%. The measured LL however was much lower. But it was reported that the clay sample felt silt like. In fact as was shown by XRD analysis, these "silt" particles were sylvite (KCl salt) crystals. After a standard was created to determine accurately the amount of KCl, it was found that the sample consisted up to an average of 40 % Sylvite. The EBS in this case is:

EBS = 0.6*(1*12) = 7.2 Å corresponding to a LL = 52 %, very close to the actual value measured in the lab: LL = 47 %. The original value of the reference smectite, the correlation line between the LL and the EBS, and the actual measured data points are given in Fig. 5.
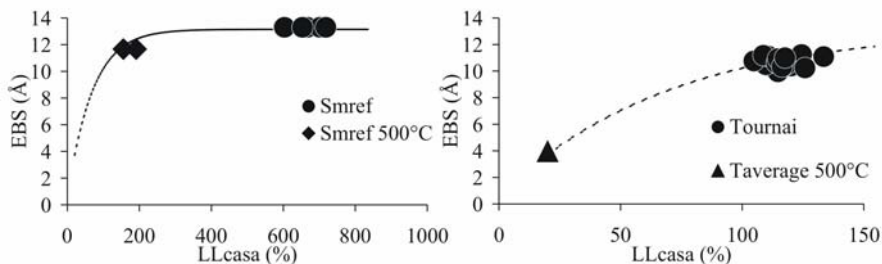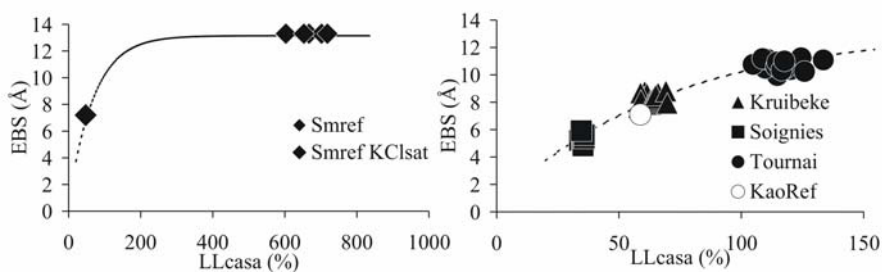

Fig. 5. The equivalent basal spacing versus the liquid limit of the reference smectite (Smref) and the same clay after exposure to a saturated salt solution (Smref KClsat). **Fig. 6.** The equivalent basal spacing versus the liquid limit of three natural clays and a reference Kaolinite(Kao ref).

The natural Tournai clay

The friction angle of a remoulded Tournai clay sample tested during a CU triaxial test is 27°. If the sample is exposed to a saturated NaCl solution, remoulded and tested, will the salt change the friction angle? From the experiment with the reference smectite and salt we know that the clay fraction decreases from 95% to 60% thus by a factor 1.58; assumed that this same factor applies to the Tournai clay - NaCl combination, the initial clay fraction of 81% will decrease to 51%, additionally the basal spacing of the 68% (10-14m) will decrease form 14 Å to 12 Å this will result in an EBS = 0.51*(0.16*10+0.07*12+0.68*12+0.09*14) = 6 Å,

LL=40% and φ'=30°. The salt increased the relative friction angle by 4°. Lab results were able to confirm this. The measured value was 31°.

Podzolinisation

Clays are often used as engineered barrier to contain hazardous waste because clays:
- are available in large quantities in low lying areas where the population density is highest and thus, the need for these industrial materials is largest
- are cheap
- have a low hydraulic conductivity
- can be easily handled and formed
- are quite stable because they are at the end of the weathering chain

A Tournai clay sample, consisting of a core of compacted natural clay, was permeated during months with a young landfill leachate. At the end, thin sections of this clay sample were examined. The analysis showed that the processes observed such as smectitisation and secondary chloritisation strongly resembled to the process of podzolisation observed in the field. This indicates that if the laboratory test is representative for the conditions present in the base of a landfill the clay used in the clay barrier will slowly transform into kaolinite.

What does this mean for the changes in terms of geotechnical properties?

In Fig. 6 the position of the three natural clays is shown as well as the position of a "pure" Kaolinite. The process of kaolinitisation will have the largest impact on the Tournai and Soignies clays. Kruibeke clay will not change that much. Although the process is beneficial for the Tournai clay in terms of gaining undrained shear strength and decreasing the compression index, the Soignies clay will be affected the other way round. The Tournai clay will show next to the gain in "strength" a decrease of the specific surface and cation exchange capacity. For the Soginies clay it will be the opposite.

This example shows once more the benefit of using the EBS concept to relate clay mineral knowledge to quantify changes of clay in terms of its engineering properties, this knowledge can be used to choose the right clay for the right task.

Conclusions

The behaviour of clayey soils is related to the microstructure and the clay mineralogy. This clay mineralogy changes if clays are used in divers engineering applications. In environmental engineering clays are frequently used as seal to contain hazardous waste. If clays are used as seal they will be exposed to e.g. brines and heat. The effect of this exposure was analysed on three natural soils with a complex mineralogy, representative of the common natural clay an engineer will work with in practise. The microstructure of clays can be studied in various ways but

with small modifications in sample preparation, the X ray diffraction technique is a very suitable method. A link between the result obtained by X ray diffraction analysis and geotechnical properties can be made using the equivalent basal spacing concept. The changes presented like exposure to heat and brines caused collapse of the interlayer space resulting in a quantifiable decreased in Atterberg limits and compressibility. It was shown that if the reaction of clay minerals when exposed to certain conditions is known from clay mineralogical literature, quantitative predictions of the changes in various geotechnical properties can be given. Finally it was shown that once the mineralogical alteration process during permeation of domestic landfill leachate through the clay barrier is recognised comparison to natural analogues can be made, and based on this knowledge suitable clay deposits can be chosen to limit the changes in geotechnical properties during the technical life of the clay seal.

Acknowledgements

References

Head K.H. (1992) Manual of soil laboratory testing. vol 1. Soil classification and compaction tests. Second edition. John Wiley & Sons.

Keijzer T.J.K. (2000) Chemical osmosis in natural clayey materials. Ph.D. thesis, Universiteit Utrecht.

Manwal (2001) Manuel relatif aux matières naturelles pour barrières argileuses ouvragées pour C.E.T. et réhabilitation de dépôtoirs en Région wallonne. Version 1. Marcoen JM, Tessier D, Thorez J, Monjoie A, Schroeder Ch. (eds). Ministère de la Région wallonne, Direction générale des Ressources naturelles et de l'Environnement Belgium.

Mitchel J.K. (1993) Fundamentals of Soil Behaviour. Second edition. John Wiley & Sons Inc.

Muir-Wood D. (1990) Soil behaviour and critical state soil mechanics. Cambridge university press.

Schmitz R.M. van Paassen L.A. (2003) The decay of the liquid limit of clays with increasing salt concentration. Ingeokring Newsletter. Dutch association of Engineering geology. 9: 10-14.

Schmitz R.M. Dosquet D. Illing P. Rodriguez C. Ourth A-S Verbrugge J-C. Hilligsman S. Schroeder C. Bolle A. Thorez, J. Charlier R. (2001) Clay – leachate interaction: a first insight. In: 6th KIWIR International Workshop on Key Issues in Waste Isolation Research. P. Delage (ed). Ecole Nationale des Ponts et Chaussèes, pp 245-269.

Schmitz R.M. Schroeder Ch. Charlier, R. (2002) A correlation between clay mineralogy and atterberg limits. In: Proceedings International Workshop of Young Doctors in Geomechanics. V. De Gennaro and P. Delage (eds). Ecole Nationale des Ponts et Chaussées, pp 27-30.

Terzaghi K., Peck R.B. (1967) Soil Mechanics in Engineering Practice. Second edition. John Wiley &Sons Inc.

Van Paassen L. (2002) The influence of pore fluid salinity on the consolidation behaviour and undrained shear strength development of clayey soils. Memoirs of the Centre of Engineering Geology in the Netherlands. TU-Delft. Vol: 216.

Wendehorst R. (1996) Bautechnische Zahlentafeln. 27. Auflage. Teubner, Stuttgart.

Wetzel A. (1990) Interrelationship between porosity and other geotechnical properties of slowly deposited, fine grained marine surface sediments. Marine Geology. 92: 105-113. Elsevier Amsterdam.

Suction induced by static compaction

Sara Tombolato, Alessandro Tarantino (✉), and Luigi Mongiovì

Dipartimento di Ingegneria Meccanica e Strutturale, Università degli Studi di Trento, via Mesiano 77, 38050 Trento, Italy
saratombolato@yahoo.it / tarantin@ing.unitn.it / mongiovi@ing.unitn.it

Abstract. The paper aims at investigating suction induced by static compaction in clay specimens. To this end, kaolin powders prepared at target water contents were statically compacted in a shearbox apparatus. Trento (TNT) high-suction tensiometers (0-1800 kPa) were installed through the loading pad to monitor suction changes during the loading-unloading paths. Specimens were compacted at water contents ranging from 0.22 to 0.30 and at vertical stresses of 300, 600, and 1200 kPa. This made it possible to explore a broad spectrum of compaction conditions. Experimental results are presented and discussed in the paper. The most striking aspect of the results is that suction of unloaded specimens increased as degree of saturation increased. This can be explained by the dependency of the main wetting curve upon void ratio.

Keywords: compacted soil, hydro-mechanical coupling, negative pore water pressure, suction.

Introduction

Compaction water content and compactive effort are known to have a significant influence on the subsequent mechanical and hydraulic behaviour of compacted fine-grained soils (Gens 1996). This influence of compaction procedure is frequently attributed to the different soil fabrics that are produced when the compaction procedure is varied. It is often implied that these changes in soil fabric produce entirely different soils, in the sense that different constitutive parameters will be required to model soil behaviour within the context of an elasto-plastic critical state framework. Recently, it has been emphasised that some effects can be simply modelled by taking into account the variation in the initial compaction-induced state (Sivakumar & Wheeler 2000; Wheeler & Sivakumar 2000; Barrera 2002). Different compaction water contents and compactive efforts produce different suction and stress histories and these could be sufficient to explain differences in the subsequent behaviour.

The information available about suction history is the suction measured on the sample at the end of the compaction process, after removing the sample from the compaction mould. However, the suction of the unloaded sample may not be representative of the entire suction history.

Suction changes occurring during the compaction process are generally unknown. The lack of this type of information was the main motivation for the experimental program described herein. There was indeed another motivation for investigating suction changes during compaction. When processing data on post-compaction suction measured on about 30 samples compacted at different water contents and compaction efforts, it appeared that suction increased as degree of saturation increased. This behaviour is surprising, as suction would be expected to decrease for increasing degree of saturation.

The paper presents an experimental programme aimed at investigating the changes in suction that occur during the compaction process. To this end, kaolin powders prepared at target water contents were statically compacted in a shearbox. Trento (TNT) high-suction tensiometers (Tarantino & Mongiovì 2002, 2003) were then installed in the loading pad to monitor suction changes during the loading-unloading paths. Specimens were compacted at water contents ranging from 0.22 to 0.30 and at vertical stresses of 300, 600, and 1200 kPa.

Previous investigation

An experimental programme on the hydro-mechanical behaviour of statically compacted Speswhite kaolin has been underway at the University of Trento. Within this experimental programme, samples were compacted at water contents ranging from 0.24 to 0.34 and vertical stresses of 300, 600, and 1200 kPa. After removal from the compaction mould, wet mass, dry mass, and total volume of the samples were measured. This made it possible to calculate water content, dry density, and degree of saturation after compaction. In addition, matric suction was measured using Trento tensiometers. The water retention curves of samples compacted at different vertical stresses are shown in Figure 1. The retention curves moves rightward as compaction vertical stress increases and, hence, void ratio decreases. This can be explained by the dependency of the retention curve on void ratio (Romero and Vaunat 2000, Gallipoli et al. 2003).

The *moisture-dry density* compaction curves for compaction vertical stresses of 300, 600, and 1200 kPa are shown in Figure 2, where contours of equal degree of saturation and of equal suction are also indicated. The optimum seems to be reached only by the curve corresponding to the compaction vertical stress of 1200 kPa, at a degree of saturation slightly greater than 0.9. The other two curves only develop on the 'dry' side of optimum. The contours of equal suction were obtained from a bi-linear interpolation of post-compaction suction data. Using bi-linear interpolation, data showed little variation. Nonetheless, contours of equal suction showed a clear trend. The most striking aspect of these data is that contours have a positive slope. This means that, if the soil is compacted at constant water content, suction increases as the degree of saturation increases. This result was unexpected, as contours of equal suction have been reported to have negative slope (Romero 1999, Barrera *et al*. 2000). To better understand the mechanisms of suction changes in compacted soils, an experimental program was carried out.
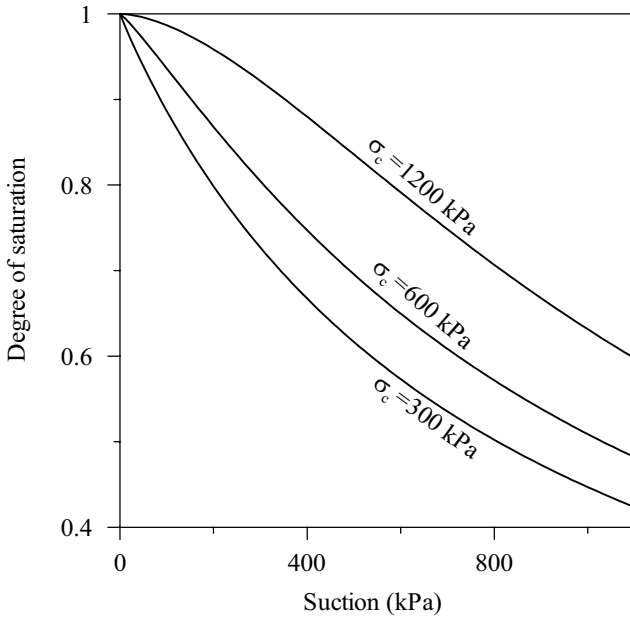
Fig. 1. Water retention curves of samples compacted at different vertical stress σ_c.
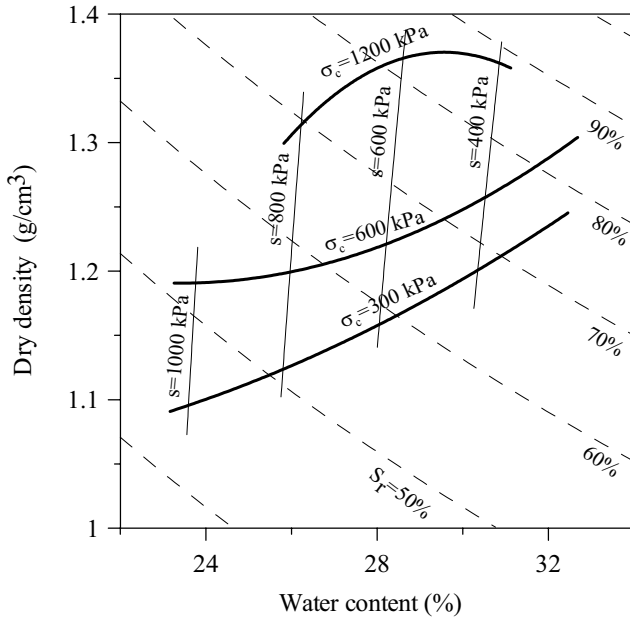
Fig. 2. Static compaction curves for Speswhite kaolin at different compaction vertical stress (thick lines), contours of equal degree of saturation (dashed lines) and contours

Material and specimen preparation

The soil used in this experimental programme is natural processed clay (Speswhite kaolin). Clay fraction (d<0.002 mm) is about 0.6, the remaining fraction being silt (0.002 mm<d<0.075 mm). Plastic and liquid limit are 0.32 and 0.54 respectively and the clay can be classified as non-active. The clay was supplied as dry powder in paper bags. The water content of the powder was that imposed by the average relative humidity in the laboratory. To prepare the moist powder, the soil was first laid in a large plastic container to obtain layers of about 5 mm height. The soil was sprayed with demineralised water and then thoroughly mixed. Lumps were then cut using a spatula sharp blade. The soil was finally sieved on a 1.18 mm sieve. The moist powder was placed in a plastic bag and stored in a high humidity room for at least one week to allow moisture equalisation.

Experimental equipment and procedure

The soil was compacted in the shearbox body shown in Figure 3. To prevent pore water losses due to evaporation, the shearbox was made airtight by sealing the gap between the two halves and the gap between the retaining plate and the lower half with silicone grease. The gap between the loading pad and the upper half was covered with a latex membrane smeared with slow setting silicone. This membrane was glued to the loading pad and clamped over the upper half. This simple anti-evaporation system proved effective in maintaining constant specimen suction during the test. Two tensiometers were installed in the loading pad and kept in place by a small cap (not shown in the figure), which was tightened to the loading pad by means of three screws. The annular gap between the tensiometer and the inner surface of the hole was sealed with an O-ring.
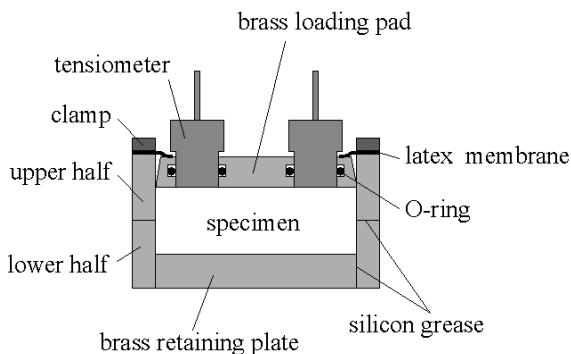
Fig. 3. Schematic layout of the monitored-suction shearbox.

Vertical displacements were measured with a potentiometer transducer having 10 mm stroke and measured accuracy of 0.003 mm (standard deviation). Vertical load was applied with a lever-arm loading system with 10:1 beam ratio.

The water content of the moist powder was first determined by taking a small amount of soil. The moist powder was poured into the shearbox body from a small height. The excess moist powder was levelled off and the loading pad was positioned on the top surface of the specimen. At this stage, dummy tensiometers were positioned in the loading pad. A vertical stress of 300 kPa was applied, thus producing a large vertical settlement. The latex membrane was clamped to the shear box upper half to ensure constant water content. Dummy tensiometers were removed and replaced with two tensiometers, after applying a paste to the tensiometer porous ceramic to make contact with the specimen. The tensiometer cap was then set in place and tightened to the loading pad. The procedure for suction measurement included pre-measurement and post-measurement checks of the porous ceramic saturation as described by Tarantino (2003).

The specimen was kept under constant vertical stress (300 kPa) for sufficient time to allow pore water pressure equalisation (about 1 day). Afterwards, the sample was unloaded and kept under quasi-zero vertical stress (5 kPa) for a period of time sufficient for pore water pressure equalisation. Two loading-unloading cycles were then applied, by increasing the vertical stress up to 600 kPa and 1200 kPa respectively.

Vertical settlements recorded during load increments were relatively large and often exceeded the travel of the vertical displacement transducer. As a result, it was not always possible to back calculate void ratio at the end of each load increment or decrement. To cope with this problem, the degree of saturation of the sample under quasi-zero vertical stress (5 kPa) was estimated using the retention curves plotted in Figure 1. The degree of saturation under loading was then calculated from the vertical swelling measured upon the subsequent unloading. At the end of the test, the shearbox was dismantled and the water content of the specimen was measured.

Results

Three tests were carried out on specimens having water content of 0.22, 0.26, and 0.30. The results from the test on the sample having water content of 0.26 are shown in Figure 4, where vertical stress, vertical displacement, and suction are plotted versus time.

The values of suction recorded by the two tensiometers are in agreement (differences are less than 10 kPa), except for the values recorded under 1200 kPa vertical stress. This discrepancy was also observed in the test on sample with 0.30 water content. The reason for this difference is not clear and it is perhaps associated with the large sudden increment applied to the sample (from 0 to 1200 kPa). It is worth noting that suction recorded after unloading from 1200 kPa is greater than suction recorded after unloading from 600 kPa, which is in turn greater than

suction recorded after unloading from 300 kPa. This result confirms the trend shown in Figure 2. The results from the three compaction tests are shown in Figure 5, where the paths followed during the compaction process are plotted in terms of suction and degree of saturation. For the test at water content of 0.22, suction measured at quasi-zero vertical stress decreased as the degree of saturation increased, in contrast to the other two tests.
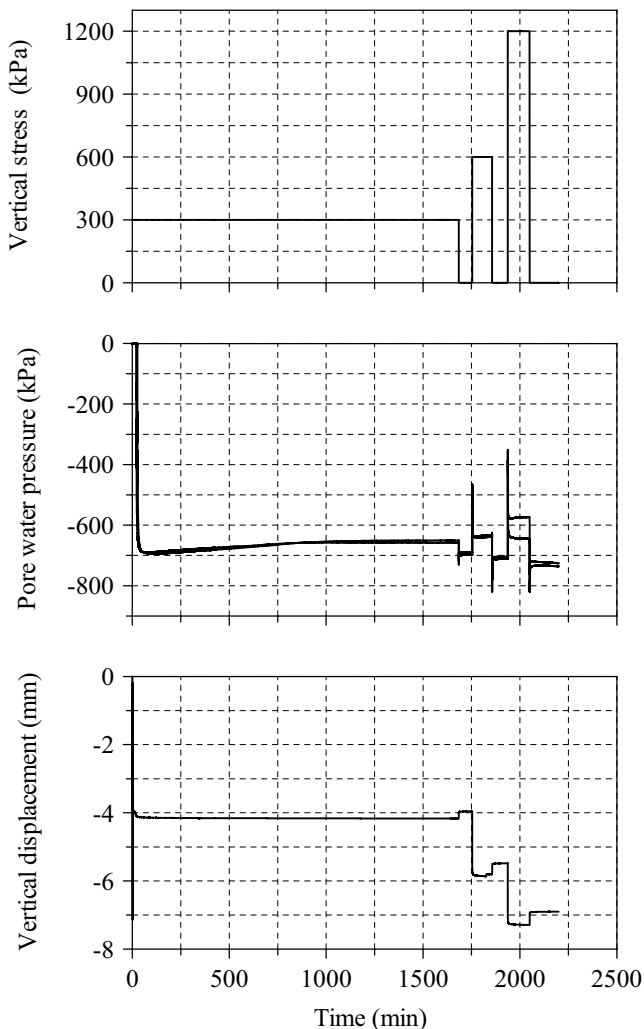
Fig. 4. Compaction test on sample having water content of 0.26.
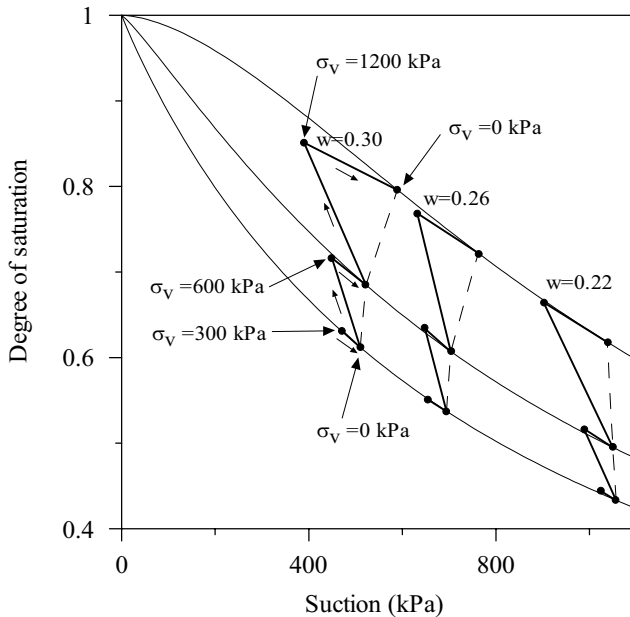
Fig. 5. Results of compaction tests in terms of degree of saturation versus suction.

Discussion

The loading stages are associated with an increase in degree of saturation (water content is constant and void ratio decreases). The resulting hydraulic path is therefore a wetting path. Since the sample is experiencing the highest degrees of saturation ever, the sample moves along a 'main' wetting path. In contrast, the unloading stages are associated with a decrease in degree of saturation and the resulting path is therefore a 'scanning' drying path.

In all the tests, specimens were subject to 'virgin' compression, in the sense that they were experiencing the highest vertical stress ever. Compression was therefore very large and the degree of saturation increased significantly. On the other side, the unloading process produced small ('elastic') swelling and the degree of saturation slightly decreased.

A qualitative representation of the path followed during the loading-unloading process is shown in Figure 6 (plane *suction – degree of saturation*). When first loading at 300 kPa, the soil moved on the main wetting curve (point A in Figure 6a). The subsequent unloading moved the soil to B, along the scanning curve. If the water retention curve was independent of void ratio, suction would be expected to decrease significantly during loading at 600 kPa (B-C-D) and slightly increase upon the subsequent unloading (path D-E). As a result, the loading-unloading process would have the overall effect of decreasing suction. If so, the

contours of equal suction in the plane water content-dry density would have a negative slope.

(a)

(b)
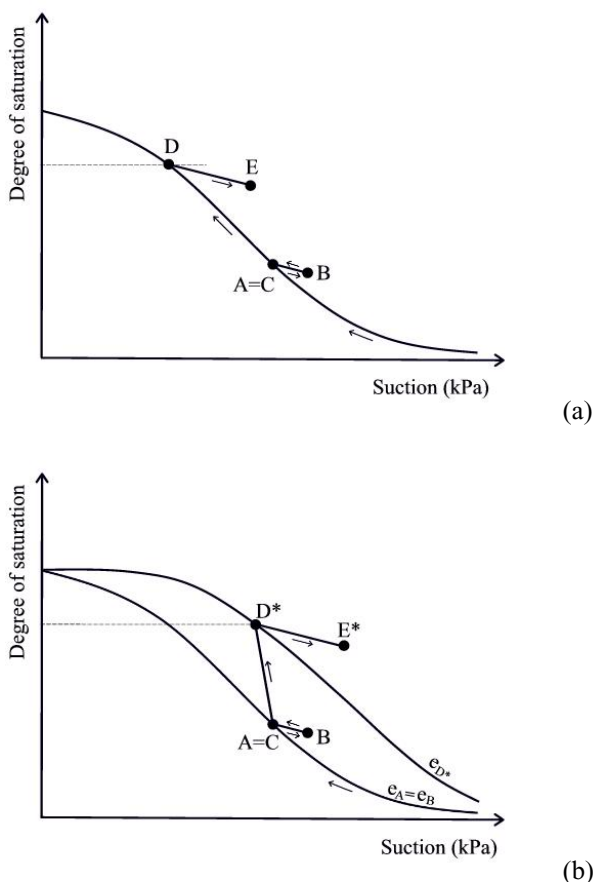
Fig. 6. Interpretation of compaction tests: a) water retention curve independent of void ratio; b) water retention curve dependent of void ratio.

However, the experimental results on specimens having water contents of 0.26 and 0.30 have shown that suction slightly increased after the subsequent unloading. This suggests that the main wetting curve moves as void ratio changes. In particular, the curve moved rightward for decreasing void ratio

The path followed during compression is qualitatively represented in Figure 6b. The first compression at the vertical stress of 300 kPa moved the soil to point A, which laid on the main wetting curve associated with the void ratio e_A. Upon the subsequent unloading, the void ratio increased slightly, the degree of saturation slightly decreased and the soil moved along the scanning curve to point B. For

sake of simplicity, let us assume that $e_B \cong e_A$ so that the unloading stage did not produce any leftward movement of the main wetting curve.

The loading at the vertical stress of 600 kPa then produced a decrease in void ratio and an increase in degree of saturation. At the same time, the main wetting curve moved rightward. The main wetting curve is the lower bound of the hysteresis domain, which delimits all possible attainable states. As a result, the main wetting curve dragged the soil to point D★. Since the soil was forced to remain on the main wetting curve, the change in suction was less than that occurring for the case of incompressible soil (rigid main wetting curve). Upon unloading, the soil moved along a scanning drying curve to point D*. For tests at water content of 0.26 and 0.30, Point D* was positioned on the left side of point A. This could explain the positive slope of the contours of equal suction observed in the specimens at water content of 0.26 and 0.30. In contrast, the specimen at water content of 0.22 showed indeed a negative slope. Because of the greater stiffness (suction is higher), the main wetting curve moved less in this latter case.

Conclusions

The experimental program described in the paper has been underway to gain better insight into an apparent anomalous behaviour regarding observed cases where increasing suctions were noted at increasing degrees of saturation for compacted specimens. Samples compacted at high vertical stress were found to have higher post-compaction suction than those compacted at lower vertical stress (at the same water content).

Three compaction tests have been carried out in a shearbox, with the facility to monitor suction during the loading-unloading cycles. Tests results have emphasised that suction changes occurring during the loading-unloading process (at constant water content) are associated with two main mechanisms: 1) the variation of the degree of saturation; 2) the movement of the main wetting curve. When the first mechanism predominates, contours of equal post-compaction suction have negative slope in the plane *water content – dry density*, as commonly reported in the literature. However, when the soil is highly compressible, it is the movement of the main wetting curve that controls suction, which increases even though the degree of saturation increases.

References

Barrera, M. (2002). *Estudio experimental del comportamiento hidro-mecánico de suelos colapsables*. PhD Thesis, Universitat Politècnica de Catalunya, Barcelona, Spain.

Barrera, M., Romero, E., Lloret, A. and Gens, A. (2000). Collapse tests on isotropic and anisotropic compacted soils. *Experimental Evidence and Theoretical Approaches in Unsaturated Soils, Proceedings of an International Workshop*, A. Tarantino and C. Mancuso (eds), Trento, 33–45. Balkema: Rotterdam

Gallipoli, D., Wheeler, S.J. & Karstunen, M. (2003). Modelling the variation of degree of saturation in a deformable unsaturated soil. *Géotechnique*, 53(1):105-112.

Gens, A. (1996). Constitutive modelling: application to compacted soils. *Proc. 1ˢᵗ Int.Conf. Unsaturated Soils*, *E.E. Alonso & P. Delage (eds.), Paris*, 3: 1179-1200. Balkema: Rotterdam

Romero, E. (1999). *Characterisation and thermo-hydro mechanical behvaoiur of unsaturated Boom clay: an experimental study*. Phd Thesis, Universitat Politècnica de Catalunya, Barcelona, Spain.

Romero, E. & J. Vaunat. Retention curves of deformable clays (2000). *Experimental Evidence and Theoretical Approaches in Unsaturated Soils, Proceedings of an International Workshop*, A. Tarantino and C. Mancuso (eds), Trento, 91-106. Balkema: Rotterdam

Sivakumar, V. & Wheeler, S.J. (2000). Influence of compaction procedure on the mechanical behaviour of an unsaturated compacted clay. Part 1: Wetting and isotropic compression. *Géotechnique*, 50(4):359-368.

Tarantino A. & Mongiovì L. (2002). Design and construction of a tensiometer for direct measurement of matric suction. *Proceedings 3ʳᵈ International Conference on Unsaturated Soils*, Recife, Brasil, 1: 319-324.

Tarantino, A. & Mongiovì, L. (2003). Calibration of tensiometer for direct measurement of matric suction. *Géotechnique*, **53(**1): 137-141.

Tarantino, A. (2003). Panel report: Direct measurement of soil water tension. Proc. 3nd Int. Conf. on Unsaturated Soils, Recife, Brasil, in press.

Wheeler, S.J. & Sivakumar, V.(2000). Influence of compaction procedure on the mechanical behaviour of an unsaturated compacted clay. Part 2: Shearing and constitutive modelling. *Géotechnique*, 50(4): 369-376.

Suction of compacted residual soils

S. Tripathy [1], E.C. Leong [2], and H. Rahardjo [3]

[1]Post doctoral Fellow, Laboratory of Soil Mechanics
Bauhaus University Weimar, Germany
[2] and [3] Associate Professors, Nanyang Technological University, Singapore
(E-mail: snehasis.tripathy@bauing.uni-weimar.de)

SYNOPSIS - Compacted soils are used in many civil engineering works such as pavement, backfills and soil covers. Though it is understood that compacted soils have degrees of saturation less than 100%, the unsaturated soil properties of compacted soils are seldom determined. Matric suction, the difference between pore-air and pore-water pressures, is an important stress-state variable of unsaturated soil and is a function of soil structure and soil moisture content. In this paper, the matric suctions of two residual soils (mudstone and sandstone) from Singapore, compacted at three compaction efforts and at various placement conditions (viz. dry density and water content), are presented. Matric suctions of the soil specimens were determined using two methods: (a) null-type axis translation technique and (b) high suction probe. The soil-water characteristic curves of the compacted soils were also established from compacted soil specimens via pressure plate tests and salt solution tests. In the determination of the soil-water characteristic curves, the compacted soil specimens were saturated prior to the pressure plate tests. The matric suctions of the soils at the as-compacted condition can also be obtained from the soil-water characteristic curve. The matric suctions of the compacted soils from the null-type axis translation technique, high suction probe and soil-water characteristic curve are compared and discussed with respect to the dry density, degree of saturation and compaction effort.

INTRODUCTION

Residual soils are formed in place by the weathering of the parent rocks in response to climate, topography, and drainage conditions. About two thirds of the land area of Singapore comprises of residual soils occupying the central and western part of Singapore. Owing to the extensive areas covered by the residual soils, these soils are commonly used in many civil engineering works. Normally, the soils are placed and compacted when used as pavement material or backfill material.

The structure and fabric in compacted soils depend upon the compaction conditions (viz., compaction effort, water content and dry density). As in the case of all compacted soils, the soils are unsaturated immediately after compaction. The po-

tential of these soils to absorb and retain water depends primarily on the initial matric suction. Matric suction is the negative pore-water pressure in the soil when referenced to pore-air pressure and is defined as the difference between pore-air and pore-water pressures. Matric suction is an important stress-state variable of unsaturated soil and is a function of soil type, soil structure and soil moisture content.

The wetting of the compacted residual soils and the subsequent drying due to evaporation and evapo-transpiration may influence the shear strength and the hydraulic behaviour. The shear strength and unsaturated hydraulic conductivity are commonly determined from the soil-water characteristic curve. The relationship between soil water content and matric suction is known as the soil-water characteristic curve (SWCC).

In this paper, the matric suctions of two compacted residual soils from Singapore were measured by a null-type axis translation apparatus and a high suction probe. Compacted soil samples were prepared at several dry densities and water contents. The matric suctions of the compacted soils were obtained from null-type axis translation tests and high suction probe tests. Drying or desorption SWCCs were also obtained by saturating the compacted soil specimens before commencement of the SWCC tests using pressure plate and salt solution tests. Matric suctions of the compacted soils measured by the null-type axis translation apparatus, high suction probe and estimated from the SWCC were compared and discussed with respect to the dry density, degree of saturation and compaction effort.

Properties of soils

Two residual soils namely, mudstone and sandstone residual soils from the Jurong sedimentary formation in the western part of Singapore were used in this study. Soils were collected from two different locations. The soils were air-dried and coarse fragments were removed by sieving the pulverized soils through 425 μm sieve. The soils were then mixed with predetermined quantities of distilled water and stored in closed polythene bags for two weeks for the moisture equilibration. The compaction characteristics of the soils were determined utilizing three different compaction efforts. The compaction efforts used were, standard Proctor (ASTM 1998a), enhanced Proctor and modified Proctor (ASTM 1998b). For the enhanced Proctor compaction effort, the weight of the ram, the height of drop of the ram and the number of blows applied per each soil layer were identical with that of the modified Proctor compaction test. However, the number of compaction layers was only three instead of five layers. The compaction curves together with the compaction conditions of the soils used in the tests are shown in Fig. 1. In Fig. 1, MS indicates mudstone and SS indicates sandstone.
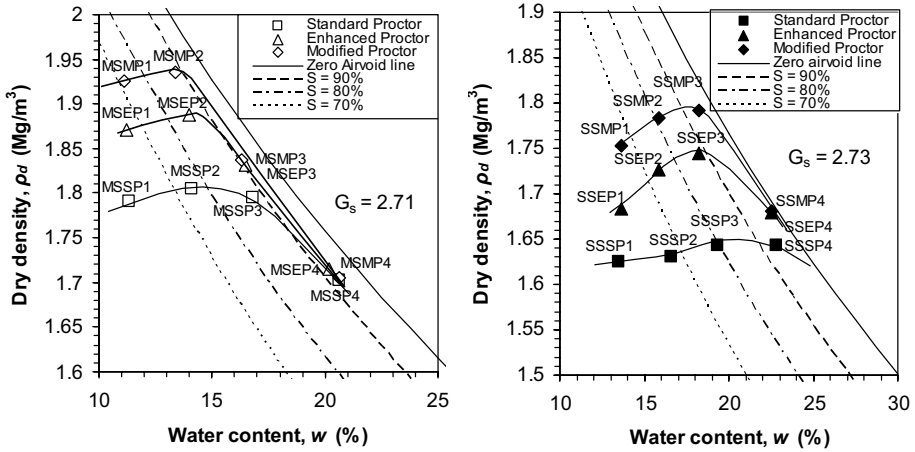
Fig.1. Compaction curves of the mudstone and sandstone residual soils.

Table 1. Properties of the soils used

Properties	Mudstone	Sandstone
Liquid limit (%)	42	53
Plastic limit (%)	28	36
Plasticity index (%)	14	17
Specific gravity	2.71	2.73
Gravel (%)	7	9
Sand (%)	40	23
Silt (%)	42	46
Clay (%)	11	22
USCS	CL	MH

The properties of the soils are shown in Table 1. The compaction conditions of the soils were chosen such that they were of the same water content but at different dry densities and also such that they were of the same dry density but at different water contents. The compacted soil samples had water contents on the dry side of optimum, near the optimum and also on the wet side of optimum water content of the compaction curves. In Fig. 1, the compacted samples were numbered from 1 to 4 on each compaction curve starting from the driest sample. The term SP, EP and MP indicate the standard Proctor, enhanced Proctor and modified Proctor, respectively. From each of the compacted soil sample, three soil specimens were prepared for the tests. One was used for null-type axis translation test, one for the high suction probe test and one for the SWCC test. Each soil specimen was 50 mm in diameter and 30 mm high. A total of 24 specimens were tested in the null-type axis translation apparatus, 16 specimens were tested using the high suction probe. The SWCCs' of 22 specimens were determined using the pressure plate apparatus and salt solution tests.

Apparatus used and Test procedure

The apparatus used for the determination of the matric suctions of the soil samples were a null-type axis translation apparatus and a high suction probe. The null-type axis translation apparatus is described in Fredlund and Rahardjo (1993) with a 15-bar ceramic disk. The high suction probe used was similar to the devices proposed by Ridley and Burland (1993) and Guan and Fredlund (1997). The high suction probe was fabricated at the Nanyang Technological University, Singapore (He 1999). The features of the high suction probe are a 5 bar ceramic disk, a very small water reservoir below the ceramic disk, a pore-water pressure transducer (Entran EXP-101W-250A) and a data acquisition system. The pore-water pressure transducer has a working pressure range of about 3500 kPa. The ceramic disks in both the devices were saturated prior to all the tests. In the case of null-type axis translation tests, the water reservoir below the ceramic disc was flushed before the saturation process and also prior to testing a soil specimen. Distilled and de-aired water was used for preparing the soil samples, to saturate the ceramic disks and also in the water reservoirs below the ceramic disks. The soil specimens tested were weighed before and after the tests. No significant change in weight of the specimens were found in either tests with all the soil specimens tested indicating that the specimens were tested at constant water content. To ensure good contact between ceramic disk and the soil specimen in both the null-type axis translation apparatus and the high suction probe, a mass of 1 kg was placed on top of the soil specimen. The soils tested do not have a significant salt content as the soil samples were prepared with distilled water. Leong *et al.* (2003) reported that these two soils have an osmotic suction of about 10 kPa. Therefore, it is reasonable to assume that only matric suction was measured utilizing the two devices. All the tests were conducted in a near constant temperature environment of 25 ± 3^0C.

The soil water characteristic curves of the saturated soil specimens were established using a volumetric pressure plate, a 5 bar pressure plate, a 15 bar pressure plate and also by salt solution tests. The salt solution tests were used for inducing higher range of suction in the soil specimens (i.e., above 1500 kPa). The volumetric pressure plate with hysteresis attachment was used to saturate the compacted soil specimens. The soil specimens were weighed periodically to check the change in weight. Once the saturation process was over indicated by a near constant weight of the soil specimens, matric suction was applied to the soil specimens in the volumetric pressure plate up to a matric suction of 200 kPa. The specimens were then transferred to a 5 bar pressure plate and then to 15 bar pressure plate and finally, to the desiccators with salt solutions for the salt solution tests. Several sodium chloride (NaCl) solutions of different salt concentration were used to induce different relative humidity in the desiccators. The relative humidity is related to total suction via the thermodynamic relationship. The suction achieved from a salt solution is given in ASTM (1998c). For each matric suction applied during the desorption process, the weight of the soil specimens were monitored till there was negligible change. The typical equilibrium time of the soil specimens in the pressure plate tests was about 3 to 4 days at each matric suction value. The typical

equilibrium time of the soil specimens in the salt solution tests was more than 2 months. No significant change in volume was noted during saturation of the soil specimens and also during the SWCC tests.

Results and discussion

Matric suction

Figure 2 shows the matric suction versus elapsed time plots for the null-type axis translation tests. As can be seen from the figures, the equilibrium condition was attained in about 60 to 300 minutes for all the soil specimens tested.

Fig. 3 shows the pore-water pressure measurements of the soil specimens using the high suction probe. As can be seen in Fig. 3, the time required for equilibrium was less than 15 minutes. There was also a tendency for some soil specimens (e.g., MSSP2, MSEP1) to show an increase in pore-water pressure (i.e., less negative) after the equilibrium condition was reached. This was attributed to presence of minute air bubbles forming in the water reservoir of the high suction probe. The matric suctions of the soil specimens from the high suction probe tests and the null-type axis translation tests are compared in Table 2. The matric suctions measured by both the null-type axis translation apparatus and high suction probe were comparable. However, the high suction probe was able to measure the matric suction of the soil specimens in a relatively shorter time.

Fig. 4 shows the as-compacted water content, degree of saturation and void ratio versus the matric suctions of the soil specimens of both the mudstone and sandstone soils for the three compaction efforts. The matric suction values in Fig. 4 are from the null-type axis translation tests. In Fig. 4, the horizontal lines show the respective water content, degree of saturation and void ratio corresponding to the optimum compaction condition for each compaction effort. The vertical lines indicate the corresponding matric suction values for the optimum compaction condition for each compaction effort. Fig. 4 shows that the matric suction decreased with an increase in the compaction water content for all the compaction efforts studied. In general matric suction decreased with an increase in compaction effort (Fig. 4a & 4d). For any given degree of saturation, some variation in the matric suction was observed (Fig. 4b & 4e). Matric suction was found to increase with an increase in compaction effort for the soil specimens with water content less than the optimum water content (i.e., degree of saturation
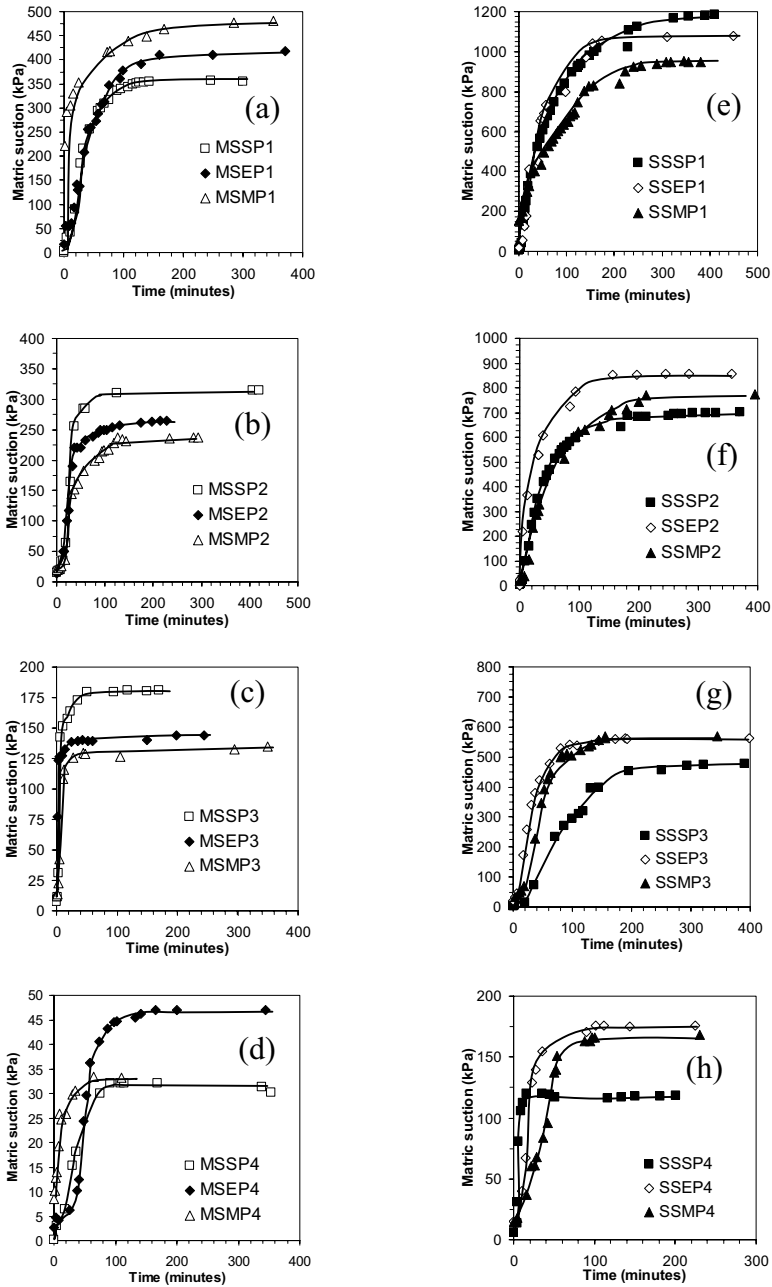
Fig. 2. Time versus matric suction of soil specimens from null-type axis transla-tion tests, (a), (b), (c), and (d) for mudstone soil, (e), (f), (g), and (h) for sandstone soil.

of about less than 90%). The effect of compaction effort seems to be secondary when the soil was compacted at optimum compaction conditions and above. The effect of structure and fabric changes on the matric suction was distinct for all the compaction efforts studied, the notable boundary being the optimum water content and maximum dry density of the soils. Similar observation has also been made by Leong and Rahardjo (2002) for compacted residual soils.
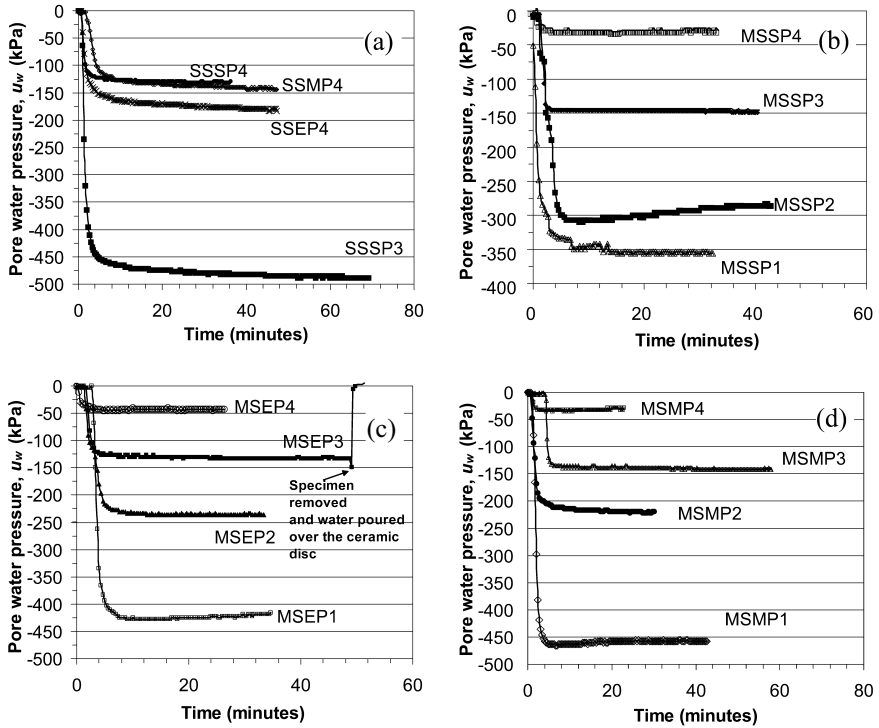
Fig. 3. High suction probe test results, (a) for sand stone soil, (b), (c), and (d) for mudstone soil.

For a given compaction effort at any void ratio, there can be two matric suction values, one being on the dry side of optimum and the other on the wet of optimum condition (Fig. 4c & 4f). This is attributed to the saturation levels the compacted soils achieved with increasing water content. Also, the soil structures of the specimen on the dry side of optimum and on the wet side of optimum are different.

Soil-water characteristic curves

The soil-water characteristic curves of the soil specimens at different compaction conditions and compaction efforts are shown in Fig. 5. Although the suction

induced in the soil specimens by the pressure plate test is matric suction and by the salt solution tests is total suction, it is believed that at higher suctions total and matric suctions are equivalent (Fredlund and Xing 1994). In general, the sandstone residual soil specimens absorbed more water after saturation than the mudstone residual soil specimens. This is expected, since the liquid limit and clay content in sandstone residual soil was higher. Differences in the air-entry values of the soil specimens can be observed. However, for both residual soils, the air-entry values lie in the range of 20 – 40 kPa. No significant difference was observed in the SWCC band for both the soils within the range of matric suction studied. The matric suction corresponding to the initial compaction water contents of the soil specimens were determined from the SWCCs' (Fig. 5) and are also shown in Table 2.

Table 2. Matric suction of the soil specimens from different tests

Soil specimens	Initial water content, w (%)	Initial degree of saturation, S_r (%)	Initial void ratio, e_0	Matric suction (kPa)		
				From Null-type axis translation test	From high suction probe test	From SWCC* test
Mudstone						
MSSP1	11.4	59.90	0.514	355	352	700
MSSP2	14.1	76.20	0.501	310	300	400
MSSP3	16.8	89.30	0.510	175	143	200
MSSP4	20.6	94.30	0.592	30	28	35
MSEP1	11.2	67.70	0.448	420	425	1000
MSEP2	14.0	87.10	0.436	260	236	550
MSEP3	16.5	93.22	0.480	140	132	200
MSEP4	20.2	94.35	0.580	45	43	80
MSMP1	11.1	73.94	0.407	475	460	1050
MSMP2	13.4	90.67	0.401	240	219	320
MSMP3	16.3	92.87	0.476	130	136	120
MSMP4	20.2	94.87	0.589	30	32	75
Sandstone						
SSSP1	13.5	55.20	0.668	1200	…	>10,000
SSSP2	16.6	68.40	0.663	690	…	>10,000
SSSP3	19.3	81.13	0.649	475	486	1000
SSSP4	22.8	95.84	0.649	120	132	22
SSEP1	13.2	59.05	0.610	1050	…	…
SSEP2	15.7	75.18	0.570	855	…	3000
SSEP3	18.3	90.20	0.554	560	…	1000
SSEP4	22.5	99.80	0.614	175	180	220
SSMP1	13.7	68.50	0.546	950	…	…
SSMP2	15.5	81.39	0.520	775	…	>9000
SSMP3	18.1	96.30	0.513	550	…	900
SSMP4	22.2	99.00	0.612	165	143	150

* From the first drying cycle after wetting from as-compacted condition
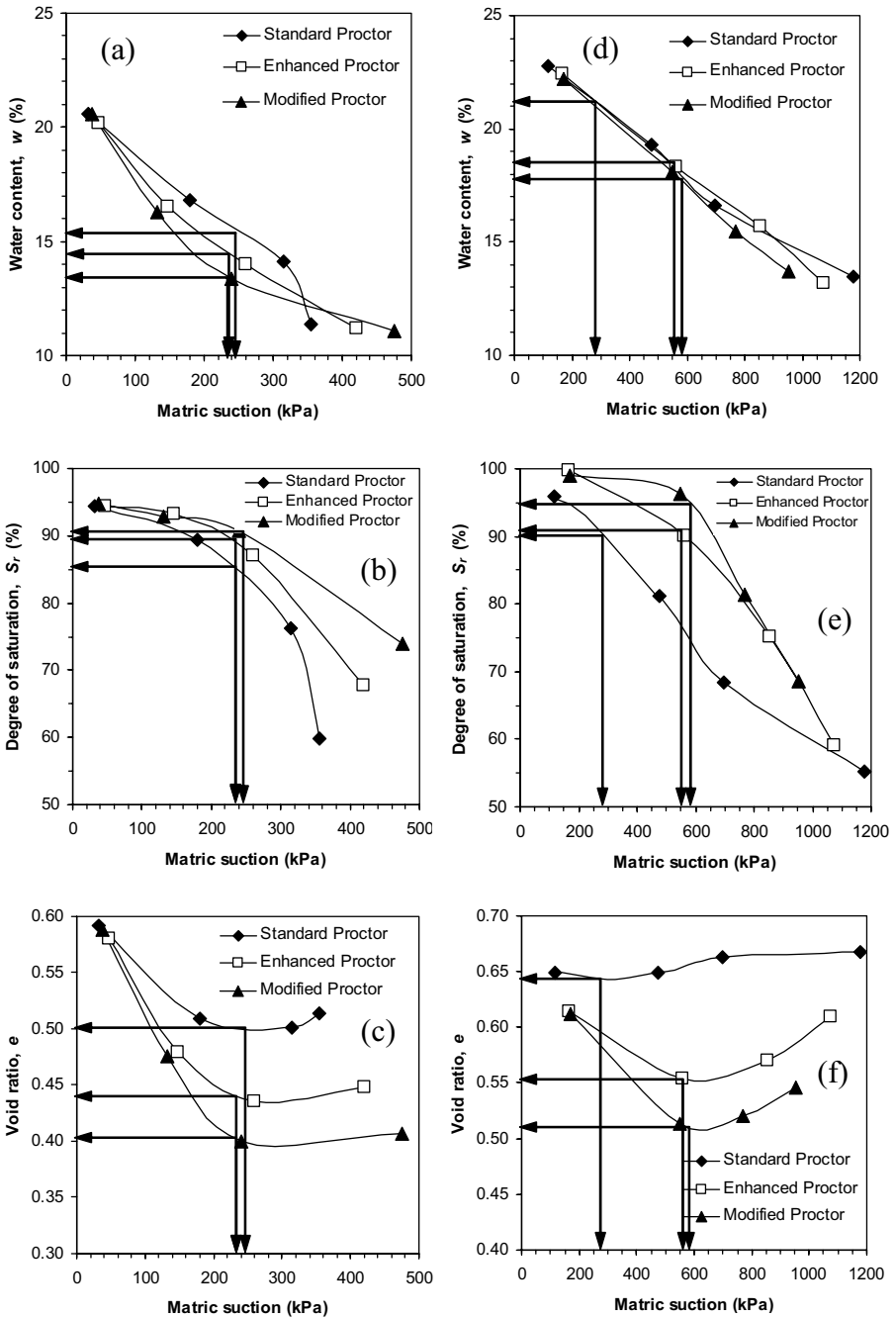
Fig. 4. As-compacted water content, degree of saturation and void ratio versus matric suction, for mudstone residual soil (a, b, c) and sandstone residual soil (d, e, f).
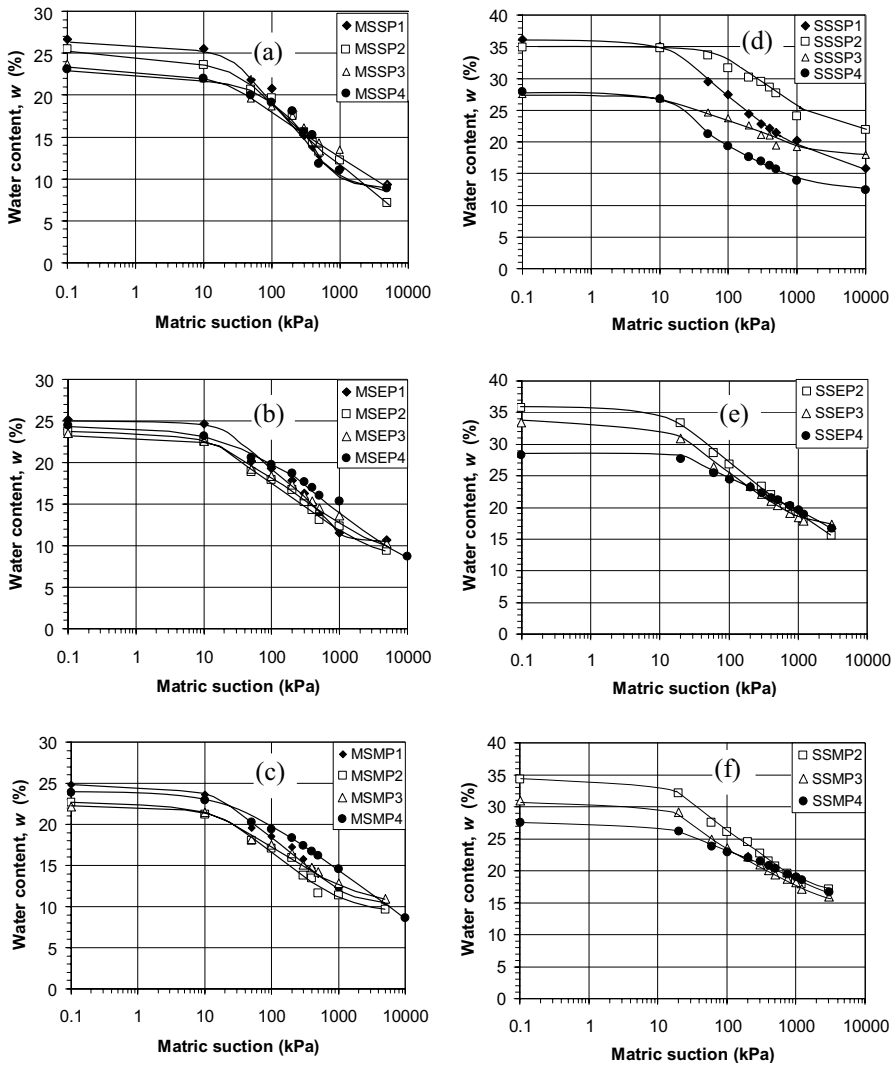
Fig. 5. Soil-water characteristic curves for mudstone residual soil samples (a, b, c), and for sandstone soil samples (d, e, f).

Comparing the matric suctions determined from the null-type axis translation apparatus and high suction probe with those obtained from SWCCs in Table 2, it can be noted that above 90% degree of saturation, matric suction remained almost unaffected due to wetting and subsequent drying cycle. The compaction effort and wetting-drying have a significant influence on the matric suction of the specimens, particularly for samples prepared on the dry side of optimum conditions and those with degrees of saturation less than about 80%. Very high suctions were found for

the sandstone residual soil specimens. This is attributed to the higher clay content of the sandstone residual soil.

Conclusions

The matric suction of several compacted soil specimens of two residual soils were measured by a null-type axis translation apparatus and a high suction probe. The matric suction obtained using these two devices were compared with the matric suctions obtained from desorption SWCCs of the compacted soil specimens. The SWCCs were determined after saturating the soil specimens. The following conclusions were drawn from the investigation:

(1)   The matric suction of compacted soil specimens determined using the null-type axis translation apparatus and the suction probe were comparable. The variation in measurements of matric suctions was within about ±15 kPa. However, the equilibrium time required in the high suction probe was only about 15 minutes compared with the equilibrium time in the null-type axis translation apparatus of 60 to 300 minutes.

(2)   Matric suction decreased with an increase in compaction effort. The effect of structure and fabric changes on the matric suction was distinct at the optimum condition of the soils for all the compaction efforts studied. Above 90% degree of saturation, the matric suction of the soil specimens did not show great variations.

(3)   Compaction effort has a significant influence on the matric suction of the specimens that were first wetted and then dried, particularly for samples prepared on the dry side of optimum and with a degree of saturation of less than 80%. The matric suction remained unaffected by the wetting-drying cycle for soil specimens that had an initial degree of saturation of more than about 90%.

Acknowledgement

References

ASTM (1998a). Test method for laboratory compaction characteristics of soil using standard effort (12400 ft-lbf/ft3 (600 kN-m/m3)), ASTM D698. 1998 Annual Book of ASTM Standards, 04.08, Soil and Rock (II), pp. 77-84. West Conshohocken, PA: American Society of Testing materials.

ASTM (1998b). Test method for laboratory compaction characteristics of soil using modi-fied effort (56000 ft-lbf/ft3 (600 kN-m/m3)), ASTM D1557. 1998 Annual Book of ASTM Standards, 04.08, Soil and Rock (II), pp. 126-133. West Conshohocken, PA: American Society of Testing materials.

ASTM (1998c). Standard test method for measurement of soil potential (suction) using fil-ter paper, ASTM D5298-94. 1998 Annual Book of ASTM Standards, 04.08, Soil and Rock (II), pp. 157-162. West Conshohocken, PA: American Society of Testing materi-als.

Fredlund, D.G. & Rahardjo, H. (1993). Soil Mechanics for Unsaturated Soils. John Wiley & Sons, Inc., New York.

Fredlund, D.G. and Xing, A. (1994). Equations for soil-water characteristic curve, Cana-dian Geotechnical Journal: 37, 521-532.

Guan, Y. & Fredlund, D.G. (1997). Use of the tensile strength of water for the direct meas-urement of high soil suction. Canadian Geotechnical Journal, 34, 604-614.

He, L.C. (1999). Evaluation of instrument for measurement of suction in unsaturated soil. MEng thesis, Nanyang Technological University, Singapore.

Leong, E.C. and Rahardjo, H. (2002). Soil-water characteristic curves of compacted soils. Proc. Intl. Conf. of Unsaturated soils, Brazil, Juca, de Campos and Marinho (eds), 271-276.

Leong, E.C., Tripathy, S., and Rahardjo, H. (2003). Total suction measurement of unsatu-rated soils with a device using the chilled-mirror dewpoint technique. Geotechnique: 53 (2), 173-182 .

Ridley, A.M. & Burland, J.B. (1993). A new instrument for the measurement of soil mois-ture suction, Geotechnique: 43 (2), 321-324.

Creation of artificial loess soils

A. Zourmpakis, D.I. Boardman, and C.D.F. Rogers

Department of Civil Engineering - the University of Birmingham – United Kingdom

Abstract. Loess is a loose, open-structured metastable soil of aeolian origin, predominantly composed of 20-60 µm quartz particles bonded together by clay particles and, in some cases, carbonate compounds. When dry it can withstand high overburden stresses, whilst upon saturation it collapses creating potentially enormous engineering problems. The mechanisms controlling this metastable behaviour involve the disintegration of inter-particle clay and chemical bonding and variations in the pore water pressures (i.e. suctions) during saturation.

The paper describes methods of creation of artificial loess samples using an airfall approach to allow the variation of bonding constituents, arrangements and formation processes. The amount of powdered clay added to primary quartz particles (ground silica) was varied and three methods for activation of clay bonding were employed, i.e. water spray, capillary wetting and steaming. The reproducibility of the synthetic loess created was determined through oedometer testing of the resulting samples, the results of which are reported together with those for undisturbed samples of mid-European loess. Similarities and differences are discussed in the context of the likely bonding mechanisms. It is concluded that creation of reproducible synthetic loess samples, while controlling its constituents, makes possible the individual examination of the different parameters that control bonding in loess.

Introduction

Loess is a widespread aeolian deposit that can be found in abundance in North and South America, Europe, western Russia, central Asia and China. It essentially consists of irregularly shaped silt-sized (20-60 µm) primary quartz particles (Rogers and Smalley, 1993). This silt was produced by high energy earth-surface processes, such as cold weathering and glacial grinding (i.e. abrasion resulting from movements of continental glaciers). With the retreat of the continental glaciers and/or due to fluvial transportation, the silt was deposited along the flood plains of rivers where it was then transported, sorted, and redeposited by wind action. Although principally consisting of quartz particles, loess deposits also contain feldspars, micas, carbonates and clay minerals.

As a result of their genesis and constitution, loess deposits form remarkably open structures with the interstitial clay sized particles congregating at the quartz particle contacts. This open structure is maintained by a process of bonding, the strength of which increases with time. The open structure is metastable and, while the bonding mechanisms can hold it together under considerable thickness of overburden, under conditions of additional loading and/or wetting it will collapse (Derbyshire *et al.* 1995). This metastability results in the costly and potentially dangerous problems of hydroconsolidation and subsidence, the effects of which (especially in China and Eastern Europe) are enormous for infrastructure, urban and rural developments. For example, in a small settlement in the Chinese district of Lanzhou, 101 out of 168 buildings were damaged or destroyed during a 10 year period as a result of loess hydroconsolidation.

The purpose of the work reported herein was to examine the feasibility of creating synthetic loess and thereby gain a better insight into the constituents and processes that create bonds in loess, and the factors affecting them. One particularly important aspect was the use of different methods of clay bond activation for comparison; to achieve reproducibility and to simulate the behaviour of natural loess. This was achieved by oedometer testing of the resulting samples to evaluate their collapse characteristics. Care was taken to mimic the aeolian origin as well as the arid environment that most loess deposits were created in.

Bonding mechanisms and interstitial clay

In general the bonding mechanisms that can be identified in loessial soils are Van der Waals bonding between the quartz particles making up the fabric structure; clay chemical bonding where the ionic variability on the surface of the quartz particles facilitates attraction by charged interstitial clay particles, with subsequent wetting causing clay bridges to be formed; suctions, or negative pore water pressure, due to limited amounts of interstitial water contained within the loess structure, an effect that has been shown to be greater than predicted according to traditional soil mechanics (Hornbaker *et al.* 1997); carbonate bonding between quartz

particles; and other salt bonding such as gypsum ($CaSO_4$) and hydrous iron oxide (FeO.OH).

Among these identified bonding mechanisms, clay bonding is of major importance. The amount of clay in loess soils varies between deposits. In clay rich deposits "clay shirts" cover most of the disintegrated grains (Figure 1) while in loess containing less clay, the dry clay powder will naturally be drawn to the points of contact between the silt particles where the forces will be necessarily much greater, prior to the formation of stronger bonds once the clay is wetted. This will occur in more humid, perhaps seasonal, conditions and/or when very small amounts of rain wet the soil surface progressively during the extended depositional progress. The authors suggest that the clay also settles by aeolian distribution, though with much lower velocity winds than are needed for the transportation of the silt particles. It is possible also that clay particles could be attached to silt particles following drying in flood plains and would then be transported with the silt. However the consistent distribution of the clay particles found in many types of loess is hard to explain in this case since only very small amounts of water in the otherwise arid environment appear to be involved in the clay bond activation process (i.e. it is considered to be in insufficient quantities to cause redistribution of the clay particles). Such a hypothesis receives much support from the literature, although terminology often varies.
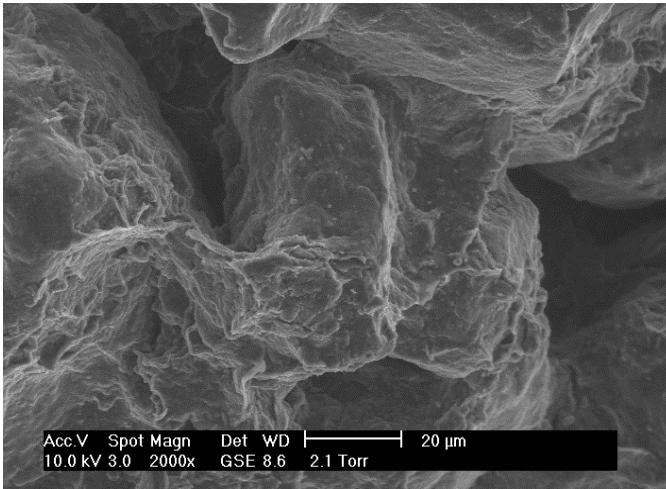
Fig. 1 Clay coating of silt in Pegwell Bay loess

For example Osipov and Sokolov (1995) suggest that contact between sandy and coarse-dusty grains and in dusty-clayey aggregates is realised through the clay minerals that constitute these "shirts". This suggests that clay bonding accounts for a large proportion of the overall bonding in loess and therefore its destruction leads to a major structural rearrangement of the fabric of the soil.

The airfall model

The oedometer was used to examine the importance of the different types of bonds that exist in loess. Usually oedometer testing is applied to carefully prepared samples of undisturbed material. The problem arising from the use of natural undisturbed loess samples is that many of the variables in the soil cannot be controlled and therefore it is difficult for their importance in the collapse process to be properly quantified. The airfall model was developed to address this issue and was tested against the results of undisturbed samples from China (Assallay *et al.* 1997) and three sites in the UK (Dibben 1998). The airfall method allows a range of variables that affect collapsibility to be tested, notably:

- particle size, shape and distribution
- voids ratio
- particle density
- types of fluid present, and
- the nature and amount of clay present.
- The main limitations to the method that Assalay (1998) and Dibben (1998) developed for the creation of artificial samples are:
- By controlling the amount of material deposited in the oedometer rings, comparable samples with similar initial voids ratio were created. The drawback was that excess material was forced into the rings to achieve the constant densities, disturbing the samples' initial structure.
- The way clay content affects the voids ratio and mass of the sample in the oedometer ring was not taken into consideration.

Materials used for the creation of artificial loess

Assallay (1998) used as a bonding material English China Clay (ECC), a pure form of kaolinite that has limited surface activity and is less chemically interactive with pore water than other minerals. For these reasons, and in order to make comparisons with Assallay's work, ECC Grade 50 was used in the study reported herein. The dominant mineral composition of ECC is well ordered kaolinite and muscovite, with minor constituents being quartz, feldspar and tourmaline. The silt fraction of loess was simulated by ground silica LG 120 provided by Tarmac Ltd. UK which was sieved to yield a grading very similar to natural loess in which the silt particles typically lie in the range 20-60 μm (Figure 2).
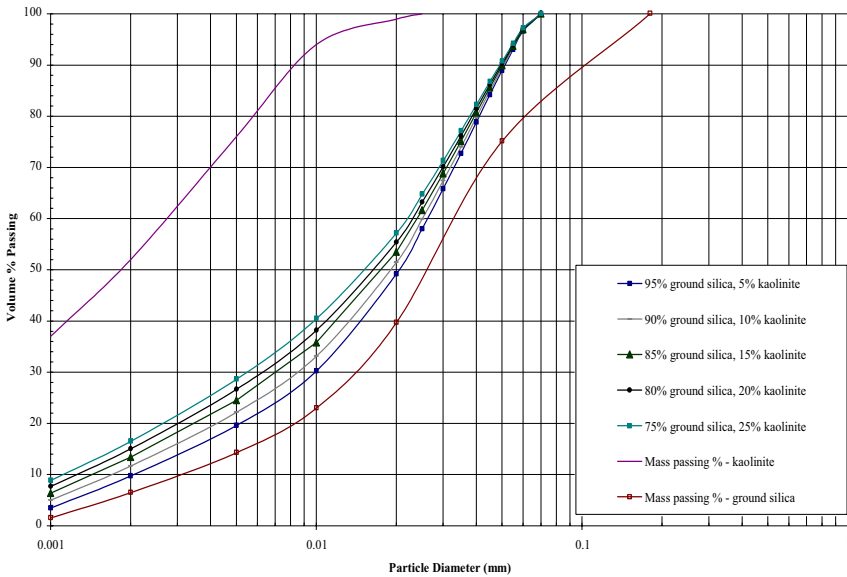
Fig. 2 Particle size distributions of kaolinite, Silica LG 120 and their mixtures

Sample preparation methods

Both the silica LG120 and the powdered clay were oven dried at 105 C^{o} for 24 hours. Then the silica LG120 was sieved through a 63 μm sieve and any coarser material discarded. The remaining material was placed in a mixer and clay was added to the different clay contents required (5%, 10%, 15%, 20% and 25% by weight) prior to mixing at low speed for 60 minutes (see Figure 2 for particle size distributions). The material was then transferred into a mortar and it was very well manually rubbed together (i.e. gently crushed) by using a rubber pestle for 20 minutes making sure that breakdown of individual particles was avoided. Finally the material was placed in an oven at 105 C^{o} and left for 24 hours.
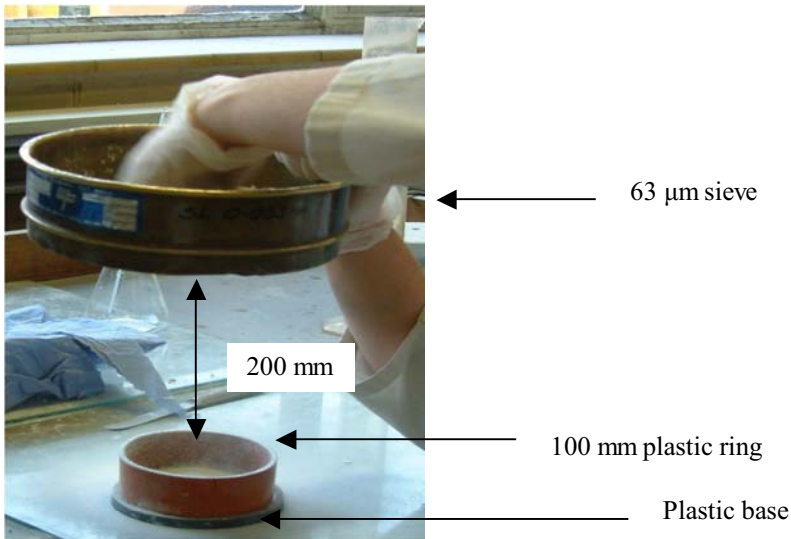
Fig. 3 Creation of a sample with the use of the airfall technique

The principle of the airfall method is that the material is deposited into a mould directly by sieving from a 63μm sieve that is at a height of approximately 200 mm above the mould (Figure 3). This method simulates the process of natural airfall sedimentation of loess and allows the particles to adopt an orientation according to their properties and ambient conditions. The purpose of subsequently moistening the material is to allow the bonding substances to "weld" the silt particles together and form a granular-framed, metastable structure (Assallay, 1998).

Three ways of wetting were utilised: by fine spray of distilled water to the top of the specimen progressively during its preparation; by applying the distilled water to the bottom of the sample so that it permeates through the silty material due to capillary rise; and placing the sample over boiling distilled water such that the water vapours permeate the sample and eventually activate the bonds. For the capillary rise and steaming methods, a plastic mould with a series of holes at the bottom was used to accommodate the samples. For the spraying method, a 100mm ring was placed on top of a plastic base (Figure 3) and material was deposited to a height of 1-2 mm using the airfall method. The surface of the sample was subsequently sprayed until the surface of the sample appeared saturated. The next layer of material was then deposited and fine sprayed, the process being repeated until a sufficient volume of material existed for the extraction of an oedometer sample. All samples were then oven dried at 50° C for a period of 24 hours, this temperature simulating the arid environments in which loess is often formed.

Initial sample characterisation

The results of Atterberg limit and specific gravity (G_s, small pyknometer method) tests performed according to BS 1377 (BSI, 1990) are presented in Tables 1 and 2. The natural undisturbed materials were sampled from Kent (UK), Vienna (Austria) and Kozlontui (Bulgaria).

Table 1. Plastic and Liquid limits, plasticity indices and specific gravity data for artificial samples.

	PL (%)	LL (%)	PI	Gs (Mg/m^3)
ECC	33	57	24	2.64
Silt LG 120	(non plastic)	30	-	2.64
5% ECC	(non plastic)	27	-	2.64
10% ECC	19	26	7	2.64
15% ECC	20	26	6	2.64
20% ECC	21	26	5	2.64
25% ECC	21	26	5	2.64

Table 2. Plastic and Liquid limits, plasticity indices and specific gravity data for natural samples

Loess source	PL (%)	LL (%)	Gs (Mg/m^3)
United Kingdom	Upper 21 Lower 19	Upper 35 Lower 27	Upper 2.76 Lower 2.68
Austria	18.9	30.1	2.73
Bulgaria	(non plastic)	26.5	2.68

Oedometer testing

A rear lever loading (Bishop Type) oedometer was used. The tests were 'single oedometer tests' which consisted of loading the specimen incrementally to a specific level of vertical stress while allowing the sample to come to equilibrium under the applied stresses, flooding the samples with water and where appropriate further incremental loading. The loading sequence used in general was of 5.0, 12.5, 25.0, 50.0, 100.0, 200.0, 400.0, 800.0, 1600.0, 2000.0 and 2400.0 kN/m^2. For the samples to reach their equilibrium under the applied stress a period of 24 hours was generally sufficient. The samples were flooded with de-ionised water either at 12.5 kPa (wet test) or 2000.0 kPa (dry test). Vertical compression ($\pm$ 3μm) was measured using an electronic transducer connected to a data logger.

Results

All three bond activation methods could be employed only for the creation of samples at 5% ECC content. Figure 4b compares the change in voids ratio when wetted at 12.5 kPa. Fine spraying created samples with the most open structure (e_o = 1.90), followed by steaming (e_o =1.35) and then capillary rise (e_o =1.09) (see Figure 4a). Fine spraying and steaming samples exhibited a similar reduction of voids ratio upon wetting (Δe = 0.26) while that for the capillary rise sample was very small (Δe = 0.01). Steaming and capillary rise samples exhibited exactly the same final voids ratios, contrary to the fine spraying sample that had a notably high final voids ratio of 0.90. The wet (past 12.5 kPa) behaviour for all three samples was similar, with two curves being coincident (Figures 4a and 4b).

When the capillary rise and steaming methods were attempted with ECC contents over 5%, intense cracking (often 2-3 mm wide) appeared on the surface of the samples making them unsuitable for oedometer testing. Samples with more than 5% ECC content could be created only with the use of the fine spraying method.

The 5% ECC clay samples exhibited significant differences in initial voids ratios when different bond activation methods were used, but relative consistency was achieved using any one technique. For the 10% - 25% ECC content samples, in spite of employing only the fine spraying method, there were significant differences in initial voids ratio (Figure 5), while final voids ratios proved remarkably similar.
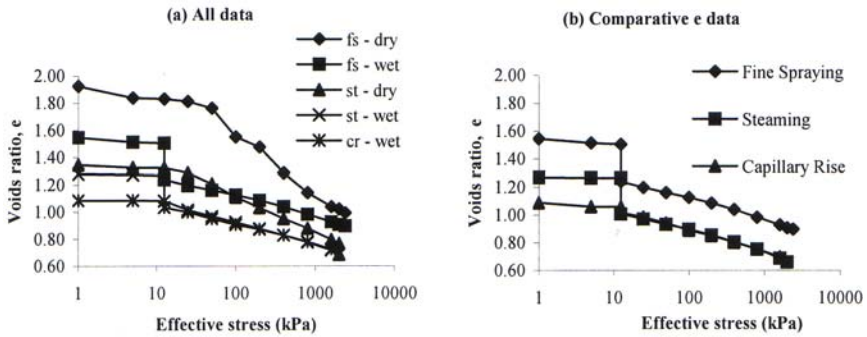
Fig. 4 Collapse behaviour of 5% ECC artificial samples created with the use of different bond activation methods
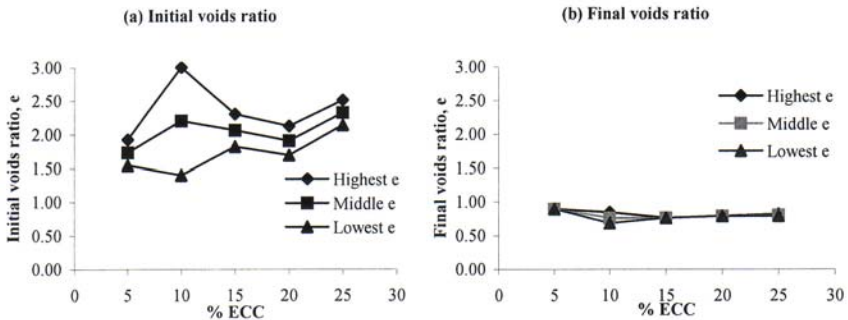
Fig. 5 Variation of initial and final voids ratios for 10% - 25% ECC samples created using the Fine Spraying method

In this work it was noticeable that the greatest variation, and hence sensitivity to clay content, was for 10% ECC (Figure 5), which interestingly also had the higher plasticity index of the artificial samples. Nevertheless among the 10% ECC tests carried out there were dry and wet tests that illustrated very good consistency both in terms of initial and final voids ratio as well as collapse behaviour (Figure 6a).

Another interesting feature of the collapse process concerns the consolidation curves (Figure 7a) of the same 10% ECC samples upon wetting as in Figure 6b. The sample with the highest initial voids ratio does not progressively collapse as the other samples do, instead a sudden breakage of the bonds takes place after 3 minutes. Also the change of voids ratio (Δe) upon wetting is approximately proportional to the initial voids ratio value (e_o), as illustrated in Figure 7b.
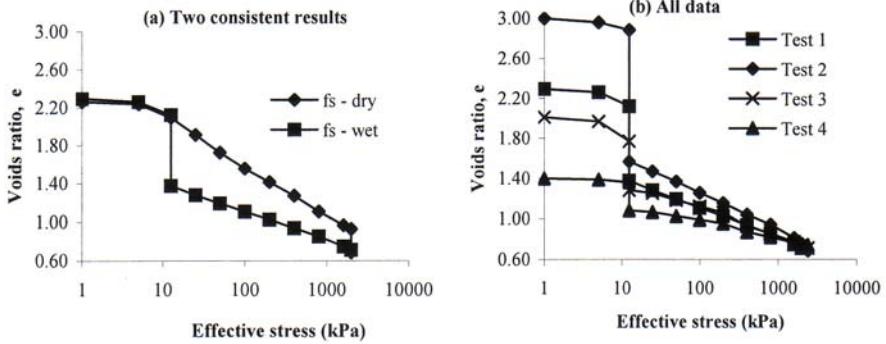
Fig. 6 Collapse behaviour of artificial samples containing 10% ECC created using the Fine spraying method
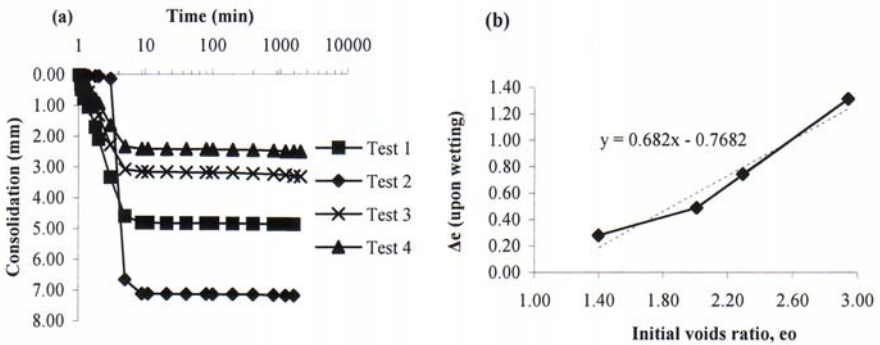
Fig. 7 (a) Consolidation curves of 10% ECC samples upon wetting at 12.5 kPa, (b) Influence of the initial voids ratio on the collapse behaviour of the 10% ECC samples upon wetting at 12.5 kPa

In Figure 8 the collapse behaviour of natural undisturbed material from the United Kingdom, Austria and Bulgaria is plotted against a typical 5% ECC artificial sample under dry loading (i.e. saturation of the samples at 2000.0 kPa). The consolidation curves exhibit a very similar trend with a similar degree of collapse upon wetting.
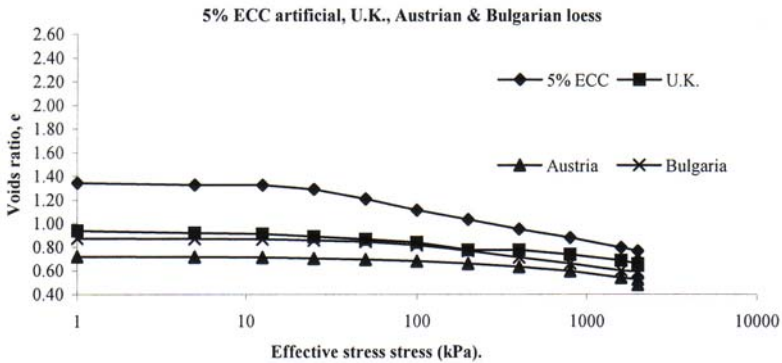
Fig. 8 Comparative data on collapse behaviour of artificial (5% ECC), U. K., Austrian and Bulgarian loess under dry loading (Austrian and Bulgarian results after Boardman *et al* 2001).

Conclusions

When the three bond activation methods are compared, the most realistic simulation of natural loess appears to derive from the use of the steaming method. The samples have relatively low initial voids ratios and exhibit a considerable amount of collapse upon wetting. The fine spraying method results in samples with high initial voids ratios while the capillary rise method underestimates the importance of the clay bonding that disintegrates upon wetting since the capillary rise samples illustrate a very small degree of collapse upon wetting. The main disadvantage of the steaming method is that excessive cracking appears at the surface of the samples during the wetting and drying cycles for ECC percentages more than 5%. The only method that allows the creation of samples with more than 5% ECC is the fine spraying method. Therefore creation of artificial samples simulating low clay content natural samples should be made with the use of the steaming method and when inapplicable due to high clay contents, the fine spraying method should be used.

Reproducibility in terms of final voids ratio is easily accomplished, as shown in Figure 5b. In terms of initial voids ratio the steaming method produced samples with consistent results (Figure 4a), but this high level of consistency could not be achieved when the fine spraying method was employed mainly due to external factors (the amount of water sprayed cannot be accurately controlled, the height of each of the layers deposited is not uniform). Nevertheless, if a large number of tests are carried out and samples with very high or low initial voids ratio are statistically ignored, a satisfactory level of consistency can be achieved. Even for sam-

ples at different ECC contents, the average initial void ratio values do not appear to deviate significantly (Figure 5a)

The initial voids ratio also controls the behaviour of the material upon wetting as illustrated in Figure 7b, where the initial voids ratio is directly proportional to the degree of collapse. Very high initial voids ratio also affect the way this collapse takes place, as shown in Figure 7a where it can be observed that the sample with an initial voids ratio marginally higher than 3 exhibited a sudden disintegration of clay bonds and consequent collapse after 3 minutes, such behaviour had not been the case for the other samples in which the collapse initiated from the moment water was introduced.

The experimental results indicate that the use of the airfall model, and in particular when the steaming bond activation method is employed, simulates natural loess deposits well. The artificial samples had higher initial voids ratios than the natural samples, but this should be expected since they were created in such a manner to simulate their aeolian origin. The consolidation curves of artificial and natural samples (Figure 8) are very similar, indicating that tests on artificial loess can provide a valuable insight to the way different factors influence the behaviour of natural loess.

References

Assallay, A.M., Rogers, C.D.F., Smalley I.J. (1997). Formation and collapse of metastable particle packings and open structures in loess deposits. Eng. Geol., 48: 101-115

Assallay, A.M. (1998). Structure and Hydrocollapse Behaviour of Loess. PhD Thesis, Loughborough University, UK.

Boardman, D. I., Rogers, C. D. F., Jefferson, I., Rouaiguia, A. (2001). Physico-chemical characteristics of British loess. Proc. International Conference on Soil Mechanics and Geotechnical Engineering, Istanbul.

British Standards Institution (1990). Methods for testing soils for civil engineering purposes. BS 1377, HMSO, London.

Derbyshire, E., Dijkstra, T. A., & Smalley, I. J., (1995a). Genesis and Properties of Collapsible Soils. Kluwer, Dordrecht, 413p

Dibben, S.C. (1998). A Microstructural Model for Collapsing Soils. Ph. D. Thesis, Nottingham Trent University, UK.

Hornbaker, D.J., Albert, R., Albert, I., Barabasi, A-L., & Schiffer, P. (1997). What keeps sandcastles standing. Nature 387, 765.

Osipov, V. I., & Sokolov, V. N. (1995). Factors and mechanisms of loess collapsibility. Proc of the NATO advanced workshop on Genesis and Properties of Collapsible Soils: 49-63

Rogers, C.D.F., Smalley, I.J. (1993). The shape of loess particles. Naturwis-seschaften 80: 461-462

Analysis of the mechanical response of an artificial collapsible soil

G.M. Medero[1], F.. Schnaid[1], W.Y.Y. Gehling[1], and D. Gallipoli[2]

[1] Federal University of Rio Grande do Sul, Brazil
[2] University of Durham, UK

Abstract. Natural collapsible residual soils are a common occurrence in Brazilian unsaturated deposits. The work presented in this paper is part of a larger project designed to identify the most important parameters controlling the mechanical behaviour of this type of material. A laboratory testing programme has been carried out in artificially unsaturated cemented samples reproducing some of the characteristics of natural collapsible soils. A technique for sample preparation has been developed, which has resulted in specimens with high values of void ratio and various degrees of cementation. In particular, it has been decided to use soil cemented mixtures with expanded polystyrene particles which has led to light samples with low density, meta-stable mechanic structure, and good workability. These artificial samples have been subjected to direct shear and oedometer tests, including conventional and suction-controlled oedometer tests. Oedometer tests have been used to characterize the behaviour of this material and to quantify the potential collapse due to loading and wetting. From the observed behaviour it is suggested that the initial void ratio, cement agent and initial suction are all important factors influencing the potential collapse of the soil. For saturated artificial soil samples the critical state lines in the (v, ln p')-plane and (q, p')-plane have also been calculated by using an approximated procedure based on the results of direct shear tests.

1 Introduction

This paper presents some initial results from an undergoing laboratory programme aimed at studying the mechanical behaviour of collapsible unsaturated artificial residual soils.

A technique of sample preparation has been developed to reproduce in the laboratory artificial soil samples that imitate the main characteristics of natural collapsible soils. The choice of using artificially prepared soil specimens rather than natural ones is mainly due to the difficulty in sampling natural specimens from deposits of highly heterogenic collapsible soils. In addition, during the laboratory testing of artificial samples, the main variables affecting collapsibility could be controlled together with the boundary conditions applied to the specimens in order

to analyse the sensitivity of the collapse behaviour to the various factor involved. In particular, it has been possible to evaluate the influence on the mechanical behaviour of the variation of both the initial void ratio and the cement agent.

A number of preliminary tests have been carried out with the objective to verify the fundamental characteristics of the artificial soil such as, for example, the saturated permeability. This study has also focussed on the investigation of the structure of the soil samples including the distribution of cement bondings between particles and the homogeneity and reproducibility of specimens reconstituted in the laboratory. This initial investigation has included falling head permeability tests, unconfined compression tests and visual inspection of different sections cut through a number of reconstituted samples (for further details see Medero, 2001).

A series of oedometer tests has been subsequently carried out under different conditions including saturated tests, collapse tests and suction controlled tests to determine the collapse potential of the meta-stable structure of the artificial soil. In addition to studying the response under oedometer conditions, a series of direct shear tests has also been performed on artificial samples which had been previously saturated in an attempt to predict the critical state soil parameters.

The research is currently under development and additional series of tests on artificial soil samples are presently being designed to evaluate alternative techniques of sample preparation and to extend the results obtained from the first experimental programme to more complex laboratory tests and different initial conditions for the artificial soil.

Sample Preparation

One of the main objectives of the present research is the selection of a suitable auxiliary material to be included in the soil mixture in the form of small particles during the preparation of the sample to help achieving high values of void ratio. These particles are deemed to interact with the surrounding soil mass in a similar fashion to the air entrapped in the soil pores, allowing soil specimens to be moulded with a high initial value of void ratio without altering the mechanical response of the soil mass. For the complete description of the sample preparation technique the reader is referred to the work by Medero (2001).

Among a number of alternatives, a mixture of soil (residual soil of Arenito Botucatu) + cement + water + particles of expanded polystyrene has been chosen as a suitable option to reproduce some of the structural features of collapsible specimens. In this mixture, small particles of polystyrene (Figure 1) work like a void within the soil mass and allow samples with high values of void ratio to be obtained.

It is here important to notice that two conditions should be met to justify the insertion of the polystyrene into to the soil:

1.   the polystyrene has a very small stiffness when compared to soil particles and the addition of polystyrene does not produce samples having different stiff-

ness and strength from a soil sample without polystirene at the same value of void ratio, i.e. the polystyrene particles act as a void in the soil mass.

2. for a given void ratio, the same hydraulical conductivity is obtained for a sample made exclusively of soil and a sample reconstituted as a soil-polystyrene mixture. This has been tested experimentally for values of void ratio up to 0.6 (the maximum void ratio which is possible to obtain for reconstituted samples without polystyrene).

The results obtained from falling head permeability tests performed on soil samples with and without polystyrene (but with the same value of void ratio) indicate that the presence of polystyrene does not affect the overall permeability of the sample (see Medero, 2001). Furthermore, the hydraulical conductivity of a soil-polystyrene sample at a value of void ratio of 1.3 has an order of magnitude of 10^{-3} m/s, which is within the range measured in natural soil samples by using in-situ permeability tests.
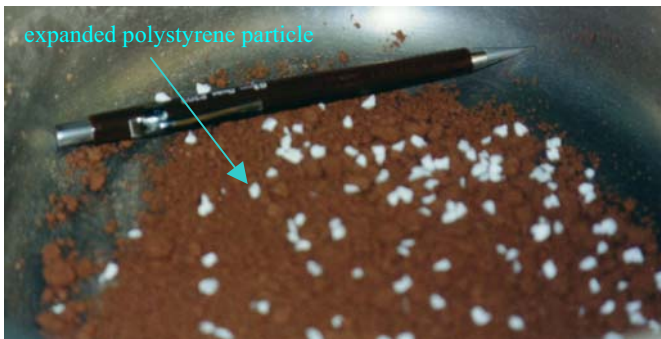
(a) mixture during the moulding process

(b) soil-polystyrene sample

(c) typical cross-section of a sample

Fig. 1. The Sample preparation technique.

The influence of the size of the polystyrene particles on the hydraulic conductivity of the samples has also been examined by Medero (2001) by performing falling head permeability tests on various soil-polystyrene samples with a void ratio 1.3, each sample reconstituted in the laboratory by mixing the soil with different sets of polystyrene particles having different size distributions. Again the experimental results indicate that the value of the hydraulic conductivity is not significantly affected by the size distribution of the polystyrene particles used for the mixture.

A possible drawback to this technique, however, is given by the fact that the presence of polystyrene can alter the overall distribution of suction which would be obtained at the same value of initial void ratio if the sample did not contain polystyrene particles.

Samples of the mixture soil-polystyrene with an initial void ratio of 1.3 have been chosen for the tests described in the following part of the present paper. This is considered to be a value representative of natural collapsible soils encountered in Brazil as indicated by the values of void ratio reported by Bressani et al. (1995); Horn (1997); Barros (1997) and shown in Table 1.

Table 1. Tropical soils (Bressani et al., 1995; Horn, 1997; Barros, 1997)

Occurrence in Brazil	Void Ratio (average)	Degree of Saturation [%] (average)
Rio Grande do Sul - Porto Alegre	0.91	43.5
Rio Grande do Sul - Porto Alegre	0.94	29.9
Rio Grande do Sul - São Leopoldo	0.90	51.2
São Paulo (Rua 13 de Maio – Bela Vista)	1.30	68.6
São Paulo (Alameda dos Guaramomis – Moema)	1.26	81.5
Sorocaba	1.70	68.0
Campinas (UNICAMP)	1.50	39.4
Guairá	2.00	52.1
Bauru	0.69	35.3
São Carlos	1.00	45.0
Campinas	1.42	46.3
São Paulo (Caxingui)	0.65	76.0
São Paulo (Cidade Universitária – USP)	0.67	82.0

The sample preparation consists of three steps, as described by Medero (2001):

1. Mix the soil with Portland cement (1% in mass) until a perfect homogeneity is obtained;
2. Add water to the soil to reach the optimum water content (16% water content);
3. Insert expanded polystyrene particles previously prepared in specified sizes and shapes.

At this stage the mixture has to be carefully prepared in order not to crush the polystyrene and to avoid concentration of particles, as shown in Figure 1.

The open soil structure obtained by using this sample preparation technique is similar to that observed in natural collapsible soils, where packets made of elementary soil particles join together to form another level of structure of a granular type. In this material it is therefore possible to distinguish two classes of pore spaces having significantly different sizes, i.e. the smaller pore spaces between the elementary particles inside the packets and the larger pore spaces between the packets of elementary particles. This has also been confirmed by initial results obtained from the application of the Scanning Electron Microscopy (SEM) technique to the analysis of the structure of artificially prepared soil samples (Medero, in press). These results indicate that the fabric and bonding characteristics of the artificial samples are qualitatively similar to those of natural collapsible soils as shown by the Scanning Electron Microscopy (SEM) analyses of natural residual soils that have been published by several authors (Nakahara, 1995; Kratz De Oliveira, 1999; Horn, 1997; Cunha, 1997; Bastos, 1999).

Experimental Results and Analysis

Collapse Potential

The collapse potential, according to the classical definition by Jennings & Knight (1957) for soil samples under oedometer conditions, is given by:

$$\frac{e_i - e_f}{1 + e_o} \qquad (1)$$

where e_o is initial void ratio and e_i and e_f are the values of void ratio obtained from the oedometer curves at natural water content and at saturation respectively under the same applied vertical stress. The difference $e_i - e_f$ coincides therefore with the change in void ratio observed upon wetting at a given applied vertical stress, as postulated by Jennings and Knight (1975).

In this work a typical collapse test has been conducted by applying the chosen value of vertical load to the sample at its initial water content and leaving the soil to consolidate until no further vertical displacements have been measured. The soil has been subsequently flooded with water and left to settle again until no further increase of vertical displacement have been recorded.

For oedometer tests carried out under suction controlled conditions, the vertical stress ha been applied by increments while suction has been maintained constant throughout the experiment. The potential collapse occurring at a given vertical stress due to a reduction of suction has then been estimated as the difference between the volumetric strains obtained from the two oedometer curves corresponding to the initial and final values of suction under the same value of applied vertical stress.

A summary of the collapse tests performed in this work is presented in Figure 2 and 3. Figure 2 shows the results from the tests on the cemented samples without polystirene particles with an initial value of void ratio of 0.6. The figure presents the collapse potential measured at different values of vertical stress together with the corresponding values of volumetric strains due to loading + wetting and to sole loading (the collapse potential being the difference between these two values). Under a given value of applied vertical stress the volumetric strains caused by loading + wetting and by sole loading are calculated according to the following two equations respectively:

$$\frac{e_o - e_f}{1 + e_o} \qquad (2)$$

$$\frac{e_o - e_i}{1 + e_o} \qquad (3)$$

Inspection of Figure 2 indicates that the samples having a void ratio of 0.6 do not exhibit collapse for all four stress values considered.

Figure 3 shows the results obtained from similar tests performed on cemented samples mixed with polystyrene particles having an initial void ratio of 1.3. These samples present a markedly different response from those shown in the previous figure as the amount of collapse undergone upon wetting is significantly larger. In particular, the results suggest that a maximum value of collapse is achieved for an intermediate value of the vertical stress around 100 kPa. The amount of collapse tends to reduce for increasing values of vertical stress due to the progressive breakage of meta-stable structure of the soil skeleton under higher loads. At very high stress levels where the soil structure has been broken by compression, the voids are reduced and the collapse becomes negligible. A similar behaviour has already been reported by Balmaceda (1991) and Futai (1997, 1999).

An additional reason for the smaller collapse observed at higher stress levels is that increasing compression of the soil at constant water content generates a progressive reduction of suction from its initial value. The subsequent reduction in suction upon saturation tends therefore to be of smaller magnitude for samples subjected to higher levels of vertical stress.
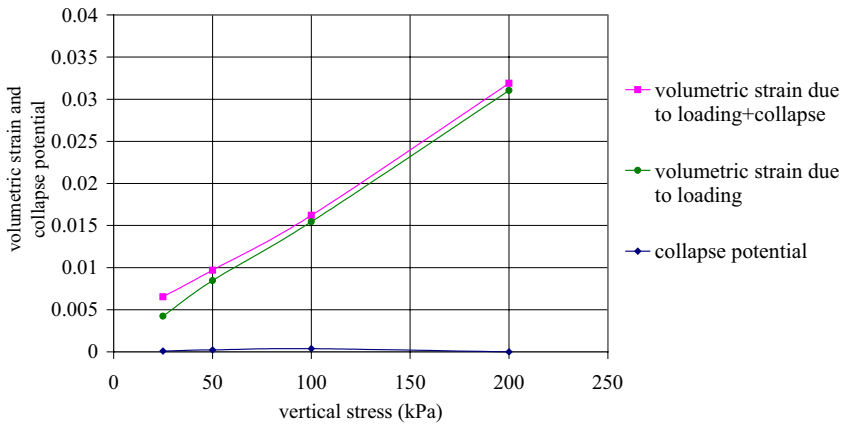
Fig. 2. Collapse potential for the soil + cement configuration.
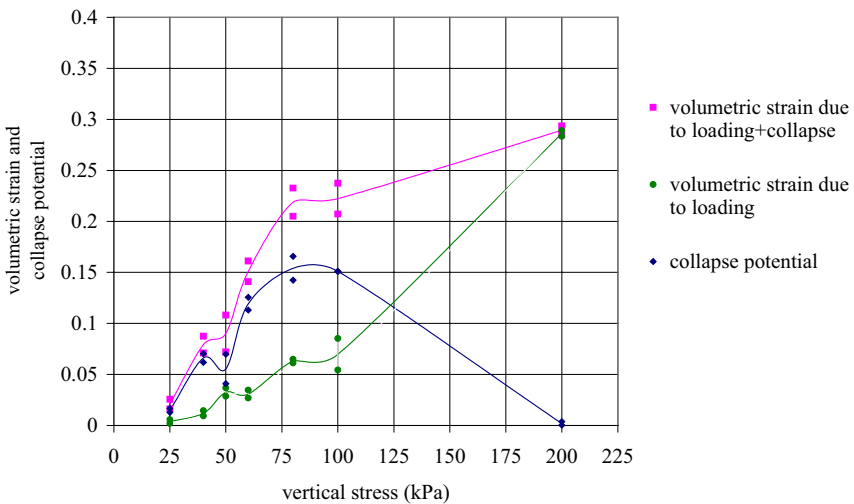
Fig. 3. Collapse potential for the soil + cement + polystyrene configuration.

From the observed behaviour shown in Figure 3 it becomes clear that the use of polystyrene to obtain a high void ratio produces a collapsible sample that exhibits characteristics of behaviour similar to those observed in natural collapsible soils. The structure of these artificial samples is not as complex as those of natural soils but they can be useful to investigate the variables that control soil collapsibility.

Table 2. Critical state parameters

Parameter	Value
M	0.88
λ	0.30
Γ	3.10

Critical State Analisys

An attempt has been made to define the critical state envelope for saturated samples of the mixture soil-polystyrene with an initial value of void ratio of 1.3. In the lack of triaxial tests, the critical state lines in the (q, p')-plane and the (v, ln p')-plane have been indirectly defined by using the results from direct shear tests. In particular, the direct shear tests have provided for each tested sample the values at critical state of the vertical stress σ, the shear stress τ and the specific volume v. The stress variables σ and τ measured at critical state for each sample have then been used to calculate the critical state line in the (τ, σ)-plane. The Mohr circles corresponding to the critical stress state for each tested sample have been subsequently calculated by imposing the following two conditions: a) the Mohr circle corresponding to the critical stress state for a given tested sample has to be tangent to the critical state line in the (τ, σ)-plane at the point corresponding to the critical stress state obtained from the direct shear test of that sample and b) the centre of the Mohr circle for any tested sample has to lie on the σ axis. From the definition of the Mohr circles it has been possible to calculate the corresponding values of the principal stresses for each sheared sample (at this stage a simplifying assumption has been introduced that the two lower principal stresses are coincident as in triaxial compression tests) and, consequently, the values of the deviator stress, q and mean net stress, p'. These results, together with the experimental values of specific volume, v at critical state, have been used to represent in Figure 4 the critical state lines for the saturated artificial soil. In accordance with the critical state lines shown in Figure 4, Table 2 presents the corresponding values of the slope M of the critical state line in the (q, p')-plane, the slope λ of the critical state line in the (v-ln p')-plane and the intercept Γ of the critical state line in the (v-ln p')-plane for a value of the mean net stress p' equal to one.
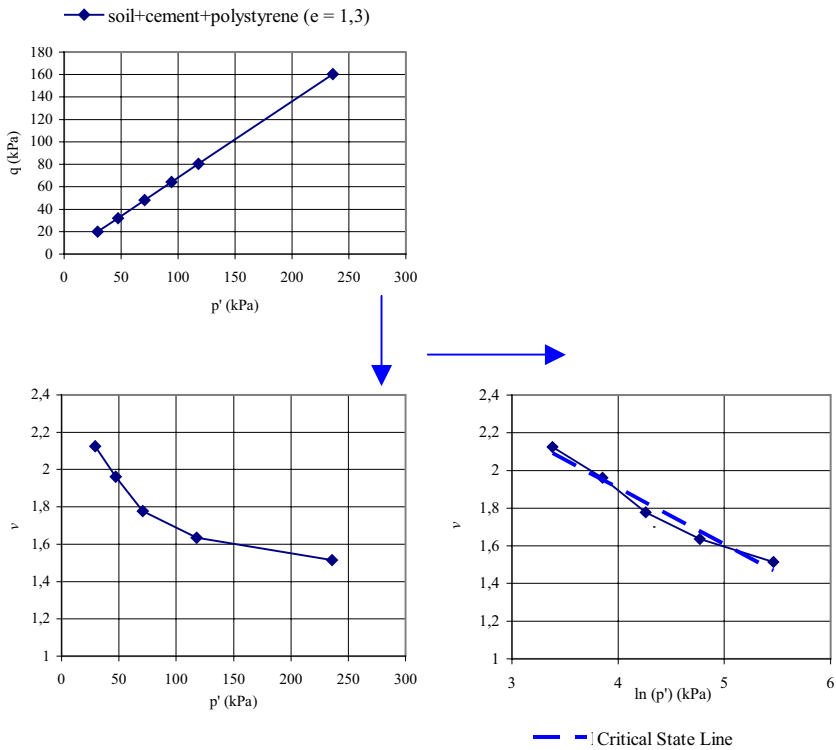
Fig. 3. Critical State Line

Conclusions

The paper presents some preliminary results from an undergoing study on the effects of cement content and initial void ratio on soil collapsibility. Artificially cemented specimens with initial void ratio of 0.6 and 1.3 have been prepared and tested in the laboratory in series of oedometer tests with and without suction control and direct shear tests. The technique of sample preparation, designed to achieve high values of initial void ratio such as 1.3 (typical of Brazilian collapsible residual soils), is one of the most relevant contributions of this work. Introduction of polystyrene particles in the soil mixture has proved to be a good option to achieve high values of initial void ratio without changing the material response in terms of strength, stiffness and permeability. The results presented in the paper indicate that this technique enables samples of meta-stable structure to be obtained

at known cement contents and large values of initial void. An investigation on the reproducibility, homogeneity and workability of these artificial soil specimens has also confirmed that this sample preparation technique is a particularly attractive option for the study of collapsible materials. A series of laboratory tests has been carried out to characterize the soil collapsibility for samples having initial values of void ratio of 0.6 and 1.3 and to define the critical state parameters for samples moulded at an initial void ratio of 1.3. Further research is currently being performed to expand the results obtained from the present laboratory programme to triaxial suction controlled conditions and to explore alternative techniques for the preparation of artificial samples representative of natural collapsible soils. One of the objectives of the current research is also to investigate the influence of the different factors affecting collapsibility on the definition of the load-collapse curve introduced by Alonso et al. (1990) and to develop an adequate analytical model for reproducing the soil behaviour observed in the laboratory.

Abbreviations

e_o - initial void ratio; q – deviator stress;
p' - mean net stress; v - specific volume;
M - slope of the critical state line in the (q, p')-plane;
λ - slope of the critical state line in the (v, ln p')-plane.

References

ALONSO, E. E.; GENS, A.; JOSA, A. A constitutive model for partially saturated soils. Géotechnique, London, v.40, n.3, p.405-430, 1990.

BALMACEDA, A. R. Suelos compactados un estudio teorico y experimental. Barcelona, 1991. 434p. Tesis Doctoral – Universitat Politècnica de Catalunya, Barcelona.

BARROS, J. M. C. Módulo de cisalhamento dinâmico de solos tropicais. São Paulo, 1997. 437p. Tese de Doutorado em Engenharia – Escola Politecnica da Universidade de São Paulo. Departamento de Estruturas e Fundações – Brasil.

BASTOS, C.A.B. Estudo geotécnico sobre a erodibilidade de solos residuais não saturados. Porto Alegre, 1999. 269p. Tese de Doutorado em Engenharia - Curso de Pós-Graduação em Engenharia Civil, Universidade Federal do Rio Grande do Sul – Brasil.

BRESSANI, L.A.; HORN, M.R.; GEHLING, W.Y.Y. Alguns resultados experimentais de um solo residual de granito. In: ENCONTRO SOBRE SOLOS NÃO SATURADOS, 1995, Porto Alegre. Anais... Porto Alegre: CPGEC – UFRGS, 1995. p.272-280.

CUNHA, L. O. B. P. Estudo da Condutividade Hidráulica de Solos Não Saturados da Região Metropolitana de Porto Alegre. Porto Alegre, 1997. 109p. Dissertação de Mestrado em Engenharia - Curso de Pós-Graduação em Engenharia Civil, Universidade Federal do Rio Grande do Sul

FUTAI, M. M. Análise de ensaios edométricos com sucção controlada em solos colapsíveis. Rio de Janeiro, 1997. 253p. Tese de Mestrado. COPPE/UFRJ – Brasil.

FUTAI, M. M.; ALMEIDA, M. S. S.; FILHO, F. C. S.; CONCIANI, W. Experimental and theoretical evaluation of the maximum collapse. In: XI PANAMERICAN CONFERENCE ON SOIL MECHANICS AND GEOTECHNICAL ENGINEERING, 1999, Foz do Iguaçu. Anais… v. 1, p.267-274.

HORN, M.R.. Estudo do comportamento mecânico de um solo residual de granito não saturado. Porto Alegre, 1997. 81p. Dissertação de Mestrado em Engenharia (Geotecnia) - Curso de Pós-Graduação em Engenharia Civil, Universidade Federal do Rio Grande do Sul – Brasil.

JENNINGS, J. E.; KNIGHT, K. A guide to construction on or with materials exhibiting additional settlement due to collapse of grain structure. In: REGIONAL CONFERENCE FOR AFRICA ON SOIL MECHANICS & FOUNDATION ENGENEERING, 6, 1975, Durban. Proceedings... Rotterdam: A. A. Balkema, 1975. 2v., v.1, p.99-105.

JENNINGS, J. E.; KNIGHT, K. The addition settlement of foundations due to a collapse of structure of sandy subsoils on wetting. In: INTERNATIONAL CONFERENCE ON SOIL MECHANICS AND FOUNDATION ENGENEERING, 4, 1957, London. Proceedings... London: Butterworths Scientific Publications, 1957. 3v., v.3a, p.316-319.

KRATZ DE OLIVEIRA, L.A. Utilização do ensaio pressiométrico na previsão da colapsividade e de parâmetros geotécnicos em solos não saturados. Porto Alegre, 1999. 143p. Dissertação de Mestrado em Engenharia - Curso de Pós-Graduação em Engenharia Civil, Universidade Federal do Rio Grande do Sul - Brasil.

MEDERO, G.M. Análise do comportamento mecanico de um materíal colapsivel. Porto Alegre, 2001. 148p. Dissertacao de Mestrado em Engenharia - Curso de Pos-graduacao em Engenharia Civil, Universidade Federal do Rio Grande do Sul - Brasil.

MEDERO, G.M. Análise de comportamento de material colapsível. Porto Alegre, in press. Tese de Doutorado em Engenharia - Curso de Pós-Graduação em Engenharia Civil, Universidade Federal do Rio Grande do Sul – Brasil.

NAKAHARA, S. Determinação de Propriedades de um Solo Não Saturado Através de Ensaios Pressiométricos e de Laboratório. Porto Alegre, 1995. 143p. Dissertação de Mestrado em Engenharia – Curso de Pós-Graduação em Engenharia Civil, Universidade Federal do Rio Grande do Sul – Brasil.

Fabric Evolution of an Unsaturated Compacted Soil during Hydromechanical Loading

Olivier Cuisinier and Lyesse Laloui

Soil Mechanics Laboratory - Swiss Federal Institute of Technology Lausanne (EPFL), Lausanne, Switzerland

e-mail : Olivier.Cuisinier@epfl.ch / Lyesse.Laloui@epfl.ch
Phone: (+) 41 21 693 23 01
Fax: (+) 41 21 693 41 53

Abstract: The main goal of this paper is to present the first results of a study performed to provide insights into the relationship between the hydromechanical stress path experienced by a compacted soil and the modification of its pore space geometry. A new oedometer employing the axis translation technique was used to characterize the hydromechanical behaviour of the tested material. The fabric of the tested samples was determined using the mercury intrusion porosimetry technique under 4 stress levels and two different suctions. From this information, the macro and micropore volume variations were then determined. The results showed that mechanical loading produced a progressive reduction of the macropore volume and a significant increase of the micropore volume beyond a stress of 250 kPa. The obtained results tend to demonstrate that suction strengthens soil fabric, as the initial "double structure" of the tested material was not destroyed in the case of the unsaturated sample by the loading up to 1 000 kPa, whereas, the saturated sample exhibited a more homogenous fabric.

Introduction

Soil structure corresponds to the combination of fabric, meaning the geometrical arrangement of soil particles, and of interparticle bondings that stem from cementations and physical-chemical interactions (Yong and Warkentin, 1975). The influence of bonding on soil mechanical behaviour has been widely studied (e.g. Leroueil and Vaughan, 1990), and it is well known that principal soil mechanical properties are directly related to the soil's initial internal fabric (e.g. Lambe, 1958). Nevertheless, there is a lack of knowledge concerning the fabric modification that results from hydraulic and/or mechanical loadings. This kind of informa-

tion is, however, of great importance since hydraulic conductivity or water retention curves, for example, depend widely on soil fabric (e.g. Brustaert, 1968; Richard et al., 2001), and that data represent essential parameters in geotechnical and geoenvironmental engineering.

In this context, some authors have attempted the characterisation of soil fabric and its evolution during mechanical loading performed under a saturated state. Delage and Lefebvre (1984), using mercury intrusion porosimetry and scanning electron microscopy, have shown that, during consolidation, only the largest pores collapse at a given stress increment and small pores are only compressed when all the macropores have been completely destroyed by the loading. These results were confirmed by the work presented by Griffiths and Joshi (1989) and Lapierre et al. (1990). Simms and Yanful (2001) have investigated the relationship between suction changes and induced fabric modifications. Their results have demonstrated that soil fabric is extremely sensitive to any suction variation. However, only a few authors have studied fabric evolution during mechanical loading of an unsaturated soil (Al-Mukhtar et al., 1996; Qi et al., 1996). These authors have used remoulded Boom clay, which is a swelling material, and a synthetic model clay named Na-laponite, respectively. However, their interest was essentially focused at the clay particle level and the initial fabric of these materials was very different from the "double structure" encountered in natural or compacted soils (Collins and Mc Gown, 1974). Consequently, it is difficult to extrapolate their conclusions towards natural or compacted soils.

Considering these observations, a study was undertaken to characterise the evolution of soil fabric during mechanical loading. The suction controlled oedometer used is presented in the first part of the paper. The mercury intrusion porosimetry technique was selected in order to determine the soil sample's internal pore space geometry. Its basic principle is explained in the second part of the paper. Two suction levels were investigated (0 and 200 kPa). The first obtained experimental results are presented in the third part of the paper. The final point outlines the main conclusions that could be inferred from these first results and further research that will be undertaken in the framework of this study.

Suction Controlled Oedometer

Two kinds of devices were used to perform the mechanical tests: basic oedometers and a suction controlled oedometer, especially developed for this study (Fig. 1). This last device employs the air overpressure method for suction control. The ceramic disc at the base of the sample had an air entry value of 500 kPa. An air pressure/volume controller regulated the air pressure, u_a, inside the sample. The water pressure at the base of the sample, u_w, was maintained constant with a water pressure/volume controller. The imposed matric suction, s, is equal to $u_a - u_w$. The maximum vertical mechanical stress, σ_v, was 1 MPa. It was transmitted to the soil sample through the upper chamber of the device, which corresponds to a water tank made with a flexible membrane (see Fig. 1). This water was pressurized with

a pressure/volume controller. All the controllers used had a precision of ± 1 kPa and ± 1 mm^3. The sample diameter was 6.35 cm and the initial height about 1.2 cm. This relatively low height was necessary to reduce the time to reach equilibrium after the imposition of a given suction to the soil sample. The vertical load and the suction were increased step by step. Each stress step required a duration of at least 24 h in order to reach deformation equilibrium. In some cases, several days were required to reach equilibrium. In the case of the basic oedometer, sample height was about 1.5 cm and the diameter was 6 cm.
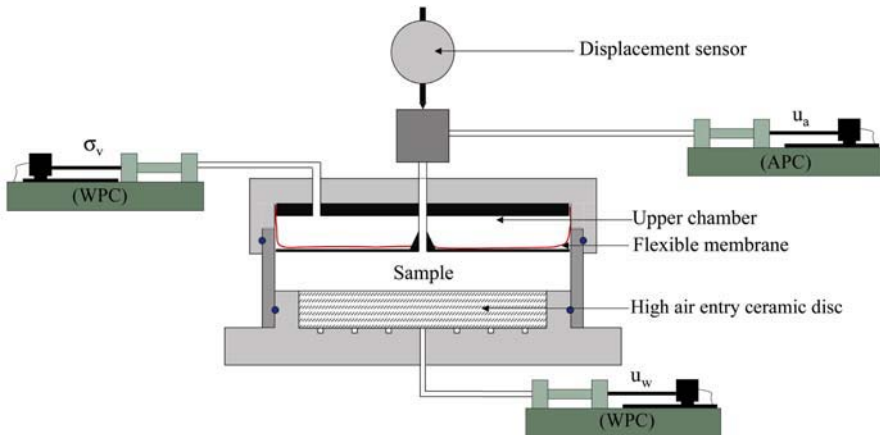
Fig. 1. Suction controlled oedometer (APC: air pressure controller; WPC: water pressure controller).

Mercury Intrusion Porosimetry (MIP)

The theoretical bases for the determination of soil fabric with MIP is very similar to those of the pressure plate test. In the case of MIP, the non-wetting fluid is mercury and air is the wetting fluid. The mercury pressure is increased step by step and the intruded volume of mercury is monitored for each pressure increment. Assuming that soil pores are cylindrical flow channels, Jurin's equation can be used to determine the pore diameter associated with each mercury pressure increment.

Due to technical requirements, tested samples must be totally dry in order to perform a MIP test. Among the available dehydrating methods, oven drying and air-drying should be avoided since they induce strong soil pore geometry modification. According to Delage and Lefebvre (1984), the freeze-drying method is the least disturbing preparation technique for water removal. Hence, this method was selected for our study although it gives less reproductive results than oven drying (Penumadu and Dean, 2000). The samples were quickly frozen with liquid nitrogen (temperature of -196 °C) and then placed in a freeze-drier for approximately

1 day. The samples were kept inside desiccators until the MIP tests were performed using a Porosimeter 2000 (Carlo Erba Instruments).

A MIP test gives the cumulative mercury volume intruded as a function of the pore radius. To further interpret MIP data, Juang and Holtz (1986) have proposed using the pore size distribution, PSD, of the sample, defined as follows:

$$f(\log r_i) = \frac{\Delta V_i}{\Delta(\log r)} \tag{1}$$

where ΔV_i is the injected mercury volume at a given pressure increment corresponding to pores having a radius of $r_i \pm (\Delta \log r_i)/2$. It is necessary to use a logarithmic scale because a wide range of pore radius, meaning several orders of magnitude, are investigated. The PSD curves that are presented in this paper were all determined using a constant value for $\Delta(\log r)$ equal to 0.3.

Tested Material

The tested soil was a sandy loam from the eastern part of Switzerland, a morainic soil of the Swiss Central Plateau. The plasticity index of the soil was about 12 % and its liquid limit about 30 %. All the samples used in this study were prepared using the same procedure. After sampling in the field, the soil was air-dried, and after several days it was gently crushed and aggregates between 0.4 and 2 mm were selected by sieving. They were then wetted up to a mass water content of about 15 % and stored in an airtight container for at least one week in order to reach moisture equilibrium. The material was then statically compacted directly inside the desired oedometer up to a dry density of 14 kN.m^{-3}. In a last stage the samples were saturated. In the case of tests conducted under suction higher than 0, the desired suction was applied in several steps after the saturation phase prior to the application of the mechanical loading.

Hydromechanical Behaviour

The test program was set up in order to determine the mechanical behaviour of the selected material and its fabric evolution during loading. In order to achieve this last objective, several samples were prepared. Each was loaded up to a different maximum stress (15, 60, 250 and 1 000 kPa) under constant suction. At the present time, the program under null suction has been completed and one unsaturated test has been already conducted. This sample was loaded up to 1 000 kPa under a suction of 200 kPa (test Unsat). The obtained oedometric curves are plotted in Figure 2 for the saturated tests and in Figure 3 for the test conducted under a suction of 200 kPa. The mechanical parameters determined from these curves are the elastic compression index Cs, the plastic compression index Cc and the preconsolidation stress $p_0(s)$. These data are grouped in Table 1.

Test number	SAT	Ch1	Ch2	Max	Unsat
Applied suction (kPa)	0	0	0	0	200
Maximum applied stress (kPa)	15	60	250	1 000	1 000
$p_0(s)$ (kPa)	n.a.	15-20	15-20	15-20	90
Cc	n.a.	-0.30	-0.27	-0.28	-0.41
Cs	n.a.	-0.05	-0.06	-0.04	-0.18

Table 1. Mechanical parameters.
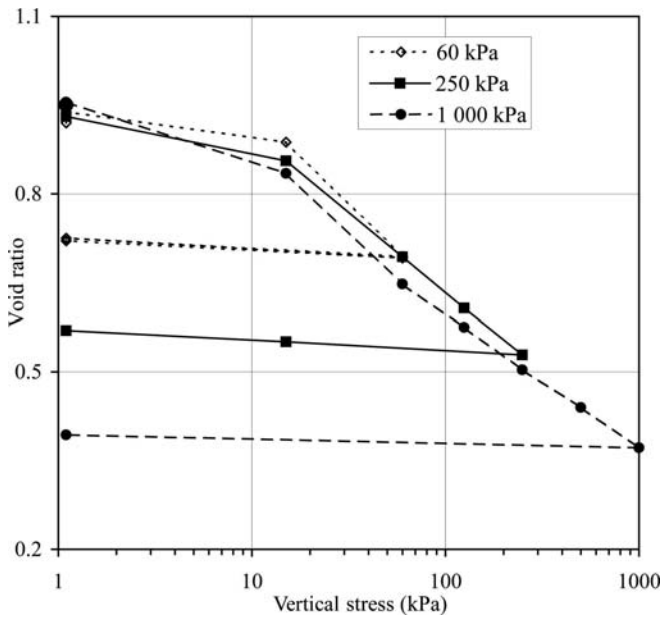
Fig. 2. Compression curves under null suction (tests Ch1, Ch2 and MAX).

The stress $p_0(s)$ is significantly higher in test Unsat than in the saturated tests and the parameter. This observation is very similar to the majority of existing data in the literature (e.g. Alonso et al. 1990). The value of Cs determined in test Unsat is significantly higher than Cs obtained in the saturated tests. This might be related to the fact that the unloading was performed in several steps during test Unsat whereas the unloading was done in one step in the saturated tests. On the other hand, it is interesting to note that the slope Cc is significantly lower in test Max, performed under null suction, than in test Unsat despite the applied suction being equal to 200 kPa in test Unsat. Geiser (1999) observed the same kind of behaviour on a silt and this author correlated the air entry value of the material with the suction for which Cc is maximal. Sivakumar and Wheeler (2000) obtained similar behaviour for lightly compacted kaolin. They demonstrated that this mechanical behaviour depends on the initial density of the material. In the case of the sample compacted under 400 kPa, Cc increases with suction, whereas in the case of the

sample compacted under 800 kPa, Cc decreases continuously with suction. The material behaviour observed in the tests presented in this paper is certainly related to the relatively loose initial density of the samples related to their low density. That conclusion is supported by data obtained by Cuisinier (2002) on a compacted swelling soil.
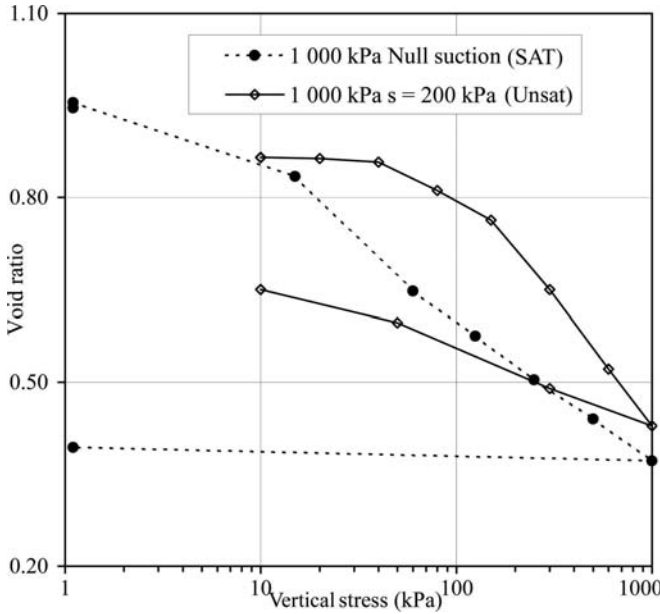
Fig. 3. Comparison of the compression curves under null suction and s = 200 kPa.

Fabric Evolution during Mechanical Loading

Saturated state

In order to validate the experimental procedure set up to determine the PSD with MIP, two MIP tests were undertaken from sample MAX. The results are plotted in Figure 4a for the injection curves and 4b for the PSDs. No significant differences were seen and hence repeatability was considered to be satisfactory.

It can be seen that the amount of injected mercury is directly related to the maximum pressure experienced by the sample: the higher the applied stress, the lower the injected mercury volume (Fig. 5). From the total volume of intruded mercury, it was possible to determine the porosity of the sample. The differences between theoretical values of the whole sample's porosity determined from oedometer tests

and porosity values estimated from the MIP test were always lower than 0.05. These results confirm that samples fabric was not significantly affected by the freeze-drying procedure. The PSD of test SAT allows the identification of two different pore classes inside the samples just prior to mechanical loading (Fig. 6). This indicated that the preparation technique allows the forming of samples with a "double structure", with micro and macropores, similar to compacted soil fabrics. The limit between the two pore classes could be situated approximately at a pore radius of 0.6 µm. Knowing this limit, it is possible to estimate the micro and microporosity of samples and their values in the different tests (Tab. 2).

   Together with the PSD curves, these data allow a representation of the modification of sample fabric during loading performed under a saturated state (Fig. 6). It appeared that the void ratio reduction occurs by the diminution of the amount of macropores without significant modification of the microporosity up to a vertical stress of 250 kPa. Beyond this value, a significant increase of the microporosity could be evidenced from PSD curves. The initial double structure of the samples is destroyed progressively and that confirms that void ratio reduction occurs by a progressive destruction of soil pores as stated by Delage and Lefebvre (1984). It is, however, interesting to note that a significant amount of macropores were not destroyed by the loading in test MAX.
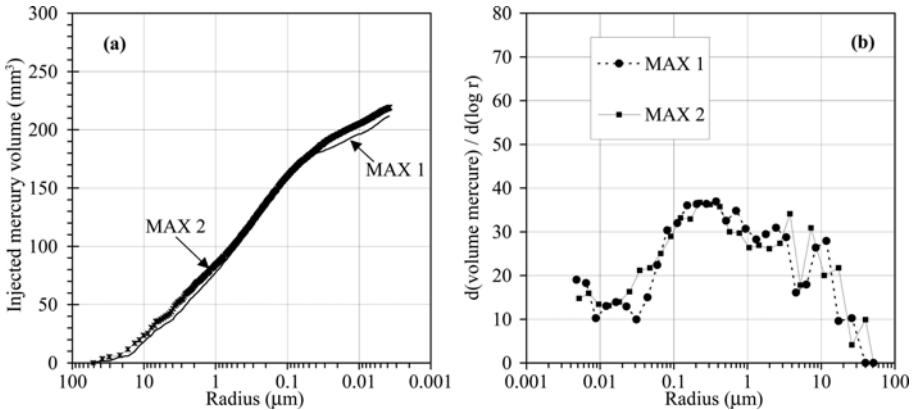
Fig. 4. Repeatability between MIP tests: (a) mercury injection curves; (b) PSD.

Test number	SAT	Ch1	Ch2	Max
Total pore volume (mm^3.g^{-1})	293.3	269.8	236.8	207.2
Total porosity	0.45	0.42	0.39	0.35
Macropore volume (mm^3.g^{-1})	179.5	155.4	119.9	89.1
Macroporosity	0.28	0.24	0.20	0.15
Micropore volume (mm^3.g^{-1})	113.8	114.4	117.6	118.1
Microporosity	0.17	0.17	0.19	0.20

Table 2. Modification of macro and microporosity during mechanical loading.
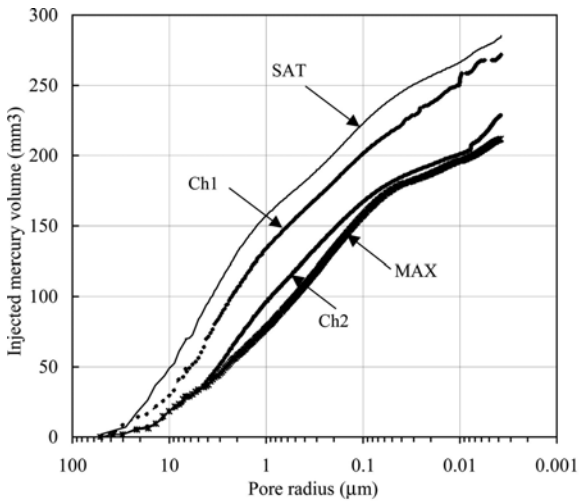
Fig. 5. Mercury injection curves of saturated samples loaded up to different vertical stress.
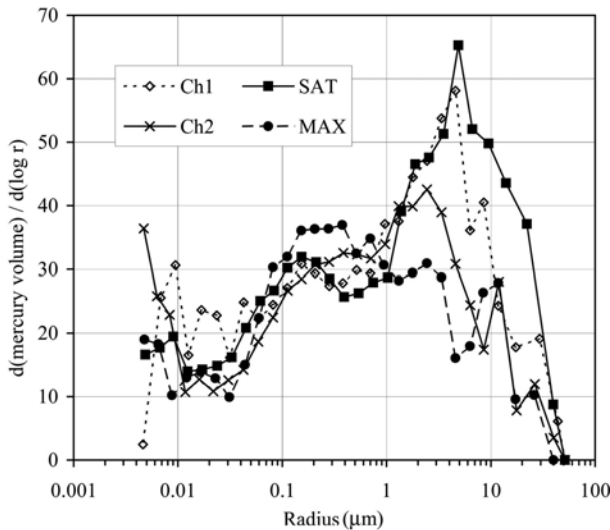
Fig. 6. PSD curves of the saturated samples loaded up to different vertical stress.

Suction Influence on the Deformation Process

The study of suction influence on the deformation process was undertaken by comparing MIP data obtained in the case of tests MAX and Unsat, as both samples were loaded up to the same vertical stress (Fig. 7 and 8). The MIP data are incomplete for the test Unsat as the minimal investigated radius was equal to only about 0.05 μm due to a technical problem encountered on the porosimeter. Consequently, it was not possible to determine the porosity of the unsaturated sample quantitatively from the data plotted in Figure 7.

Figures 7 and 8 tend to demonstrate that suction had a strong influence on the deformation process. It can be seen that the Unsat sample clearly exhibited a "double structure", whereas the sample MAX had a more homogenous fabric, as discussed previously. However, only pores lower than 8-9 μm seem to be affected by the applied suction. The amount of void having a radius comprised between 5 and 1 μm is lower in sample Unsat than in sample MAX, whereas the amount of pores smaller than 1 μm is the highest in sample Unsat. Two aspects could explain this phenomenon. First, fabric modifications produced by the suction imposition phase in test Unsat have to be taken into account. Simms and Yanful (2001) have shown that drying produced shrinkage of the macropores that shrink due to suction increase. This produces an increase of the micropore volume. Consequently, we can suppose that before the loading phase, the volume of micropores was higher in sample Unsat than in sample MAX. Second, as evidenced in the saturated tests, micropores are not significantly affected by mechanical loading. These two points could explain the differences between the samples MAX and Unsat.

An important observation is that after the loading/unloading phase, there are still macropores in the Unsat sample. This is similar to what was observed in test MAX. This might be related to the procedure employed to prepare the samples but additional data are needed to interpret these data further.
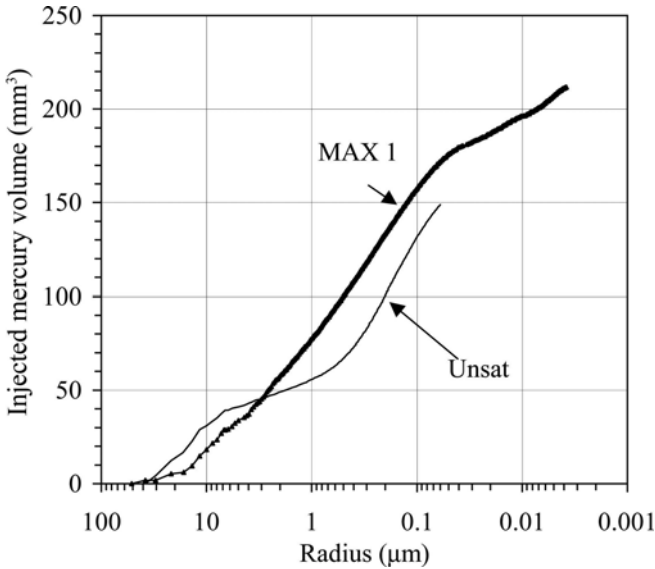
Fig. 7. Comparison of Max and Unsat tests mercury injection curves.
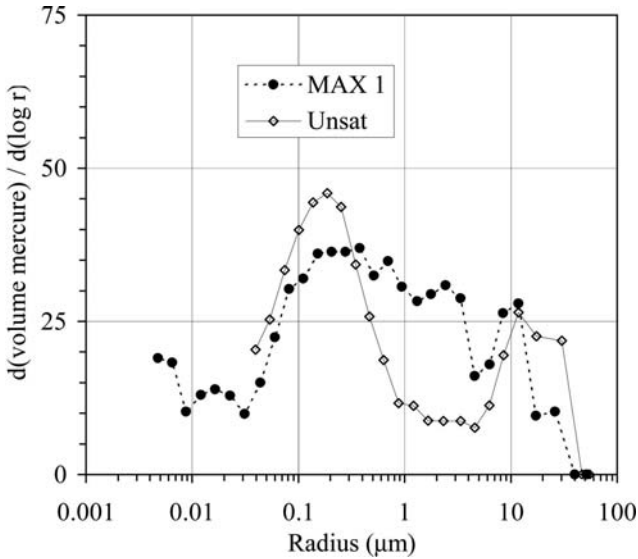
Fig. 8. Comparison of Max and Unsat tests PSD curves.

Conclusion

The paper presents the first results of a study undertaken to characterise the hydromechanical behaviour and the evolution of fabric as a function of the imposed stress/suction path of a compacted soil.

The unsaturated test was performed with a new suction controlled oedometer using the air overpressure method. The mechanical behaviour was determined under two suctions: 0 and 200 kPa. The pore space geometry of the soil was determined with mercury injection porosimetry. The MIP tests performed after the saturated mechanical tests have shown that stress increase produced a progressive destruction of the macroporosity which became significant for applied stresses higher than approximately 250 kPa. In addition, after an applied stress of 250 kPa, a significant increase of micropore volume was observed. The data already obtained under an applied suction of 200 kPa suggest that suction has a strong influence on the deformation process of soil. It seems that, for the same applied mechanical stress, fabric is strengthened by suction. In addition, the amount of micropores is higher in the unsaturated sample than in the saturated sample. Also, an important observation was the fact that all macropores did not disappeared following the application of stress/suction.

Additional tests will be performed under suctions of 100 and 200 kPa to characterise fabric modification fully as a function of suction and applied load and to depict the modification of the fabric that stems from suction variation. Then, the consequence of structural modification on other parameters, such as air permeability or water retention, will be undertaken.

Acknowledgements

References

Al-Mukhtar, M., Belanteur, N., Tessier, D. and Vanapalli, S.K., 1996. The fabric of a clay soil under controlled mechanical and hydraulic stress states. Applied Clay Science, 11, pp. 99-115.

Alonso, E.E., Gens, A. and Josa, A., 1990. A constitutive model for partially saturated soils. Géotechnique, 40, pp. 405-430.

Brustaert, W., 1968., The permeability of a porous medium determined from certain probability laws for pore-size distribution. Water Resources Research, 4, pp. 425-434.

Collins, K. and Mcgown, A., 1974. The form and function of microfabric features in a variety of natural soils. Géotechnique, 24, pp. 223-254.

Cuisinier, O. 2002. Hydromechanical behaviour of compacted swelling soils (in french). PhD thesis, INPL, Nancy, France, 165 p.

Delage, P. And Lefebvre, G., 1984. Study of the structure of a sensitive Champlain clay and of its evolution during consolidation. Canadian Geotechnical Journal, 21, pp. 21-35.

Geiser, F. 1999. Mechanical behaviour of an unsaturated silt – Experimental study and constitutive modelling (in French). PhD thesis, Lausanne, Switzerland, 224 p.

Gens, A. And Alonso, E.E., 1992. A framework for the behaviour of unsaturated expansive clays. Canadian Geotechnical Journal, 29, pp. 1013-1032.

Griffiths, F.J. And Joshi, R.C., 1989. Change in pore size distribution due to consolidation of clays. Géotechnique, 39, pp. 159-167.

Juang, C.H. and Holtz, R.D., 1986, A probabilistic permeability model and the pore size density function, Int. Journal of Numerical and Analytical Methods in Geomechanics, 10, 543-553.

Lambe, T.W., 1958, The engineering behaviour of compacted clays, Journal of the Soil Mechanics and Foundation Division, ASCE, 84, pp. 1-35.

Lapierre, C., Leroueil, S. and Locat, J., 1990. Mercury Intrusion and Permeability of Louisville clay, Canadian Geotechnical Journal, 27, pp. 761-773.

Leroueil, S. and Vaughan, P.R., 1990. The general and congruent effects of structure in natural soils and weak rocks. Géotechnique, 40, pp. 467-488.

Penumadu, D. and Dean, J., 2000. Compressibility effect in evaluating the pore size distribution of kaolin clay using mercury intrusion porosimetry, Canadian Geotechnical Journal, 37, pp. 393-405.

Qi, Y., Al-Mukhtar, M., Alcover, J.F. and Bergaya, F., 1996. Coupling analysis of macroscopic and microscopic behaviour in highly consolidated Na-laponite clays. Applied Clay Science, 11, pp. 185-197.

Richard, G., Cousin, I., Sillon, J.F., Bruand, A., and Guérif, J., 2001. Effect of compaction on the porosity of a silty soil: influence on unsaturated hydraulic properties. European Journal of Soil Science, 52, pp. 49-58.

Simms, P.H. and Yanful, E.K., 2001. Measurement and estimation of pore shrinkage and pore distribution in a clayey till during soil-water characteristic curve tests, Canadian Geotechnical Journal, 38, pp. 741-754.

Sivakumar, V. and Wheeler, S.J., 2000. Influence of compaction procedure on the mechanical behaviour of an unsaturated compacted clay. Part 1: wetting and isotropic compression, Géotechnique, 50, pp. 359-368.

Yong, R.N. and Warkentin, B.P., 1975. Soil properties and behavior. Developments in Geotechnical Engineering, 5. 449 p.

Measurement of osmotic suction using the squeezing technique

N. Peroni[1] (✉) and A. Tarantino[2]

[1]Dipartimento di Fisica e Ingegneria dei Materiali e del Territorio, Università Politecnica delle Marche, Via Brecce Bianche, 60131 Ancona, Italy, nicoletta_p@yahoo.it

[2] Dipartimento di Ingegneria Meccanica e Strutturale, Università degli Studi di Trento, via Mesiano 77, 38050 Trento, Italy, tarantin@ing.unitn.it

ABSTRACT: The paper presents an experimental determination of the osmotic component of suction by means of the squeezing technique. Soil was mixed with distilled water at different water contents and squeezed at different pressures. Osmotic suction was estimated from electrical conductivity of water extracted from the soil and two different empirical relationships were used to estimate osmotic suction. Experimental results have shown that osmotic suction depends upon the extraction pressure and the initial water content. The osmotic suction measured using the squeezing technique was then compared with the difference between total suction (measured with transistor psychrometer) and matric suction (measured with axis translation technique).

INTRODUCTION

The total suction ψ is made of two components, the matric suction s and the osmotic suction π ($\psi = s + \pi$). Both matric and osmotic suction depends on water content, although this dependency is controlled by different physical mechanisms. Matric suction is controlled by the interaction of soil particles with the pore water whereas osmotic suction depends on the concentration of ions dissolved in the pore water. Most researchers have focused on the relationship between water content and matric suction. Nonetheless, the osmotic suction may also play an important role in the hydro-mechanical behaviour of clayey soils.

Osmotic suction is present in both saturated and unsaturated soils. However, osmotic suction remains nearly constant in saturated soils (unless the soil is exposed to chemical contamination) whereas it can change significantly in unsaturated soils. As the soil losses water by evaporation, the concentration of the dissolved ions increases, and the osmotic component of suction also increases. A change in pore water concentration affects the interaction between clay particles and, hence, the mechanical behaviour of unsaturated fine-grained soils. As a re-

sult, the osmotic suction shall be regarded as a potential stress variable for unsaturated clayey soils.

The assessment of the osmotic component of suction is also important to match matric and total suction measurements. When determining water retention curves of clayey soils, more than one technique is required to cover the entire suction range. In the low suction range, measurement techniques are commonly based on migration of free water (e.g. axis-translation technique and tensiometer) and matric suction is measured. In the high suction range, measurement techniques are based on vapour migration (e.g. psychrometer) and the total component of suction is measured. When tracing the water retention curve over the entire range of suction, it is necessary to match matric and total suction measurements through the assessment of the osmotic suction.

Techniques for measuring soil osmotic suction are based on the extraction of pore water from the soil sample for the purpose of determining the amount of soluble salts contained in the extracted liquid. Several methods of pore water extraction are available, namely the immiscible liquid displacement or gas extraction method, the centrifuging method, the saturation extract method and the mechanical squeezing method (Iyer, 1990). The immiscible liquid displacement method and the gas extraction method can only be used for sand or silty soils whereas the centrifuging method is reported to be quite satisfactory especially with sands and silts (Iyer, 1990). The saturation extract method and the high pressure squeezing technique are employed for pore water extraction from clays and clay shales.

The pore fluid squeezer technique has shown to give the most reasonable measurement of osmotic suction (Krahn & Fredlund, 1972; Wan, 1996). This technique consists in squeezing a soil specimen to extract the macropore water and then measuring its electrical conductivity. This can be related to the total concentration of dissolved salts, which can in turn be related to the osmotic suction of the soil.

Romero (1999) has made significant contribution to the measurement of osmotic component of suction. The author validated two empirical relationships to correlate the electrical conductivity to the osmotic suction. To this end, the osmotic suction determined via electrical conductivity was compared to the osmotic suction determined from the relative humidity of the air in equilibrium with the extracted pore water (transistor psychrometer). Substantial agreement was observed between the two methods.

Furthermore, Romero (1999) assessed the validity of the squeezing technique by calculating the osmotic suction as the difference between total and matric suction values, obtained by Wan (1996) using non-contact and contact filter paper respectively. The values of total minus matric suction were found to closely agree with the values of osmotic suction estimated on the basis of the electrical conductivity.

In general, the results of the squeezing technique measurements appear to be affected by the magnitude of the extraction pressure applied (Engelhardt & Gaida, 1963; Iyer, 1990) and this influence is found to depend on the type of soil.

This paper presents an experimental investigation on the osmotic suction of kaolin using the squeezing technique. Osmotic suction was estimated from electri-

cal conductivity of pore water extracted from the soil, using the two relationships validated by Romero (1999). The effects of the extraction pressure and the initial water content of the soil were first analysed. Then, the osmotic suction measured from electrical conductivity was compared with the difference between total suction (measured with transistor psychrometer) and matric suction (measured with axis translation technique).

EXPERIMENTAL APPARATUS

Osmotic suction was investigated using the pore fluid squeezer. It is a heavy-walled stainless steel cylinder with a squeezer piston (Figure 1). A concave seat was centrally machined in the upper part of the piston to accommodate a high resistance steel sphere and allow the centring of the vertical load. The vertical load was applied to the piston through a hydraulic load frame. A rigid ertalon disc and a neoprene disc were placed between the piston and the upper base of the soil sample. The former ensured a uniform load distribution on the specimen and the latter ensured that water did not escape through the annular gap between the piston and the inner wall of the cylinder.
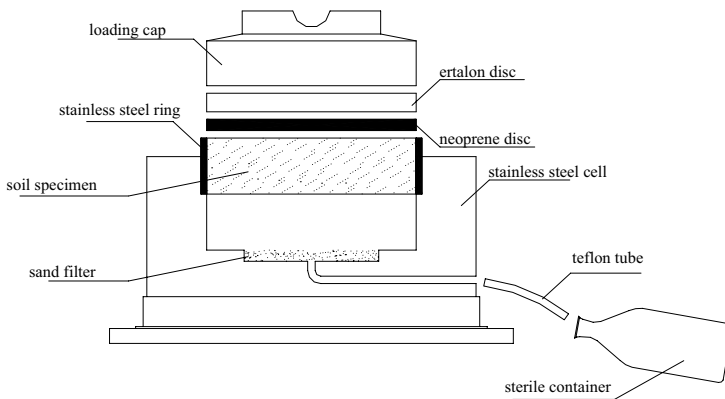
Fig. 1. Scheme of pore fluid squeezer (Peroni, 2002).

The soil specimen, having diameter of 56 mm and height of 15 mm, was placed on a sand filter. The sand filter was used in place of ceramic porous stone, bronze porous disc, or geotexile because it is permeable, chemically inert and does not experience significant grain crushing when loaded at high vertical stresses. As shown later in the paper, chemical inertness of washed sand was verified measuring the electrical conductivity of distilled water maintained in contact with the sand for 24 hours. The measured electrical conductivity appeared negligible

(20 μS/cm). The sand filter was placed at the bottom of the stainless steel cell and connected to a sterile container using a 3 mm diameter teflon tube. The extracted liquid was collected into the sterile container.

TEST MATERIAL AND SPECIMEN PREPARATION

Commercial processed kaolin (Rotoclay HB Goonvean, St.Austen, UK) was used in the present research work. The physical properties of the material are summarised in Table 1.

Table 1. Properties of Rotoclay kaolin

Property	Reference	Value
Principal mineral	Product information	kaolinite
Specific gravity (G_s)	ASTM D854	2.65
Liquid Limit (LL)	ASTM D4318	52%
Plastic Limit (PL)	ASTM D4318	35%
Plastic Index (PI)	ASTM D4318	17%
Activity (A)	-	0.68
Particle Sizes:		
Silt (0.002÷0.074 mm)	ASTM D422	75%
Clay (<0.002 mm)	ASTM D422	25%
Maximum dry unit weight (γ_{dmax})	ASTM D698	14.3 kN/m^3
Optimum water content (w_{opt})	ASTM D698	28.5%

To prepare the samples, kaolin powder was sprayed with distilled water ($EC < 20$ μS/cm) to target gravimetric water contents (ranging from 29.6% to 52.3%). These water contents were sufficiently high to extract an adequate amount of pore water for measurement of electrical conductivity. At the same time, they were sufficiently low to avoid excessive dilution of pore water. The moist powder was hand-mixed and stored in a plastic bag for one day to allow moisture equalisation.

EXPERIMENTAL PROCEDURE

Before placing the soil sample inside the pore fluid squeezer, every part of the apparatus was first washed with alcohol and then rinsed three times with distilled water, in order to reduce contamination of the pore liquid as much as possible.

Sand was put at the bottom of the pore water squeezer. In order to assure that the sand did not alter the chemical content of the pore liquid, it was first washed with chlorine solution, then rinsed three times with distilled water and finally dried at a temperature of 105 °C for 24 hours.

The remoulded soil sample was placed into the pore fluid squeezer and then covered with the neoprene disc and the ertalon disc. Finally the piston was placed on the specimen and the squeezer was connected to the sterile container by a teflon tube. The tube connections were sealed with parafilm in order to avoid evaporation of pore water.

Vertical stress was applied in steps to a predetermined extraction pressure and held until no more water was expelled (at least 24 hours). For initial gravimetric water contents lower than the plastic limit PL of the soil, especially at the lower extraction pressures, it was necessary to repeat the procedure two or three times in order to collect a representative amount of pore water.

Before measuring the electrical conductivity, the extracted liquid was filtered with a vacuum pump system and an ultra-fine White HAWP glass fibre filter paper, having pore diameter less than 1 μm. Filtration is necessary to retain colloidal flocculated clay particles which could alter conductivity readings (Romero, 1999).

An electrical conductometer was used to measure the conductivity of pore water. The instrument can automatically correct the measurement to account for temperature changes. Osmotic suction was estimated from the electrical conductivity of the extracted water using the following empirical relationships:

$$\pi = 0.0191\ EC^{1.074} \qquad \text{(U.S.D.A., 1950)} \qquad (1)$$

$$\pi = 0.0240\ EC^{1.065} \qquad \text{(Romero, 1999)} \qquad (2)$$

where π is the osmotic pressure in kPa and EC the electrical conductivity in μS/cm. Both expressions are based on exponential correlations between electrical conductivity and osmotic suction. The first expression was proposed by the U.S.D.A. Agricultural Handbook N.60 (1950) (quoted in Fredlund & Rahardjo, 1993) and was obtained with water solutions containing mixture of dissolved salts; the second one was determined with homoionic NaCl solutions by Romero (1999). The two curves led to quite close osmotic suction values (differences were less than 15% for osmotic suctions greater than about 40 kPa).

In the present study, two sets of squeezing tests were performed. The first one was performed on samples prepared at different initial gravimetric water contents (from 29.6% to 52.3%), applying the same extraction pressure of 3 MPa. The maximum water content was chosen according to the procedure for free pore water squeezing proposed by ASTM D4542 (1993). This recommends an initial water content less than the liquid limit to avoid leaching of dissolved salts with consequent alteration of the original saline content of the pore water. The second group of tests was performed on kaolin samples at the same initial gravimetric water content ($w = 32\%$) applying different extraction pressure (3, 12, 28 and 35 MPa).

EXPERIMENTAL RESULTS AND INTERPRETATION

Experimental results obtained by the two sets of squeezing tests are shown in Figure 2 and Figure 3. There seems to be good agreement between the two empirical expressions used to correlate osmotic suction with the electrical conductivity.

The variation of the osmotic suction versus the initial gravimetric water content is shown in Figure 2. It can be seen that osmotic suction decreases as the initial water content of soil increases. In particular, its variation is more significant in the water content range from 29.6% to 40%, whereas it seems to approach a constant value at higher water contents. The variation of the solute concentration and, hence, of the osmotic suction with water content has also been reported by Iyer (1990) when using the saturation extract technique.

The variation of the osmotic suction versus the extraction pressure is shown in Figure 3. It can be observed that estimated osmotic suction decreases as the extraction pressure increases. The reduction in osmotic suction is relatively small, being about 25% of the value at the lowest extraction pressure. It then appears that the squeezing pressure has less influence than the initial water content on the osmotic suction.

The variation of osmotic suction with the extraction pressure can be explained by considering the interaction between the soil water with the clay particles. In a dry clay powder, adsorbed cations are strongly held by the negatively charged clay particles. Cations in excess of those needed to neutralise the electronegativity of the clay surface and associated anions are present as salt precipitates (Mitchell, 1976). Upon wetting, these precipitated salts go into the free solution contained in the macro-porosity which is mainly the pore water being extracted by squeezing technique at low extraction pressures. As the squeezing pressure is increased, the salts contained in micro-porosity water (diffused double layer) will not be dissolved in the free water due to the "restrictive membrane effect" (Mitchell, 1976). Cations would tend to diffuse away from the micro-porosity level desiring to equalise concentration throughout. However, the diffusing tendency is restricted by the negative electrical field originated at particle surfaces which acts a restrictive semipermeable membrane separating regions of high concentration midway between particles and the low concentration zones in the solution surrounding the peds. The adsorbed cations will tend to increase liquid concentration at the particle mid-plane to counterbalance the higher squeezing pressure. As a result, salt concentration of the extracted pore water and, hence, osmotic suction, decrease as the squeezing pressure increases.

Iyer (1990) reported different values of pore water concentrations when applying different squeezing pressures. He found that concentrations of cations of the squeezed water at pressures less than 20 MPa remained approximately constant, becoming representative of the macro-porosity and the outer double layer. At higher squeezing pressures, concentration decreased supposedly due to the mixing of the free pore water with water in the double-layer. Iyer (1990) suggested that this threshold squeezing pressure should be established for each soil. However, this threshold squeezing pressures could not be detected for soil tested (Fig. 3).
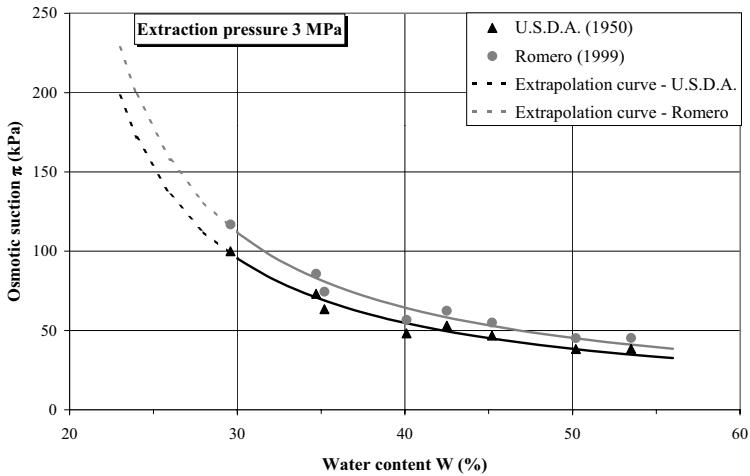
Fig. 2. Osmotic suction versus gravimetric water content (Peroni, 2002)

The investigation was completed by comparing the osmotic suction estimated from extracted pore water to the difference between total suction (measured with transistor psychrometers) and matric suction (measured with a suction controlled oedometer using axis translation technique). To this end, samples for total and matric suction measurement were prepared at the same target water content, using the same soil adopted for pore water extraction technique.
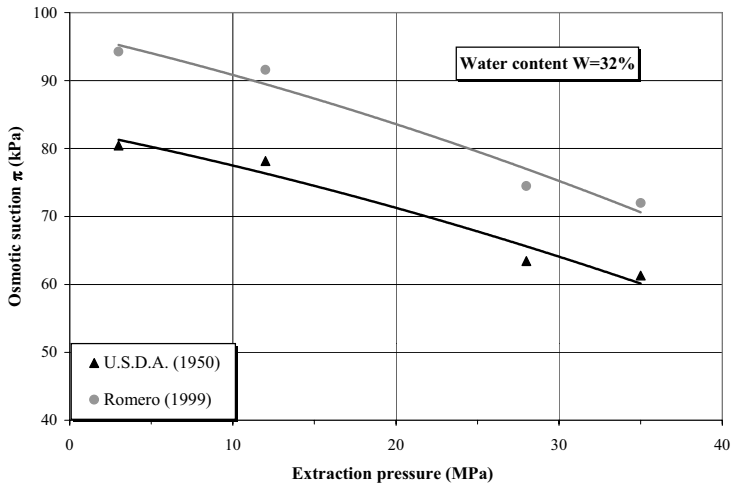
Fig. 3. Osmotic suction versus extraction pressure (Peroni, 2002)

Kaolin samples were moistened with distilled water at the predetermined water content of approximately 23% and were dynamically compacted (Proctor Standard procedure) at the same initial dry unit weight (γ_{dmax} = 14 kN/m^3). This water content was a compromise solution. The water content needed to be closest to the range of water contents investigated by the squeezing technique (29.6% to 52.3%). However, higher water contents would have produced very low total suctions, which would have been difficult to measure with the transistor psychrometer.

Ten specimens having a diameter of 15 mm and a height of 12 mm were cut from the compacted samples and used to measure total suction using the transistor psychrometers. The SMI transistor psychrometer (Woodburn et al., 1993) allows the measurement of the relative humidity of the air within a confined space and it can be used to measure total suction values from 0.5 MPa to greater than 10 MPa.

All specimens were used to determine a single total suction value in order to minimise the measurement errors and the effect of dishomogeneity in water content and structure. Every total suction measurement lasted one hour. The average total suction value was approximately 0.60 MPa.

Three specimens having a diameter of 50 mm and a height of 20 mm were cut from compacted samples and used to estimate matric suction using an axis-translation oedometer.

The kaolin specimens were subject to an initial suction of 0.4 MPa and then wetted under constant net vertical stress applying the following matric suction path: 0.4 MPa, 0.3 MPa, 0.2 MPa, 0.1 MPa and 0.01 MPa. Suction was reduced maintaining constant the air pressure at 0.5 MPa and slowly increasing water pressure (air over pressure technique). During each matric suction decrement, water volume inflow/outflow were monitored. This made it possible to back calculate gravimetric water content at the end of each suction decrement. It was found that matric suction corresponding to the gravimetric water content of 23% was approximately 0.35 MPa. As a consequence the difference between the total and the matric suction was estimated as π = 0.25 MPa.

To determine the osmotic suction corresponding to the water content of 23%, it was necessary to extrapolate the data obtained in the range 29.6% to 52.3% (Fig. 2). The extrapolation function was defined on the basis of simple physical assumptions.

Romero (1999) have showed that the relationship between osmotic suction π and concentration of the salt solution is approximately linear in the range 0-1000 kPa when using homoionic solutions:

$$\pi \propto C \tag{3}$$

where C is the concentration of the solution, defined as the mass of salts to mass of extracted water ratio. The concentration C of the pore water is given by:

$$C = M_{salt} / M_{w\,free} \tag{4}$$

where M_{salt} is the mass of salts dissolved in water and $M_{w\,free}$ is the mass of free pore water. The latter can be expressed as:

$$M_{w\,free} = M_w - M_{w\,bonded} \tag{5}$$

where M_w is the total mass of water and $M_{w\,bonded}$ is the mass of bonded water. If M_s is the mass of the solids, w is the water content and w_{bonded} is the water content associated with the bonded water, we can combine equations (3), (4), and (5) as follows:

$$\pi \propto M_{salt} / [M_s\,(w\text{-}w_{bonded})] \tag{6}$$

As a first approximation, we can assume that the mass of dissolved salts is independent of water content. Accordingly, the extrapolation function takes the form:

$$\pi = A / [(w\text{-}B)] \tag{7}$$

where A and B are fitting parameters. Data shown in Fig. 2 were then interpolated using equation (7) and the parameters A and B were determined using the least square method. The extrapolation curves are shown in Fig. 2 as dashed lines. At water content of 23%, the osmotic suction was found to be 0.20 MPa and 0.23 MPa when using equations (1) and (2) respectively. The average osmotic suction was then 0.21 MPa, a value that is very close to the one obtained from the difference between total and matric suction (0.25 MPa). It would therefore seem that this extrapolation function can be used to estimate osmotic suction to the range of low degrees of saturation, where pore water is difficult to extract from the unsaturated soil.

CONCLUSIONS

An experimental program was carried out to assess the reliability of the squeezing technique for measuring osmotic suction. A pore fluid squeezer was used to extract pore water from kaolin samples. Electrical conductivity of extracted pore water was measured and related to osmotic suction using two different relationships proposed in the literature.

To investigate the role of initial water content tests were performed at different water contents and constant squeezing pressure. To investigate the role of the squeezing pressure, tests were performed at different squeezing pressures and constant water content.

Experimental results have shown that osmotic suction depends upon the initial water content and the extraction pressure. However, changes in osmotic suction in response to squeezing pressures appear small when compared to the osmotic suction changes associated with changes in initial water content.

The osmotic component estimated using the squeezing technique was then compared with the difference between total suction (measured with transistor psychrometers) and matric suction (measured with axis translation technique). To this end, an extrapolation function based on simple physical assumptions was proposed to extrapolate osmotic suction to the range of lower water contents. This

function fits satisfactorily the experimental data. Most of all, the extrapolated osmotic suction seems to be good agreement with the difference between the total suction and the matric suction.

This good agreement seems to support the reliability of the squeezing technique for osmotic suction measurements, as well as the extrapolation method used to estimate osmotic suction at the lower water contents. The results also seem to support the validity of the two empirical relationships proposed in the literature used to correlate osmotic suction to the electrical conductivity.

Acknowledgements

REFERENCES

ASTM (1993) "Annual book of ASTM standards", *Vol. 04.08, Philadelphia.*

Engelhardt, W.V. e Gaida, K.H., 1963, "Journal of Sedimentary petrology", *Vol. 33, pp. 919-930.*

Fredlund, D.G. & Rahardjo, H. (1993) "Soil mechanics for unsaturated soils" *John Wiley & Sons, Inc. New York.*

Krahn, J. E Fredlund, D.G., 1972 "On total, matric and osmotic suction", *Soil Science, Vol. 114, n.5, pp.339-348.*

Iyer, B., 1990 "Pore water extraction-comparison of saturation extract and high-pressure sqeezing", *Physo-chemical aspects of soil and related materials, ASTM STP 1095, K.B. Hoddinott and R.O. Lamb, Eds., American Society for Testing and Materials, Philadelphia, pp. 159-170.*

Mitchell J. K. (1976) "Foundamentals of soils behavior" *Ed. J. Wiley & Sons, New York.*

Peroni, N. (2002) "Contributo allo studio delle proprietà idrauliche e della deformabilità di un terreno insaturo" *PhD Thesis, Università degli Studi di Ancona, Italy.*

Romero, E. (1999) "Characterisation and thermo-hydromechanical behaviour of unsaturated Boom Clay: an experimental study", *PhD Thesis, Universitad Politecnica de Cataluna.*

U.S.D.A. (1950) "Diagnosis and improvement of saline and alkali soils" *Agricultural Handbook n. 60.*

Wan, A.W.L. (1996) "The use of thermocouple psychrometers to measure in situ suctions and water contents in compacted clays" *PhD Thesis, University of Manitoba.*

Woodburn J.A., Holden J. & Peter P. (1993) "The transistor psychrometer: a new instrument for measuring soil suction", *in S.L.Houston and W.K. Wray (eds.), Unsaturated soil – Geotechnical Special Publications n. 39, ASCE, Dallas: 91-102.*

The use of different suction measurement techniques to determine water retention curves

M. Boso[1], E. Romero[2], and A. Tarantino[1]

[1] Dipartimento di Ingegneria Meccanica e Strutturale Università degli Studi di Trento, Italy
[2] Departament d'Enginyeria del Terreny, Cartogràfica i Geofísica, Universitat Politècnica de Catalunya, Spain

Introduction

One of the problems of determining the water retention curve is that many techniques are often required to cover the entire range of suction. In particular, this applies to clayey soils where suction range can extend over hundreds of MPa. Each measurement technique is capable of measuring a limited range of suction and therefore provides only a part of the retention curve.

Techniques for suction measurement can involve either liquid or vapour transfer. The former measure matric suction, the latter measure the total suction.

The suction measurement techniques can be also distinguished between direct and indirect. A direct technique consists of measuring water tensile stress, while indirect techniques exploit thermodynamic and physical laws to link suction with other measurable variables, e. g. the relative humidity of the pore air.

To compare different measurement techniques it is necessary to perform tests on similar samples, but because of the several assumptions underling each technique, suction data may not be fully consistent. The different stress paths followed on the application of these techniques may significantly affect water retention properties of the material. As a result, the stress paths followed must also be accounted for when comparing suction measurements from different techniques.

This paper presents water retention data obtained with three different techniques: the axis translation technique, the extended range transistor psychrometer and the high-suction tensiometer.

The axis translation technique is an indirect method that involves the control of air pressure and water pressure as boundary conditions. It was implemented following two different procedures in two pressurised cells (oedometer and shearbox cells) to investigate the low suction range. These tests were performed at constant vertical net stress.

The extended range transistor psychrometer is an indirect method for total suction measurement and measures the relative humidity in equilibrium with the soil (vapour phase equilibrium). It was used to investigate the high range of suction and measurements were performed under null net stress.

The intermediate zone of the retention curve was covered by the high-suction tensiometer. This is a direct measurement technique and the equilibrium is achieved through the liquid phase. Also in this case measurements were performed under null net stress. These techniques were used to trace the main drying curve of a reconstituted clayey silt.

An attempt was made to overlap the suction ranges explored by each technique in order to verify their consistency, as well as to study the effects of the stress paths followed on water retention characteristics.

Tests were performed on samples normally consolidated from slurry which were subsequently dried. One test was performed directly starting from slurry.

Tested material and specimen preparation

The material studied was taken from the Campus Nord of the Universitat Politècnica de Catalunya of Barcelona. Physical properties of the silty/clay material are shown in Table 1. The clay fraction is constituted predominantly by illite (Barrera 2002).

To fabricate the samples, a slurry was prepared at a water content 1.5 times the liquid limit. For nearly all the tests, the slurry was consolidated at a vertical effective stress of 100 kPa. In the case of the oedometer test, the slurry was directly poured into the oedometer cell. For tests using the high-suction tensiometer and the transistor psychrometer, the consolidated slurry was air-dried to target water contents. The samples were sealed into plastic bags and stored in a high-humidity chamber for moisture equalisation.

Table 1. Basic properties of the BCN silt.

Clay (%)	Silt (%)	Sand (%)	γ_s (kN/m^3)	w_h* (%)	w_L (%)	w_P (%)	$I_P = w_L - w_P$
20	43	37	26.6	1.8	31.8	16.0	15.8

* hygroscopic humidity (mass basis) at a relative humidity of 50%

The mercury intrusion porosimetry was used to determine the pore size distribution of the consolidated slurry before and after a main drying path with no external stress applied (Delage et al. 1996). Fig. 1 shows the two pore size density functions, in which a clear mono-modal distribution is observed that corresponds to the dominant matrix structure of the slurry condition.

The consolidated slurry exhibits a dominant pore size at 4.9 μm. On main drying to a suction of around 500 kPa, the consolidated slurry undergoes shrinkage at expense of the dominant pore size, defining a new mode at a lower value of 850

nm. The estimated suction needed to desaturate the dominant pore size (air-entry value) of the consolidated slurry is around 60 kPa, as estimated from the Laplace equation. The estimated value for the consolidated slurry after undergoing the drying path is around 340 kPa.
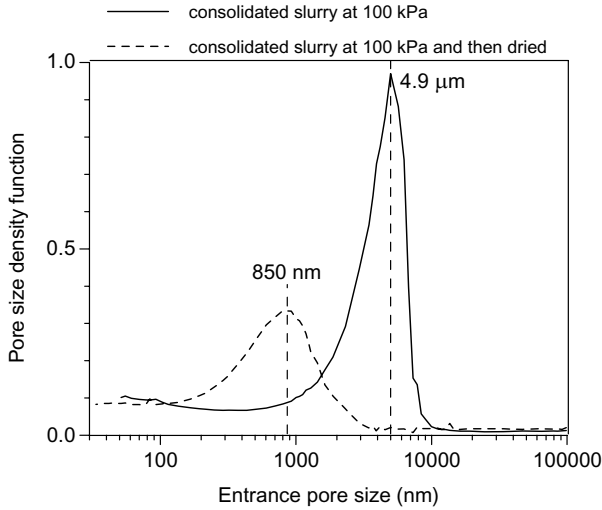
Fig. 1. Pore size density functions of the consolidated slurries. The dashed line represents the condition after undergoing a main drying path with no external stress applied.

The drying process of a normally consolidated soil under nearly saturated conditions and with no external stresses applied has many similarities with the mechanical consolidation of the same saturated soil (Toll 1995). An oedometer test was performed on a normally consolidated and saturated sample to complement this mechanical information. The virgin compression line displayed a slope of - $\delta e / \delta(\ln\sigma'_v) = 0.081$. On subsequent unloading – reloading paths the saturated material displayed a slope of 0.017.

Experimental equipment and procedures

Axis translation technique

The procedure consists of increasing pore air pressure to a constant value u_a, greater than the atmospheric pressure, in order to translate the pore-water pressure in the positive range, where it can be easily controlled/measured (Hilf 1956). The axis translation technique was implemented in pressurised oedometer and direct

shearbox cells. The cells were equipped with an HAEV ceramic disc to ensure the continuity between the pore-water and the water in the measuring system and with a peristaltic or ram pump to flush out the air bubbles accumulated below the ceramic.

Two different procedures were followed to apply matric suction: a) air overpressure technique, in which a constant air pressure was maintained and water pressure was regulated (oedometer cell), and b) water sub-pressure technique, in which a constant water pressure was applied and air pressure was varied (direct shear cell).

The first procedure was applied on slurry that was directly poured into the oedometer cell. The first stage of the procedure consisted of alternatively increasing the air pressure and the vertical stress in order to maintain the net vertical stress below 30 kPa. These air pressurisation and loading stages were carried out under nearly water undrained conditions until the desired air pressure (u_a = 600 kPa) and vertical net stress ((σ_v-u_a) = 30 kPa) were reached. During the initial process, significant vertical settlements were recorded due to the presence of occluded air bubbles in the slurry and the soil extrusion through the gap between the loading cap and the oedometer ring. Di Mariano (2000) observed significant vertical settlements during the air pressurisation process at high degree of saturation and suggested increasing air pressure at slow rates and before any loading path.

Towards the end of the process an elastic response was obtained while cycling the vertical net stress, which indicated that air overpressure technique was correctly applied. Afterwards the water drainage was open to apply a target water pressure at the base of the sample and hence a target suction. The drying path was carried out at constant (σ_v-u_a) = 30 kPa, while changing water pressure in a stepwise procedure. The water outflow was measured by a burette connected to the water pressure line. The applied suction steps were 0.01, 0.05, 0.1, 0.2, 0.5 MPa, according to the hydro-mechanical path shown in Fig. 2a). At the end of the test the sample was extracted from the cell and its water content was measured.

The second procedure (water sub-pressure technique) was applied in the shearbox cell on samples previously consolidated at a vertical effective stress of 100 kPa. The experimental procedure consisted in applying a vertical net stress of 100 kPa (the same as the consolidation stress) and then increasing matric suction to the target value by increasing air pressure around the sample and keeping water pressure atmospheric below the HAEV ceramic. The stress path followed during preparation of the sample and the drying path in the controlled-suction shearbox cell are shown in Fig. 2b). After consolidation the sample was unloaded, reloaded in the box cell at the same vertical stress and then suction was increased to the target value. At the end of the shear test the sample was extracted from the cell and its water content measured (Boso in prep.).
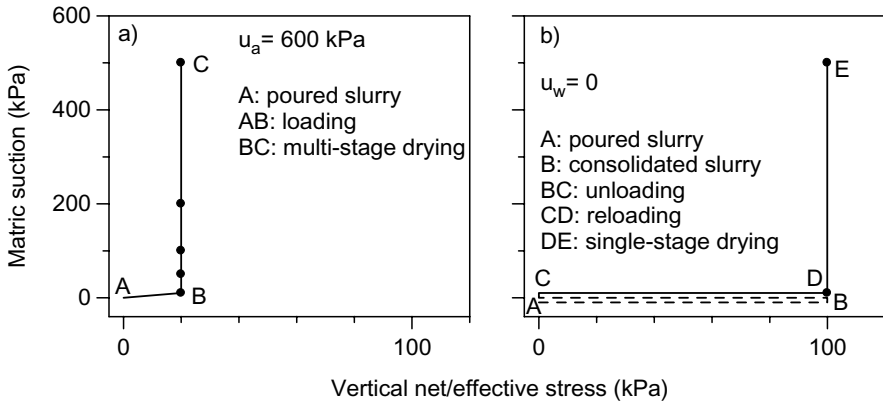
Fig. 2. Stress paths followed: a) air over-pressure technique (loading, multi-stage drying); b) water sub-pressure technique (consolidated slurry, reloading, single-stage drying).

Extended range transistor psychrometer

Transistor psychrometers (SMI, Woodburn et al. 1993) with an extended measuring range were used to complement the retention curve information in the total suction range from 1 to 70 MPa. The psychrometer probe is shown in Fig. 3b and consists of two transistors, which act as wet bulb and dry bulb. The output voltage produced by the transistor can be related to the relative humidity (or total suction) through a suitable and extended calibration (Mata et al. 2002).

Measurements were performed on six specimens cut from the same sample. After each measurement, the specimens were air-dried for some hours at the relative humidity of the laboratory (50%), stored for one day for moisture equalisation, weighed and total suction measured again. At the end of the multi-stage drying procedure, the specimens were weighed, oven-dried and the water contents were back-calculated. The stress path followed during this multi-stage drying procedure with no external stresses applied is shown in Fig. 4a.

High-suction tensiometer

The tensiometer allows direct measurement of the negative pore water pressures (water tensile stress). Fig. 3a shows a schematic layout of the tensiometer (Tarantino & Mongiovì 2002).

Reliable measurement of water tensile stress requires adequate saturation of the porous ceramic. Saturation of the ceramic was checked before and after measurements according to the procedure described by Tarantino (2003).

Two kinds of measurement were performed: monitoring matric suction during a continuous drying process ('dynamic' procedure) and measuring suction under constant water content ('static' procedure).

The 'dynamic' determination was achieved by placing the sample along with the tensiometer on a balance. The changes in sample mass and suction were continuously monitored by a data acquisition system. Water content was estimated considering the changes in sample mass as changes in water.

This procedure assumes that the matric suction in the sample is uniform. However, it can be partially affected by the excessive evaporation along the boundaries in contact with the air of the laboratory. In order to slow down this evaporation the bottom surface of the sample, where evaporation took place was covered with a synthetic textile. The stress path followed during this continuous drying procedure with no external stresses applied is shown in Fig. 4b.

The 'static' determination was achieved by constant water content measurements performed on the same sample air-dried to target water contents at null stress using a multi-stage procedure. Before each measurement the sample was left to equalise in plastic bags placed in a high-humidity chamber for two days at least. During measurement, the sample was wrapped in clingfilm in an attempt to minimise evaporation. Special attention was given to the isolation of the paste that 'connects' the tensiometer to the sample. The stress path is similar to the one shown in Fig. 4b, but the drying path CD was in steps.
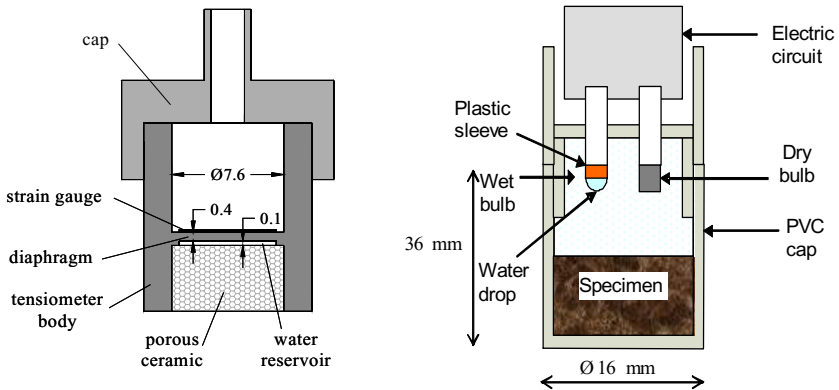

Fig. 3. (a) Schematic layout of the tensiometer (Tarantino & Mongiovì 2002). (b) Transistor psychrometer probe (Woodburn et al. 1993).
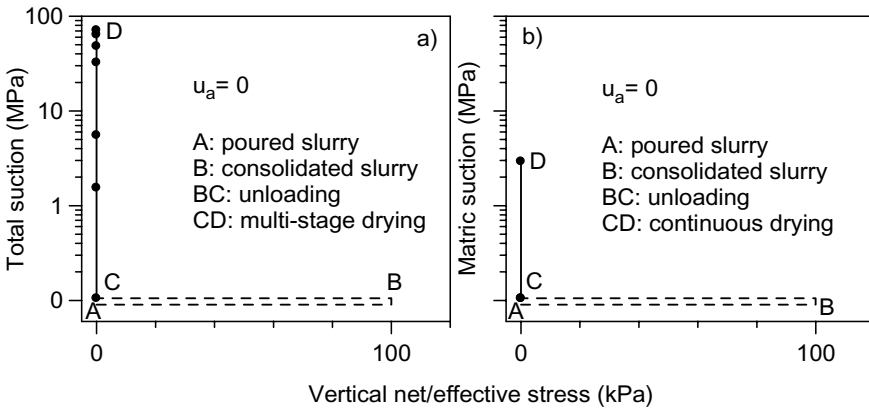
Fig. 4. Stress paths followed: a) psychrometer (consolidated slurry, unloading and multi-stage drying); b) tensiometer "dynamic curve" (consolidated slurry, unloading and continuous drying).

Test results and interpretation

Fig.5 shows test results obtained with the controlled-suction oedometer (air over-pressure technique), with the tensiometer using the 'dynamic' and 'static' procedures and with the psychrometer. It is interesting to note that the suction ranges covered by these instruments and techniques could overlap each other, making it possible to compare the experimental procedures.

Tensiometer data display approximately the same drying curve, showing that both 'dynamic' and 'static' procedures are equivalent if the same stress paths are followed and adequate experimental procedures are implemented. In the following, the directly measured suctions with tensiometer will be used as the reference data for the comparison of the different experimental results, due to its good reproducibility and the extension of the overlapping with the different techniques.

As shown in Fig. 5, controlled-suction oedometer and tensiometer test results tend to converge following approximately a linear relationship between the logarithm of matric suction and the water content. However, for equivalent matric suctions over 100 kPa, the water stored using controlled-suction technique is lower than the measured one using the tensiometer.

This difference can partly be explained by the non-uniform matric suction distribution when axis translation technique is used. Matric suction is only controlled at the bottom of the sample by liquid water transfer. At the top boundary of the sample in contact with the relative humidity of the air chamber, another suction (total component) is applied through vapour transfer. Numerical simulations performed by Romero (1999) have shown that the upper part of the sample undergoes

drying by vapour transfer at early stages of the equalisation phase due to the high-applied total suction.

However, this evaporative flux reduces as the relative humidity of the air chamber increases. Meanwhile, matric suction along the sample height tries to equalise to the applied value at the bottom boundary in contact with the ceramic disc. Finally, under steady-state conditions, a non-uniform matric suction distribution is attained with a higher value at the top boundary due to the evaporative flux that has not vanished. In this way, slightly higher values of matric suction are expected compared to the applied one when plotting the retention curve with the mean value of the water content (Romero 1999). Consequently, axis translation data are shifted towards lower matric suctions compared to tensiometer data.

Fig. 5 also shows a comparison between tensiometer and psychrometer data. In both cases the same stress paths were followed and measurements were carried under atmospheric conditions (Fig. 4a and 4b). However, the comparison is still not straightforward, as the psychrometer measurement is associated with total suction, while the tensiometer is related to the matric component.
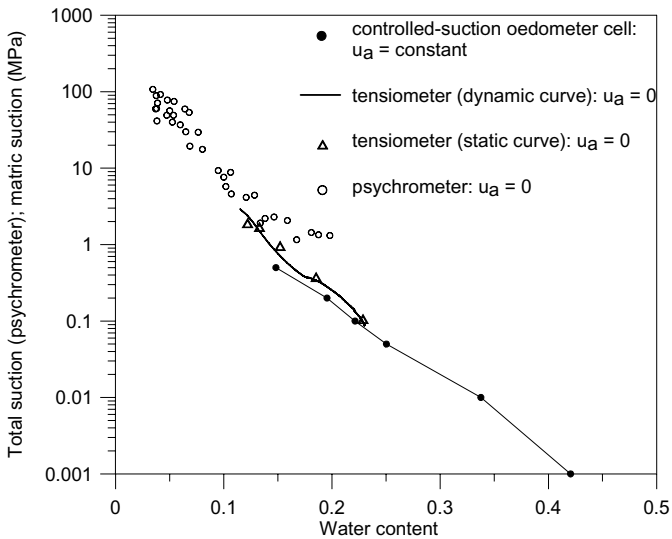

Fig. 5. Psychrometer, tensiometer and air over-pressure technique data.
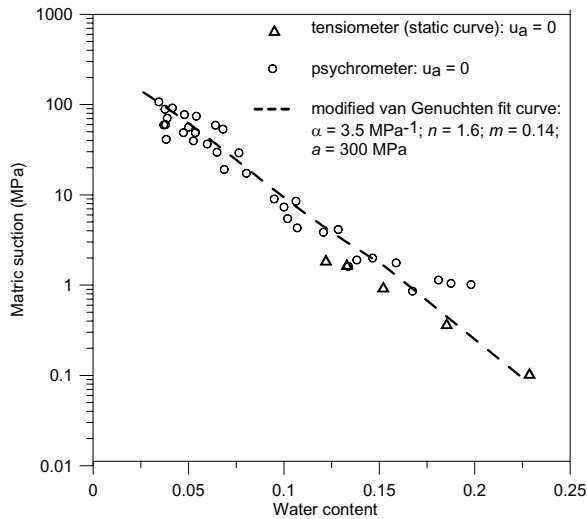
Fig. 6. Tensiometer and psychrometer data (total minus osmotic suction). Modified van Genuchten's fitting curve.

To compare psychrometer with tensiometer data, an osmotic suction of about 0.3 MPa was tentatively assumed. This value was chosen on the basis of osmotic suction data published in the literature. Romero (1999) measured an osmotic suction of around 0.4 MPa in a kaolinitic/illitic clay with 75% of clay minerals using squeezing technique. Fredlund and Rahardjo (1993) reported an osmotic suction of 0.2 MPa for a glacial till that was measured with the same fluid extraction technique.

Fig 6 compares psychrometer data plotted as total minus osmotic suction with tensiometer data. Despite the osmotic suction shifting, there is still a gap between tensiometer and psychrometer data, which can be associated with two aspects. On the one hand, the low resolution of the psychrometer at low total suctions, as the relative humidity values in the vicinity of the dew point.

On the other hand, the osmotic suction of the pore-liquid interacting with a silty/clay structure may significantly differ from the osmotic suction of the same solution isolated from the soil (Mata et al. 2002). In addition, the common assumption of constant osmotic suction is not appropriate, especially when suction increase is associated with vapor transfer, which induces an increase in pore-water concentration and the consequent increase in the osmotic component (gap between the two techniques at suctions higher than 1 MPa).

Test results shown in Fig. 6 were fitted using a modified form of the van Genuchten's equation (1980), where water content w is defined as a function of matric suction s (Romero & Vaunat 2000):

$$\frac{w}{w_{sat}} = S_r = C(s)\left[\frac{1}{1+(\alpha s)^n}\right]^m \tag{1}$$

$$C(s) = 1 - \frac{\ln\left[1+\dfrac{s}{a}\right]}{\ln(2)} \tag{2}$$

Parameters n, m and α are the same as used in van Genuchten's expression, w_{sat} represents the water content stored under saturated conditions, and S_r is the degree of saturation. Equation (2) forces the curve to be linear in a semi-log scale in the high suction range. Material parameter a represents the intersection with the y-axis at null water content of this linear part. A non-linear curve-fitting algorithm using least-squares method was used to determine parameters n, m and α, assuming $a = 300$ MPa. Fitted parameters were $n = 1.6$, $m = 0.14$ and $\alpha = 3.5$ MPa^{-1}.

Fig. 7 shows the results of the two procedures followed on the application of the axis translation technique compared to the reference data of the tensiometer. A conventional consolidation test performed on previously consolidated sample is also included in the figure to complement the information of the drying process in the low suction range where the soil is nearly saturated. The vertical effective stress was transformed in mean effective stress assuming a constant lateral coefficient at rest $K_0 = 0.6$ throughout the virgin loading path. It can be noted that at low suction range tensiometer data and controlled suction oedometer data lie on the normal consolidation line. This seems to confirm that the effect of a suction change in a saturated soil under zero total stress is equivalent to the effect of a change in mean effective stress (Blight 1965).

Toll (1995) put forward a conceptual model in which a unique water content – suction relationship is assumed to exist (virgin drying line) for an initially saturated and normally consolidated soil subjected to drying with no external stress applied. This unique curve, in which all the differences in stress and suction history should be erased, will follow the virgin consolidation line up to a point where the suction reaches the air-entry value.
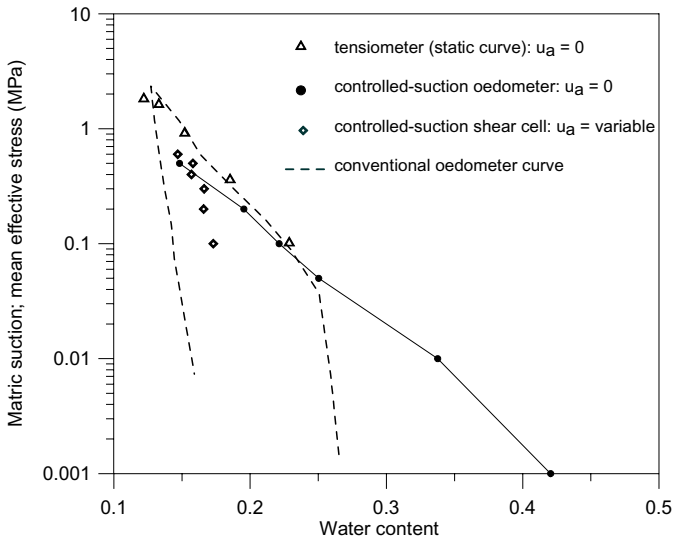
Fig. 7. Tensiometer and axis translation data. Virgin consolidation line obtained from oedometer test.

Based on porosimetry data an air entry value of about 340 kPa was estimated for the slurry dried up to a suction of 500 kPa. It is therefore difficult to explain the reason why the tensiometer readings follow the virgin consolidation line beyond this desaturation limit and up to about 2 MPa, while the axis translation curve clearly evolves towards lower suction values. It is possible that the suction measured with tensiometer was overestimated. Water evaporation from the paste causes a local drop in water content in the measuring zone. When suction is low soil permeability is relatively high and the evaporated water is promptly replaced with pore-water moving from the core of the sample. In contrast, when suction is high the permeability is lower and pore-water flow rate cannot counterbalance the water evaporation rate. As a result water content in the measuring zone remained lower than the average one and suction is therefore overestimated.

The significant differences observed in Fig. 7 between the data of controlled-suction oedometer and the controlled-suction shearbox are mainly related to the different stress paths followed (Fig. 2). The loading history and the air pressurisation process have an important effect on the low-suction range of the retention curve. Here the curve is highly dependent on the void ratio, which affects the water storage capacity (meniscus and bulk water contained in the macropores) and the air-entry value of the soil (Romero & Vaunat 2000; Karube & Kawai 2001). The effects of the stress path followed when the sample was previously consolidated result in an overconsolidated state from a hydraulic point of view ('over-dried' state according to the terminology of Toll (1995)). The retention curve obtained in the shearbox cell displays a 'stiff' response in terms of water content changes, until it reaches the main drying line of the retention curve obtained in the

oedometer cell. However, the limited data at elevated suctions hinders a further interpretation of the results.

Conclusions

The paper has presented a comparison of different suction measurement techniques as well as different possible procedures using the same technique. A first comparison has concerned 'static' and 'dynamic' measurement of suction using high suction tensiometer. 'Dynamic' measurement is extremely appealing from the practical point of view as it makes it possible to obtain water retention curve in a relatively short time.

Experimental results have shown that 'dynamic' determination may be quite accurate provided evaporation rate is sufficiently slowed down. Water retention from tensiometer and axis translation oedometer data in the low suction range seems to confirm that suction changes in saturated samples under zero total stress produce the same effect as a change in mean effective stress. Although expected this result is not trivial.

In the intermediate range, matric suction seems to be underestimated when using the axis translation technique and overestimated when using the tensiometer with no perfect isolation of the sample. In both cases, this error was attributed to pore-water evaporation. It should be noted that water evaporation can be prevented when using the tensiometer provided the sample is placed in an airtight container. In contrast evaporation is much more difficult to prevent when using axis translation technique. The use of the humid air to pressurize the cell can certainly reduce evaporation rate but is likely to not prevent it completely.

Psychrometer data, which are associated with total suction, seem to indicate an osmotic component of suction much higher than osmotic suction of the solution extracted from the soil. This discrepancy may be due to the excessive dilution of the liquid extracted from the soil. However the problem needs further investigation.

References

Barrera, M. 2002. *Estudio esperimental del comportamento hidro-mecànico de suelos colapsables.* PhD Thesis, Universitat Politècnica de Catalunya, Spain.

Blight, G. E. 1965. A study on effective stresses for volume change. *Proc. Conf. Moisture Equilibria and Moisture Changes in Soil beneath Covered Areas*: 259-269.

Boso, M. in preparation. Mechanical characterization of unsaturated soils with control and measurement of suction. PhD Thesis, Unìersità degli Studi di Trento, Italy.

Delage, P., Audiguier, M., Cui, Y.-J. & Howat, D. (1996). Microstructure of a compacted silt. *Can. Geotech. J.*, 33: 150-158.

Di Mariano (2000). *Le argille a scaglie e il ruolo della suzione sulla loro deformabilità.* PhD Thesis, Università di Palermo e di Catania, Italy.

Hilf, J. W. 1956. An investigation of pore water pressure in compacted cohesive soils. *US Bureau of Reclamation, Tech. Mem. 654, Denver: US Bureau of Reclamation.*

Karube, D. & Kawai, K. 2001. The role of pore water in the mechanical behaviour of unsaturated soils. *Geotechnical and Geological Engineering* 19: 211-241.

Mata, C, Romero, E., Ledesma, A. 2002. Hydro-chemical effects on water retention in bentonite-sand mixtures. *3ʳᵈ Int. Conf. on Unsaturated Soils, Recife, Brazil:* 283-288.

Romero, E. 1999. *Characterization and thermo.hydro-mechanical behaviour of unsaturated Boom clay: an experimental study.* PhD Thesis, Universitat Politècnica de Catalunya, Spain.

Romero, E., Vaunat, J. 2000. Retention curves of deformable clays. *Experimental evidence and theoretical Approaches in Unsaturated soils*, Tarantino & Mancuso (eds). Balkema, Rotterdam, 91-106.

Tarantino, A., Mongiovì, L. 2002. Design and construction of a tensiometer for direct measurement of matric suction. *3ʳᵈ Int. Conf. on Unsaturated Soils*, Recife, Brazil, 1: 319-324.

Tarantino, A. 2003. Panel report: Direct measurement of soil water tension. *3ʳᵈ Int. Conf. on Unsaturated Soils*, Recife, Brazil, in press.

Toll, D. G. 1995. A conceptual model for the drying and wetting of soil. *1ˢᵗ Int. Conf. on Unsaturated Soils*, Paris, 2: 805-810.

van Genuchten, M. Th. 1980. A closed form equation for predicting the hydraulic conductivity of unsaturated soils. *Soil Sci. Soc. Am, J.* 44: 892-898.

Woodburn, J.A., Hold. J. & Peter, P. 1993. The transistor psychrometer: a new instrument for measuring soil suction. Unsaturated Soils. *Geotechnical Special Publication* Nº 39, Dallas, S.L. Houston and W.K. Wray (eds). ASCE, 91-102.

Measurement of Suction of Thick Textured Soil using Filter Paper Method and Equivalent Tensiometer – EQT

C.F. Mahler and C.A.R. Mendes

Department of Civil Engineering - COPPE/UFRJ – Federal University of Rio de Janeiro, Brazil

Abstract: This paper is a study of the correlation between the humidity, density and matrix suction of non-plastic soil taken from a region located near the city of Rio de Janeiro. The study was conducted through laboratory tests, using mini-lysimeters and equipment that indirectly measured the humidity through soil suction: in effect, an automated tensiometer, an equivalence tensiometer (EQ2), a TDR and a specially adapted system, which measures the suction in situ, using filter paper. The electronic instruments were connected to a data logger and placed in three mini-lysimeters. Cycles of wetting and drying of the confined material were simulated. The soil was characterised. This characterisation enabled the determination of physical indexes, density, plasticity, grain size, porosity, and the characteristic curve of water retention, using the Richards pressure pan (cooker) test. The results obtained by the instruments, humidity and matrix suction, were compared with the characteristic curve. Overall, the equipment was satisfactory. The low presence of clay in this soil, around 7%, and its associated high porosity, were factors in limiting water retention. The equilibrium time of the soil humidity and the filter paper, obtained at intervals of fifteen days, presented better results than the weekly intervals (seven days). The equivalence tensiometer EQ2 compared to the filter paper presented quite efficient results for high suction values.

1 Introduction

Studies for developing understanding of physical processes in the soil, such as dynamic hydrogeological behaviour, have become increasingly important for geotechnical engineering, geology and agronomy. This paper offers a contribution to these studies by determining the suction in soil, using filter paper (Whatman nº 42) and an equivalent tensiometer, EQ2 (Delta-T devices).

The filter paper method is an efficient and economical technique for determining suction in the soil. The filter paper method can be used to obtain both matrix and total suction (Fredlund & Rahardjo, 1993). However, depending upon the domain of suction that is being studied, the time needed to obtain the equilibrium for the total suction could need to be extended. In this research, two different time spans were tested: one and two weeks.

Minimal knowledge of the capability of an equivalent tensiometer, to determine the suction in unsaturated and tropical soils, was also a motivator to test the effectiveness of this equipment.

2 Methodology

The tests were carried out in the laboratories of UFRJ, using minilysimeters mounted in COPPE (Figure 1).

Fig 1. Mini-lysimeter and the instrumentation

Each mini-lysimeter was filled with approximately 40 kg of soil retired of an A horizon, of a plain-soil section, with a texture of sandy clay. The clay fraction was 7% (Embrapa/Snlcs, 1988 a e b). In the lower part of the tanks, between the soil

and the drain, a layer of very small stones was placed, separated by a Geotextil sheet.

A soil with high porosity was chosen because it was intended manufacture wetting and drying cycles at very short intervals.

2.1 Equivalence tensiometer– EQT

This tensiometer has a common *Theta* sound (Delta–T Devices, Cambridge, UK) and an equilibrium body, as can be seen in figure 2. This tensiometer uses electronic humidity sensors to obtain higher suctions. These values cannot be measured by the conventional tensiometers due to cavitation phenomena. The sensor consists of a theta sound mounted in a porous material body, which is specially projected. The water retained in this body achieves equilibrium with the matrix potential of the soil around the theta sound.

Fig 2. Equivalent Tensiometer – Equitensiometer EQT (Delta – T Devices, UK, 2000).

The EQT senses the capacitance measurement, and only gives correct readings when the equilibrium in the interior of the body occurs. During the equilibrium time the potential matrix of the soil can be altered by the hysteresis. The lower the matrix potential, the quicker the alteration and the lower the effect of the hysteresis. As in nature, the velocity of the change of the matrix potential, in general, is less than 0,1 hPa/min. The effect of the hysteresis, in practical use, is much lower than these values.

The application of this equitensiometer is very advantageous because it does not require normal maintenance, as do common tensiometers, which need the water column filled when the suction is high. The EQT is very adaptable and can be used for studies of the water stress in plants, due to its capacity to function well in drier soils. It usually comes calibrated and this calibration can be adapted for use in the laboratory.

This equipment measures suction in a domain between 0 to –1000 kPa (10 atm), but precision occurs in the domain –100 kPa to – 1000 kPa, with an error

of ± 5 %. The accuracy of the lecture of suctions between 0 and -100 kPa, is of ± 10 kPa.

To date, tests of EQT in salt soils have not been representative. The conductibility of the soil, in the tests carried out, meant that it could not be guaranteed that the EQT would perform well in these types of soils. The tests indicated that the high concentration of sodium has a negative influence on the stability of the results with the passing of time. Several TDR sound responses show a dependence on the change of the temperature. The equilibrium in congealed soils is not affected, but the measured values are not reliable and present highly elevated values. The response time is very promising. However, the equilibrium pressure in relation to the automized tensiometers is limited, ≥ 6 kPa/h. There is no useful information in relation to long-term stability.

The lack of information in the available literature, and in the equipment manuals, indicates that the physical and chemical soil characteristics of the soil have minimal influence on the measured results. The humus content, soil structure, grain size, density and pH, seem not to influence the measurements. The equivalent tensiometer was coupled to a *Data Logger*. The variation of the suction was measured at defined intervals and was continuous.

2.2 Filter Paper

In this case, Whatman nº 42 paper was used (Chandler & Gutierrez, 1986). Two filter paper discs, were placed in a PVC tube measuring 25,0 cm length, and 25 mm diameter (1"Ø). This gadget, proposed by Mahler & Dias de Oliveira (1997), is very simple although it requires special care, in relation to evaporation, when removing the filter paper from the tube. The tubes are made with PVC (Mendes, 2000) and a special piece of plastic is glued inside the tube on the side that is placed within the soil, in order to prevent the paper from coming into contact with the inner wall of the tube (Figure 3). This procedure was necessitated to prevent wetting of the paper, a causal consequence of water bubbles that could form in the walls of the tube. The paper filter discs were retrieved with the help of callipers, placed in freezer bags and then in a isopore box, where less temperature changes occurs. At this point, they were transported to the place where they were weighed in a analytical balance with four decimals of error 0,0001g (Crilly & Schreiner, 1991). They were then placed in a oven with a temperature of 105 ºC for twenty four hours. After completion of the drying process, they were weighed again and the matrix suction was calculated using the formulae proposed (Fawcett and Collis-George, 1967) in Fredlund and Rahardjo (1993).

The filter paper was left in the tube in the soil for two time periods: one and two weeks. The results obtained from the tube that was placed in the soil for a two-week period were within the more acceptable confidence band and were therefore adopted as reference in this research.

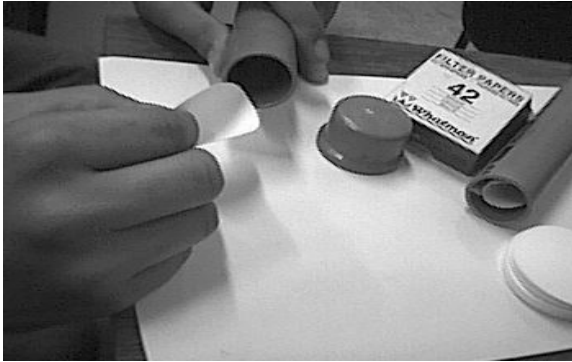**Fig. 3.** Placement of the filter paper in the PVC tube.

2.3 TDR and Soil-Water Characteristic Curve

At the beginning of the tests in the mini-lysimeter, a TDR probe (Tetha Probe – ML2, Delta-T devices) was also placed in the soil, to determine the water content. Figure 4 presents results of the Richard pressure plate used to obtain the soil-water characteristic curve.
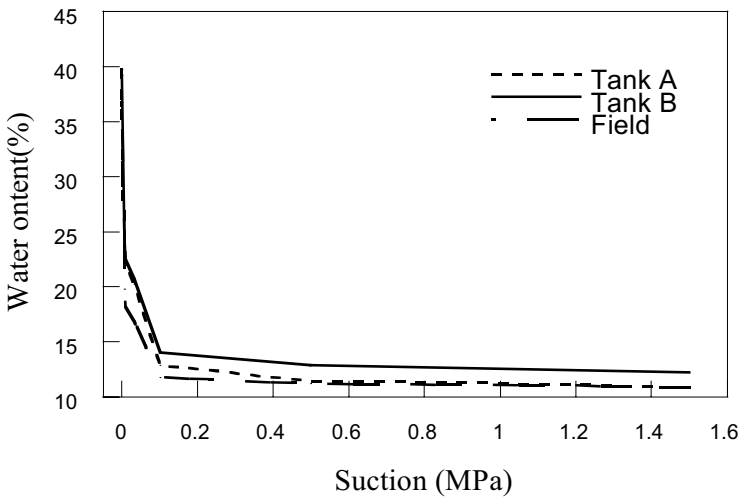

Fig. 4. Soil Water Characteristic Curve

3 Results

The results presented the expected variations, mainly to the suctions less than –100 kPa, even for the equivalent tensiometer and the filter paper. Calibration for the suctions less than –100 kPa, was possible by installing high precision electronic tensiometers in the mini-lysimeters (Mendes et all, 2001). The suction increased as the soil dried until values greater than –100kPa were reached. After this point, readings of the filter papers every fifteen days were more accurate then readings every seven days. With values above –100 kPa both pieces of equipment began to present better results (see Figure 5).

The initial water content in tank B (39,7 %) was greater than that in tank A (37,7 %). Consequently the infiltration in tank B was slower during the saturation process than in tank A. The water content, in both tanks, became simultaneously lower as the suction became higher, in absolute value. The same results were obtained in the Richards pressure panel (figure 4).

The suction in the two boxes was different. Figure 5 shows that in box A higher suctions were observed. This fact can be explained by the apparent density of the soil, which, in the field, showed values of approximately 1,67 g/cm3. When the soil was placed in the tanks, the apparent density changed to 1,64 g/cm3 in tank A, and 1,59 g/cm3 in tank B. Thus, the condition of the soil in tank A remained nearer to the condition of soil in the field. The soil inserted in tank B became more sandy in texture, with a higher porosity. It was also observed that the wetting and drying process in tank B was quicker.

Considering that the values measured were not greater than –350 kPa, a comparative analyses for values higher than –100 kPa. is presented in Figure 5. The normal tensiometers do not measure values higher than –100 kPa. A study in three levels were proposed: –100 kPa, –200 kPa e –300 kPa.

The results obtained in the Richards pressure pan showed that the values in tank B are higher for suction of –100 kPa, –200 kPa and –300 kPa. The values of residual humidity, for the samples encountered in tank B, were larger than in tank A and these were greater than that encountered in the field.

In the tests for values of suction higher than –100 kPa, the results obtained with the equivalent tensiometer were higher than those obtained with the filter paper. Figure 6 shows suctions measured in the two tanks from approximately –100 to –150 kPa. After a suction of approximately –100 kPa the values presented in tank B were higher.

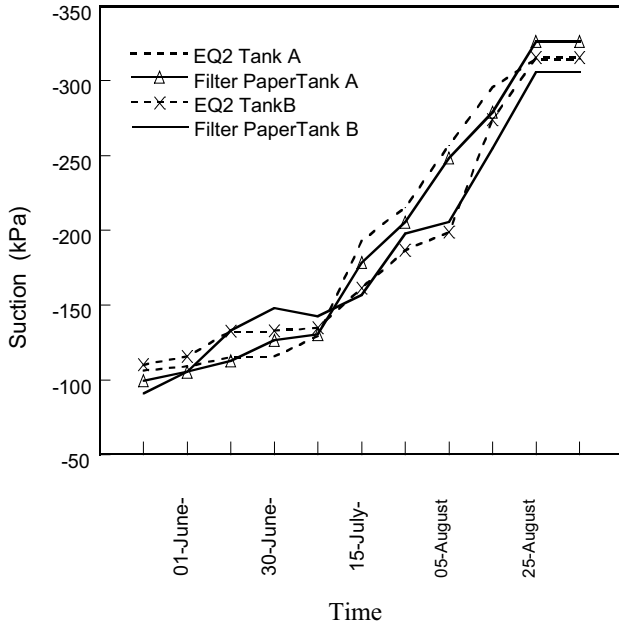**Fig 5.** Suction values higher than –100 kPa, measured with the Filter paper Method and the EQT
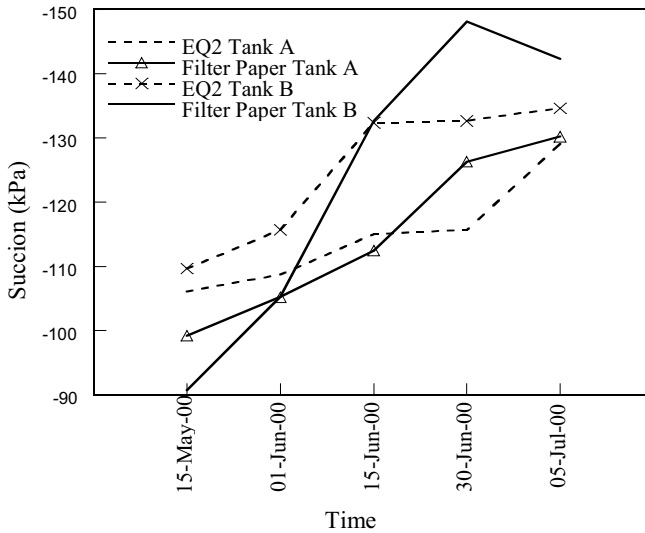

Fig 6. Comparison between the results obtained with the Filter Paper Method and the Equivalent Tensiometer EQT for values between –100 kPa and –150 kPa.
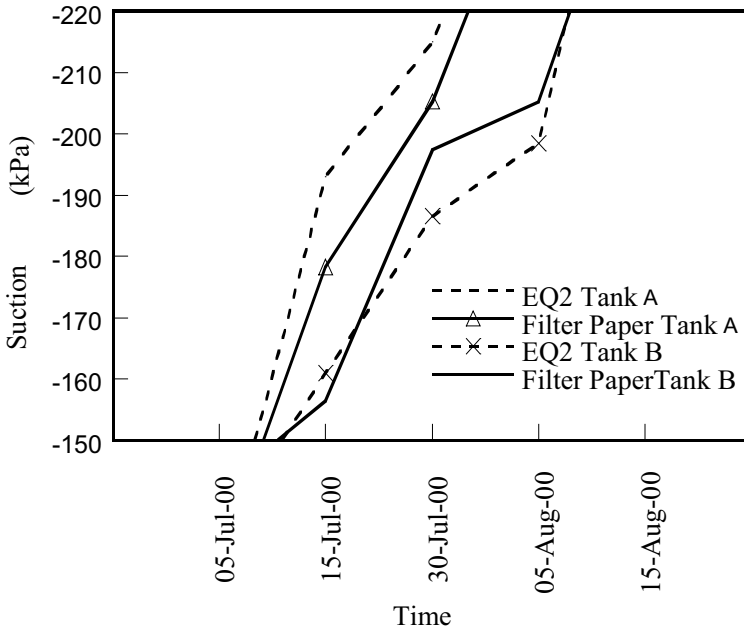
Fig. 7. Suction measured with the filter paper and equivalent tensiometer near –200 kPa.

For values of suction near –200 kPa (figure 7), the results of EQT were greater than the values observed with the filter paper method in tank A. However in tank B the opposite was observed. The values of suction presented in tank A were also higher than the values observed in tank B.

For values of suction near–300 kPa (figure 8), the values measured in tank A with the equivalent tensiometer EQT were higher. These results repeated in tank B. As suction values near –200 kPa higher values of suction were observed in tank A.

The dates obtained with the Tetha Probe – ML2 (Delta-T devices), presented water content values very coherent with the values of the soil water characteristic curve. These results were correlated with the suctions corresponding to values of –100 kPa, –200 kPa and –300 kPa. This permitted to obtain curves suction x water content in the mini-lysimeters. The water content values measured were 27,5 %, 14.5%,14,0% for tank B, and 17,5 %, 13,5%, 12,5% for tank A.

Fig. 8. Comparison between the results obtained with the Filter Paper and the Equivalent Tensiometer (EQ2) for suctions near –300 kPa.
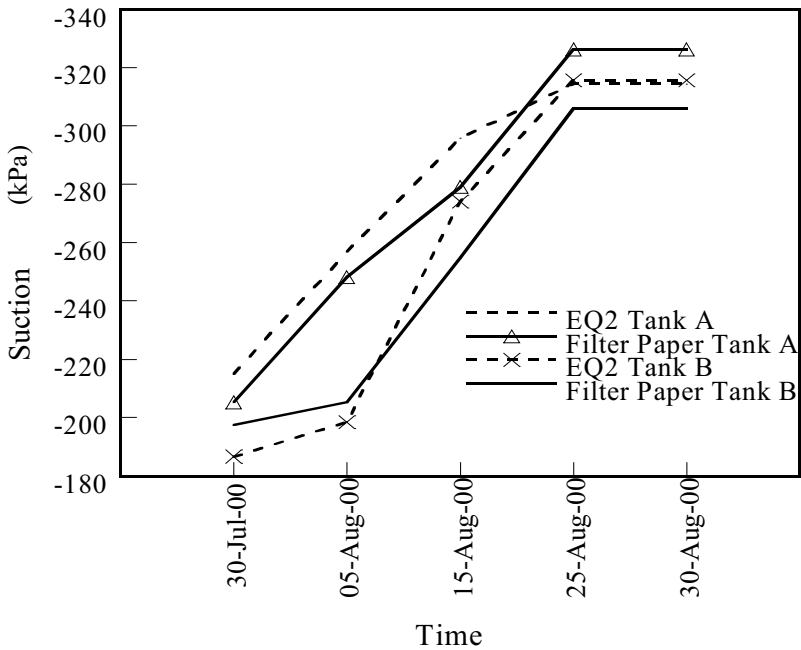
4 Final Comments

After six months of research the soil used under the conditions presented showed a limit in the drying process of –350 kPa. The soil used in this research is non plastic, although it also has a low presence of clay. Chandler & Gutierrez (1986) observed that the filter paper technique leads to better results when applied in clayey soils. In the case studied here, in the two boxes, a good similarity between the results presented by the filter paper method and by the equivalent tensiometer could be observed, despite the non plastic soil that was used. In this case, the type of soil with low clay fraction can be the answer to the suction limit, because it is in the clay fraction where the higher suction can occur. The results obtained with the use of the TDR probe were very good and showed to be a good complement in this research. Also in this soil the filter paper method presented good results. The equivalent tensiometer (EQT) also presented good results. The time responses presented by the equivalence tensiometer were very good. However, the filter paper showed to present better results after two weeks measurements. The mini-lysimeter, as a laboratory system to study soils, water movements in the soil and,

in parallel, to test new equipment's and prepare students, showed to be an economical, good and simple action.

Acknowledgements

References

Chandler, R. J. & Gutierrez, I. C., 1986. "The Filter-paper Method of Suction Meansurement". Geotechnique, vol. 36, nº12, pp. 265-268.

Crilly, M.S., Schreiner, H.D. & Gourley, C.S., 1991. A simple field suction measurement probe. Geotechnics in the African Environment, Proceedings of the Tenth Regional Conf. for Africa on Soil Mechanics & Found. Eng., Maseru, 291-298.

Delta - T Devices, 2000. Instruments for Environmental and Industrial Measurement, http://www.delta - t.co.UK

Embrapa, Brazilian Company of Research on Agriculture. Study of soils of Rio de Janeiro State leading to classification and correlation. 1988 a e b, 208p. (in Portuguese)

Fawcett, R.G. and Collis-George, N., 1967. A Filter-Paper Method for Determining the Moisture Characteristics of Soil, Australian J. Exp. Agriculture and Animal Husbandry, vol. 7, pp. 162-167.

Fredlund, D. G. & Rahardjo, H., 1993 "Measurement of Soil Suction". In: Soil Mechanics for Unsaturated Soil, chapter 4, New York, USA, John Wiley & Sons, Inc.

Mahler, C. F. & Dias de Oliveira, L. C., 1997. " Measurement of total suction in situ of porous soils of São Paulo using the filter-paper method ". Symposium of Recent Developments in Soil Mechanics, COPPE/UFRJ, June de 1997.

Mahler, C.F., Mendes, C.A.R., Souza, A.P. e Fernandes, N.F., 2002. Measuring the matrix potential of water in the soil through instrumentation installed in Mini-Lysimeters. UNSAT 2002 – 3rd Int. Conf. on Unsaturated Soils, ABMS, Recife, Brazil, March.

Mendes, C. A. R. 2000. Water measurement in the soil with automatic instruments installed in laboratory mini-lysimeters for environmental studies. Rio de Janeiro, 116p (COPPE/UFRJ, M.Sc., Civil Engineer Department, Master Dissertation). (in Portuguese).

Laboratory measurement of matric suction in pyroclastic soil using vacuum and high-suction tensiometers

M.V. Nicotera[1] and A. Tarantino[2]

[1] Dipartimento di Ingegneria Geotecnica, Università degli Studi di Napoli Federico II, Via Claudio 21, 80125 Napoli, Italy, nicotera@unina.it (✆)

[2] Dipartimento di Ingegneria Meccanica e Strutturale, Università degli Studi di Trento, via Mesiano 77, 38050 Trento, Italy, tarantin@ing.unitn.it

Abstract: The paper presents suction measurements on pyroclastic soils using vacuum tensiometer and high-suction tensiometers. Laboratory measurements with the vacuum tensiometer aimed at assessing the performance of this instrument, which had to be used for field measurement of matric suction. These measurements were also used to develop and validate a numerical model for predicting air cavity growth in the vacuum tensiometer. The model was intended to be a tool for detecting possible malfunctioning of the tensiometers in the field. Measurement with high-suction tensiometers aimed at corroborating the results of vacuum tensiometer measurements. When using high-suction tensiometers, contact can be better controlled and suctions approaching the limit value of the vacuum tensiometers (about 80 kPa) can be measured with no risk of cavitation.

Keywords: field measurement, laboratory testing, matric suction, vacuum tensiometer, high-suction tensiometer

Introduction

The hills in the urban area of the city of Napoli (Italy) are frequently affected by slope failures occurring in unsaturated pyroclastic soils. Previous studies have shown that these failures are mainly caused by loss of suction brought on by infiltrating rainwater (Nicotera 1998, 2000; Scotto di Santolo, 2000; Evangelista et al. 2002). To design landslide countermeasures and early warning systems, it is essential to monitor suction in the field. Vacuum tensiometers (range 0-80 kPa) were therefore installed at four slopes, the tensiometers being part of a broader set of instruments (psychrometers, tiltmeters, rain gauge, and radiometer).

After installation, suction was continuously recorded by the vacuum tensiometers and it soon appeared that some tensiometers were not functioning properly. Matric suction readings, after apparently reaching equalisation, did not remain

stable but systematically decreased regardless of the meteorological conditions. Furthermore, some instruments emptied and became inoperative in a very short time. A laboratory investigation was then set up to gain better insight into the unreliable response of some field tensiometers and to possibly define appropriate experimental procedures.

The main problem in vacuum tensiometer measurement is the continuous desaturation of the instrument. It is practically impossible to avoid air bubble formations inside a vacuum tensiometer. If the tensiometer is left without flushing, the quantity of air will continue to increase until it eventually occupies the whole tube. The higher the soil matric suction the faster the air growth.

The accumulation of air in the tensiometer can cause faulty responses of the instrument. In some cases, the excessive accumulation of air can be detected. For example, suction may be found to decrease in dry periods. In contrast, it may be difficult to interpret tensiometer readings during wet periods. The increase in pressure recorded by the vacuum gauge may be due to either air accumulation in the body tube or decrease in soil suction. Furthermore, the readings may appear reliable and stable even if they are actually incorrect (Ridley et al. 1998). The growth of the air cavity may counterbalance the decrease in water pressure due to the equalisation process and the tensiometer readings remain stable.

The key problem in tensiometer measurements is therefore how to detect the excessive accumulation of air in the body tube and, hence, the faulty response of the instrument. The approach proposed in this paper lies on a very simple idea. If the rate of air cavity expansion could be theoretically predicted, the prediction could be compared the actual air accumulation, estimated from the amount of water injected into the tensiometer to periodically refill it. Any discrepancy would indicate that the measurement is likely to be inaccurate. In turn, this would indicate that either the instrument has been incorrectly installed (poor contact, porous cup not perfectly saturated or cracked during installation) or that matric suction in the soil has exceeded the maximum measurable value.

To develop and validate a theoretical model for air cavity expansion, it was necessary to perform a controlled laboratory test to investigate the response of vacuum tensiometer and to monitor the growth of the air cavity. This test was carried out at the Geotechnical Laboratory of the Università di Napoli Federico II. The pyroclastic soil was placed in a caisson and a vacuum tensiometer was then permanently buried in the soil. Its measurement was then compared with that of a portable tensiometer, inserted into the soil at regular intervals.

Even under controlled laboratory conditions, two problems may still affect vacuum tensiometer measurement, the contact between the soil and porous ceramic cup and the tensiometer response at suctions approaching the limit value of 80 kPa. To corroborate the laboratory measurements using the vacuum tensiometer, measurements were performed on undisturbed pyroclastic samples at the Università di Trento using the TnT high-suction tensiometer. Using this probe, the contact between the soil and tensiometer ceramic filter could be better controlled and suction greater than 60 kPa could be measured without any problem of cavitation.

The paper describes the experimental tests performed at both institutions, and a comparison will be made between the measurement data obtained using the two types of tensiometers. The problems encountered in the measurement of suction in this coarse material (pyroclastic soil) are then illustrated and discussed. Finally, the theoretical model used to predict air cavity growth in the tensiometer is shortly presented.

Tensiometers

Vacuum tensiometer

Two types of vacuum tensiometers were used in this experimental program, the Jet Fill tensiometer and the Quick Draw tensiometer (Soilmoisture Equipment Corp.). The Jet Fill tensiometer consists of a transparent stiff nylon tube, a ceramic porous cup, a differential vacuum gauge located remote from the tip, and a reserve supply of water mounted in a storage container at the top of the tensiometers (Fig. 1a). A manual pump can be used to replace any air that may form within the measuring system with water from the storage container. The reading of vacuum gauge is obviously altered by air flushing and thus each time that air is removed an equalisation process will start.

The Quick Draw tensiometer is a portable tensiometer and consists of a ceramic tip connected to the vacuum gauge by means of a capillary tube, in order to reduce to minimum the time required to make a reading (Fig. 1b). The apparatus is equipped with a knob (null knob), which permits manual adjustment of the water pressure inside the instruments. This knob can be operated to reduce the response time of the instrument.
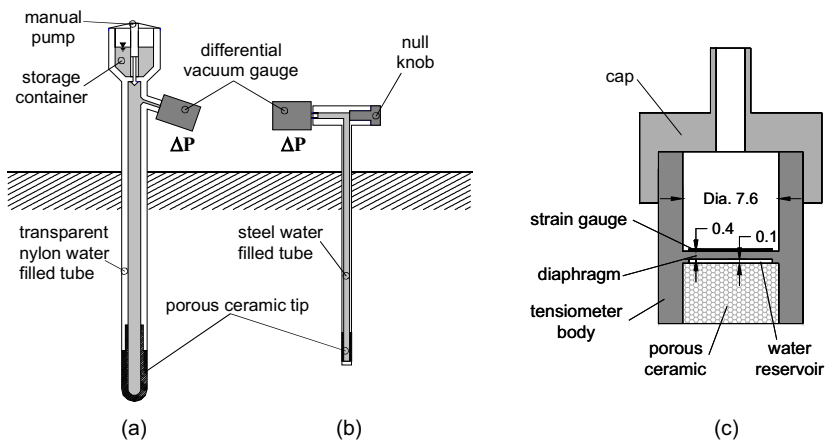

Fig. 1. (a) Jet Fill Tensiometer; (b) Quick Draw Tensiometer; (c) Trento tensiometer.

High-suction tensiometer

The high-suction Trento tensiometer (Tarantino and Mongiovì 2002; 2003) has retained the main features of the tensiometer developed by Ridley and Burland (1995). Modifications were introduced to the diaphragm design. As shown in Fig. 1c, it is positioned at mid–height of the stainless steel body in contrast to the IC tensiometer, where the diaphragm forms a wall of the top section. This ensures a quasi-symmetric geometry, which may be preferable if calibration is performed in the positive range and extrapolated to the negative one. Most of all, it allows direct calibration in the negative range. The disadvantage of such a design consists in bonding the strain gauge down to a hole.

Material and methods

The pyroclastic soil (*pozzolana*) had a grain size distribution ranging from silty sand to sandy silt (clay fraction was less than 10%). To test the vacuum tensiometers in the laboratory, a caisson provided with bottom drainage was filled with a 0.1 m^3 sample of remoulded *pozzolana,* placed using the wet tamping procedure. The initial porosity of the sample was 0.63 and the initial water content was 0.15.

A vacuum tensiometer and a TDR gauge were permanently buried in the soil sample whereas a portable tensiometer was repeatedly pushed into it to measure matric suction at different depths. The caisson was placed in a temperature-controlled room.

The test consisted of applying drying and wetting cycles. The sample was dried in steps by repeatedly exposing the sample top surface to the room air. After each drying step, the sample surface was covered to allow moisture equalisation. Wetting was achieved in steps by either filling the bottom caisson drainage with a predetermined amount of water or sprinkling water on the top surface of the sample. After each wetting stage, the sample top surface was covered and the bottom drainage was closed to allow moisture equalisation.

The test allowed the analysis of the response time of the tensiometer following either a change in the sample water content or a re-saturation servicing operation. In addition, it was possible to monitor the rate of air cavity growth and to estimate the water retention curve of the soil (the average water content could be estimated by weighing the caisson).

Suction measurement using high-suction tensiometers was carried out on undisturbed samples. Two sample tubes containing undisturbed samples were shipped to the Università di Trento. To slowly push out the *Pozzolana* sample, the first tube was placed in a motorised hydraulic horizontal extruder. Unfortunately, the soil and the tube had strongly cemented together. As a result, the force applied by the extruder ruptured the tube attachment, making it impossible to extrude the sample. The tube was then hit with a hammer in an attempt to take out the sample. The soil could be finally extracted from the tube, but in a completely loose state. Another method was then adopted to obtain an undisturbed sample. The second

sample tube was cut along two generatrices using a circular saw so as to split the sample in two parts. It was then decided to keep the soil in the half sample tube, to ensure that the original structure of the soil was not destroyed.

The initial water content of the sample was estimated by measuring the water content of a small piece cut from the sample. The sample was then air dried to a target water content (estimated by weighing the sample together with the half tube), sealed in two plastic bags and stored in a high–humidity room for at least one week to allow moisture equalisation. After suction measurement, the sample was air dried to a lower water content following a similar procedure.

The main problem of suction measurement in pyroclastic soils is the contact between the tensiometer ceramic filter sample and the sample, because these soils are poor in clay. To ensure contact, some pyroclastic soil was first sieved on the 0.075 mm sieve. The fraction passing through this sieve was mixed with tap water to obtain a soil paste, which was used to make contact between the sample and the ceramic filter. Tap water was used in place of demineralised water to minimise dissolution of soil minerals.

The soil paste was not sufficient to ensure 'connection' of the instrument with the sample. It was necessary to slightly push the tensiometer against the soil using the caps shown in Fig. 2. The caps were tightened to a plate, which was in turn clamped over the edge of the half sample tube. An O-ring was positioned in the tensiometer hole to avoid evaporation of water from the measurement area.
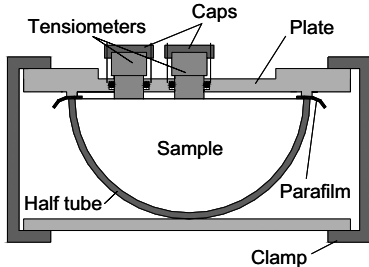

Fig. 2. Schematic layout of the arrangement used for suction measurement on the undisturbed sample.

To detect poor contact between the sample and the tensiometer ceramic filter, it was necessary to isolate the mass of air surrounding the sample to avoid evaporation of pore water and keep constant the water content of the sample during measurement. If the contact is poor, the tensiometer measures the suction of the paste (used to make contact with the sample) and not that of the sample. The water content of the paste decreases rapidly because of water evaporation into the surrounding air and, hence, suction decreases almost linearly with time. This suction decrease can be taken as an indication of poor contact, provided the sample is isolated and its water content is kept constant. Parafilm was interposed between the plate and the half tube to prevent pore water evaporation (Fig. 2).

Experimental results

One of the aims of the laboratory investigation was to determine the response time of the vacuum tensiometer, in an attempt to better interpret field response of these instruments. The response time of the vacuum tensiometers is presented in Fig. 3 for both the Jet Fill tensiometer and the Quick Draw tensiometer. As expected, the response time increases as matric suction increases. However, it is worth noticing that the response time of the Jet Fill tensiometer is about one order of magnitude greater than that of the Quick Draw tensiometers. The slow response of the Jet Fill tensiometer at high matric suctions makes it difficult to monitor suction changes associated with daily rainfall.
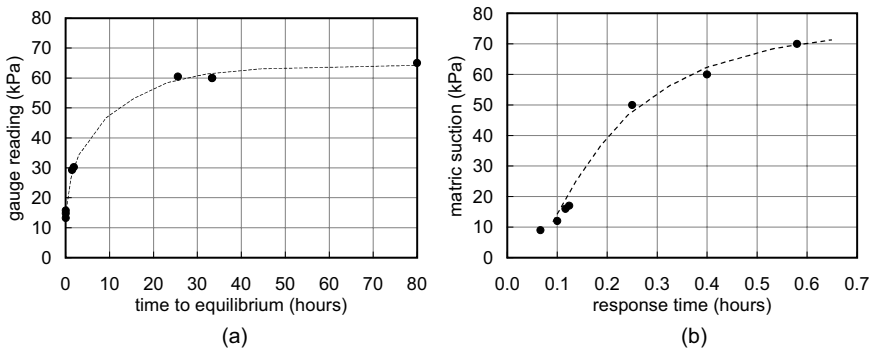

Fig. 3. Response time of (a) Jet Fill tensiometer and (b) Quick Draw tensiometer.

Suction measurement using the high-suction tensiometers were performed on the undisturbed *pozzolana* sample, having an initial water content of 0.187 and subsequently air dried to water contents of 0.171, 0.15, 0.12, and 0.099 (estimated by weighing the sample). Results of these measurements are shown in **Fig. 4**a. In all measurements, with the exception of w=0.099, suction remained constant with time, indicating that a good contact between the soil and the ceramic filter could be achieved.

The response time of the TNT tensiometer is presented in Fig. 4b. It can be noticed that equalisation was reached in a very short time at water contents w of 0.187, 0.171, and 0.15. It was little longer when the sample had water content of 0.12 and 0.10, probably because of the time required draining water from the soil paste. Because of the reduced size of the water reservoir, the response time of the Trento tensiometer is clearly lower than that of the Quick Draw tensiometer.

The water retention curve of the remoulded *pozzolana* is shown in Fig. 5. It was determined using the values of matric suction measured by the jet fill tensiometer and the average water content of the remoulded *pozzolana* sample estimated by weighing the soil together with the caisson. In the figure, the water retention curve is compared with the values of water content-matric suction measured on the undisturbed sample using the high-suction tensiometers and also with the water re-

tention curve of undisturbed samples of pozzolana from the formation of the Neapolitan Yellow Tuff (Nicotera et al. 1999).

The water retention curve of the *pozzolana* undisturbed sample is close to that of the remoulded *pozzolana* at relatively low suctions. At high suctions, the curve relative to the undisturbed sample departs from that of the remoulded soil. This is not unexpected. The remoulded sample had higher porosity and partially lost particle bonding. As a result, matric suction in the remoulded soils is lower at given water content. Nonetheless, the water retention data on the undisturbed sample seems to corroborate the data on the remoulded soil, and therefore the consistency of the measurement carried out with the Jet Fill tensiometer. It is also interesting to note that the water retention curve on the undisturbed *pozzolana* sample moves towards the one measured on undisturbed samples of Yellow Tuff pozzolana. This would suggest that *pozzolana* is a rather homogeneous soil as far as the water retention characteristics are concerned.
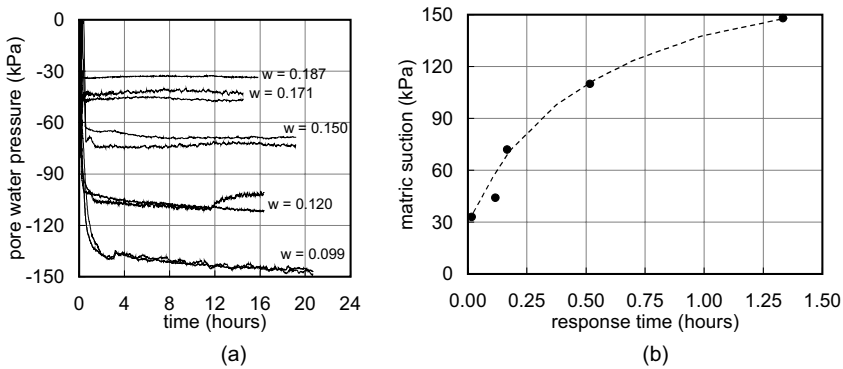

Fig. 4. Results of high-suction tensiometer measurement: (a) suction versus time curves at different water contents; (b) response time versus suction.
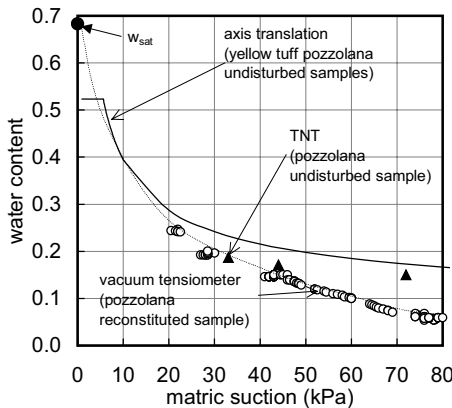

Fig. 5. Matric suction-water content relationship for the *pozzolana* compared with water retention curve of yellow tuff *pozzolana*

Prediction of air cavity growth

It is usually recommended to saturate vacuum tensiometer with deaired water to slow down the growth of the air cavity in the tensiometer tube and hence to prolong suction measurement. However, it is difficult to refill the instruments with deaired water in the field. Furthermore, if maintenance is carried out correctly, the instrument will never completely empty of air and the concentration of air in the water filling the tensiometer will progressively increase.

To analyse the process of desaturation in the tensiometer tube, it may be convenient to consider first the ideal condition of tensiometer filled with perfectly deaired water and then the more realistic condition of tensiometer filled with non–deaired water.

When the tensiometer is filled with deaired water, the initial concentration of air in the tensiometer is virtually zero whereas the concentration of dissolved air in the pore water corresponds to the atmospheric pressure (according to Henry's law). Because of the concentration gradient, air diffuses from the pore water (and from the pore air if air phase is continuous) towards the water filling the tensiometer tube. The diffusion process proceeds until the concentration gradient of dissolved air between the pore water and the tensiometer water vanishes. The air diffusing towards the water filling the tube does not affect the functioning of the instrument provided air does not come out of solution. This may happen if a gas/liquid interface is present in the liquid.

Imperfections exist in the inner surface (e.g. cracks, interstices, etc.) of the tensiometer tube and these provide an ideal trap for tiny amounts of air or water vapour that can remain stable even after thorough deairing of the instrument (Marinho and Chandler 1995; Ridley et al. 1998). These entrapped gaseous nuclei act as drains for dissolved air. When the porous cup is placed in contact with the soil, water pressure in the tensiometer tube decreases and the small gas nuclei enlarge. Accordingly, the air pressure in these gas nuclei reduces (below the value corresponding to the concentration of dissolved air in water) and hence air comes out of solution into these small cavities.

The diffusion process towards the entrapped cavities produces a progressive increase of air pressure inside these cavities. It is then likely that some of these entrapped cavities do not remain stable and an amount of air is released in form of free bubbles in order to restore equilibrium of the nucleus liquid-gas interface (convex on the water side). Because of buoyancy, the free bubbles collect in the top section of the tensiometer tube and eventually form a gaseous cavity that occupies the entire cross section of tensiometer tube.

The gas pressure in the large cavity atop the tube is always less than atmospheric (the gas-liquid interface is flat). As a result, air diffuses towards the large cavity driven by the concentration gradient and the large cavity progressively grows in size. The cavity is fed by the air from outside the tensiometer that crosses the ceramic filter and moves upward by diffusing through the water filling the tube and also by the air bubbles that detach from the tube's wall. Eventually, the air cavity enlarges so as to empty the tensiometer completely.

The rate of air cavity growth depends on matric suction. As matric suction increases, the air pressure in the large cavity decreases and air diffusion takes place at faster rate because of the higher concentration gradient. The rate of air cavity growth also depends on the degree of saturation of the surrounding soil. If pore air is continuous, air has direct access to the high air entry porous cup and the impedance of the surrounding soil has not significant role in the process. On the other hand, if the air phase is discontinuous, soil impedance acts in series with porous cup impedance and hence can strongly affect the air diffusion into the tensiometer. As a result, air collects more rapidly when the degree of saturation of soil is low.

When the tensiometer is filled with non-deaired water, the growth of the large cavity at the top of the tube is analogous to the one described for tensiometer filled with de-aired water but it is obviously faster. Here the large cavity is also fed by the relatively large amount of air dissolved in the water filling the tube, in addition to the air diffusing from outside the tensiometer.

In conclusion, two main processes produce air cavity growth in a tensiometer filled with non−deaired water: releasing of free bubbles from entrapped gaseous nuclei and diffusion of dissolved air towards the large cavity formed at the top of the tensiometer tube. The former is the triggering mechanism of cavity formation, the latter is the feeding mechanism.

Modelling of the desaturation process

The process of air cavity growth results from the interaction of many physical mechanisms that can be represented by differential equations. These are the dissolution of air into water (Henry's law), air diffusion through the water filling the tensiometer (Fick's law), water transition from liquid phase to gaseous phase (Kelvin's equation), changes in air pressure in response to volume and mass changes (ideal gas law).

A simplified model of vacuum tensiometer was analysed in order to predict the air cavity growth rate in the vacuum tensiometer installed in the pyroclastic soil at the natural water content (pore air phase is continuous). The model is illustrated in Fig. 6. It consists of a tube of length L with an inner section A. The tube top end is sealed while the bottom end is closed by an high air entry value porous disk (section A_p, thickness L_p, porosity n_p). This disk represents the tensiometer tip. The tube is partially filled (L_w indicates water column length) with aired water (C_a indicates dissolved air concentration) and partially with air and water vapour (l indicates the length of air filled portion). The instrument tip was assumed to be in perfect contact with the surrounding soil and soil impedance was assumed negligible.

The system of differential equations governing the diffusion process into the tensiometer was derived and solved using a numerical algorithm based on finite difference method (Nicotera and Scotto di Santolo 2002).
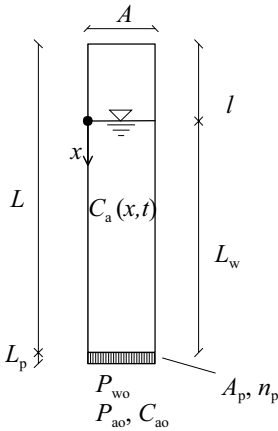
Fig. 6. Simplified model of vacuum tensiometer.

Numerical simulation of air cavity growth

The results of the numerical simulations are shown in Fig. 7a. The calculated dimensionless cavity length l/L is plotted versus the dimensionless time factor $D_w t/L^2$ for the case of $L=1$ m, where D_w is the air diffusivity in water and t is the time. Curves are plotted for different matric suction values (ranging from 50 kPa to the maximum measurable suction). As expected, the rate of air cavity growth increases as matric suction and air diffusivity increase. The length l of the air cavity forming after 2, 5, 10 and 15 days is plotted versus matric suction in Fig. 7b. It can be noted that air accumulation in the tensiometer becomes more significant as matric suction approaches the limit value of about 80 kPa.
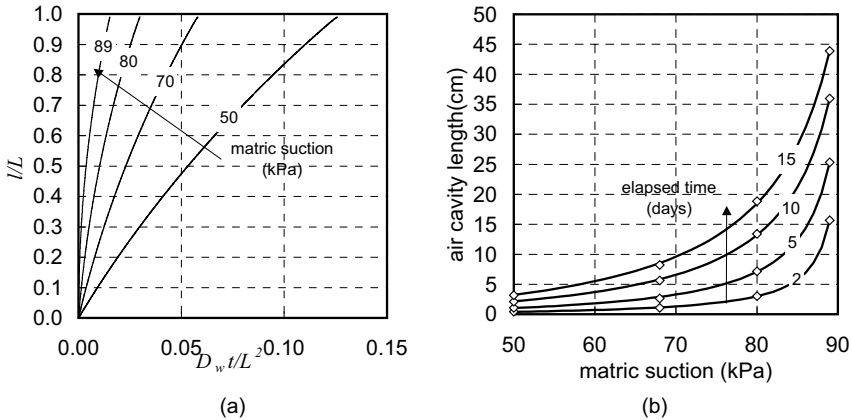

(a)   (b)

Fig. 7. (a) Dimensionless air cavity length versus dimensionless time factor. (b) Air cavity length versus matric suction at different elapsed times.

The experimental data obtained in laboratory are compared with the results from the numerical simulations in Fig. 8. For matric suction less than 65 kPa, the numerical simulations are in satisfactory agreement with the experimental data. At higher matric suctions, the numerical simulations underestimate air growth rate and this difference is probably due to the releasing of free bubbles from entrapped gaseous nuclei on the tensiometer inner wall, which has been disregarded in the numerical model. As a first approximation, the air cavity length at higher matric suctions can be estimated from the curves corresponding to matric suction 10 kPa higher. For example, the curve corresponding to a matric suction of 80 kPa can be used to estimate the cavity length at matric suction of 70 kPa.
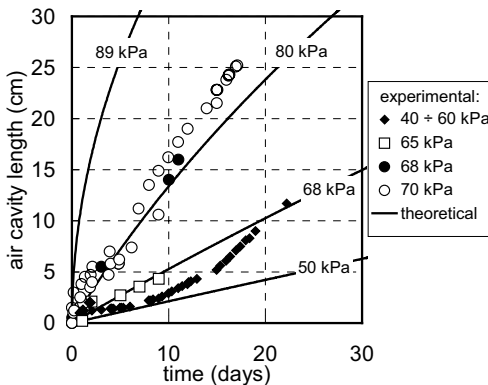

Fig. 8. Air cavity length versus time: experimental results and numerical predictions.

Conclusions

The paper has presented laboratory measurements of matric suction on pyroclastic soils (*pozzolana*) using vacuum tensiometer and high-suction tensiometers. Measurements with the vacuum tensiometer aimed at assessing the performance of this instrument, which had to be used for field measurement of matric suction. Measurement with high-suction tensiometers aimed at corroborating the results of vacuum tensiometer measurements.

The high-suction tensiometers were used to measure suction of an undisturbed *pozzolana* sample. Experimental results have shown that it was possible to ensure contact between the tensiometer porous filter and the soil, even though the paste used to make contact with the soil was poor in clay fraction. Furthermore, these measurements have shown that water retention data were consistent with those obtained on a remoulded sample using the vacuum tensiometer.

Measurements using the vacuum tensiometer have made it possible to develop and validate a numerical model for predicting air cavity growth in the tensiometer tube. The model was intended to be a tool for detecting possible malfunctioning of the field tensiometers. The model could predict satisfactorily the rate of air cavity growth at suctions less than 65 kPa, whereas it tended to underestimate the rate of growth at greater suctions (65 kPa$<s<$80 kPa).

Acknowledgements

References

Evangelista A, Pellegrino A, Scotto di Santolo A (2001). Misure in sito di suzione nelle coltri piroclastiche del napoletano. In: Evangelista A, Pellegrino A (eds.) *Campi sperimentali per lo studio della stabilità dei pendii*. Benevento, Hevelius, pp 19-25.

Nicotera MV (1998) *Effetti del grado di saturazione sul comportamento meccanico di una pozzolana del napoletano*. PhD Thesis, Università di Napoli Federico II.

Nicotera MV, Evangelista A, Aversa S (1999) Determinazione della curva caratteristica e delle funzioni di permeabilità di una pozzolana non satura. Atti del XX Convegno Nazionale di Geotecnica. Bologna, Pàtron, pp. 213-221.

Nicotera MV (2000) Interpretation of the shear response upon wetting of natural unsaturated pyroclastic soils. In Tarantino A, Mancuso C (eds.) *Experimental Evidence and Theoretical Approaches in Unsaturated Soils.* A.A. Balkema, Rotterdam, pp 177-192.

Nicotera MV, Scotto di Santolo A. (2002) Taratura di apparecchiature per la misura di suzione in sito. Internal Report, Dipartimento di Ingegneria Geotecnica, Università di Napoli Federico II.

Ridley AM, Burland JB (1995) Mesasurement of suction in materials which swell. Applied Mechanics Reviews, 48(10): 727-732.

Ridley AM, Marsland F., Patel A (1998). Tensiometer, their design and use for civil engineering purposes. Geotechnical Site Characterisation, *Proc. 1ˢᵗ International Conference on Site Characterisation*, 2: 851-856. Atlanta, USA.

Scotto di Santolo A (2000) *Analisi geotecnica dei fenomeni franosi nelle coltri piroclastiche della Provincia di Napoli*. PhD Thesis, Università di Napoli Federico II.

Tarantino A, Mongiovì L. (2002) Design and construction of a tensiometer for direct measurement of matric suction. *Proceedings 3rd International Conference on Unsaturated Soils*, Recife, Brasil, 1, pp 319-324.

Tarantino A, Mongiovì L. (2003) Calibration of tensiometer for direct measurement of matric suction. *Géotechnique* 53(1): 137-141.

Tarantino A (2003) Panel report: Direct measurement of soil water tension. Proc. 3nd Int. Conf. on Unsaturated Soils, Recife, Brasil, in press.

EXPANSIVE SOILS

Volume Change Behaviour of Fine Grained Soils

A. Sridharan

Honorary Professor, Department of Civil Engineering, Indian Institute of Science, Bangalore – 560 012 INDIA

Abstract. Soils in arid and semi-arid zones undergoes volume changes due to wetting. Depending upon the type of clay minerals present, degree of saturation, externally applied load and bonding, the fine grained soils either swells or compresses. One of the parameter that affects the volume change behaviour is the primary clay mineral present in their clay size fraction. A simple method of identifying the same has been presented. It has been brought out that in an expansive unsaturated undisturbed soil, the diffuse double layer repulsion, the stress state and the bonding play significant role in their volume change behaviour. In non-expansive fine grained unsaturated undisturbed soils, the shearing resistance at particle level (including the matrix suction and bonding) and fabric play a significant role in influencing the volume change behaviour. While both the mechanism co-exist, one of them play a dominant role depending upon the primary clay mineral is swelling or non swelling.

1 Introduction

Soils in arid and semi-arid zones have received considerable attention from volume change behaviour point of view. They are mostly unsaturated because the water tables in the arid and semi-arid zones are usually deep. Wetting and drying take place resulting in desiccation bonds. Presence of suction in unsaturated soils makes them exhibit stress-strain response that is atypical of saturated soil deposits. In particular, these soils suffer large swelling and collapse strains upon increase in moisture content under constant applied stress. Whether the soils will swell or collapse upon wetting depends upon the insitu stress state, reduction of suction caused by wetting, mobilisation of double layer repulsion, and presence of bonding between particles due to desiccation and other means.

The range of soils to be found in arid zones is extremely wide and it is difficult to isolate common distinctive feature. However, it can be said that some arid region's soils are distinctively expansive and some are distinctively collapsible and then often present a bonded structure. To increase the complexity, all the above mentioned characteristics may be present in a given soil in some proportion but some characteristics may dominate. Presence of the type of clay minerals play a role in their volume change behaviour. Thus the important parameters that control

their volume change behaviour could be stated as the type of soil (the clay minerals present), the degree of saturation (the suction pressure), the degree of bonding, and the level of the applied stress. In this paper, an attempt has been made to identify the soils which could be grouped as expansive or collapsible and to identify mechanism(s) controlling their volume change behaviour and the factors affecting the same.

2 Natural Soils

Natural fine grained soils which are susceptible for volume changes could be conventionally described through the classical plasticity chart. Figure 1 presents the plasticity chart of number of soils tested for their liquid limit and plastic limit as per standard procedures. The results presented in Figure 1 has been broadly identified either predominantly kaolinitic soils or montmorillonitic soils. The primary clay mineral present in these soils identify them either kaolinitic or montmorillonitic. It is seen that these natural soils are spread along the Casagrande's 'A' line irrespective of the type of primary clay mineral present. In other words, the conventional representation of these natural soils in the plasticity chart does not distinguish them either they are kaolinitic or montmorillonitic.

Figure 2 presents the same soils presented in Figure 1, represented through their sediment volume in kerozene (V_k) and in water (V_d). The sediment volume test (the free swell test) is performed by pouring a 10 g specimen of the dry soil sample into a 100 mL graduated cylinder containing about 40 mL of distilled water (Sridharan et al. 1986c). The suspension was stirred repeatedly and made upto 100 mL mark with distilled water and left undisturbed to attain an equilibrium state of volume. At the end of the equilibrium period, the sediment volume of the soil or clay in water was noted and expressed as cc/gm. The same procedure is repeated with carbon technochloride/kerozene. It has been shown by Sridharan et al. (1990) that the sediment volume in non-polar liquid CCl_4 and in kerozene are essentially same.

It is seen in Figure 2, that the results are disposed in two distinct groups : the swelling montmorillonitic soils with minimum value of about 1.0 to 1.2 cc/gm in kerozene with all the points lying on a plateau. The sediment volume in water go upto about 14 cc/gm, the non-swelling kaolinite clays were positioned well above the plateau and occupied sediment volume > 1.1 cc/gm in kerozene. The value in kerozene go upto about 2.8 cc/gm for kaolinite. This property of occupying a higher sediment volume in kerozene is typical of non-swelling soils which is
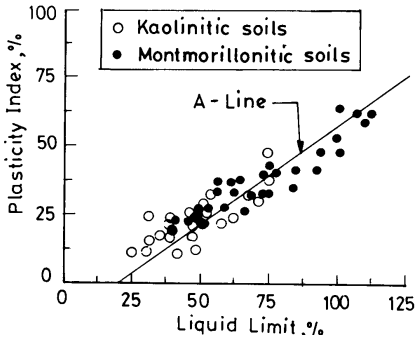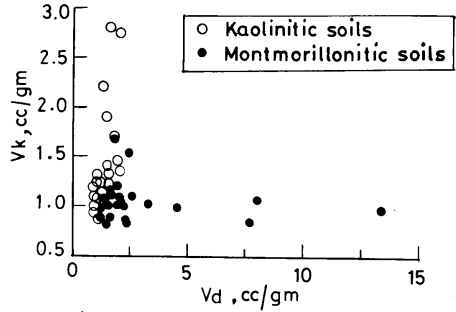
Fig. 1. Plasticity Chart

Fig. 2. Relationship between V_k and V_d

attributed to flocculation. Very low sediment volume (1.0 cc/gm) in kerozene and high sediment volume in water (≈ 14 cc/cm) is typical of highly swelling soils (Sridharan et al. 1986c) which is attributed to diffuse double layer swelling. Thus the results presented in figure 2 indicate a simple method of identifying the soils either swelling or non-swelling fine grained soils.

Figure 3 presents the liquid limit obtained with water and with CCl_4 as pore fluids for different natural soils by cone penetration method. It is noticed that the non-swelling kaolinitic soils gives higher liquid limit in CCl_4 than in water.
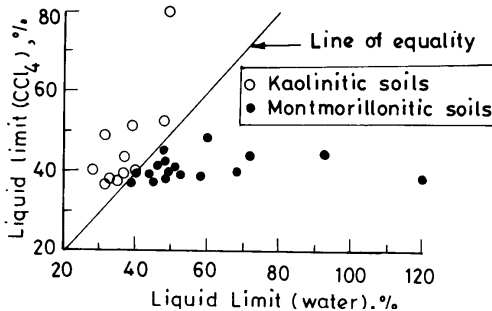
Fig. 3. Comparison of liquid limits in Water and CCl_4

Swelling soils show higher liquid limit in water than in CCl_4. The line of equality demarcates the kaolinitic soils from montmorillonitic. It is seen from Figures 2 and 3 that there is a distinct behaviour of sediment volume/liquid limit whether they are kaolinitic or montmorillonitic with respect to the pore fluid used. However in the conventional plasticity chart they do not classify differently.

3 Mechanisms controlling the liquid limit behaviour of fine grained soils

Sridharan and Rao (1975) have discussed the possible mechanisms governing the liquid limit of fine grained soils. Figure 4 shows the effect of dielectric constant, ε on the liquid limit of kaolinite and montmorillonite. These clays have been chosen as they represent the extreme types of clay minerals and any natural soil is likely to behave in between these two extremes. The liquid limit results are presented on volume basis to take care of the unit weights of the organic fluids which varies. It is distinctly seen that the two clays behave strikingly opposite manner with respect to change in the dielectric constant. For montmorillonite, the liquid limit decreased significantly from a value of 866% for water ($\varepsilon = 80.4$) to 149.2% for hexane ($\varepsilon = 1.89$) whereas the liquid limit increased from 127% (for water) to 230% (for hexane) for kaolinite.

For kaolinite, a change in the dielectric constant does not bring about appreciable change in double layer thickness (Sridharan and Jayadeva 1982); the decrease of dielectric constant however enhances the interparticle attraction, the interparticle shearing resistance and the extent of particle flocculation. The increase in voids space for pore fluid entrapment facilitated by the enhanced particle flocculation on lowering the dielectric constant of the pore fluids is responsible for the higher liquid limits of the non-swelling clay specimens. For montmorillonite, the increase of dielectric constant of the pore medium causes an increase in the diffuse double layer thickness, the same is reflected as higher liquid limit of the swelling clays. Thus two distinct mechanisms control the liquid limit behaviour of clays depending upon the clay is kaolinite or montmorillonite.

Figure 5 shows percent swell obtained in the conventional oedometer as a function of exchangeable sodium in soils (Sridharan et.al 1986b). It is fairly established that the magnitude of sodium as exchangeable ion indicates the level of the diffuse double layer (Mitchell 1976). An increase in exchangeable sodium indicates an increase in double layer repulsion and hence an increase in percent swell. Figure 6 shows for montmorillonitic soils, the liquid limit bears a fairly good correlation with exchangeable sodium. Magnitude of monovalent ions as the exchangeable ions is more important than the magnitude of cation exchange capacity itself for contributing to swelling (Sridharan et al. 1986b). This once again confirms that the liquid limit of montmorillonitic soils, is primarily governed by the magnitude of diffuse double layer repulsion (Sridharan, et al. 1986b).
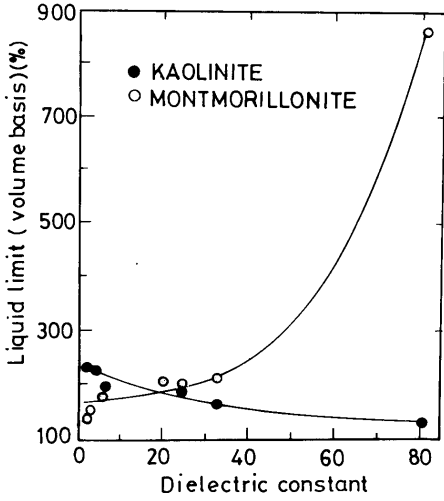
Fig. 4. Effect of Dielectric constant on liquid limit
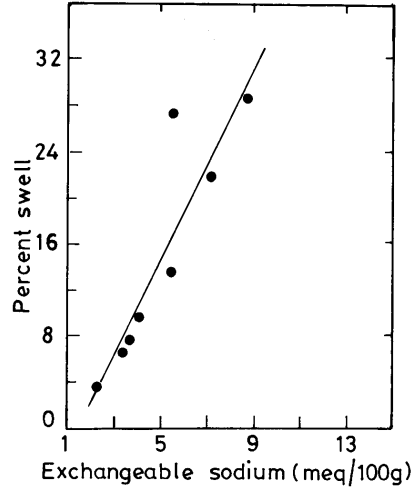
Fig. 5. Effect of exchangeable sodium on percent swell
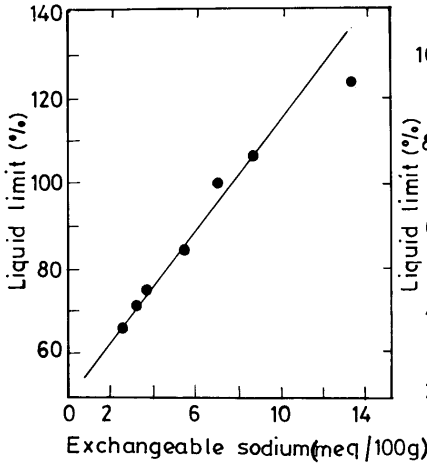
Fig. 6. Effect of exchangeable sodium on liquid limit
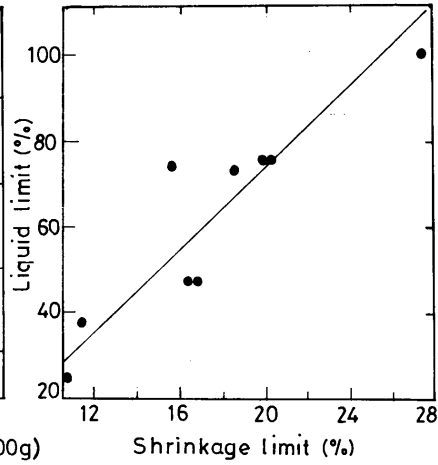
Fig. 7. Shrinkage limit vs. liquid limit for kaolinitic soils

Figure 7 shows liquid limit of kaolinitic soils bearing a good correlation with the shrinkage limit. Shrinkage limit can to a great extent indicates the fabric of the soil (Lambe 1958). Larger the shrinkage limit, the fabric is more open, and flocculated. Smaller the shrinkage limit, the fabric is relatively more oriented. Since fabric controls to a great extent the liquid limit of kaolinitic soils, it has a good corre-

lation with the shrinkage limit (Sridharan & Rao 1975, Sridharan et al. 1988). From the above discussion, it is fairly clear that the basic properties, viz., liquid limit and the sediment volume are governed by two different mechanisms, depending upon the principal clay mineral is kaolinite or montmorillonite.

4 Double layer theory and void ratio - pressure relationship

The Gouy-Chapman diffuse double layer theory has been the most widely used approach to relate clay compressibility to basic particle - water - cation interaction (Bolt 1956; Bolt and Miller 1955; Mitchell 1960; Sridharan and Rao 1973; Sridharan and Jayadeva 1982 to name a few). Bolt (1956) and van Olphen (1963) presented methods for calculating pressure - void ratio relationship in a clay - water electrotype system. Sridharan and Jayadeva (1982) improved the procedure given by Bolt (1956) and van Olphen (1963) and presented the diffuse double layer theory in a lucid form that could be readily used for understanding the engineering behaviour of clays. Many researchers have concluded the validity of the Gouy-Chapman theory for predicting the void ratio - pressure relationship qualitatively and under certain circumstances quantitatively (Bolt 1956; Bolt and Miller 1955; Mitchell 1960; 1976; Sridharan and Jayadeva 1982; Sridharan and Choudhury 2002 to name a few).

Figure 8 shows the basic relationship between the mid-plane potential, u and the non-dimensional parameter Kd for various $(dy/d\xi)_{x=0}$ value.

$$\left(\frac{dy}{d\xi}\right)_{x=o} = (B/S)\sqrt{2\pi/\varepsilon nkT} \tag{1}$$

$$K = \sqrt{8\pi e'^2 v^2 n/\varepsilon kT} \tag{2}$$

$$e = G\gamma_w Sd \tag{3}$$

where, n = concentration of ions in the bulk fluid, k = Boltzmann constant, T = temperature absolute, B = Base exchange capacity, S = Specific surface of the soil, ε = Dielectric constant of the bulk fluid, v = valency of the exchangeble ions, e' = 4.8×10^{-10} esu, G = specific gravity of soil solids, γ_w = unit weight of water and d = half the distance between the parallel plates

Van't Hoff equation (Eq. 4) relate the pressure, p and the mid-plane potential, u as:

$$p = 2nkT(\cosh u - 1) \tag{4}$$

Although Figure 8 shows that the u-Kd relationship depends on $(dy/d\xi)_{x=o}$ it has been shown by Sridharan and Jayadeva (1982) that the u-Kd relationship is almost unique for the clay-water electrolyte system usually encountered in geotechnical engineering and is given as:

$$u = 2.35 - 4.375 \log_{10} Kd \tag{5}$$

Figures 9, 10 and 11 show some selected typical examples of how experimental results compare with the theory (Sridharan and Jayadeva 1982; Sridharan et al. 1986a).
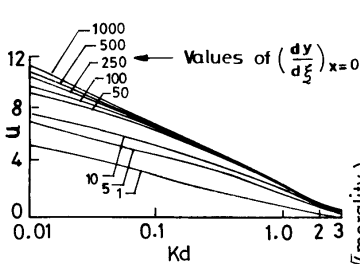
Fig.8 u – Kd relationship
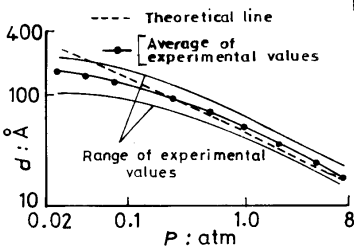
Fig.9. d vs p relationship for montmorillonites
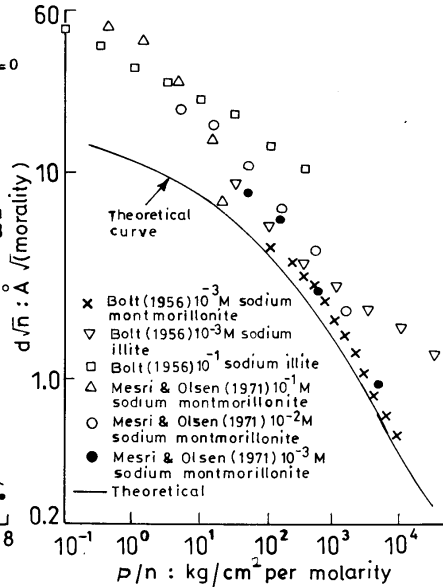
Fig.10. Comparison of experimental results with theory

Figure 9 shows the log d vs. log p results obtained for several montmorillonites having different specific surfaces. Figure 10 shows (using the results of Bolt 1956; Mesri and Olsen 1971), how the theoretical d√n-log(p/n) relationship compares with the experimental results. Figure 11 shows the comparison of experimentally obtained swelling pressure with the dry density, γ_d of a swelling soil compacted at different moisture contents. As per the double layer theory, the swelling pressure is primarily a function of the separation distance, 2d, which is a direct function of the dry density when all the other soil/fluid parameters are same. The initial molding water content should not influence the relationship as per diffuse double layer theory.
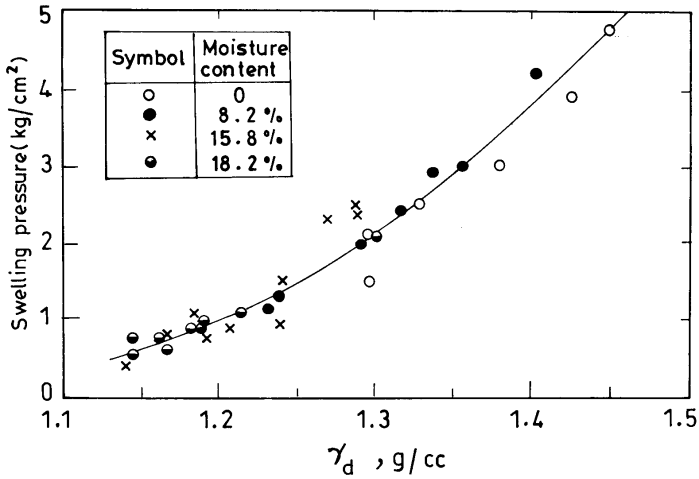
Fig.11. Effect of dry density on the swelling pressure

The typical results shown in figures 9, 10 and 11 indicate that the Gouy-Chapman diffuse double layer theory can explain to a great extent, satisfactorily the pressure-volume chnge behaviour of clays. Further, it has been brought out in the literature that the prediction of the Gouy-Chapman theory is better for the sodium montmorillonite clay - water system than for other clays (Sridharan and Choudhury 2002). It has been brought out by Sridharan and Choudhury (2002) that while the theoretical equation for Na-montmorillonite based on Gouy-Chapman theory could be stated as:

$$u = 2.1 - 4.583 \log_{10} Kd \qquad (6)$$

The experimental results shows u to be related to Kd as:

$$u = 2.81 - 3.375 \log_{10} Kd \qquad (7)$$

The above discussion brings out the potential use of Gouy-Chapman theory for prediction of pressure - void ratio relationship of montmorillonitic clays with suitable modifications.

5 Volume Change Behaviour

5.1 Saturated clays

Several factors are responsible for volume changes in natural and compacted clays. Since the understanding of the volume change behaviour of clays, compression/swelling, appears to depend on a better understanding of the physico-mechanisms which are involved, it is worthwhile considering the basic mechanisms controlling the same.

5.2 Basic mechanisms controlling compressibility of clays

Sridharan and Rao (1973) based on the available results reported in the literature and on their own experimental results proposed basically two mechanisms controlling the volume change behaviour. They are, mechanism 1, wherein the compressibility of a clay is primarily controlled by the shearing resistance at the near contact points and volume changes occur by shear displacement and/or sliding between particles and mechanism 2, in which compressibility is primarily governed by the long range electrical repulsive forces (primarily double layer repulsive forces). Although these effects operate simultaneously, the published results indicate that mechanism 1 primarily governs the volume change behaviour of non-expanding lattice type of clays like kaolinitic soils and mechanism 2 that of expanding lattice type of clays like montmorillonitic clays.

Some typical experimental results are presented to bring out the dominant presence of mechanism 1 and 2 controlling the volume change behaviour of clays. Figure 12 shows the pressure - void ratio relationship of kaolinite (w_L = 49% w_p = 29%), with pore fluid as CCl_4 and water obtained in a conventional oedometer (Sridharan and Rao 1973). The kaolinite clay can withstand the same pressure at much higher void ratio with CCl_4 as fluid compared to water. For kaolinite clay, the required shearing resistance with CCl_4 as fluid is realised at much higher void ratio than with water as pore fluid. Figure 13 shows the change of pore fluid from CCl_4 to water at a specified pressure brings down the void ratio. Lesser void ratio is required to withstand the same external pressure with water as pore fluid. The typical results presented brings out the shearing resistance controlling the volume change behaviour in kaolinite.

Figure 14 present the effect of pore fluid on the one-dimensional consolidation of montmorillonite (w_L = 305% w_p = 44%; Sridharan and Rao 1973). As against what has been seen for kaolinite (Figure 12), quite opposite behaviour can be noticed for montmorillonite. Because of larger diffuse double layer repulsion,
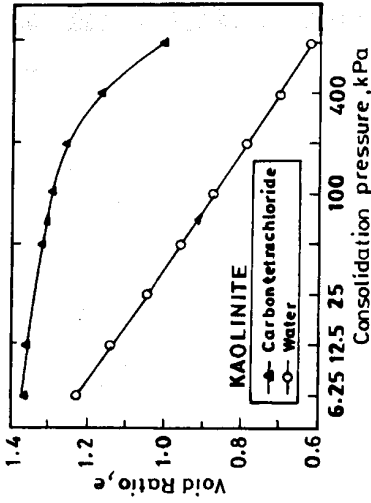
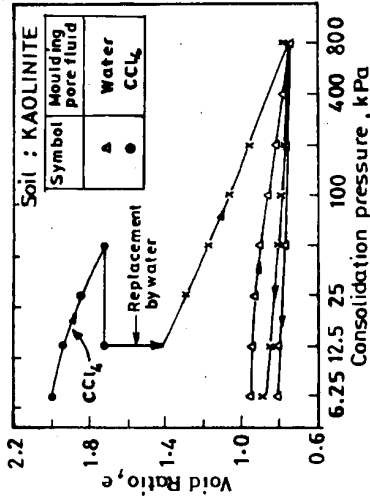Fig.12. Void ratio vs pressure for kaolinite

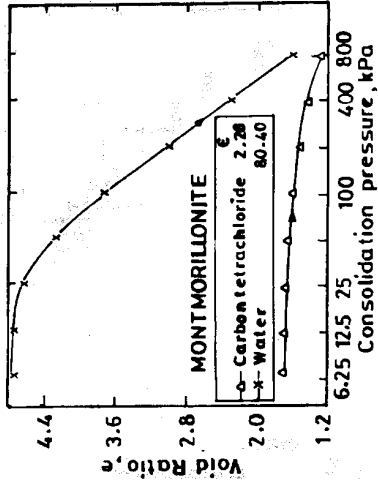Fig.13. Void ratio vs pressure for kaolinite
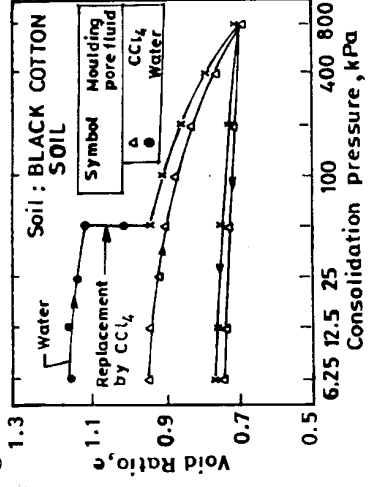
Fig.14. Void ratio vs pressure for montmorillonite

Fig.15. Void ratio vs pressure for B.C. soil

same external pressure is withstood with water as pore fluid at much higher void ratio than with CCl_4 as pore fluid. Diffuse double layer is significantly depressed with low dielectric constant fluid like CCl_4 ($\varepsilon = 2.284$) when compared with the dielectric constant of water ($\varepsilon = 80.4$). Figure 15 shows the sudden collapse when the existing fluid of water is replaced by CCl_4 for the montmorillonite clay at a specified external pressure. The change of water by CCl_4 depressed the diffuse double layer bringing in significant reduction in the void ratio. Thus the results presented in Figures 12 through 15 supports the two basic dominating mechanisms controlling the volume change behaviour of saturated clays either it is kaolinitic or montmorillonite.

5.3 Partly saturated clays

As has been noticed for saturated clays, partly saturated clays are also controlled by the two mechanisms discussed above, depending upon either the clay is kaolinitic or montmorillonitic. Figure 16 shows the compacted partly saturated kaolinitic clay (compacting water content = 11%, initial dry density = 1.14 g/cc, w_L = 49%, w_p = 29%, percent clay = 54%) tested in a conventional oedometer (Sridharan et al. 1973). The void ratio - pressure relationship has been shown before soaking and after soaking the sample. The samples were consolidated under partly saturated condition upto a specified pressure and then soaked till equilibrium has reached keeping the external pressure constant. The kaolinite collapsed at all soaking pressures, even at a nominal pressure of 6.25 kPa. Similar results have been obtained for other initial conditions also. The compression curves for the soaked soils are potted in terms of conventional effective stress, whereas those for partly saturated condition are in terms of applied stress (The negative pore water pressure/suction pressure, the attractive and repulsive pressures are not known under partly saturated condition). Irrespective of soaking pressures, it is observed that all the compression curves join almost into a single curve after soaking. The effect of stress path seems to be negligible on the e-p curve.

Figure 17 illustrates results on black cotton soil which is an expansive soil (w_L = 101%, w_p = 28% and percent clay fraction = 30%). The results are from conventional oedometer on compacted soil (compacting water content = 11.5%, compacting dry density = 1.23 g/cc). Similar results have been obtained for other initial densities and water contents (Sridharan et al. 1973). Unlike what has been noticed for kaolinite (Fig. 16), swelling has taken place even upto an external pressure of 25 kPa and at higher pressures collapse has taken place. As one would expect, for the black cotton soil, the amount of swelling is more when externally applied pressure is less. Similarly the compression/collapse is more when applied pressure is more. Depending upon the initial density and compacting water contents, swelling/compression can take place at lower/higher external pressure.

It has been brought out earlier that mechanism 1 and 2 controls the volume change behaviour of saturated system depending upon the nature of clay mineral

present. The results presented in Figure 16 shows that compression/collapse takes place because of the reduction in shearing resistance at the particle level due to reduction in effective stress brought out by negative pore water pressure tending to zero, the electrical repulsive forces increase and the attractive forces decrease due to saturation (Sridharan and Rao 1973, Sridharan et al. 1973) . Hence, it is seen that the compression/collapse is primarily due to the reduction in the shearing resistance brought about by reduction in the effective stress. As per mechanism 1, the shearing resistance at particle level controls the volume change behaviour. Equilibrium reaches when the shearing resistance mobilised due to reduction in void ratio equals the shearing stress at particle level due to the externally applied pressure.

The results presented in Figure 17 bears evidence for the mechanism 2 operating in expansive soils. Upon saturation, diffuse double layer repulsion gets mobilised showing heave if the externally applied pressure is less than the swelling pressure in soils at that initial void ratio. When the externally applied pressure is more than the swelling pressure, compression takes place till the repulsive pressure mobilised equals the externally applied pressure. Thus it is seen that the mechanism controlling the volume change behaviour of partly saturated clays are also the same as the saturated clays. It is worth mentioning here that the level of the external effective pressure acting plays a role whether an expansive soil will swell or compress. Partly saturated kaolinitic soils will always compress even at very low external pressure acting.

6 Undisturbed Natural Soils

6.1 Non-swelling soil

In the previous paragraphs, the volume change behaviour of saturated kaolinite, montmorillonite, black cotton soils under remoulded conditions have been examined and it has been brought out that the mechanisms controlling their volume change behaviour is distinctly different. In the following paragraphs, the volume change behaviour of unsaturated undisturbed as well as remoulded soils are considered.

Figure 18 shows the oedometer test results of soils both undisturbed (UND) and remoulded to insitu density and water contents (REM) are presented (Sridharan and Allam 1982). The undisturbed soils are partly saturated and are allowed to get saturated in the oedometer at a nominal pressure of 6.25 kPa. The different soils
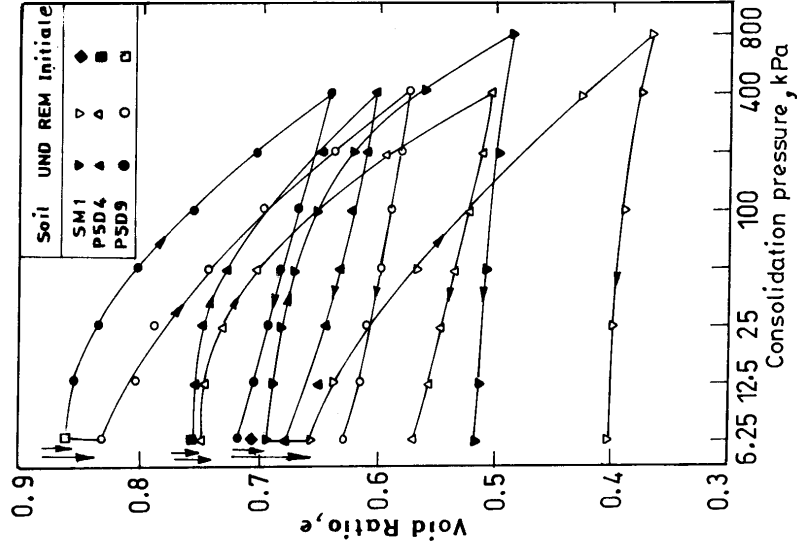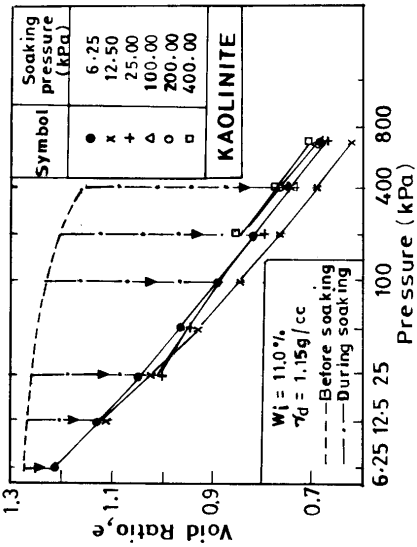
Fig.18 Effect of soaking for Natural soils

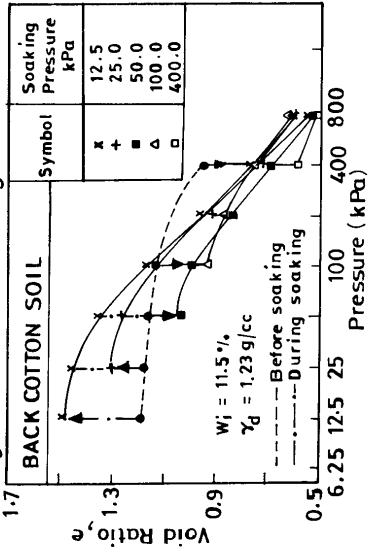Fig.16 Effect of soaking on void ratio

Fig.17 Effect of soaking on void ratio

SM1, P5 D4 and P5 D9 have relatively low liquid limits (32 to 48%) and plasticity index values (13.4 to 20%). The percentage of silts and clays present is also (18 to 40%). The clay mineralogical investigation shows that they are composed of mainly non-expanding lattice structured clay minerals. Free swell test data (Fig. 2) indicates that these soils are of relatively non-swelling type. Figure 18 shows in both their undisturbed and remoulded conditions compression taking place upon soaking at the initial pressure of 6.25 kPa, greater compressions occurring for soils in the remoulded condition. The total compression at the end of the loading cycle of the test is also more for the remoulded condition. Flat rebound curves, or in other words, small expansions on unloading are an indication that swelling is due to elastic rebound and straightening of bent particles indicating that the soil is of a non-swelling type. The above discussions brings out that the soils SM1, P5 D4 and P5 D9 are governed by mechanism 1, wherein the shearing resistance at parti-cle contacts governs the compression behaviour.

For undisturbed soils, the presence of desiccation bonds between soil particles augments the intrinsic effective stress present between them and thus the shearing resistance at particle contacts. The larger shearing resistance present at the particle level enables the undisturbed soil to support the external load at a higher void ratio compared with the remoulded soil where this intrinsic effective stress is not pre-sent as the desiccation bonds are disrupted by remoulding. The desiccation bonds are less affected by soaking is evidenced by the smaller compressions taking place for undisturbed soils.

6.2 Swelling Soils

Figure 19 presents typical oedometer test results on undisturbed and remoulded samples of primarily expansive soils. P7D4 and P3D11 soils have relatively large liquid limits 44.5% and 52%; plasticity index values of 16.5 and 19%; the per-centage of silt and clays of 49% and 32% respectively. The clay mineralogical in-vestigation shows that they are mainly composed of expanding lattice - structured clay minerals. The free swell test data also confirms their swelling nature. Figure 19 shows that these soils in both their undisturbed and remoulded states swell upon soaking at the initial pressure of 6.25 kPa, the magnitude of swelling being more for the remoulded state. The swelling is noticeable, although slight, for the undisturbed state.

The desiccation bonds present in the undisturbed soils cement soil particles to-gether to form larger particles or crumbs resulting in reduced effective specific surface areas. On soaking at the initial pressure of 6.25 kPa, the bonds present prevent the component particles from mobilising diffuse double layers between themselves. While the increased repulsion between the crumbs causes the soil to swell, the swelling is small compared with that undergone by the remoulded soil with its relatively larger effective specific surface and thus repulsive force. During the loading cycle of the consolidation test, the remoulded soil is able to mobilise 2

the necessary interparticle repulsion to support the external pressure at a higher void ratio, owing to its larger effective specific surface than the undisturbed soil. The compression curve for the remoulded soil thus lies above that for the undisturbed soil (Fig. 19). Further, it may be seen that the amount of rebound is larger for the remoulded soil as can be expected. The results presented in Figure 19 indicate that mechanism 2 wherein diffuse double layer repulsive forces govern the volume change behaviour.

Figure 20 present the consolidation test results of soils essentially containing expanding lattice structured clay minerals in their fines. The NG2 and NG3 soils have liquid limits of 44.5% and 35.5%; plasticity indices of 19.% and 13%, silt and clay of 60.5% and 47%; and sand contents of 33.5% and 48% respectively. On soaking at the initial pressure of 6.25 kPa, the soil in their remoulded state swell, while in their undisturbed state they compress (only limited results are presented for want of space). Further, the rebound curves are steeper and the recovery ratios are greater for the remoulded state. Although the soils are expanding lattice type, they show compression upon soaking at a nominal pressure of 6.25 kPa in their undisturbed state like non-expanding lattice type of soils (Fig. 18) because of crumbs formed due to desiccation bonds making them larger size particles with lesser surface areas. In the case of remoulded soils, the soil swells on soaking indicating that the repulsive forces dominate and the volume changes are governed by essentially diffuse double layer forces; i.e., mechanism 2. From the results presented in Figures 19 and 20, it is seen that "swell sensitivity" exists. The amount of swell upon soaking is more for remoulded state than for undisturbed state. Swell sensitivity could also be negative since the remoulded soil swells whereas the undisturbed soil compresses upon inundation.

7 Conclusions

Partly saturated fine grained soils collapse or swell when they are allowed to get saturated depending upon the type of primary clay mineral present in their clay size fraction and the external stress acting. Swelling/non-swelling soils (montmorillonitic/ kaolinitic) cannot be differentiated by the conventional plasticity chart. Simple sediment volume test/free swell test with pore fluid as water and non-polar fluid like CCl_4 helps to identify the fine grained soils either swelling/non-swelling.
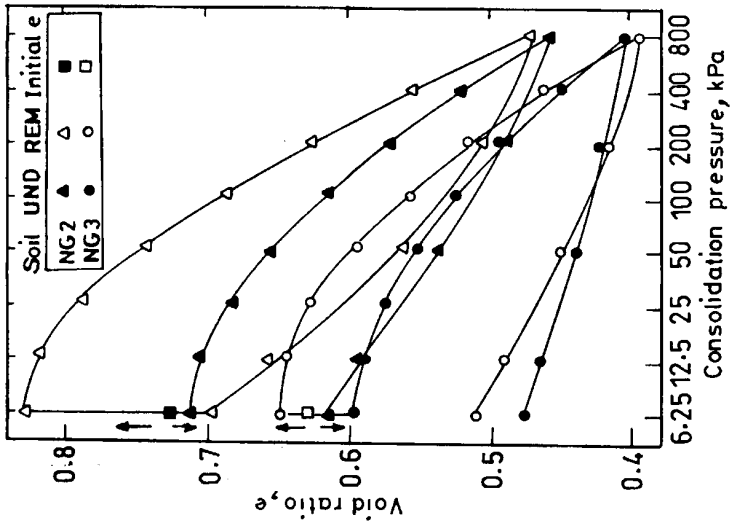
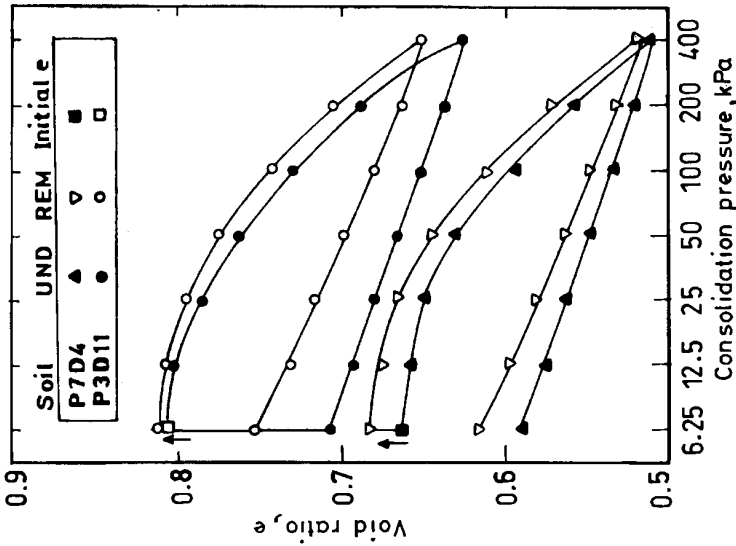Fig.20. Effect of soaking on void ratio for swelling soils

Fig.19. Effect of soaking on void ratio for swelling soils

Distinctly two different mechanisms control the liquid limit/volume change behaviour of fine grained soils either they are swelling or non-swelling soils. While shearing resistance at particle level and fabric control the liquid limit/volume change behaviour of kaolinitic soils (mechanism 1), diffuse double layer repulsion plays a dominant role in the liquid limit/volume change behaviour of montmorillonitic soils (mechanism 2). While both the two mechanisms operate simultaneously in a natural fine grained soils, one of them dominates depending upon the type of clay minerals present and their percentages. Gouy-Chapman theory enables to predict the swelling of montmorillonitic clays qualitatively and quantitatively under certain circumstances.

Bonding, externally applied stress and type of clay mineral present play important roles in the compression/swelling behaviour of non-expansive/expansive natural undisturbed partly saturated soils. Upon wetting, the unsaturated bonded specimen (undisturbed) collapses/swells by an amount smaller than that of the unsaturated unbonded (remoulded) specimen depending upon the magnitude of externally applied stress. Undisturbed (bonded) expansive soils can even show compression upon wetting even under very light external stresses, whereas the remoulded sample can show large swelling.

In this paper, the volume change behaviour of fine grained soils containing primary clay mineral either kaolinite or montmorillonite have been discussed. It is possible that many natural fine grained soils may contain mixed clay minerals without exhibiting the behaviour distinctly either to be kaolinitic or montmorillonitic in the free swell test. This aspects needs further investigation.

8 References

Bolt GH (1956) Physico-chemical analysis of the compressibility of pure clays. Geotechnique 6:86 73

Bolt GH, Miller RD (1955) Compression studies of illite suspensions. Proc. Soil Sci. Soc. Of Am. 19: 285 288

Lambe TW (1958) The structure of compacted clay. Jl Soil Mech and Found divn ASCE 84:1654

Low PF (1980) The swelling of clay II montmorillonites. J Soil Sci Soc Am 44:667 676

Mesri G, Olson RE (1971) Consolidation characteristics of montmorillonite. Geotechnique 21: 341 352.

Mitchell JK (1962) The application of colloidal theory to compressibility of clays. Proc of seminar on interparticle forces in clay-water-electrolyte system. Melbourne CS&I RO 2-92 2-97

Mitchell JK (1976) Fundamentals of soil behaviour. John Wiley, New York.

Sridharan A (1991) Engineering behaviour of clays - A fundamental approach. Indian Geotech J 21:1-136.

Sridharan A, Allam MM (1982) Volume change behaviour of desiccated soils. J of the Geotech Div Proc ASCE 108:1057 1071.

Sridharan A, Choudhury D (2002) Swelling pressure of sodium montmorillonites. Geotechnique 52:459 462.

Sridharan A, Jayadeva MS (1982) Double layer theory and compressibility of clays. Geotechnique 32:133 144.

Sridharan A, Rao GV (1973) Mechanisms controlling volume change behaviour of saturated clays and the role of effective stress concept. Geotechnique 23: 359 382.

Sridharan A, Rao GV (1975) Mechanisms controlling the liquid limit of clays. Proc. Istanbul Conf. on Soil Mech and Found Eng 1:75-84

Sridharan A, Rao SM (1988) A scientific basis for the use of index tests in identification of expansive soils. Geotech. testing J. 11:208 212.

Sridharan A, Rao GV, Pandian RS (1973) Volume change behaviour of partly saturated clays during soaking and the role of effective stress concept. Soils and Foundations 13 : 1 15.

Sridharan A, Rao AS, Sivapullaiah PV (1986a) Swelling pressure of clays. Geotechnical Testing J 9:24 31.

Sridharan A, Rao MS, Murthy NS (1986b) Liquid limit of montmorillonite soils. Geotechnical Testing J 9:156 164.

Sridharan A, Sudhakar M. Rao, Sathyanarayana Murthy (1986c) A rapid method to identify clay type in soils by the free swell technique. Geotechnical Testing J 9: 198 203.

Sridharan A, Rao SM, Murthy NS (1988) Liquid limit of kaolinitic soils. Geotechnique 38: 191 198.

Sridharan A, Sudhakar M Rao, Sanjeev Joshi (1990) Classification of expansive soils by sediment volume method. Geotechnical Testing J 13: 375 380

van Olphen H (1963) An introduction to clay colloid chemistry for clay technologists, geologists and soil scientists. Interscience, New York.

Volume change behaviour of cohesive soils

M. Dobrowolsky

University of Kaiserslautern, Department of Soil Mechanics and Foundation Engineering, dobrow@rhrk.uni-kl.de

1 Abstract

The volume behaviour of partly saturated soils is investigated within the scope of a subproject of the DFG-Research Group "Mechanik teilgesättigter Böden". The subproject III, Prof. Helmig, is parallely involved with our work for the description of the moisture transport in cohesive soils, which will later be integrated into our concept.

The subject of this paper are the constraints on geotechnical structures due to temperature and moisture changes. The demand for a suitable constitutive equation exists since such effects are only minimally resp. not at all observed the well-known literature. There are different research papers in the literature dealing with the subject "expansive soils", like e.g. from: [15], [5], [10], [11], [12], [13], [7], [6] and others. But most of these papers concentrate solely on the axial swelling heave and hence, the resulting swell pressure. Systematic investigations for constraints for any state of stress or deformations under the consideration of variable water content, temperature and void ratios are still unavailable and are trying to be completed in the context of this research work. The investigation results leads into an approach of a constitutive relation, which is subsequently implemented into a numerical programme.

2 Constitutive relation

An objective constitutive equation is to be developed to describe the volume change behaviour of fine grain soil due to moisture and temperature changes. The volume change behaviour due to swelling

$$I_\varepsilon^{SW} = f_1 \left(e_0, w(t), I_{\sigma'}, T, t \right) \tag{1}$$

as well as due to shrinking

$$I_\varepsilon^{SN} = f_2 \left(e_0, w(t), I_\sigma, T, t \right) \tag{2}$$

is considered. Dependencies existing by the initial void ratio e_0, the effective stress $I_{\sigma'}$, the degree of saturation S_r, the time t and the temperature T. As an inverse to equation (1), the swell pressure-strain relationship can also be written as a product relation

$$I_\sigma^{SW} = I_{\sigma\max}^{SW} \cdot f_3(I_\varepsilon^{SW}, e_0, w(t), T, t) \tag{3}$$

whereby $I_{\sigma\max}^{SW}$ is the 1st invariant of the stress tensor, which occurs due to swelling at a constant volume . The maximum of $I_{\sigma\max}^{SW}$ is likewise dependant on the mentioned parameters and can be written as

$$I_{\sigma\max}^{SW} = P_a \cdot f_4(w_0) \cdot f_5(e_0) \cdot f_6(T) \tag{4}$$

whereby P_a is the atmospheric pressure.
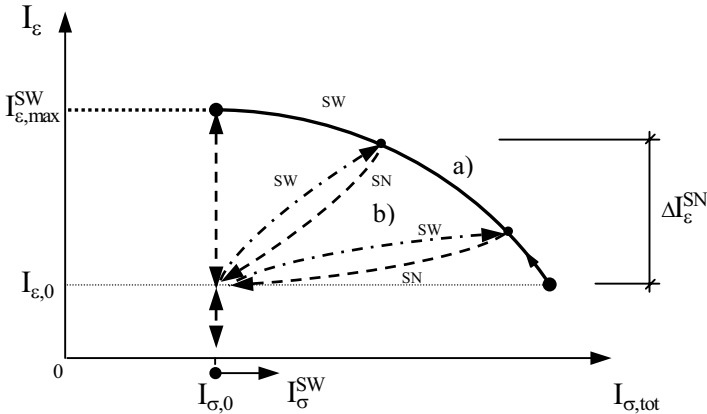
Fig. 1.   Deformations due to swelling and shrinkage of a soil sample

For expansive soils both the initial stress condition as well as the swelling constrains act together in situ. For the following model only the spherical components of the stress tensor are considered. The 1st invariant of the total stress consists of the preloading pressure and the swelling pressure:

$$I_{\sigma,tot} = I_\sigma^{SW} + I_{\sigma,0} \tag{5}$$

The qualitive evolution of the deformation behaviour due to swelling, curve a) in fig. 1, is known from the literature, e.g. [15]. It is generally to be assumed for shrinkage, that this can occur for any state of deformation or stress and a subsequent absorption will once again occur, curve b) in fig. 1. With a decrease in total stresses $I_{\sigma,tot}$, the incremental volumetric shrinkage strain $\Delta I_\varepsilon^{SN}$ expands and reaches its peak value when the swell stress $I_\sigma^{SW} = 0$. For the developed model

the interaction between the stress state and the volume change behavior is considered by the compression and swelling index with respect first of all and among others to the degree of saturation.

3   Test material

The material chosen for the test is kaolinite (finely ground clay IBECO-Uniton) which is described in [3]. In table 1 the clay mineral composition according to factory specifications and some soil-physical parameters are displayed.

Table 1:   Clay fractions and soil-physical parameters

Clay minerals	Kaolinite > 40%
	Illite < 20%
	Smectite < 5%
Liquid limit	$w_L = 54,0 \%$
Plastic limit	$w_P = 21,3 \%$
Water absorption value after 4 h	$w_A = 73,5 \%$

The kaolinite is able to adhere to water in different manners. Therefore the soil water is distinguished in two components:

- Adsorption water, which is accumulated on the mineral surfaces and as well as inside the material.

- Capillary water, which is retained in the pores by means of surface tension.

Both parts of water are in equilibrium. The experimentally determined water content of a specimen must be separated in both parts for the description of the soil-moisture tensions, which is only a function of the capillary water.
The adsorption water can be calculated from the water film thickness and specific surface of the soil in the saturated condition. A model was developed, e.g. by [14], which can determine the adsorpitve adhered part of the total water content for saturated conditions. This model is however not suitable for the purposes of this work since the adsorption water content must be known for any case of unsaturation. A relationship between the mentioned water components is to be experimentally determined by means of multiphase absorption.

4   Test procedure

The aim of the investigations is the determination of the functions for the equations (1) to (4) as well as the values of the mentioned material parameters. There are four series of tests, which are considered. For the first series, the oedometer tests listed in table 2 are temporarily conducted.

Table 2:   Test programme, series 1

Initial degree of saturation S_{r0} [-]	Initial void ratio e_0 [-] / Temperature T [°C]				
	0,68		0,78		0,88
0,68	20	5	20	35	20
0,78	20	5	20	35	20
0,88	20	5	20	35	20

All specimens in this series are watered from the value $S_{r,0}$ to saturated conditions ($S_r=1,0$). The investigations for series 1 concentrate on the time dependent development of $I_{\sigma,max}^{SW}$. $S_{r,0}$, e_0 and T are the variable parameters.

Oedometer tests are likewise performed in series 2. The effects from swelling strain I_ε^{SW} as well as skrink deformations I_ε^{SN} to I_σ^{SW} are also investigated, see fig. 1.

$$I_\sigma^{SW} = f(I_\varepsilon^{SW}, I_\varepsilon^{SN}, ...) \tag{6}$$

The initial void ratio e_0 and degree of saturation $S_{r,0}$ as well as the test temperature T are the variable parameters.

The three dimensional swelling strain behaviour, by irrigation on all sides of the specimen will be investigated in triaxial tests in series 3. Some pre-tests are performed with a foam cover in a standard triaxial cell. The results are compared with those from the oedometer tests. The variables are hereby again e_0, $S_{r,0}$ and T.

Multi-level saturation tests in an oedometer are performed in series 4. It is investigated whether the value $I_{\sigma,max}^{SW}$ is reached for multi-level absorption, see fig. 2, which appears by immediate saturation. The results should provide information concerning the stress equilibrium, which was already addressed in chapter 3, and the time dependences of I_σ^{SW}.
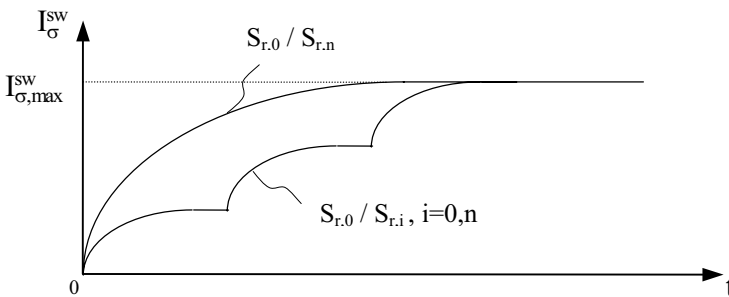
Fig. 2. Series 4: Multi-Level absorption, $I_\varepsilon^{SW} = 0$, $S_{r,0}$=0,68, $S_{r,n}$=1,0, $S_{r,i}$=0,78 / 0,88 / 1,0 , T= 20°C

5. Test implementation

The aim of the different test series is to observe the materials swelling, shrinking and creeping under consideration of the initial and boundary conditions. The initial and boundary conditions are affected by: The primary stress condition $I_{\sigma,0}$, the temperature T, the void ratio e_0, the degree of saturation S_{r0}, the relative humidity H, the soil sample preparation whereby the most important points here are whether the stress equilibrium, as is described in chapter 3, is already reached or not and with which preload the sample was produced, see fig. 3.

a)   **b)**
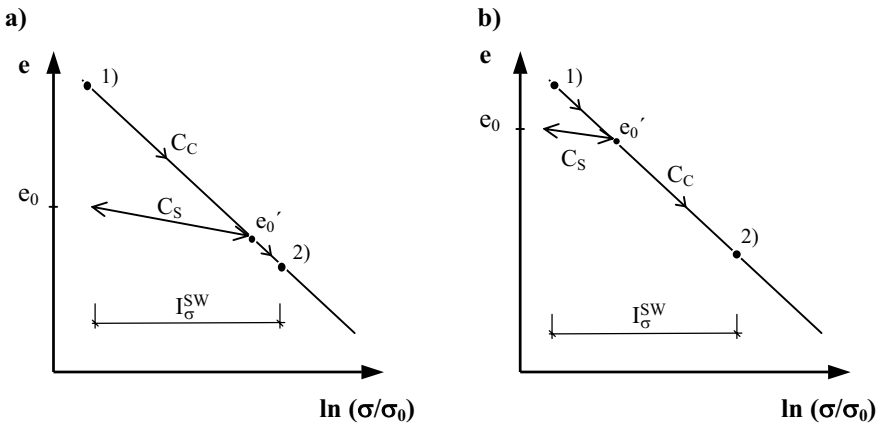
Fig. 3. Stress-void ratio diagramme in a semi-logarithmic scale

Figure 3 shows the semi logarithmic relationship between the stress and the void ratio of a saturated soil. For the sake of simplicity the behaviour of unsaturated soils is abutted to that of saturated soils.

From point 1), the material is compressed to a value of $e_0{}'$ by means of a static compression and is then once again released. The initial void ratio e_0 is reached after relaxation of the specimen. For reloading due to I_σ^{SW} until point 2), the effects from C_S resp. C_C are significant in curves a) resp. curve b). These effects must be considered during both the sample production and the test itself.

5.1 Series I

Cylindrical specimens with a diameter of d=100 mm and a height of h_0=20 mm are mounted in a oedometer cell with a treated inner surface to provide smooth sliding, fig. 4. The finely ground clay is mixed with a specified water content in a mixer at time t_0 with a value of w_0 for the sample production.

It is statically compressed with a preload pressure σ_v, until the desired void ratio e_0 is achieved. It was investigated in some pre-tests at which time the swelling process ended after mixing of the sample with w_0. It is thereby warranted, that the swelling due to w_0 already vanished at the beginning of the test. The tests of series 1 take place with a constant volume of $\varepsilon_z=0$ and a testing termperature of T=20°C. The swelling is investigated in dependance of the fabrication time of the specimen and the test time.

$$I_\sigma^{SW} = P_a \cdot f(t, ...) \rightarrow I_{\sigma,max}^{SW} \tag{7}$$

Furthermore, the test are performed with constant volume

$$\varepsilon_z = 0 \rightarrow I_{\sigma max}^{SW} = P_a \cdot f_7(e_0, w_0, T, I_\sigma) \tag{8}$$

for the determination of $I_{\sigma,max}^{SW}$.

Fig. 4. Oedometer device with additional load cell

5.2   Series II

The oedometer tests of series 2 are built upon equation 8 of series 1. A specified deformation in the z direction is permitted for the determination of I_σ^{SW} as a function of I_ε^{SW} after reaching the maximum swelling stress.

$$\varepsilon_z \neq 0 \rightarrow I_\sigma^{SW} = f_8(I_\varepsilon^{SW}, e_0, w_0, T, I_\sigma, t) \tag{9}$$

The samples in the oedometer ring subsequently shrink due to applied a vacuum at the top and bottom plate and are once again absorbed thereafter to maintain the curves b) in fig. 1.

Pre-tests are conducted for shrinkage in which the samples are placed between two porous stones free of preloading stresses, see fig. 5. The samples have been statically compressed in a cylinder after mixing in such a way that the desired initial soil values have been reached.

The samples were subsequently pressed out of the cylinder, porous stones with applied filter paper have been arranged on the sample ends and the desiccation under isothermal conditions subsequently results. Filter paper on the surfaces enabled an unstrained sliding of the sample. The axial and the radial displacements of the specimen were determined with a slide gauge and the water content of the soil material is detected by weighing.

Fig. 5.   Four specimens in the shrinkage test

5.3   Series III

The pre-tests of series III are carried out to develop a convenient fabrication method in order to ensure a homogeneous and isotropic behaviour in the axial and radial direction of the specimen. These tests are also of interest relating to the results of series I and II.

The cylindrical sample with a homogeneous initial degree of saturation $S_{r,0}$ is inserted into a hollow foam cylinder without any membrane on the surfaces [see Fig. 6]. The foam covers the soil specimen and provides the stability of the soil grains due to pressure induced by water inflow and it allows deformations in all directions due to the swelling process. To provide the soil from excess pore air pressure, a vertical drainage is inserted inside the specimen.

The samples are subjected to different hydrostatic pressures up to $\sigma_0 = 100$ kPa. In this phase, the specimen begins to saturate. The test time, the temperature and the inflow quantity of deaerated water in the specimen are measured. Furthermore,

the deformation of the soil sample is recorded from beginning to end. While the specimen is going to saturate ($S_r \rightarrow 1,0$), the effective stress of the material decreases and totally vanishes when the specimen is fully saturated ($I_{\sigma'} = 0$). The temperature as well as the total cell pressure remains constant during the swelling process.

It can be seen from the test results that the radial deformation is about 85 % to 100 % of the axial deformation in the final state. Further investigations with concentrating on the differences in the deformation will follow. It is assumed in the first step that the triaxial swelling behaviour is reasonably homogenous.

Tests subjected to high effective stress states ($I_{\sigma'} > 0$) as well as investigations of the volume change behaviour considering watering and dewatering paths are planned to be carry out with a modified triaxial cell.

Fig. 6. Specimen in its "foam corset" after test completion

5.4   Series IV

Further multiple step absorption tests are performed in the oedometer machine with an identical replica of the specimen used in series 1. The samples are absorbed in three steps whereby a constant value of I_{σ}^{SW} must occur at the beginning of the next step, compare fig. 2. The resutls are subsequently compared with results from series 1.

6.   Analysis of the test results

6.1   Series I

The saturation takes place in the oedometer by fixed top plate, $\varepsilon_z = 0$. The swelling pressures due to $S_{r,0}$ are already abated at the beginning of the test. Figure 7 exemplarily shows the results of a swelling pressure test with constant volume and an initial stress $\sigma_z = 8{,}0$ kPa in semi logarithmic form. The sample pertaining to figure 7 was almost saturated after roughly one hour and I_σ^{SW} reached 91 % from $I_{\sigma,max}^{SW}$.
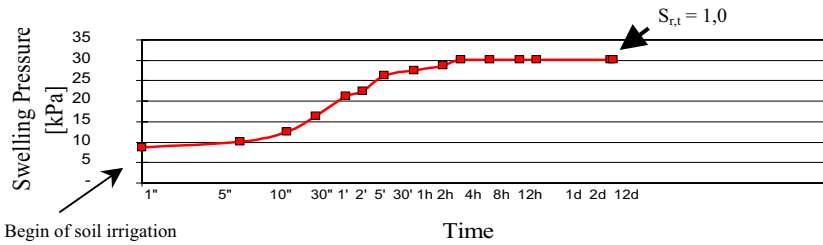
Fig. 7. Swell pressure-time curve, $e_0 = 0{,}78$, $S_{r0}=0{,}88$, T= 20 °C , $\Delta I_\varepsilon = 0$

The maximum swell pressure $I_{\sigma,max}^{SW} = 3 \cdot \sigma_{z,max}^{SW}$ occurs after t = 4 h. Figure 8 displays further results from series 1.
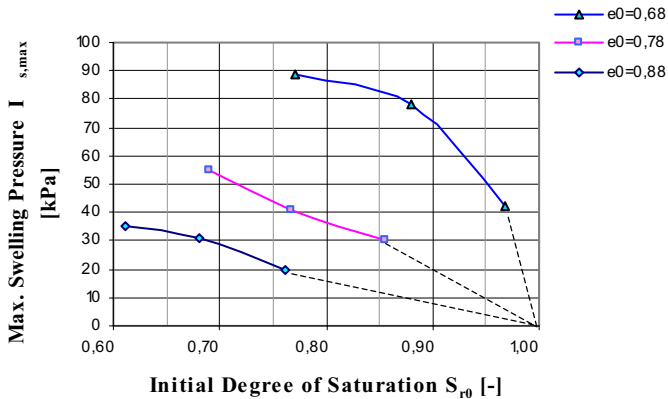
Fig. 8. Max. swell pressure in dependence of the initial saturation as well as the void ratio

The results in figure 8 show that the swelling pressure is significantly reduced with increasing void ratio and thereby a decreasing sample stiffness. The same tendancy exists for fixed e_0-values and increasing initial saturation. All samples were loaded with same preloading pressure $\sigma_v = 8$ kPa.

6.2   Series II

The samples swell up to a value of I_ε^{SW} and a subsequent loss of moisture occurs and in turn, a shrinkage of the sample. Variable parameters are e_0, w and T. A test result is examplarily displayed in figure 9.

It is evident that both the volume and density remain relatively constant after the shrinkage limit w_s is reached. The water tensions cause larger deformations as far as this shrinkage limit.
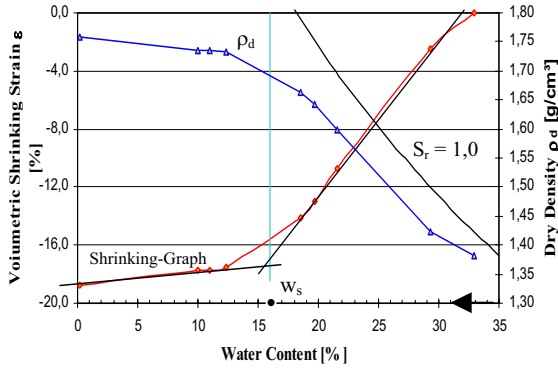
Fig. 9. Results from a shrinkage test, $e_0 = 0,88$, $Sr_0=0,98$, $w_0=0,32$, T= 20 °C

The results of three shrinkage tests with different initial degree of saturations and constant initial void ratio are expressed in figure 10. The curves of the lower water contents are similar to each other, but the almost saturated sample ($w_0=0,25$) exhibits a noteworthy larger degree of shrinkage.
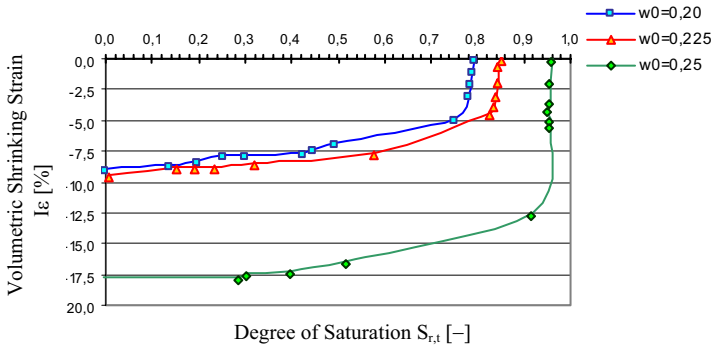
Fig. 10. Compilation of three shrinkage curves with different initial saturation., $e_0 = 0{,}68$, T= 20 °C, σ_v = const.

The preloading pressure σ_v is kept constant for all three tests. The swell time at the beginning of the tests is 24 h. An excessive hydrostatic pressure results from the preloading and is removed within this period and the sample relaxes.

6.3   Series III

The samples are subjected to an isotropic stress level of $I_\sigma= 300$ kPa 24 hours after mixing the material with the initial water content w_0.
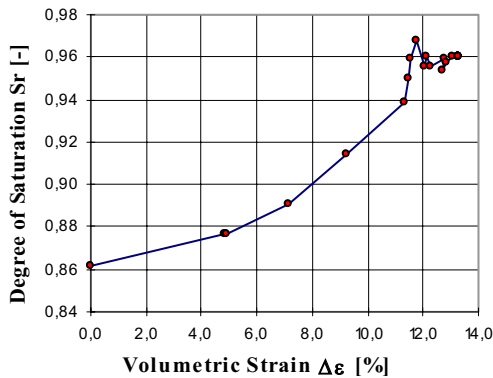
Fig. 11. Volumetric strain – degree of saturation curve, $e_0 = 0{,}78$, w_0=25,0 %, T= 20 °C, $I_{\sigma'\,(Sr\approx1,0)}= 0$ kPa

The swell strain versus saturation curve is exemplary expressed in figure 11. The sample was irrigated for 7 days until the maximum volumetric swell strain was reached. Further maximum swell strains after saturation for different initial degrees of saturation $S_{r,0}$ are shown in figure 12. The samples had three different initial void ratios.
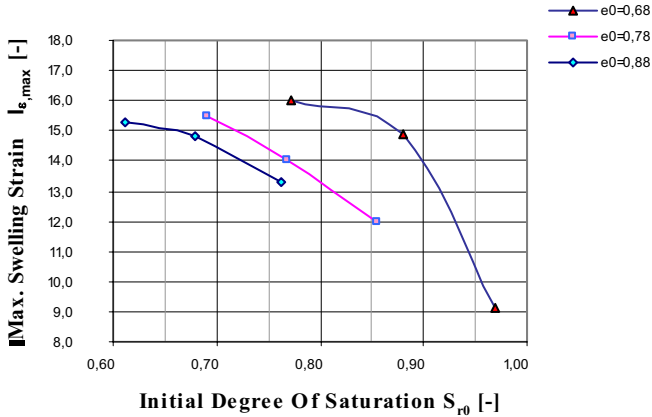
Fig. 12. Relationship of the maximum swell strain to the initial degree of saturation with different initial void ratios, T= 20 °C, $I_{\sigma'} = 0$ kPa, σ_v = const.

The swell strains increase with an decrease in the initial void ratio as well as a decrease in initial degree of saturation. Additional tests must show whether every curve possesses a common plateau with a decrease in initial degree of saturation.

7.   Future developments

The temperature and the absorption resp. desiccation time effects on the swell tests and shrinkage tests are to be investigated more closely. The tests are continued in every series, whereby the pre-tests in series 2 are completed and the main investigations can be started. The boundary conditions from series 3 are adjusted with those from series 1.

The available amount of data allows only an approximate determination of the necessary parameter values. The constitutive relations shall then be implemented in a finite element programme and initial – boundary conditions shall be investigated.

We are expecting specifications from the subproject III from the DFG-Research Group, under management of Prof. Dr.-Ing. Rainer Helmig, concerning the time progression of a homogeneous distribution of the degree of saturation in samples as well as subsoil sectors and relations for the description of the moisture transport in soil depending on the temperature T, water content w_0 and the void ratio e_0.

References

1. Brauns, J. & Schneider, H. & Gottheil, K.: Wasserverlust und Schrumpfen bei mineralischen Dichtungen aus geotechnischer Sicht, In: geotechnik 23, Nr. 1, 2000
2. Bucher, F. & Jedelhauser, P. & Mayor, P.-A.: Quell-, Durchlässigkeits- und Schrumpf-Versuche an Quarzsand-Bentonit-Gemischen, Technischer Bericht , Institut für Grundbau und Bodenmechanik, ETH Zürich, 1986
3. Dobrowolsky, M. & Becker, A.: Adsorptions- und Desorptionsverhalten durchströmter bindiger Böden, Schriftenreihe Geotechnik, 4. Workshop Weimar „Teilgesättigte Böden" , 2002
4. Fredlund, D.G. & Rahardjo, H.: Soil mechanics for unsaturated soils, Canada: John Wiley & Sons. 517pp., 1993
5. Gadre, A.D. & Chandrasekaran, V.S.: Swelling of black cotton soil using centrifuge modelling, Journal of Geotechnical Engineering, ASCE, Vol. 120, No. 5, 1994
6. Gens, A. & Alonso E. E.: A framework for the behaviour of unsaturated expansive clays, Canadian Geotechnical Journal 29, pp. 1013-1032, 1992
7. Gudehus, G. & Külzer, M. & Meier, T.: Zustandsgrenzen und Anisotropie aufbereiteter Seetone ohne und mit Salz, In: geotechnik 26, Nr. 1, 2003
8. Hiltmann, W. & Sribrny, B.: Tonminerale und Bodenphysik, Band 5
9. IBECO Bentonit-Technologie GmbH, Technisches Datenblatt Tonmehl IBECO-Uniton, Mannheim, 1998
10. Katti, R.K. & Katti, A.R.: Behaviour of saturated expansive soil and control methods, A.A. Balkama/Rotterdam, 1994
11. Richards, B.G.: Pressure on a retaining wall by an expansive clay, 9th International Conference in soil Mechanics and Foundation Engineering, Tokyo, pp. 705-710, 1977
12. Richards, B.G.: A method of analysis of the effects of volume change in unsaturated expansive clay on engineering structures, Australian Geomechanics Journal, V G9, pp. 27-41, Sydney, 1979
13. Richards, B.G. & Peter, P. & Martin, R.: The determination of volume change properties in expansive soils, Fifth International Conference on Expansive soils, Adelaide, pp. 179-186, 1984
14. Schick, P.: Anwendung eines Zwei-Komponenten-Modells der pF-Kurve auf Strukturänderungen in Böden, In: Bautechnik 79, Heft 2, 2002
15. Solomon, T.A.: Foundation pits in saturated highly expansive soils, publication of the department of soil mechanics and foundation engineering, University of Kaiserslautern, Heft 8, 2002
16. v. Soos, P.: Eigenschaften von Böden und Fels; ihre Ermittlung im Labor. In Grundbautaschenbuch, 6. Auflage Teil 1, Ernst & Sohn, Berlin, 2001
17. Wendling, S. & Meißner, H.: Soil water suction and compaction influence on desiccation cracks of mineral liners, Department of soil mechanics and foundation engineering, University of Kaiserslautern, 2001
18. Zou, Y.: Der Einfluss des gebundenen Wassers auf die Leitfähigkeit und die mechanischen Eigenschaften feinkörniger Böden, Veröffentlichung des Institutes für Boden- und Felsmechanik der Universität Fridericiana in Karlsruhe, Heft 144, 1998

Swelling Pressures and Wetting-Drying Curves of a Highly Compacted Bentonite-Sand Mixture

S.S. Agus and T. Schanz

Laboratory of Soil Mechanics, Bauhaus-University Weimar, Germany

Abstract. This paper presents preliminary results of research on hydro-mechanical characterisation of a highly compacted bentonite-sand mixture for its potential use as buffer material in nuclear waste disposal system. Development of swelling pressure with change in suction is presented. Wetting curve of the material was derived from the test as suction was reduced from its initial value using vapour equilibrium technique as well as via axis-translation technique. For comparison, three-dimensional free swell tests were also performed by inducing different suction paths into several specimens such that wetting and drying curves could be obtained. No significant swelling pressure development was observed as the specimens were wetted from as-prepared and oven-dried states to about 10000 kPa suction. Comparison with the three-dimensional free swell test results leads to a conclusion that from dry state to about 10000 kPa suction, the maximum swelling pressure upon saturation is suction independent. It is also shown that swelling pressure curve, wetting-drying curves and void ratio-suction relationship generally exhibit hysteresis. Moreover, the results indicate that even at high suction, void ratio change plays an important role in determining the shape of the wetting curves.

Keywords: buffer material, hydromechanics, swelling pressure, wetting-drying curves, hysteresis

1. Introduction

There have been growing interests of research on the use of highly compacted expansive clay, bentonite and bentonite-sand mixtures as buffer materials for nuclear waste disposal system. Intensive studies have been performed on the characterisation of their properties, such as Romero et al. (2001, 2003), Fleureau et al. (2002), Herbert and Moog (2002), Lloret et al. (2003) and many others. Although the behaviour of the sealing material is affected by temperature (Romero et al. 2003), during the stage where isothermal processes take place (i.e., during construction until placement of the canister), information pertaining the characteristics of the sealing element are also required and important. In this phase, the material is unsaturated and thus unsaturated processes, such as unsaturated flow of water in liquid as well as in vapour forms are likely to occur. Although in the

field, there exist other liquid transports besides water, in this study only water as wetting fluid is concerned.

For expansive material, such as bentonite, introduction to water causes swelling of the material. In the case of constant volume condition, as water is absorbed by the bentonite, swelling pressure is developed. Many factors have been cited by Sridharan et al. (1986) to control the magnitude of swelling pressure. However, in the case where only one material at a particular dry density is concerned and only water is considered as wetting fluid at isothermal condition, the magnitude of swelling pressure only depends on the amount of water uptake as it controls the separation distance between two clay platelets, by which the swelling pressure develops when the swelling is constrained. The amount of water uptake can be related to suction through wetting-drying curve. As suction is decreased from its initial value, water is absorbed and thus swelling pressure develops.

This paper presents some preliminary results of research on characterisation of hydro-mechanical properties of a highly compacted bentonite-sand mixture for its potential use as buffer material for medium and high-level nuclear waste disposal systems. The material tested possesses special concerns, particularly in Germany, since a field test was conducted at Sondershausen location, in which the material under investigation was used in a form of a brick.

2. Material Used

The bentonite used is a commercially available calcium bentonite (Calcigel) from southern part of Germany, whilst the sand is a quartz sand sieved through 2-mm mesh. The bentonite and the sand were mixed at a ratio of 50/50 dry mass with 11% water content. Properties of the bentonite, the sand and the mixture are listed in Table 1. The mixture was subsequently compacted in a cylindrical form. The compacted specimens were cured in a closed container at room temperature until their weights were constant, resulting in cylindrical specimens with a diameter of 5 cm and a height of 2 cm. The average dry density and the average water content of the as-prepared specimens were 2 Mg/m^3 and 8.7%, respectively, with an average void ratio of 0.285. By using this method fabrication and field conditions of the brick specimens of the same mixture that were used in the field test, was simulated. As it had reached constant mass under room condition (i.e., air dry), the compacted specimen was most probably in its residual state with respect to water content with the initial suction around 22000 kPa (see sub-section 4.3 for the determination).

Figure 1 shows the plot of cumulative intruded pore volume versus pore diameter as obtained from mercury intrusion porosimetry (MIP) tests on freeze-dried specimens. Three different conditions of the compacted specimen, namely as-prepared, oven-dried and swollen (at water content equal to 19%) conditions were used. Three different pores, namely micropores, mesopores and macropores, have been distinguished in the figure. The determination of the three-pore categories is shown for the case of the as-prepared specimen and the same method is

used for the other two specimens. The micropores correspond to intra-aggregate pores; the pores inside the clay aggregates, while the meso- and macropores seem to signify the pores between the clay aggregates (inter-aggregate pores) and the pores between the clay aggregates and the sand particles. It is shown that the as-prepared and the oven-dried specimens, exhibit 'well-graded' pore-size distributions with pore diameters ranging from about 0.001 μm to approximately 1000 μm.

Table 1. Properties of material used

Properties	Bentonite	Sand	Mixture
Specific gravity	2.65	2.65	2.65
Liquid limit	130	n.a.	70
Plasticity index	97	n.a.	47
Montmorillonite content (%)	60-70	n.a.	30-35
Clay fraction (%) [*]	83	-	42
D_{10} (mm)	-	0.25	-
D_{30} (mm)	-	0.40	-
D_{60} (mm)	-	0.70	0.3
External specific surface area (m^2/gr) [*]	69	-	-
Total specific surface area (m^2/gr) [**]	493	-	-
Cation exchange capacity (meq/100 gr) [+]	49	n.a.	-
USCS classification	CH	SP	CH

[*] Determined using BET method
[**] Data from Schmidt et al. (1992)
[+] Data from Herbert and Moog (2002)
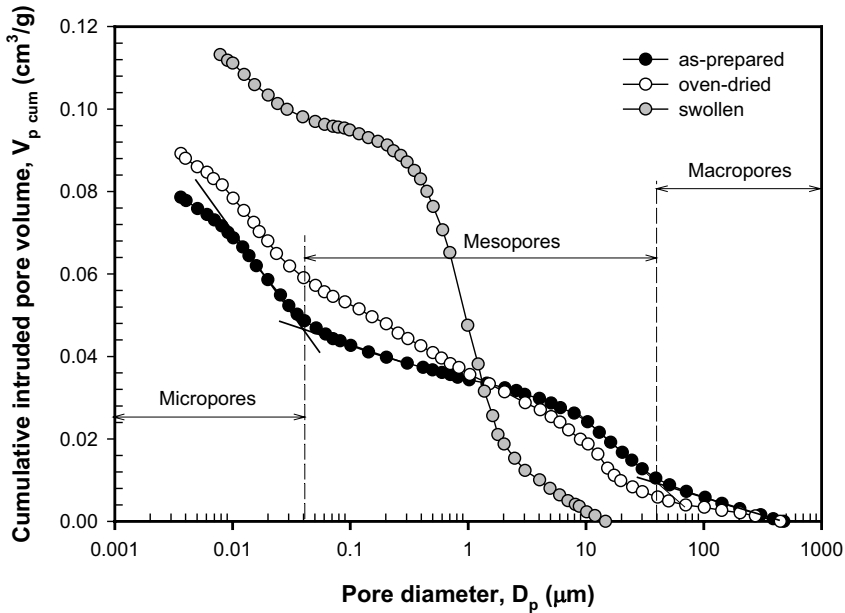
Figure 1. MIP test results of the material tested in different conditions

The plot also shows that drying does not significantly change the pore-size distribution, whereas wetting remarkably affects the pore-size distribution. Upon wetting to 19 % water content, the size of the macropores is reduced, while the size of the micropores remains essentially unaffected resulting in a more uniform pore-size distribution. There is a significant increase in volume of the mesopores compensating a reduction in volume of the macropores. The unremarkable change of the pore-size distribution curve following drying indicates that the compacted specimen was close to its corresponding residual void ratio where drying only slightly reduces the void ratio contrary to wetting. The specimen preparation method adopted in this study causes rearrangement of the clay particles and the sand grains such a way that it results in a very stable structure possibly without having any collapse behaviour. The collapse behaviour exists when the material is compacted dry of optimum to an intermediate density having a metastable structure due to aggregation of the clay platelets or aggregation of the clay platelets and the sand particles.

The theoretical total pore volume of the as-prepared specimen as computed from volume-mass relationships is 0.113 cm^3/g, whereas the theoretical total pore volumes for the oven-dried and the swollen specimens are 0.120 cm^3/g and 0.226 cm^3/g, respectively. In spite of assumptions involved in the analysis of the MIP tests like cylindrical-tube pores, etc., based on Figure 1, one can always determine the minimum water content required to saturate the micropores. This information is important as the term 'microstructures' that are assumed to be al-

ways saturated in most of the current modelling approaches, do not necessarily refer to the micropores as the micropores may not be saturated in the real situation. The material near canister desiccates upon heating and its water content may go much below the lower limit. The minimum water content required to saturate the micropores of the as-prepared specimen is 8.5%, whilst the lower limit of water content needed for the oven-dried and the swollen specimens to be at saturation are 8.3 % and 14.4 %, respectively.
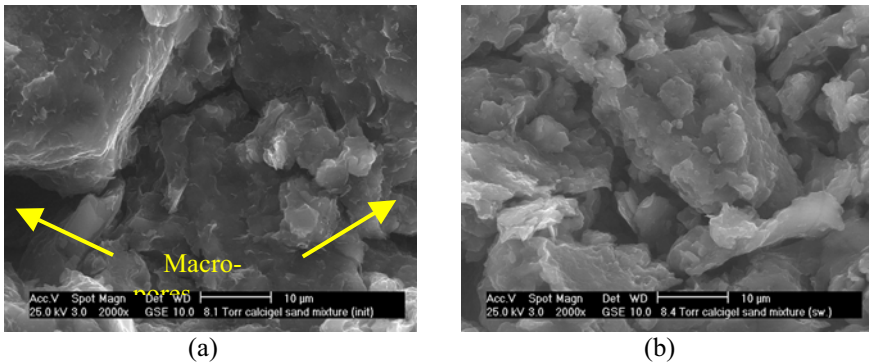
Figure 2. ESEM photo of the specimen (a) as-prepared condition and (b) swollen condition

Figure 2(a) shows an Environmental Scanning Electron Microscope (ESEM) photo of the as-prepared specimen. It is seen in the figure the existence of two macropores with a size of approximately 10 μm and channel-like pores apparently connecting two macropores. The macropores apparent in the figure are indeed in the smallest size as the magnification used in the ESEM does not allow showing any larger pores. The ESEM photo of the specimen at swollen condition as portrayed in Figure 2(b), does not seem to indicate any pores as large as those hypothesised as macropores in Figure 2(a).

3. Experimental Program

Swelling pressure (SP) tests were conducted using the Barcelona constant volume (isochoric) cells as described in Villar et al. (2001). Two methods have been used to induce suction into the specimen, namely, vapour equilibrium technique (VET) and axis-translation technique (ATT).

In the VET, total suction is induced using water vapour generated by molal salt solutions of different concentrations and by saturated salt solutions. The salt solutions used were prepared according to ASTM Standard (1997) E 104-85 and were each subsequently placed in an Erlenmeyer flask. The water vapour in the vapour space above the solution was circulated at a constant rate through the specimen top and bottom boundaries using an air pump. To date, no attempt has been made by the authors to obtain the optimum vapour flow rate for the test on

this material. It is important to note that excessively high vapour flow rate may create heat, which may result in condensation on the specimen tested especially at high relative humidity, while extremely low flow rate means an intolerably long time is required to complete one series of experiments. The applied suction was calculated using Kelvin's law (Fredlund and Rahardjo 1993):

$$\psi = \frac{-RT}{M_w (1/\rho_w)} \ln(RH) \tag{1}$$

where R is the universal gas constant ($=8.31432$ J/mol K), T is the absolute measured temperature in K, M_w is the molecular weight of water ($=18.016$ kg/kmol), ρ_w is the unit weight of water in kg/m^3 as a function of temperature and RH is measured relative humidity defined as u_v/u_{vo} with u_v is partial pressure of pore-water vapour in the specimen and u_{vo} is saturation pressure of water vapour over a flat surface of water at the same temperature.

The tests were performed at room temperature where there existed a temperature fluctuation of about 2 ^{o}C. Therefore, the applied suctions might deviate from the target values as a result of a change in u_{vo}. A preliminary investigation was carried out to determine the actual suction applied to the specimen. The applied suction was determined by measuring the relative humidity (RH) of the vapour space using a polymer capacitance sensor, which can perform measurement at high RH values or low suctions without having condensation problem. It was found that the temperature fluctuation caused a temperature gradient in the system or in the test arrangement, causing a large suction deviation at low targeted suctions. A maximum error of 50% was noticed at a targeted suction of about 3000 kPa. The preliminary investigation has also shown that the use of this method must be limited to a minimum suction of 2000 kPa when a temperature fluctuation of 0.5 ^{o}C and only a 30% maximum deviation from targeted suction are allowed (Agus and Schanz, 2003). No attempts have been made to find out the actual temperature fluctuation in the specimens.

Unlike the VET, in the ATT, matric suction is applied. Pore-air pressure (u_a) was altered from the top of the specimen while maintaining pore-water pressure (u_w) at the bottom of the specimen constant at atmospheric value. The difference between the pore-air pressure and the pore-water pressure (u_a-u_w), results in the applied matric suction. No attempt was made to measure the actual applied matric suction. In both methods, the weight of the cell and the specimen was measured periodically until reaching constant value in each suction increment to obtain equilibrium besides the swelling pressure equilibrium. Using the both tests, the wetting curve of the material under constant volume condition can also be obtained.

In addition of the constant-volume test, three-dimensional free swell (TDFS) test was also performed using VET. The specimen's weight was determined and its dimensions were measured using a digital calliper until equilibrium was achieved. As the material swells or shrinks upon suction change, the equilibrium is deemed based on volumetric water content instead of specimen's mass as in the test on non-expansive materials. The TDFS tests performed in this study were

also meant to obtain the main wetting and the main drying curves of the material as different suction paths were introduced into the specimens.

Both the SP and the TDFS tests are still ongoing, hence, only parts of the results are presented herein. The actual suction applied and the suction paths used in the SP and the TDFS tests are summarised in Table 2.

Table 2. Actual suction and suction paths applied

Specimen	Technique used	Condition before test	1st suction (kPa)	2nd suction (kPa)	3rd suction (kPa)	4th suction (kPa)
SP-1[*)]	VET	As-prepared	13663	10255	-	-
SP-2	ATT	As-prepared	500	300	100	50
SP-3[*)]	VET	Oven-dried	39204	23764	13663	-
TDFS-1	VET	As-prepared	5805	10255	13663	23764
TDFS -2	VET	As-prepared	10255	13663	23764	39204
TDFS -3	VET	As-prepared	13663	23764	39204	149408
TDFS -4	VET	As-prepared	23764	39204	149408	294278
TDFS -5[*)]	VET	As-prepared	39204	23764	13663	10255
TDFS -6[*)]	VET	As-prepared	294278	39204	23764	13663

[*)] Test is still in progress, thus, computations are performed based on their average initial water content

4. Results and Discussion

Although two different water transfer mechanisms were involved in the experiment (vapour in the case of VET and liquid in the case of ATT), for simplicity, it is assumed herein that both processes have the same impact on the specimen tested. Moreover, although the VET results in total suction, whereas the ATT gives matric suction, at high suction both methods yield almost the same suction value. Thus, results obtained from both techniques can be combined to give single wetting-drying curves. This is also assumed to be true for the swelling pressure. Oven-dried condition is assumed to be at 1,000,000 kPa suction as has been proved with thermodynamical considerations by Croney and Coleman (1948).

As mentioned earlier, one should pay a particular attention to the SP test using VET as there is a possible increase in the temperature of the system caused by the use of the air pump. The heating gives additional temperature gradient between the system and the water vapour above the salt solution and thus creates excessive amount of condensed water in the system. To investigate this effect, a preliminary observation was performed using a coarse sand specimen. As the residual water content of the coarse sand used is expectedly located at a very low suction, for the suctions encountered in the VET, only negligible amount of water uptake would exist. The results of this investigation as shown in Figure 3, clearly indicate that for suctions less than 40000 kPa, there was a remarkable amount of water uptake

in the coarse sand, which could result in a significant error in the wetting and dry-ing curves determination for the coarse sand and thus for the highly compacted bentonite-sand mixture. The water uptake of the system (mainly the porous plate used) as a function of suction was further utilised to give correction in the analy-ses of the data.
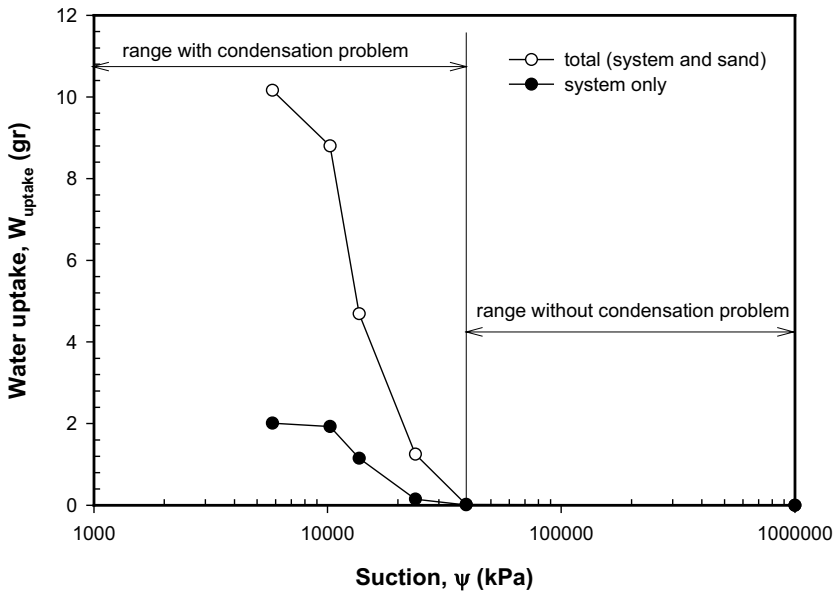
Figure 3. Water uptake as a result of condensation problem in SP test using VET

4.1. Swelling Pressure as a Function of Suction

Figure 4 shows the development of swelling pressure on a semi-log plot as the compacted specimen was wetted from different initial states. The maximum swelling pressure determined by saturating the as-prepared specimen with dis-tilled water is also shown in the figure. Specimen SP-1, which started from as-prepared condition, is shown to exhibit a rapid increase in swelling pressure, close to the maximum swelling pressure, as it was wetted to about 10000 kPa. However, the swelling pressure corresponding to about 10000 kPa suction in this specimen seems to be erroneous as can be explained by its corresponding wetting curve described in the next sub-section. A slightly lower swelling pressure than the maximum value developed in specimen SP-2 upon wetting from as-prepared condition to 500 kPa (OA) and subsequently increased towards the maximum value (AB). By large, swelling pressure did not develop for specimen SP-3 fol-lowing wetting to a suction of about 10000 kPa.
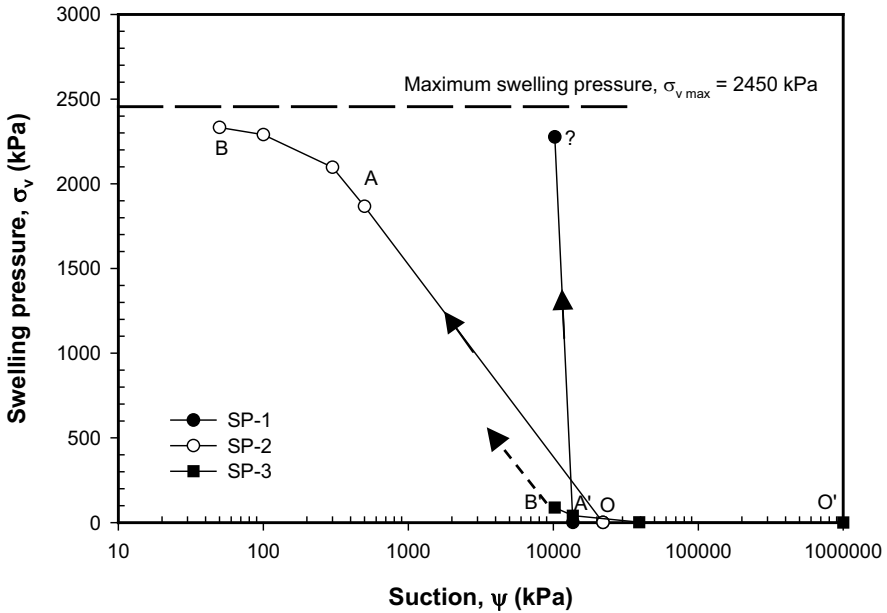
Figure 4. Swelling pressure developed upon wetting from different initial condition

4.2. Wetting Curves under Constant Volume Condition

Figure 5 shows the wetting curves of the material at constant volume condition as derived from the measurement of water uptake during the swelling pressure (SP) test plotted in semi-log scale. For specimen SP-1, there was a significant increase in water content as the specimen was wetted via water vapour transfer to about 10000 kPa suction. A linear relationship in the semi-log plot is noted for specimen SP-2 from its initial state to a suction of 50 kPa, while no information is available above the as-prepared initial suction (i.e., 22264 kPa; see sub-section 4.3) as it is impossible to maintain constant volume during drying. Since the water content-suction relationship generated from the VET and the ATT results on identical specimens is continuous, it is believed that the data point denoted by the question mark in Figure 5 is peculiar and exhibits a large deviation from where it should be. The authors believe that this could be due to condensation of water vapour during the test as addressed before. The correction factor using Figure 3 can only account for the condensation of water vapour in the porous plates, whereas the amount of condensed water within the specimen cannot be justified. Hence, in relation to this, it is suggested that an appropriate flow rate be used in the SP test if more reliable data are to be obtained.

On contrary to the swelling pressure development with decreasing suction, water content, w for specimen SP-2 increases linearly on the semi-log plot all the way from as-prepared condition (O_1) to a suction of 50 kPa (B_1). Approximately, 5% increase in water content (about 98% of the total increase in water content to reach saturation) results in the development of about 80% of the maximum swelling pressure. The remaining rise in water content up to saturation contributes to the rest 20% of the maximum swelling pressure. The possible rapid development of swelling pressure following saturation from B_1 is plausible since the inter-aggregate pore space of the specimen at this condition (B_1) is most probably so suppressed such that absorption of a small amount of water upon wetting from 50 kPa suction, which causes internal swelling of the bentonite, will be directly reflected in a rapid macroscopic change in void ratio. As the void ratio change is restrained, accordingly, the swelling pressure is rapidly increased. This may not be the case when the material is compacted at low density, in which the internal swelling due to wetting from a high degree of saturation is not directly accompanied by the rapid macroscopic change in void ratio as it can be partly accommodated in the inter-aggregate pore space.

Comparison of the swelling pressure development of specimen SP-3 with its corresponding wetting curve under constant volume condition as shown in Figure 5 reveals an interesting phenomenon. It is seen that a large increase in water content (or absorption of a large amount of water), is not accompanied by a significant increase in the swelling pressure upon wetting to about 10000 kPa suction (see path O'B' as compared to O_1'B_1'. Based on this, one may then be tempted to conclude that the maximum swelling pressure developed by saturating the dry specimen is of the same magnitude as that of the as-prepared specimen. Thus, the maximum swelling pressure at full saturation is independent of the initial suction of the specimen wetted from initial suction ranging from 10000 kPa to 1,000,000 kPa (completely dry state), which is indeed in the residual range.

The absorbed water in the as-prepared and in the completely dry specimens upon wetting to any suction greater than 10000 kPa seems only to satisfy the adsorptive force due to surface hydration of the bentonite platelets without inducing significant swelling pressure development. It is apparent that the swelling pressure only significantly develops when the surface hydration is satisfied and the effects of the capillary component of suction come into picture. The corresponding water content at the suction value, below which the mechanical effects, such as swelling pressure development resulting from a reduction in suction, become apparent (i.e., in this case about 9% and 7% for the as-prepared and the oven-dried specimens, respectively), has an important role in the swelling pressure-suction relationship. At this water content, the specimen has a certain equilibrium osmotic suction, at which the swelling pressure develops following further wetting due to osmotic process. In the authors' opinion, below this water content, if it is believed that capillary force is only one of two components of matric suction, the concept of osmotic suction loses its meaning and the term of total suction may only mean the adsorptive force, which is the other component of matric suction.

Figure 5 also depicts the discontinuity of the curves for specimen SP-1 and SP-3, which indicates that the wetting curve of the material under constant volume condition also exhibits hysteresis. The curve for specimen SP-3 is obviously the main wetting curve as it starts from completely dry state. One could then imagine that if the drying test could be performed on the specimen at constant volume condition, the curve for specimen SP-1 could have been like that drawn as long-dashed line in Figure 5 (O'_1O_1), which might be the main drying path.
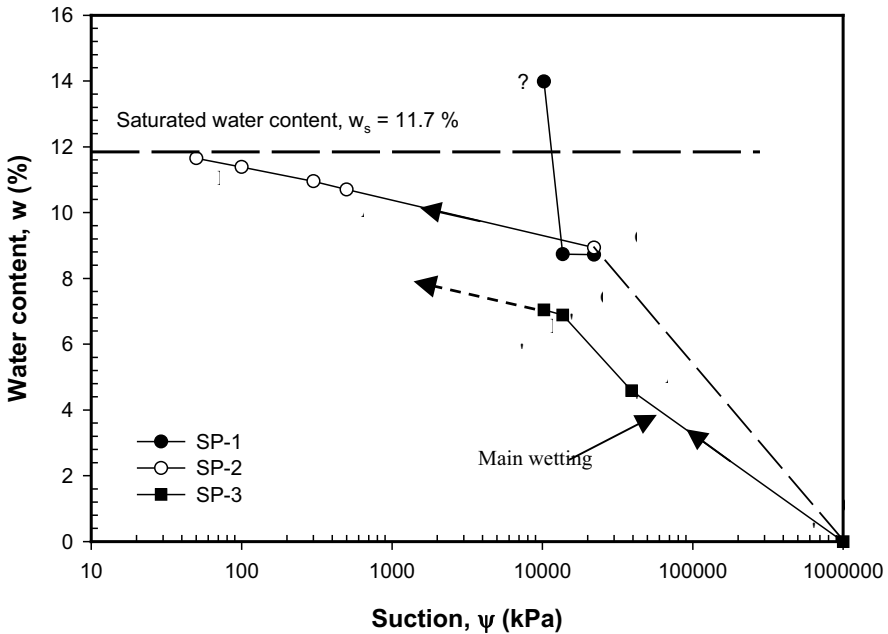
Figure 5. Wetting curves determined at constant volume condition

4.3. Initial Suction Determination and Wetting-Drying Curves under Free Swell Condition

The average initial suction of the specimens used is determined using the results from the three-dimensional free swell (TDFS) tests. The volumetric water contents of specimens TDFS-1 to TDFS-6 after the first suction cycle are plotted in a semi-log graph as shown in Figure 6. A power function is fitted through the data points and by substituting the average initial volumetric water content into the equation the average initial suction can then be determined (ψ_{init} = 22264 kPa). The initial suction as determined by mass basis using gravimetric water content-suction plot (not shown herein) is 23568 kPa.

Figure 6. Determination of initial suction

The scanning curves for the material under three-dimensional free swell condition are shown in Figure 7. The main drying and the main wetting curves are drawn based on the scanning curves. For comparison, the wetting curves at constant volume condition shown in Figure 5 are also plotted in this figure as dash-dotted lines. Both the main wetting and the main drying curves seem to follow linear curves for suctions below the initial suction for the as-prepared specimen (i.e., about 22000 kPa). The 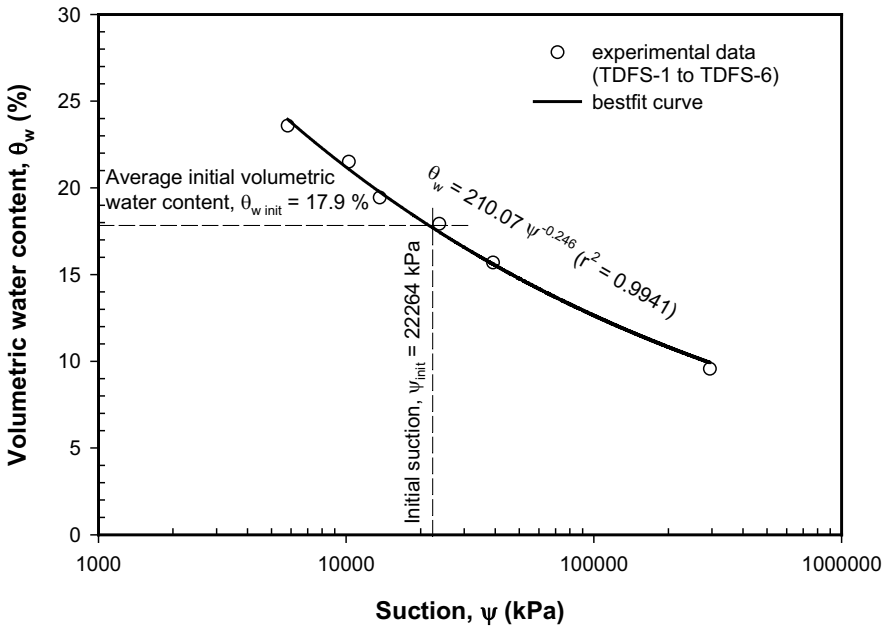main wetting curve can be approximated by a bilinear water content-suction relationship with a breaking point at about 22000 kPa, whereas the main drying curve exhibits a trilinear relationship with two breaking points, at 25000 kPa and 350000 kPa, respectively. No information on the main drying and the main wetting paths are available for suctions lower than 5000 kPa as restricted by the limitation of VET in applying low suctions.

One can obviously see that the main wetting curve at constant volume condition does not coincide with that of at free swell condition. Similarly, the wetting curve for the as-prepared condition does not follow the same path as the wetting curve at free swell condition. It is however contradictory with the findings from Loiseau et al. (2002), where it has been shown that the wetting path at confined condition and the wetting path at free swell condition for a highly compacted mixture of Kunigel clay and Hostun sand coincide at high suctions (greater than 10000 kPa). It has been concluded that the difference is due to the macropores, which exist at high suctions and start to disappear when the constant volume

specimen was wetted to suction lower than 10000 kPa. A similar phenomenon has also been observed by Lloret et al. (2003) for a Spanish bentonite. Up to a suction of about 15000 kPa, the water in the specimen only belongs to the intra-aggregate pores, where void ratio has no role in the water content-suction relationship.
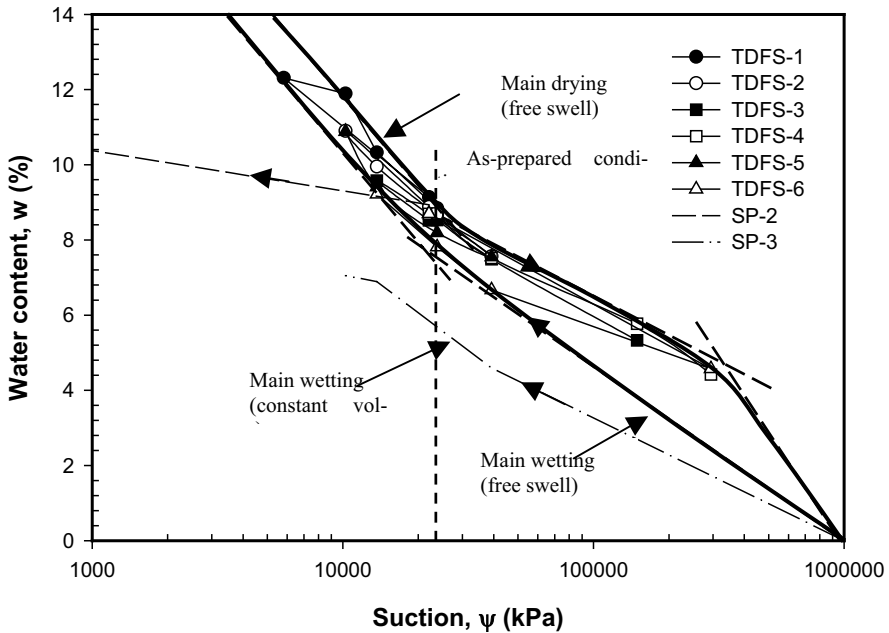
Figure 7. Wetting and drying curves at free swell condition

On contrary, the results presented herein may indicate that even at high suctions, the void ratio change plays an important role in determining the shape of the wetting curve. A part of the change in water content during wetting at suction higher than 10000 kPa belongs to the inter-aggregate pores, which can only occur following the change in void ratio. This fact can be seen clearly in the case of the as-prepared specimen, where none of the wetting paths of the three specimens, TDFS-1 to TDFS-3, whose the first path is wetting, coincides with the wetting path of the specimen SP-2.

4.4. Void ratio-Suction Relationship

Figure 8 shows scanning curve of void ratio-suction relationship of the material as obtained from the three-dimensional free swell (TDFS) tests. Similarly, the main drying and the main wetting curves for this relationship can also be constructed based on the scanning curves and are shown as thick solid lines in the

figure. The main drying and the main wetting curves show bilinear void ratio-suction relationship with breaking points corresponding to residual void ratios occur at slightly different intermediate suctions. The average as-prepared condition almost coincides with the residual void ratio as determined for the main drying curve. This residual void ratio corresponds to 9.5% water content, which is in turn the shrinkage limit of the material when obtained at conditions similar to the as-prepared specimen.

Generally, only small amount of increase in void ratio is found upon wetting from as-prepared condition as well as from completely dry state. This is attributed to the fact that in general, the highly compacted bentonite-sand mixture used in this study is categorised as an 'inactive' material as compared to other materials that have been proposed for nuclear waste disposal barriers. This has actually been reflected in the swelling pressure development as shown earlier. The maximum swelling pressure of 2450 kPa for a dry density of about 2 Mg/m^3 is considered low as compared to more than 40000 kPa swelling pressure for compacted MX-80 (sodium bentonite) specimens of the same density that have been tested recently by Herbert and Moog (2002). Iwata et al. (1995) has addressed that calcium bentonite may exhibit a hinge structure, where there exist a dead volume such that swelling is restrained as a result of a strong edge-to-face bonding of clay particles. The presence of sand also contributes to the lower swelling pressure of the material as at the same dry density, the actual dry density of the bentonite is lower. Thus, to achieve the same swelling characteristic as the sodium bentonite, a higher dry density is desirable for calcium bentonite.
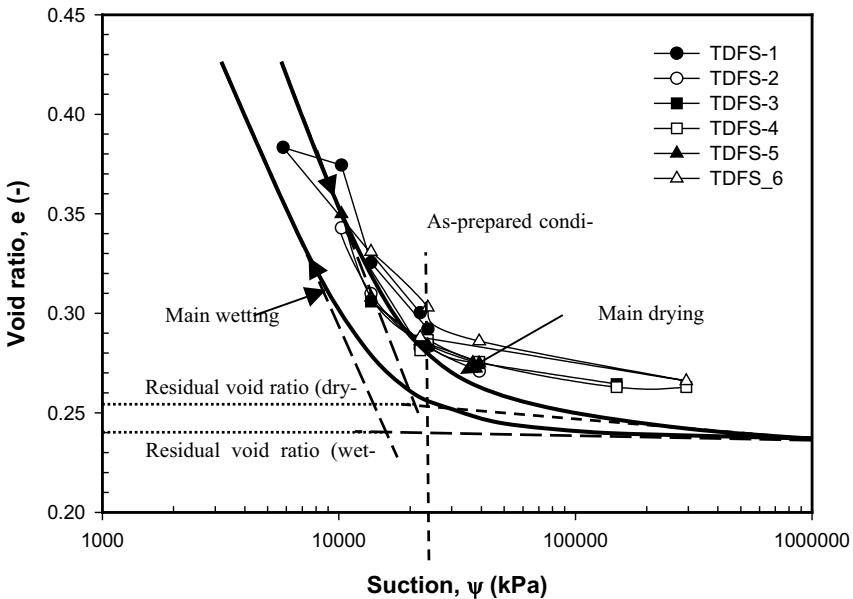

Figure 8. Void ratio-suction relationship obtained from TDFS tests

5. Conclusions

Some preliminary results of an experimental study on a highly compacted bentonite-sand mixture have been presented. The swelling pressure as a function of water content, the wetting curve under constant volume as well as under free swell condition and the void ratio-suction relationship for the material have been shown and discussed. The swelling pressure-suction curve does not seem to have the same pattern as the wetting curve under constant volume condition. The experimental results show that the swelling pressure does not develop remarkably upon wetting from as-prepared and completely dried conditions to suction higher than 10000 kPa. This fact is also seen in the void ratio-suction relationship, which indicates that the as-prepared specimen is in its residual range close to the shrinkage limit when determined for that particular condition.

The wetting curve under constant volume and the wetting-drying curves under free swell conditions generally exhibit hysteresis. The results also indicate that although it is small, the change in void ratio has a significant contribution in determining the water content-suction relationship of the highly compacted bentonite-sand mixture used in this research. The study on the material at residual range does not only highlight its physical effects, such as void ratio and water content increases with suction decrease but may also provide a better understanding of suction components in expansive materials and their respective effects on the hydro-mechanical properties. The study is far from complete; therefore, more experimental results are desirable to give a clearer picture about the hydro-mechanical behaviour of the material.

Acknowledgement

References

Agus S.S., Schanz T. (2003) Vapour equilibrium technique for tests on a highly compacted bentonite-sand mixture. In Proceedings of the International Conference on Problematic Soils, Nottingham, United Kingdom: 467-474.

ASTM Standard (1997) E 104-85. Maintaining constant relative humidity by means of aqueous solutions. Annual Book of ASTM Standard. 11.03. Atmospheric Analysis. ASTM International West Conshohocken. Philadelphia: 781-783.

Croney D., Coleman J.D. (1948) Soil thermodynamics applied to the movement of moisture in road foundations. In Proceedings of the 7th International Congress for Applied Mechanics. London 3: 163-177.

Fredlund D.G., Rahardjo H. (1993) Soil mechanics for unsaturated soils. John Wiley & Sons, Inc., New York.

Fleureau J.M., Verbrugge, J.C., Huergo P.J., Correia A.G., Kheirbek-Saoud S. (2002) Aspects on the behaviour of compacted clayey soils on drying and wetting paths. Can. Geotch. J. 39: 1341-1357.

Iwata S., Tabuchi B., Warkentin, B.P. (1995) Soil-water interactions. Mechanisms and applications. 2nd Edition. Marcel Dekker, Inc. New York.

Herbert H.J., Moog H.C. (2002) Untersuchungen zur Quellung von Bentoniten in hochsalinaren Lösungen. Abschlussbericht GRS–179, Foerderkennzeichen 02 E 8986 5 (BMBF). Gesellschaft für Anlagen und Reaktorsicherheit (GRS)mbH. Germany.

Lloret A., Villar V., Sànchez M., Gens A., Pintado X., Alonso E.E. (2003) Mechanical behaviour of heavily compacted bentonite under high suction changes. Géotechnique 53(1): 27-40.

Loisseau C., Cui Y.J., Delage P. (2002) Air conductivity of a heavily compacted swelling clay-sand mixture. In Proceedings of the 3rd International Conference on Unsaturated Soils (UNSAT 2002), Recife, Brazil (Eds. Jucá JFT, de Campos TMP, Marinho FAM), Swets & Zeitlinger, Lisse, 1: 383-388.

Romero E., Alonso E.E., Gárcia I., Knobelsdorf J. (2001) Microstructural changes affecting air permeability through an unsaturated 80/20 sand-bentonite mixture. In Proceedings of the 6th International Workshop on Key Isuues in Waste Isolation Research (KIWIR 2001). Ecole National des Ponts et Chaussées, Paris: 1-8.

Romero E., Gens A., Lloret A. (2003) Suction effects on a compacted clay under non-isothermal conditions. Géotechnique 53(1): 65-81.

Schmidt W., Sitz P., Kessler J. (1992) Physicalische und chemische Eigenschaften von Bentonite als Verfüll- und Versigelungsmaterial bei der Endlagerung radioaktiver Abfälle. Technischer Bericht 93-37, Nagra, Wettingen, Switzerland.

Sridharan A., Rao A.S., Sivapullaiah P.V. (1986) Swelling pressure of clays. Geotech. Testing J. GTJODJ. 9(1): 24-33.

Villar M.V., Rivas P., Campos R., Lloret A., Romero E., di Mariano A. (2001) First report on thermo-hydro-mechanical laboratory tests. Report 70-IMA-L-0-86 (FEBEX Project). Ciemat. Spain.

Results and interpretation of bentonite resaturation experiments with liquid water and water vapour

Klaus-Peter Kröhn

Gesellschaft für Anlagen- und Reaktorsicherheit (GRS), Theodor-Heuss-Str. 4, 38122 Braunschweig, Germany

Abstract. Most countries favour compacted air-dry bentonite for engineered barriers in final repositories for nuclear waste. While the hydrophilic properties of bentonite appear to be ideally suited for minimising any contact of water with the waste the process of resaturation is not fully understood yet. In order to investigate the dynamics of water uptake several resaturation experiments with liquid water as well as with water vapour have been performed. A series of tests concerning the uptake of liquid water in compacted MX-80 bentonite samples has been completed recently. The experiments provide uptake rates and moisture distributions as a function of time. Analogous experiments with water vapour are presently running. Some first results are presented. The data gained is used to check new conceptual models which explain resaturation by flow of liquid water and by diffusion of water vapour, respectively. In the new models the effects of hydration on the local pore water content and the change of porosity corresponding to the amount of hydrated water are considered. The results strongly suggest that vapour diffusion plays a significant - if not dominant - role in the resaturation process of bentonite.

Introduction

Geotechnical barriers are an integral part in the design of nuclear waste repositories. One of their main tasks is to protect the waste against any contact with water from the host rock in order to prevent a mobilization of toxic or radioactive material. For this purpose compacted bentonite is worldwide considered to be an ideal material because water entering the bentonite will be hydrated in the interlamellar

space (interlayer) of the clay particles thereby causing a swelling of the bentonite with a corresponding drastic decrease of permeability and porosity.

In order to predict the process of resaturation under repository conditions several numerical codes have been developed. But an analysis of the existing THM-codes revealed deficiencies in the underlying conceptual models for the hydraulic part that lead to the development of alternative conceptual models (Kröhn 2003). These new conceptual models are rather simple but contrary to the above mentioned models include the process of hydration and a direct coupling of hydration with a corresponding change of porosity.

Checking numerical models for bentonite resaturation still states a major problem for two reasons. Firstly, the uptake process is not yet completely understood and thus no strictly reliable mathematical description exists. Secondly, the effort to measure one of the most important quantities, the water content as a continuous function of time and space is extremely high. Very few experiments are known that provide a distribution of the water content within a bentonite body (Börgesson 1984, 2001; Pusch 1980; Pusch and Kasbohm 2001; Huertas et al., 2000). They were performed with different degrees of physical and geometrical complexity and basically, these experiments provide either sufficient spatial distributions or local temporal variations but not both.

The present paper attempts to bridge this gap. In order to get more insight into the processes involved during resaturation new uptake experiments with most simple physical and geometrical conditions are performed on one hand and new basic conceptual and numerical models for the bentonite resaturation have been developed on the other hand. The experimental results already available are presented here with a comparison to results of the new numerical models.

Conceptual models

Assumptions, boundary and initial conditions

Bentonite can take up liquid water as well as water vapour. Thus two models, one for the uptake of liquid water and one for the uptake of water vapour are considered. For the purpose at hand the resaturation of bentonite is restricted to a one-dimensional problem using the following assumptions:

- isothermal conditions,
- fixed position of the bentonite particles in space,
- distinction between water in the pore space and the interlamellar space,
- equal densities of hydrated water and of fresh water and
- equal values of increase of interlayer and of reduction of pore space.

Depending on the type of model one boundary is connected to an infinite volume of either liquid water or vapour saturated air. The other boundary is closed.

The bentonite has a certain initial water content. Movement of water is restricted to the pore space and is controlled by the respective flow law. Additionally, water is drawn from the pore space into the interlamellar space of the clay particles due to the difference of the chemical potential between the pore water and the hydrated water. This process locally reduces the available pore space by the same amount by which the interlayer volume increases. Hydration is therefore a sink for water flow within a correspondingly shrinking pore space.

Advection model

In the model for uptake of liquid water - the "advection model" - only two processes are considered: Darcy flow and hydration. Hydration of liquid water is a rather fast process (Pusch and Yong 2003). Thus, in the advection model it is assumed to be instantaneously resulting in a steep moisture front. Water flow in the advection model is driven by a pressure gradient which is constituted by the hydraulic pressure at the inflow boundary and the suction of the unsaturated bentonite at the moisture front. This model has been checked using an uptake experiment by (Kahr et al. 1986) and is described in more detail by (Kröhn 2003).

Vapour Diffusion model

Processes considered

Two main differences exist between the advection model and the model for uptake of water vapour, the "vapour diffusion model". Firstly, the main water transport mechanism in the vapour diffusion model is assumed to be the diffusion of water vapour in air instead of Darcy flow. Secondly, the flow rate of water between the pore space and the interlamellar space, called "hydration rate" further on is assumed to be finite and to depend on the differences of the chemical potential of pore water and hydrated water.

Balance equation

The case of water flow in an unsaturated bentonite can be regarded as a flow in a porous medium with a locally varying porosity Φ and a locally varying sink r for the water. In the vapour diffusion model the porosity is assumed to be a function of the water content which is calculated separately integrating the local hydration rates over time. While the porosity and the vapour partial density ρ are variables in time and space the coefficient D for binary gas diffusion is a constant under the isothermal conditions that are considered here. For the sake of simplicity the tortuosity τ is assumed to be constant as well. The resulting mass balance equation for the vapour in the pore space reads:

$$\frac{\partial(\Phi\rho)}{\partial t} - \tau D \frac{\partial}{\partial x}\left(\Phi \frac{\partial\rho}{\partial x}\right) = r \tag{1}$$

Quantification of the sink term mainly requires the calculation of the local hydration rate. This rate depends on the chemical potential Π_p of the water vapour in the pore space and the chemical potential Π_i of the interlamellar water. The chemical potential Π_p can be derived from thermodynamic considerations and is under isothermal conditions only a function of the relative humidity r_h (e.g. (Kahr et al. 1986)).

$$\Pi_p = \frac{RT}{M_w}\ln r_h \tag{2}$$

using the universal gas constant R, temperature T and the molar weight of water M_w. Under equilibrium conditions that are characterized by $\Pi_i = \Pi_p$ an adsorption isotherm can be measured which yields a unique function of relative humidity r_h vs. water content w (Mooney et al. 1952; Kahr et al. 1986). Thus for any arbitrary water content w one fictitious value $r_{h\,eq}$ exists for the relative humidity under equilibrium conditions which allows to calculate the chemical potential Π_i as

$$\Pi_i = \frac{RT}{M_w}\ln\left(r_{h\,eq}(w)\right) \tag{3}$$

As a first approximation a linear function for the adsorption isotherm is assumed in the present version of the vapour diffusion model. It is further assumed that the local hydration rate per unit mass of bentonite $\dot{m}$ is linear proportional to the potential difference $\Delta\Pi = \Pi_p - \Pi_i$ with a constant proportionality factor a:

$$\dot{m} = a\,\Delta\Pi = a\left(\frac{RT}{M_w}\ln\frac{r_h}{r_{h\,eq}(w)}\right) \tag{4}$$

The product of the constants a, R, T, and $1/M_w$ in Eq. (4) can be interpreted as the specific reference mass flux $\dot{m}_{ref}$. This flux occurs theoretically when the actual relative humidity exceeds the equilibrium relative humidity corresponding to the actual water content by the factor e. It follows that the factors a or $\dot{m}_{ref}$ can be calculated using any arbitrary known set of $\dot{m}$, r_h and $r_{h\,eq}$. In order to obtain an appropriate sink term the relative humidity has to be substituted by the ratio of vapour partial density ρ to the vapour partial density ρ_{sat} at vapour saturation and, finally, the mass specific sink $\dot{m}$ has to be transformed into the volumetric sink r by multiplying $\dot{m}$ with the bentonite dry density ρ_d:

$$r = \rho_d \, \dot{m}_{ref} \, \ln \frac{\rho}{\rho_{sat} r_{h\,eq}(w)} \tag{5}$$

Uptake experiment with liquid water

Experimental equipment and measuring procedure

Air-dry MX-80 bentonite with an initial water content of about 10% was filled into cylindrical steel cells illustrated in Fig. 1. The specimen had a length of 10 cm and a diameter of 5 cm. The bentonite was compacted layer wise in order to minimize density changes due to wall friction and the resulting initial average dry density was about 1500 kg/m³. In order to mirror the conditions at the Äspö Hard Rock laboratory the bentonite was saturated with water from the Baltic Sea. Starting in a buret the Äspö solution flowed with minimal hydraulic pressure through a flexible tube into the cylinder where it was distributed by means of a system of circular and radial grooves on the surface of the locking solid cylinder and a frit. Thus a uniform and continuous water supply over the front plane of the cylindrical bentonite specimen was achieved which allows to describe the water uptake as a one-dimensional process. The interface between frit and bentonite is called "inlet" further on. The amount of water drawn into the bentonite was measured over time using the buret. Water uptake took place under a constant temperature of 20 °C.

After a predefined period of time the water-carrying tube to the measuring cell was disconnected. The cell was opened on both sides and the bentonite specimen was pushed out of the cell. During this process bentonite slices with a thickness of a few millimetres were cut off. The thickness of each slice was measured before cutting. The slices were weighed, dried 24 hours at a temperature of 105 °C and weighed again in order to assess the water content. The integral value for each slice was assigned to the midpoint of the respective slice for the graphical representation of the data.

Each individual uptake test yields one profile for a specific time period. In order to check the accuracy of the measuring procedure most tests were repeated. The longest test period was about half a year.
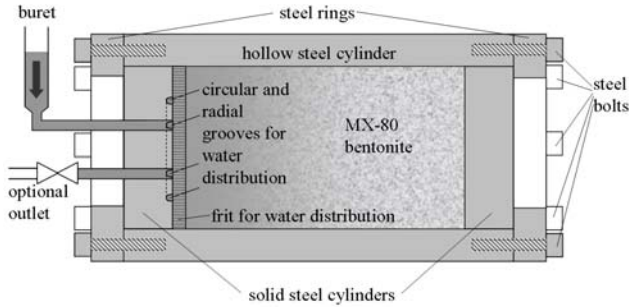
Fig. 1. Principal sketch of the measuring cell
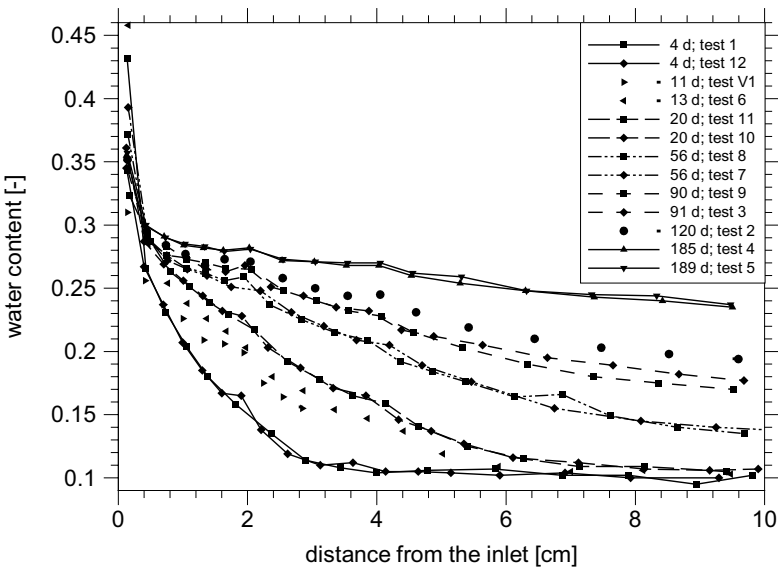
Fig. 2. Measured water content distributions for uptake of liquid water

Results and interpretation

The moisture distributions gained are shown in Fig. 2. With the exception of the first data point the profiles demonstrate a remarkable reproducibility.

First, the high water content in a zone close to the inlet has to be discussed. All curves in Fig. 2 show that within the first three millimetres much more water has been taken up than the expected theoretical maximum of 0.31 $kg_{water}/kg_{dry\ bentonite}$. A close inspection of the data for the respective first slice reveals that the meas-

ured water content is not dependent on the test period contrary to any cross-section more distant from the inlet.

It appears that the initial swelling has led to a decompaction of the inlet zone which in turn caused a slight compaction of the still dry parts of the bentonite. The effect is illustrated by the dry density distribution of the bentonite slices (see Fig. 3). Within the time period covered by the measurements no further density changes have been observed.

Except for the inlet zone the water content distributions are characteristic for a diffusion-like water transport. Here it is most important to note that the local water content is continuously rising with time even in the second slice of each specimen which represents the cross-section at a distance of about 4 mm from the inlet. The water content amounts to 26.7 % after four days, to 30.0 % after 185 days and appears to be still increasing afterwards (see Fig. 4). During these 185 days a lot more water had passed through this cross-section than would have been necessary to fully saturate the second slice. Thus the water supply cannot be the limiting factor for the water uptake in this slice.
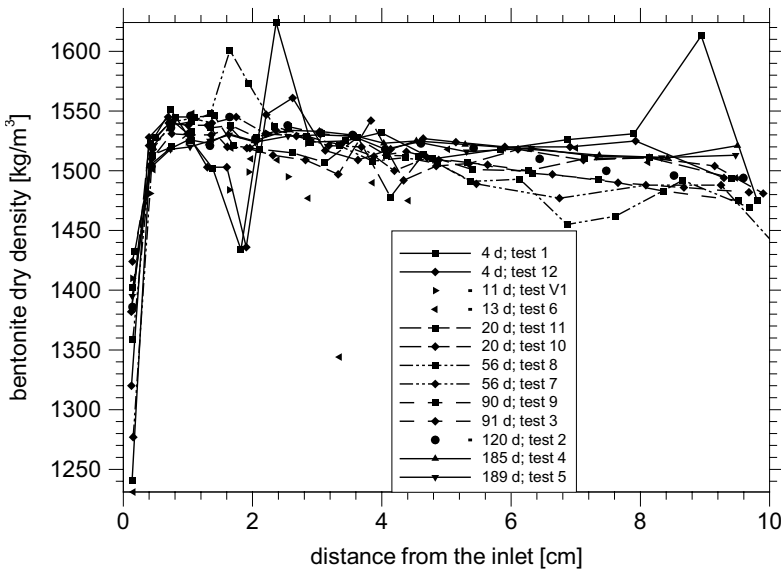
Fig. 3. Measured bentonite dry density distributions for uptake of liquid water

There are two ways to explain this observation. Firstly, non-pressurized liquid water entering the bentonite is initially pulled into the pore space by capillary forces (Pusch and Yong 2003). In a zone where filled and empty channels coexist the swelling of the water filled channels may entrap the air in some of the empty channels. Further water uptake in these domains would invoke air solution, evaporation and subsequent hydration of vapour, transport of water molecules by surface diffusion on the clay particles or other slow processes.

Fig. 4. Measured water content vs. time at several locations for uptake of liquid water

The second explanation is based on the assumption that liquid water is initially sucked into the bentonite by capillary forces and that all water entering afterwards evaporates at the established interface between liquid water and air. Water transport further into the bentonite takes places only by means of vapour diffusion in t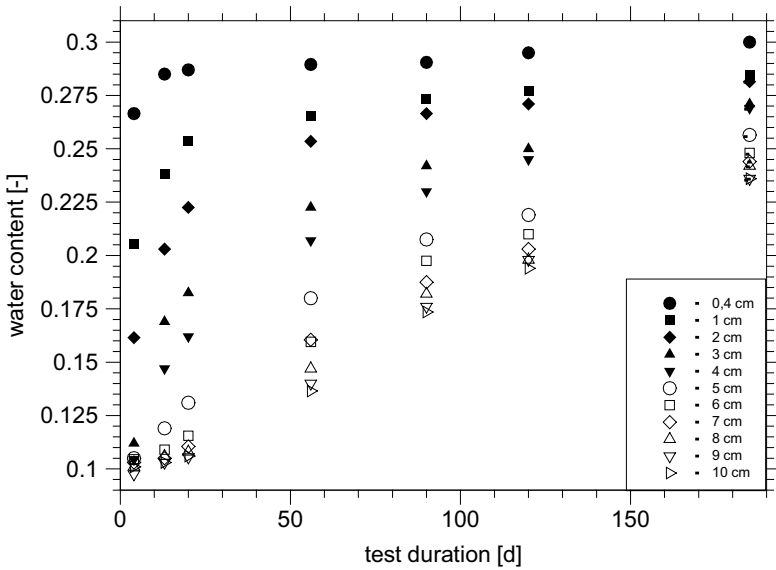he gas phase. The relative humidity is therefore monotonic decreasing with the distance to the water-air interface. At the same time the relative humidity provides an upper limit for the local water content according to the adsorption isotherm. As the vapour saturation of the air can only reached asymptotically by diffusion the saturation of the bentonite is then an asymptotic process either. This second explanation was checked utilising uptake experiments with water vapour.

Uptake experiment with water vapour

Currently running at GRS is a new series of uptake tests in which the measuring cells described above are used to investigate the dynamics of uptake of water vapour. Five cells, five gas washing bottles and a pump are coupled in a series connection with flexible tubes constituting a closed gas circuit with highly vapour saturated air as illustrated in Fig. 5.
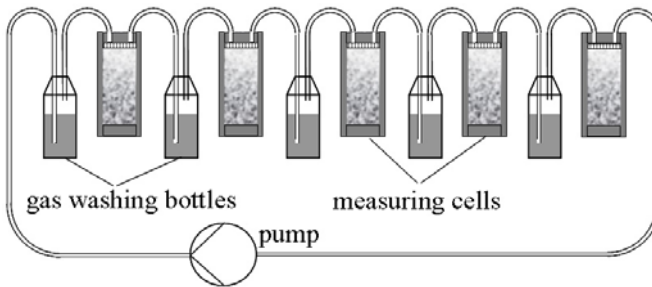
Fig. 5. Connection diagram of the measuring cells for the vapour uptake tests

First results concerning the water content are given in Fig. 6. The most obvious difference to the respective moisture profiles from the experiments with liquid water can be found at the inlet zone. The water content rises comparatively slow, thus confirming the assumption of an initially fast uptake of liquid water by capillary forces. Otherwise, the profiles are characteristic again for diffusion-like processes.
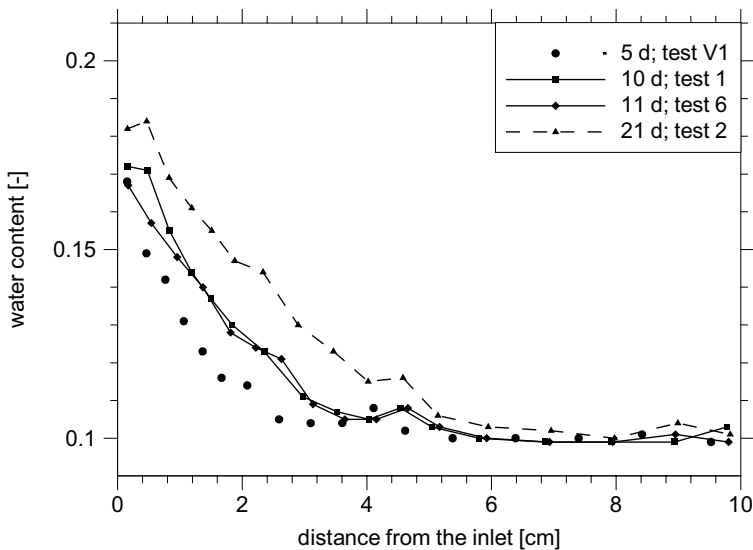
Fig. 6. Measured water content distributions for uptake of water vapour
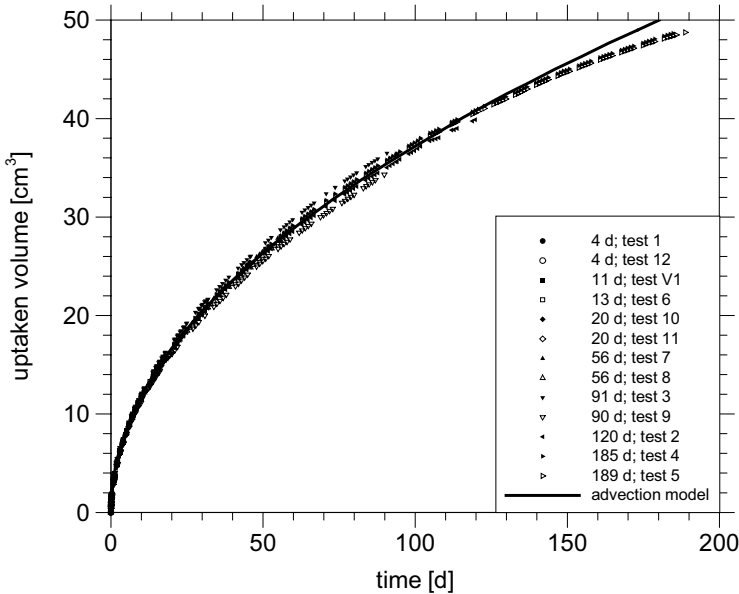
Fig. 7. Measured volume of up taken liquid water and results of the advection model

Comparison of experimental and model results

The time-dependent uptake of liquid water could be satisfyingly reproduced with the advection model using realistic input parameters (see Fig. 7). However, the steep moisture front predicted by the advection model could not be observed. Obviously, the actual processes involved are as little captured by this model as by the well-known empirical Fickian type law with the constant "diffusion coefficient". But while the empirical "diffusion constant" has to be recalibrated for different physical conditions like for increased temperature the data for the advection model are already known for a wide spectrum of different conditions. The advection model is therefore still valuable to predict integral quantities like water uptake rates, total water content or others.

The time-dependent moisture distribution in the experiments for uptake of water vapour could be reproduced fairly well with the vapour diffusion model (see Fig. 8). The amount of hydrated water as well as the trend of the distributions coincides well with the measured data. Only the uptake dynamic seems to be somewhat off. Recalling that the uptake rates are simply approximated here with a linear relation to the difference of the chemical potential, additionally using only a linear approach for the adsorption isotherm the agreement is satisfying.

Fig. 8. Measured water content for vapour uptake and results of the vapour diffusion model
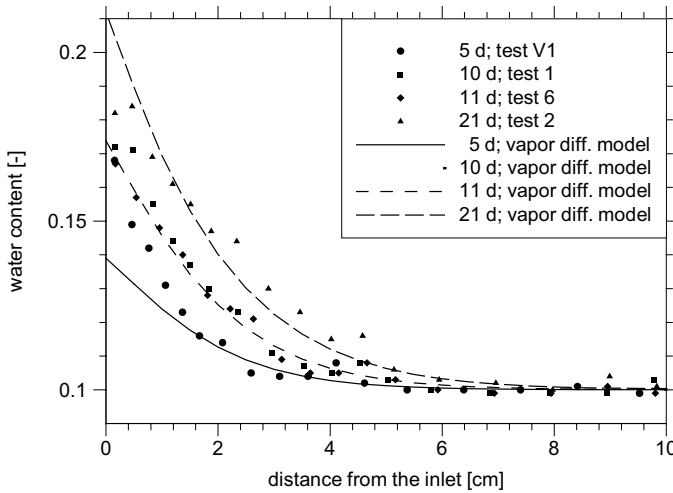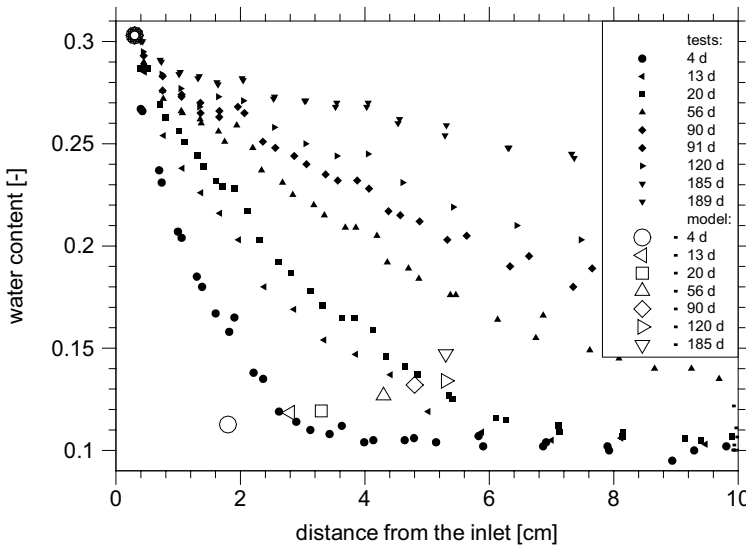

Fig. 9. Measured water content for liquid water uptake and results of the vapour diffusion model

Interesting conclusions can be drawn from a comparison of the results of the vapour diffusion model with the data from the uptake experiment with liquid wa-

ter as illustrated in Fig. 9. Even without regarding the increased water content at the inlet zone that has been discussed earlier it becomes clear that about one half of the hydrated water can be explained by means of binary gas diffusion.

An increase of the diffusion coefficient of less than a factor of ten could suffice to provide the total amount of hydrated water by vapour diffusion. Such an increase may occur if binary gas diffusion fades to Knudsen diffusion in an advanced stage of saturation. Knudsen diffusion becomes dominant if the mean free path length of a gas molecule is longer than the diameter of the flow channel. As a very rough approximation the clay particles can be considered to be cylindrical discs with a diameter of 300 nm and a thickness of less than 40 nm. Since the mean free path length of a water molecule in air is approximately 100 nm it appears to be reasonable to take Knudsen diffusion as a possible transport mechanism into consideration in further investigations.

Summary and conclusions

The uptake experiments provide a reliable data base for the evolution of water content and bentonite dry density as a function of time and space both for the uptake of Äspö-solution and for the uptake of water vapour. In the case of an uptake of liquid water the measurements show a fast increase of the water content within a distance of two to three centimetres from the inlet. The trend of the earliest measured curve confirms the assumption of an initial fast suction of water into the pore space by capillary forces. At the inlet zone swelling leads to a displacement of the clay particles and thus to a decrease of the bentonite dry density. But the resulting compaction of the bentonite in the remaining part is very low so that the assumption of homogeneity is not too much violated by swelling effects. The fact that no further density changes occur after 4 days of saturation justifies the model assumption of a fixed position of the bentonite particles in the specimen as a good approximation except for the first few millimetres.

The advection model for uptake of liquid water can describe the water uptake of the specimen as a whole, but does not reproduce the time-dependent moisture distributions within the specimen. However, it is an improvement of the empirical "diffusion" law because it is applicable for a wider variety of physical situations.

First results from the uptake experiments with water vapour show a considerable increase of the water content within a short time. The vapour diffusion model using a binary gas diffusion approach is able to reproduce the time dependent water content distributions even if the hydration dynamics have to be improved yet. This is a strong evidence for the importance of vapour diffusion for the saturation of bentonite on one hand and the validity of the vapour diffusion model on the other hand.

A comparison of the results of the vapour diffusion model and of the experiments with liquid water indicates that a considerable part of the water uptake is due to vapour diffusion. Assuming that binary gas diffusion fades to Knudsen diffusion in an advanced stage of saturation it could even be possible to explain the

bentonite saturation exclusively by vapour flow due to an increasing diffusion co-efficient. In that case the uptake of liquid water may be limited to the wetted bentonite surface.

Acknowledgements

References

Börgesson L (1984): Water Flow and Swelling Pressure in Non-Saturated Bentonite-Based Clay Barriers. Clay Barriers for Isolation of Toxic Chemical Wastes, International Symposium, May 28-30, Stockholm

Börgesson L (2001) Compilation of laboratory data for buffer and backfill materials in the Prototype Repository. SKB, International Progress Report IPR-01-34

Huertas F, Fuentes-Cantillana JL, Jullien F, Rivas P, Linares J, Farina P, Ghoreychi M, Jockwer N, Kickmaier W, Martinez MA, Samper J, Alonso E, Elorza FJ (2000) Full-scale engineered barriers experiment for a deep geological repository for high-level radioactive waste in crystalline host rock (FEBEX project). European Commission, final report EUR 19147 EN

Kahr G, Kraehenbuehl F, Müller-Vonmoos M, Stoeckli HF (1986) Wasseraufnahme und Wasserbewegung in hochverdichtetem Bentonit. NAGRA, Technischer Bericht 86-14

Kröhn K-P (2003) New conceptual models for the resaturation of bentonite. Applied Clay Science, Vol. 23

Mooney R W, Keenan AG, Wood LA (1952) Adsorption of Water Vapour by Montmorillonite; I: Heat of Desorption and Application of BET Theory. Journal of the American Chemical Society, Nol. 74, No. 6

Pusch R (1980) Water uptake, migration and swelling characteristics of unsaturated and saturated, highly compacted bentonite. KBS Report 80-11, SKBF, Stockholm

Pusch R, Kasbohm J (2001) Can the Water Content of Highly Compacted Bentonite be Increased by Applying a High Water Pressure? SKB, Technical Report 01-33

Pusch R, Yong R (2003) Water saturation and retention of hydrophilic clay buffer - microstructural aspects. Applied Clay Science, Vol. 23

MECHANICAL BEHAVIOUR

Shear strength of unsaturated bentonite buffer material

A. Farouk, J. Kos, and L. Lamboj

Department of Geotechnics, Faculty of Civil Engineering,
Czech Technical University, Prague, Czech Republic

Abstract. There are two widely accepted approaches to determine the shear strength of unsaturated soils: the effective stress approach (Bishop, 1959) and the independent stress state variables approach (Fredlund et al., 1978). The main difference between these two approaches lies in how to reduce the effect of increasing matric suction. Bishop's coefficient χ can be calculated using φ^b ($\chi = \tan\varphi^b / \tan\varphi'$) and vice versa. However, Bishop's approach with the coefficient χ "of the matric suction efficiency" seems to be closer to the reality since there is a difference between decreasing φ^b and the experimental results, which have proved that the effective friction angle slightly increases with increasing matric suction. The coefficient χ decreases with increasing suction as a result of decreasing both the total area of water-solid contacts and number of particles connected by water menisci. This explains why the parameter χ decreases with increasing porosity. Thus, the maximum effect of matric suction can be reached with higher water content as a result of two opposite influences: decreasing matric suction and increasing number of particles connected by water menisci (matric suction efficiency χ).

The analysis of this problem is based on the experimental programme of the bentonite buffer material under unsaturated conditions. Pure bentonite as well as bentonite mixtures with siliceous sand and graphite were tested. Samples with extremely different porosities were prepared under compaction pressures ranging from 300 kPa to 100 MPa and then tested in the triaxial apparatus.

1 Introduction

The basic principles related to the understanding of unsaturated soil mechanics were formulated mainly in the 1970's [1]. However, the behavior of unsaturated soils is more complex and more difficult to be described than that of saturated ones. There are many problems that can arise when dealing with unsaturated soils. Some of these problems were reported by Jennings [2] who stated that the most important problem when dealing with unsaturated soils is the shear strength variation as a function of soil suction. However, some of the additional strength gained in unsaturated soils is due to the negative pore water pressures. These negative

pore water pressures increase the effective stress, increase the matric suction, and thus increase the shear strength. Matric suction is attributed mainly to capillary actions in the soil structure and is considered as the key factor that influences the mechanical properties of unsaturated soils [3]. In general, the strength of a soil usually decreases with increasing water content since increasing the amount of adsorbed water leads to increase the separation of particles and thus, weakens bonds and softens cements that hold the soil particles together [4].

For most cases, unsaturated soils can be considered as the main source of most geotechnical engineering problems. Many examples of the application of unsaturated soil concepts can be found in transportation projects such as roads and railway embankments, and in environmentally sensitive projects such as waste containment in land fill sites and nuclear storage installations, which is the case on this study.

This work investigates the shear strength and the suction of the bentonite-sand-graphite mixture proposed to be utilized as a geotechnical barrier to seal the high-level radioactive fuel waste repositories prepared to be used in the Czech Republic. However, understanding the suction characteristics of unsaturated barriers is necessary to analyse and predict their material performance in any waste management program. That is why much knowledge was needed about the mechanisms of how suction changes as a result of external loading as well as more information about the strength of the bentonite-sand-graphite buffer at different suction values and, as a result, under different degrees of saturation.

As a part of the whole program planned to study shear strength characteristic of this mixture under different degrees of saturation, a relatively dry, highly compacted samples with water content less than 13% were prepared and then tested using a standard triaxial apparatus. Matric suction inside samples was expected to be very high, and thus, it was impossible to measure it experimentally. A simple soil model, in which the soil particles are modelled as a system of spheres, was adopted to calculate matric suction numerically. Finally, it was possible to combine and analyse the calculated suction along with the shear strength parameters obtained from the triaxial test.

2 Tested material

In the last twenty years, worldwide research of a potential use of bentonites as an efficient barrier in the disposal of radioactive waste has been conducted [5]. The material to be studied in the current work consists of 85% of highly plastic bentonite clay, 10% siliceous sand, and 5% graphite mixed by dry weight. The used bentonite, which is known as RMN (i.e., taken from the locality Rokle at the west side of the Czech Republic, Milled, and Not activated) is a grinded, homogenizated, non-activated calcium-rich bentonite (i.e., Ca-type montmorillonite). Siliceous sand (PR33) with grain sizes ranging from 0.1 to 0.6 mm was added to the bentonite to reduce the swelling pressure, while graphite with 94-96% carbon content is added to increase the thermal conductivity of the mixture. Using the data of

the Atterberg limits and the plasticity chart, the mixture was classified as clay with extremely high plasticity according to the Unified Classification System. Typical properties of this mixture in the powder state are illustrated in Table (1).

Table 1. Typical physical and hydro-physical properties of the studied bentonite-sand-graphite mixture in powder state [5].

Soil property	Value
Unit weight, (ρ)	843 kg/m³
Dry density, (ρ_d)	788 kg/m³
Specific weight, (ρ_s)	2405 kg/m³
n	67 %
W_{Cn}	7.5 %
WS	23 %
WL	121 %
WP	44 %
IP	77 %

3 Testing program

A laboratory-testing program was planned and carried out in order to fulfill the objective of this study. The testing program was divided into two main groups. The first group deals with the specimens that have 100% degree of saturation so as to evaluate the effective shear strength parameters, c' and ϕ', and to compare the behaviour of saturated soils with that of unsaturated ones. The second group consists of unsaturated and relatively dry highly compacted specimens with water content ranging between 1 and 12.7%.

Three subgroups of samples, with three different water contents, 1.0, 7.5, and 12.7% (i.e., with three different degrees of saturation, 6.0, 43.0, and 74.0 respectively) were tested in the triaxial device using the undrained test method, "UU". Each subgroup comprised six samples that had the same initial degree of saturation, while each subgroup was further subdivided into three sets of samples tested under three different confining pressures (0.0, 0.5, and 1.0 MPa). To obtain accurate results, each set contained two samples, S1 and S2, that were tested by applying the same confining pressure, σ_3, then applying and measuring the deviator stress, σ_d, and the longitudinal strain, ε_y, until the failure point was reached. Then, it was possible to consider the average values of these measurements for each set.

4 Specimen preparation

Specimen used to determine the effective strength parameters were prepared by mixing its components together by weight to achieve the prescribed mixing ratio (85% bentonite, 10% sand, and 5% graphite). A considerable amount of distilled water was added gradually to the mixture until a uniform color and consistency was achieved. Then, the mixture was stored in an airtight container for five days to homogenize the water content. Specimens were prepared in a mould. The specimens were 38.5 mm in diameter, 83.0 mm in height, 147.0 gm in weight, and nearly 98.0 % degree of saturation. Before testing, they were re-saturated using a backpressure of 500 kPa.

The unsaturated highly compacted samples were prepared using a constant volume mould at a prescribed density and water content. A two-part split thick-walled mould, that had the same diameter of the required samples, was assembled inside an outer hollow thick-walled steel cylinder. Then, a guiding solid steel cylinder with the same diameter of the sample was put inside the mould. After that, a predetermined weight of the bentonite-sand-graphite mixture in its powder state was put inside the mould until it was completely filled. Another solid steel guiding cylinder was put on the upper surface of the powder that filled the mould and then the whole set was placed in a hydraulic press. The powder was compressed under a static compacting effort of about 100 MPa until the guiding cylinders were fully pushed inside the mould. It may be interesting to mention that the lengths of the two guiding cylinders were pre-specified so that when they are fully pushed inside the mould, this produced specimens of 38.4 mm diameter, 76.2 mm height, 163.25 gm in weight (with water content of about 7.5%, which was the water content of the delivered bentonite powder), dry unit weight of about 1.72 gm/cm^3, and nearly 43.0 % degree of saturation.

To have samples with different water contents (i.e., to control the degrees of saturation), some samples were dried in oven at 80° C to a pre-determined weight, which led, after four days, to samples with about 1.0% water content, and 6.0% degree of saturation. Samples with water contents higher than 7.5% were prepared before compaction by spraying a predetermined amount of distilled water to the powder with agitation until the desired water content was achieved. Then, the mixture was stored in an airtight container for about six days before compaction in order to regulate the propagation of the sprayed water through the whole weight of the mixture. The initial weight of the mixture being filled to the mould was increased proportionally to the expected water content. However, exact values of the water contents and degrees of saturation were re-evaluated after testing. The main steps used for preparing the highly compacted unsaturated samples are shown in Fig. (1).
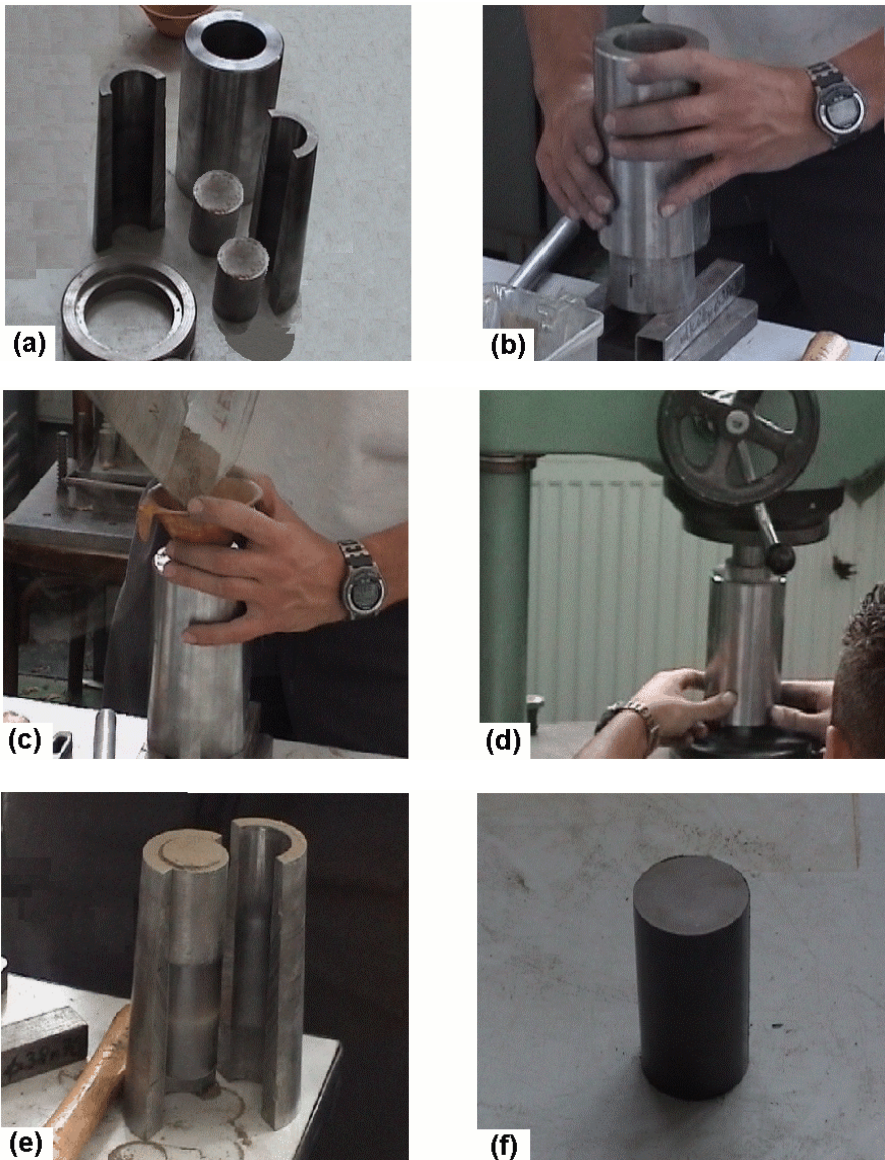
Fig. 1. Steps used for preparing the unsaturated highly compacted samples, (a) The two split mould, and the steel cylinders; (b) Assembly of the mould; (c) Filling the mould with the bentonite mixture; (d) Placing the mould in the compression machine; (e) The sample and guiding cylinder inside the mould just after compaction; (f)Compacted sample ready to be tested.

5 Testing procedures

The experimental testing program used in the current study was executed in the Center of Experimental Geotechnics (CEG) at the Faculty of Civil Engineering in Prague using a 50 kN triaxial machine manufactured in England by "Wykeham Farrance Int. Co. Ltd". The cell used in the current study was also designed and built by "Wykeham Farrance Int. Co. Ltd". This cell is the standard triaxial cell that can test specimens having a length of 3.00 inches and a diameter of 1.50 inches, which is considered as the standard diameter for testing soils free from stones, [6]. To evaluate the effective shear strength parameters, consolidated Isotropic undrained compression tests were applied to three initially unsaturated samples consolidated against backpressure to produce saturation, then a constant strain rate of about 0.004 mm/min was used during the shearing stage. Due to the fact that any redistribution of the pore-water pressure was expected to be too small as a result of the low water content inside them, the unsaturated and relatively dry highly compacted samples were consolidated using undrained testing method.

6 Experimental results and discussion

Fig. (2) represents the effect of degree of saturation on the stress strain behaviour for samples at different degrees of saturation under 0.5 MPa confinning pressure. The curves shows relatively linear performance for different degrees of saturations untill a strain of about 2.0%. Afterwards, the shear strength increases slowly for a few increments of strains with the maximum deviator stress generally being reached at axial strains of between 2.5% and 3.2%. However, the same behaviour was also observed when testing samples with similar degrees of saturation under the effect of different confining pressures. The modulus of elasticity in case of 1.0% water content ranged between 500 and 600 MPa, for 7.5% water content it was between 400 and 500 MPa, while for water content of about 12.7% the modulus of elasticity ranged between 300 and 350 MPa. The values of modulus of elasticity increase with increasing confining pressures. In general, this indicated that samples of lower water contents are stiffer than those of higher ones, as expected.

Fig. (3) shows Mohr circles representation of the results obtained from undrained tests performed on samples with 1.0% water content. In general, the pore pressures inside the relatively dry highly compacted samples were not measured during shear. That is why the results of shear strength were related to the total stress without a knowledge of pore pressure at failure. Typical curved envelopes could be drawn tangent to the Mohr circles of the samples at failure. These envelopes clarified the curved relationship between shear strength and total normal stress for the tested samples with different degrees of saturations under undrained conditions.
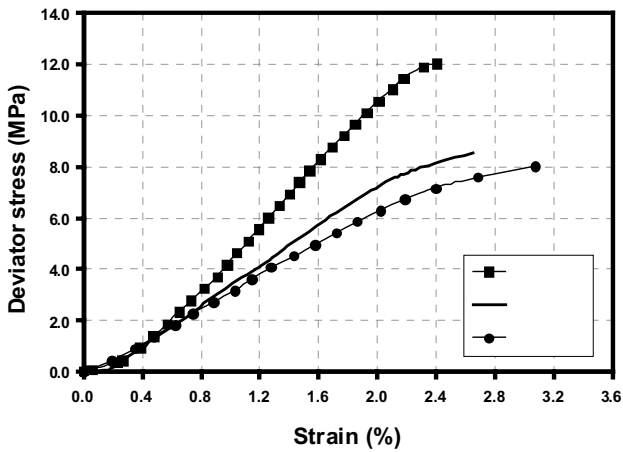
Fig. 2. Effect of degree of saturation on the stress strain behaviour at 0.50 MPa confining pressure.
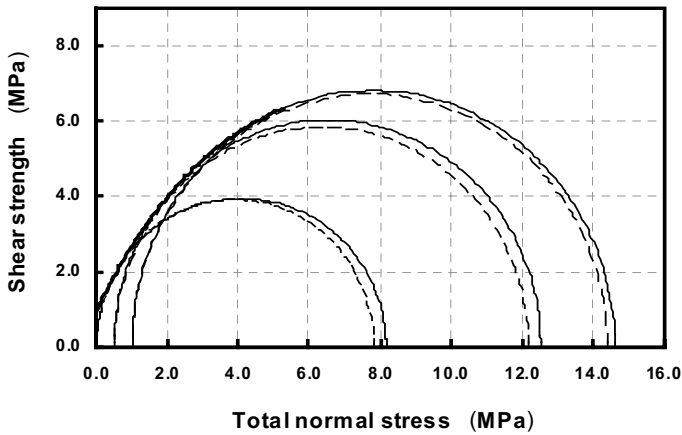

Fig. 3. Mohr coulomb circles for unsaturated highly compacted samples with 1.0% water content at different confining pressures.

The curved failure envelopes for all tested samples are shown together in Fig. (4). From this figure, it can be seen that the friction angle of this material decreases while its cohesion increases as a result of increasing confining pressures. At the same confining pressure, the friction angle increases with decreasing water contents as can be seen from the following results:

Water content	Friction angle, ϕ	Cohesion, c	$(c / \tan \phi)$
12.7%	39-32°	1.5-1.9 MPa	1.9-3.0 MPa
7.0%	49-41-40	1.2-1.5-1.55 MPa	1.0-1.7-1.9 MPa
1.0 %	57-52-41	1.2-1.4-2.20 MPa	0.8-1.1-2.6 MPa
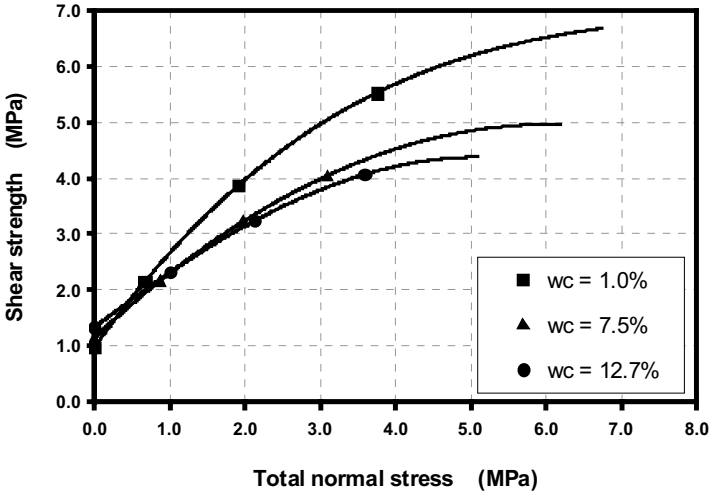
Fig. 4. Failure envelopes for unsaturated highly compacted samples with different water content.

The interpretation of the effect of decreasing water content on the cohesion is not so simple. This can be due to the growing influence of imperfections in the connections between soil particles by water menisci. The amount of these imperfections increase with decreasing saturations, especially for dried samples (wc=1.0%). The friction angle is also affected since it has some values within 52 and 57 degrees, which seems to be unrealistically high. This can be explained that when the confining preparation pressure decreased the sample expanded and the number of particles connected by water rapidly decreased. These losses in cohe-

sion led to a steeper Mohr-Coulomb envelope and extremely high value of friction angle. This observation can be supported by the tensile strength tests conducted in the Center of Experimental Geotechnics at the Faculty of Civil Engineering in Prague. The tensile strength was tested by bending beam specimens that have a cross-section of 40×40 mm^2, length of 200 mm, and water contents of 7.5 and 1.0%. The results of these tests showed that the tensile strength is practically the same (up to 0.9MPa).

Finally, the results shown above could be used in the discussion of numerical solutions for the unsaturated soil strength. The discussion presented hereinafter depends on the two widely known approaches used to express the shear strength of unsaturated soils (i.e., Bishop's [7] and Fredlund's [8]). However, some authors prefers Bishop's approach, which is based on the following equation, where χ can be called "the coefficient of the effectiveness of matric suction".

$$\tau = c' + [(\sigma - u_a) + \chi(u_a - u_w)]\tan \phi' \tag{1}$$

Moreover, many authors argue that the measurement of the parameter ϕ^b used in equation (2) proposed by "Fredlund" is difficult, time consuming and requires very sophisticated equipment.

$$\tau = c' + (\sigma - u_a) \tan \phi' + (u_a - u_w)\tan \phi^b \tag{2}$$

Other authors argue that Bishop's parameter, χ, which depends on many factors can be heavily quantified. From the point of view of these arguments and counter-arguments, the main difference between Bishop's [7] and Fredlund's [8] equations lies in how to reduce the effect of increasing matric suction. In fact, some studies showed that Bishop's parameter χ can be calculated using ϕ^b and vice versa (i.e., $\chi = \tan \phi^b/\tan \phi'$ and $\tan \phi^b = \chi \cdot \tan \phi'$). Therefore, results of unsaturated shear strength analyses using one of these approaches can be used as a base for the other. However, when describing the processes inside the highly compacted unsaturated samples of the bentonite buffer material tested in this study, Bishop's equation seems to be more realistic. With a decreasing water content and degree of saturation, the matric suction (or better to say its potential) increases, but the shear strength increase loses. This retardation can be expressed using a decreasing value of ϕ^b or χ. Contrary to decreasing ϕ^b, the friction angle of a drying soil increases rather than decreases. On the other hand, the decreasing effectiveness of matric suction, χ, can be explained. With decreasing saturation of a soil as the result of drying or expansion, the matric suction increases, but the cross-section area of average water meniscus decreases and the share of soil particles connected by water menisci decreases too and then shrinkage appears in the form of micro cracks. Bishop's equation seems to be unnecessarily complicated for many tasks from the practical point of view. The evaluation of air pressure, water suction and parameter χ is necessary. In many cases, the effect of air pressure can be ignored because its influence is less than uncertainties in the pore-water pressure, u_w, and the parameter, χ. For example, the air pressure is equal to the atmospheric in soils of low water content, while the air volume is very small in almost fully saturated soils. In these cases the Bishop equation can be simplified as:

$$\tau = c' + (\sigma - \chi'.u_w)\tan \phi' \qquad (3)$$

Where, $(\chi'.u_w)$ is the weighted mean of water suction and insignificant air pressure, which can be calculated as; $(\chi'.u_w) = -(c - c')/\tan \phi'$.

7 Conclusions

Tests on highly compacted bentonite samples of low water content show the typical behavior of this kind of material. The Mohr circles envelope is curved. When the confining pressure is increased, the friction angle decreases, while the cohesion increase. This can be explained as the effect of increasing number of particles connected by water. The number of imperfections decreases and the effectiveness of suction and cohesion increase. From this point of view, Bishop's approach to the calculations of the unsaturated soil strength using the parameter, χ, (of the suction effectiveness), seems to be more realistic for describing the processes inside the tested material.

Acknowledgement

References

[1] Fredlund, D. G. (2000): "Historical developments and milestones in unsaturated soil mechanics" Proceedings of the 1st Asian Conference on Unsaturated Soils (UNSAT-ASIA 2000), ISBN 90 5809 139 2, pp. 53-68.
[2] Jennings, J. E. B. (1961): "A revised effective stress law for use in the prediction of the behavior of unsaturated soils" Conf. on pore pressure and suction in soils, organized by British Nat. Soc. of Int. Soc. Soil Mech. Found. Eng. At Inst. Civil Eng., London, England: Butterworths, pp. 26-30.
[3] Blatz, J.; Tang, X.; Graham, J.; and Wan, A. (1999): "Psychrometer techniques for measuring suction in the triaxial test" 52nd Canadian Geotec. Conference.
[4] Favaretti, M. (1995): "Tensile strength of compacted clays" Proc. of the 1st International Conference on Unsaturated Soils, Paris, vol. 1, pp. 51-56.
[5] Pacovsky, J.; et al. (2001): "Experimental research of prefabricated bentonite barriers used for high radioactive waste isolation in deep underground disposal" Report GACR reg. Č. 103 / 99 / 1288, Center of Experimental Geotechnics (CEG), Faculty of Civil Engineering, CTU, Prague.

[6] Bishop, A. W.; and Henkel, D. J. (1962): "The measurement of soil properties in the triaxial test" Second edition. Edward Arnold (publishers) Ltd., London.

[7] Bishop, A. W. (1959): "The principle of effective stress" Teknish Ukeblad, vol. 106, no. 39, pp. 859-863.

[8] Fredlund, D. G.; Morgenstern, N. R.; and Widger, R. A. (1978): "The shear strength of unsaturated soils" Canadian Geotechnical Journal, vol. 15, no. 3, pp. 313-321.

Evaluation of Yielding in Unsaturated Clays Using an Automated Triaxial Apparatus with Controlled Suction

James Blatz, David Anderson, Jim Graham, and Greg Siemens

Department of Civil Engineering, University of Manitoba
Winnipeg, Manitoba, CANADA

Abstract. Research in the field of unsaturated soil mechanics for high plastic clays is very active. One area of considerable current interest is development of general constitutive models for unsaturated clay based sealing materials in a framework that can be implemented in numerical modeling tools (Alonso *et al.* 1990, Delage and Graham 1995, Toll 1990). In particular, more quantitative information is required to define the features of yielding, failure and strain hardening for predictive modeling applications. Soil suction must be controlled and independently measured in laboratory tests. This will allow examination of behaviour along any stress path that can be expected to occur in engineering applications which will provide the necessary material information to calibrate and validate proposed constitutive frameworks.

   This paper presents details of laboratory tests in a custom triaxial system with stress path automation and independently controlled and measured suction (Blatz and Graham 2000, 2003). Details describing the equipment will be given along with selected results for the yield, strength, and strain hardening behavior of a high-plastic sand-clay material at suctions from 5 MPa to 160 MPa and isotropic pressures from 1 MPa to 6 MPa. The results demonstrate the importance of independent measurement and control of suction along well controlled loading paths for interpreting the behaviour of unsaturated high plastic clays.

Introduction

In many geoenvironmental engineering applications, silty and sandy native soils are often mixed with smectitic clay to form 'impervious' seals. Many conceptual deep geological waste repositories propose a 50:50 mixture of heavily compacted sand and bentonite clay as a sealing material (known as 'buffer') to form an advective and sorbing barrier to transport of radionuclides. The buffer is subject to heat loading from unspent waste fuel in the storage containers (the sand acts to improve heat transfer and limit shrinkage.) Coupling between heat and moisture near the container results in temperature gradients that cause drying at the container surface and wetting near the host rock. The processes of wetting and drying

affect the hydro-mechanical characteristics of the buffer material significantly (Graham *et al.* 1997). Different behaviour can be expected at different water contents and corresponding degrees of saturation (Wheeler *et al.* 2003). The differences in behaviour are caused by varying water contents in the material and associated changes in soil suction.

In order to understand the behaviour of unsaturated soils, laboratory testing procedures must be developed that allow examination of the soil properties at different suction levels. Measurements from the laboratory can then be used to define material properties for use in numerical modeling tools designed to analyze complex interactions that occur in many engineering applications.

Many researchers have developed equipment that incorporates controlled suction. A number of different techniques have been used depending on the suction levels being examined (Escario and Sáez 1986, Cui and Delage 1996, Cunningham *et al*. 2003). As well as *controlling* suction, many methods have been developed for *measuring* soil suction in laboratory experiments (Ridley and Burland 1993, Fredlund and Rahardjo 1993, Cunningham *et al*. 2003). However, in many cases these two systems have not been integrated to provide control of suction with simultaneous independent measurement, especially for high suctions experienced in high plastic clays. This can result in significant difficulties when interpreting test results. In some cases, soil suctions are assumed to be in equilibrium when the volume strains equilibrate. This is not always valid. In other cases, suctions are assumed to be constant during application of external stress conditions. This often is not the case (especially in high plastic compacted clays) in constant mass tests, where total mean stresses are altered. This paper demonstrates how independent suction measurement and control is essential to properly interpret test results for examining the behaviour of unsaturated clays. It deals specifically with some of the features of yielding under isotropic and shear stress loading conditions.

Results from triaxial tests on densely compacted sand-bentonite buffer are presented along with details of the testing apparatus used to independently control and measure soil suction. The specimens were subjected to various suction levels using a vapour equilibrium technique. Selected specimens included two embedded psychrometers that provided direct measurements of suction during triaxial testing. The results provide information regarding the yield behaviour of densely compacted buffer.

Materials and Specimen Preparation

Before mixing, the constituent bentonite and sand were stored in an oven at 104 C for a minimum of 48 and 24 hours respectively. After removing the materials from the oven, the containers were sealed with plastic wrap and a rubber band to ensure moisture was not pulled from the air into the materials. The materials were allowed to equilibrate with room temperature for 90 minutes before measurements and mixing commenced.

The required dry weights of the constituent bentonite clay, silica sand, and distilled deaired water for buffer specimens were pre-determined from target 'reference' values, water content = 19.42% and dry density = 1.67 Mg/m^3 and verified by quality control tests. Mixing of the constituents followed standardized procedures used at the University of Manitoba that are outlined in Blatz *et al.* (1999). Water content measurements were taken 48 hours after mixing to evaluate the actual water content of the material. This water content was then to determine the wet soil mass needed for compaction to meet the density requirements.

Specimen Compaction

Specimens were compacted in a rigid one-dimensional static compaction mould. Procedures developed at the University of Manitoba for preparing triaxial specimens of sand-bentonite were followed (Blatz *et al.* 1999). Triaxial specimens were compacted to a nominal height of 100 mm and diameter of 50 mm. Specimens were compacted in five equal lifts using the constant lift height (20 mm) criterion. The constant lift height criterion was adopted in this work to ensure specimen consistency with past research projects on Reference Buffer Material (RBM). The technique produces specimens with minimal water content and density variations. It is noted that Cui and Delage (1996) demonstrate that stress-based compaction procedures produce a material that is more comparable with what occurs in engineering applications. However, for comparison with past research, the specimens in this work were compacted using the strain-based method. Following compaction, specimens were immediately placed in constant-suction environments for the first phase of the testing.

Experimental Method and Facility

The triaxial apparatus (Figure 1) has been described in detail in Blatz and Graham (2000). The capabilities and operation of the triaxial apparatus, including control and measurement of suction, will be presented briefly. More details will be provided during discussion of the experimental results.

The triaxial apparatus was designed to examine the behaviour of soils at cell pressures up to 10 MPa and temperatures up to 100C. The original equipment has recently been augmented by an automated control of cell pressure and shear loading using a custom-designed data acquisition and control system. The system is centered round a Rockwell Programmable Logic Controller (PLC) that interfaces with a standard desktop computer running the commercially available RSView software. The software interface was also custom designed to allow user-defined control recipes related to the external load conditions, measured soil suction, and measured volumetric strain. The capabilities of the system have provided considerable improvement in controlling stress paths. This has resulted in much easier and more consistent interpretation of yield behaviour of the specimens. The sys-

tem was commissioned in the summer of 2002 and has been used for all testing since that point.

Suction Measurement Using Psychrometers

The psychrometers used for suction measurement are commercially available Wescor PST-55 stainless steel psychrometers. These were selected due to their quick response times, small uniform cylindrical tip geometry, and the durability of the steel shield compared to the ceramic tipped alternative. The psychrometer sensor measures 5mm in diameter and 7mm in length. The psychrometers were controlled and measured using a Campbell Scientific CR-7 measurement and control system. Details of the installation procedure for incorporating these sensors in the center and top of specimens have been discussed by Blatz *et al.* (1999).

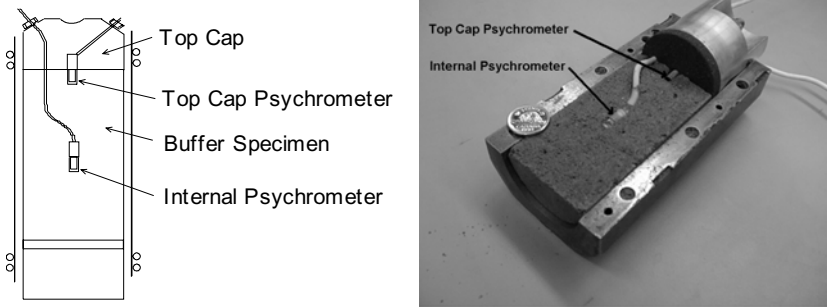**Fig. 1.** Automated triaxial system with controlled suction

Fig. 2. Schematic of psychrometer layout (left) and photograph (right) of psychrometers following excavation of specimen (after Blatz *et al*. 1999)

Figure 2 shows the location of the psychrometer sensors in a typical specimen. A quality control specimen was compacted to test the compaction apparatus and to ensure that the internal psychrometer was not damaged during compaction. After compaction, the specimen was carefully trimmed to expose the internal psychrometer with minimal disturbance (Figure 2). The photograph illustrates the psychrometer location and the wire that leads to the external data acquisition system. These psychrometers provide point measurement of total suction (matric plus osmotic suction) in the range of 1MPa to 8MPa during all stages of testing. The buffer specimens have an initial as-compacted suction of 4MPa. The psychrometers have worked well for examining increases or decreases in suction from the initial as-compacted suction to the limits indicated.

Controlled Suction Triaxial Apparatus

Constant suction conditions can be created using relative humidity environments generated by ionic solutions in sealed chambers. Here, solutions of sulphuric acid and distilled, deaired water were used to create a range of partial vapour pressures in desiccators as a function of the acid concentration. Using relationships between partial vapour pressure and acid concentration, solutions were used to generate suctions from 5 MPa to 160 MPa.

Figure 3 (after Blatz and Graham 2003) shows a simplified diagram illustrating the triaxial apparatus and vapour equilibrium system that allows for controlled suction in the triaxial cell. The desiccator (a) containing an ionic solution mixed to generate a target suction level is connected to a pump (b) using plastic tubing approximately 6.5 mm in diameter from the head space above the level of the ionic solution in the desiccator and finally to the triaxial cell.
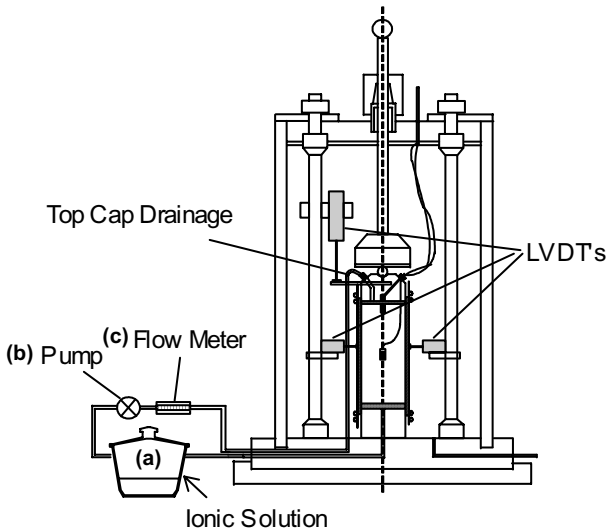
Fig. 3. Schematic of controlled suction system for triaxial cell after Blatz and Graham (2000)

An air flow meter (c) is installed between the desiccator and the triaxial cell to monitor vapour flow through in the system. When the pump is engaged, vapour from the headspace of the desiccator (with a known partial vapour pressure and therefore suction) is pumped along the tubing to the base of the triaxial cell. From the triaxial base, vapour enters the porous stone beneath the specimen. The vapour then moves along the periphery of the specimen through Amaco #2044 woven geotextile placed in strips around the specimen. The geotextile is placed vertically in strips similar to filter paper drains used for saturated specimens. Geotextile strips provide a pathway for vapour movement along the exterior of specimens while being rigid enough to maintain drainage under externally applied cell pressure. The geotextile is able to maintain a continuous flow path for the vapour at cell pressures up to approximately 2.5 MPa. The geotextile strips are long enough to cover the top and bottom porous stones and provide a continuous passageway for vapour flow.

When vapour reaches the top of the specimen, it enters the top porous stone and continues through piping to the base of the cell, where it is circulated back into the desiccator headspace. This is a closed, constant-mass system with respect to the water vapour and ionic solution. As water vapour moves along the outside of a specimen at the porous stone and geotextile interfaces, it exerts a total suction on the soil specimen according to the partial vapour pressure generated by the ionic solution. The specimen transfers water to, or takes water from, the vapour depending on the soil suction gradient between the ionic solution and the specimen. During application of suction using this system, the soil suction at the center and top of the specimen is monitored using embedded psychrometers. As drying proceeds,

water moves from the specimen into the desiccator and alters the ionic concentration. This must be accounted for in establishing the suction level and is another reason why independent measurement of suction is important.

Results

The following sections include representative results from specimens with embedded psychrometers (up to 8MPa suction) and specimens without psychrometers (initial suctions greater than 8MPa). Initial suctions greater than 8MPa were generated by placing compacted specimens with initial suctions of 4MPa in desiccators with target suction levels up to 160MPa for a period of 30 days that ensured equilibrium with the head space environment, Tang *et al*. 2002). The specimens were then tested using the triaxial system that has been described previously, though it is noted that the suctions were now outside the range of the psychrometer measurement. In these cases, the relationship regarding the measured response of soil suction to applied external stresses at lower soil suctions were extrapolated to higher suctions. Work is ongoing to examine the capability of new sensors that will provide a much greater range of suction measurement.

Response of Suctions to External Loading

An important consideration in testing unsaturated specimens in the triaxial cell is the response of soil suction to external loading. A series of specimens containing two psychrometers (Figure 2) examined the response of the soil suction to isotropic and shear loading.

After installation in the test cells, specimens were allowed to equilibrate for 24 hours prior to loading. A series of isotropic pressure increments were then applied with 24 hour intervals to attain volume and suction equilibrium. All drainage lines were shut off during the loading to ensure that specimens were undrained in both the gas and liquid phases. We have called this creating a 'constant mass' condition. Since the material was unsaturated, loading was accompanied by compression strains. Figure 4 shows the changes in soil suction measured by the two psychrometers due to the applied cell pressure increments. Figure 4 also shows the same data plotted with respect to time. The measurements show that with undrained conditions in both the air and gas phases, soil suction decreases with increasing mean stress.

The response appears broadly linear ($\Delta S/\Delta p$=-0.83) as has been previously reported by Tang *et al*. (2002) who also show that the relationship is reversible, at least in this stress range. The response at the center of the specimen and at the top of the specimen are broadly similar, indicating that the 24 hour equilibration period is sufficient to ensure that the soil suction is uniform throughout the specimen before the next isotropic stress increment.

Figure 5 shows the response of soil suction to shear loading (deviator stress) in a standard triaxial compression test.
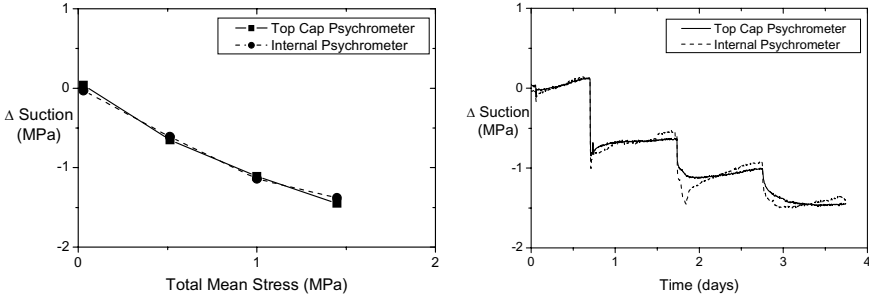

Fig. 4. Measured suction change due to increments in total mean stress and with time
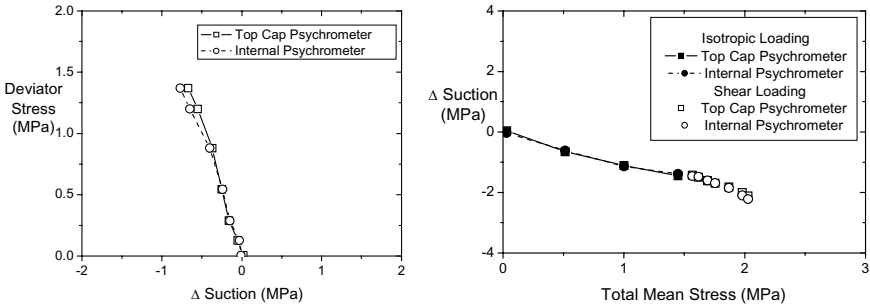

Fig. 5. Change in suction due to 3:1 triaxial shear loading and summary of change in suction due to both total mean stress and shear loading conditions

Figure 5 shows that suction is decreasing as the axial load is applied (along a 3:1 triaxial stress path with constant cell pressure), however the accompanying figure shows that in fact the suction response again appears to be linked to the change in mean stress associated with the shearing stress path examined.

In fact, the slope of the relationship is broadly similar to that of the soil suction response associated with the change in mean stress alone. Once again, the suction responses in both psychrometers are in close agreement after 24 hours. Some deviation in the suction measured by the two instruments occurred at higher shear stress conditions. This may be due to different yielding and localized strain effects at the center of the specimen compared with the top of the specimen in the 'dead

zone'. The agreement is still acceptable as the difference in measured suction levels is approximately 7% of the absolute value of suction.

The slope of the change in suction due to changes in mean stress has been termed the 'isotropic suction response relationship'. This relationship has been found consistent by three different researchers over a number of confining pressures and suction ranges. The response is believed to be related to compression of the soil skeleton and the resulting changes in saturation that occur when volumetric straining results from externally applied pressures consistent with what has been presented in other work (Wheeler *et al*. 2003). This is an important feature of behaviour that is currently being explored in more detail and one that is not observed in drained tests where constant suction are achieved using axis translation.

Shrinkage Characteristics

In order to examine the behaviour of buffer at suctions beyond the measurement capabilities of the psychrometers in this test program, suctions during triaxial testing had to be inferred from initial suctions and the isotropic suction response relationship already discussed. (The relationship was assumed to remain unchanged at higher suctions). An alternative is to relate measurable volume changes and water contents to suctions through a Soil Water Characteristic Curve.

Measurements of the dimensions and masses prior to placement in the desiccators and after equilibration (30 days) allowed for assessment of the changes in water content and density associated with the change in suction from the as-compacted state to the target suction value. The results were used to determine the soil water characteristic curve (SWCC) shown in Figure 6 and the volumetric shrinkage curve shown in Figure 7. Suction data in Figures 6 and 7 have taken into account the mass balance correction that occurs inside the sealed desiccators as the vapour transfer proceeds to equilibrium. (This is the reason that the final suction in the figures is not exactly the same as the target suction set in each desiccator.)

As the suction increases the measured volumetric shrinkage increases nonlinearly to an apparent upper limit of about 8% volume strain at approximately 30MPa suction (Figure 7). It is postulated that shrinkage beyond the 30 to 40MPa level is inhibited through transfer of stresses from the clay phase to the sand phase of the material. Initially the buffer material behaviour is believed to be dominated by the clay, with sand simply acting as filler in the clay matrix. With increasing suctions, it is proposed that bulk volumetric shrinkage occurs until the clay matrix becomes small enough to fit within the void space provided by the sand skeleton. This is noted in Figure 7 as the non-linearity that occurs at 8 to 10 % strain.
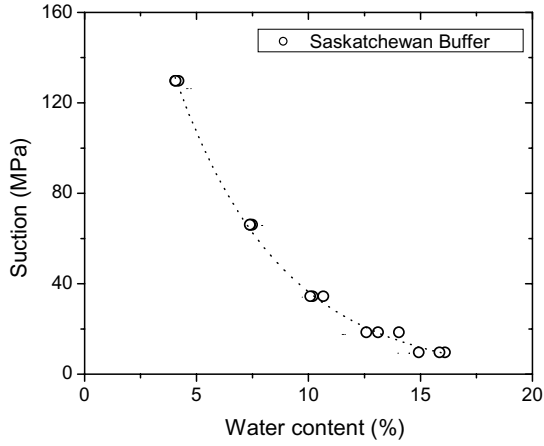
Fig. 6. Soil Water Characteristic Curve for Saskatchewan buffer
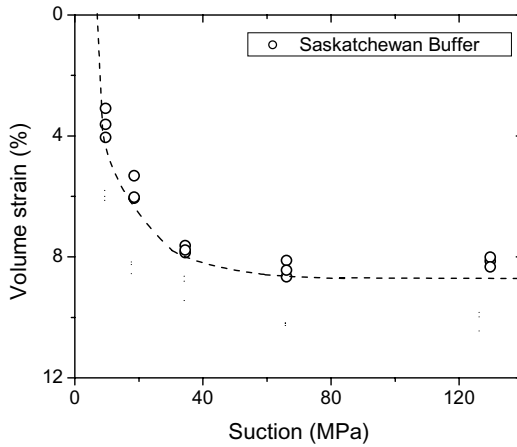
Fig. 7. Shrinkage behaviour of Saskatchewan buffer

This suggestion is supported by observations of stiffness and strength that approach those of the sand component at suctions greater than 30MPa as well. Further increases in suction no longer increase the volumetric straining of the buffer mixture but the water content will continue to decrease as water is pulled from the clay, which continues to shrink in the spaces in the sand skeleton. The relationship in Figure 7 for volumetric shrinkage versus total suction, is not therefore the formal 'shrinkage limit', which is defined as a water content. Parallel studies to those

in Figure 7 have been done with Wyoming bentonite. Similar results are obtained, but the limit of volumetric shrinkage is 12% instead of the 8% for the Saskatchewan bentonite in Figure 7. Future work will explore these relationship by testing specimens of pure bentonite to compare their shrinkage limits to those of sand-bentonite buffer mixtures. This concept is important for modeling. Two separate soil models may be required to describe the full range of behaviour of the buffer as volumetric strains occur.

Yielding Under Isotropic Compression

Figure 8 shows volume strain versus logarithm of total mean stress for specimens of Saskatchewan buffer specimens made with target suction levels of 10, 20, 40, 80, and 160 MPa. As mentioned earlier, the loading paths during isotropic compression in these constant–mass tests has been assumed to follow a path $\Delta S/\Delta p = -0.83$ and are not along constant-suction traces. Figure 8 indicates that the behaviour under initial loading was stiff and that this is followed by less stiff behaviour beyond an apparent yield stress (or load yield (LY) pressure) for all suction levels.

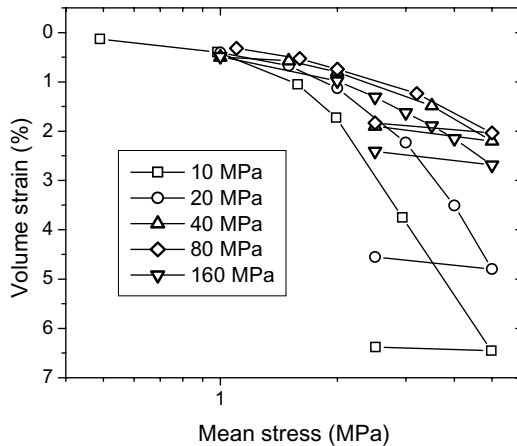**Fig. 8.** Compression results for Saskatchewan buffer at various suction levels

Definition of the yield stress is clearer at lower suction levels as compared to higher suction levels. As expected, the response to unloading after reaching the maximum mean stress value (5 MPa) was also stiff. The slope of the unloading section was comparable (though slightly stiffer) to the initial portion of the loading curve.

Figure 9 (after Blatz and Graham 2003) shows stress paths in mean stress versus total suction space for two specimens that were placed in the triaxial cell following compaction and isotropically compressed in increments up to 2MPa. By compressing the specimens beyond their initial 'as compacted' isotropic yield point, the position of the initial load yield line is known, as is the new load yield line formed by plastic hardening to the new maximum mean stress of 2MPa. The specimens were then unloaded to 1MPa, corresponding to an overconsolidation ratio equal to 2.0. The controlled suction system described earlier was then used to dry the specimens to higher suctions. This is shown in Figure 9 where the stress paths show an increase in suction at a constant total mean stress. Following the applied suction increases, the two specimens were again loaded isotropically and their new yield points interpreted. Again the consistent slope for the decrease in suction associated with increasing mean stress is apparent.
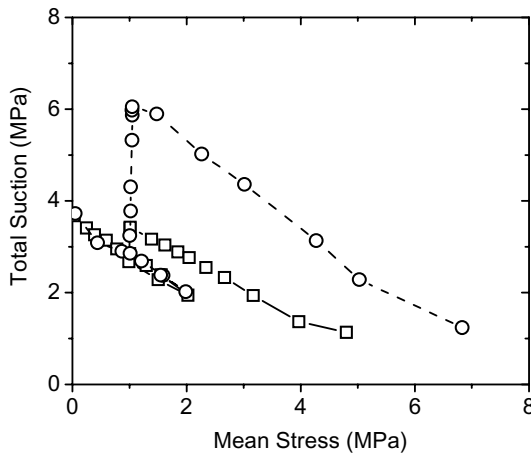

Fig. 9. Compression behaviour observed in controlled suction tests (after Blatz and Graham 2003)

When the yield points at each suction level are summarized (Figure 10), the variations in the load yield pressure can be examined. Specimens in the range of suction measured with the by psychrometer (4 to 8 MPa) show acceptable agreement with the additional specimens up to final suction values of 140 MPa (corresponding to a target suction level of 160 MPa). In all cases the final suctions have been corrected to take into account the decreases in soil suction associated with mean stress. This consideration is most important at the lower suction levels where the applied mean stress can be similar to the soil suction level. It is also interesting that the load yield pressure does not appear to increase significantly after suctions above 30MPa, which is the approximate limit of volumetric shrinkage due to increased suctions.
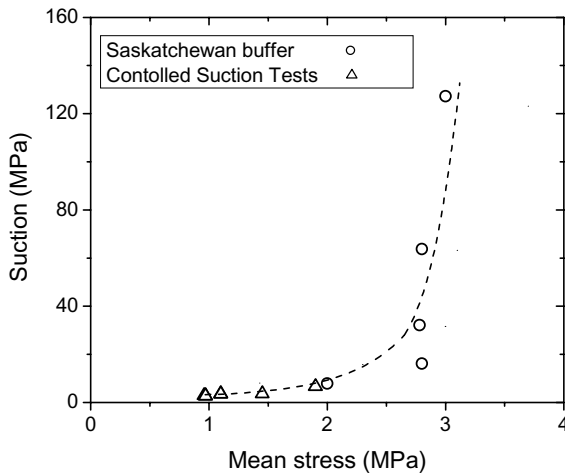
Fig. 10. Interpreted load yield curve for compacted buffer

Yielding Under Triaxial Shearing

After isotropic compression was completed, triaxial shearing was undertaken at a constant rate of 0.0139 mm/min. (This took the specimens to 20% axial strain in approximately 24 hours. During shearing, the cell pressure was adjusted to maintain target ($\Delta q/\Delta p$) stress paths where q is deviator stress ($\sigma 1 - \sigma 3$) and p is total mean stress ($\sigma 1 + 2\sigma 3$)/3. The chosen shearing rate was based on measurements with embedded psychrometers to ensure that suction throughout the specimens was constant during shearing (Blatz *et al.* 1999). Figure 11 shows a typical set of stress paths that were followed in q-p space during shearing at specific target suctions. The peak and end-of-test values for q and p are shown in the Figure. The plots in q-p space show that significant strain-softening occurs after specimens have reached peak shear strength for cases with constant-p and the $\Delta q/\Delta p = 3$:-1 stress paths. The stress path control was achieved using the automated stress path control system described previously.
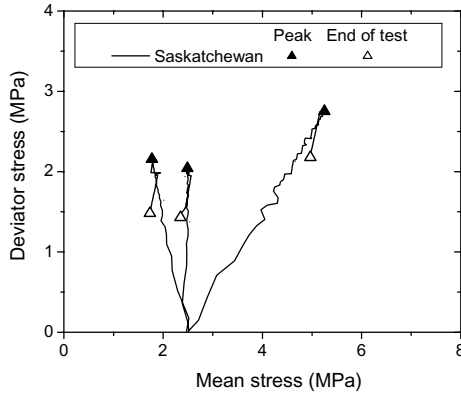
Fig. 11. Typical triaxial shearing paths followed
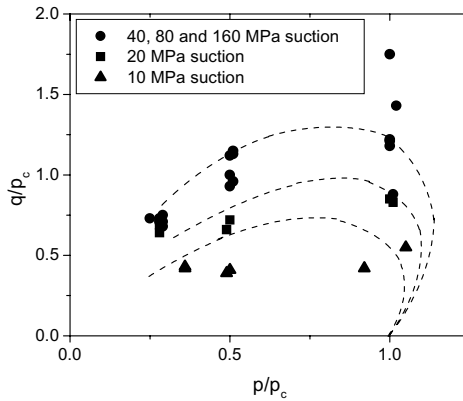
Fig. 12. Normalized yield loci

The yield points in these tests could be interpreted relatively easily using plots of specific volume versus logarithm mean stress. By normalizing the deviator stress and total mean stress at yield using the preconsolidation pressure, yield loci for the shearing stress paths could be drawn for the various initial target suctions. Figure 12 shows normalized q and p data for the buffer material at all suction levels. The figure also suggests possible yield loci. The normalized yield loci have broadly similar shapes, but increase in size with increasing suction. Again, however, after a suction of approximately 30MPa (corresponding to the limit of volumetric shrinkage), the loci tend to coalesce. This indicates that after 30 MPa suction, the yield loci appear independent of suction level. This is again attributed to

transition from a clay-dominated behaviour to sand-dominated behaviour when shrinkage is sufficient to allow the sand component to carry external forces.

Discussion and Conclusions

Results have been presented to demonstrate the reliability of suction control using the vapour equilibrium technique and suction measurement using thermocouple psychrometers. Details of the methods and the triaxial apparatus have been introduced and reference given to other publications with more detailed background information. Implementation of these two techniques (suction control and suction measurement) in triaxial testing has been shown, along with data that demonstrate the importance of assessing changes in suction that occur in association with mean stress increments. The data also show that the changes in suction appear relatively independent of the deviator component of the stress tensor.

Shrinkage tests showed that the sand-bentonite 'buffer' in this program exhibits a limit of volumetric shrinkage at a suction of approximately 30MPa. The limit of shrinkage is believed to result from a stress transfer of stresses from the clay component to the sand component of the mixture. A transition from clay-dominated behaviour to sand-dominated behaviour has considerable impact on the mechanical response under subsequent external stresses. When suctions are less than 30MPa, the material behaves as a compacted clay. At suctions greater than 30 MPa, the material appears to transition to a purely frictional sand behaviour.

Combinations of isotropic loading and deviator loading were use to investigate yielding behaviour as a function of soil suction. The results again showed a transitional behaviour corresponding to the 30MPa suction level consistent with the shrinkage tests. The greatest improvement that can be implemented for future testing will be to develop suction measurement beyond the current 8MPa limitation. Considerable effort is being directed at finding new technologies that will remove this barrier and provide information on suction responses at suctions higher than 8MPa. These high suctions are rare in the published literature but are likely common in practice in clay-rich soils, especially in dry climates.

The results in this paper present only a small part of an research effort that has been ongoing for 20 years to elucidate the behaviour of the compacted clay-based sealing materials for use in an underground repository environment.

Acknowledgements

References

Alonso, E.E., Gens, A., and Josa, A. 1990. A constitutive model for partially saturated soils. Geotechnique, 40: 405-430.

Blatz, J.A., and Graham, J. 2003. Elastic plastic modeling of unsaturated high plastic clay using results from a new triaxial test with controlled suction. Géotechnique Special Symposium in Print on Unsaturated Soils, 53(1): 113 – 122.

Blatz, J.A., and Graham, J. 2000. A method for controlled suctions in triaxial testing. Géotechnique, 50(4): 465 – 470.

Blatz, J.A., Tang, G.X., Graham, J., and Wan, A. 1999. Psychrometer techniques for measuring suction in the triaxial test. Proc. of 52nd Canadian Geotechnical Conference, Regina, Vol.1, pp. 617-622.

Cui, Y.J. and Delage, P. 1996. Yielding and plastic behaviour of an unsaturated compacted silt. Geotechnique, 46(2):291-312.

Cunningham, M.R., Ridley, A.M., Dineen, K., and Burland, J.B. 2003. The mechanical behaviour of a reconstituted unsaturated silty clay. Géotechnique Special Symposium in Print on Unsaturated Soils, 53(2): 183 – 194.

Delage, P. and Graham, J. 1995. Understanding the behavior of unsaturated soils requires reliable conceptual model. State of the Art Report, Proceedings, 1st Int. Conf. on Unsaturated Soils, Paris, France, 1995, 1223-1256.

Escario, V. and Sáez, J. (1986). The shear strength of partly saturated soils. Géotechnique 36, No. 3, 453-456.

Fredlund, D.G. and Rahardjo, H. 1993. Soil Mechanics for Unsaturated Soil. A Wiley- Interscience Publication. John Wiley & Sons, Inc., New York, NY.

Graham, J., Chandler, N.A., Dixon, D.A., Roach, P.J., To., T., Wan, A.W.L. 1997. The buffer container experiment: results, synthesis, issues. AECL Whiteshell laboratories, Pinawa, Manitoba. AECL-11746.

Ridley, A.M. and Burland, J.B. 1993. A new instrument for the measurement of soil moisture suction. Geotechnique 43(2):321-324.

Tang, G.X., Graham, J., Blatz, J.A., Gray, M. and Rajapakse, R.K.N.D. 2002. Suctions, stresses and strengths in unsaturated sand-bentonite. Journal of Engineering Geology, 64(2): 147-156.

Toll, D.G. 1990. A framework for unsaturated soils behavior (discussion). Geotechnique, 41(1):159-161.

Wheeler, S.J., Sharma, R.S., and Buisson, M.S.R. 2003. Coupling of hydraulic hysteresis and stress – strain behaviour in unsaturated soils. Géotechnique Special Symposium in Print on Unsaturated Soils, 53(1): 41 – 54.

Wheeler, S.J. and Sivakumar, V. 1995. An elasto-plastic critical state framework for unsaturated soil. Geotechnique, 45(1):35-53.

Wiebe, B.J. 1996. The effect of confining pressure, temperature, and suction on the strength and stiffness of unsaturated buffer. M.Sc. Thesis, Department of Civil and Geological Engineering, University of Manitoba, (Winnipeg, Manitoba).

A triaxial device for unsaturated sand – New Developments

C. Lauer and J. Engel

Institute of Geotechnical Engineering, TU Dresden, Germany
`carsten.lauer@mailbox.tu-dresden.de`

Summary. Investigation into the mechanical and hydro-mechanical behaviour of unsaturated sand requires special laboratory equipment for testing and preparing the specimens. In this paper, the requirements for a triaxial testing device for unsaturated sand are presented. With respect to the requirements for testing unsaturated sand (axis-translation technique), measuring small overall and pore-water volume change, and the control or measurement of small values of suction, a new triaxial device has been developed. It consists of a double-walled triaxial cell, a modular loading frame including the axial power unit, and a pc for controlling and data logging. The device enables the determination of the shear strength, the SWCC, and the hydraulic conductivity of unsaturated sand.

Keywords: Unsaturated sand, SWCC, double-walled triaxial cell

1 Introduction – Requirements

To understand the mechanical and hydraulic behaviour of unsaturated soils it is necessary to receive accurate measurements. A perfect test equipment should allow the full control over all stresses and strains. However, this aim can only approximately be reached. Unsaturated soils are mixtures of solids, pore-water and pore-air. Thus, it is necessary to develop test equipment for controlling the volume change as well as the stress change of all three phases. In this paper, a new triaxial device for sand and silt samples is presented. The special requirements are:

– the sand specimen have to be prepared with a reproducible fabric and different densities,
– the transducers must allow the registration of very small changes of deformations during the consolidation stage and of large deformations during the shear stage,
– to control the suction in a wide range, the axis–translation technique should be used,
– with the axis–translation technique it should be possible to adjust a suction gradient between the top and the bottom of the specimen.

For this reason, it is necessary to consider the mechanical and hydraulic properties of the soils. In the first phase, triaxial tests were carried out on dry Hostun sand to achieve results with a conventional and a new developed cell and, moreover, reference results of the saturated state. Tests on a reconstituted silt are planned for a later stage.

2 Soil Mechanic Properties of saturated Hostun sand

First, all laboratory tests were performed on dry Hostun sand. Hostun sand has been used for many tests in different soil mechanical laboratories. Thus, test results for saturated conditions are well documented [8, 6, 4, 13]. This results in a reliable data base to check the own test results in the design stage of the equipment.

2.1 Classification

Hostun sand is a uniformly-graded granular siliceous medium sand with a mean particle size of $d_{50} = 0.355$ mm and a coefficient of uniformity of $C_u = 1.43$. Fig. 1 shows the grain size distribution. The grain shape of Hostun sand
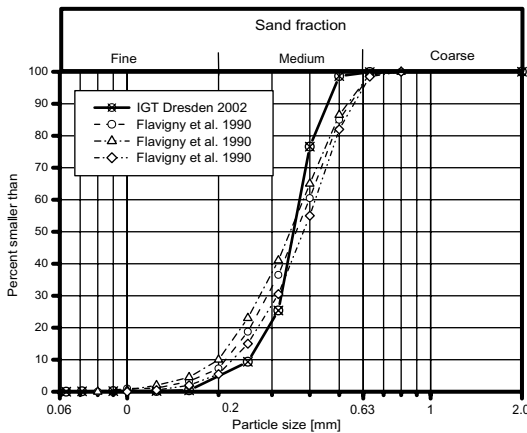

Fig. 1. Grain size distribution

is angular (Fig. 2). Fig. 3 shoes the results of a X-Ray Powder Diffraction (XRD). According to this the principal component is silica (SiO_2) with a slight fraction of potash feldspar ($KAlSiO_8$). More classification parameters have been listed in Table 1.
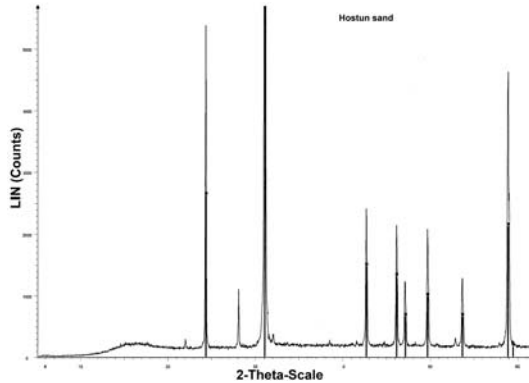
Fig. 2. Grain shape of Hostun sand

Fig. 3. Qualitative phase analysis by X-Ray Powder Diffraction (XRD)

Table 1. Material parameters of Hostun sand

maximum void ratio	max e	[-]	1.032
minimum void ratio	min e	[-]	0.647
density of the solid particles	ρ_S	g/cm^3	2.643

2.2 Triaxial Tests on dry Hostun sand

The shear strength of saturated Hostun sand was obtained from drained triaxial compression tests. All tests were carried out with a conventional triaxial testing device without lubricated ends. Specimens with a diameter of 5.0 cm and a height of 12.5 cm ($H/D = 2.5$) were used. This geometry of the specimens is identical to those in the newly developed double-walled triaxial cell for unsaturated soils. To prepare specimens with high densities a special pluviation technique, and specimens with low densities a combination of pluviation and a modified dry funnel method was used. Both methods will be described later. The surrounding latex membrane is of 0.35 mm thickness. The constant vertical displacement speed was 0.5 mm/min. In Fig. 4 the influence of the lateral stress σ_3 on the peak friction angle φ_p for samples with low and high initial relative densities I_D is shown. The test results correspond with the data given by [6], [4] and AL ISSA (1973, cited in [3]).

To characterize the stiffness of the specimens the secant modulus at 50% shear strength E_{50} was used. It's value was determined from the stress-strain curves of the drained triaxial compression tests. As is generally known, the quantity of the stiffness modulus depends on the minor principal stress σ_3 (Fig. 5). The stress dependency could be described by equation 1 where σ_{ref} is a free, selectable reference stress which is here assumed to 100 kPa.
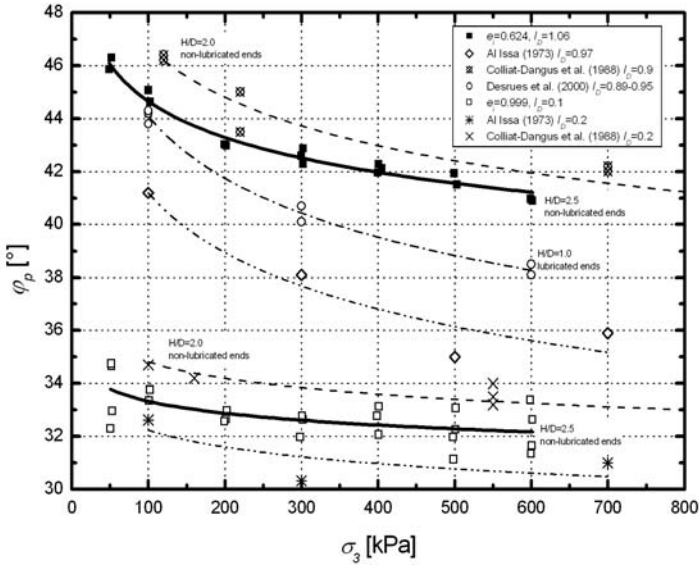
Fig. 4. Influence of lateral stress σ_3 on φ_p

$$\frac{E_{50}}{\sigma_{ref}} = v \left(\frac{\sigma_3}{\sigma_{ref}} \right)^w \qquad (1)$$

endequation The coefficient v and the exponent w, which describes the stress dependency, are specified in Fig. 5 for loose and dense Hostun sand. The experimentally determined values for E_{50} for loose Hostun sand correspondent to tests results from [6]. In contrast, for dense Hostun sand only the values at σ_3=100 kPa are comparable. The differences between the values for E_{50} for a certain lateral stress are considerable. For example E_{50} is determined to 53.9 and 93.2 MPa for σ_3=600 kPa. The unloading and reloading stiffness E_{ur} from dense Hostun sand was determined from drained triaxial compression tests with three unloading and reloading stress paths at 50, 70 and 90 % of the mobilization of the peak friction angle. All tests were performed on dry sand using different cell pressures (σ_3=200, 400 and 600 kPa). The amplitude of the unloading and reloading cycles was defined to 12.5 % of $\sigma_{1,max}$ obtained in the triaxial compression. This special testing procedure had been chosen to obtain measurable quantities of stress-strain changes and to investigate the elastic behaviour without hysteresis effects [11]. For the unloading and reloading path, the modulus coefficient v_{ur}=3758 was determined. In consequence of the small amplitude of vertical deformation - $\Delta\varepsilon_1$ is approximately $7.5\cdot10^{-5}$ - the stiffness is higher than in conventional tests with full reloading.

$$\frac{E_{ur}}{\sigma_{ref}} = v_{ur} \left(\frac{\sigma_3}{\sigma_{ref}} \right)^{w_{ur}} \qquad (2)$$
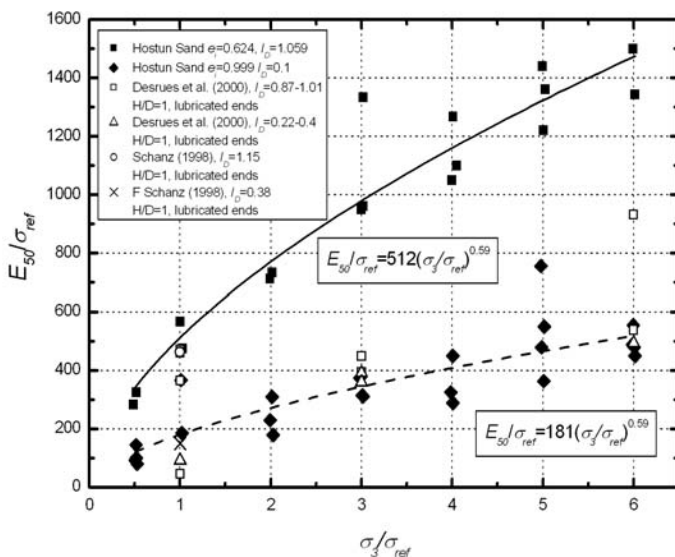
Fig. 5. Triaxial stiffness E_{50} of Hostun sand

It seems that there is no unique stress dependency ($w_{ur} \approx 0$) for the tested range of lateral pressures.

The initial stiffness is defined as the tangent on the stress-strain curve at $\varepsilon_1 = 0$. The parameters v_i and w_i, which describe the stress dependency of the initial stiffness modulus E_i (tangent modulus), are given in table 2.

Table 2. Initial stiffness for Hostun sand

	e_i	v_i	w_i
dense Hostun sand	0.641	840	0.38
loose Hostun sand	0.999	492	0.32

3 Requirements on the Equipment for Testing Unsaturated Sand

The preliminary laboratory tests on Hostun sand (shear strength, SWCC) have shown that there is an enormous request on the measuring accuracy and the measuring range. Therefore, a new triaxial testing device has been developed. It is intended to use this new equipment for the determination of the shear strength, the SWCC, and the water conductivity of unsaturated sand as well as silt.

During each test, the overall and the pore-water volume change of the specimens should be measured. The measuring system has to be optimized for the requirements, which are summarized in Tab. 3.

In general, the deformations of dense and loose sand during isotropic consolidation or oedometric stress path ($\varepsilon_2 = \varepsilon_3 = 0$) are relatively small. Assuming an average stiffness $E_{oed} = 23.3$ MPa for dense Hostun sand [10] and vertical stress of 400 kPa, a vertical displacement of 2.15 mm is calculated for specimens with a height of 12.5 cm. Calculating the vertical displacement due to a change of axial loading $\Delta\sigma_1 = 100$ kPa during the unloading and reloading stress path ($E_{ur}^{ref} = 175.2$ MPa [10]) yield to a vertikal displacement about 0.07 mm. This requires the registration of the vertical displacement and the radial deformation with a high resolution and high accuracy. The vertical displacement transducer should allow a measuring accuracy of $\pm 1\,\mu$m. Triaxial tests with isotropic loading path have shown an overall volume change of $\varepsilon_v = 0.015$ at $\sigma_1 = \sigma_3 = 800$ kPa [6].

Due to technical problems (deformation of the testing equipment, compression of air-bubbles in the volume change system), the accurate measurement is difficult. Therefore, the technical solutions for the planned triaxial device have to be adapted to the problems of measuring small volume changes.

During shearing with vertical deformation up to 20% (2.5 cm) of the specimens height, the overall volume change is much higher. In the preliminary tests and published test data for dense Hostun sand at low stresses the resulted volumetric strains were measured in the range of $\varepsilon_v = 0.09...0.12\%$ and for loose specimen $\varepsilon_v = 0.01...0.025\%$. Also, for the determination of the

Table 3. Required measuring accuracy for testing unsaturated sand

	Consolidation and oedometric stress path		Shearing stage		SWCC, k_w
	($S_r = 1$)	($S_r < 1$)	($S_r = 1$)	($S_r < 1$)	
ε_3	$< \pm 0.005$	$< \pm 0.005$	$< \pm 0.005$	$< \pm 0.005$	$< \pm 0.005$
Δh	± 0.001 mm	$\pm 1\,\mu$m	± 0.01 mm	$\pm 1\,\mu$m	$\pm 1\,\mu$m
Δs		$\leq \pm 0.3$ kPa		$\leq \pm 0.3$ kPa	$\leq \pm 0.3$ kPa
$\Delta V_{pw,i}$		$\leq \pm 1.25$ cm^3		$\leq \pm 1.25$ cm^3	$\leq \pm 1.25$ cm^3

SWCC the accuracy, and the resolution of the pressure transducers and regulation valves must be very high to enable the measuring of changes during the transition zone. The accuracy of matric suction measurement or control by the axis-translation technique depends on the accuracy and resolution of pore-air and pore-water pressure control and measurements. For tests with unsaturated sand, the precise control of the matric suction is very important. In soil-physics matric suction increments of $s = 0.3$ kPa are normally used. During the transition zone, there are significant changes of pore-water

volume (s=0.5 kPa: ΔV_{pw}=37 cm^3), while the changes during the residual and saturation zone are negligible. For the determination of the volumetric water content Θ with an accuracy of $\pm$0.005 the change of pore-water volume has to be measured with an accuracy of $\pm$1.25 cm^3 The overall volume change due to applied matric suction will be much smaller than during consolidation.

For the determination of the unsaturated conductivity it must be possible to apply a matric suction gradient to the sand specimen. A great amount of pore-water passes through the specimens if it is nearly saturated. Whereas, with decreasing saturation, the water conductivity decreases rapidly. The saturated hydraulic permeability for Hostun sand was experimentally determined for different densities. The relationship between the saturated permeability and the void ratio e is linear ($k_{10} = (6.1\,e - 1.3)10^{-4}$ m/s).

4 Equipment for Testing Unsaturated Sand

4.1 Specimen Preparation

Systematical investigations in the mechanical and hydraulic behavior of soils are only useful, if uniform and reproduceable specimens are guaranteed. Hence, for the laboratory determination of mechanical or hydraulic parameters of unsaturated specimens the reproduceable fabric of the specimens is important.

On the base of these assumptions it was decided to prepare the sand specimens by pluviation. The aim is that afterwards no further work at the specimens is necessary and that the top of the specimen is plane. For this reason the pluviator, shown in figure 6, has been developed. First, a defined amount of sand is given in the sand reservoir at the top of the pluviator. Through a central outlet the sand falls on a aluminium cone, which distributes the concentrated sand stream in all directions. The sand bounce against the perspex wall. To ensure a uniform sand-rain over the entire cross section of the specimen the sand pass two rings with several thin rods. The second one is rotated 90 degree towards the first one. Finally a close-meshed sieve is installed. The result is a very fine and uniform sand rain. With this method it is possible to produce specimens with a reproducible density (initial void ratio e_i=0.624, I_D=1.059). According to [5] the maximum density of Hostun sand is reached by pluviation with a low depositional intensity (0.15 g sec^{-1} cm^{-2}). The drop height seems to be insignificant by low pouring rates. After pluviation the surface of the specimen is absolutely plane.

Loose specimens were prepared with a combination of pluviation and drawing up a closed meshed sieve. First a defined amount of dry sand is pluviated with a high drop height (29.8 cm) in a thin-walled tube (0.5 mm) standing in the air-tight split mold. At the bottom of the tube a closed-meshed sieve is installed. After pluviation the tube with the sieve is slowly drawn up. Due to the problems associated with the preparation of loose
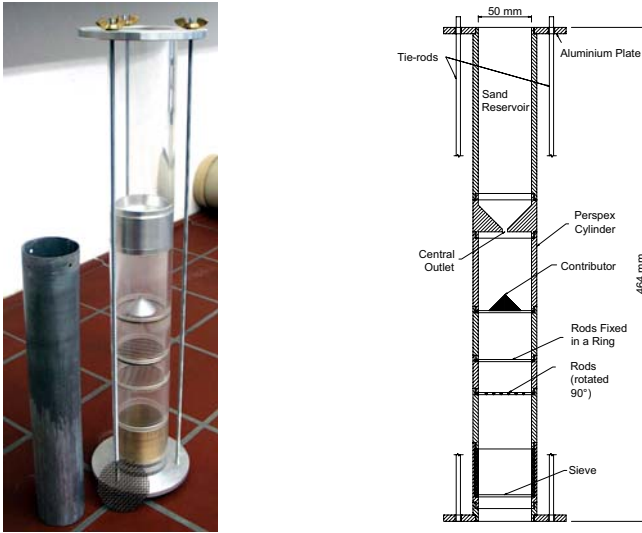
Fig. 6. Pluviator

specimens (e. g. contraction at the top) the deviation of the desired density is greater than for dense specimens. The reproducible initial void ratio with the described method is e_i=0.999 (I_D=0.102).

First indication for uniform and replicable sand specimens is a repeatable peak friction angle and the repeatability of the stress-strain curves (Fig. 7). Both criteria are appropriate, which can be shown with the test results of the drained triaxial compression test on dry Hostun sand. Whereas, the fluctuations of the density, the peak friction angel and the stress-strain curves for the loose specimens are greater than for dense specimens. It can be assumed that the reconstituted sand specimens are uniform and replicable. It is planned to specify the homogenity of the microstructure with convenient methods (e. g. digital imaging techniques, mercury intrusion porosimetry).

4.2 Double-walled Triaxial Cell

The total volume change of an unsaturated soil specimen is the sum of the pore-air and pore-water components of volume change. For the determination of the total volume change different methods can be used, for instance: (1) measuring pore-water and air-volume change; (2) measuring total volume change in real double-wall triaxial cell or in modified triaxial cells with an insert; (3) contacting or non-contacting internal instrumentation for axial and radial strain measurements; (4) determining of the total volume change by imaging technique (X-ray radiography, Digital imaging processing and analysis techniques) or Laser measurement.
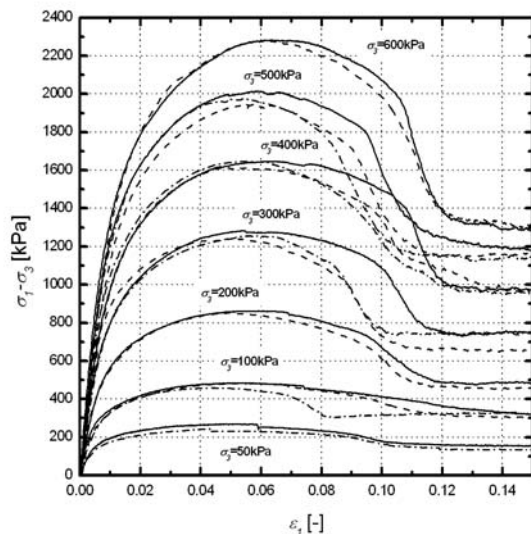
Fig. 7. Stress-strain curves for dense specimens (e_i=0.624, I_D=1.059)

With the help of the internal instrumentation, it is possible to measure ε_1 and ε_3 very accurately. However, most of them are manufactured for investigation in the small strain stiffness of soils or the pre-failure behaviour. The resolution of the imaging technique is poor [14], and even the air-volume change is difficult to measure (compressibility of air, environmental effects e.g. temperature) [16].

For future tests with axial strains up to 20% of specimen height, a double wall cell has been manufactured to measure the total volume change of the unsaturated specimen.

Over the past years several double-wall triaxial cells have been built [1, 2, 15]. Main focus was on the measurement of the volume change of the cell fluid. The whole constructive design of this new cell has been tuned to this aspect. The goals are (1) to reduce axial deformations of the cell; (2) to avoid clearance volume e.g. threads, quick connects; (3) ensure optimal deairing of the cell; (4) small volume of the inner cell; (5) unhindered specimen preparation by air pluviation; and (6) design of an optimal measuring system for unsaturated sand specimen.

The cell has been designed for specimens with a diameter of 50 mm and 125 mm height (height to diameter ratio of 2.5). The radial deformation of the specimen is measured by monitoring the flow of the cell fluid into or out of the triaxial cell. Errors due to the deformation of the cell wall are avoided by applying the same pressure in the outer and inner cell.

The cell consists of a head plate, a base plate, and a basis plate (Fig. 8) made of stainless steel. To avoid any splices the head plate is manufactured
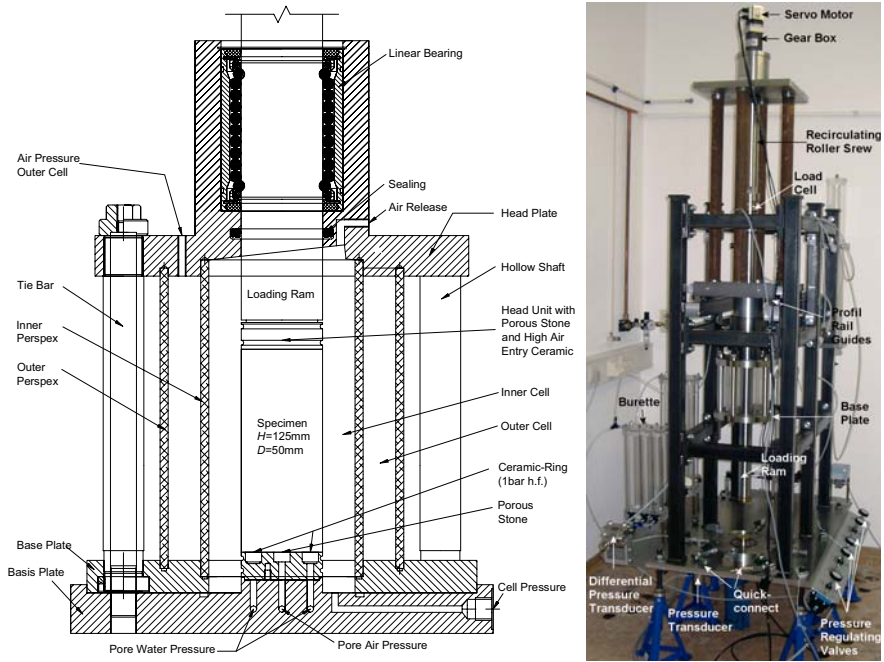
Fig. 8. Double-walled triaxial cell and modular loading frame

in one piece. The loading ram is guided by a linear roll bearing which is installed in the upper part. It has the same diameter like the specimen. The sealing between loading ram and head plate can be solved by using a rod seal with a high sealing efficiency, low friction, and a minimal stick-slip effect. Therefore, the loading ram must have a hard-chromium plated surface with special demands on the surface profile.

During cell filling, it is possible to bleed air with an lateral air release installed at the highest point of two inclined levels. For the cell walls, acrylic pipes are used. The inner and outer cell have a diameter of 9 cm and 11.5 cm respectively. Thus, the diameter of the inner cell enables radial deformation of the specimen or even the development of shear bands by compression tests with large axial deformation (20% from specimen height). The inner cell, with a relative small volume, is filled with silicon oil of a low viscosity and the outer cell with air.

The head plate, the perspex walls, and the base plate are held together by hollow shafts. The perspex walls are collected in fluts with o-ring seals which lie in a second flut. When the cell is put together the flut is completely filled with the o-ring sealing. There ist no place left for the cell liquid. The cell is connected by five 16 mm diameter stainless steel tie bars with the basis

plate. To prevent the flow of silicone oil between the two plates an o-ring sealing is installed. The diameter of the o-ring sealing is nearly the same as the diameter of the inner cell.

There are five stainless steel connections for the supply with the different media. The tubes are connected with the cell by special quick connectors with minimal spillage and air inclusion ($0.3\,\mathrm{cm^3}$) while the connecting or disconnecting process.

A stainless steel ball valve without any clearance volume is installed in front of every connection. The pressure transducers (cell, pore-water and pore-air pressure) are durably screwed in T-pieces. They point to the bottom to prevent the air from becoming trapped. There are two connections for the cell pressure and the pore-water pressure, and one for the pore-air pressure.

To separate pore-water from pore-air pressure a base pedestal is connected with the basis plate. Leakage is prevented by an o-ring seal. Even the tubes for the pore-water pressure and the pore-air pressure are sealed with o-rings. Two tubes for pore-water pressure end in a water compartment under a high-air-entry ceramic-ring (1 bar high flow). It is possible to measure the pore-water pressure and flush the diffused air. The pore-air pressure is applied to the specimen through a porous stone. At the end of the loading ram (top of the specimen), the same unit is installed. Changing the units to apply or to measure higher matric suction is simply possible. With two ceramic discs it is possible to apply the same or different matric suction(s) at the top and the base of the specimen. This ensures a shorter equalization stage [12], a nearly uniform distribution of matric suction about specimen height, and a defined matric suction gradient above the specimen height.

The absorption of water by the acrylic cell wall [1, 15] and even the diffusion from water and air through the rubber membrane [9] are well-known. This effects were avoided using silicon oil as cell fluid. Another advantage is, that oil has a lower surface tension than water. The surfaces in the inner cell will be well wetted and the risk of any air bubbles in the tubes is much lower than using deaired water. The greater compressibility of oil demanded the observation of the volume change due to different cell pressure stages.

Loading Frame

The cell is surrounded by a loading frame. The axial force is produced by a servo motor with a gearbox. The rotation of the electric motor is changed to linear motion using a recirculating roller screw. The fastest vertical deformation speed is at $25\,\mathrm{mm/min}$ and the slowest, but still continuous, is less than at $0.0001\,\mathrm{mm/min}$.

During the preparation of the sand specimens by pluviation the cell is run up and driven backwards on profil rail guides without any vibration. When the specimen is prepared the cell is driven to the starting position and dropped down for connection with the basis plate.

Measuring the Axial Stress and Vertical Deformation

The vertical tensile or compression force is measured out of the double-walled cell by a 10 kN load cell. The load cell is installed between the loading ram and the recirculating roller screw without any fetch. Lateral forces can not be excluded because of the length of the loading ram. However, preliminary tests with conventional load cells have shown that lateral forces have an enormous effect on the measurement. To solve this problem, a special load cell with an integrated lateral force compensator has been used. The maximal deviation measuring the axial stress is smaller than 1.53 kPa by a resolution of 0.16 kPa.

The axial displacement of the specimen is measured externally to the cell with an opto-electronical displacement transducer which enables an accuracy of ± 0.001 mm. The measuring range is 35 mm.

Pressure control and measurement

The air pressure is adjusted manually with precision pressure control units. For the cell pressure, a pressure regulating valve with an adjustable range from 0.15 up to 10 bar and for the pore-water pressure and the pore-air pressure four pressure regulating valves with a adjustable range from 0.03 up to 2.1 bar are used. The sensitivity is less than 0.032 kPa.

The pore-water and the pore-air pressure are measured with pressure transducers with an effective range from 0 to 3.5 bar. The accuracy is less than 0.04% from the final value (0.14 kPa). The cell pressure can be measured with an accuracy less than 0.25% from the final value (10 bar).

Volume change of the specimen and the pore-water

The volumetric deformation of the unsaturated specimen is measured by monitoring the flow of the cell fluid into or out of the double-wall cell with double-walled burettes. Also, the flow of the pore-water into or out of the specimen can be observed with burettes. Therefore, modular burettes-units consisting of three burettes have been built. The height of the oil respectively the water column is measured by differential pressure transducers. Detailed information concerning the accuracy and resolution are given in [7]. By circulating the pore-water in the pore-water drainage system with peristaltic pumps (Fig. 9) it is possible to flush the diffused air out of the water compartement under the ceramic plate. The peristaltic pumps are controlled via pc.

Data logging

All transducers are connected to a pc with a 16 channel-measurement card. The developed software allows a continuous recording of the data. High resolution of the measurement is ensured by using a 16-bit card.
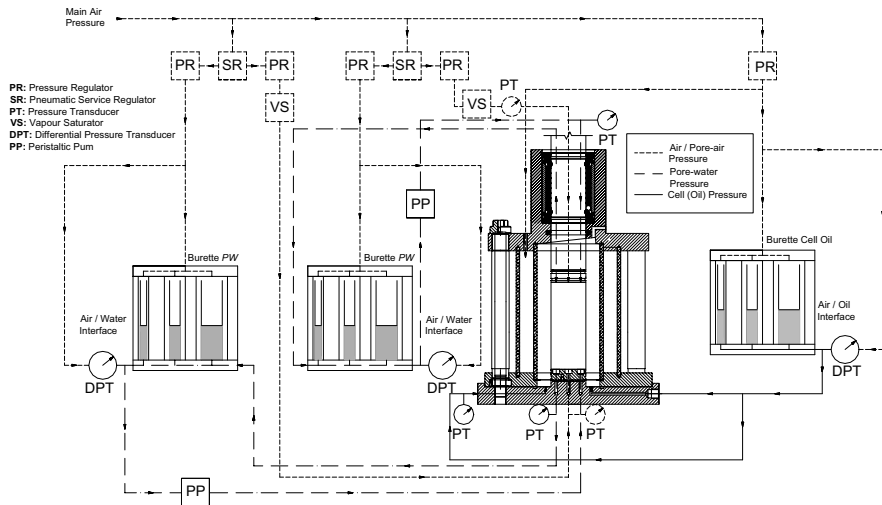
Fig. 9. Scheme of the instrumentation of the double-walled triaxial cell

5 Outlook

The planned tests will be carried out in different stages. At first functional tests are intended for checking the apparatus and the instrumentation. This stage includes (1) tests (triaxial compression, isotropic compression) on saturated specimens and the comparison with other test results (e. g. literature, other triaxial testing apparatus); and (2) the comparison of test results (shear strength) acquired with a conventional and the new equipment ($w =$const.); (3) investigation in the influence of membrane penetration and the error estimation of the volume change measurement.

Thereafter a scientific testing programm for the determination of the (1) relationship between saturation and shear strength; (2) soil-water-characteristic curve; and (3) the unsaturated conductivity will be started. The SWCC and the unsaturated conductivity will be examined for different isotropic stresses with recording the total volume change. The aim is to develop and to test models, which describe the SWCC and the unsaturated conductivity for deformable unsaturated soils. When the investigations on the mechanical and hydromechanical behaviour of sand are finished, a silt will be tested.

Acknowledgements

References

1. W. F. Anderson, A. K. Goodwin, I. C. Pyrah, and T. H. Salman. Equipment for one-dimensional compression and triaxial testing of unsaturated granular soils at low stress levels. *Geotechnical Testing Journal*, 20(1):74–89, 1997.

2. S. Aversa and M. V. Nicotera. A triaxial and oedometer apparatus for testing unsaturated soils. *Geotechnical Testing Journal*, 25(1):3–15, 2002.

3. J. Biarez and P.-Y. Hicher. *Elementary Mechanics of Soil Behaviour-Saturated Remoulded Soils*. A.A. Balkema, Rotterdam/Brookfield, 1994.

4. J. L. Colliat-Dangus, J. Desrues, and P. Foray. Triaxial testing of granular soil under elevated cell pressure. In R. C. Chaney R. T. Donaghe and M. L. Silver, editors, *Advanced Triaxial Testing of Soil ans Rock*, pages 290–310, Baltimore, 1988.

5. A. Cresswell, M. E. Barton, and R. Brown. Determining the maximum density of sands by pluviation. *Geotechnical Testing Journal*, 22(4):324–328, 1999.

6. J. Desrues, B. Zweschper, and P.A. Vermeer. Database for tests on Hostun RF sand, 2000.

7. J. Engel, C. Lauer, and M. Pietsch. A modular triaxial testing device for unsaturated soils. In *GTMM 2003 International Symposium on Geotechnical Measurements and Modelling*, Karlsruhe, 2003. Accepted for publication.

8. E. Flavigny, J. Desrues, and B. Palayer. Le sable d'hostun. *Rev. Franc. Géotechn.*, 53:67–70, 1990.

9. S. Leroueil, F. Tavenas, P. La Rochelle, and M. Tremblay. Influence of filter paper and leakage on triaxial testing. In R. T. Donaghe, R. C. Chaney, and M. L. Silver, editors, *Advanced Triaxial Testing of Soil and Rock, ASTM STP 977*, pages 189–215, Philadelphia, 1988. ASTM.

10. Y. Lins and T. Schanz. Determination of hydro-mechanical properties of sand. In T. Schanz, editor, *Int. Conf. From experimental evidence towards numerical modelling of unsaturated soils*, Lecture Notes in Applied Mechanics. Springer, 2003.

11. H. Müllerschön. *Spannungs-Verformungsverhalten granularer Materialien am Beispiel von Berliner Sand*. PhD thesis, Universität Stuttgart Institut füt Mechanik Lehrstuhl II, 2000. Bericht Nr. II-6.

12. E. Romero, J.A. Facio, , A. Lloret, A. Gens, and E. E. Alonso. A new suction and tempretature controlled triaxial apparatus. In *Proceedings of the Fourthteenth International Conference on Soil Mechanics and Foundation Engineering*, pages 185–188, Hamburg, 1997.

13. T. Schanz. Zur Modellierung des mechanischen Verhaltens von Reibungsmaterialien. Habilitationsschrift, 1998.

14. G. K. Scholey, J. D. Frost, L. C. F. Presti, and M. Jamiolkowski. A review of instrumentation for measuring small strains during triaxial testing of soil specimens. *Geotechnical Testing Journal, GTJODJ,*, 18(2):137–156, 1995.

15. S. J. Wheeler. The undrained shear strength of soils containing large gas bubbles. *Géotechnique*, 38(3):399–413, 1988.

16. D. Wulfsohn, B. A. Adams, and D.G. Fredlund. Triaxial testing of unsaturated agricultural soils. *J. agric. Engng Res.*, 69:317–330, 1998.

Undrained Isotropic Compression of Soil

Jack P. Oostveen

University of Technology Delft, Dept. of Civil Engineering, Geotechnics

Stevinweg 1

NL 2628 CN Delft

Email: j.oostveen@citg.tudelft.nl
Tel.: 0031.15.2785423 Fax: 0031.15.2783328

Abstract.
This paper deals with a theoretical description of the undrained and drained behaviour of unsaturated soils under isotropic load. By taking into account the compressibility of the solid mass and the fluid/gas mixture inside the pores a theoretical relation between the pore water coefficient (B) and the saturation (S_r) is derived, which is shown to be similar to measured data given in the literature. The approach described involves natural strains, schematizations of the solid mass and the fluid/gas mixture and the use of different boundary conditions for respectively B=1 and B<1.

Keywords: *grade of saturation, (un)saturated soil, (un)drained, fluid/gas-mixture, dissolved gas, gas bubbles, isotropic compression, excess pore water pressure*

Introduction

In the classical approach of stress analysis in soil mechanics it is assumed that the solid mass as well as the pore water are incompressible compared to the compressibility of the structure of the solid skeleton. As a consequence of this assumption it has been suggested that compression of the soil mass occurs due to inter-particle slippage in the solid grain structure only, even in case of an isotropic load. In the unsaturated situation the amount of gas/air is considered to take care of the compressibility of the "pore water" system.

In this study the compressibility of both the solid mass and the pore water are considered in more detail starting from other basic assumptions.

Before any expression for the isotropic compression of soil can be derived some general aspects have to be noted. The non-linearity of soil properties necessitates the usage of natural strain. Incremental loading may change the saturation and porosity of soil. In addition some basic aspects of the soil constituents have to be considered, like the compression of the solid mass, the fluid phase and gas/air.

Then, the resulting mechanical properties of the gas-fluid mixture and their effects on unsaturated soil behaviour can be evaluated.

Solid mass

The soil volume can be considered as a cube with $V_{soil}=\Delta x \Delta y \Delta z$ containing the solid mass, outlined by an inner block with $V_{solid}=a\Delta x.a\Delta y.a\Delta z$ [**Figure 1**].
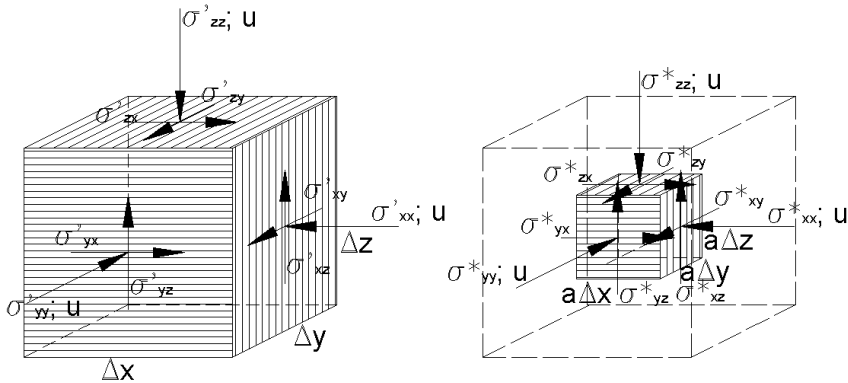

Figure 1. Scheme of the 3D soil/solid model

Because the solid volume V_{solid} is $(1-n)V_{soil}$, which is also equal to $a^3 V_{soil}$, the sides of the inner solid cube depend on the porosity: $a = \sqrt[3]{(1-n)}$. Following Terzaghi, in stress analysis in soil mechanics soil stress is decomposed in effective stress and water pressure. The effective stress is defined as the average ratio of the intergranular forces acting on the surface of the soil "cube" with a relative surface area of 1. Here an additional solid stress measure is introduced, taking the average intergranular forces acting on the surface of the inner block of solid mass with a relative surface area of a^2. So this solid stress measure depends on both the effective stress and the porosity. This can be written as $p_{solid,ij}=\alpha_n p'_{ij}$ with $\alpha_n=(1-n)^{-2/3}$ and i,j=1,2,3. The water pressure working on this solid cube is the same as on the total soil cube. By indicating ∂ as increment and taking into account the flexibility of the bulk of the solid structure, β_{solid}, the following relation (1) for isotropic load can be derived:

$$\left. \begin{array}{l} \partial \varepsilon_{solid} = \dfrac{\partial V_{solid}}{V_{solid}} = \beta_{solid} \partial p_{solid} \\ \partial p_{solid} = \partial(\alpha_n p' + u_{water}) \end{array} \right\} \Rightarrow \begin{array}{l} \partial \varepsilon_{solid} = \beta_{solid}\partial(\alpha_n p' + u_{water}) \\ \text{with } \alpha_n = (1-n)^{-2/3} \end{array} \tag{1}$$

Obviously for fully undrained condition at which p'=0 equation (1) becomes:

$$\partial \varepsilon_{solid} = \beta_{solid}\partial u_{water} \tag{2}$$

Fluid phase

Taking into account the compressibility of pore water, the following relationship (3) based on the flexibility of the bulk of water, β_{water}, can be expressed:

$$\partial\varepsilon_{water} = \beta_{water}\partial u_{water} \qquad (3)$$

Gas phase

In addition to the water mentioned above, a portion of gas (organic soils) or air may be present in the pores of the soil. While the volume of water can be written as $V_{water}=nS_rV_{soil}$, the total volume of gas/air is $V_{gas}=n(1-S_r)V_{soil}$. In general, assuming a constant temperature for gas/air the isothermal stress-strain relationship can be based on the law of Boyle, from which (4) can be derived for small increments:

$$\partial(pV) = 0 \Rightarrow \partial\varepsilon_{gas} = -\frac{\partial p_{gas}}{p_{gas}} \qquad (4)$$

Considering the unsaturated condition, the influence of gas or air on the total soil behaviour is very important. Several conditions by which gas can be present in soil, can be distinguished, e.g.:

- Air, not fully surrounded by pore water, occurs in the vadose zone.
- Gas bubbles, confined by the freatic pore water.
- Dissolved gas, confined by the freatic pore water

Here the second and third conditions of the gas confined by the freatic water are considered

Gas bubble

In case of the gas bubbles the gas is encased by water and cut off from the open air (Figure 2). The interaction between gas and surrounded water satisfies equilibrium of stresses. Taking into account the surface tension of water ($u_{surface}$) at the water/gas-interface the gas pressure inside the bubble will be different from the water pressure. With surface tension q and radius r of the gas bubble this phenomenon can be expressed by (5):

$$p_{gas} = p_{atm} + u_{water} - \frac{2q}{r}$$
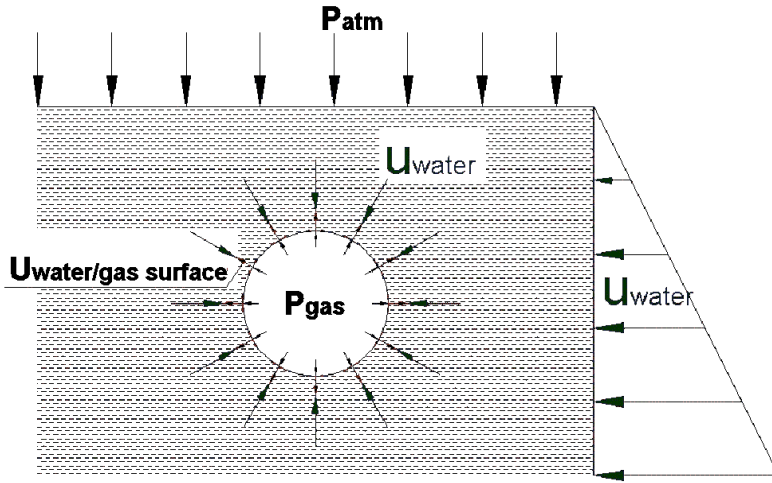$$\text{and } u_{surface} = \frac{2q}{r} \qquad (5)$$

Figure 2. gas bubble (schematically)

From (4) and (5) follows for small changes (6):

$$\left.\begin{array}{l} \partial\varepsilon_{gas} = 3\dfrac{\partial r}{r} = -\dfrac{\partial p_{gas}}{p_{gas}} \\[2mm] \partial p_{gas} = \partial u_{water} + \dfrac{2q}{r}\dfrac{\partial r}{r} \end{array}\right\} \Rightarrow \partial\varepsilon_{gas} = -\dfrac{1}{p_{atm} + u_{water} - \dfrac{2}{3}\dfrac{2q}{r}}\partial u_{water} \qquad (6)$$

And the incremental change of the pressure inside the gas bubble dp_{gas} can be written as (7):

$$\partial p_{gas} = \dfrac{p_{atm} + u_{water} - \dfrac{2q}{r}}{p_{atm} + u_{water} - \dfrac{2}{3}\dfrac{2q}{r}}\partial u_{water} \qquad (7)$$

Figure 3 illustrates (7) for the initial situation at a range of 1E-9 m$<r_0<$1E-3 m for surface tension q=73E-6 kN/m. It shows that for relatively large initial $r_{gas\ bubble;0}>$1E-5 m the ratio $dp_{gas}/du_{water}\downarrow1$, which means the effect of $u_{surface}$ on this ratio is negligible. For small initial $r_{gas\ bubble;0}<$1E-7 m the ratio is $dp_{gas}/du_{water}\uparrow1,5$. This means that $u_{surface}$ causes an incremental increase of dp_{gas} of about 150% of du_{water}, by which rather high gas pressures inside the small bubbles can occur. It also shows that the higher the initial water pressure $u_{water;0}$ is the smaller the gas bubbles are for which $u_{surface}$ can be neglected.

Due to the increase of the u_{water} onto the gas bubble $r_{gas\ bubble}$ decreases, while because $u_{surface}$ is proportional to the reciprocal of its radius $u_{surface}$ will increase. However, when $r_{gas\ bubble}$ is decreasing, the volume of the bubble decreases too and p_{gas} inside the bubble will increase. This is illustrated by Figure 4 and Figure 5, at which u_{water} increases from 0 kPa to –5000 kPa with a load increment of du_{water}=5 kPa.
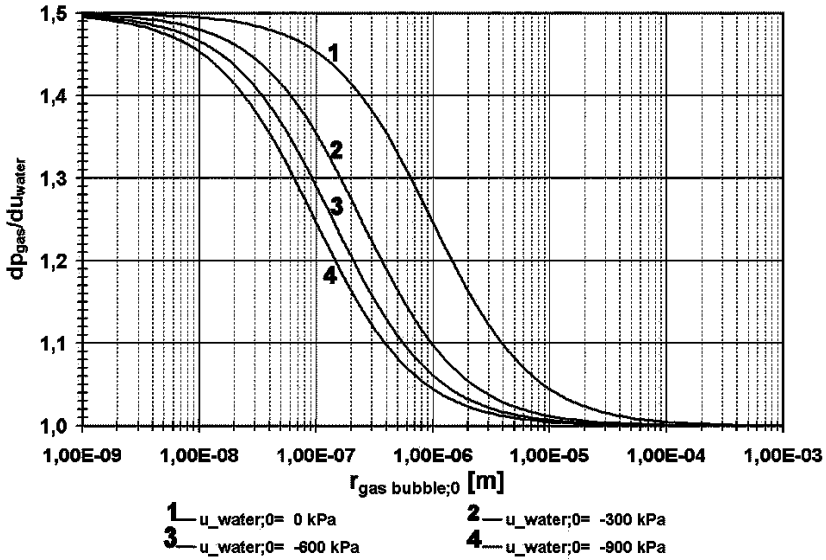
Figure 3. relation $r_{gas\ bubble;0}$, dp_{gas} and du_{water} for several initial $u_{water;0}$
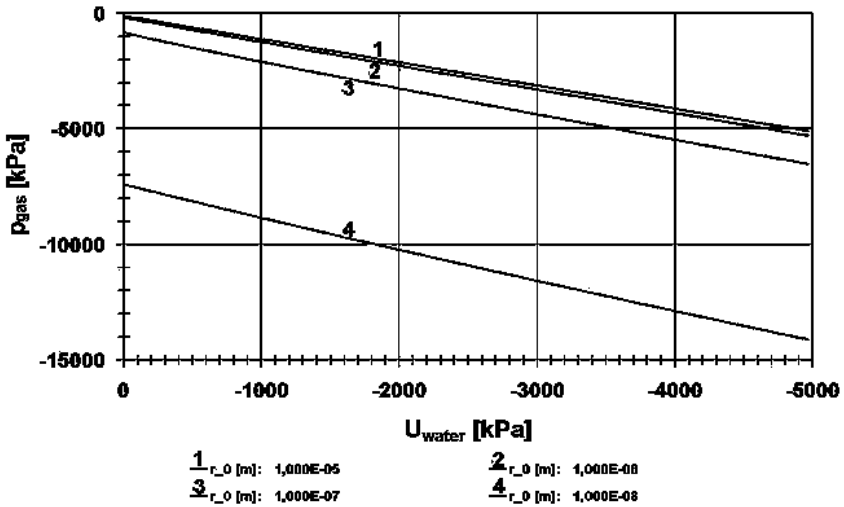
Figure 4. relation u_{water}-dp_{gas} for compression of gas bubbles starting at several r_0

Figure 4 shows that the increase of p_{gas} under an increasing u_{water} is dependent on the radius of the gas bubble at the beginning of the compression at u_{water}=0. So while for a large gas bubble $p_{gas}=p_{atm}+u_{water}$ because $u_{surface}$ can be neglected, for small bubbles p_{gas} is higher and can be written by (8):

$$p_{gas} = \alpha_s \left(p_{atm} + u_{water} \right)$$

$$\text{with } \alpha_s = 1 - \frac{2}{3} \frac{u_{surface}}{p_{atm} + u_{water}} \tag{8}$$
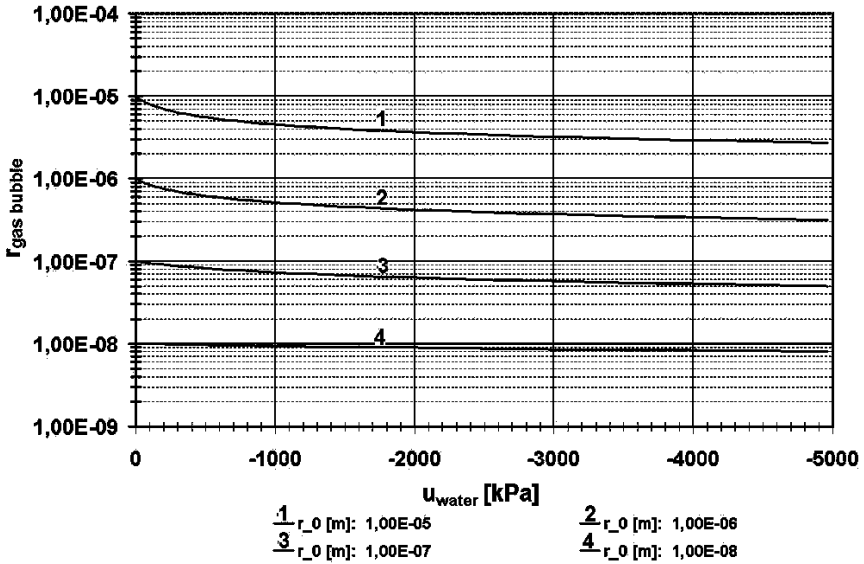

Figure 5. relation u_{water}-ε_{gas} for compression of gas bubbles starting at several r_0

Figure 5 demonstrates that the decrease of the radius of the gas bubble is limited. This limitation of the compression of the gas bubble has been caused by the increase of the stiffness of the air, which is proportional with p_{gas}. Because for very small gas bubbles the increase of p_{gas} is substantially more than for the larger bubble, the stiffness of the very small bubble is substantial higher too. For very small gas bubbles (r_0=1E-8 m) and at u_{water}=500 kPa the compression of V_{gas} is about ε_{gas}=2% while for large bubbles (r_0>1E-6 m) the compression will be about ε_{gas}=45%. For u_{water}=5000 kPa the compression is respectively ε_{gas}=20% and ε_{gas}=75%.

For the same case of compression of gas bubbles shown in Figure 4, Figure 6 shows the development of the ratio dp_{air}/du_{water} as a function of r_{gas} for several initial r_0 while u_{water} decreases from 0 kPa to -5000 kPa. Figure 7 shows the development of α_s as a function of the radius of the gas bubble and u_{water}. According to Figure 6 and Figure 7 no specific value of p_{gas} can be defined. To take into account the range of sizes of gas bubbles a mean value of α_s has to be applied and the general equation for gas (4) becomes (9) with α_s>1. It is obvious that for the larger bubbles at which the surface tension can be neglected, $\alpha_s \approx 1$.

$$\partial \varepsilon_{gas} = - \frac{1}{\alpha_s \left(p_{atm} + u_{water} \right)} \partial u_{water} \tag{9}$$
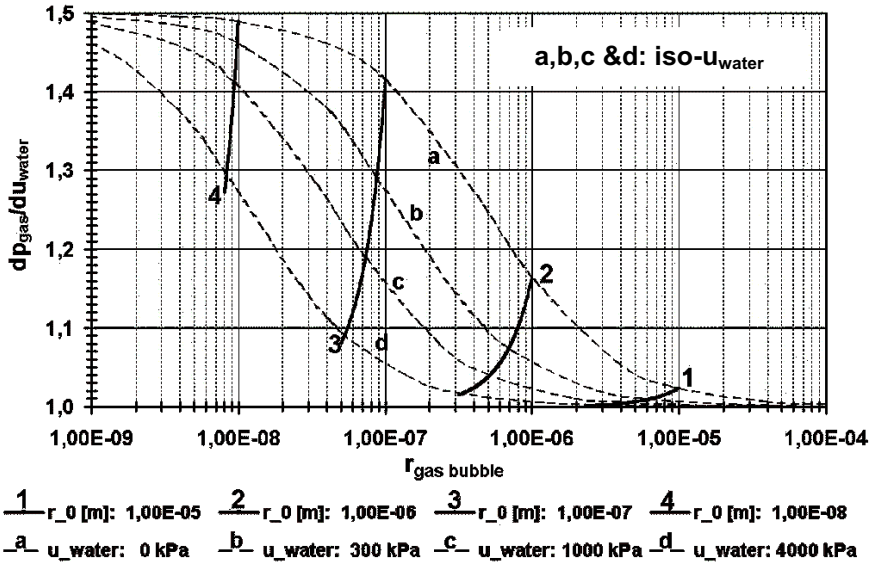
Figure 6. Relation of r_{gas} with dp_{air}/du_{water}
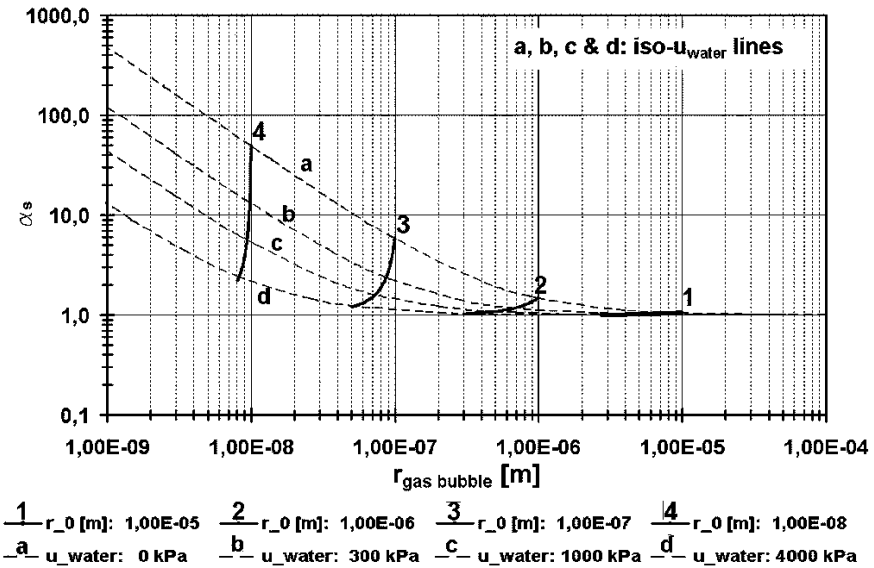

Figure 7. Relation u_{water} with α_s

Dissolved gas

In addition to the free gas an amount of dissolved gas is present in the pore water. Henry's law states that at a constant temperature, the density of gas, which dissolves in a given volume of liquid, is directly proportional to the gas pressure (Schuurman, 1966 & Barends, 1979). Considering especially for the very small gas bubbles, that the gas pressures are much higher than the water pressure, a flow of gas molecules penetrating the contractile skin of water will occur until an equilibrium condition is reached. Generally the volume of dissolved gas at which that equilibrium has been reached is about 2% of the volume of water at an atmospheric pressure ($V_{dissolved\ air}=0,02V_{water}$).

The dissolved gas has almost no influence on the specific weight of water and the stiffness of gas has practically no effect on the stiffness of water (Fredlund, 1993). Because of the conservation of mass and the isothermic law of gas, according to $\varepsilon_{gas}=-dp_{gas}/p_{gas}=-d\rho_{gas}/\rho_{gas}$, under atmospheric pressure both the density and the stiffness of gas is low, this indicates relative high pressures inside the pockets of dissolved gas. The same physical molecular force, which causes the surface tension between water and free gas, will also influence the gas/water relation in respect to the dissolved gas.

At an increasing isotropic load the volume of gas, both the free gas bubbles as well as the dissolved gas will be compressed further. By that the relative volume of dissolved gas decreases too. However by compressing the gas bubbles the gradient of the pressures between the free gas inside the bubble and the water pressure will increase by which a new flow of gas molecules will dissolve into the water mass until a new equilibrium has been reached at which $V_{dissolved\ gas}=hV_{water}$. Meanwhile the flow of gas molecules into the water causes a decrease of the volume of the gas bubble by which the pressure gradient over the contractile skin increases. The more this pressure gradient increases, the more gas molecules will dissolve in water, until the limit: the gas bubble has been dissolved at all.

Therefore concerning the compression, the equations (6) and (7) as elaborated by Figure 3 and Figure 6 for the free gas bubbles are valid for the small dissolved gas pockets too. Therefore the strain stress relation of dissolved air can be written like (10).

$$\partial\varepsilon_{dissolved\ gas} = -\frac{1}{\alpha_{s_{dissolved\ gas}}\left(p_{atm}+u_{water}\right)}\partial u_{water} \tag{10}$$

Because the volume of dissolved gas in water is essentially independent of gas or water pressures (Fredlund, 1993) and proportional to the volume of water, the compensated incremental flow from the free gas bubbles to dissolve gas has to be equal to that incremental volume change of dissolved gas by the load increment.

Noticed, from Figure 4, Figure 5 and Figure 6 the phenomenon described in this chapter, concerns mainly the gas bubbles, which were initially very small and at which the surface tension causes high gas pressures inside the bubbles. So, probably it should concern a relatively small amount of the total gas volume.

Fluid-gas mixture

While the relative volume of free gas can be written as $V_{free\ gas}/V_{pore} = (1-S_r)$, for water - including the dissolved gas - that will be $(V_{water} + V_{dissolved\ gas})/V_{pore} = S_r$. With $V_{dissolved\ gas} = hV_{water}$ the relative volume of pure water is $V_{water}/V_{pore} = S_r/(1+h)$ and for the dissolved gas $V_{dissolved\ gas}/V_{pore} = hS_r/(1+h)$.

Concerning the conservation of mass and the isothermic law of gas the volume change of free gas by compression and the flow by dissolving gas can be derived as (11):

$$\varepsilon_{gas} = -\left[1 + \frac{\chi h S_r}{(1+h)(1-S_r)}\right]\frac{1}{\alpha_s\left(p_{atm} + u_{water}\right)}\partial u_{water} \tag{11}$$

$$with: \chi = \frac{\rho_{dissolved\ gas}}{\rho_{gas}}\frac{\alpha_s}{\alpha_{s_{dissolved\ gas}}}$$

Now the change of volume of the water/gas mixture, which should be equal to the change of pore volume, can be derived by (12):

$$\varepsilon_{pore} = \left\{\frac{S_r}{1+h}\beta_{water} - \left[(1-S_r) + \frac{\chi h S_r}{(1+h)}\right]\frac{1}{\alpha_s\left(p_{atm} + u_{water}\right)}\right\}\partial u_{water} \tag{12}$$

Incremental change of saturation

The saturation, S_r has been defined to be proportional of the volume of water and dissolved gas related to the total volume of the gas-water mixture, which is equal to the pore volume at which the $V_{water} = S_r V_{pore}$ and $V_{gas} = (1-S_r)V_{pore}$. When the water-gas mixture is loaded by a pressure increment, by the difference of stiffness between the water and the gas changes of the volumes of water and gas are different and not proportional to each other's. Therefore after each loading increment the new proportion of water and gas has to be determined.

After some derivation the incremental change of the saturation can be written for small increments as (13)

$$\partial S_r = S_r\left(1-S_r\right)\left(\partial\varepsilon_{water} - \partial\varepsilon_{gas}\right) \tag{13}$$

This becomes with (3) and (12) into (14):

$$S_r^* = S_r + S_r\left(1-S_r\right)\left(\beta_{water} + \left[(1-S_r) - \frac{\chi h S_r}{(1+h)}\right]\frac{1}{\alpha_s\left(p_{atm} + u_{water}\right)}\right)\partial u_{water} \tag{14}$$

Figure 8 shows the results of the change of saturation by an incremental increasing of the pore water pressure ($du_{water} = 5$ kPa), which is similar to the effect of backpressure. Here is $h=0,02$, while $\alpha_{s;free\ gas} = 1$ and $\chi = 0,1$.
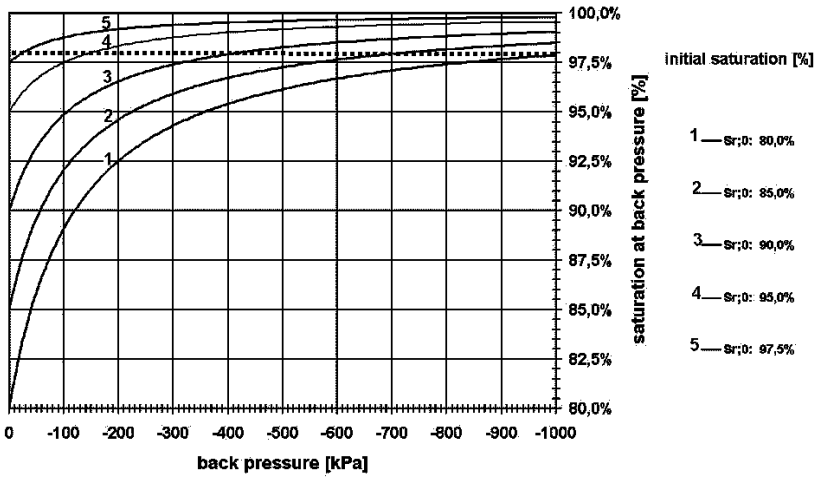
Figure 8. influence of increasing pore pressure on the saturation

Incremental change of porosity: n

The porosity, n has been defined by the proportionality of the volume amount of the solid mass and the pore volume related to the total soil volume by which the $V_{solid}=(1-n)V_{soil}$ and $V_{pore}=nV_{soil}$. When a volume of soil has been loaded, because of the different stiffness of the solid mass and the mass by which the pores are filled, the changes of these distinguished volumes are not proportional to each other's. Therefor after each load increment the new proportionality of the pore volume has to be determined. After some derivation the change of the porosity can be written for small increments as (15).

$$\partial n = n(1-n)(\partial \varepsilon_{pore} - \partial \varepsilon_{solid}) \tag{15}$$

with (1) and (12) that becomes into (16):

$$n^* = n + n(1-n)\left[\left\{\frac{S_r}{1+h}\beta_{water} - \left[(1-S_r)+\frac{\chi h S_r}{(1+h)}\right]\frac{1}{\alpha_s\left(p_{atm}+u_{water}\right)}-\beta_{solid}\right\}\partial u_{water} - \alpha_n\beta_{solid}\partial p'\right] \tag{16}$$

Undrained isotropic compression.

The undrained situation can be distinguished by two kinds of conditions depending on the properties of the composite materials: solid mass, water and the contents of gas or air. Especially the compressibility of these components is highly responsible for the actual boundaries.

At first depending on the compressibility of the gas/water mixture this composite component can be compressed more than the solid mass, where also during the

undrained state the solid grain interaction forces will partly bear the load. With the Skempton pore pressure coefficient B, this can be written as:

$$p' < 0 \rightarrow \partial u = B \partial p \text{ and } \partial p' = (1 - B) \partial p \text{ with B<1} \tag{17}$$

The isotropic compression of the soil skeleton will determine the total volume deformation highly. The pore volume will change proportionally to the compression of the solid mass ($\partial n = 0$), while according the undrained condition the mass of the gas/water mixture inside the pore volume does not change at all. The volume of the gas/water mixture is changing by an increase of the water pressure only, which has to be in equilibrium with the increase of the total and effective stresses. From (15) the boundary can be written as:

$$\partial n = n(1-n)(\partial \varepsilon_{pore} - \partial \varepsilon_{solid}) = 0 \implies (\partial \varepsilon_{pore} - \partial \varepsilon_{solid}) = 0 \tag{18}$$

Secondly, if the saturation of the gas/water mixture is such as high, the compressibility of that composite element is less than that of the solid mass and during the undrained state the gas/water mixture will bear the load:

$$p' = 0 \rightarrow \partial u = \partial p \text{ and } \partial p' = 0, \text{ so with B=1} \tag{19}$$

Cause to that situation the pore volume will vary according to the compressibility of the gas/water mixture as well as the compressibility of the solid mass. Because the compressibility of the gas/water mixture differs from the compressibility of the solid mass dn≠0.

B<1: Undrained situation with unsaturated water condition, at which interaction forces between the grains can be developed

By the boundary (18) as well as the equations (1) and (12) the basic relation between load, pore pressure and effective stress can be derived:

$$\left\{ \frac{S_r}{1+h} \beta_{water} - \left[(1-S_r) + \frac{\chi h S_r}{(1+h)} \right] \frac{1}{\alpha_s (p_{atm} + u_{water})} - \beta_{solid} \right\} \partial u_{water} - \alpha_n \beta_{solid} \partial p' = 0 \tag{20}$$

From this relationship (20) after some derivation dp' (21), du$_{water}$ (22) and dε (23) can be derived as a function of the total load dp:

$$\partial p' = \frac{\left\{ \dfrac{S_r}{1+h} \beta_{water} - \left[(1-S_r) + \dfrac{\chi h S_r}{(1+h)} \right] \dfrac{1}{\alpha_s (p_{atm} + u_{water})} - \beta_{solid} \right\}}{\left\{ \dfrac{S_r}{1+h} \beta_{water} - \left[(1-S_r) + \dfrac{\chi h S_r}{(1+h)} \right] \dfrac{1}{\alpha_s (p_{atm} + u_{water})} - (1-\alpha_n) \beta_{solid} \right\}} \partial p \tag{21}$$

$$\partial u_{water} = \frac{\alpha_n \beta_{solid}}{\left\{ \dfrac{S_r}{1+h} \beta_{water} - \left[(1-S_r) + \dfrac{\chi h S_r}{(1+h)} \right] \dfrac{1}{\alpha_s (p_{atm} + u_{water})} - (1-\alpha_n) \beta_{solid} \right\}} \partial p \tag{22}$$

$$\partial \varepsilon = \frac{\alpha_n \beta_{solid} \left\{ \dfrac{S_r}{1+h} \beta_{water} - \left[(1-S_r) + \dfrac{\chi h S_r}{(1+h)} \right] \dfrac{1}{\alpha_s (p_{atm} + u_{water})} \right\}}{\left\{ \dfrac{S_r}{1+h} \beta_{water} - \left[(1-S_r) + \dfrac{\chi h S_r}{(1+h)} \right] \dfrac{1}{\alpha_s (p_{atm} + u_{water})} - (1-\alpha_n) \beta_{solid} \right\}} \partial p \tag{23}$$

From equation (22) obviously the Skempton (1954) pore pressure coefficient B is (24):

$$B = \frac{\alpha_n \beta_{solid}}{\left\{ \dfrac{S_r}{1+h} \beta_{water} - \left[(1-S_r) + \dfrac{\chi h S_r}{(1+h)} \right] \dfrac{1}{\alpha_s \left(p_{atm} + u_{water} \right)} - (1-\alpha_n) \beta_{solid} \right\}}$$

(24)

Because B<1 the following conditions for the situation mentioned here can be derived from (24):

$$S_r > \frac{(1+h)\left[1 + \alpha_s \left(p_{atm} + u_{water} \right) \beta_{solid} \right]}{\left[h(1-\chi) + 1 + \alpha_s \left(p_{atm} + u_{water} \right) \beta_{water} \right]}$$

(25)

All derivations of the equations (6) to (12) and (20) to (25) are based on the small deformation.

B=1: Undrained situation with sufficient saturated water conditions, at which no interaction forces between the grains can be developed.

It is obvious the situation mentioned here at which B=1 can be derived direct from (24):

$$S_r \frac{(1+h)\left[1 + \alpha_s \left(p_{atm} + u_{water} \right) \beta_{solid} \right]}{\left[h(1-\chi) + 1 + \alpha_s \left(p_{atm} + u_{water} \right) \beta_{water} \right]}$$

(26)

Because B=1, only the pore pressure will increase proportionally to the isotropic load, while the increase of the effective stress is equal to zero, so for the condition mentioned here the deformation can be derived by (27):

$$\partial \varepsilon = \left\{ n \left(\frac{S_r}{1+h} \beta_{water} - \left[(1-S_r) + \frac{\chi h S_r}{(1+h)} \right] \frac{1}{\alpha_s \left(p_{atm} + u_{water} \right)} \right) + (1-n)\beta_{solid} \right\} \partial p$$

(27)

$$n^* = n + n(1-n) \left\{ \frac{S_r}{1+h} \beta_{water} - \left[(1-S_r) + \frac{\chi h S_r}{(1+h)} \right] \frac{1}{\alpha_s \left(p_{atm} + u_{water} \right)} - \beta_s \right\} dp$$

(28)

Pore water coefficient B

By supposing compression only, the undrained isotropic compression of soil has been derived. Among the derived equations, the pore water coefficient B (24), characterizing the isotropic compression, can be compared with Skempton (1954) (30) as well as Bishop (1973) (31). This coefficient, rewritten by (29), has been assumed as a function of the porosity, bulk moduli of the solid mass and water, the content of dissolved gas and the initial state of pore pressure and/or the applied backpressure.

$$B = \cfrac{1}{1 + \cfrac{1}{\alpha_n}\left\{\cfrac{\cfrac{S_r}{1+h}\beta_{water} - \left[(1-S_r) + \cfrac{\chi h S_r}{(1+h)}\right]\cfrac{1}{\alpha_s\left(p_{atm} + u_{water}\right)} - \beta_{solid}}{\beta_{solid}}\right\}}$$

(29)

$$Skempton : B = \cfrac{1}{1 + n\cfrac{C_v}{C_c}}$$

(30)

$$Bishop : B = \cfrac{1}{1 + n\cfrac{C_w - C_s}{C - C_s}}$$

(31)

Here $\dfrac{S_r}{1+h}\beta_{water} - \left[(1-S_r) + \dfrac{\chi h S_r}{(1+h)}\right]\dfrac{1}{\alpha_s\left(p_{atm} + u_{water}\right)} - \beta_{solid}$ in (29) is characterizing the compressibility of the soil as effected by pore water only and is similar to C_v in (30) and (C_w-C_s) in (31). C_c in (30) and $C-C_s$ in (31) are similar to β_{solid} in (29) and expresses the compressibility of the solid mass, loaded by the effective stresses, while n in (30) and (31) is replaced by $\alpha_n^{-1}=(1-n)^{2/3}$ in (29). Obviously from the derived equation (29) and depending on the magnitude of β_{solid} the B=1 can also exists for values lower than $S_r=1$. For $S_r=1$ the pore pressure coefficient B will be 1 because $B \rightarrow \alpha_n/(\alpha_n-1)>1$
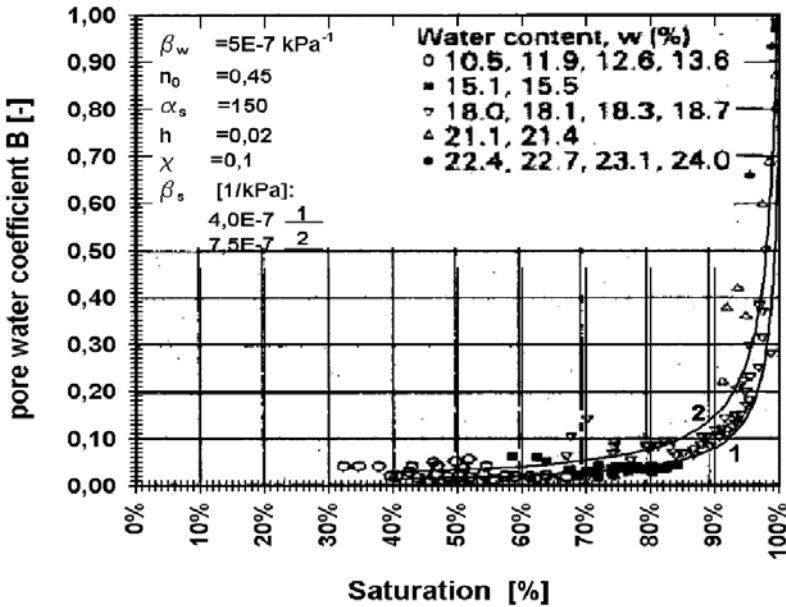

Figure 9. B-S_r relationship comparing with Peorian loess (Campbell by Fredlund, 1993)

Figure and Figure 9 show some theoretical results comparing to data from literature (Campbell by Fredlund, 1993). The equations (24) as well as (21) and (22) have been elaborated in Figure by an incremental increase of the isotropic compression load (dp=-100 kPa) and updating the grade of saturation and porosity after each load increment. Figure 9 shows for the same case the relation between the load and the generated pore water pressures. The theoretical curve for both figures has been fitted depending on the combination of β_s and α_s mainly. The parameter χ has a rather low sensitivity, because the volume of dissolved gas is very low (h=0,02).

A satisfied fit of the given data has been got iteratively between both figures by α_s=150 and consequently β_s=4E-7 kPa. The porosity n_0=0,45 has been estimated from the given water content.

From these results it should be concluded in relation to the Peorian loess at which $\beta_{solid} \approx \beta_{water}$ and α_s is relatively large the condition B=1 cannot be reached under normal conditions. Consequently to the high value of α_s and Figure 7 a large amount of the gas bubbles should be very small.
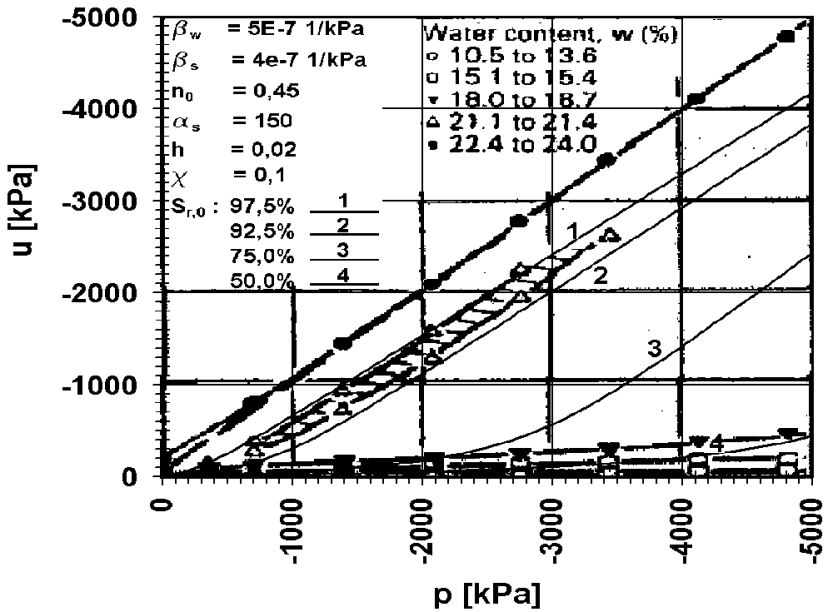
Figure 9. p-u_{water} relationship comparing with Peorian loess (Campbell, by Fredlund 1993)

Figure 10 shows the same relation as Figure 9 for a material with a lower stiffness (β_{solid}=2E-6 kPa) and α_s=20, consequently to the theoretical condition at which $\beta_{solid} > \beta_{water}$ the condition B=1 can be reached sooner or later due to an increasing isotropic load. The higher β_{solid} respectively S_r the faster that condition has been reached.

Figure 10. p-u$_{water}$ relationship due to increasing isotropic load

Conclusion

By taking into account the compressibility of solid mass and the fluid/gas mixture inside the pores, a theoretical relation between the pore water coefficient B and the saturation $S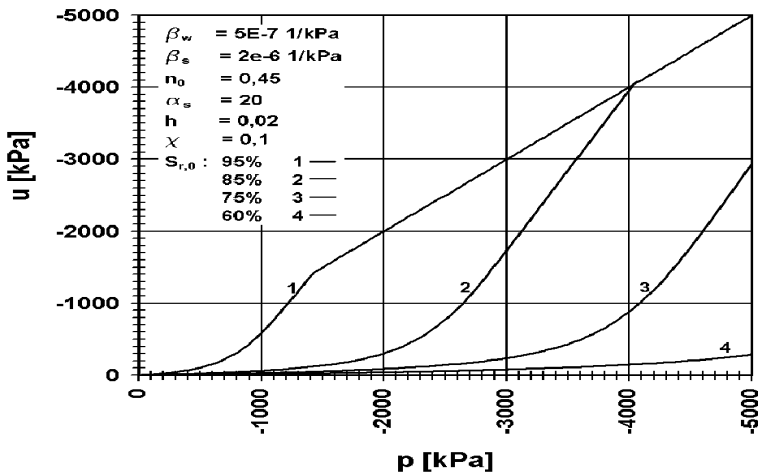_r$ is derived. This theoretical relationship between S_r and B is shown to be similar to measured data given in the literature. Furthermore the approach results in a theoretical model describing the isotropic undrained behaviour quiet well. The theoretical results are showing that soil behaviour depends strongly on the interaction of solid mass and the fluid/gas mixture. The theory can be elaborated for drained situation, creep as well as for one-dimensional compression. In such case accompanying laboratory tests are needed to verify the model.

Literature

Barends, F.B.J. (1979). "The Compressibility of an Air-Water Mixture in a Porous Medium". *L.G.M. mededelingen*, published by Delft Soil Mech. Lab., The Netherlands, part 20, no. 1, pp49-66.

Bishop, A.W. (1954). "The Use of Pore Pressure Coefficients in Practice". *Geotechnique*, vol. 4, no 4, pp 148-152.

Bishop, A.W. &Hight, D.W. (1977). "The Value of Poisson's Ratio in Saturated Soils and Rocks Stressed under Undrained Conditions". *Geotechnique*, Vol. 27, no 3, pp 369-384.

Fredlund, D.G. &Rahardjo, H. (1993). *Soil Mechanics for Unsaturated Soils*. New York, John Wiley & Sons. ISBN 0-471-85008-X.

Oostveen, J.P. (2002). "Uncertainties in Settlement Predictions". *Learned and Applied, Soil Mechanics out of Delft,* Ed. Barends, F.B.J. & Steijger, P.M.P.C., A.A.Balkema Publishers. ISBN 90-5808-357-3

Oostveen, J.P. (?). Report in progress

Schuurman, E. (1966). "The Compressibility of an Air/Water Mixture and a Theoretical Relation between the Air and Water pressure". Geotechnique, vol. 16, no 4, pp 269-281.

Skempton, A.W. (1954). "The Pore Pressure Coefficients A and B". *Geotechnique*, vol. 4, no 4, pp.143-147.

Hydro-mechanical behaviour of a clayey silt under isotropic compression

C. Buenfil, E. Romero, A. Lloret, and A. Gens

Departament d'Enginyeria del Terreny, Cartogràfica i Geofísica,
Universitat Politècnica de Catalunya, Barcelona, Spain

1 Introduction

Experimental studies concerning the mechanical response of unsaturated soils during compression under isotropic conditions have been mainly focused on the compressibility variation and yield properties at different suction levels (Sivakumar 1993, Rampino *et al*. 1999, 2000, Chen *et al*. 1999). However, few experimental studies have been focused on the coupled hydro-mechanical response at low suctions (Romero 1999, Barrera 2002), in which mechanical actions play an important role in the water retention properties of the soil. The low-suction range of the water retention curve as a function of the gravimetric water content is highly dependent on void ratio. The changes of this volumetric variable induced by mechanical actions affect mainly the water storage capacity of the soil at saturation, the air-entry value on drying and the air-occlusion value on wetting (Romero & Vaunat 2000, Karube & Kawai 2001).

The paper contains some results of a laboratory investigation performed on low-density clayey silt with the aim of studying the hydraulic response on isotropic loading at low suctions. The results of this experimental study provide a consistent picture of the coupled hydro-mechanical response of the soil, in which the loading paths clearly affect the shape of the water retention curves and the consequent hydraulic response of the soil.

Test results were interpreted within the framework of an elastoplastic model (Alonso *et al*. 1990) and bounding retention curves (Vaunat *et al*. 2000), which separate a domain of attainable states from unattainable states in the water content : suction plane and explain the water content changes observed on isotropic loading.

2 Characterization of the tested soil

2.1 Tested material and compaction procedures

Laboratory tests were performed on a low plasticity clayey silt from Barcelona. It has a liquid limit of w_L=28%, a plastic limit of w_P=19%, a clay-size fraction $\leq 2\,\mu m$ of 19%, a silty fraction of 47% and unit weight of the solids of γ_s=26.6 kN/m^3. The dominant mineral of the clay fraction is illite (Barrera 2002). The hygroscopic water content (mass basis) of the soil at laboratory conditions (relative humidity 47%) is about 1.7%.

Samples (38 mm diameter and 76 mm high) at a prescribed water content of 12.0% were prepared at a dry unit weight of γ_d=14.7 kN/m^3 (degree of saturation of S_r=40%), by one-dimensional static compaction under constant water content and at a constant piston displacement rate of 0.2 mm/min. Maximum fabrication vertical net stress was 0.3 MPa. Lateral stresses were measured by an active lateral stress system, resulting in a lateral stress coefficient at rest of K_0=0.48. Suction after compaction, s=270 kPa, was measured using a high-range tensiometer (Ridley & Burland 1993).

A relatively low dry unit weight was selected with the aim of inducing an open structure, which was susceptible to undergo important void ratio changes on loading and in turn to induce important changes of the water retention properties of the soil.

2.2 Water retention curves

Retention curves of the clayey silt were obtained using a controlled-suction oedometer cell. Samples (50 mm diameter and 10 mm high) were prepared following the same compaction procedure described before. In this case, two contrasting void ratios were selected: e=0.82 and e=0.57. The larger void ratio was representative of the as-compacted state. The lower value corresponded to a state reached after undergoing an important compression on loading.

Axis translation technique with a constant air pressure was used to apply suctions ranging between 550 kPa and a value close to zero. The water pressure was applied by a GDS Instruments Ltd. pressure/volume controller connected to a high air-entry value ceramic (HAEV of 1.5 MPa), which allowed the measurement of water volume changes. Suctions lower than 8 kPa were controlled by placing the pressure controller below the oedometer level (negative water column). Suction data above 15 MPa at nearly the same void ratios (e=0.55 and e=0.75) were obtained by Barrera (2002) using psychrometer technique.

The retention curves were obtained at a constant vertical net stress of (σ_v-u_a) = 20 kPa following multi-stage wetting and subsequent drying paths. At this stress level, the loose sample developed some collapse on wetting. Nevertheless, the void ratios during hydration and subsequent drying did not change signifi-

cantly, and the data could be considered as representative of constant volume retention curves.

The relationships between suction and water content in wetting and drying paths for both densities have been plotted in Fig. 1. As observed, the wetting and drying retention curves are sensitive to void ratio changes.
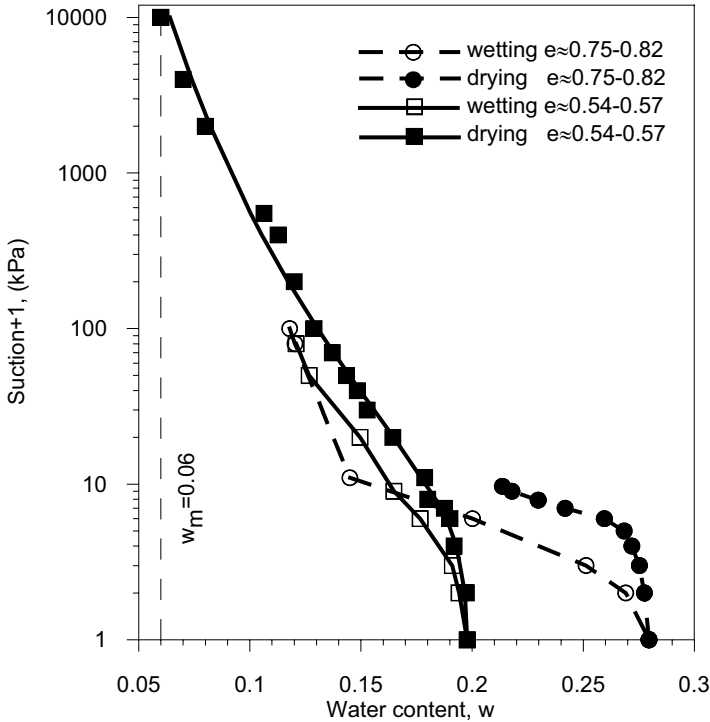

Fig. 1. Wetting and drying retention curves of the clayey silt at two contrasting void ratios.

Water in aggregated structures containing micro and macropores, like that of the tested material, is assumed to be retained by capillary effects (free water) and water adsorption mechanisms (adsorbed water) (Barbour 1998, Romero *et al.* 1999 and Vanapalli *et al.* 1999). Inside micropores, where adsorbed water is predominant, the water content is unaffected by mechanical effects, and inside macropores, where free water is predominant, the water content is sensitive to mechanical actions (Romero *et. al.* 1999). The water content that separates these two storage zones in the tested material was estimated at a value of w_m=6% by Barrera (2002), following an equivalent procedure to that described by Romero *et. al.* (1999). As observed in Fig. 1, water contents are higher then this value, indicating that mechanical actions produce changes in the macroporosity, affecting free wa-

ter contained in these large interconnected pores, while not greatly influencing soil microporosity. The water content at null suction depends on the void ratio and therefore the curves markedly diverge to reach the water contents corresponding to their saturated conditions. Moreover, the changes in void ratio also affect the air-entry value on drying. The low-density soil has a lower air-entry value (5 kPa) compared to the high-density soil (10 kPa). Void ratio effects are also detected in the crossing of the two wetting branches, as a consequence of their influence on the air-occlusion value (water-entry value) of the curves.

On first wetting before compaction, the soil follows the 'main wetting curve', which acts as a state boundary curve in the w:s plane. This 'main wetting curve' changes on subsequent compaction at constant water content, due to its dependence on void ratio. The as-compacted state after this compression process is not located on this 'main wetting curve'. In this way, a subsequent wetting phase will follow a 'scanning curve' with a slope steeper than the slope of the main curve. When the scanning curve reaches the intersection with the main curve, the state of the soil will proceed along this main curve on further wetting. This behavior is especially clear in the wetting branch of the low-density soil shown in Fig. 1, in which a decrease in suction starting from the as-compacted condition (w=12%) to a suction of s=10 kPa causes only a small increase in water content. A similar behavior was observed on wetting by Delage & Suraj de Silva (1992), testing a compacted eolian silt.

3. Experimental program

3.1 Controlled-suction equipment

An improved controlled-suction triaxial cell similar to the equipment described in Romero *et al.* (1997), Romero (1999) and Barrera (2002) was used to perform the tests. The deformation response was monitored with local axial (miniature LVDTs adhered to the membrane) and radial (electro-optical laser system mounted on two diametrically opposite sides) transducers.

Suction was applied simultaneously via axis translation technique on both ends of the sample, maintaining a constant air pressure and modifying the water pressure. Both top and bottom platens have a combination of two porous discs: a peripheral annular coarse one connected to the air system and an internal disc with a high air-entry value ceramic (HAEV of 1.5 MPa) connected to the water system. This double drainage ensured a significant reduction of the equalization time.

Water content changes were registered measuring the water volume that crossed both HAEV discs by means of two double wall burettes with differential pressure transducers. The measured water volume changes were corrected taken into account the amount of air diffused through the ceramic discs and the leakage through the pipes. In this way, delicate effects concerning the inflow and outflow of water during loading could be successfully examined.

Two stepper motors operating air pressure regulators were used to apply the deviator and confining stresses.

3.2. Stress paths followed

Three isotropic compression tests (A, B, and C shown in Fig. 2) were performed at different suctions. Equalization stages A1-A2, B1-B2 and C1-C2, to bring the as-compacted suction to the different target suctions, are shown in Fig. 2 (A1, B1, C1 represent the as-compacted states). Isotropic compression paths (A2-A3, B2-B3 and C2-C3) are also indicated.
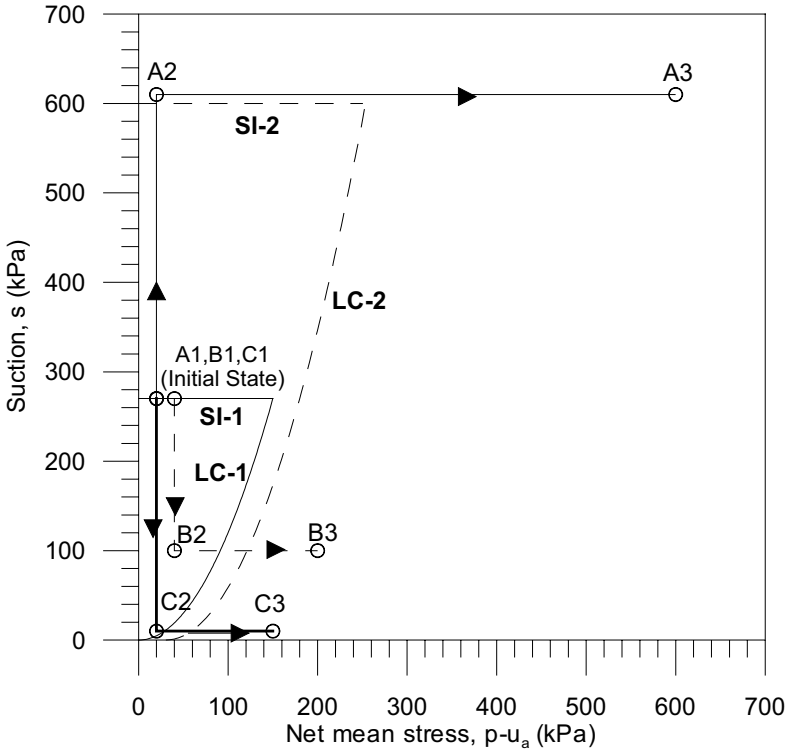

Fig. 2. Stress path followed on the clayey silt. Yield curve evolutions.

Equalization stages were carried out to apply target suctions of 10, 100 and 600 kPa. Equalization was assumed to be achieved when water content and deformations became stable, or according to Sivakumar (1993) and Rampino *et al.* (1999), once water flow was lower than water content changes of 0.04% per day.

Equalization period was about 250 hours at a target suction of 10 kPa. All the equalization stages were performed under a constant mean net stress (p-u_a)=20 kPa and a deviator stress q=10 kPa. These low values were chosen to avoid collapse on wetting and to allow the detection of the yield stress (p_0-u_a) in the subsequent isotropic compression path under constant suction.

Some small collapse (irreversible deformation) was observed when suction was maintained below 10 kPa in the oedometer test used to find the retention curve of the low-density soil. This fact was associated with the dragging of the 'loading-collapse' *LC* yield locus, as proposed by Alonso *et al*. (1990). The initial position of the *LC-1* curve that corresponds to the as-compacted state is shown in Fig. 2. As observed, the wetting paths under isotropic conditions evolved in the elastic domain, developing small reversible swelling strains. On the other hand, during the drying path under isotropic conditions to reach a suction of 600 kPa, the soil underwent irreversible shrinkage that was associated with the dragging of the 'suction increase' *SI* yield surface, as proposed by Alonso *et al*. (1990). The strain hardening induced by this drying process, which enlarged the elastic domain, was also reflected by the new position of the *LC-2* curve indicated in Fig. 2. The initial (*SI-1*) and final positions (*SI-2*) of the *SI* yield loci are shown in Fig. 2.

The increase of mean net stress (p-u_a) was applied at a stress rate of 1.8 kPa/hr, under a constant deviator stress q=10 kPa. This stress rate was considered adequate to avoid water pressure build-up. This condition was verified when measuring negligible compression strains after maintaining a constant confining stress for at least 24 hours at the end of the compression ramp. The maximum mean net stress of each test was chosen to determine the yield stress at different suctions and to display enough post-yield response due to the dragging of the *LC* yield locus.

4. Experimental results

Fig. 3 displays the time evolution of different volumetric variables during the suction equalization stages. The following volumetric variables were selected: void ratio e, water ratio e_w (volume of water to volume of solids) and degree of saturation $S_r = e/e_w$. The water ratio $e_w = G_s w$ was considered as the work conjugate volumetric variable associated with suction, in the same way as the volumetric variable void ratio e was associated with the net stress variable (Romero & Vaunat 2000). As expected, water inflow and some swelling were observed when suctions of 10 kPa and 100 kPa were applied, and water outflow and shrinkage were measured when suction was increased to 600 kPa. The small changes detected in the equalization stage at $s = 100$ kPa indicated that the initial as-compaction suction was close to this value. During the suction increase path it was easier to expel water than induce shrinkage deformation on soil skeleton, and e_w/e reduces. It was also admitted that when suction increased over the *SI-1* yield locus (refer to Fig. 2), which bounds the transition between elastic and virgin states, both simultane-

ous irreversible strains and irrecoverable water ratios developed affecting in a po-roplastic way soil behaviour (Vaunat *et al.* 2000).

   Fig. 4 shows the changes of the different volumetric variables undergone by the soil during the different compression paths. As observed, the evolution of variable *e* displayed clear pre- (associated with reversible processes) and post-yield zones. Yield stresses increase at higher suctions in accordance with the elastoplastic model of Alonso *et al.* (1990). Post-yield response on variable *e* was associated with the dragging of the loading-collapse *LC* yield curve that was sketched in Fig. 2. The post-yield compressibility decreased at higher suctions, also in accordance with the model. A common yield stress in the e:ln(p-u_a), e_w:ln(p-u_a) and e/e_w:ln(p-u_a) planes was identified for all the volumetric variables along the compression paths at suctions of 100 and 600 kPa. In these paths, the evolution of the degree of saturation displayed an increasing trend on loading in the post-yield range, as a consequence of the higher efficiency of the loading mechanism in deforming soil skeleton (macropore volume reduction) than expelling water (emptying of macro-pores). No significant degree of saturation changes were detected in the pre-yield range of these paths. These experimental tendencies were similar to those reported by Rampino *et al.* (1999, 2000).
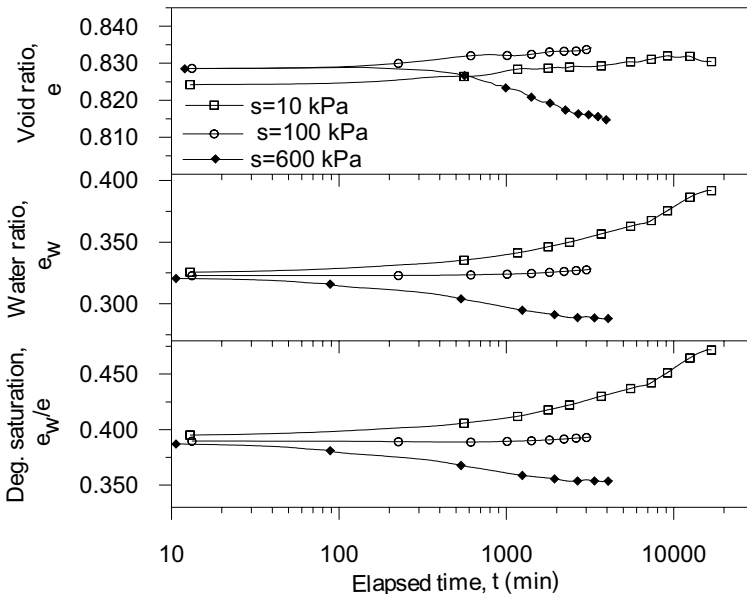

Fig. 3. Evolution of void ratio, water ratio and degree of saturation during the suction equalization stages.

The same figure shows a clear tendency of water ratio increase in the loading path at $s = 10$ kPa. In this case, the important increase of degree of saturation was associated with two mechanisms: soil skeleton deformation due to the higher post-yield compressibility (macropore volume reduction) and flooding of macropores. The second mechanism was a consequence of the important macropore volume and size reduction undergone by the material on loading. This new pore network was more eager for retaining water, due to the higher air-occlusion value of the wetting branch of the retention curve induced by the decrease of the void ratio (refer to Fig. 2). Sivakumar (1993) presented test results that also displayed water inlet during a ramped compression.
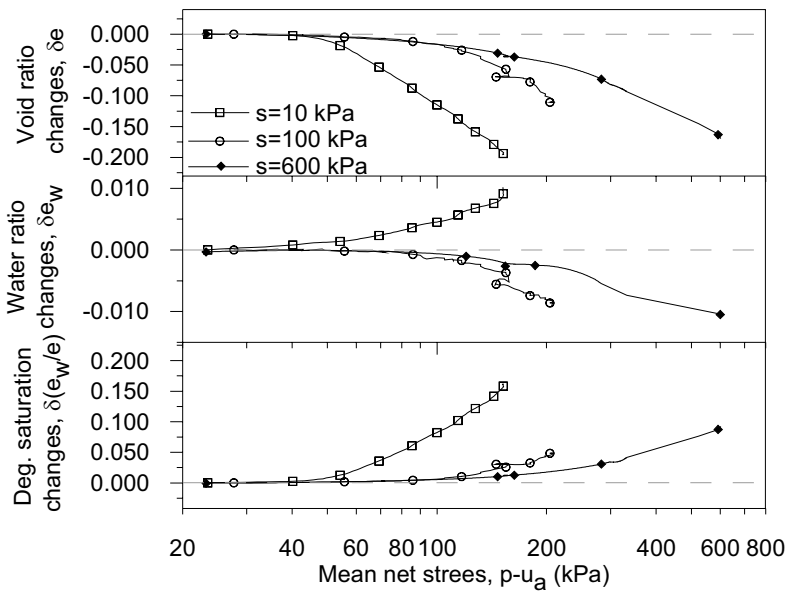

Fig. 4. Changes in void ratio, water ratio and degree of saturation during the isotropic compression paths.

The hydraulic response can be plotted in a e_w:ln(s) plane. In Fig. 5, the 'main wetting and drying curves' for the as-compaction state (e_I=0.75-0.82) are indicated by MC$_{D1}$ (Main Curve for suction Decrease) and MC$_{I1}$ (Main Curve for suction Increase), following the same nomenclature of the hydro-mechanical model proposed by Vaunat *et al.* (2000). These bounding wetting and drying curves at a constant void ratio enclose the scanning region and separate attainable states (inside this region) from unattainable states. As pointed out previously, when the soil undergoes a reduction in the macropore volume, the shape of these main curves changes (MC$_{D1}$ to MC$_{D2}$ and MC$_{I1}$ to MC$_{I2}$, as shown in Fig. 5), increasing their

air-entry value on drying and their air-occlusion value on wetting, and decreasing the water ratio at saturation.

In the first test at high suction (A1-A2-A3 in Fig. 5), the soil underwent an important macropore volume reduction on suction equalization (shrinkage A1-A2) and the subsequent isotropic compression path A2-A3. The volumetric strains undergone by the soil, induced the movement of the main drying curve from MC_{I1} to MC_{I2}. During the suction increase stage, the state of the sample moved initially on a 'scanning curve' until the MC_{I1} curve was reached. Afterwards, the state of the soil remained on this bounding curve and it followed its movement. On loading, due to the constraint that the zone on the right side of MC_I is unattainable, the soil state is pushed (path A2-A3) by the movement of the main drying curve, causing a small decrease in water ratio at constant suction.

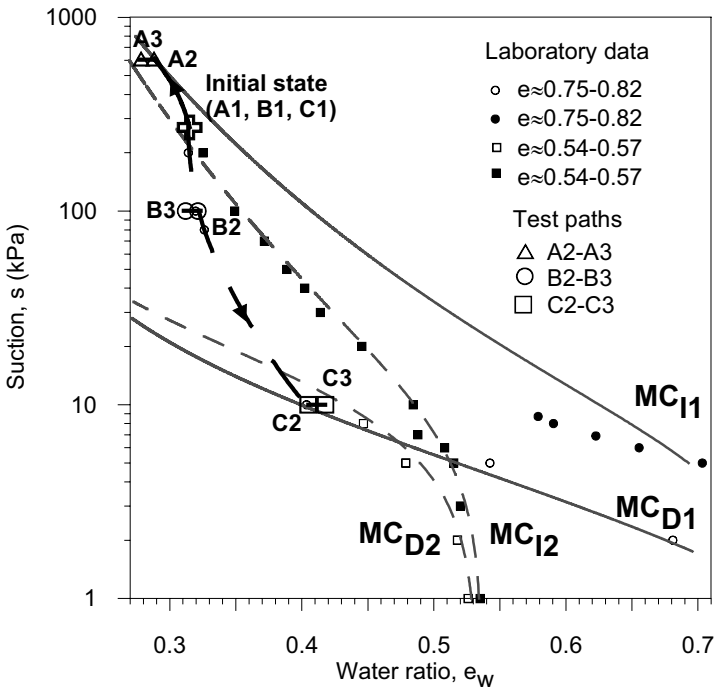**Fig. 5.** Paths followed in the e_w:ln (s) plane. Main wetting and drying curves.

In the second test at medium suction (B1-B2-B3 in Fig. 5), the changes in the main drying and wetting curves were negligible during the suction equalization stage (B1-B2), because the volumetric strains undergone by the soil were small. The state of the soil during this wetting path remained inside the attainable zone,

following a 'scanning curve' with a small increase in water ratio. Vaunat *et al*. (2000) assumed a reversible response within this scanning zone. During the subsequent isotropic compression path B2-B3, the void ratio decreased from e=0.83 to 0.72, inducing a slight movement of the main curves. However, the state of the soil still remained inside the scanning zone between both main curves. Within this zone, Romero & Vaunat (2000) and Vaunat *et al*. (2000) assumed a reversible response of water ratio changes induced by loading/unloading paths. The elastic hydraulic stiffness against net stress changes proposed by these authors predicted a water ratio decrease on loading, which was the same response observed in the loading path B2-B3.

In the third test performed at very low suction (C1-C2-C3 in Fig. 5), the changes in MC_{D1} and MC_{I1} were also negligible during the suction equalization stage (C1-C2), because the swelling strains undergone by the soil were small. As in the previous test, the soil initially followed an elastic path over a 'scanning curve' ending at a final state C2, which was probably near the main wetting curve MC_{D1}. During the compression path C2-C3, important plastic volumetric strains were developed, which induced the movement of the main wetting curves from MC_{D1} to MC_{D2}. In this case, it is particularly important the increase in the air-occlusion value of the soil due to the decrease in the pore diameter caused by the compression process. As observed, the new position MC_{D2} intersects the initial MC_{D1} at s<10 kPa. It was assumed that the state of the soil remained on this bounding wetting curve and it followed its movement. On loading, due to the constraint that the zone on the left side of MC_D is unattainable, the soil state is pushed (path C2-C3) by the movement of the main wetting curve, causing an increase in water ratio at constant suction.

5. Conclusions

A series of three isotropic compression paths at different suctions were performed in a fully-instrumented triaxial cell to study the coupled hydro-mechanical response of a clayey silt, which was statically compacted at a very low dry density. This low value was selected to induce an appreciable change of the void ratio and the water retention properties of the soil on loading.

The experimental technique, involving suction equalization and ramped compression stages, was described in detail. The local instrumentation of axial and radial strains installed in the triaxial cell, as well as the continuous recording of the soil water volume changes with automatic burettes, allowed the careful monitoring of the coupled hydro-mechanical response and the successful examination of delicate effects concerning the inflow and outflow of water during loading.

Retention curves for compacted states at two contrasting void ratios were obtained to show the main effects induced by the compression process. The comparison between these retention curves showed some insight about its dependence on void ratio, which affects the water storage capacity of the soil at saturation, the air-entry value on drying and the air-occlusion value on wetting.

The experimental results showed the important role played by the mechanical path in modifying the water retention properties of the soil. Three equalization stages were selected at suctions 10, 100 and 600 kPa, which corresponded to a zone in the retention curve plot close to the bounding 'main wetting curve', a zone in the 'scanning domain' between both main curves, and a zone close to the bounding 'main drying curve'. On loading at a suction of 100 and 600 kPa, the sample expelled water, whereas at a suction of 10 kPa there was a clear tendency to absorb water due to the formation of a denser structure with a higher air-occlusion value. This fact is explained in terms of the movement and the change of shape on loading of the bounding drying and wetting curves, which depend on the void ratio and delimit the domain of attainable states.

Mechanical results at different suctions, such as the post-yield compressibility and the yield stress of the loading paths, were interpreted within the framework of the elastoplastic model of Alonso *et al*. (1990). Water content changes observed on isotropic loading were interpreted within the framework of bounding retention curves proposed by Vaunat *et al*. (2000), which separate a domain of attainable states from unattainable states in the water content : suction plane.

Acknowledgements

References

Alonso EE, Gens A, Josa A (1990) A constitutive model for partially saturated soils. Géotechnique 40 (3): 405-430.

Barbour SL (1998) Nineteenth Canadian Geotechnical Colloquium: The soil-water characteristic curve - A historical perspective. Can Geotech J 35: 873-894.

Barrera M (2002) Estudio experimental del comportamiento hidro-mecánico de suelos colapsables (in Spanish). Ph.D. thesis, Universitat Politècnica de Catalunya, Barcelona, Spain.

Chen Z-H, Fredlund DG, Gan JK-M (1999) Overall volume change, water volume change, and yield associated with an unsaturated compacted loess. Can Geotech J 36: 321-329.

Delage P, Suraj de Silva GPR (1992) Negative pore pressure and compacted soils. In: Ovando E, Auvinet G, Paniagua W, Díaz J (eds) Raul J. Marsal vol, Sociedad Mexicana de Mecánica de Suelos, México, pp 225-232.

Karube D, Kawai K (2001) The role of pore water in the mechanical behaviour of unsaturated soils. Geotechnical and Geological Engineering 19: 211-241.

Rampino C, Mancuso C, Vinale F (1999) Laboratory testing on unsaturated soil: equipment, procedures and first experimental results. Can Geotech J 36: 1-12.

Rampino C, Mancuso C, Vinale F (2000) Experimental behaviour and modelling of an unsaturated compacted soil. Can Geotech J 37: 748-763.

Ridley AM, Burland JB (1993) A new instrument for the measurement of soil moisture suction. Géotechnique 43(2): 321-324.

Romero E, Faccio JA, Lloret A, Gens A, Alonso (1997) A new sution and temperature controlled triaxial apparatus. In: Proc 14th Int Conf on Soil Mechanics and Foundation Engineering, Hamburgo. Balkema, Rotterdam, pp 185-188.

Romero E (1999) Characterization and thermo-hydro-mechanical behaviour of unsaturated Boom clay: an experimental study. Ph.D. thesis, Universitat Politècnica de Catalunya, Barcelona, Spain.

Romero E, Gens A, Lloret A (1999) Water permeability, water retention and microstructure of unsaturated Boom clay. Engineering Geology 54: 117-127.

Romero E, Vaunat J (2000) Retention curves of deformable clays. In: Tarantino A, Mancuso C (eds) International Workshop On Unsaturated Soils: Experimental Evidence and Theoretical Approaches in Unsaturated Soils, Trento, Italy. A.A. Balkema, Rotterdam, pp 91-106.

Sivakumar V (1993) A critical state framework for unsaturated soil. Ph.D. thesis, University of Sheffield, Sheffield, U.K.

Vanapalli SK, Frendlund DG, Pufahl DE (1999) The influence of soil structure and stress history on the soil-water characteristic of a compacted till. Géotechnique 49(2):143-159.

Vaunat J, Romero E, Jommi C (2000) An elastoplastic hydro-mechanical model for unsaturated soils. In: Tarantino A, Mancuso C (eds) International Workshop On Unsaturated Soils: Experimental Evidence and Theoretical Approaches in Unsaturated Soils, Trento, Italy. A.A. Balkema, Rotterdam, pp 121-138.

The concept of "apparent" Compression Index

M. Bardanis[1] and M. Kavvadas[2]

[1]Doctoral Student, National Technical University, Athens, Greece
[2]Associate Professor, National Technical University, Athens, Greece

Abstract. One-dimensional consolidation tests are often performed without accurate control of the initial degree of saturation, since most commercially used testing apparatuses do not permit back-pressuring. As a result, the initial degree of saturation is often less than unity and, thus, the measured 'Apparent' Compression Index can be very different than the value corresponding to a fully saturated sample. Similar differences are caused by most oedometer tests being performed up to a maximum stress lower than the maximum pre-consolidation pressure. Oedometer tests on undisturbed samples, on initially unsaturated samples of reconstituted soil, and a data-base of commercial oedometer tests are presented in order to exhibit the effect of high maximum preconsolidation pressure, cementation and initial unsaturation. Finally, expressions for the volumetric deformation of unsaturated soils proposed by Alonso et al. (1990) are used to explain different trends exhibited by the 'Apparent' Compression Index for low- and high-plasticity soils.

1 Introduction

Oedometer testing is an essential part of both commercial and research geotechnical investigation as it yields important parameters of soil behaviour. These tests are carried out routinely by commercial laboratories in a standardised manner, usually involving loading up to 800 kPa, as this value requires a five-day loading sequence (50-100-200-400-800 kPa) compatible with a working week, and because 800 kPa exceeds the applied pressure in most typical projects. Results reported by these tests typically include the Compression Index C_c, the Recompression Index C_r, the preconsolidation pressure σ'_{prec}, the void ratio versus vertical stress curve, the one-dimensional modulus of deformation E_s and the vertical strain versus vertical stress curves. Given these parameters and knowing the stress change that the structure will induce, settlements during one-dimensional consoli-

dation may be calculated using C_c (most usual method) or the void ratio-stress curve or the one-dimensional modulus of deformation E_s. Given, however, that commercial oedometer tests usually yield dubious results especially regarding C_c, due to the relatively low maximum stress applied, an investigation of the effects influencing the measured value of C_c is justified.

2 Identification of the problem

A conventional oedometer test can yield 'correct' values of the parameters involved if the loading sequence is such that several points of the void ratio versus vertical stress compression curve (with the vertical stress axis in logarithmic scale) lie on a straight segment of the curve, past a transitional curved segment of this curve around a value of the vertical stress termed the 'apparent' preconsolidation pressure (as it may not be due to actual gravitational preconsolidation but other structure-inducing agents). Casagrande 1936, proposed his well-known geometrical construction (empirical) for the determination of this value from a void ratio-vertical stress curve. More recent methods (Burland 1990) determine this value by the comparison of the one-dimensional compression curves for the undisturbed samples of soil to the one-dimensional compression curves for reconstituted samples of the same soil. Regardless of the method used for the determination of the 'apparent' preconsolidation pressure, it is obvious that the 'correct' or 'true' value of the Compression Index is determined if the applied maximum stress is significantly higher than 'apparent' preconsolidation pressure, thus including the linear portion of the compression curve. Using therefore a loading sequence up to only 800 kPa will most probably yield incorrect values of the compression parameters because these parameters are affected by the maximum pressure applied in the geological history of the material (gravitational pre-consolidation), other structure-inducing agents such as cementation, and the initial degree of saturation of the tested specimen. Such values are 'apparent' values of Compression Index, $C_{c,app}$, with the exception of fully saturated, uncemented soils subjected to a maximum pre-consolidation pressure up to about 400 kPa in their geological history.

In order to exhibit the magnitude of the difference between 'true' and 'apparent' values of the Compression Index, oedometer tests were carried out on undisturbed samples of two marls and two clays from Greece. The properties of these soils are presented in Table 1. Corinth marl is a highly cemented low- to medium-plasticity marl found in the greater area of the city of Corinth (regarding the cementation and the engineering behaviour of the Corinth marl, see Kavvadas et al 1993, 2002). St. Anargiri clay is a medium-plasticity clay sediment found in north-western Athens in layers intercalating with the medium-plasticity marl found in the same area. Amaroussion clay is a medium- to high-plasticity clay sediment also found in northern Athens in the greater area of the Olympic Sports Centre. All of these soils are either cemented and/or over-consolidated and in-situ are usually unsaturated (due to the dry climate and the relatively deep ambient water table).

Undistorted samples of these soils were loaded one-dimensionally to very high stresses (4.8 or 6.4 MPa depending on the soil) and the one-dimensional compression curves obtained are presented in Fig. 1. As it is shown in Table 1, values of the 'apparent' Compression Index (calculated for the portion of the curves between 400 and 800 kPa as would be the case for a commercially performed oedometer test) are found to be significantly lower as a result of the preconsolidation, cementation or initial degree of saturation of these natural soils.

Table 1. Properties of soils, undisturbed samples of which were consolidated one-dimensionally.

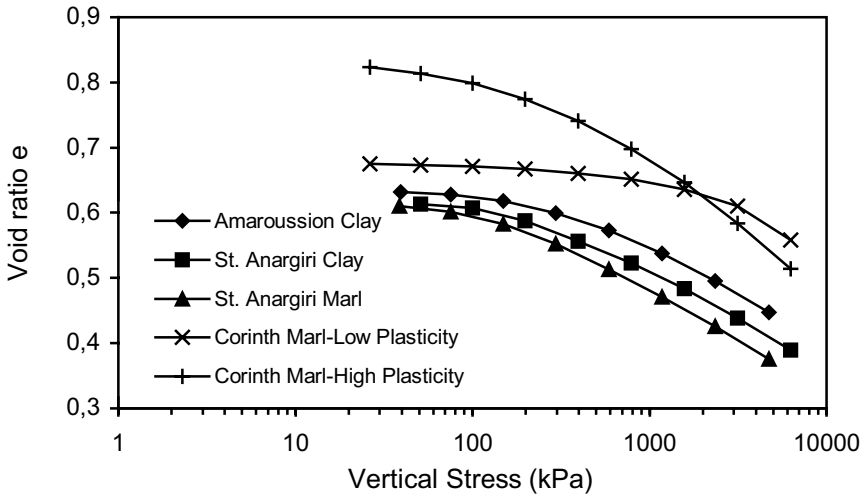| Material	w_L	w_p	I_p	S_{ro}	'Apparent' C_c	'True' C_c
	(%)	(%)		(%)		
Corinth Marl (Low I_p)	30,5	25,0	5,5	90,3	0,032	0,170
Corinth Marl (High I_p)	34,0	22,5	11,5	90,9	0,144	0,232
St. Anargiri Marl	31,5	16,0	15,5	76,4	0,135	0,166
St. Anargiri Clay	40,5	20,0	20,5	77,6	0,114	0,163
Amaroussion Clay	47,5	23,0	24,5	83,0	0,103	0,157

Fig. 1. 1-dimensional compression curves from oedometer tests on undisturbed samples of various clays and marls from Greece.

3 The effect of the initial degree of saturation

In order to exhibit the effect of initial degree of saturation, a number of conventional oedometer tests were specially designed. Reconstituted clays consolidated one-dimensionally from slurries yield one-dimensional compression curves that are practically linear (Dineen 1997; Bardanis 1998, 1999) or only slightly concave upwards (Burland 1990; Chandler 1999). In any case, one-dimensional compression curves from tests on reconstituted clays (intrinsic compression curves as referred to by Burland 1990) do not have any inflection points, provided the samples are initially fully saturated. Bardanis 1998, 1999, presented results from tests on reconstituted soils consolidated from various initial water contents and indicated that changes in the inclination of the intrinsic compression curves or even the appearance of an inflection point at very low stresses similar to that obtained from one-dimensional compression curves from natural soils are due to initial values of the degree of saturation lower than unity.

In order to investigate this further and isolate the effect of initial degree of saturation from preconsolidation and cementation, tests on reconstituted Speswhite Kaolin were performed at even lower initial water contents than those reported by Bardanis 1999. Speswhite Kaolin is procured commer-cially as a dry powder, has a liquid limit of 64%, plastic limit 32% and Gs=2.61. One-dimensional compression curves from these tests are pre-sented in Fig. 2 (SK stands for Speswhite

Kaolin and the number next to it for the initial water content of the slurry as a per-centage of the liquid limit, e.g. 075, 75% of 64% = 48%). Initial parts of the curves appear to deviate from linearity as initial water content of the slurry -and therefore initial degree of saturation- decreases and a value of 'apparent' precon-solidation pressure can be determined. The existence of this 'apparent' precon-solida-tion pressure and the curvature of these curves leading to significant dif-ferences between 'true' and 'apparent' values of Compression Index are at-tributed solely to initial degree of saturation. As shown in Fig. 3, 'apparent' pre-consolidation pressure values decrease exponentially as ini-tial degree of satura-tion increases (Fig. 3a), fitting nicely a value of ap-proximately 1 kPa for Sro=100% when 'apparent' preconsolidation pres-sure is plotted in logarithmic scale (Fig. 3b). Similar trends are obtained if 'apparent' preconsolidation pressure is plotted against the suction corre-sponding to the values of initial degree of satu-ration calculated from these tests (suction values from soil-water characteristics of reconstituted Speswhite Kaolin determined by Dineen 1997). The 'apparent' pre-consoli-dation pressure increases exponentially with initial suction past the air-entry value of kaolin which is 1300 kPa (Dineen 1997) as presented in Fig. 3c and fits a linear change when the 'apparent' preconsolidation is plotted in logarithmic scale (Fig. 3d).

'Apparent' values of the Compression Index are usually smaller than the 'true' values (Fig. 4). 'Apparent' Compression Index values (between 400 and 800 kPa) larger than the 'true' values for high values of the initial de-gree of saturation in-dicate that the effect of initial degree of saturation di-minished greatly even below 400 kPa and therefore this is due to the in-trinsic compression curve being slightly concave upwards.
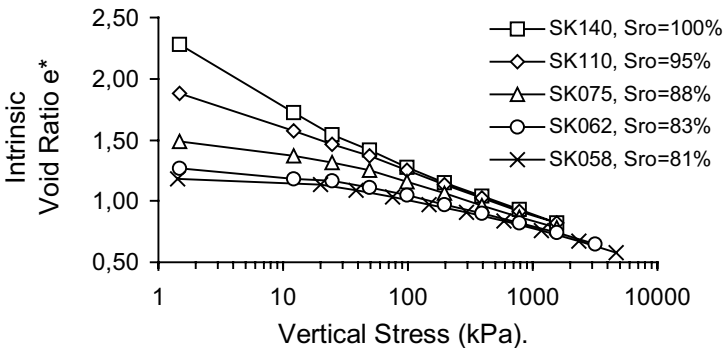

Fig. 2. 1-dimensional compression curves on reconstituted Speswhite Kaolin with various initial water contents (SK140, SK110 and SK075 from Bardanis 1999).
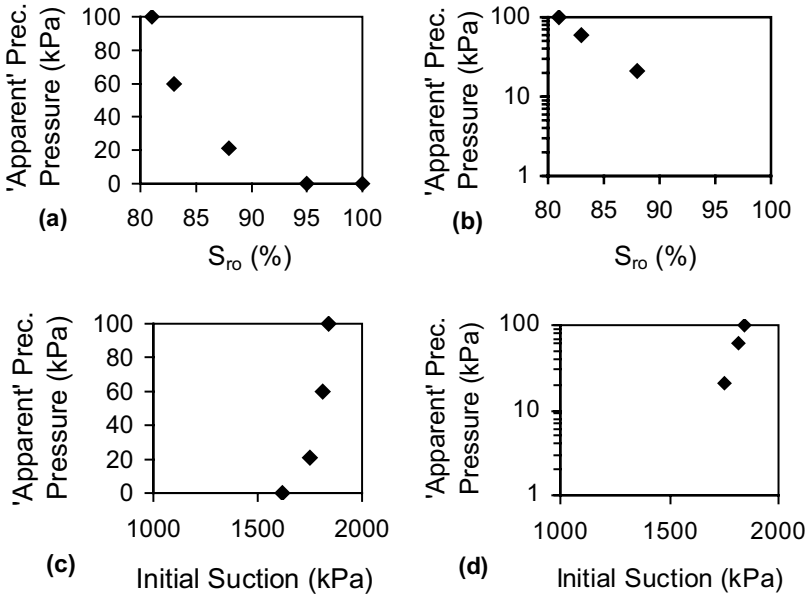
Fig. 3. 'Apparent' Preconsolidation Pressure of reconstituted Speswhite Kaolin consolidated 1-dimensionally from various initial water contents with initial degree of saturation (normal (a) and logarithmic scale (b) for 'apparent' preconsolidation pressure) and with corresponding initial suction (normal (c) and logarithmic scale (d) for 'apparent' preconsolidation pressure).
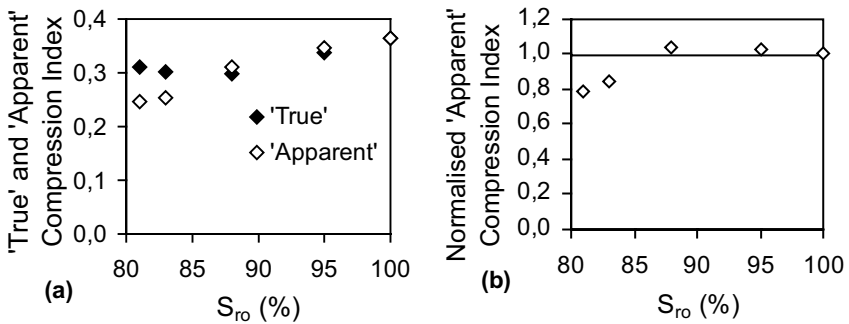

Fig. 4. 'True' and 'Apparent' Compression Index (absolute values (a) and normalised values of 'apparent' compression index) with initial degree of saturation from reconstituted Speswhite Kaolin consolidated from one-dimensionally from various initial water contents.

4 Commercial oedometer tests

Bardanis and Cavounidis 2001a, collected available empirical relations for the Compression Index and evaluated them on the basis of commercial oedometer testing practice on clayey soils in Greece (Bardanis and Cavounidis 2001b), identifying the restrictions imposed by the maximum loading pressure limited to 800 kPa in most tests. Fig. 5 shows the change of the reported Compression Index values from tests where the loading sequence did not exceed 800 kPa ('apparent' values) with initial degree of saturation, for all data in the data-base (Fig. 5a) and data for soils with very low (<20%) and very high (>70%) values of liquid limit w_L (Fig 5b). 'Apparent' Compression Index values from all soils against initial degree of saturation plot in such a way that there seems to be a change corresponding from a large increase to a small decrease of the compression index with increase of the degree of saturation from a centrally located value (Fig. 5a). If soils with the smallest and largest values of liquid limit are selected from the data-base and their 'apparent' compression index is plotted against their initial degree of saturation, then Fig. 5b is obtained where compression index decreases with increasing degree of saturation for low liquid limit soils and increases with increasing degree of saturation for high liquid limit soils. Changes of compression index with degree of saturation for these extreme liquid limit values frame conveniently the data for all soils.
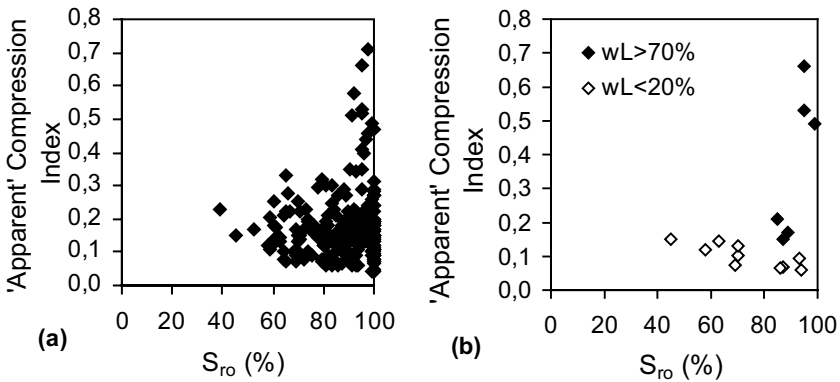

Fig. 5. 'Apparent' Compression Index against Initial Degree of Saturation for all samples in commercial oedometer tests data-base (a) and samples of soils with liquid limit below 20% and liquid limit above 70% (b).

5 Analytical expressions

Having identified partial saturation and 'apparent' preconsolidation pressure as the controlling parameters of whether 'true' or 'apparent' compression parameters will be obtained during oedometer testing, a mathematical framework was sought for the description and explanation of the compression parameters measured in commercial oedometer tests.

Alonso et al 1990, proposed a hardening plasticity constitutive model for slightly or moderately expansive unsaturated soils using two independent sets of stress variables: the excess of total stress over air pressure p and the suction s. Volume changes relative to net mean stress and suction changes are treated independently and determined by six parameters (geometrically defined in Fig. 6): κ, the elastic stiffness parameter for changes in net mean stress, $\lambda(s)$, the stiffness parameter for changes in net mean stress for virgin states of the soil, p_o, the preconsolidation stress, κ_s, the elastic stiffness parameter for changes in suction, λ_s, the stiffness parameter for changes in suction for virgin states of the soil and s_o, the hardening parameter of the suction increase yield curve. Incremental changes in specific volume v (v=1+e) are therefore: $dv= -\kappa \, dp/p$ (for elastic changes in net mean stress for constant suction s), $dv= -\lambda(s) \, dp/p$ (for plastic changes in net mean stress for constant suction s), $dv= -\kappa_s \, ds/s$ (for elastic changes in suction for constant net mean stress p) and $dv= -\lambda_s \, ds/s$ (for plastic changes in net mean stress for constant net mean stress p). The stiffness parameter for changes in net mean stress for virgin states of the soil, $\lambda(s)$, varies with suction s and is predicted by Eq. 1:

$$\lambda(s) = \lambda(0) \, [(1-r) \exp(-\beta s) + r] \tag{1}$$

where $\lambda(0)$ is the value of the stiffness parameter for zero suction, r and β are curve-fitting parameters. Given this variation of the stiffness parameter for changes in net mean stress (decrease with suction) a value of net mean stress p_t can be determined at which a transition occurs (Fig. 7). If net mean stress p remains lower than p_t, then specific volume will be higher for virgin compression of reconstituted soil without prior drying than specific volume for virgin compression at constant suction s of reconstituted soil with prior drying to suction s. If net mean stress however is higher than p_t, then the opposite is true. Using Eq. 1 and assuming virgin compression of reconstituted soil with and without prior drying, this transitional value of net mean stress is obtained by equating the two values of specific volume. Thus p_t is derived:

$$\ln(p_t/p^c) = \kappa_s \ln[(s+p_{at})/p_{at}] \, / \, \{\lambda(0)[(1-r)(1-\exp(-\beta s))]\} \tag{2}$$

if drying prior to compression does not exceed suction s_o, or:

$$\ln(p_t/p^c)=\{\kappa_s \ln[(s_o+p_{at})/p_{at}]+\lambda_s \ln(s/s_o)\}/\{\lambda(0)[(1-r)(1-\exp(-\beta s))]\} \tag{3}$$

if drying prior to compression exceeds suction s_o (p_{at} is the atmospheric pressure and p^c an arbitrary reference pressure).
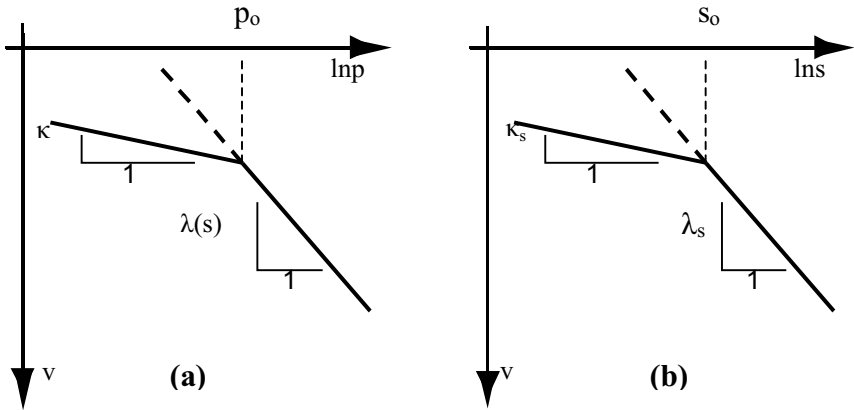
Fig. 6. Volumetric change parameters according to Alonso et al 1990, for net mean stress (a) and suction changes (b).

Regarding preconsolidation pressure p_o, that changes with suction and is given by Eq. 4 (Alonso et al 1990):

$$(p_o/p^c) = (p_o*/p^c)^{[\lambda(0) - \kappa]/[\lambda(s) - \kappa]}$$

(4)

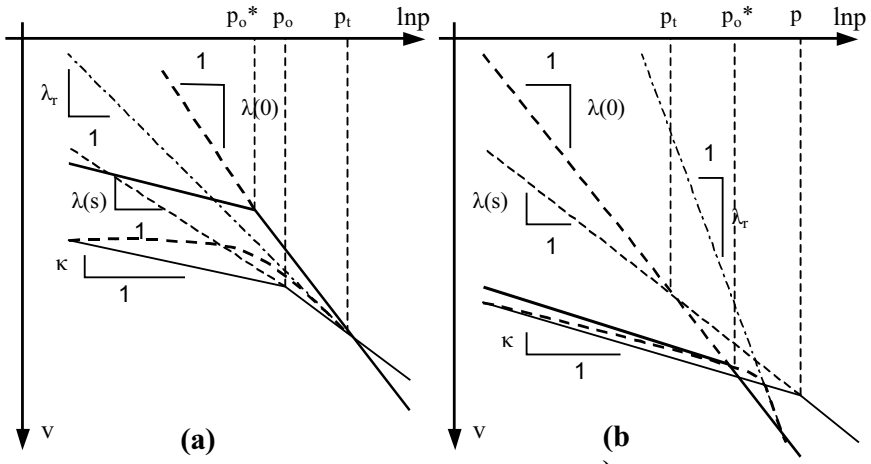where p_o* is the preconsolidation pressure at zero suction.

Fig. 7. Possible volumetric changes during loading of initially unsaturated clayey soil for maximum preconsolidation pressure below (a) and above transitional pressure p_t (b).

Let's consider now the following two situations. In the first case (Fig. 7a) a soil has been loaded to a value of net mean stress $p_o^* < p_t$ and then unloaded without drying prior to loading and the same soil has been loaded to the corresponding value of net mean stress $p_o < p_t$ and then unloaded to the same value of net mean stress as before but with drying to suction s prior to loading. If this soil is reloaded to a net mean stress smaller than p_t, reported values of the stiffness parameter λ_r (the 'apparent' compression index in oedometer tests stopping at relatively low stress) will be lower than the reported fully saturated stiffness parameter value $\lambda(0)_{rep}$ for the initially fully saturated sample (Fig. 7a). In the second case (Fig. 7b) a soil has been loaded to a value of net mean stress $p_o^* > p_t$ and then unloaded without drying prior to loading and the same soil has been loaded to the corresponding value of net mean stress $p_o > p_t$ and then unloaded to the same value of net mean stress as before but with drying to suction s prior to loading. If this soil is reloaded to a net mean stress larger than p_t and p_o^* but lower than p_o, reported values of the stiffness parameter λ_r (the 'apparent' compression index in oedometer tests stopping at relatively low stress) will be higher than the reported fully saturated stiffness parameter value $\lambda(0)_{rep}$ for reloading of the initially fully saturated sample to the same stress (Fig. 7b). In the cases described above, drying may be prior to loading or after that, as long as the preconsolidation pressure (with the effect of suction as described by Alonso et al 1990 included) is the one corresponding to the suction s caused by drying and the preconsolidation pressure in the case of the fully saturated soil. Also $\lambda(0)_{rep}$ is always smaller than $\lambda(0)$ for loading to relatively low net mean stress (below p_t and p_o^* respectively in Figs. 7a and 7b). If p_t is postulated to be higher than the value corresponding to vertical stress of 800 kPa for high plasticity soils and lower than this value for low plasticity soils (for the same preconsolidation pressure p_o), then this postulated behaviour describes the differences between low- and high-plasticity soils in Fig 7 (low-plasticity soil behaviour in Fig. 7b and high-plasticity soil behaviour in Fig. 7a).

6 Conclusions

Lower than required maximum applied pressures (typically 800 kPa) and lack of control of the initial degree of saturation S_{ro}, can lead to miscalculation of the Compression Index in conventional commercial oedometer tests with measured ('apparent') values of the Compression Index typically smaller than the 'true' values. A specially designed series of oedometer tests was performed in order to exhibit the effect of S_{ro} on the Compression Index. Tests on 'structured' soils were used to exhibit the effect of the combination of maximum preconsolidation pressure, cementation and S_{ro} on the Compression Index if loading is limited to relatively low stress. A large data-base of commercial oedometer tests on soils from Greece was used to illustrate the identified problems. S_{ro} lower than unity results in the Compression Index being underestimated unless very high stresses are applied. The problem can be overcome by saturating the samples prior to loading by back-pressuring, although the effect of irreversible changes in the state of the soil

would still be recorded if the initial degree of saturation was very low (close to the residual degree of saturation). Similarly, heavy preconsolidation and cementation result in underestimation of the Compression Index unless the maximum applied pressure is well above the preconsolidation pressure of the material. The miscalculation of the Compression Index by reporting 'apparent' values could be overcome by employing in design calculations the void ratio versus stress curves instead of the Compression Index, although this may complicate numerical analyses with commercial computer programs. It is shown that the framework proposed by Alonso et al 1990 can explain that oedometer tests on initially unsaturated low-plasticity soils yield higher values of $C_{c,app}$ than tests on fully saturated soils preconsolidated to the corresponding maximum stress and reconsolidated to the same stress below preconsolidation pressure p_o. The opposite is true for high-plasticity soils; oedometer tests on initially unsaturated high-plasticity soils yield lower values of $C_{c,app}$ than tests on initially fully saturated soils preconsolidated to the corresponding maximum stress and reconsolidated to the same stress below transitional net mean stress p_t. Future research aims to compare the results of conventional and hydraulic oedometer tests, to incorporate suction measuring devices in the cells of conventional oedometers in order to know both the initial degree of saturation and the suction, and finally to verify the differences in the behaviour of low- and high-plasticity soils.

Acknowledgements

References

Alonso EE, Gens A, Josa A (1990) A constitutive model for partially saturated soils. Géotechnique. 40: 405-430.

Bardanis ME (1998) An experimental study of the 'robustness' of the Intrinsic Compression Line. M.Sc. Thesis, Imperial College of Science, Technology and Medicine, University of London.

Bardanis ME (1999) An experimental study of the properties of intrinsic compressibility of one clay and one marl. In: Proceedings 13th Young Geotechnical Engineers Conference, Santorini, Greece, pp 88-97.

Bardanis M, Cavounidis S (2001a) Empirical relations between the compression index of clayey soils and their physical characteristics (in Greek). In: Proceedings 4th Hellenic Conf on Geotechnical & Geoenvironmental Engng, pp 123-130.

Bardanis M, Cavounidis S (2001b) Comparison between compression index from empirical relations and tests on clayey soils from Greece (in Greek). In: Proceedings 4th Hellenic Conf on Geotechnical & Geoenvironmental Engng, pp 131-138 (in Greek).

Burland JB (1990) On the compressibility and shear strength of natural clays Géotechnique. 40: 327-378.

Casagrande A (1936) The determination of the pre-consolidation load and its practical significance. In: Proceedings 1st Int Conf on Soil Mech & Found Engng, pp 60-64.

Chandler RJ (1999) Clay sediments in depositional basins: the geotechnical cycle. Quart J of Engng Geol & Hydrogeology. 33: 7-39.

Dineen K (1997) The influence of soil suction on compressibility and swelling. Ph.D. Thesis, Imperial College of Science, Technology and Medicine, University of London.

Kavvadas MJ, Anagnostopoulos AG, Georgiannou VN, Bardanis ME (2002) Characterisation and engineering properties of the Corinth marl. In: Tan et al (eds) Proceedings Int Workshop 'Characterisation and Engineering Properties of Natural Soils'. AA Balkema Publishers, pp 1435-1459.

Kavvadas M, Anagnostopoulos AG, Kalteziotis N (1993) A framework for the mechanical behaviour of the cemented Corinth marl. In: Proceedings Int Symp on Hard Soils - Soft Rocks, Athens, Greece, pp 577-583.

Behaviour of unsaturated cohesive soils subjected to cyclic loads

T. Becker[1] and T. Li[2]

[1] University of Kaiserslautern, Germany, Department of Soil Mechanics and Foundation Engineering `beckerth@rhrk.uni-kl.de`
[2] Northern Jiaotong University, China, Institut of Tunnel and Geotechnical Engineering `taoli@center.njtu.edu.cn`

1 Introduction

Cyclic or alternating load impact provoked e.g. by wind or traffic loads is one of the most important types of soils strains. Beside this mechanical impact, unsaturated soils are sometimes subjected to cyclic loads as a result of changing pore water pressures by infiltration or evapotranspiration. Therefore, it is necessary to distinguish between the mechanical and the hydraulic cyclic load impact on unsaturated soils.

In contrast to saturated cohesive soils, the behaviour of unsaturated cohesive soils subjected to mechanical induced cyclic loads is similar to the one of non-cohesive soils. In some cases, the result of the ongoing alternating load effect is not an increase, or more generally said, a significant change of the pore water pressure resp. the matric suction, but rather an increase in the stiffness of the soils skeleton below a critical stress state depending on the number of load cycles. This effect is typically known as the cyclic shakedown in sands, i.e. the decrease of plastic strain increments when approaching the elastic state and is also called the 'ratcheting-effect', especially for metallic materials.

Besides the mentioned number of load cycles, the plastic deformation of cohesive soils depends on the stress state as well as the initial void ratio, the initial degree of saturation, the load frequency and the cyclic load amplitude. Most importantly, the impact of matric suction concerning the 'ratcheting-effect' is not yet clearly clarified for unsaturated soils. Systematic cyclic triaxial tests and oedometric compression tests are carried out on a remoulded cohesive soil to evaluate the influences on matric suction and the degree of saturation on the plastic deformations. The results of these investigations yield to a constitutive relation based on an elastoplastic two-surface model developed by Li [7].

2 Experimental investigations

In order to ensure good specimen reproducibility, an artificial soil is used for the laboratory tests. The model mixture is characterized as a silty soil

containing 97 % stone powder from a phorphyrite and 3 % Na-Bentonite and thus covers a wide range of geotechnical applications. Because of the homogenous grain size distribution of the stone powder in combination with the bentonite, the mixture comprises a constant plasticity and is extremely suitable to simulate the conditions of a natural silt without any significant variations in it's physical composition. The non-swelling behaviour and in particular, the sensitivity of the pore pressure to the void ratio, have been considered by using this compound. Taking typical engineering applications into account, e.g. build-up of a dam or a footing ground, the tested specimens are produced with a compaction degree range of 95 % $\leq D_{pr} \leq$ 98 %.

The grain size distribution of the model soil is shown in Figure 1. More soil parameters are displayed in table 1.
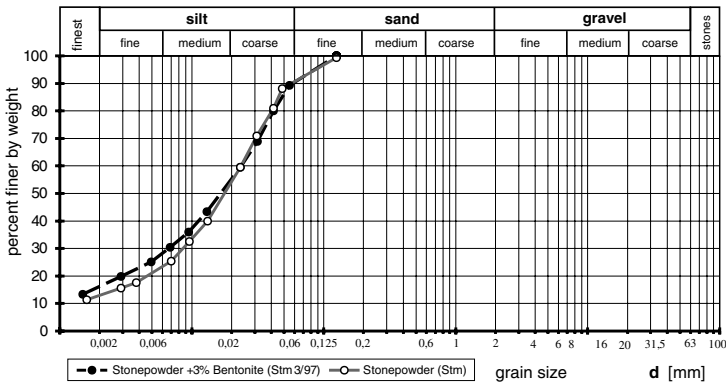

Fig. 1. Grain size distribution of the used soil mixture

The experimental investigations of the stress-strain behaviour are carried out with a triaxial cell for cylindrical soil specimens and an oedometric compression cell, both equipped with a small tip tensiometer. The triaxial cell furthermore consists of an independent two circuit load system for separate axial and radial loading of the soil specimen. The loads can be applied as isotropic and/or deviatoric total or effective stresses. The triaxial apparatus is modified in three parts: a) a tensiometer for measuring the matric suction inside the specimen, b) a load cell at the top of the specimen and c) an air pressure control system to apply excess pore air pressure to the specimen during the axis translation procedure. A detailed description of these modifications is given in [2]. Similar to the modifications of [14], the tensiometer is mounted inside the specimen to fit the special conditions of cyclic loading and to avoid contact problems between the ceramic tip of the tensiometer and the inner soil surface.

The applied excess pore air pressure is controlled by a pressure transducer in the air supply system and a second transducer at the bottom of the spec-

Table 1. Soil parameters, Stm 3/97

Parameter	value
optimum of dry density	1.81 t/m^3
optimum of water content	16.4 %
grain density	$2,65$ t/m^3
saturated hydraulic conductivity	$1 * 10^{-10}$ m/s
liquid limit	34 %
plasticity index	13 %
water absorption	56 %
compression index C_c ($S_r = 1$)	0.053
swelling index C_s ($S_r = 1$)	0.002
angle of internal friction φ	$22°$
cohesion c ($S_r = 1$)	10 kPa

imen in the pedestal. In combination with the axis translation method, the system is able to measure and control excess pore air pressure and matric suction up to $(u_a - u_w) \leq 285\ kPa$. The overall volume change of the soil specimen is measured by radial and axial applied LVDT's. The water volume change is taken into account by weighing the sample before and after loading outside of the cell. Cyclic loading is possible with frequencies $f \leq 0.1\ Hz$ in deviatoric tests and with $f \leq 1\ Hz$ in standard tests.

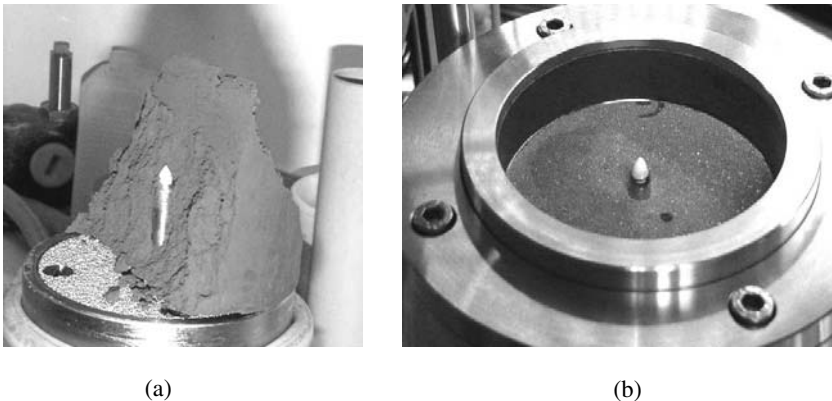(a)   (b)

Fig. 2. (a) Enlarged specimen with tensiometer after a triaxial test; (b) Bottom of oedometric compression cell with mounted tensiometer

The cylindrical specimens with a height of 12 cm and a diameter of 10 cm are statically compacted due to the anisotropic structure and water content distribution as a result of dynamic compaction, e.g. from proctor mode. Before being mounted on the pedestal, the sample is drilled in the center of the

bottom to install the tensiometer without rupturing the soil. The tensiometer itself is shielded by a stainless steel sleeve to provide mechanical impact to the acrylic glass tube. A tensiometer is installed in the exact same manner in the center of a conventional oedometric compression cell. The dimensions of the specimen measure 2 cm in height and 10 cm in diameter. Figure 2 shows a disturbed sample after a triaxial test with the contact zone of the tensiometer tip and the soil on the left side and a picture of oedemetric compression cell on the right.
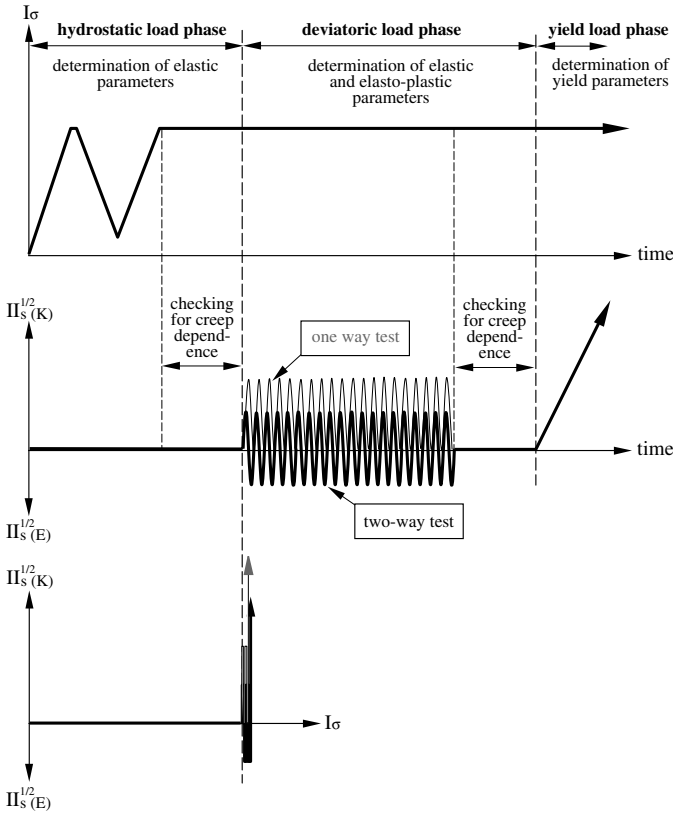

Fig. 3. One-way and two-way stress path during cyclic loading

The triaxial tests are carried out as drained cyclic one-way and two-way tests. In a one-way test there is no change in the main stress direction during cyclic loading, while in a two-way test, the main stress directions are alternating above and below the isotropic stress level. The regular stress path for a one-way test as well as for a two-way test is shown in Figure 3. The oedometric compression tests are performed according to the German standard

(DIN 18135, Entwurf 06/99) with two unloading/reloading stress paths at different stress levels.

3 Test results and Interpretation

Figure 4 shows the soil water characteristic curve (SWCC) for an absorption path. The measurement in the range of $0 \leq (-u_w) \leq 300$ kPa is performed with a tensiometer and the values in the range of 10^4 to 10^5 kPa are determined with the vacuum desiccator method, see [11].
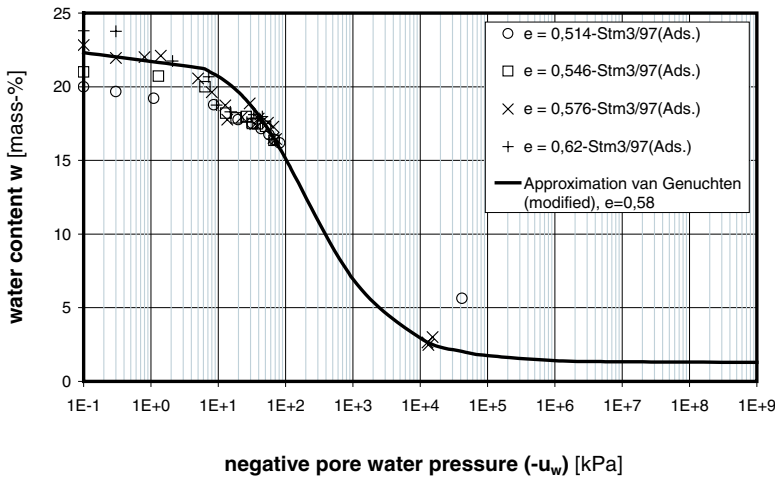

Fig. 4. Soil water characteristic curve (SWCC) for absorption paths of the used soil mixture approximated with *van Genuchten* according to Eq. 1

Van Genuchten's approximation [13] is modified for the mathematical formulation of the soil water and pressure relation in the following form

$$w = w_r - (w_s - w_r) \left[\frac{1}{\left[1 + (\alpha \ (-u_w))^{\sqrt{m}} \right]^m} \right], \tag{1}$$

with

w_r = residual water content for the maximum suction of the soil,
w_s = water content of the fully saturated soil,
α = constant form factor ($\alpha = 0.008$) for the investigated soils,
m = form parameter with respect to the void ratio,
$(-u_w)$ = negative pore water pressure for atmospheric conditions or the matric suction.

The form parameter m can be described in a very simple way as a linear function of the void ratio e.

The swell and compression index (C_s, C_c) can be determined for effective stresses from odeometric compression tests with respect to the matric suction resp. to the degree of saturation, considering Eq. 1 and the actual void ratio. Both parameters decrease as expected with increasing negative pore water pressure (Figure 5).
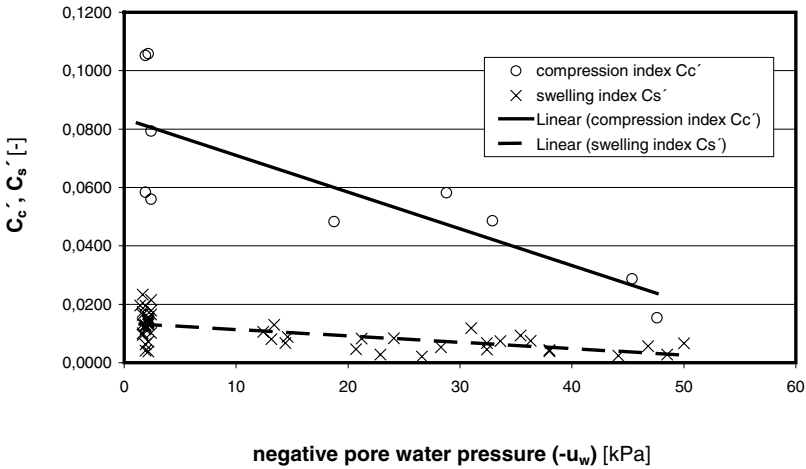

negative pore water pressure (-u$_w$) [kPa]

Fig. 5. Effective compression and swelling index depending on the soils suction

The evolution of the total deviatoric strains during the cyclic load phase is expressed for the axial as well as for the radial specimen direction in Figure 8. For initial load paths, the stiffness is defined with the initial shear modulus G_0. The ongoing load process due to the cyclic loading leads to a higher shear modulus G_1 for the first load cycles and subsequently to a degradation of the shear modulus (G_N) until the last load cycle is reached.

The degradation of the shear modulus is a function of the number of load cycles, the initial soil parameters (void ratio and degree of saturation) as well as the cyclic load amplitude. A simple expression is given with

$$G_N = G_1 N^b, \tag{2}$$

where N is the number of load cycles and b is a form factor with respect to the aforementioned parameters. For a constant value of the initial void ratio as well as for a constant stress amplitude, the parameter b is expressed in Figure 7 with respect to the negative pore water pressure.
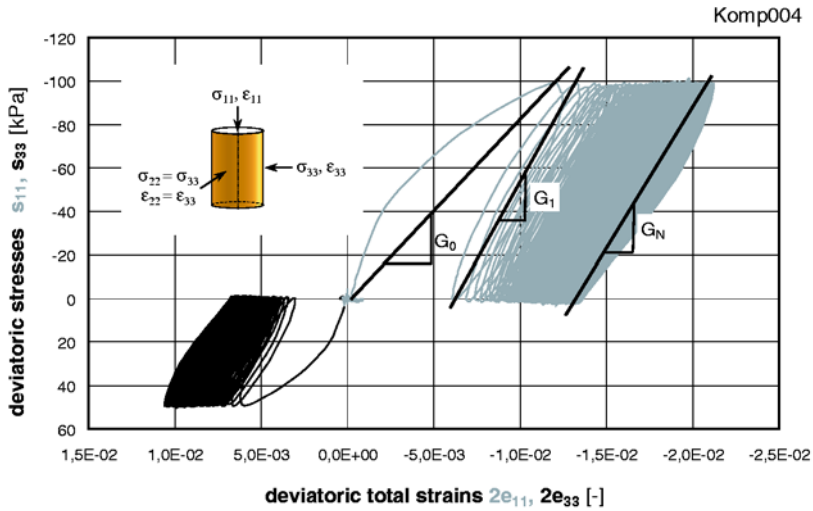
Fig. 6. Evolution of the total deviatoric strains in a drained one-way triaxial compression test

These results must be completed for other values of the initial void ratio and leads into the description of the plastic modulus in the constitutive relation (Section 4.4).
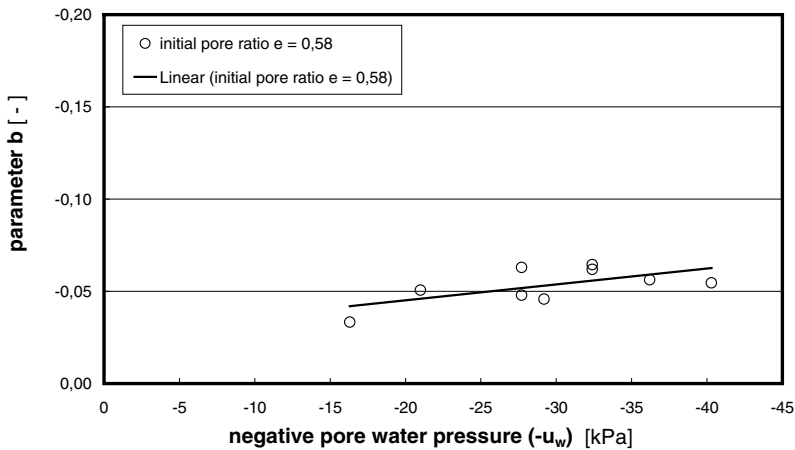

Fig. 7. Dependence of the parameter b on the negative pore water pressure u_w

Beside the shear modulus degradation, the soil behaviour shows a strain hardening, i.e. an increase in volumetric strains due to the cyclic loading. From the results in Figure 8 it can be seen that the total volumetric strains increase with the number of load cycles while the average value of the negative pore water pressure remains constant.
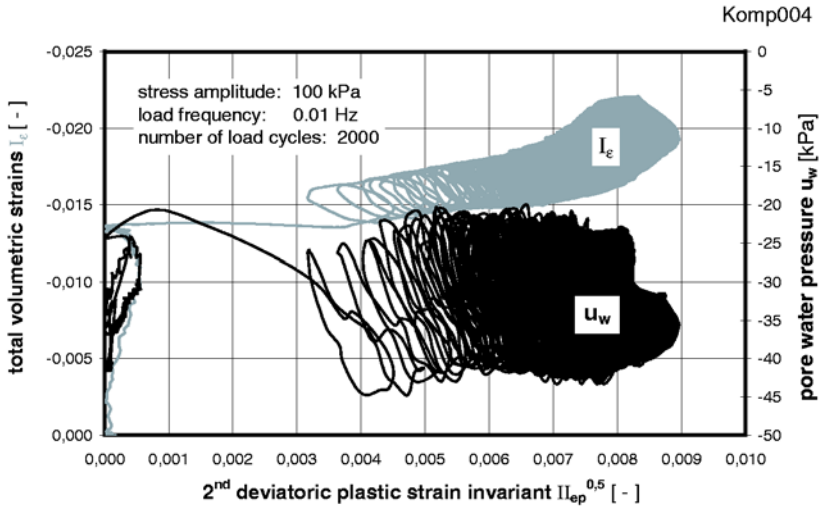

Fig. 8. Total volume change during isotropic and deviatoric stress path in a drained one-way compression test

Measurements of the water content before and after the cyclic load phase detected that there is no significant loss of water during the cyclic phase. An explanation for this behaviour is the alternating expansion and contraction of the pore volume in which the pore water is bound to the grain surfaces.

As a result of plastic deformation in the soil, the void ratio decreases and the degree of saturation increases simultaneously. In contrast to the behaviour of saturated cohesive soils, the pore water pressure in the unsaturated condition is not affected by the cyclic impact in the drained test even though the load frequency of the tests are 0.01 Hz, i.e. a load velocity of 120 kPa/min. Further investigations for undrained boundary conditions and other values of the initial void ratio are still pending for the moment.

4 Numerical modelling

4.1 Conceptual model

A two-surface model is used to describe the behaviour of such low plasticity cohesive soils under cyclic load impact. The model based on the work of Li [7, 8], who formulates the behaviour of Kaolinite for fully saturated and undrained soil conditions with respect to the bounding surface model [5, 6] and the modified Cam-Clay model [12]. Modifications of this model are carried out for the implementation of unsaturated behaviour and for drained conditions.
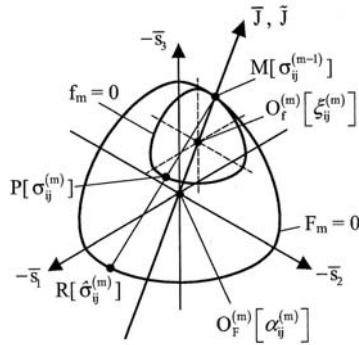
(a) section in deviatoric plane
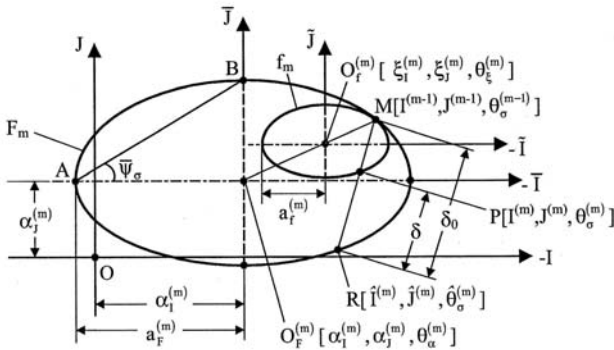
(b) section in I-J plane

Fig. 9. Boundary and loading surface of the two-surface model from [7]

The single load cycle is modelled considering the Masing rule [9] and each load reversal point in the stress space is defined as a memory center for the ongoing load path.

The bounding surface represents the isotropic prestress state and the inner loading surface the actual stress state and the stress direction, see Figure 9. The bounding surface is allowed to expand and the loading surface is allowed both to expand and to translate, considering a mixed hardening behaviour, i.e. a combination of isotropic and kinematic hardening.

The mathematical formulation takes place in the three dimensional stress space and is represented by a transformed stress tensors for the bounding surface as well as for the loading surface with respect to their centers. The stress state of the bounding surface is given by the stress tensors $\overline{\sigma}_{ij}$ and $\alpha_{ij}^{(m)}$, where $\alpha_{ij}^{(m)}$ is the shift tensor between the bounding surface center ($O_F^{(m)}$, see Figure 9) and the origin of the stress space (O)

$$\overline{\sigma}_{ij} = \sigma_{ij} - \alpha_{ij}^{(m)}; \qquad \alpha_{ij}^{(m)} = \beta_{ij}^{(m)} + \frac{1}{3}I_\alpha^{(m)}\delta_{ij}. \tag{3}$$

The index (m) identifies the actual number of load cycles. The associated invariants are given in [7]. Similar to $\overline{\sigma}_{ij}$ in Eq. 3, the stress tensor of the loading surface $\widetilde{\sigma}_{ij}$ describes the stress state with respect to its center ($O_f^{(m)}$, see Figure 9) and $\xi_{ij}^{(m)}$ is the assigned shift tensor.

The bounding surface is defined by Eq. 4 and the loading surface by Eq. 5. Both surfaces, which are proportional to each other, have an elliptical form in the I - J plane and their main axis are parallel.

$$F_m\left[\overline{\sigma}_{ij}, a_F^{(m)}\right] = \overline{I}^2 + \overline{r}^2\left(\overline{\theta}_\sigma\right)\overline{J}^2 - \left[a_F^{(m)}\right]^2 = 0, \tag{4}$$

$$f_m\left[\widetilde{\sigma}_{ij}, a_f^{(m)}\right] = \widetilde{I}^2 + \widetilde{r}^2\left(\widetilde{\theta}_\sigma\right)\widetilde{J}^2 - \left[a_f^{(m)}\right]^2 = 0, \tag{5}$$

where

$\overline{\sigma}_{ij}, \widetilde{\sigma}_{ij}$ = transformed stresses corresponding to the center of the boundary resp. the loading surface,

$\overline{I}, \widetilde{I}$ = 1st invariants of the transformed stress tensor corresponding to $\overline{\sigma}_{ij}, \widetilde{\sigma}_{ij}$,

$\overline{J}, \widetilde{J}$ = 2nd invariant of the transformed stress tensor corresponding to $\overline{\sigma}_{ij}, \widetilde{\sigma}_{ij}$,

$\overline{\theta}_\sigma, \widetilde{\theta}_\sigma$ = corresponding Lode angles in deviatoric planes,

$a_F^{(m)}, a_f^{(m)}$ = corresponding radius of the major axis of the Cam-Clay ellipse with respect to the number of load cycles m,

$\overline{r}, \widetilde{r}$ = relation of minor and major radius of the Cam-Clay ellipse.

The critical state is specified by the extended Mohr-Coulomb yield criterion for unsaturated soils. Thus, the parameters $\overline{r}$ and $\widetilde{r}$ are functions of the corresponding Lode angles θ_σ. An approach of Agryris et al. [1] is used to ensure a smooth transition of the yield function in the deviatoric plane.

4.2 Mixed hardening of the two-surface model

In accordance to the modified Cam-Clay model [12], the plastic volumetric deformation ϵ_v^p is the unique hardening parameter for the bounding surface, i.e.

$$a_F^{(m)} = \frac{da_F^{(m)}}{d\epsilon_v^p} d\epsilon_v^p. \tag{6}$$

The isotropic hardening of the bounding surface is then given by

$$a_F^{(m)} = a_F^{(0)} \exp\left\{\chi_0 \left[(\epsilon_v^p)_0 - (\epsilon_v^p)_m\right]\right\}; \qquad \chi_0 = \frac{1 + e_0}{C_c - C_s}, \tag{7}$$

in which $a_F^{(0)}$ is the prestress state of the soil, defined as

$$a_F^{(0)} = a_{Fi} \exp\left\{\chi_i \left[(\epsilon_v^p)_i - (\epsilon_v^p)_0\right]\right\}; \qquad a_{Fi} = \frac{c}{\tan\varphi}. \tag{8}$$

The parameter a_{Fi} represents the tension cut-off with respect to the effective cohesion c and the effective angle of internal friction φ of the soil. Taking the unsaturated conditions into account and considering a non shrinking behaviour, the model parameters C_c, C_s and c in Eq. 7 and 8 are defined with respect to the degree of saturation S_r.

Besides the isotropic loading, the bounding surface is also subjected to deviatoric loads depending on the actual stress state of the loading surface. That leads to a kinematic hardening formulation considering the shifting tensor of the loading surface. Hence, Equation 9 is based on the geometrical relationship of both similar surfaces, the bounding surface and the loading surface, and represents the center of the bounding surface with

$$\alpha_{ij}^{(m)} = \sigma_{ij}^{(m-1)} - \frac{a_F^{(m)}}{a_f^{(m-1)}} \left[\sigma_{ij}^{(m-1)} - \xi_{ij}^{(m-1)}\right]. \tag{9}$$

The Eq.s 7 and 9 together describe the isotropic and kinematic (mixed) hardening of the bounding surface in the general three dimensional stress space.

In the same way as Eq. 9 and with the assumption of no significant changes in the pore pressure during the cyclic loading (which is a result of the laboratory tests), the center of the loading surface is given by

$$\xi_{ij}^{(m)} = \sigma_{ij}^{(m-1)} - \frac{a_f^{(m)}}{a_f^{(m-1)}} \left[\sigma_{ij}^{(m-1)} - \xi_{ij}^{(m-1)}\right]. \tag{10}$$

To describe now the hardening of the loading surface, the memory center (point M, Figure 9) is used in the way of [5, 6]. It defines the contact point between the boundary and the loading surface. The stress reversal during the cyclic loading points towards the loading surface and tends to come into

contact with the opposite point of the loading surface (point P, Figure 9). Using a three dimensional radial mapping rule of this stress path, a new conjugating point (point R, Figure 9) exists on the bounding surface when extrapolating the stress path to this surface. As a result of the similar shape of both surfaces and with some geometrical and mathematical effort, described in [7], the stress tensor $\hat{\sigma}_{ij}^{(m)}$ of the conjugating point R can be denoted as

$$\hat{\sigma}_{ij}^{(m)} = \sigma_{ij}^{(m-1)} + \frac{a_F^{(m)}}{a_f^{(m)}} \left[\sigma_{ij}^{(m)} - \sigma_{ij}^{(m-1)} \right]. \tag{11}$$

The geometric relations between the points P, R and M in Figure 9 are a measure for the hardening of the loading surface during cyclic loading, expressed later on as the plastic modulus (see Section 4.4).

Other than the model parameters given in the Eq.s 7 and 8, all stresses mentioned above must be defined as effective stresses depending on the degree of saturation of the soil. To achieve this, Bishop's Equation [3] for atmospheric conditions is used

$$\sigma_{ij} = \sigma_{ij}^{tot} - S_r u_w \delta_{ij}, \tag{12}$$

where

$$\begin{aligned}
\sigma_{ij} &= \text{effective stress of the soil,} \\
\sigma_{ij}^{tot} &= \text{total stress,} \\
S_r &= \text{degree of saturation,} \\
u_w &= \text{pore water pressure.}
\end{aligned}$$

The negative pore water pressure of the unsaturated soil $u_w = f(e, S_r)$ can be easily obtained from laboratory tests from the SWCC (see Figure 4) providing a smooth transition between unsaturated and saturated conditions. The approximation of the SWCC (see section 3) is given by van Genuchten [13].

4.3 Constitutive relation for drained conditions

Based on the assumption of additive strain decomposition in kinematics, the total strain increment is given as

$$d\epsilon_{ij} = d\epsilon_{ij}^e + d\epsilon_{ij}^p, \tag{13}$$

where

$$\begin{aligned}
d\epsilon_{ij}^e &= \text{total elastic strain increment,} \\
d\epsilon_{ij}^p &= \text{total plastic strain increment.}
\end{aligned}$$

Considering Eq. 13, the general elastic stress-strain relation turns into

$$d\sigma_{ij} = [E] \left(d\epsilon_{ij} - d\epsilon_{ij}^p \right), \tag{14}$$

with $[E]$ being the elastic constitutive matrix. σ_{ij} is replaced by $\overline{\sigma}_{ij}$ for the bounding surface and by $\widetilde{\sigma}_{ij}$ for the loading surface. The elastic material response consists of a deviatoric as well as a volumetric part

$$d\epsilon_{ij}^e = de_{ij}^e + \frac{1}{3}d\epsilon_{kk}^e\delta_{ij} \tag{15}$$

and can be calculated from isotropic resp. deviatoric unloading and reloading stress paths in triaxial tests with

$$(a) \quad d\epsilon_{kk}^e = \frac{dI_\sigma}{3K_0}; \qquad (b) \quad de_{ij}^e = \frac{ds_{ij}}{2G_0}. \tag{16}$$

The initial bulk modulus K_0 and the initial shear modulus G_0 are determined for unsaturated conditions with respect to the degree of saturation S_r.

The total plastic strain increments can be separated in the same way as Eq. 15

$$d\epsilon_{ij}^p = de_{ij}^p + \frac{1}{3}d\epsilon_{kk}^p\delta_{ij}. \tag{17}$$

The general deviatoric plastic strain increments which are based on the normality condition and take some volumetric plastic deformations occurring from non-deviatoric incremental stress components into account, are given as

$$(a) \ de_{ij}^p = d\lambda\left(\frac{\partial f_m}{\partial s_{ij}} - \frac{1}{3}\frac{\partial f_m}{\partial s_{kk}}\delta_{ij}\right); \qquad (b) \ d\lambda = \frac{1}{h}\frac{\partial f_m}{\partial \sigma_{ij}}d\sigma_{ij}. \tag{18}$$

$d\lambda$ is a proportionality factor and $h = f(\sigma_{ij}, \epsilon_{ij}^p, m, S_r)$ is the so called plastic modulus. In accordance to Meißner [10], the volumetric plastic strain increments arising from the incremental isotropic stress paths are given by a volumetric flow rule with

$$d\epsilon_{kk}^p = dI_\epsilon^p = d\lambda \, D_L. \tag{19}$$

Taking the experimental results into account, that the average value of the pore water pressure remains constant, but plastic strains occur during the cyclic load phase, the parameter D_L can be taken to fit the drainage conditions during and after the cyclic load path. D_L is determined from triaxial tests (compressions tests as well as extension tests) under deviatoric conditions.

Now assuming an associated deviatoric flow rule for a cohesive soil, the second part in the brackets of Eq. 18(a) can be neglected and Eq. 17 together with the Eq. 18 and 19 leads to

$$d\epsilon_{ij}^p = \frac{1}{h}\frac{\partial f_m}{\partial \sigma_{ij}}d\sigma_{ij}\left[\frac{\partial f_m}{\partial s_{ij}} - D_L\frac{\delta_{ij}}{3}\right]. \tag{20}$$

Replacing Eq. 20 in Eq. 14 and rearranging them (e.g. in [4, 7, 10]) yields the general elasto-plastic incremental stress-strain relation for strain hardening and drained conditions

$$d\sigma_{ij} = [D] \ d\epsilon_{ij}, \tag{21}$$

with the elasto-plastic constitutive matrix

$$[D] = \left[[E] - \frac{[E] \frac{\partial f_m}{\partial \sigma_{ij}} [E] \left[\frac{\partial f_m}{\partial s_{ij}} - D_L \frac{\delta_{ij}}{3} \right]}{h + \frac{\partial f_m}{\partial \sigma_{ij}} [E] \left[\frac{\partial f_m}{\partial s_{ij}} - D_L \frac{\delta_{ij}}{3} \right]} \right]. \tag{22}$$

4.4 Plastic modulus of the bounding and the loading surface

The plastic modulus h in Eq. 22 describes the evolution of the incremental plastic deformations in the soil for all possible load paths (initial loading, loading, unloading and reloading). Both, bounding surface and loading surface are similar and of the same circumference for initial loading. In this case, the plastic modulus is defined by the hardening rule of the bounding surface considering the consistency condition

$$dF_m = \frac{\partial F_m}{\partial \overline{\sigma}_{ij}} d\overline{\sigma}_{ij} + \frac{\partial F_m}{\partial a_F^{(m)}} da_F^{(m)} = 0. \tag{23}$$

Also considering that F_m is a homogenous function in σ_{ij} and $\overline{\sigma}_{ij}$ for initial pure isotropic loading, which means that only normal stresses exist in the soil skeleton, the total plastic strain increment is given by

$$d\epsilon_{kk}^p = \frac{1}{H_m} \frac{\partial F_m}{\partial \overline{\sigma}_{ij}} d\sigma_{ij} \frac{\partial F_m}{\partial \overline{\sigma}_{kk}}. \tag{24}$$

Eq. 6 together with Eq. 24 in Eq. 23 and rearranging for H_m leads to the plastic modulus of the bounding surface

$$H_m = \left[\frac{\partial F_m}{\partial \overline{\sigma}_{ij}} \frac{\partial \alpha_{ij}^{(m)}}{\partial a_F^{(m)}} - \frac{\partial F_m}{\partial a_F^{(m)}} \right] \frac{\partial F_m}{\partial \epsilon_{kk}^p} \frac{\partial F_m}{\partial \overline{\sigma}_{kk}}. \tag{25}$$

Solving the derivations in Eq. 25 (e.g. in [7]) for $a_F^{(0)}$ resp. $a_F^{(m)}$, leads to the conditional equation for the plastic modulus of the bounding surface for initial loading H_0 and for ongoing loading events H_m.

Apart from the isotropic loading events, the plastic modulus of the loading surface is defined by the interpolation rule according to Section 4.2. The mathematical description depends on the distance between point P and its conjugating point R ($\delta = \overline{PR}$) as well as the distance between M and R ($\delta_0 = \overline{MR}$) in Figure 9.

The plastic modulus h_P at point P is then determined from a linear interpolation between the known values H_M and H_R, Figure 10. The geometrical relation is given in Eq. 26.

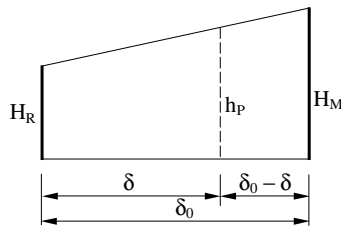$$h_P = H_R + (H_M - H_R)\frac{\delta_0 - \delta}{\delta_0}. \tag{26}$$

Fig. 10. Interpolation of the hardening modulus h_P by radial mapping of the known values H_M and H_R, notations according to Fig. 9

Again, from the similarity of both surfaces, the geometrical relations can be rearranged and the actual plastic modulus of the loading surface is denoted in a general form with respect to the number of load cycles as

$$h_m = H_m + (H_M - H_m)\left(1 - \frac{a_f^{(m)}}{a_F^{(m)}}\right)^\gamma.\tag{27}$$

H_m is the plastic modulus of the bounding surface from Eq. 25 and $H_M = (H_l; H_u; H_r)$ is the plastic modulus defined for loading (H_l), unloading (H_u) and reloading (H_r) during cyclic impact. Those modulus depending on the initial soil and stress parameters as well as the cyclic load parameters (frequency, the number of load cycles and the cyclic load amplitude). Furthermore, γ is a scalar form function that reflects the pseudo degradation of the shear stiffness depending on the total plastic deformations.

4.5 Verification

For the verification of the aforementioned model, the mathematical formulation is implemented by the user subroutine UMAT in the ABAQUS© finite element code. The numerical simulation of element tests as well as the solution of some boundary value problems associated to cyclic loadings in geotechnical engineering is still pending.

The quality of Li's basic model [7] is determined for saturated and undrained conditions in element test simulations for static and cyclic one-way and two-way tests. The results of both the measured as well as the simulated two-way test represented by the stress-strain relation and the excess pore water degradation are displayed in Figure 11.

As one can see, there is a good agreement between the simulation and the measurement regarding to the stress-strain relation (left side in Figure 11). The unloading and reloading paths show a realistic behaviour in accordance to the different values of the plastic modulus. Similar to this, the hysteresis loops of each load cycle are displayed with an appropriate comparability.
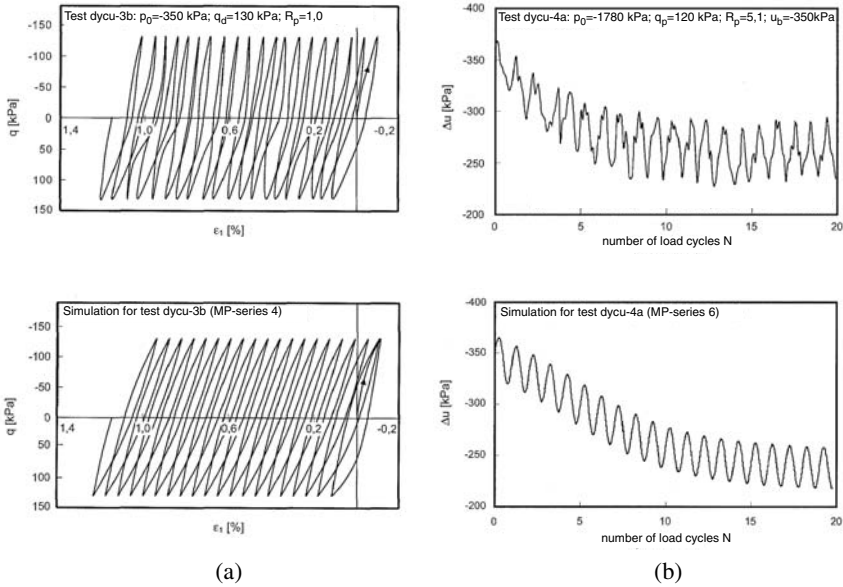
Fig. 11. Comparison between the measured (upper graphs) and simulated soils behaviour (lower graphs) for saturated conditions in an undrained two-way test: (a) deviatoric stress-strain curve; (b) excess pore water pressure changing with number of load cycle (OCR=5.1), from [7]

The changing of the excess pore water pressure is displayed on the right side of Figure 11 corresponding to the number of load cycles. The cyclic loading leads to a degradation of the excess pore water pressure, which is expected for an overconsolidated soil. The simulation also shows a good comparison to the measured behaviour.

5 Conclusion

Triaxial tests and oedometric compression tests are carried out to determine the pre- and post-behaviour as well as the behaviour during cyclic loading of unsaturated low plasticity cohesive soils. It can be deduced from the test results that on one hand, no significant changes in the pore water pressure occur for certain stress levels during the non-monotone load phase even though plastic deformations simultaneously arise with a decreasing void ratio. On the other hand and as a consequence of the unsaturated conditions of the soil, volumetric plastic deformations evolve from deviatoric stress paths.

Both effects are incorporated into an incremental two-surface cap model based on [7] and modified for unsaturated soils under drained conditions. The basic parameters of the Cam-Clay model ($e_i, C_s, C_c, \varphi, c$ and G) can be

identified from two series of standard triaxial and oedometric compressions tests with respect to the unsaturated conditions which contains unloading and reloading stress paths. The special parameters for the description of the hardening modulus are determined from cyclic triaxial tests. Due to the fact that the cyclic stiffness of the soil depends on the initial void ratio, the prestress state as well as the cyclic stress amplitude and the initial shear modulus, some laboratory effort is necessary to find the required parameters, most importantly for the dependence of the initial shear modulus on the pore pressure. Apart from this, the SWCC must be determined with respect to the void ratio of the soil.

The model includes the incremental volumetric plastic deformations during and after the cyclic load phase considering a dilation parameter D_L. The incremental plastic deformations in deviatoric load paths are described by the plastic modulus for all possible load cases (loading, unloading and reloading).

It can be stated for the saturated conditions that the model of Li [7] shows a good agreement with the laboratory test results. The verification for unsaturated conditions are still pending.

Acknowledgement

References

1. J.H. Argyris et al. Recent developments in finite element analysis of PCRV. 2nd *International Conference on SMIRT*, 1973. Berlin.
2. Th. Becker and H. Meißner. Direct suction measurement in cyclic triaxial test devices. *Proc. of 3rd Int. Conf. on Unsaturated Soils*, 2002. Recife, Brasil.
3. A. W. Bishop. The principle of effective stress. *Teknisk Ukeblad*, 106(39):859–863, 1959. Oslo, Norway.
4. W.F. Chen and E. Mizuno. *Nonlinear analysis in soil mechanics*. Elsivier, Netherlands, 1990.
5. Y.F. Dafalias and L.R. Herrmann. A bounding surface soil plasticity model. *International Symp. on Soils under Cyclic and Transient Loading*, pages 335–345, 1980. Swansea.
6. Y.F. Dafalias and L.R. Herrmann. Bounding surface plasticity ii: Application to isotropic cohesive soils. *Journal of Engineering Mechanics, ASCE*, 112(12):1263–1291, 1986.
7. T. Li. *Zweiflächen-Stoffmodell für wassergesättigte bindige Böden unter zyklischer Beanspruchung*. Dissertation, Universität Kaiserslautern, Fachgebiet Bodenmechanik und Grundbau, 2002. 183 Seiten.
8. T. Li and H. Meißner. Two-surface plasticity model for cyclic undrained behavior of clays. *Journal of Geotechnical and Geoenvironmental Engineering, ASCE*, 128(7):613–623, 2002.

9. G. Masing. Eigenspannungen und verfestigung beim messing. In *Proc. snd Int. Conf. for Applied Mechanics*, pages 332–335, Zürich, Switzerland, 1926.

10. H. Meißner. *Tragverhalten axial oder horizontal belasteter Bohrpfähle in körnigen Böden.* Veröffentlichungen des institutes für bodenmechanik und felsmechanik der universität fridericiana in karlsruhe, heft 93, Universität Karlsruhe, Karlsruhe, 1983.

11. H. Meißner and S. Wendling. Soil water suction and compaction influence on desiccation cracks of mineral liners. *Proc. of Int. Symp. on Suction, Swelling, Permeability and Structure of Clays*, 2001. Shizuoka, Japan.

12. A. Schofield and P. Wroth. *Critical State Soil Mechanics.* Mc Graw Hill, Cambrigde, London, 1968.

13. M. Th. van Genuchten. A closed-form equation for predicting the hydraulic conductivity of unsaturated soils. *Soil Sci. Soc. Am.*, (44):892–898, 1980.

14. S. Zakowicz and K. Garbulewski. Modification of triaxial apparatus for prediction of dam core behavior. *Proc. of 2nd Conf. on Unsaturated Soils*, 2:585–590, 1995. Paris.

Remarks on consolidation in unsaturated soils from experimental results

Ernesto Ausilio and Enrico Conte

Dipartimento di Difesa del Suolo, Università della Calabria, Cosenza, Italy

Abstract.

This paper presents the experimental results from several conventional oedometer tests conducted on compacted and unsaturated soils. Soil samples of medium plasticity, but with different grain size distribution and degree of saturation were tested. Some of these tests were interrupted before consolidation was achieved, and the water content of the soil was measured both before and after each test. The results point out that the recorded time-settlement curves consist of two distinct stages that are characterized by a different settlement rate. The early stage should essentially be ascribed to the faster dissipation of air pressure, while the final stage should be caused by the gradual expulsion of water from the soil. The results are also analysed using Terzaghi's theory [1] in order to ascertain whether this theory is suited to simulating the time-histories of settlement recorded during the tests.

Introduction

The consolidation of cohesive soils as the result of dissipation of excess pore pressures generated by external loading is a problem of considerable concern for geotechnical engineers. In 1925, Terzaghi [1] presented a simple theory for the analysis of one-dimensional consolidation in saturated soils, which is still widely used in practice. This theory should in principle be unsuitable to describe the consolidation processes occurring in unsaturated soils that fundamentally consist of a solid phase and two fluid phases: air and water.

In the last few decades, nevertheless, there has been a considerable improvement in the understanding of the behaviour of unsaturated soils. As a result, theoretical as well as experimental studies [2, 3, 4] have been conducted in order to analyse consolidation in such soils. As first pointed out by Barden [5], three different classes of behaviour may be singled out on the basis of the continuity of the fluid phases: for very high values of the degree of saturation of the soil, the water phase is continuous and the air phase is discontinuous; for lower values of the degree of saturation, both the air phase and water phase may be considered as continuous; finally, when the degree of saturation is low, the air phase is continuous and the water phase is discontinuous. Consolidation should be analysed using a

specific approach for each of the above classes. For example, when the soil is close to saturation, the air contained in the pores is occluded and cannot flow as a continuous fluid. In these circumstances, the air bubbles and pore water behave as a homogeneous compressible fluid flowing under water pressure gradients. As a result, the case of occluded air may be analysed using essentially the same formulation as for saturated soils provided that the pore fluid is assumed to be compressible [6]. For lower values of the degree of saturation, consolidation analysis is more complex because air and water may flow simultaneously and separately through the soil. A general formulation for one-dimensional consolidation in which the air and water phases are assumed to be continuous was, almost at the same time, presented by Fredlund and Hasan [7], and Lloret and Alonso [8]. This formulation is based on two continuity equations, one for the water phase and one for the air phase, which have to be solved simultaneously to give water and air pressures at any time and elevation. In the method developed by Fredlund and Hasan [7], the constitutive relations proposed by Fredlund and Morgenstern [9] were incorporated. Lloret and Alonso [8], on the contrary, used appropriate state surfaces to describe the mechanical behaviour of the soil. Ausilio and Conte [10] showed that the solution for one-dimensional consolidation may also be expressed in terms of the degree of settlement and the average degree of consolidation for the water phase and air phase, and derived a simple equation relating these dimensionless parameters. Afterwards, Ausilio et al. [11] also showed that when pore-air pressure undergoes an instantaneous dissipation or when excess pore-air induced by loading may be neglected, Terzaghi's theory [1] provides a good approximation to the degree of consolidation for unsaturated soils.

The main purpose of this study is to point out some features of consolidation in unsaturated soils caused by external loading. The study is based on the experimental results from several conventional oedometer tests conducted on soil samples dynamically compacted using the standard Proctor procedure. Moreover, the experimental results are analysed using Terzaghi's theory in order to ascertain whether this theory could be used, for practical purposes, to predict the settlement rate of foundations on unsaturated soils in situations more general than those considered by Ausilio et al. [11].

Soil properties

The tests were conducted on two materials that are herein indicated as soil A and soil B, respectively. Specifically, soil A is a silt with sand and clay, while soil B is a silty, clayey sand. The index properties of these soils are summarized in table 1. According to Atterberg limits and Casagrande's classification, both soils may be classified as inorganic clays of medium plasticity; activity is about unity. The organic content was about 1%. Samples of both soils were artificially prepared and compacted at optimum water content according to the standard Proctor procedure. This procedure was used in order to reproduce soils with relatively high permeability and compressibility. The average physical properties of the compacted ma-

terial are given in table 2. After compaction, soil specimens were carefully trimmed and then were subjected to conventional oedometer tests.

Table 1. Index properties of the soils used in the tests.

Soil A		Soil B	
Grain size distribution:		Grain size distribution:	
Sand	28 %	Sand	61 %
Silt	43 %	Silt	21 %
Clay	29 %	Clay	18 %
Atterberg limits:		Atterberg limits:	
Liquid limit, w_L	48.4 %	Liquid limit, w_L	32.8 %
Plastic limit, w_P	20.8 %	Plastic limit, w_P	14.4 %
Plasticity index, PI	27.6 %	Plasticity index, PI	18.4 %
Specific gravity, G_s	2.60	Specific gravity, G_s	2.69

Table 2. Soil properties after compaction

Soil A		Soil B	
Optim. water content, w_{opt}	21 %	Optim. water content, w_{opt}	16 %
Degree of saturation, S	62 %	Degree of saturation, S	78 %
Void ratio, e	0.86	Void ratio, e	0.55

Experimental results

In order to perform an analysis of consolidation in unsaturated soils, several oedometer tests were carried out. In these tests, the soil specimen was not flooded, and each load was maintained for a much longer time than in conventional tests. Figures 1 and 2 show some typical time-settlement curves recorded during the tests in response to the application of loads with different magnitude. As can be observed, each experimental curve consists of two distinct stages that are pointed out in the figures as AB and BC, respectively. During the early stage, the settlement rate is faster than that measured during the subsequent stage, when in addition most of the settlement occurs.

In order to investigate this behaviour, further tests on specimens of both soil A and soil B were performed. These latter tests, however, were interrupted at different times before consolidation was achieved, as pointed out in Figs. 3 and 4. Both before and after each test, the water content, w, and degree of saturation, S, of the soil specimen were determined.
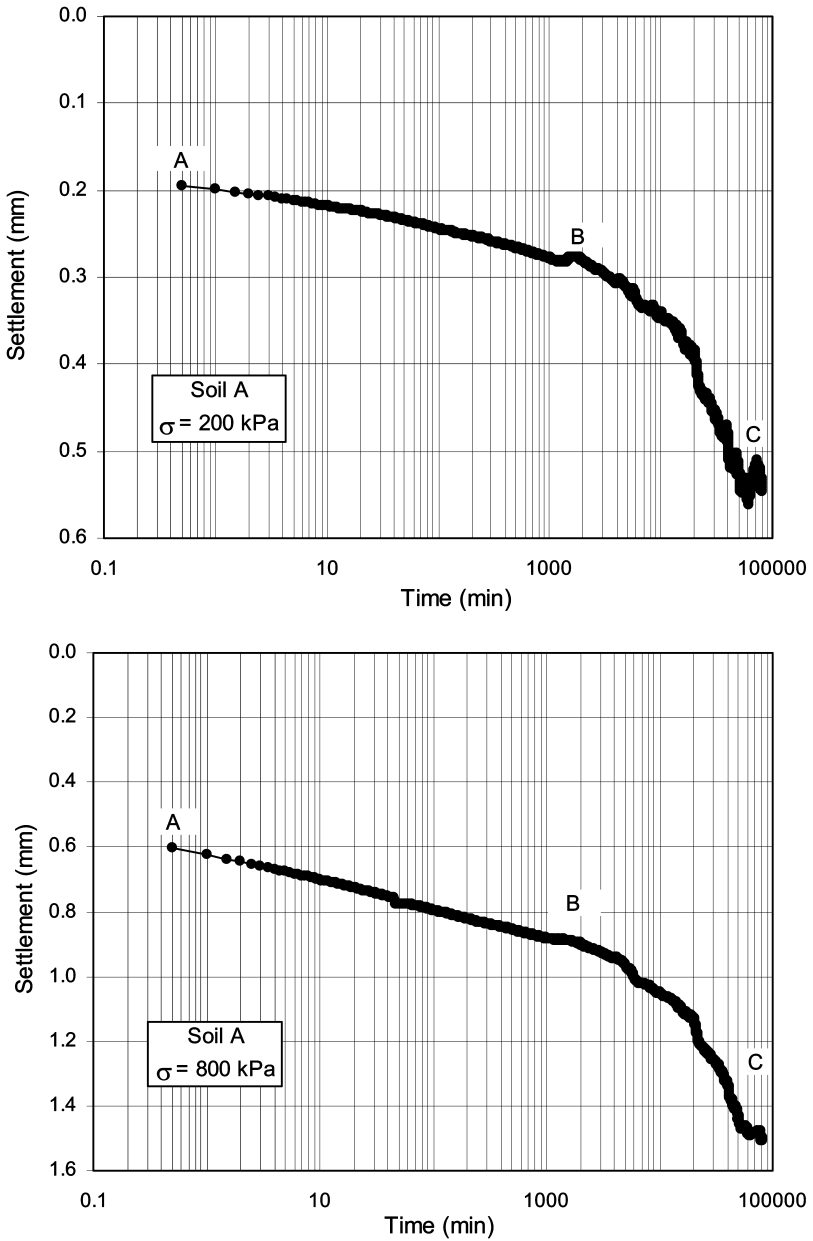
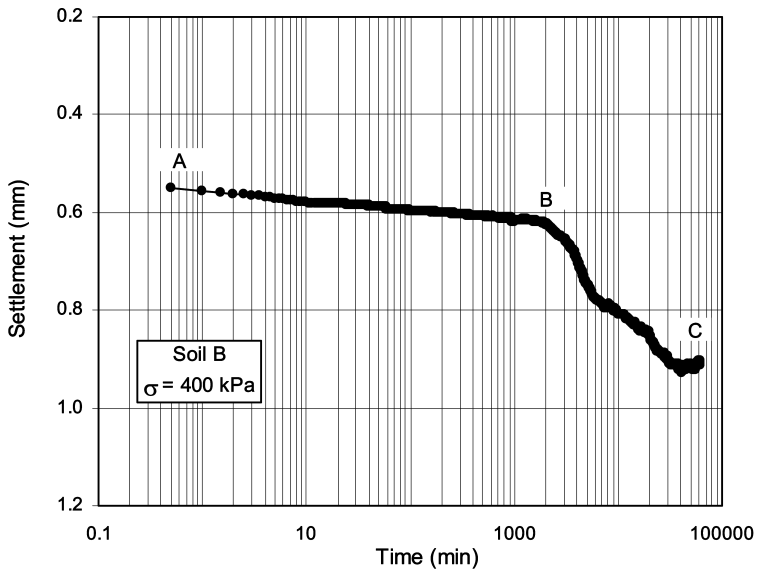**Fg. 1.** Typical time-settlement curves recorded during the tests on soil A.

Fig. 2. Typical time-settlement curve recorded during the tests on soils B.
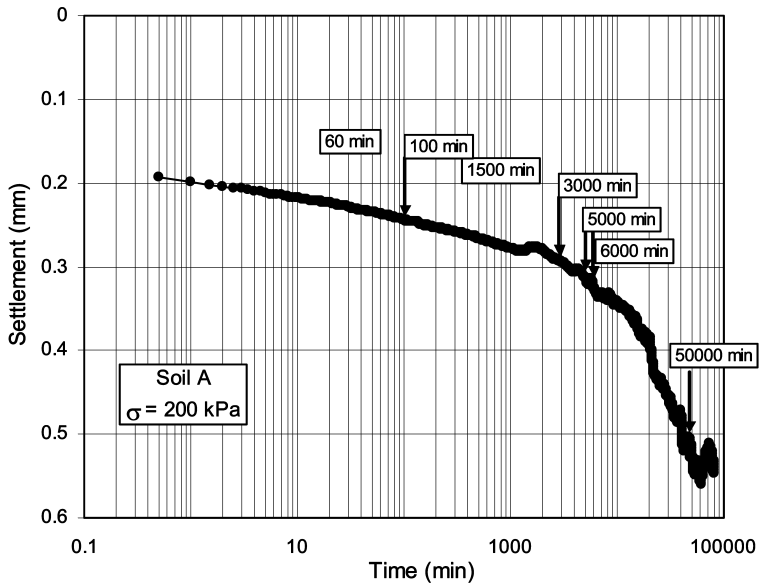

Fig. 3. The time-settlement curve recorded during a test on soil A, with indication of the time at which the other tests conducted on the same soil were interrupted.

Figures 5 and 6 show, respectively, the change in the water content, Δw, and degree of saturation, ΔS, with respect to their initial values (w_o, S_o), for all the tests carried out. As can be observed, the water content of the specimens of both soil A and soil B changes very slightly during the early stage of consolidation, and decreases markedly during the subsequent one (Fig. 5). This leads us to believe that the early stage of consolidation (AB) is essentially governed by the faster dissipation of air pressure than water pressure, while the final stage BC, when a gradual expulsion of water from the soil occurs, is due to the consequent dissipation of water pressure. Air pressure dissipation during the early stage should produce an increase in the net total stress, (σ-u_a), and a decrease in matric suction, (u_a-u_w), which are contrary effects on settlement. Moreover, the water pressure dissipation, while total stress and air pressure remain unchanged, should cause an increase in matric suction and consequently leads to a greater settlement during the final stage of consolidation. This physical interpretation is consonant with the change in degree of saturation found before and after the tests. As shown in Fig. 6, S slightly increases during stage AB whereas it significantly decreases during the final stage of consolidation. This again occurs both for soil A and soil B.

As a consequence of the above remarks, the experimental results are analysed using Terzaghi's theory [1], under the assumption that air and water flow separately and not simultaneously though the soil, during the above stages (AB and BC) of consolidation.
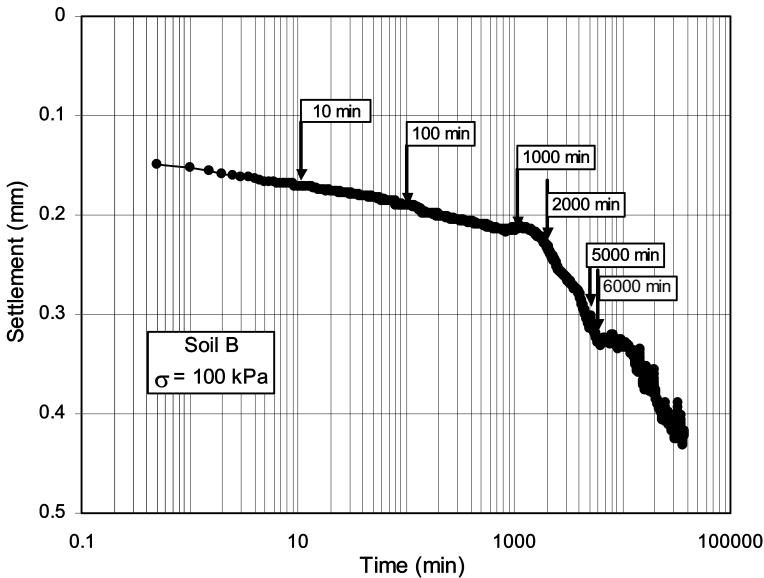

Fig. 4. The time-settlement curve recorded during a test on soil B, with indication of the time at which the other tests conducted on the same soil were interrupted.
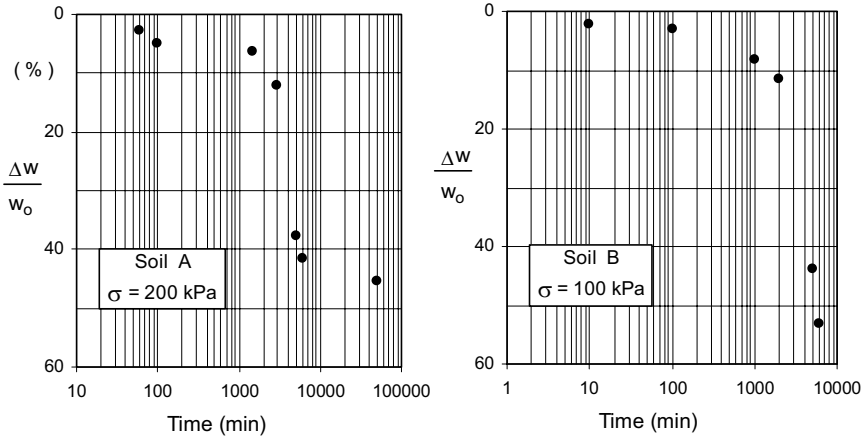
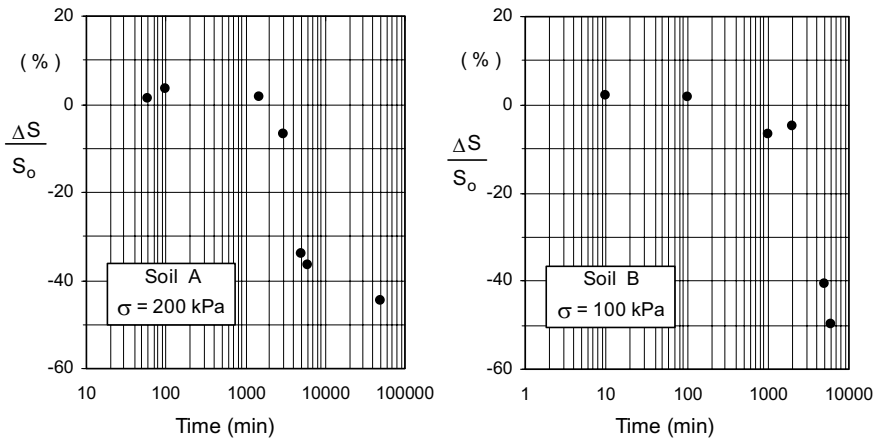**Fig. 5.** Change in water content before and after the tests.

Fig. 6. Change in degree of saturation before and after the tests.

Calculations were performed using a constant operative value of the coefficient of consolidation, c_v, for each stage. The value of c_v was chosen as that corresponding in Terzaghi's theory [1] to a degree of settlement of 50%. This latter parameter was calculated as the ratio of the settlement at a given time to the final settlement of the stage considered, after deducting the settlement recorded at the beginning of the same stage from both these values. Some comparisons of the experimental and theoretical values of settlement are shown in Figs. 7 and 8, where the values of c_v used in the calculations are also pointed out. As can be seen, the agreement between computed and measured results is fairly close.
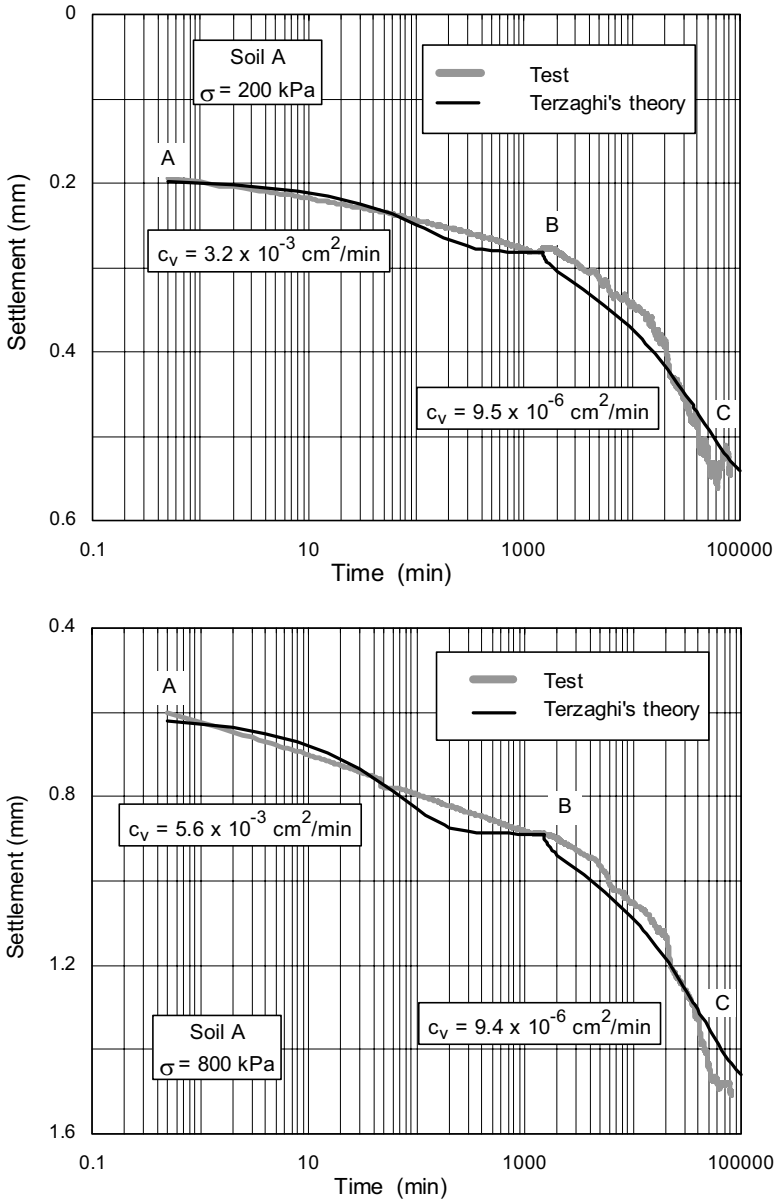
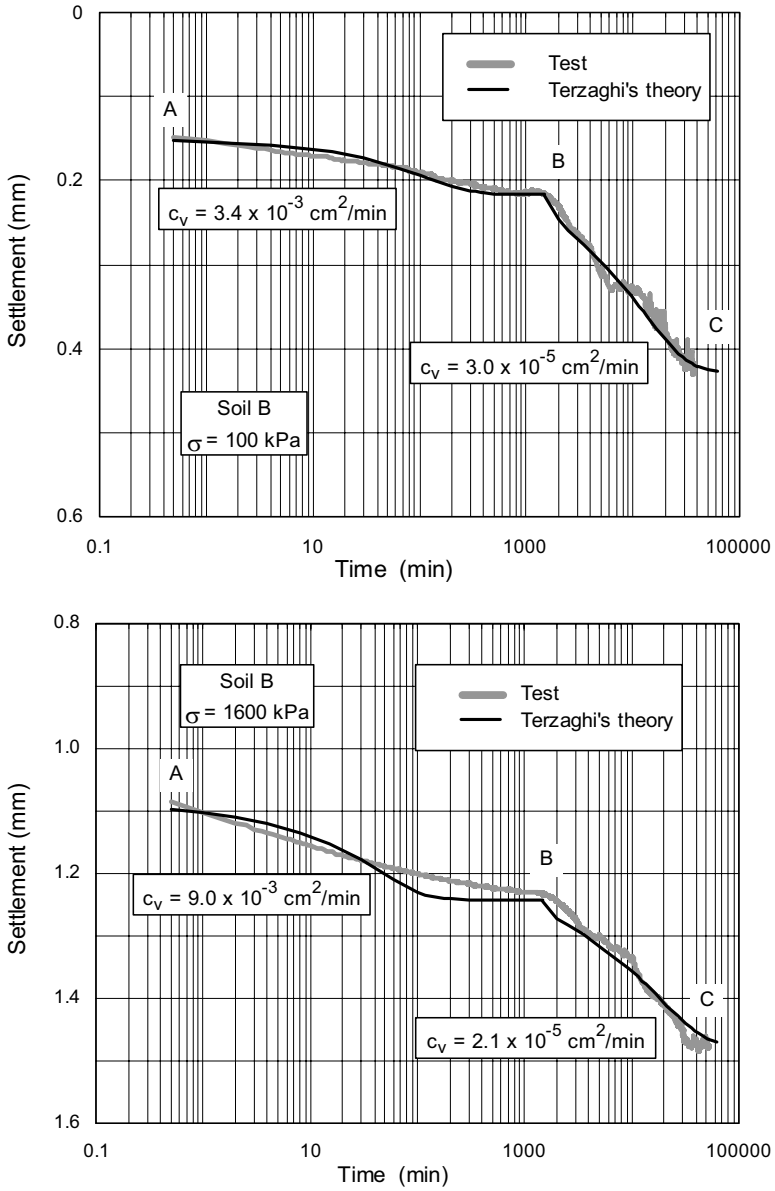**Fig. 7.** Simulation of some time-settlement curves recorded during the tests on soil A using Terzaghi's theory.

Fig. 8. Simulation of some time-settlement curves recorded during the tests on soil B using Terzaghi's theory.

Concluding remarks

Experimental results from conventional oedometer tests conducted on compacted and unsaturated soils have been presented. The results have pointed out that the time-settlement curves recorded during the tests consist of two distinct stages, which are characterized by a different settlement rate. The early stage should essentially be governed by the faster dissipation of air pressure, while the subsequent stage should be caused by the gradual dissipation of water pressure.

Moreover, it has been shown that Terzaghi's theory is suited to reasonably simulating the time-history of settlement recorded during both the above stages of consolidation.

References

[1] Terzaghi, K., Erdbaumechanik auf bodenphysikalischer Grundlage, Leipzig Deuticke, Vienna, 1925.
[2] Alonso, E. E., Gens, A., and Hight, D. W., General Report: special problem soils, Proc. European Conference on Soil Mechanics and Foundation Engineering 9, Dublin, Ireland, 1087-1146 (1987).
[3] Fredlund, D. G., and Rahardjo, R, Soil mechanics for unsaturated soils, John Wiley & Sons, New York, 1993.
[4] Rahardjo, H., and Fredlund, D. G., Experimental verification of the theory of consolidation for unsaturated soils, Canadian Geotechnical Journal 32, 749-766 (1995).
[5] Barden, L., Consolidation of compacted and unsaturated clays, Géotechnique 15, 267-286 (1965).
[6] Olson, R. E., State-of-the-art: consolidation testing, in Consolidation of soils, testing and evaluation (R. N. Yong and F. C. Townsend, Eds), American Society for Testing and Materials, ASTM STP 892, Philadelphia, 1986.
[7] Fredlund, D. G., and Hasan, J. U., One-dimensional consolidation theory: unsaturated soils, Canadian Geotechnical Journal 16, 521-531 (1979).
[8] Lloret, A., and Alonso, E. E., Consolidation of unsaturated soils including swelling and collapse behaviour, Géotechnique 30, 449-477 (1980).
[9] Fredlund, D. G., and Morgenstern, N. R., Constitutive relations for volume change in unsaturated soils, Canadian Geotechnical Journal 13, 386-396 (1976).
[10] Ausilio, E., and Conte, E., Settlement rate of foundations on unsaturated soils, Canadian Geotechnical Journal 36, 940-946 (1999).
[11] Ausilio, E., Conte, E., and Dente, G., An analysis of the consolidation of unsaturated soils, Proc. International Conference on Unsaturated Soils 3, Racife, Brazil, 239-243 (2002).

Prediction and modeling of tensile stresses and shrinkage

Thomas Baumgartl

Institute for Plant Nutrition and Soil Science, University of Kiel, Olshausenstrasse 40, 24118 Kiel

Abstract.
Volume change as a result of drying is often neglected in soil mechanics and soil hydrology, despite the important influence it has in the change of mechanical stability and water flow. Therefore, processes which lead to volume change have to be understood. Tensile stresses as the main parameter for shrinkage are a result of hydraulic and mechanical mechanisms in unsaturated soils or soil substrates. Both mechanisms have to be recognised as dependent processes. Unsaturated soils are defined as 3-phase systems. Capillary forces in soil pores act as contractive forces of the liquid phase on the solid phase. The resulting tensile stress caused by water increases with decreasing degree of water saturation. This causes shrinkage in a given soil volume, including soils with small plasticity. Mechanical stress parameters will simultaneously be changed with shrinkage, which as a result also change the hydrological parameters altering the pore system. The separation of the mechanical from the hydraulic stress is difficult. Therefore, a method was developed, which allows the determination of tensile stress under defined boundary conditions and is based on the general stress equation. Also a method is described by which this information is used for general modeling of volume change by hydraulic stress and general empirical functions used in hydraulic modeling.

Introduction

Definition of tensile stresses

Tensile stresses occur where adhesive and cohesive bondings exist. They are defined by the force per area, which has to be exerted to pull particles in opposite directions. When such bonds are broken at a maximum pulling force, a yield

strength or tensile strength will be reached. Tensile stresses can be distinguished in a mechanical and hydraulic stress. The latter defines stresses, which are caused by water menisci in a porous system. The occurrence of water menisci is, amongst other variables, mainly based on the surface tension of the liquid in the pore and the surface (repellency) properties of the pore. Both parameters control the curvature of the water menisci and thus the contractive force. In contrast to mechanical tensile stresses, hydraulic tensile stresses can be, in short term, very dynamic as a result of emptying or filling of a pore volume with a certain pore size distribution. Furthermore, due to the properties of liquid bodies, stresses are uniformly distributed within a water filled pore space with interconnected pores. Also, tensile stresses act through the water phase in an isotropic direction (neglecting the gravitational potential). Tensile stresses[1] occur in the 3-phase-system of unsaturated soils (solid-liquid-gas) as well as in quasi-saturated soils, i.e. in soil volumes, where at the boundaries of a porous volume water menisci can be detected.

Mathematically the stresses can be summarized according to the general stress equation of Terzaghi. The resulting effective stress is the sum of the mechanical and hydraulic stress. In the case of a 3-phase-system it results in the effective stress equation for unsaturated soils (Bishop, 1955), when air pressure is neglected:

$$\sigma' = \sigma - \chi \cdot u_w \qquad (1)$$

where σ' = effective stress; σ = total stress; χ = factor taking into account the degree of water saturation of the pores; u_w = neutral stress (= $-\Psi$: water potential)

The term $\chi \cdot u_w$ summarises the tensile (internal) stresses, which are responsible for volume change.

Using the concept of independent stress state variables for describing the total stress state, normal stresses can be defined by (Koolen & Kuipers, 1983; Fredlund & Rahardjio, 1993):

$$\underline{\acute{\mathbf{o}}} = \begin{bmatrix} \sigma_x & \tau_{xy} & \tau_{xz} \\ \tau_{xy} & \sigma_y & \tau_{yz} \\ \tau_{xz} & \tau_{yz} & \sigma_z \end{bmatrix} \qquad (2)$$

whereas the neutral stress is defined by

$$\underline{\mathbf{u}} = \begin{bmatrix} (u_a - u_w) & 0 & 0 \\ 0 & (u_a - u_w) & 0 \\ 0 & 0 & (u_a - u_w) \end{bmatrix} \qquad (3)$$

These stress state variables define the stress state more clearly than equation 1. However, for reasons of simplification the following concept is based on the prin

---

[1] In the following tensile stresses will be referred to as *hydraulic* tensile stresses.

ciple of the effective stress equation, which in this context can be assumed as valid.

Determination and calculation of tensile stress for constant volume

Generally, any increase or decrease of the tensile stress, which causes volume change, results in a change of the effective stress by an alteration of the orientation of the particles. With the dynamic change of the pore size distribution caused by each state of wetting and drying, the determination of the terms of the effective stress equation becomes difficult. Hence the mathematical calculation of the tensile stress as the product of χ and neutral stress is not based on constant boundary conditions. A possibility to solve this problem is to keep the volume constant, while the tensile stress changes. With the effective stress being constant:

$$d\sigma' = 0 \qquad (4)$$

According to the general stress equation, tensile stresses are defined by the product of water potential and χ-factor. The factor χ describes the stresses which are transmitted via the water phase. For saturated soils χ has to have a value of 1 to meet the effective stress equation of Terzaghi for saturated soils (2-phase-system solid-liquid). For completely dry soils this factor equals 0. In the literature this value is often defined as the degree of saturation, despite many discussions as to whether it represents a real value.

According to Richards (1966), stresses of the liquid/water phase have to be considered as the result of capillary effects and osmotic action. However, osmotic stresses do not appear in the equation describing the tensile stress. While the water menisci pull solid particles together, osmotic stresses act in the (opposite) direction to the surface of the solid phase (Fig. 1). The amount of water which coats the solid surface as a result of osmotic forces needs to be substracted from the total amount of water, which contributes to the tensile stress. This amount of water which is due to osmotic action is very much dependent on the total surface (i.e. texture) of the substrate and the chemical allocation on the surface. The volume of water which is influenced by adhesive stresses can be as high as 50% of the total water volume in saturated conditions (Waldron et al, 1961; Low, 1958). Only water which is not affected by these stresses can be considered as "free" water, which can form menisci and is able to create tensile stresses. The amount of this water corresponds with the relative water content of a soil. Therefore, χ can be approximated by the water content of soils rather than by the degree of saturation.

Using this information, equation (1) can be rewritten, using $u_w = \Psi$, to

$$-d\sigma = d(\Psi.\theta) \qquad (5)$$

where θ is the relative volumetric water content.

The same result is gained when using the stress state variables, when assuming that any stress caused by the matric potential is transmitted via the water phase. Based on the theoretical considerations given above, any change of the stress state
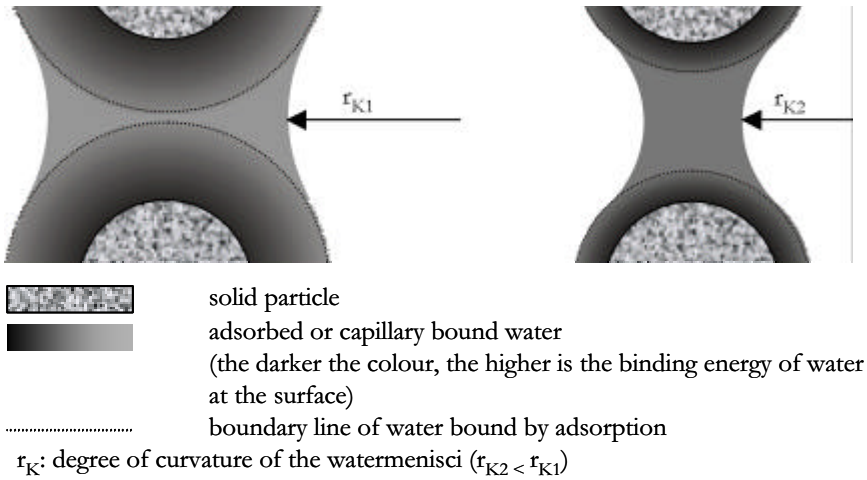
solid particle
adsorbed or capillary bound water
(the darker the colour, the higher is the binding energy of water at the surface)

.... boundary line of water bound by adsorption

r_K: degree of curvature of the watermenisci ($r_{K2} < r_{K1}$)

Fig. 1. Sketch of the adsorbed versus capillary water for different drying intensities

variable matric potential will result in an equivalent change of the total stress state. Rearrangement results in

$$\frac{-\,d\sigma}{d\psi} = \theta + \psi\,\frac{d\theta}{d\psi} \qquad (6)$$

Equation (6) describes the stresses which are caused by a change in the water matric potential by the water retention curve.

The objective of this study was to investigate whether a derivation of hydraulic parameters from the mechanical stress state by a change of the internal stress is possible and if the derived water retention curve can be validated by other means, e.g. inverse modeling of the water outflow curve.

Modeling of volume change due to tensile stress

In the case that tensile stress changes soil volume, the water retention curve which is based on a rigid pore system has to be adapted to the alteration of the pore size distribution. In order to achieve this, volume changes due to hydraulic stresses have to be included. Following the concept of Fredlund and Rahardjo (1993) or Toll (1995), who relate change of volume and moisture to each other, volume change can be modeled by the same kind of models like moisture change, e.g. by models used in hydrology which describe the water retention curve. Thus, volume changes due to mechanical stress can be considered equivalent to volume changes by hydraulic stresses. This allows a general possibility for modeling the dynamic of the water retention curve as a result of either the influence of mechanical or hydraulic stress. Using this concept, the shrinkage curve of a porous

system can be depicted by the combination of the water retention curve and the shrinkage-strain relationship, both based on the same stress state variable water potential.

A typical result is given in Fig. 2. A variety of different stages can be found for a shrinkage curve, which are described as structural shrinkage – normal shrinkage – residual shrinkage and zero shrinkage. Only in the case of normal shrinkage does the Δ moisture ratio = Δ void ratio. This range of shrinkage is usually explained by a volume reduction of saturated soils. If structural shrinkage can be defined, then moisture ratio decreases with no adequate reduction of void ratio. Often this behaviour is explained by the existence of a secondary pore system as a result of aggregate formation. This would also mean that shrinkage of a volume would eventually take place on different scales, namely the aggregate and the aggregated scale. However, structural shrinkage can also occur when the soil has been exposed to mechanical or hydraulic pre-stressing and no structural elements. Up to a certain pre-compression stress or pre-shrinkage stress, the pore system is stable in respect to mechanical or hydraulic stresses. Within this range of stresses, the tensile stress will only cause little shrinkage, because volume reduction will follow the elastic part of the stress-strain relationship. The behaviour of the shrinkage curve is in addition influenced also by mechanical stresses, which will in general regard only residual and zero shrinkage. The complete stress state of a porous systems can be well explained with such an analysis of volume change due to shrinkage at a given mechanical stress state (Groenevelt and Bolt, 1972).
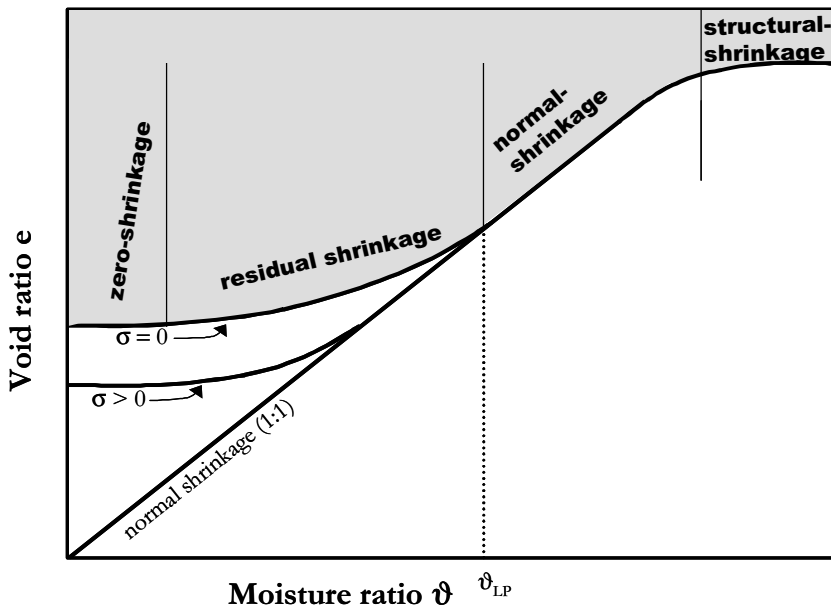

Fig. 2. Phases of the shrinkage characteristic of a structured soil

Methods and material

Determination and calculation of tensile stress at constant volume

In order to calculate the tensile stress for constant volume and to solve equation (6), an experimental design had to be developed, which allows to maintain a constant soil volume throughout any wetting and drying events. Only the knowledge of the total stress and the matric water potential are sufficient to solve equation (6) by iterative determination of the water retention curve which matches the slope of the total stress and matric water potential relationship. In order to calculate the tensile stress the total stress has to vary. this was achieved by using the swelling capacity of soils. Relatively dry soil with high swelling capacity was filled into a cylinder, which was closed on one end. The other end was placed onto a ceramic plate through which the soil was wetted and desiccated. When water is added to a relatively dry soil, the soil starts to swell. However in the test any extension of the soil volume was prevented by the metal cylinder. Swelling pressure build up due to wetting was measured by stress transducers which were attached horizontally (σ_3) and vertically (σ_1) in the centre of the metal cylinder. The soil sample was wetted via the ceramic plate until maximum saturation was reached. Desiccation by vacuum pressure resulted in water outflow, decrease of both the matric water potential and the swelling pressure. The difference between actual swelling pressure and maximum swelling pressure at saturation was equated to the tensile stress caused by the matric water potential acting via the liquid phase. Therefore

$$d\sigma_\tau = -d\sigma \tag{7}$$

where $d\sigma_\tau$ = tensile stress

Figure 3 shows the experimental setup. The dimensions of the metal cylinder were: height: 59mm; radius: 36mm. The ratio of axial an radial length was close to 1 and the soil sample. The soil was watered until saturation ($\Psi = 0$) followed by desiccation with shrinkage ceased. The derivation of the tensile stress could only be carried out as long as the swelling pressure > 0. Once the tensile stress reached a value of 0 no contact of the soil onto the cylinder wall could be proven and the soil was considered to be in the state of shrinking.

For reasons of validation of the water retention curve derived by the measurement of the tensile stress an additional test was performed with which the water retention curve was determined using the information of the change of the water matric potential with water content as a typical inverse model (outflow experiment). Both results of the water retention curve are compared.
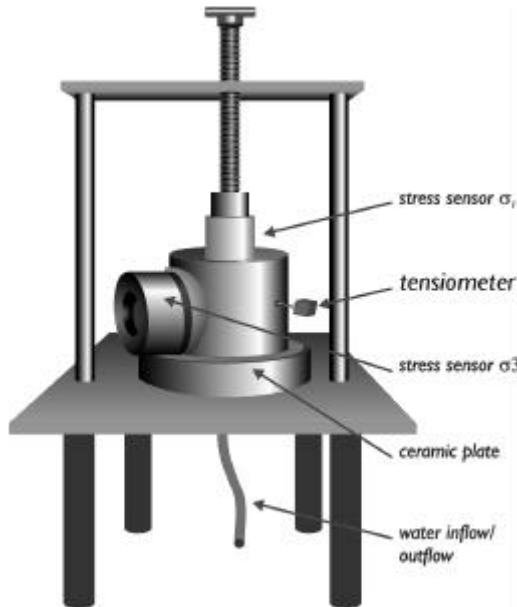
Fig. 3. Experimental setup for determination of tensile stress at constant volume

Modeling of volume change

Volume change was modeled using the hydraulic model of van Genuchten (1981). On the basis of one and the same model a set of parameters could be determined, for both, the water retention curve and shrinkage curve , which describe the water potential dependent emptying of water filled pores and the reduction of pores due to loss of volume, respectively. Based on this parameterisation, it is easily possible to create a shrinkage characteristic (equivalent to Fig. 2), by relating water content (moisture ratio) and volume loss (void ratio) to the same stress state variable water potential.

Material

In the experiments for determination of tensile stress at constant volume a soil substrate was used with a clay content of 42% (Griffith-clay, Australia). The soil was compacted to a bulk density of 1.36 g cm^{-3} with a water content of 10% g g^{-1}.

The volume change as a result of tensile stresses and decreasing water potential was determined at soil samples of the top soil of an agriculturally used field (Luvisol derived from Loess, Hildesheim, Germany)

Results

Determination and calculation of tensile stress at constant volume

Wetting of the soil through the ceramic plate created swelling pressure which was recorded as horizontal and vertical stress. The mean of both stresses of different directions was calculated by

$$\sigma_Q = (\sigma_1 + 2\sigma_3)/3 \qquad\qquad (8)$$

where σ_Q = swelling pressure

The soil was wetted until saturation and a maximum swelling pressure is reached. Thereafter the soil was desiccated by negative pressure in three steps (-25, -50 and -75 kPa). The application of a negative pressure causes reduction of the swelling pressure, matric water potential and water content (measured as water outflow) with decreasing vacuum pressures. At saturation the tensile stresses, which are caused by capillary action, are zero. With the decrease of the matric water potential the tensile stress increases while the swelling pressure decreases (Fig. 4). Using equation 6 the slope of this relationship can be modeled by fitting the data according to water retention curve. Integration enables the calculation of the tensile stresses. The calculations were pertained using the van Genuchten equation (van Genuchten, 1981). For the investigated stress range a very good correlation could be found (Fig. 4). The fitted pore size distribution, which is necessary to create tensile stresses, can be used to quantify stresses which are caused by capillary forces dependent on the water filled pore volume. The fitted pore size distribution is shown in Figure 5.

In order to validate the water retention curve obtained by using the dependence of the mechanical stress states from the matric water potential, the existing data set was used to calculate the water retention curve by inverse modeling (Simunek et al, 1998). Figure 5 shows the comparison of the results obtained. The water retention curves, which are derived on the basis of two different concepts (mechanical properties; hydraulic properties) are very similar in the range where no volume change occurs, i.e. down to water matric potentials of ca. -60 kPa in the example of Figure 5. Once the measured swelling pressure equals 0, volume reduction due to shrinkage begins. This will change the effective stress and the volume change as well as the change of the pore size distribution have to be included (Baumgartl, 2000).
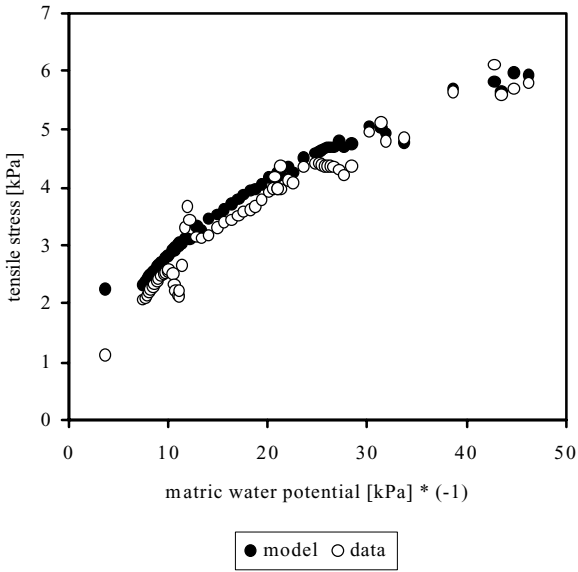
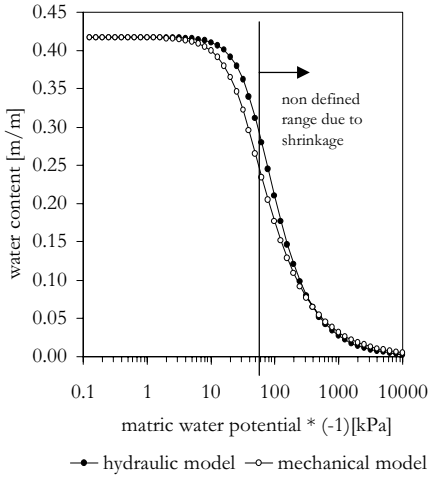Fig. 4. **Measured and modeled tensile stresses as a result of a change in water matric potential**

Fig. 5. **Modeled water retention curve based on measurements of swelling pressure (mechanical model) and water outflow curve (hydraulic model)**

Modeling of volume change

Fig. 6 shows an example of a reduction of void ratio with decreasing matric potential. At the same time the moisture ratio (i.e. the water retention curve) decreases, however, more intensively as pores are emptied of water and shrinkage cannot compensate the volume decrease. As long as the course of the two curves is parallel and the derivation is > 0, the soil will show normal shrinkage. When the air entry point of the water retention curve is not exceeded and the total volume does not change structural shrinkage can be defined. As for a stress-strain relationship a pre-consolidation value can be derived in the semi-logarithmic plot, for the shrinkage-strain relationship a pre-shrinkage stress can be defined, which is equivalent to the air-entry value of the water retention curve. In Fig. 6 this value would be around a stress (water potential) of ca. 10 hPa. Fig. 6 also shows that modeling of the volume change using the van Genuchten model fits very well the shrinkage data.

Relating moisture ratio and void ratio to the same stress state variable matric water potential results in the well known shrinkage curve. As is shown in Fig. 7 the data do not fit well at high moisture ratios, i.e. close to saturation. Using a bi-modal approach for modeling the water retention curve (see also fit of data of the moisture ratio at high matric water potentials), the fit of the shrinkage curve is significantly improved. A bi-modal pore size distribution is often used when structural elements or secondary pores have to be distinguished from textural (primary) pores. Modeling of moisture ratio and void ratio using the same (hydrological) model fits data very well and also is capable to reveal very clearly the mechanical behaviour of a soil.
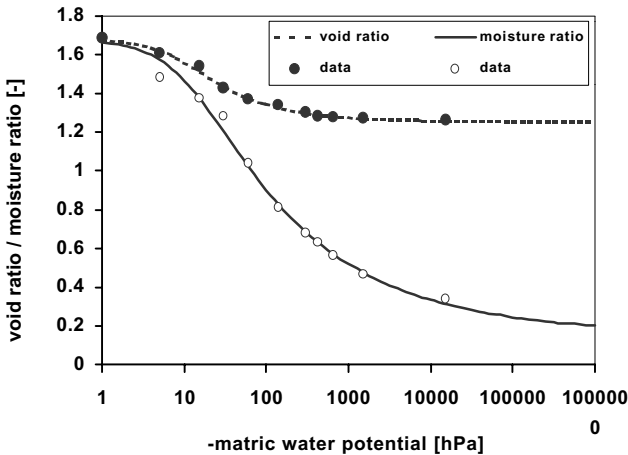

Fig. 6. Water retention and shrinkage curve described by moisture ratio and void ratio with decreasing water matric potential
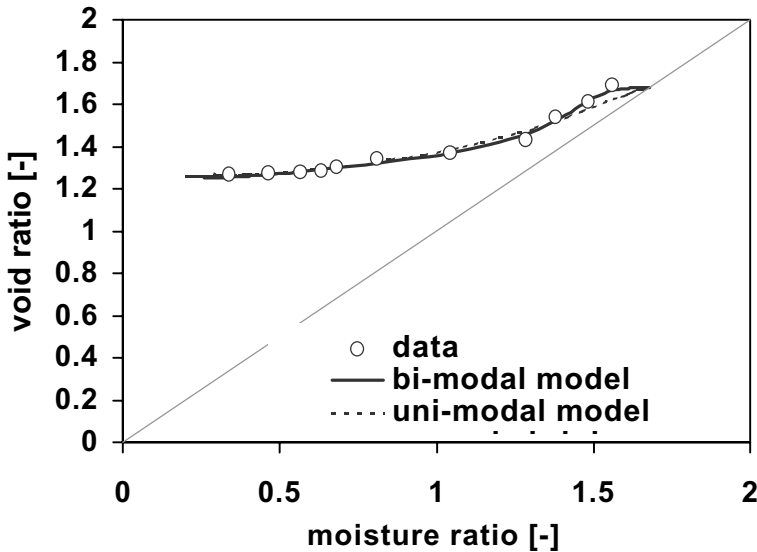
Fig. 7. Shrinkage characteristic of a top soil, modeled using a uni- and bi-modal pore size distribution

Conclusions

Mechanical and hydraulic stresses have to be considered as combined processes in case of changes of the stress state variables of the mechanical stress equation. This aspect is important when tensile stresses are determined. As each change of mechanical stress changes the hydraulic stress, pore size distributions cannot be considered as constant. Therefore, the measurement of tensile stresses, that are caused by water loss and shrinkage (hydraulic tensile stress), requires as a main precondition either the understanding of the dynamics of changes of the pore size distribution with drying or constant volume. In case of constant volume the water retention curve can be predicted by the stress state variable total stress and matric water potential. This may be of advantage in comparison of e.g. the inverse method, which is commonly used as this latter method relies on time dependent flow processes.

If tensile stresses cause a volume reduction, the course of the water retention curve is dynamic. Modeling shrinkage based on the stress state variable matric water potential, allows the combination of deformation and energy state of the bound water. For a known shrinkage characteristic the dynamic of the water retention curve can be considered easily.

The possibility to model (hydraulic) tensile stresses gives rise to the possibility to predict cracking of soils as a function of the mechanical properties. Nevertheless, the processes of the dynamics of the water retention curve have to be understood more clearly.

References

Baumgartl, T. and Horn, R. 1999. Influence of mechanical and hydraulic stresses on hydraulic properties of swelling soils. In: M.T. van Genuchten and F.J. Leij (Editors), *Characterization and measurement of the hydraulic properties of unsaturated porous media*. University of California, Riverside, California, pp. 449-458.

Baumgartl, T., Rostek, J. and Horn, R. 2000. Internal and external stresses affecting the water retention curve. In: R. Horn, J.J.H. van den Akker and J. Arvidsson (Editors), *Subsoil compaction. Distribution, Processes, consequences*. Advances in Geoecology. Catena Verlag, Reiskirchen, pp. 3-12.

Bishop, A.W. 1961. The measurement of pore pressure in the triaxial test. Pore pressure and suction in soils. Butterworths, London, pp. 38-46.

Fredlund, D.G. and Rahardjo, H. 1993. Soil mechanics for unsaturated soils. A. Wiley, New York

Groenevelt, P.H., and G.H. Bolt. 1972. Water retention in soils. Soil Sci. 113:238-245.

Low, P.F. 1958. Movement and equilibrium of water in soil systems as affected by soil-water forces. *High Res. Bd. Spec. Rept.*, No.40.: 55-63.

Matyas, E.L. and Radhakrishna, H.S. 1968. Volume change characteristics of partially saturated soils. *Geotechnique*, 18: 432-448.

Richards, B.G. 1966. The significance of moisture flow and equilibria in unsaturated soils in relation to the design of engineering structures built on shallow foundations in Australia*, Symp. on Permeability and Capillary*. Amer. Soc. Testing Materials, Atlantic City, NJ.

Simunek, J., van Genuchten, M.T. and Sejna, M., 1998. *Code for simulating the one-dimensional movement of water, heat and multiple solutes in variably saturated porous media.* US Salinity Laboratory, USDA, ARS, Riverside, CA, USA.

Toll, D. G. (1995): *A conceptual model for the drying and wetting of soil.* E. E. Alonso and P. Delage: First International Conference on unsaturated soil. Balkema, Rotterdam, Paris/France, 805-810.

van Genuchten, M.T. 1980. A closed-form equation for predicting the hydraulic conductivity of unsaturated soils. *Soil Sci. Soc. Am. J.*, 44: 892-898.

Waldron, L.J., McMurdie, J.L. and Vomocil, J.A. 1961. Water retention by capillary forces in an ideal soil. *Soil Sci. Soc. Am. Proc.*, 25: 265-267.

Tensile Strength of Compacted Clays

G. Heibrock[*], R.M. Zeh[#], and K.J. Witt[#]

[*]PHi Consult, Marburg, Germany
[#]Professorship of Foundation Engineering, Bauhaus-University Weimar, Germany

(E-mail: rainer.zeh@bauing.uni-weimar.de)

SYNOPSIS - The paper presents experimental results linking matric suction and tensile strength of compacted clays. Test results from a cohesive soil are presented and discussed with respect to the soil structure and the interaction of soil and water. It is assumed that two main groups of pores can be clearly identified in compacted clays; the pores between aggregates (interaggregate pores) and pores between particles (intraaggregate pores). Based on a description of soil-water-interaction an expected behaviour, describing tensile strength as a function of matric suction, is derived and compared with the experimental results. The laboratory test results indicate that there is a strong correlation between the pore size distribution (assessed by interpretation of the soil water characteristic curve SWCC) and the tensile strength of compacted soils. Furthermore, the test results are compared by using micro-mechanical considerations of the interaction between the skeleton of unsaturated soils (interparticle contact force) and by using numerical calculations with an elastic relationship.

1. Introduction

Tensile strength of soils is usually not taken into account when dealing with soil related problems. Generally it is accepted that soils are not capable of resisting significant tensile forces over a longer time and there is almost no information on the influence of creep on the tensile strength of fine grained, i.e. clay, soils. Thus, the focus of the paper is not to investigate the meaning of tensile strength from an engineering point of view, but from a soil mechanics perspective. The results of some relatively simple investigations may contribute somewhat to the understanding and discussion on the soil water interaction and its meaning for the behaviour of fine grained soils used as compacted clay liners in landfills.

2. Soil Structure and Soil Water Interaction

Since the early days of clay colloid chemistry investigations (Endell, 1941) it is known that the engineering properties of fine grained soils are closely related to the soil water interaction. Investigations indicated that the amount of water that is absorbed by fine soils correlates to many properties of the soil (e.g. swelling behaviour, shear strength, compressibility etc.).

Fig. 2.1a (modified from Nagaraj et al., 1990) shows a schematic drawing of the fabric (arrangement of particles) of a fine grained soil. This kind of fabric is somewhat characteristic for a clay soil compacted dry of optimum (Proctor curve). Groups of clay particles are tied together and form aggregates of a 2 - 10 µm size. Pores between these aggregates (called interaggregate pores) usually show sizes clearly above 0,1 µm (10^{-7} m). The number and the size of interaggregate pores depend on the type of compaction and the water content at compaction (and indirectly on the suction). Jasmud & Lagaly (1993) and Nagaraj et al. (1986) showed that soil water is not bonded by clay particle surface forces (diffuse double layer forces, see Fig. 2.1c) at distances larger than about 6 x 10^{-9} m to particle surfaces. Therefore, water trapped in interaggregate pores will be considered as capillary water. It is assumed that interaction of soil and water can be described by the capillary theory in these pores.

Depending on the clay type, pore fluid chemistry, the soil preparation and the water content, the particles forming an aggregate show face to face, edge to edge or edge to face orientation. Pores inside the aggregates will be called intraaggregate pores and usually show sizes clearly below 0,1 µm. The number and size of these pores is not significantly influenced by compaction but from interparticle forces (Fig 2.1b, modified from Mitchell, 1993). Water trapped in intraaggregate pores is influenced by particle surface forces and capillary forces.

A clay soil compacted wet of optimum (Proctor curve) will show low volumes of interaggregate pores. Nevertheless, boundaries between aggregates, which form mechanically weak points exist. Fig. 2.1a gives an idea on the sizes of the mentioned elements. Note that the numbers have been taken from different but few sources, and therefore should be considered as orientation values.

The simple model will be used to derive an idea of the development of tensile strength of a compacted clay soil as a function of the water content. Taking into account the described bimodal pore structure it is assumed that the overall tensile strength is determined by forces which can be transmitted from aggregate to aggregate – since the tensile strength of the aggregates themselves will obviously be higher. Therefore, tensile strength of a compacted clay could be described by the tensile strength of an equivalent soil consisting of particles of the same size and shape as the aggregates (considering that these particles will decrease in size at lower water contents) and therefore, the capillary theory may be used to describe the process of tensile strength as a function of the water content.

Fig. 2.2 (taken from Schubert, 1982) shows the development of tensile strength of lime-stone. Starting from nearly saturated conditions the tensile strength t equals capillary pressure p_k times saturation S (capillary range). When pores begin to desaturate, tensile forces have to be transmitted by water bridges between
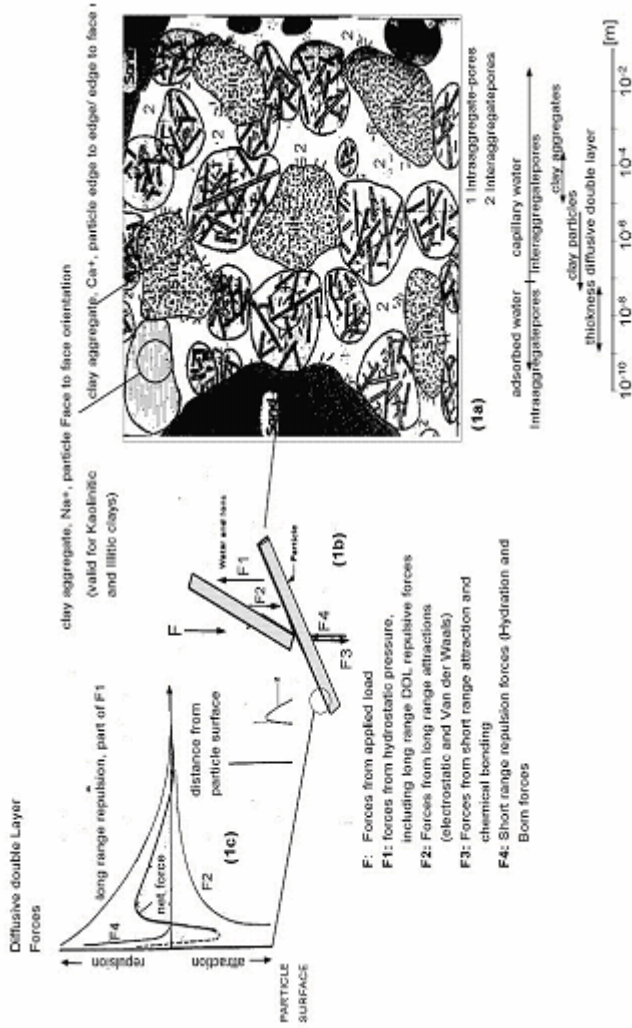
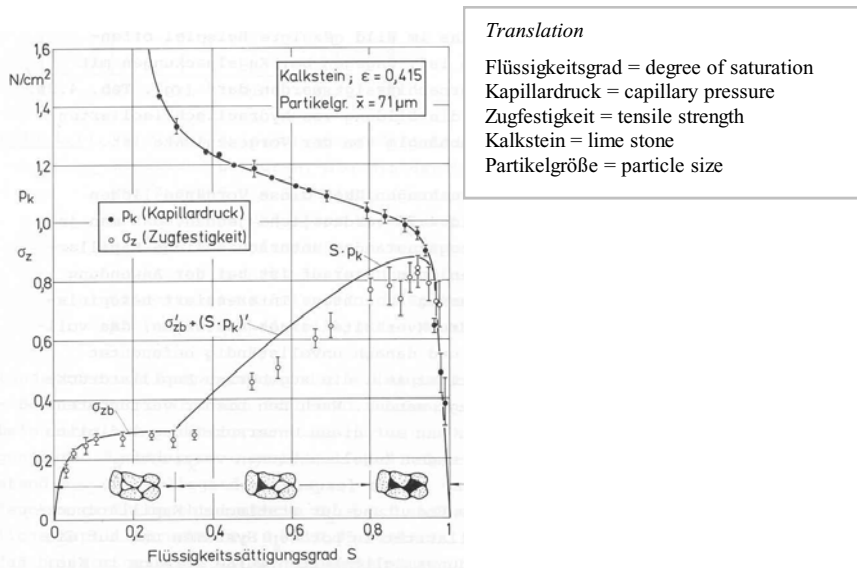**Fig. 2.1.** Fine grained soil fabric (schematic) and water (modified from Nagaraj et al., 1990)

Fig. 2.2. Tensile strength of a lime-stone (Schubert, 1982)

particles and still water filled pores. Schubert calls this stage the transition phase and he calculates the tensile strength as the sum of forces transmitted by water bridges σ_t and still saturated pores ($t = \sigma_t + (S \cdot p_k)$). When all pores have become desaturated the pendular state is reached and tensile strength is equal to σ_t.

Therefore, if we transfer this behaviour to compacted clay soils we should expect increasing tensile stresses with decreasing water contents reaching their maximum at a saturation of about 90 percent and decreasing tensile strength with further lowering of water contents.

3. Experimental Investigations

The following section describes sample preparation, the mode and results of direct tensile strength tests which were conducted by Brüggemann (1998). Furthermore, results are discussed with respect to the pore size distribution of the compacted soils assessed by interpretation of the soil water characteristic curve.

3.1 Sample Preparation and Test Procedure

Samples were Proctor compacted (3 layers compacted by 25 blows with 2,5 kg hammer) at optimum water content (e.g. 25,5 % gravimetric water content for the Kaolin samples). The sample of about 100 mm x 120 mm size was cut parallel to

the layer surfaces preparing samples from the upper, middle and lower part. Besides, the characteristic of the compaction differs over the height. Thus, differences in the soil structure and the tensile strength are expected for the samples (upper, middle and lower part). Each of the three samples is carefully trimmed using a wire-string creating three cylindrical samples of about 90 mm x 24 mm (height x diameter) size. At the end of this stage, the gravimetric water content of the samples is controlled by analysing soil residues from the trimming process. Water content losses up to 2% (related to the compaction stage) were observed. To investigate the influence of water content on tensile strength samples were air dried (at same conditions in a climatic chamber) or wetted (by spraying water on the sample surface, water content controlled by weighing the sample during the process). Subsequently, the samples were coated with wax to prevent further changes in the water content. In addition, the sample volume and hence the volumetric water content can be measured by dip-weighing. This is necessary to read the matric suction of the soil water characteristic curve measured separately from samples Proctor compacted at the same water content (middle part samples). The soil water characteristic curves were measured by Stoffregen (1997).

After wax coating the sample is stored in a climatic chamber for about 48 hours to ensure a homogeneous distribution of water in the sample. The final step is drilling bore holes of 8 mm diameter creating a hollow cylinder. A filter textile is placed in the centre of the sample, the right and left remaining part of the bore hole is filled with epoxy resin and two hooks are fastened with dowels placed in the bore holes. The reason for choosing the hollow-cylinder form is that maximum tensile stresses occur in the middle of the sample, and thus influences of 'spreading' forces to the sample are minimised (see results of elastic FE-calculations in section 4.3). Figure 3.1 shows a picture of the sample placed in the test device.

After carefully removing the wax coating the sample is placed in the test device (see Fig. 3.1) and is slowly torn apart ($\cong 0{,}06$ mm/min). Tests showed that lower velocities did not result in any changes in the measured tensile strength. During this process, tensile forces are measured. Fig 3.2 shows a typical test result. Tensile strength rises linearly with time as well as with strain until the sample rupture occurs. Axial tensile strength of the sample is defined as maximum tensile force measured during the test. Tensile strength is higher for samples taken from the lower part of the proctor sample indicating that compaction resulted in smaller interaggregate pores than in the middle and upper part of the proctor sample.
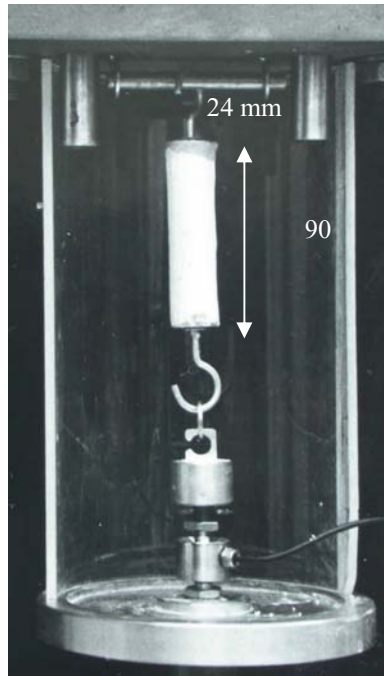
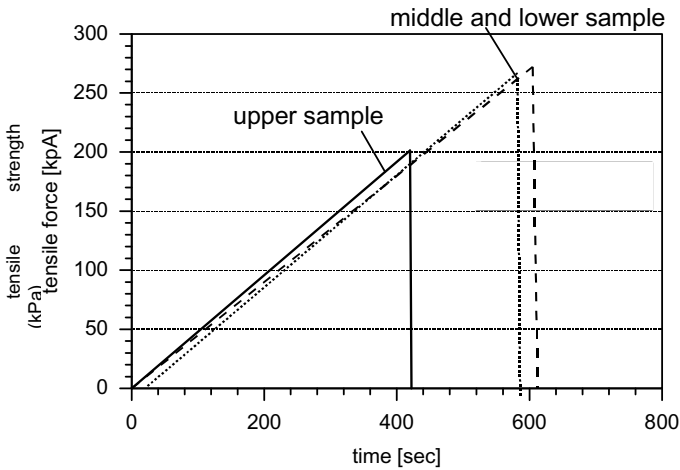**Fig 3.1.** Sample and tensile strength test device

Fig. 3.2. Typical test result of the direct tensile strength test (test at 20% water content)

3.2 Test Results

The tests were conducted at a medium plastic clay (Kaolin clay - 61 % clay, 39 % silt; Proctor density 1,55 g/cm³; Liquid limit 44,4 %, plastic limit 28,1%, shrinkage limit 25%, plasticity index 16,3 %, Proctor water content 25,5 %, activity 0,26). Figure 3.3 shows the parametrised soil water characteristic curve using a weighted sum of two Van-Genuchten functions (Durner, 1991):

$$\Theta = (\theta - \theta_r) / (\theta_s - \theta_r) = \sum w_i \, (1/(1 + \alpha \, (u_a - u_w))^{n_i})^{m_i} \qquad (3.1)$$

where $\qquad$ Θ: water saturation [-], θ: volumetric water content [-],
$\qquad\qquad$ θ_r: residual water content [-],
$\qquad\qquad$ θ_s: volumetric water content at saturation [-]
$\qquad\qquad$ w_i: weights [-]
$\qquad\qquad$ u_a: pore air pressure [kPa], u_w: pore water pressure [kPa]
$\qquad\qquad$ $u_a - u_w$: suction [kPa]
$\qquad\qquad$ m_i, n_i : parameters [-], α : skaling [1/kPa].

$d\Theta/d\log(u_a - u_w)$ describes the change in saturation with a change in suction. Therefore, if a change in suction corresponds to a relatively large change in saturation this means that many pores desaturate at the applied suction. Thus, the maximum of $d\Theta/d\log(u_a - u_w)$ gives the pore size which is most frequent (filling
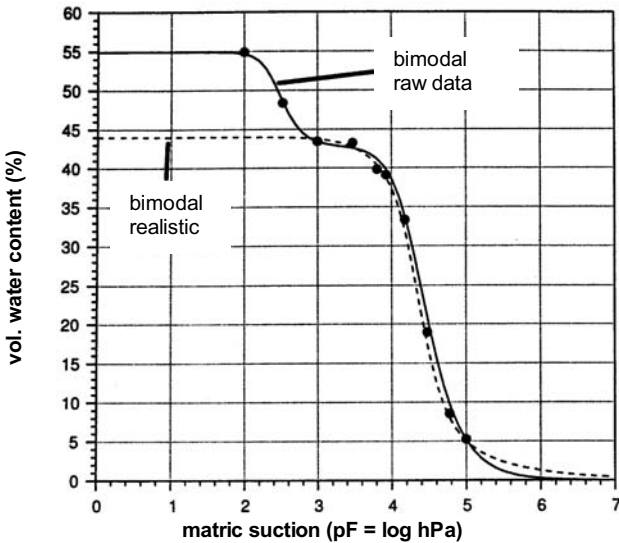

Fig. 3.3. Measured and parametrised soil water characteristic curve of Kaolin clay
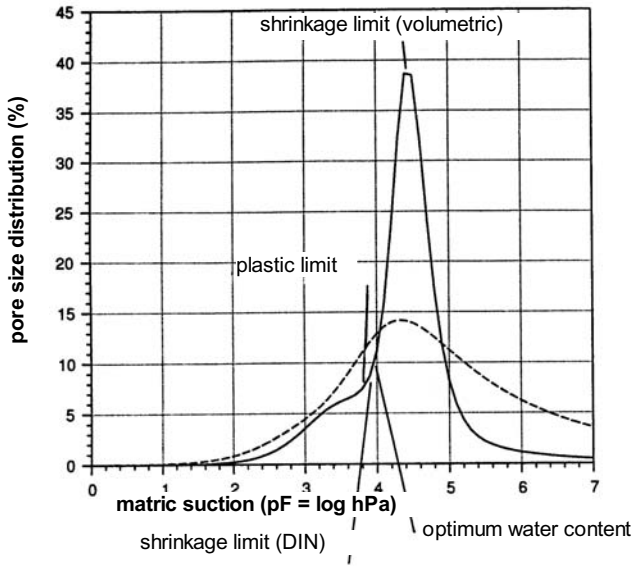
Fig. 3.4. Pore size distribution of Kaolin clay (dΘ/dlog(u_a – u_w))
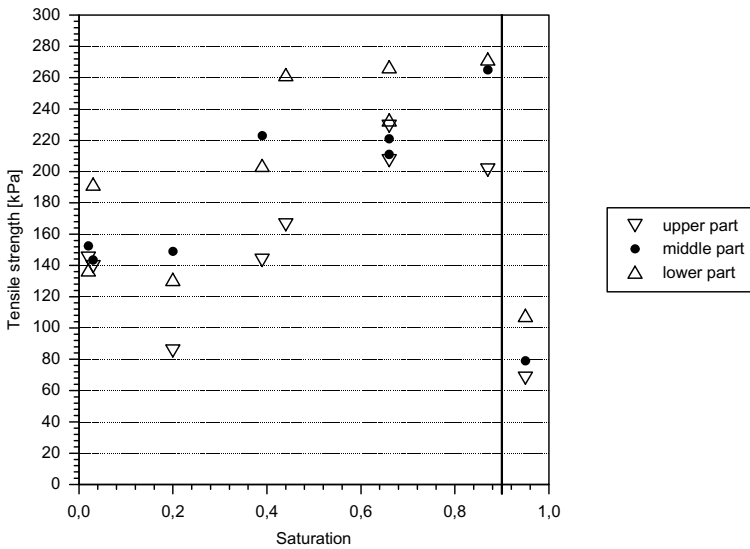

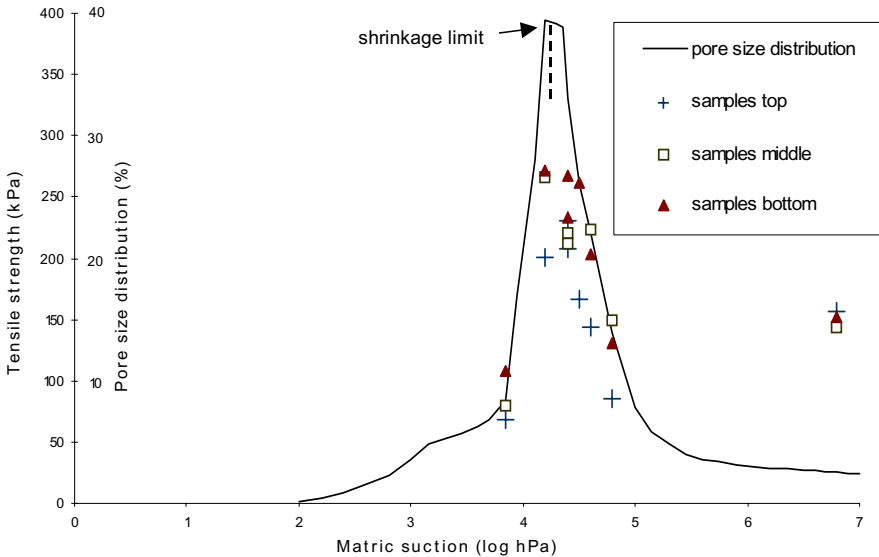**Fig. 3.5.** Tensile strength as a function of suction

Fig 3.6. Pore size distribution and tensile strength of the compacted Kaolin

the largest volume) in the soil. Assuming that the soil pore system can be described as a bundle of capillary tubes of different sizes, $d\Theta/dlog(u_a - u_w)$ gives an idea of the distribution of capillary tube diameters and thus, the pore size distribution. Fig 3.4 shows the "pore size distribution" of Kaolin clay. Two regions can be identified. One region in the range of pF = 2 to about pF =4,5 (showing a maximum at pF = 4,2 – 4,3), which belongs to pore sizes larger than 0,1 μm (diameter calculated from capillary pressure) and therefore representing the water in the interaggregate pores. A second region ranging from about pF = 4,5 to about pF = 7 linked to pore sizes clearly lower than 0,1 μm and therefore representing water in the intraaggregate pores.

Figure 3.5 shows the results of tensile strength tests as a function of saturation (Brüggemann, 1998). The maximum value of tensile strength is reached at about 87 percent saturation corresponding to suctions of about pF = 4,3. Samples with lower water contents show decreasing values of the tensile strength, except the samples with lowest water content (gravimetric) of about 0,3 %. A slight reincrease of tensile strength can be identified. Generally, the samples taken from the upper part of the Proctor sample show lower tensile strengths than the samples from the middle and lower part.

Fig. 3.6 shows the measured tensile strength values as a function of suction combined with the "pore size distribution" of the Kaolin. In addition, the suction at shrinkage limit is marked. It can be seen that maximum tensile stress is reached at suctions just below the maximum of the pore size distribution which represents

the most frequent interaggregate pores. This maximum corresponds to the shrinkage limit (determined by volumetric shrinkage tests). Thus, maximum tensile strength seems to occur when interaggagate pores are almost desaturated. The soil has left the normal shrinkage region, and forces between aggregates are transmitted more and more via water bridges. In terms of capillary theory (see section 2) this means that the soil develops from the transition to the pendular state. The next section deals with tensile forces calculated by means of the capillary theory assuming the pendular state.

4. Calculations and Comparison

According to the theory of porous solid systems (Schubert 1982, Heibrock, 1997, 1996), soil water in the pendular state occurs only in water bridges between the particles. Schubert (1982) and Molenkamp & Nazemi (2003) developed different approaches to calculate the forces between particles (smooth, rough) in the pendular state. Based on these approaches simple calculations of possible tensile strengths of homogeneous, undisturbed particle fabrics are presented, and show that the capillary theory gives the correct magnitude of tensile strength, when the pendular state is reached.

4.1 Interparticle Contact Forces

4.1.1 Calculations Based on Schubert (1982)

Schubert's calculations are theoretically based on the capillary theory of porous solid systems. In addition, different contact forms (e. g. identical spheres, spheres with different diameters, sphere to plate, etc.) are described in his book. Results of numerical calculations are combined in diagrams as shown in Fig. 4.1 b).

The following computations use i) the ratio of the water bridge volume and the sphere volume (V_l / V_s) and ii) the bridge angle β to read out the dimensionless contact force $F/\gamma \cdot x$ (compare with Fig. 4.1 a), where γ is the surface tension (for pure water and air, at a temperature of 293°K, the surface tension is $\gamma \cong 0,0727$ N/m) and x is the diameter of the sphere. Besides, the decisive tensile stress σ_t is derived from (Rumpf & Schubert, 1978)

$$\sigma_t = (1-e) \cdot F / e \cdot x^2 \qquad (4.1)$$
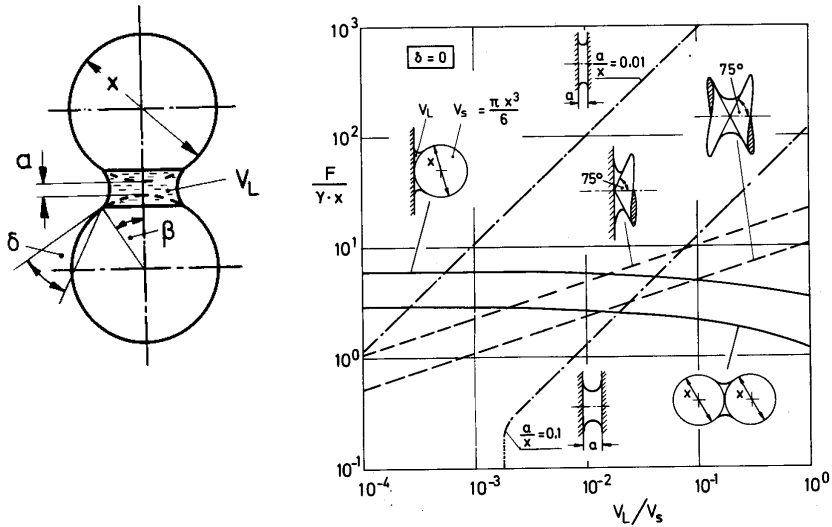
where e is the void ratio of the soil.

Figure 4.1. (a) Spheres with water bridge , (b) contact force versus contact forms and ratio of the water bridge volume and the sphere volume V_1 / V_s (Schubert, 1982)

The Kaolin clay was used for all example calculations. The average void ratio of the samples is assumed as e = 0,6 (Brüggemann, 1998). The initial sphere diameter is usually 10 to 2 µm for a Kaolin, Snyder & Miller (1985) recommend an average diameter of 5 µm. After the shrinkage process, and consequently, for thependular state, a diameter of 1 to 3 µm is expected. Table 4.1a-c represents the results based on the described assumptions i) – the tensile strength versus the contact form, the ratio V_1 / V_s and the diameter of the sphere.

Cohesive soils have naturally a mixture of the different contact forms (e. g. Mitchell, 1993). Therefore, a combination of the calculated contact form values (Table 4.1) could give similar tensile strengths as they were obtained by the laboratory tests.

The second calculation algorithm ii) uses the capillary pressure p_k (the suction) in the soil. By using the dimensionless capillary pressure $p_k \cdot x/\gamma$, the bridge angle β of the different sphere diameter is collected. According to that, the dimensionless force is collected likewise, then the tensile stress is calculated with equation 4.1. The authors consider only sphere systems with the same diameter x, no othercontact forms. As the suction value, 1995 kPa was chosen for the Kaolin (the shrinkage limit). The calculation results are represented in Table 4.2 by using two different ratios of sphere distance a/d (Fig. 4.1a). Table 4.3 shows the stresses according to the proportions of the grain size distribution of the Kaolin. It is evident that the size of the sphere distance a/d (at small values) does not play an important role for the tensile strength. The results are very similar.

**Table 4.1a.** Tensile strength σ_t (kPa) versus contact form, ratio $V_l / V_s = 10^{-2}$ and diameter **x**

Form		$x = 1{,}5$ μm	$x = 3{,}0$ μm	$x = 5{,}0$ μm
∞		80,78	40,39	24,23
	$x_1/x_2 = 2$	117,12	58,56	34,80
	$x_1/x_2 = 10$	163,17	81,59	48,95
		190,64	95,32	57,19
		3231,11	1615,01	969,33

Table 4.1b. Tensile strength σ_t (kPa) versus contact form, ratio $V_l / V_s = 10^{-3}$ and diameter **x**

Form		$x = 1{,}5$ μm	$x = 3{,}0$ μm	$x = 5{,}0$ μm
∞		90,47	45,24	27,14
	$x_1/x_2 = 2$	126,01	63,00	37,80
	$x_1/x_2 = 10$	172,86	86,43	51,86
		203,59	101,80	61,07
		339,27	169,64	101,78

Table 4.1c. Tensile strength σ_t (kPa) versus contact form, ratio $V_l / V_s = 10^{-4}$ and diameter **x**

Form		$x = 1{,}5$ μm	$x = 3{,}0$ μm	$x = 5{,}0$ μm
∞		96,93	48,47	29,20
	$x_1/x_2 = 2$	132,48	66,24	39,74
	$x_1/x_2 = 10$	177,71	88,86	53,31
		210,02	105,01	63,01
		35,54	17,77	10,66

Table 4.2. Tensile strength σ_t (kPa) versus diameter **x** (μm) and ratio of sphere distance **a/x**

	sphere distance $a/x = 0$	sphere distance $a/x = 10^{-3}$	sphere distance $a/x = 0$	sphere distance $a/x = 10^{-3}$
diameter x	bridge angle β (°)	bridge angle β (°)	σ_t (kPa)	σ_t (kPa)
2 μm	14,8	13,4	70,28	70,28
6 μm	8,6	7,6	24,23	23,02
20 μm	4,0	3,3	7,46	5,09
60 μm	1,8	1,5	2,52	0,87

Table 4.3. Tensile strength σ_t (kPa) versus grain size distribution

diameter x	proportional - grain size distribution Kaolin	sphere distance a/x = 0 σ_t (kPa)	sphere distance a/x = 10^{-3} σ_t (kPa)
2 µm	0,62	43,57	43,57
6 µm	0,24	5,82	5,53
20 µm	0,13	0,97	0,66
60 µm	0,01	0,03	0,01
total sum		50,39	49,77

4.1.2 Calculations Based on Molenkamp & Nazemi (2003)

Molenkamp & Nazemi (2003) consider the interactions between two rough spheres in detail (similar diameter, Fig. 4.2). These calculations ought to be compared to the computing for ii) above - the approach of Schubert. Fig. 4.2 shows the geometry of the problem. As a first value the dimensionless pressure differences have to be obtained –

$$\psi = (u_a - u_w) \cdot x \, / \, \gamma \tag{4.2}$$

with $(u_a - u_w)\cdot$ as suction, x as the diameter of the spheres and γ as the surface tension (in our example, the suction is 1995 kPa and the surface tension $\gamma \cong 0,0727$ N/m assuming a temperature of 293°K).

The force between the spheres is

$$F = f \, / \, x \cdot \gamma = \psi \pi Y_c^2 + 2\pi Y_c \sin(\beta + \theta) \tag{4.3}$$

with $Y_c = \sin \beta$, β as the bridge angle (Table 4.2). θ - the liquid-solid contact angle - is taken as 0. As above, the tensile strength is $\sigma_t = (1\text{-}e)\cdot F \, / \, e \cdot x^2$ and it is in accordance to the proportions of the grain size distribution of the Kaolin. The results of the calculations are represented in Table 4.4 and 4.5. Compared with the calculation results based on the approaches (ii) of Schubert (Table 4.3), higher tensile strengths are obtained.
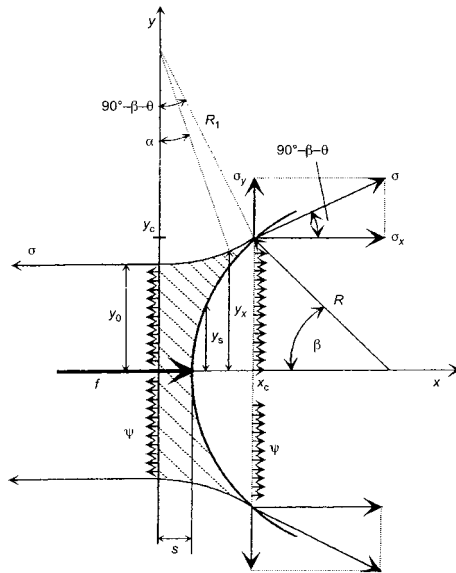
Fig. 4.2. Illustration of geometry of right-hand side of liquid bridge and actions on it (Molenkamp & Nazemi, 2003)

Table 4.4. Tensile strength σ_t (kPa) versus grain size distribution, a/x = 0 (a =2s, Fig. 4.2)

diameter x	contact force F (-)	proportional -grain size distribution - Kaolin	tensile strength σ_t (kPa)
2 μm	$1{,}6897 \ 10^{-6}$	0,62	174,60
6 μm	$5{,}1064 \ 10^{-6}$	0,24	22,70
20 μm	$1{,}2243 \ 10^{-5}$	0,13	2,65
60 μm	$2{,}2224 \ 10^{-5}$	0,01	0,04
		total sum	199,99

Table 4.5. Tensile strength σ_t (kPa) versus grain size distribution, a/x = 10^{-3} (a =2s, Fig. 4.2)

diameter x	contact force F (-)	proportional -grain size distribution - Kaolin	tensile strength σ_t (kPa)
2 μm	$1{,}2557 \ 10^{-6}$	0,62	129,76
6 μm	$3{,}9942 \ 10^{-6}$	0,24	17,75
20 μm	$8{,}3369 \ 10^{-6}$	0,13	1,81
60 μm	$1{,}5479 \ 10^{-5}$	0,01	0,03
		total sum	149,35

4.2 Numerical Analyses

Simple numerical calculations with the FE-code COMPASS (Thomas et al., 2002), using the standard elastic relationship (Hook), showed the expected stress concentration in the middle of the hollow-cylinder-sample (Fig. 4.3) and parallel the contraction in the middle of the sample (see Fig 4.4). Typical soil parameter for the Kaolin clay were taken from Brüggemann (1998) and Alonso et al. (1990) - e. g. : n = 0,4, G = 3300 kPa, ν = 0,4.
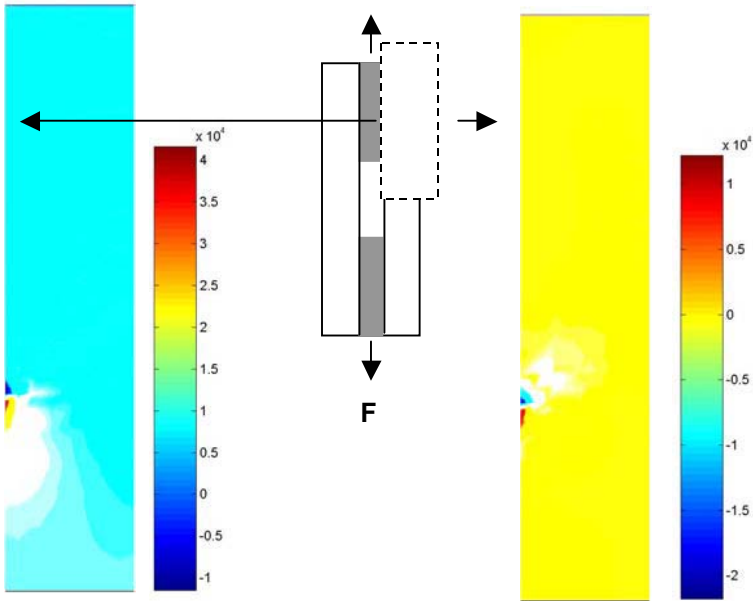

Fig. 4.3. a) Stress (Pa) in **y**-direction, sample scheme, b) in **x**-direction, after 122 s
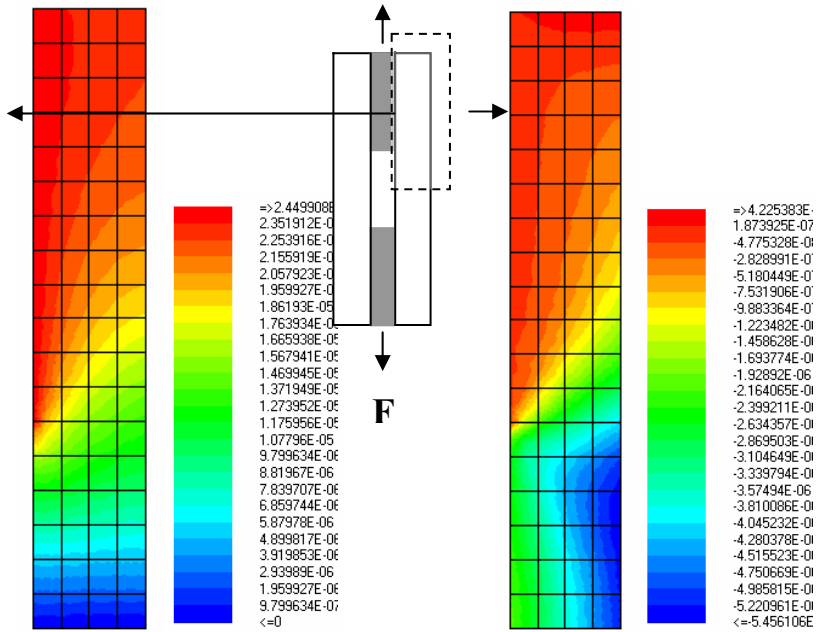
Fig. 4.4. a) Displacement (m) in **y**-direction, sample scheme, b) in **x**-direction, after 122 s

4.3 Comparison

The comparison of the test results in the laboratory and the analytic calculations based on the approaches of Schubert (1982) and Molenkamp & Nazemi (2003) shows that the correct magnitude of tensile strength could be obtained by using equations derived from the capillary theory. Obviously, the calculation of tensile strength as a product of 'total' saturation and suction overestimates tensile strength by an order of magnitude. In order to transfer the equations of Schubert / Molenkamp & Nazemi onto fine grained soils, the overall saturation S has to be replaced by S_I representing the degree of saturation of the interaggregate pores. Assuming that 7 % of the interaggregate pores remain saturated at pF = 4,3, where the maximum tensile strength was observed, the tensile strength calculated from t $= \sigma_t + (S_I \cdot p_k)$ equals 189 kN/m^2 – 289 or 339 kN/m^2 depending on the assumptions with respect to aggregate size distribution and contact form (see Tables 4.3 – 4.5). This range matches with the measured maximum values (see Fig. 3.5) although calculated tensile strength is about 20 % higher compared to the measured strength. This could be explained from the rough estimation of the still saturated part of the interaggregate pores. Assuming that the pendular state is reached at S = 0,2 and thus tensile stresses could be calculated only from forces transmitted by water bridges, the resulting tensile strength calculated from the

equation of Schubert / Molenkamp & Nazemi equals 50 kN/m^2 – 140 or 200 kN/m^2 (see Tables 4.3 – 4.5) which again matches the observed values between 80 kN/m^2 and 140 kN/m^2. The equation of Molenkamp & Nazemi seems to give a better approximation indicating that contact forces between aggregates should be described by assuming rough contact conditions.

5. Conclusion

By now, the tensile strength's characteristics of compacted clays as a function of water content have been rarely investigated. Although the results documented above are not sufficient to confine the hypothesis that tensile strength of compacted clays could be explained by capillary theory assuming that tensile strength is governed by forces that could be transmitted at the boundaries between clay aggregates, the results indicate that the basic approach is promising.

The shape of the measured tensile strengths can be explained through the capillary theory as well as the magnitude of the measured values. This does not apply to very low water contents below saturation of 0,2.

Further investigations will take different soils (high and low plastic clays) into account, and attempts will be made to identify water volumes with different water contents which are trapped in interaggregate pores.

Acknowledgements

References

Alonso, E. E., Gens, E., Josa, A. 1990. A constitutive model for partially saturated soils. Géotechnique 40, No. 4, pp. 405-430

Brüggemann, R. 1998. Zugfestigkeit verdichteter Tone als Funktion des Wassergehalts. Diplomarbeit. Institut für Grundbau und Bodenmechanik, Ruhr-Universität Bochum. unveröffentlicht

Durner, W. 1991. Vorhersage der hydraulischen Leitfähigkeit strukturierter Böden. Diss., Bayreuther Bodenkundliche Berichte, Band 20

Endell, K. 1941. Stand der Erkenntnisse über die Quellfähigkeit von Tonen, ihre innere Ursache und Bestimmung, Bautechnik, Heft 19, Berlin

Heibrock, G. 1996. Zur Rissbildung durch Austrocknung in mineralischen Abdichtungsschichten an der Basis von Deponien. Schriftenreihe des Instituts für Grundbau an der Ruhr-Universität Bochum, Heft 26

Heibrock, G. 1997. Desiccation cracking of mineral sealing liners. in: Proceedings Sardinia 1997, 6. International Waste Management and Landfill Symposium, CISA, Cagliari

Jasmund, K., Lagaly, G. 1993. Tonminerale und Tone: Struktur, Eigenschaften Anwendungen in Industrie und Umgebung. Stenkopff, Darmstadt

Mitchell, J. K. 1993. Fundamentals of Soil Behaviour. J. Wiley & Sons, London

Molenkamp, F., Nazemi, A. H. 2003. Interactions between two rough spheres, water bridge and water vapour. Géotechnique 53, No. 2, pp. 255 – 264

Nagaraj, T. et al. 1990. Discussion on « Change in pore size distribution due to consolidation of clays » by Griffith and Joshi, Géotechnique, Vol. 40 No. 2

Nagaraj, T., Murthy, S. 1986. A Critical reappraisal of compression index equations. Géotechnique 36, No. 1, pp. 27 – 32.

Rumpf, H., Schubert, H. 1978. Adhesion forces in agglomeration processes. in Onada & Hench: Ceramic processing before firing, J. Wiley a. Sons, Inc., London

Schubert, K. 1982. Kapillarität in porösen Feststoffsystemen. Springer Verlag, Heidelberg

Snyder, V. A., Miller, R. D. 1985. Tensile strength of unsaturated soils. Soil Sci. Soc. Am. J., Vol. 49: 58-65

Stoffregen, H. 1997. Bodenuntersuchungen an Kaolin. Fachgebiet der Bodenkunde und Regionale Bodenkunde, Institut für Ökologie, TU Berlin

Thomas, H. R., Cleall, P. J., Seetharam, S. C. 2002. Numerical modelling of the thermal-hydraulic-chemical-mechanical behaviour of unsaturated clay. Environmental Geomechanics. Monte Verità, pp. 125 - 136

Fine Fissuring of Clay Fill Materials for Flood Defence Embankments

Mark Dyer and Barnaby Coulson

School of Engineering, University of Durham, UK; mark.dyer@durham.ac.uk
tel 00 44 191 334 2441
fax 00 44 191 334 2390

ABSTRACT : The UK Environment Agency currently maintains over 35,000 km of coastal and flood defence embankments in England and Wales with an annual expenditure of approximately £400m. The majority of the flood defences are earth embankments built from locally available materials using traditional construction methods. Although the performance of the flood defence embankment can be jeopardised by several different failure modes, instability due to the fine fissuring of clay fill has been identified as one of the main causes of failure especially along the eastern coast and Thames Estuary. At these locations medium to highly plastic clays are commonly used as fill material. The fine fissuring of these clay fills can reduce the mass permeability of the embankment, leading to a rapid ingress of floodwater with catastrophic collapse of the inward face. As part of a wider research programme into the fine fissuring of clays, preliminary laboratory tests have been carried out into the formation of fissures for a variety of clays with different plasticities. The tests investigated an empirical relationship between the geometry of thin discs of soil with the onset of fissuring for different plastic indices.

1 Introduction

The fine fissuring of clay fill was first recognised as a major cause of flood embankment failure in the UK following the devastating North Sea floods of 1953. Cooling & Marsland (1954) carried out extensive field studies of the areas affecting by flooding in Essex and Kent and concluded that embankment failure was a result of one or a combination of the following causes:

- Erosion of the outward face by wave action
- Erosion of the inward face due to overflow
- Slipping of the inward face caused by seepage through the embankment
- Build up water pressures in underlying permeable strata resulting in uplift

The field study observed that for embankments constructed from highly plastic clays fine fissuring had developed to a depth of 0.9 – 1.2m. It was considered that in these highly fissured embankments, seepage had caused instability in the inward face prior to or during overtopping that eventually lead to breach formation. Figure 1 shows possible failure mechanisms proposed by Cooling and Marsland (loc cit).

As part of further field studies into breach formation Marsland and Cooling (1958) and Marsland (1968) conducted full-scale seepage and overtopping using a steel sheet pile cofferdam was constructed on the riverside of an 18m length of bank. The seepage of water through the bank was measured along with pore water pressures within the embankment. The test embankment was located along a length of embankment breached during the 1953 Floods. It was 3.3m high with a 1.2m wide crest and back slop of 1 in 1.5. The water level in the cofferdam was raised for overtopping to occur as a thin sheet of water flowing over the inward slopes. As a result a shallow slip developed involving a 75 cm deep vertical face at the rear crest of the bank, which lead to formation of a breach. The total time from the start of the slip to the formation of the breach was under 2 minutes

Significantly the researchers observed that at least 95% of the total seepage took place through the upper 0.9-1.2m of the bank, which corresponded to the fissured zone. Values of permeability for this fissured layer were calculated to be in the range 0.0175 - 0.04 m/s be compared with a permeability of 2.5×10^{-6} m/s for the intact clayey silt core.

Laboratory Tests

Although the field studies by Marsland and Cooling (1958) provided a valuable insight into the affect of fine fissuring on the stability of flood defence embankments constructed from clay fill, the technical literature on cracking of clay from desiccation has in general been very limited. In contrast the topic has received much more attention in the literature of soil science and agriculture but the treatment has been largely qualitative. One notable exception would be the publication by Morris et al (1992) where the authors provided a thorough review of the technical literature on shrinkage cracking along with theoretical solutions for the cracking mechanisms. In particular the paper provided a detailed explanation about the mechanism controlling crack propagation below the drying surface brought about by the development of tensile stresses at the crack tip due to matrix suction pressure that exceed tensile strength of the soil.
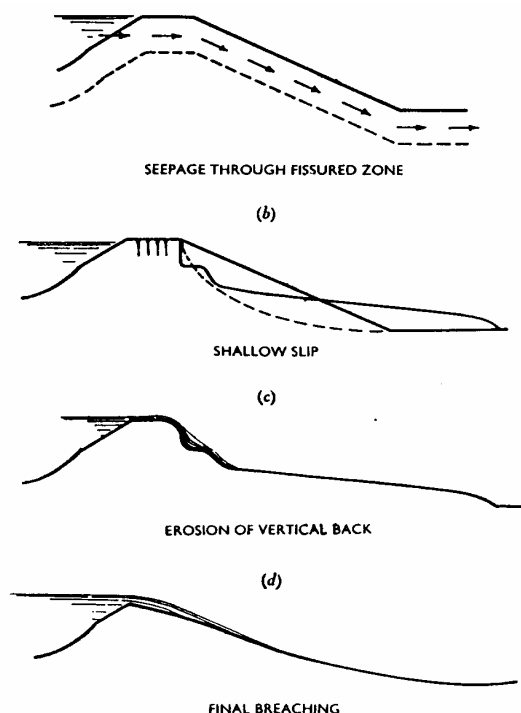
SEEPAGE THROUGH FISSURED ZONE

(b)

SHALLOW SLIP

(c)

EROSION OF VERTICAL BACK

(d)

FINAL BREACHING

Fig. 1: Potential Breach Mechanism Attributed to Fine Fissuring (after Cooling and Marsland, 1954)

Although further research needs to be carried out into the mechanics of crack formation and its affects on mass permeability, this paper presents results from a preliminary study into crack formation that simply observed the cracking of discs of clay soils allowed to air-dry in the laboratory at 20^0C. The project was carried out for a final year master degree (Coulson 2003). Different diameters and thickness of clay samples were prepared using a 66mm or 122mm diameter aluminium mould. The moulds were filled with remoulded soils in 2mm thick layers using a spatula. The discs dried on a glass plate.

Four types of clay were used in the tests. These comprised (a) silty brown glacial till from the northeast of England called Birt clay, (b) calcium bentonite, (c) kaolin in dry powder form, and (d) sample of a clay excavated from a borrow pit for a new flood defence embankment on the Humber Estuary. Table 1 lists the soil properties determined using standard laboratory tests along with soil classifications. The clays ranged from medium plasticity (Humber Clay and Glacial Till) to extremely high plasticity (Bentonite). A further fifth clay was manufactured using a mixture of kaolin and bentonite. Equal weights of oven dried kaolin and bentonite were mixed thoroughly into a slurry. The standard liquid and plastic limit tests were likewise determined.

Table 1: Properties and classifications of the four clays used in the cracking tests

Clay	Liquid Limit	Plastic Limit	Plasticity Index	Shrinkage Limit	Shrinkage Index	Clay Fraction
Kaolin	68%	34%	34 %	22%	46%	64%
Birt Clay	56%	25%	31%	15%	41%	77%
Ben-tonite	121%	62%	59%	40%	81%	91%
Hum-ber Clay	49%	25%	24%	15%	34%	78%

Results

To begin with the initial diameter and thickness of discs were such that the samples merely shrunk without cracking. To create cracks progressively thinner discs were prepared that produced a network of fine cracks, which eventually lead to a single crack propagating diametrically across the disc. The relative diameter and thickness of samples influence the onset of cracking. As a result a so-called "critical cracking ratio" was used to characterise the potential for cracking. It was defined as the ratio of the diameter to thickness of the sample when only one crack extends diametrically across the sample as shown in Figure 1. There appeared to be a relationship between "critical cracking ratio" with the plasticity index for each type of clay as well as the initial moisture content. This meant that samples with a diameter to depth ratio greater than critical value resulted in more substantial cracking (for example two cracks that extend from edge to edge) where as samples with at diameter to depth ratio less than critical resulted in smaller cracks that would only extend from one edge or were confined to the centre of the sample.

Based on these results the "critical cracking ratios" could be plotted against plasticity indices for the different clays prepared with initial moisture content at the liquid limit as shown in Figure 2. The liquid limit was chosen as the initial moisture content for ease of sample preparation. The "critical cracking ratio" can be seen to decrease as the plasticity index increased, which meant that the propensity for cracking increased with plasticity index. In comparison Figure 2 also shows that a higher "critical cracking ratio" was measured for samples prepared at a higher initial moisture content midway between the plastic limit and liquid limit. This second set of results shows a significant increase in the "critical cracking ratio" for soil samples prepared with a lower initial moisture content. The result indicates a reduced tendency for cracks to form when the initial moisture content of the samples is reduced.

Fig. 1 A diametrical crack propagating across the sample associated with the "critical cracking ratio"

Discussion

It was recognised from the outset that desiccation of clay samples from the liquid limit with no compaction would be unrepresentative of modern embankment construction. In order to investigate the cracking of clay soils with a lower initial moisture content, a compaction test was carried out on the glacial till. Using a standard compaction test the optimum moisture content was measured to be 22.5% with a corresponding bulk density of 2.006g/cm^3 and dry density of 1.637 Mg/m^3. Using this information a 105mm diameter sample was compacted at the optimum moisture content and extruded from the mould for cutting into 5 discs using a fine wire blade to minimise disturbance of the samples. The samples were placed onto a glass plate to dry in the usual manner. Based on earlier results the samples were expected to crack extensively at a thickness of 8mm that corresponded to diameter/thickness ratio of 21.0 . After drying the 8mm thick sample showed no signs of shrinkage cracking. Some very fine surface cracks were present although these were attributed to the shearing action of the cutting blade. Instead a single diametrical shrinkage crack only appeared on the thinner 5mm thick sample that corresponded to a "critical cracking ratio" of 13. This is significantly lower than the "critical cracking ratio" determined form the discs of remoulded clay prepared at an initial moisture content midway between plastic and liquid limits. If any thing
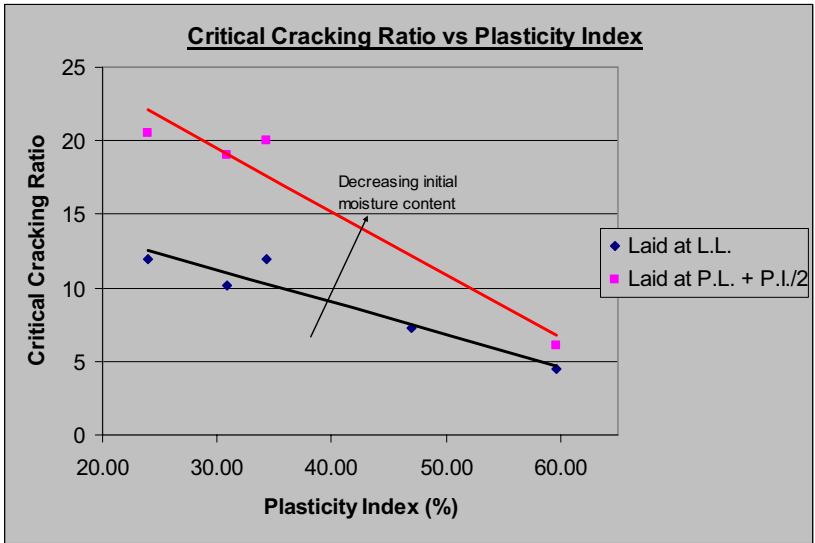
Figure 2: Relationship between critical cracking ratio and plasticity index for samples prepared at the liquid limit and midway between the plastic and liquid limit

the "critical cracking ratio" for the compacted sample is similar to the samples prepared at an initial moisture at the liquid limit. No explanation has been found for the discrepancy between the results for compacted and uncompacted samples. Unfortunately it proved impracticable to carry out compaction tests at much higher moisture contents because the soil adhered to the compaction hammer.

Nevertheless the concept of a "critical cracking ratio" provides an empirical method of characterising the tendency of a clay sample to crack due to desiccation. The results for uncompacted discs samples show a decrease in "critical cracking ratio" (i.e. increasing tendency to crack) with an increase in plasticity index for different clays ranging from a medium to highly plastic clay. A similar trend exists when plotting "critical cracking ratio" against shrinkage index. In comparison the "critical cracking ratio" is shown to increase with a decrease in the initial moisture content. The result is in line with the common practice of placing fill material near to optimum moisture content in order to minimise the risk of cracking due to desiccation. Although for dam construction fills material can often be placed wetter than optimum for the material to be more workable and less prone to hydraulic fracturing.

Even though the results are empirical and further research is needed, the tests offer an insight into the depth of soil sample required to provide the necessary restraint at the base of the sample for cracking to develop from the surface downwards. The test mirrors the drying mechanism in nature where the sample dries from the top downwards, leading to the development of tensile stresses and crack propagation. Furthermore the experiment showed that a sample without restraint at

the base could still crack at the top surface, although further research is needed to investigate the relationship between the depth of soil sample required for restraint and the soil properties.

In order for these initial results to be related to field behaviour further investigations are needed to link the "critical cracking ratio" to the rate and depth of fine fissuring along with changes to mass permeability of the fill material that can lead to breach formation as illustrated in Figure 1. These field investigations are planned in the near future at abandoned flood defences in the UK.

Conclusions

The paper introduces the concept of a "critical cracking ratio", which provides an empirical method to characterise the tendency of a clay sample to crack due desiccation. The results present a clear relationship of decreasing "critical cracking ratio" (ie. increased tendency to crack) with increase in plasticity index or shrinkage index for the clays tested. Likewise the tests demonstrate that "critical cracking ratio" increases (ie. reduced tendency to crack) when samples are placed at lower initial moisture content.

References

Cooling, L.F and Marsland, A. (1954) Soil Mechanics of Failures in the Sea Defence Banks of Essex and Kent, ICE Conference on the North Sea Floods of 31 January / 1 February 1953

Coulson B. 2003 The effect of fine fissuring of clay on the stability of flood defence embankments. MEng Final Year Report, University of Durham

Dyer MR and Gardener (1996). Geotechnical Performance of Flood Defence Embankments. Environment Agency R&D Technical Report W35.

Marsland, A. (1968) The shrinkage and fissuring of clay in flood banks. Note No. IN 39/68, Building Research Station

Marsland, A. and Cooling L.F. (1958) Tests on Full Scale Clay Flood Bank to Study Seepage and the Effects of Overtopping, Building Research Station

Morris, P.H., Graham, J., and Williams, D.J. (1992). "Cracking in drying soils." Canadian Geotechnical Journal, Vol 29, pp. 263-277

Laboratory investigation of the virgin drying of the Corinth Marl

M. Bardanis[1] and M. Kavvadas[2]

[1]Doctoral Student, National Technical University, Athens, Greece
[2]Associate Professor, National Technical University, Athens, Greece

Abstract. Marly formations are widespread in Greece with major works founded on, or excavated in them. Perhaps the most spectacular of them is the Corinth Canal, a ca. 7 kilometre long canal with very steep (average inclination 4.5 : 1) and high (up to 80 m) slopes excavated through the Corinth marl. The excellent stability of the steep canal slopes has motivated extensive laboratory investigations of the mechanical properties of the Corinth marl at the Geotechnical Department of the National Technical University of Athens since several years, the latest of which involved the drying properties of the Corinth marls. The drying portion of the soil-water characteristic curve was determined from undisturbed block samples and from reconstituted samples re-consolidated to the in-situ stresses. The air-entry pressure was found to be higher in the case of the undisturbed samples compared to the reconstituted/re-consolidated samples. Furthermore, the variation of the void ratio with suction up to the air-entry pressure was found to be close to the curve of void ratio versus effective stress from one-dimensional consolidation over the same stress range. This behaviour constitutes evidence of the validity of the effective stress principle up to the air-entry pressure. Finally, the paper concludes with estimations on the apparent cohesion change of the Corinth marl with suction.

1 Introduction

Marly formations cover a large part of Greece and present great interest from both geological and geotechnical aspects. They are neogene deposits of lacustrine, flu-

vio-lacustrine or marine origin, containing 35-75% calcium carbonate and a complementary fraction of clay minerals. The calcareous substances in the marls have come from the dissolution of carbonate rocks (e.g. limestones) surrounding the basin and subsequent sedimentation of the calcium carbonate, when its solubility in the water is reduced by changing conditions (e.g. temperature or pH changes). Marls have developed a structure, mainly in the form of "bonding" between individual particles, due to cementation caused by the deposition of calcium carbonate at the time of sedimentation or via a sustained seepage of calcium-rich pore water through the material after gravitational consolidation. Due to the cementation, marls exhibit an abnormally high stiffness and strength at low and moderate stress levels and a relatively gradual reduction of these properties when bond de-structuration is initiated with straining. As a result, the geotechnical properties of the marls are not controlled solely by the void ratio and stress history (current stress and maximum past overburden), as with typical sedimentary clays, rendering conventional geotechnical investigation and interpretation techniques insufficient (Vaughan et al, 1988). A framework for the description of the mechanical behaviour of stiff structured soils (including marls) was proposed by Kavvadas et al 1993, and Kavvadas and Anagnostopoulos 1998.

Extensive deposits of marls occur in the Corinth area, about 65km to the west of Athens, around the isthmus where the Corinth Canal was excavated in 1893. The Canal is 6.3 kilometres long and about 25 metres wide at sea level. The slopes have an average inclination 4.5 to 1, i.e., about 75 degrees with respect to the horizontal and a maximum height 75 meters above sea level plus another 10 meters below sea level. Despite the long, high and very steep slopes, the large number of tectonic faults crossing the canal (their traces are clearly visible on the canal slopes) and the intense seismicity of the Corinth area (e.g., Papazachos et al 1981) which is among the highest in Greece, the canal slopes have suffered only minor instabilities in their more than one hundred-year-long history. This type of behaviour is mainly due to the favourable mechanical characteristics of the Corinth marl, which up till now have been attributed solely to cementation. The recent construction of new railroad and highway bridges over the canal has revived interest in the behaviour of the Corinth marl and initiated further research on the mechanical characteristics of the canal marls. A new laboratory testing programme was initiated in order to investigate further the cementation of the marls and the effect of partial saturation on their behaviour. The drying portion of the soil-water characteristic curve was obtained as part of this programme. The main results of the research on the effect of partial saturation on the behaviour of the marls are presented in this paper. Since the Corinth marl exhibits many of the typical characteristics of calcareous formations and other stiff cemented soils, many of the findings of this research have more general applicability.

2 Sampling and testing programme

The mechanical properties of the Corinth marl and the influence of the cementation-induced structure have been investigated at the Geotechnical Department of the National Technical University of Athens for the last 10 years, by means of several laboratory testing programmes on samples of the lower bluish-gray marl. An overview of the results of these investigations is presented by Kavvadas et al 2002. These programmes however have not included so far investigations on the effects of partial saturation on the properties of the Corinth marl, which was part of the latest programme. During this programme, intact samples of the lower bluish-gray marl were obtained from the north slope of the Corinth Canal. The samples were obtained from the toe of the north slope at the location of the old railway bridge constructed over the canal in 1936 and destroyed in 1944 during World War II. At the toe of the north slope at this particular location the bluish-gray marl is visible at sea level (0.00 to 0.70 m) with the yellowish-white marl starting at about 1 m above sea level. To minimize the effect of drying and sampling disturbance, near-surface material was first removed and then large intact samples (about 40 cm) were carefully extracted, wrapped in cling film, placed in double plastic bags, carefully transported to the laboratory and stored at a controlled relative humidity of 100%.

During sampling, the in-situ suction was frequently measured with a Soil-Moisture Quickdraw Suction Probe. The probe can measure suctions up to 100 kPa with minimum equilibration time (85 kPa in practice). The measured suction was about 16 kPa at a height of 0.50 m above sea level for depths up to 0.50 m from the surface and about 11 kPa at depths 0.50 to 1.00 m from the surface and at the same height. Both of these mean values –although low by general standards- are higher than expected at a height of only 0.50 m above sea level.

As part of the testing programme to investigate the effect of partial saturation on the behaviour of the Corinth Marl, the drying portion of the soil-water characteristic curve was obtained using a Soil Moisture pressure plate extractor with ceramic pressure plates of 15 Bar (1500 kPa) air-entry pressure.

3 Physical properties of the Corinth Marl

Classification tests on the recently obtained samples indicate that the marl can be characterized as a low plasticity clayey silt lying either slightly
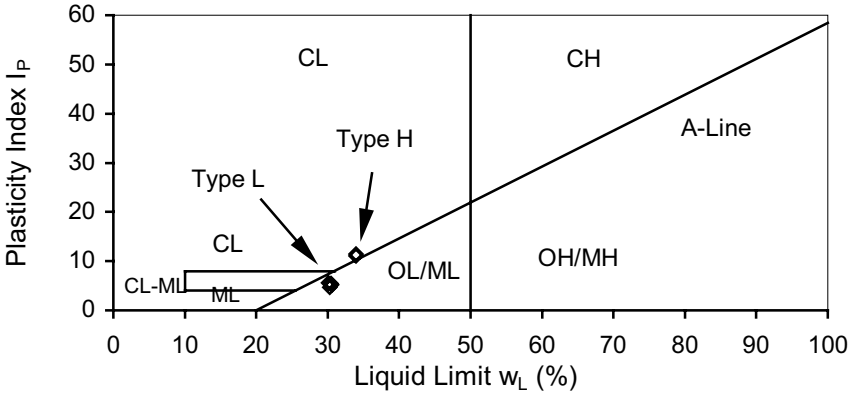
Fig. 1. Casagrande's Plasticity Chart with results for the Corinth marl.
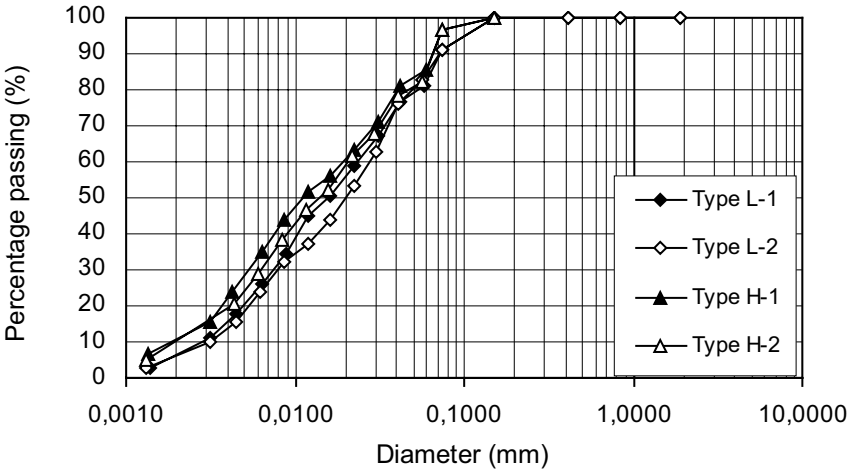

Fig. 2. Grain size distributions for the Corinth marl.

above or slightly below the A-Line on Casagrande's Plasticity Chart. Two distinct types of the material were identified: (1) Type H, of higher plasticity with an average liquid limit of 34%, plasticity index 11.5% and approximately 11% clay-size content (97% fines) and, (2) Type L, of lower plasticity with an average liquid limit of 30.5%, plasticity index 5.5% and approximately 6.5% clay-size content (91% fines). Both types of the marl have a specific gravity $G_s = 2.67$ and their natural water content varies between 24% and 25%. Fig. 1 shows Casagrande's

Plasticity Chart with the location of the two distinct types of the marl and Fig. 2 shows the grain-size distribution curves.

4 Drying Portion of the Soil-Water Characteristic Curves

The drying portion of the soil-water characteristic curve was obtained using a Soil Moisture pressure plate extractor with pressure plates of 15 Bar (1500 kPa) air-entry pressure. Carefully trimmed samples of the natural soil (trimmed using oedometer cell rings of 19 mm height and 70 mm diameter and then extracted from the rings) were placed in the apparatus. Air pressure in the cell was then raised and kept constant for 24 hours before removal of the samples. Samples were then evenly divided in two, placing one half of each sample in the 105° C oven for water content measurement and the other half of the sample in paraffin wax for void ratio measurement. The degree of saturation was calculated from the measured values of the specific gravity, water content and void ratio. The aforementioned process was repeated for samples of the same material reconstituted at an initial water content equal to 1.5 times the liquid limit and then consolidated one dimensionally to the in-situ maximum stress of the marl (800 kPa). In fact, the samples were obtained from locations very close to the slope of the canal, where the present horizontal stress is close to zero. The vertical stress prior to the excavation of the canal was about 1600 kPa (80m x 20 kN/m^3) but, due to the excavation, was reduced to the present value estimated to be about 800 kPa. Obtaining curves for both the natural and the reconstituted soil brought at the same stress level as the natural soil, aimed at investigating the differences and the possible effect of cementation on the drying characteristics of the marl.

In Fig. 3 the degree of saturation is plotted against suction. Desaturation occurred between 100 and 200 kPa for the reconstituted/reconsolidated marl and between 200 and 300 kPa for the natural marl. Comparison of the two curves shows that residual saturation occurs at pressures higher than 1500 kPa as the second point of inflection was not obtained up to the maximum suction that could be applied with the pressure plate extractor (1500 kPa). The natural marl maintained a higher degree of saturation compared to the reconstituted/reconsolidated marl at the same suction level. The same conclusion is also obtained from Fig. 4 where the gravimetric water content is plotted against suction: the natural marl was found to retain more water in its pores than the reconstituted/reconsolidated marl.
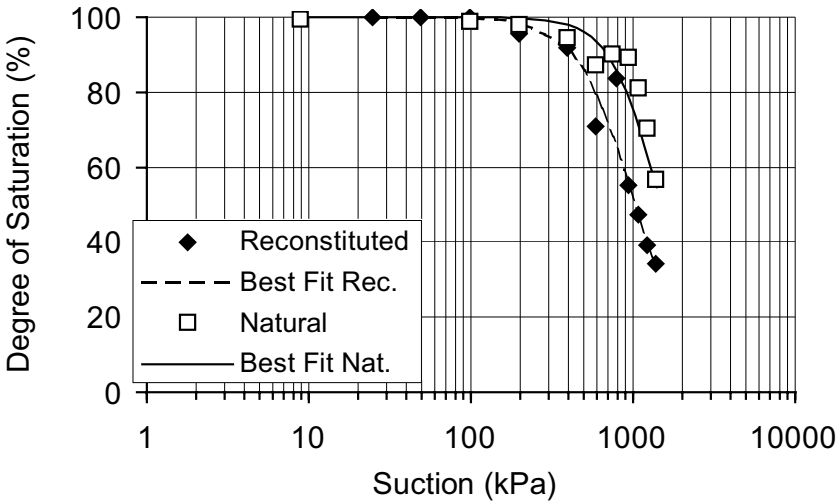
Fig. 3. Degree of saturation of natural and reconstituted/reconsolidated Corinth marl with suction (best-fit curves obtained using equation proposed by Fredlund & Xing, 1994).

The above observation is compatible with test results presented by Huang et al 1998. They obtained soil-water characteristic curves for a silty sand (10% clay, 37.5% silt and 52.5% sand) with liquid limit $w_L = 22.2\%$ and $w_P = 16.6\%$ after consolidating it first from slurry to various stresses. This soil therefore had different preconsolidation pressures prior to obtaining its soil-water characteristic curve. During these tests, the higher the preconsolidation pressure of the soil was, the higher the degree of saturation the soil could maintain for the same suction was. Preconsolidation-induced structure therefore causes soils to be able to maintain a higher water content and degree of saturation than soils with less or no such structure at the same suction level. In the case of the natural Corinth marl, the same observations can be attributed to its more pronounced structure (combination of pre-consolidation- and cementation-induced structure) compared to the reconstituted/reconsolidated material (which has only preconsolidation-induced structure). Therefore, a combination of the adsorption of the cementing agents in the natural marl (which are practically washed away or at least significantly diminished in concentration during reconstitution with distilled water) and past pre-consolidation is most likely to be the cause of the higher water-retaining capacity of the natural marl.
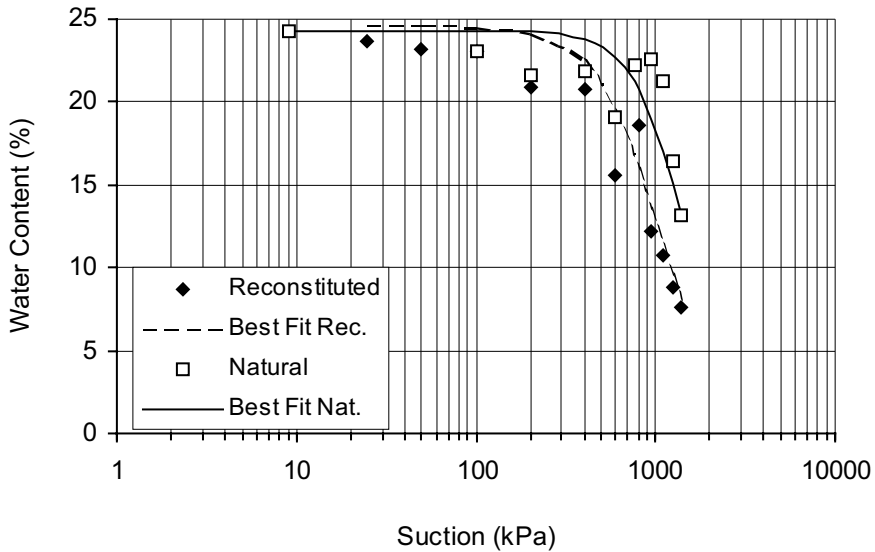
Fig. 4. Gravimetric water content of natural and reconstituted/reconsolidated Corinth marl with suction (best-fit curves obtained using equation proposed by Fredlund & Xing, 1994).

Fig. 5 investigates the effect of void ratio changes by plotting void ratio (e) against suction. Void ratio remained practically constant with increasing suction, although its calculation using paraffin wax led to large variations in the determination of its values even for the reconstituted soil. In the case of the natural marl, transition from the lower plasticity marl (majority of the samples used) to the higher plasticity one (which has a higher void ratio in its natural state) led to a void ratio increase at higher suctions. These observations notwithstanding, the void ratio was expected to remain constant as degree of saturation-water content and void ratio-water content curves indicate (Figs. 6 and 7 respectively).

The degree of saturation (S) and water content (w) are related through Eq. 1:

$$G_s \, w = S \, e \qquad (1)$$

where G_s is the specific gravity. The practically linear segment of the S-w curve observed in Fig. 6 for water content below the desaturation limit, indicates a constant S/w ratio equal to G_s/e (according to Eq. 1). The inclination of the best-fit line of points after desaturation and through the origin (as zero water content corresponds to zero degree of saturation), yields the constant void ratio of the soil after desaturation. These lines are plotted in Fig.7 and the values of void ratio corresponding to their inclinations are 0.62 for the natural marl (corresponding to a shrinkage limit of 23.1%) and 0.58 for the reconstituted/reconsolidated marl (corresponding to a shrinkage limit of 21.9%). The higher shrinkage limit of the natu-

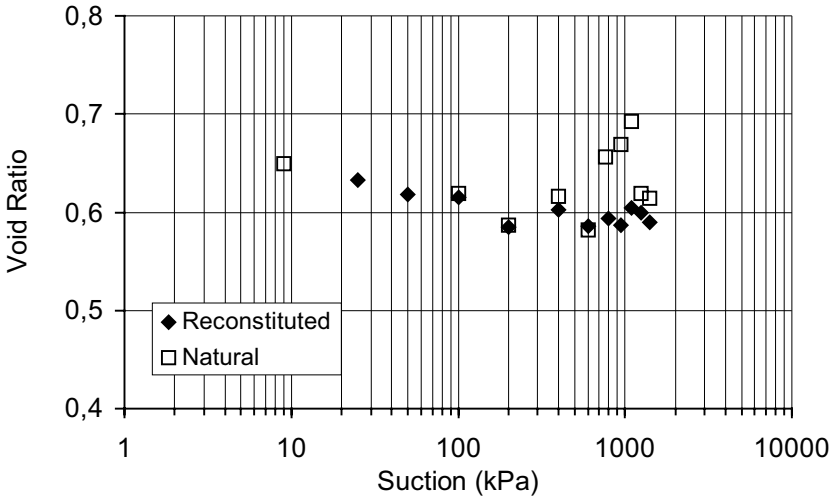**Fig. 5.** Void ratio of natural and reconstituted/reconsolidated Corinth marl with suction.
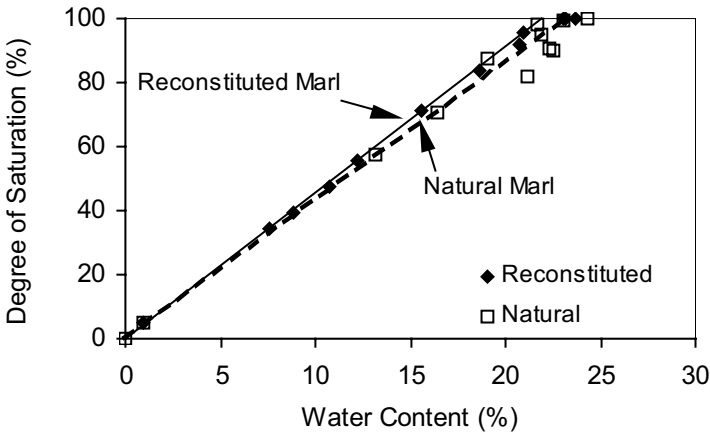

Fig. 6. Degree of saturation of natural and reconstituted/reconsolidated Corinth marl with gravimetric water content.

ral marl indicates the structure-dependence of this soil characteristic, which, although considered an index property, is not a constant (unlike the liquid and plastic limits which do not depend on structure).
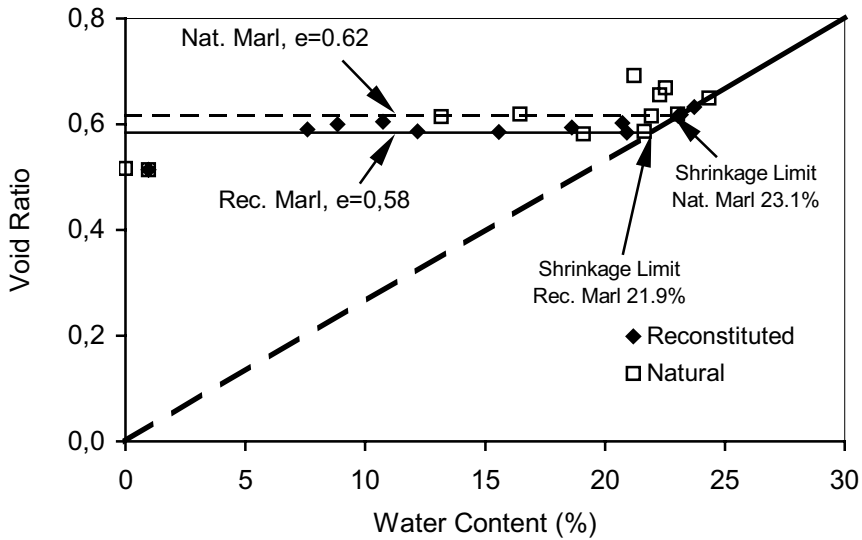
Fig. 7. Void ratio of natural and reconstituted/reconsolidated Corinth marl with gravimetric water content.

Furthermore, in agreement with results presented by Fredlund & Rahardjo 1993, if the void ratio-suction curves are compared to similar curves obtained from one-dimensional consolidation tests, there is a close agreement of calculated values of void ratio up to the suction/stress value corresponding to the air-entry pressure of the soil. This is clear for the reconstituted/reconsolidated marl (Fig. 8) but not so much for the natural marl (Fig. 9). In any case it adds to the evidence for the validity of the principle of effective stress up to the air-entry pressure and once again points out the need for refinement of the method used to measure the void ratio when obtaining the soil-water characteristic curve using pressure plate extractors.

5 Estimation of strength evolution with drying

As already mentioned, research on the characteristics of the Corinth marl aims to explain the excellent stability of the very high and steep Corinth Canal slopes. Although cementation can explain the appreciable increase of the shear strength of the natural material compared to its remoulded state, it cannot explain the long-term stability of the canal slopes. The missing strength component can certainly be attributed to its present unsaturated state (especially close to the Canal slopes).
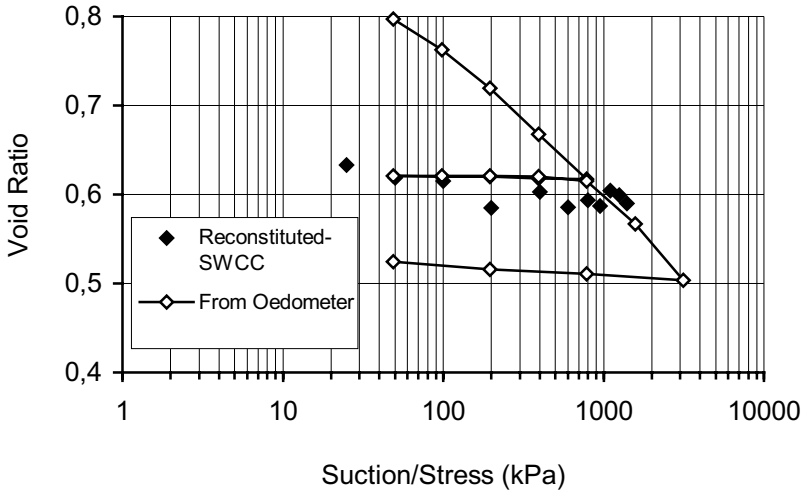
Fig. 8. Void ratio of reconstituted/reconsolidated Corinth marl during drying in the pressure extractor and 1-dimensional consolidation from slurry in oedometer.

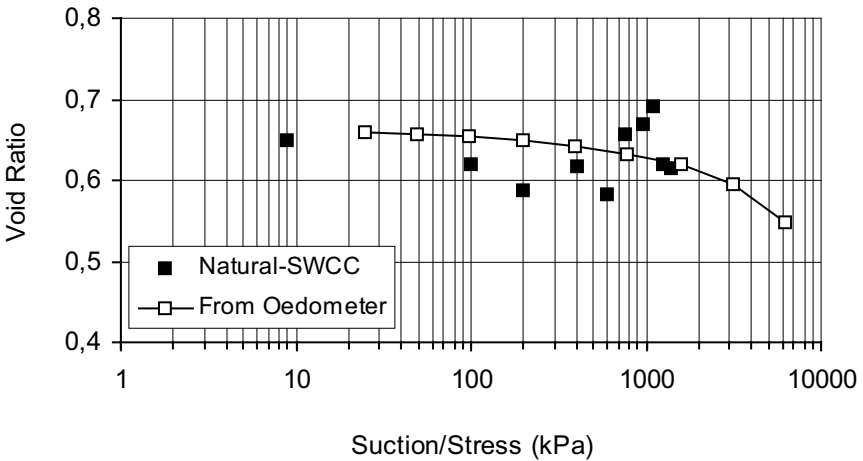**Fig. 9.** Void ratio of natural Corinth marl during drying in the pressure extractor and one-dimensional consolidation in oedometer.

The ongoing research on the properties of the Corinth marl, aims to investigate methods to measure the shear strength of the marl in its natural unsaturated state. As a preliminary report on the strength evolution with suction however, a litera-

ture review was performed on current methods for the prediction of the shear strength of unsaturated soils from the soil-water characteristic curve. This review (e.g. Fredlund et al 1996; Rassam & Williams 1999) revealed the lack of curve-fitting parameters for cemented soils like the Corinth marl, making thus unconservative the immediate application of such methods without first carrying out specific testing to measure the unsaturated shear strength. Despite the general absence of relevant data, it is generally accepted that the increase of the shear strength up to the air-entry value of the soil can be described by an 'apparent' increase in cohesion equal to the product of the suction times the tangent of the effective angle of friction (φ'). This is in agreement with the principle of effective stress being valid for suction values up to the air-entry pressure of the soil and corresponds to the increase in effective stress by the amount of the suction (introduced as negative pore water pressure in the effective stress equation). Kavvadas et al 2002, report shear strength parameters for the Corinth marl, $c' = 100$ kPa and $\varphi' = 33^o$ for low stress levels, $c' = 300$ kPa and $\varphi' = 26^o$ for moderate stresses and $c' = 0$ kPa and $\varphi' = 33^o$ for high stress levels (e.g. above 1.5 MPa). At the air entry pressure of the material (about 250 kPa), the increase in cohesion due to suction is about 150 kPa (i.e., 60 kPa for every 100 kPa of suction). Even considering suctions only up to the air entry pressure, the increase in shear strength can explain the excellent stability of the canal slopes.

6 Conclusions

A laboratory testing programme was carried out in order to investigate the virgin drying curve and the effects of partial saturation on the engineering properties of the natural and reconstituted/reconsolidated Corinth marl. Void ratio changes with suction were found to be practically negligible even up to the air-entry pressure for both natural and reconstituted samples, although the observed values are very close to the change in void ratio during one-dimensional consolidation over the same stress range, as the material is relatively stiff. The air-entry pressure of the natural marl was found to be higher than that of the reconstituted/reconsolidated material. In general, the natural marl was found to be able to retain more water in its pores than the reconstituted/reconsolidated marl for the same values of suction. The magnitude and nature of the cementation of the Corinth marl justifies such behaviour. Finally the calculated increase in shear strength due to suction can explain the excellent stability of the high and steep slopes of the Corinth canal. As part of further research, the wetting portion of the soil-water characteristic curve and the shear strength of the marl during drying will be measured.

References

Fredlund DG, Rahardjo H (1993) Soil Mechanics for Unsaturated Soils. John Wiley & Sons Inc, New York.

Fredlund DG, Xing A (1994) Equations for the soil-water characteristic curve. Can Geotech J 31: 521-532.

Fredlund DG, Xing A, Fredlund MD, Barbour SL (1996) The relationship of the unsaturated soil shear strength to the soil-water characteristic curve. Can Geotech J 32: 440-448.

Huang S, Barbour SL, Fredlund DG (1998) Development and verification of a coefficient of permeability function for a deformable unsaturated soil. Can Geotech J 35: 411-425.

Kavvadas M, Anagnostopoulos AG (1998) A framework for the mechanical behaviour of structured soils. In: Proceedings 2nd Int Symp on the Geotechnics of Hard Soils - Soft Rocks, Napoli. AA Balkema Publishers, Rotterdam, pp 603-614.

Kavvadas MJ, Anagnostopoulos AG, Georgiannou VN, Bardanis ME (2002) Characterisation and engineering properties of the Corinth marl. In: Tan et al (eds) Proceedings Int Workshop 'Characterisation and Engineering Properties of Natural Soils'. AA Balkema Publishers, Rotterdam, pp 1435-1459.

Kavvadas M, Anagnostopoulos AG, Kalteziotis N (1993) A framework for the mechanical behaviour of the cemented Corinth marl. In: Proceedings 1st Int Symp on Hard Soils - Soft Rocks, Athens, Greece, pp 577-583.

Papazachos BC, Comninakis PE, Moundrakis DM, Pavlides SB (1981) Preliminary results of an investigation of the February-March 1981 Alkionides Gulf (Greece) earthquakes. In: Proceedings Int Symp on the Hellenic Arc and Trench, pp 400-420.

Rassam DW, Williams DJ (1999) A relationship describing the shear strength of unsaturated soils. Can Geotech J 36: 363-368.

Vaughan PR, Maccarini M, Mokhtar SM (1988) Indexing the engineering properties of residual soils. Quart J Engng Geol 21: 69-84.

APPLICATIONS

From experimental evidence towards the assessment of weather-related railway embankment hazards

Gilson Gitirana Jr, Ph.D. student
Delwyn G. Fredlund, Professor Emeritus

Department of Civil and Geological Engineering, University of Saskatchewan, 57 Campus Drive, Saskatoon, SK, Canada, S7N 5A9

Abstract. Weather-related geo-hazards are a major concern for the railway industry in Canada. The financial losses that result from derailments and delays amount to millions of dollars every year. On the other hand, the assessment and management of geo-hazards is a difficult problem that involves complex coupled phenomena and numerous soil and weather parameters. The primary goal of this paper is to illustrate the manner whereby unsaturated soil mechanics can be taken from the soil property assessment level using techniques based on the soil-water characteristic curve (SWCC), to the solution of this real and highly complex problem.

First, a concise description of the weather-related geo-hazards assessment model (W-GHA model) is given. Deterministic and probabilistic aspects of the model were developed within a Decision Analysis framework. The deterministic core of the model consists of a two-dimensional stability analysis combined with the analysis of the effects of weather conditions on the pore-water pressures. According to the proposed model, weather conditions interact with the ground through the flow of liquid water, water vapour, and heat. Critical embankment stability conditions are determined using a Dynamic Programming Method (DPM) combined with Finite Element based stress fields. The soil system is ultimately represented by a series of partial differential equations (PDE's) governing conservation of mass and momentum. A discrete stochastic analysis is implemented within the proposed framework.

Several unsaturated soil property functions are required as input to the system of PDE's. The hydraulic conductivity (i.e., coefficient of permeability), vapour diffusion coefficient, thermal conductivity, volumetric specific heat, and shear strength are all nonlinear functions physically related to the SWCC. The methodology by which these soil property functions can be inter-related to the SWCC is presented. The theoretical model illustrates the manner whereby it is possible to quantitatively assess embankment stability based on weather conditions. The methodology is feasible and yet relatively comprehensive.

1 INTRODUCTION

This paper presents theoretical and practical aspects associated with a weather-related geo-hazard assessment model (W-GHA model) developed for railway embankments. The study was carried out taking into account the specific needs of the Canadian Pacific Railway (CPR). However, the W-GHA model should be applicable to the railway industry in general. Special focus is given to the saturated/unsaturated soil modelling and the assessment of unsaturated soil property functions. First, a description of the problem background is given, explaining the decision situation the railway industry faces. A description of how the railway could benefit from a geo-hazard assessment model is given, making the case for the potential benefits of using unsaturated soil mechanics to assess weather-related geo-hazards. Secondly, a description of the *Decision Analysis* framework for railways is given, embracing the deterministic and probabilistic features of the model. The following section presents the W-GHA model, describing the unsaturated soil theories required to assess weather-related geo-hazards in addition to explaining the required weather and soil parameters. The method of assessing the unsaturated soil properties is described, emphasising the central role played by the soil-water characteristic curve, SWCC. Finally, a framework for frequency and sensitivity analyses is provided.

1.1 Problem background

Geo-hazards create a serious impact on the performance of the Canadian railway networks. The most important impact involves a compromise of deadlines, an expense for the repair of railway track and damaged sites, and the safety exposure for employees and the public. As a result, the minimization of geo-hazards impacts is an issue of great concern for the railways. The railway industry faces a serious dilemma; namely, the industry operates networks with tens of thousands of kilometres of line, crossing several types of geographical terrain, soil, and weather conditions from coast to coast (see the CPR network on Fig. 1). It is extremely difficult to protect and/or remediate every site under significant risk. At the same time, risks must be managed in an affordable manner.

The importance of geo-hazards is illustrated through derailment statistics. Figure 2 presents the number of main-track derailments reported by the Canadian railways to the Transportation Safety Board of Canada (TSB 1994) combined with data from the following years (TSB 2001). The '*main track*' is defined as a track extending through yards and between stations whereas '*non-main track*' is composed mostly of sidelines and yards. Figure 2 shows that Canadian *main-track* derailments have declined by a factor of almost three between 1980 and 1988, fol-

lowed by a roughly level trend thereafter, despite a peak of derailments in 1996. A series of equipment improvement initiatives undertaken during the 1980's were essentially exhausted after 1988, explaining in part why derailments have levelled or even increased thereafter.
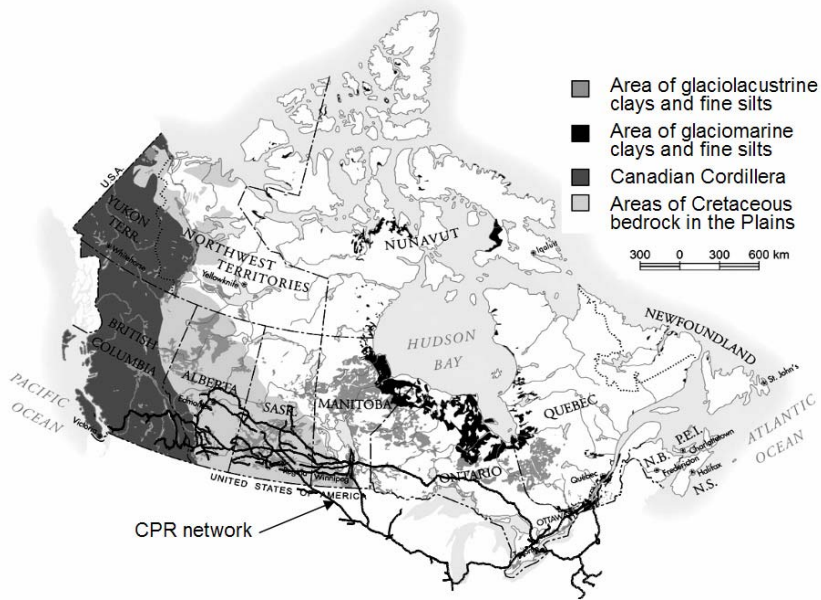

Fig. 1. Canadian Pacific Railway network and main landslide areas according to the type of terrain (terrain data from Office of Critical Infrastructure Protection and Emergency Preparedness 2001).
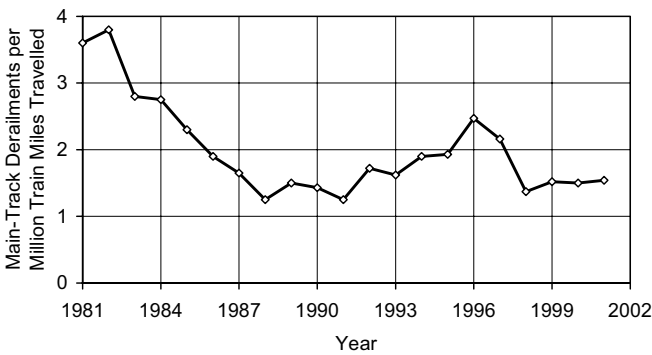

Fig. 2. *Main-track* derailment data provided by the Transportation Safety Board of Canada (1994 and 2001).

In 2001, the Transportation Safety Board provided more detailed rail occurrence statistics, including *non-main track* data. Figure 3 presents the total number of derailments classified by assigned factors, along with the number of fatalities and injuries caused by derailments from 1992 to 2001. Geometry and roadbed factors are closely related to geo-hazards whereas equipment factors are associated to mechanical failures and defects. Action factors are related to inappropriate train and track operation. Figure 3 shows that the number of fatalities and injuries caused by derailments can be considered small when compared to the numbers of fatalities and injuries associated with crossing and trespasser accidents, which reaches the hundreds annually. A high number of derailments suggest a potentially high financial impact. Clear trends for the entire period from 1992 to 2001 are non-existent, but the number of derailments is relatively constant as shown in Fig. 3. One important observation shown by the data is that the cross-section geometry and roadbed factors have a significant contribution to the number of derailments, demonstrating the importance of geo-hazards for railway safety.

1.2 Geo-hazards affecting Canadian railways

The geo-hazards affecting the Canadian railway networks can be classified into five categories; namely, debris flows, embankment failures, rock falls, volume change (subsidence and frost heave), and erosion washouts. Figure 4 groups together the first four categories as "slope and subgrade failure and/or serviceability" problems. Most geo-hazards are clearly a direct function of weather conditions and are usually triggered by severe weather conditions/storms. Embankment failures and debris flows represent relatively low frequency and high impact hazards, while other categories have higher frequencies but a lower impact.

In the past, geo-hazards have received the same emphasis as equipment-related hazards, but there has been less success in dealing with geo-hazards due to the complexity of assessing ground conditions. Improvements in real-time hazard detection systems and the implementation of track inspection programs have somewhat improved the situation. Detection instrumentation systems are effective but are an expensive option that still requires a great deal of technological improvement. Inspection programs only partially assist in identifying track geometry problems because washouts and slides can quickly cause roadbed deterioration. In order to adequately identify geometry related problems, an economically prohibitive number of inspection teams would have to be dispatched.

Improvements in geo-hazard assessment techniques can assist in indicating appropriate inspections frequencies, thereby providing a way to rationalize railway resources. CPR has implemented slope hazard assessment and management programs. The programs are showing promise but limited results are available. One such example is the rock slope program implemented during the mid 1970's, using a *qualitative* priority rating system (ranking method). While *qualitative* assessment methods satisfy many practical needs, the advantages of *quantitative* methods cannot be ignored. Morgenstern (1997) presents a list of advantages of *quantitative* assessment approaches. Mackay (1997) showed that the CPR hazard

management programs would greatly benefit from a procedure for *quantitative* as-sessment. Most geo-hazards are triggered by severe weather conditions, and therefore a *quantitative* hazard assessment method meeting the needs of CPR should involve quantification of the influence of weather. The quantification of weather effects can be done through a soil-atmospheric moisture exchange model (Wilson et al. 1994).
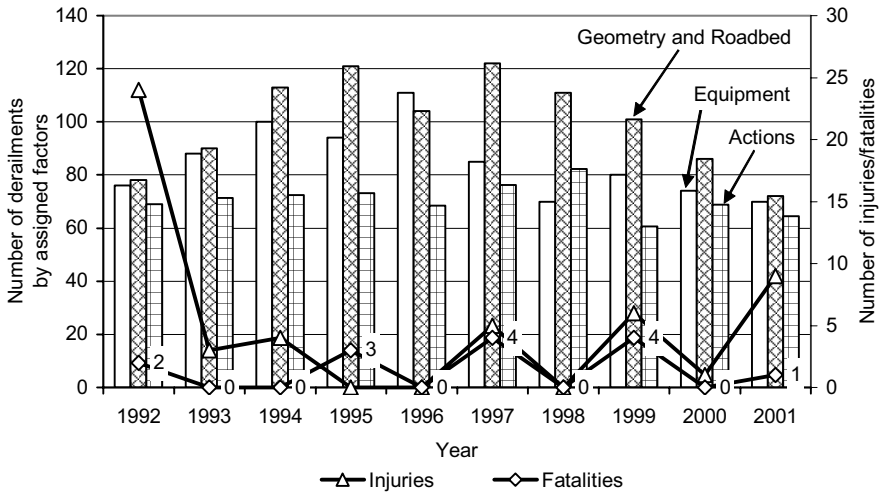

Fig. 3. *Main-* and *non-main* track derailments by assigned factors and inju-ries/fatalities due to derailments (data from Transportation Safety Board of Can-ada 2001).
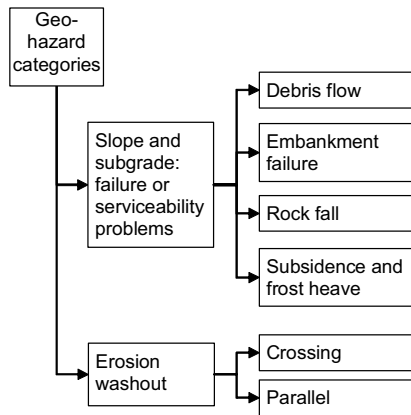

Fig. 4. Categorization of geo-hazards

The framework for the assessment of weather-related geo-hazards under study will be limited to embankment ruptures. The general framework should also be applicable for the assessment of the other categories of geo-hazards. Infiltration and exfiltration are considered in this paper, but the influences of freezing and thawing processes are not considered.

1.3   Soil-water characteristic curve as a hazard gauge

Embankment hazards are strongly related to the reduction in soil suction within the embankment. Soil suction varies according to the amount of water stored within the embankment. On the other hand, changes in the amount of water within the soil are associated with the weather conditions and soil properties. The relationship between the amount of water being stored in the soil and soil suction is given by the soil-water characteristic curve, SWCC (Figure 5). Typical unimodal SWCC's can be defined using four soil parameters; namely, the air-entry value, ψ_b, the residual suction, ψ_{res}, the residual degree of saturation, S_{res}, and a parameter defining the sharpness of the transitions at the bending points, 'a' (Gitirana Jr. & Fredlund 2003). The shape of the SWCC is a function of the pore-size distribution in the soil, amongst other factors.

Figure 6 presents an analogy, explaining the fundamental concept behind the W-GHA model. According to this analogy, the soil comprising an embankment can be viewed as a 'water tank'. The SWCC works as a gauge, an indication of the water level within the 'water tank'. The water level is lowered through evaporation and downward seepage and raised through infiltration from rainfall. The embankment *factor of safety*, F_s, and the embankment hazard level vary according to the water level. A low water level corresponds to a lower level of hazard (higher F_s), while higher water levels produce greater hazards (lower F_s). The rigorous model for the assessment of embankment hazards presented herein is based on the 'water tank' concept and on the *factor of safety*. However, it is also possible that a more crude approach could rely directly on the water level within the 'water tank'. Such an approach would still capture the main factors controlling the stability of railway embankments.
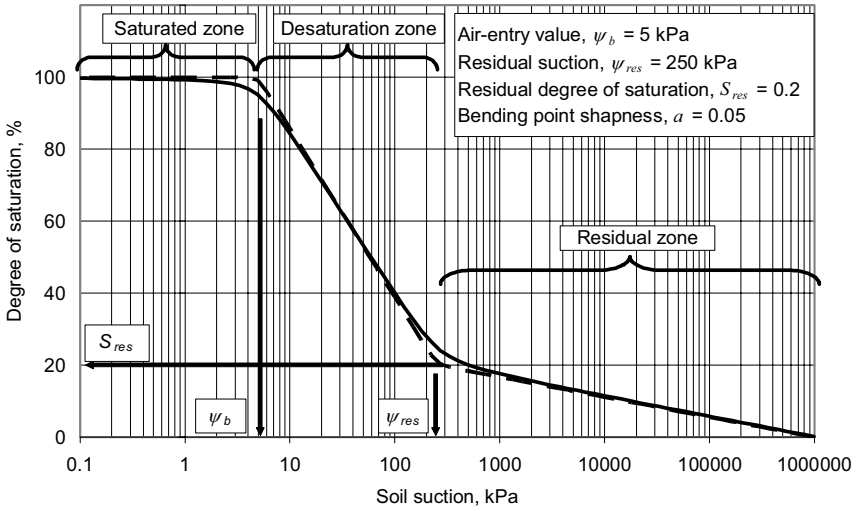
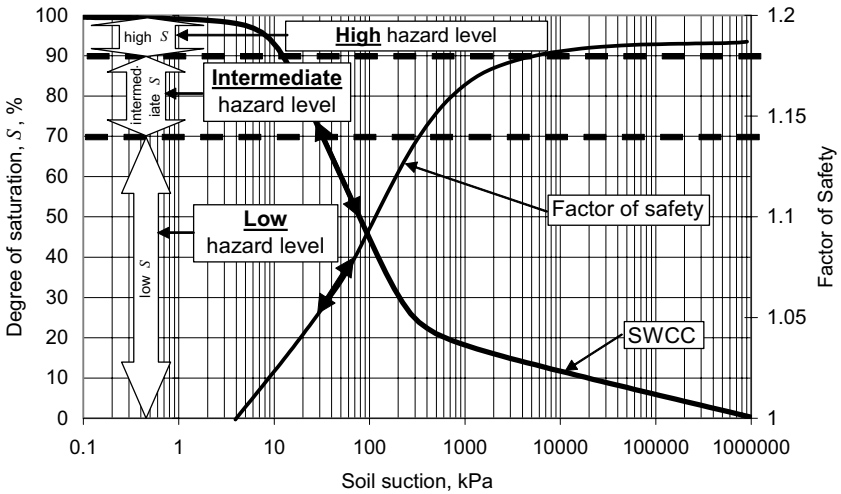**Fig. 5.** Soil-water characteristic curve conceptualization.

Fig. 6. SWCC as a water level and embankment hazard gauge.

2   DECISION ANALYSIS MODEL FOR WEATHER-RELATED GEO-HAZARDS

The W-GHA model is composed of deterministic and probabilistic elements that are developed within a *Decision Analysis* framework. Einstein et al. (1978) and Einstein (1997) present some applications of the *Decision Analysis* technique to geotechnical engineering problems. According to the definition given by Keeney and Raiffa (1976), *Decision Analysis* provides a structure for systematically analysing difficult situations. Bunn (1984) emphasized that *Decision Analysis* should not be viewed as a substitute for the personal judgement of decision makers, but as a complement. Bunn's observations are similar to the views of several researchers with regard to the role of probabilistic analysis in geotechnical engineering. These authors recommend the use of a reliability-based analysis not as a substitute, but along with the past experience accumulated after generations of geotechnical engineering (Whitman 1984, Fell 1994, and Morgenstern 1995).

According to Clemen (1996), there are four basic sources of difficulty in decision analysis. These are: (1) problem complexity; (2) inherent uncertainty of the situation; (3) decisions involving multiple objectives; and (4) problems where different perspectives lead to different conclusions. The W-GHA model is a complex, multidisciplinary model that brings together concepts of geotechnical and hydrological engineering for a complex problem. There are also inherent uncertainties due to soil properties and weather conditions. The third source of difficulty listed above can be considered to be 'not important' if the analysis of geohazards is kept sufficiently narrow.

All railway objectives presented in the next section depend on the minimization of hazards. The minimization of hazards can be expressed in terms of the single objective to maximize the factor of safety for the problem at hand. The fourth type of difficulty listed above should be of minor importance when compared to the previous sources of difficulty, as long as broadly accepted geotechnical engineering approaches are undertaken.

The *Decision Analysis* flowchart has seven steps (Fig. 7). The first two steps in the *Decision Analysis* cycle, 'identification of decision situations' and 'identification of alternatives' are presented in this section. Step number three, 'decomposition and modelling' is presented later. Systematic criteria for the selection of best alternatives and systematic steps in a sensitivity analysis can be learned from the *Decision Analysis* approach. The choice of a best alternative can be temporarily eliminated and the problem reduced to a *reliability-based* analysis problem.
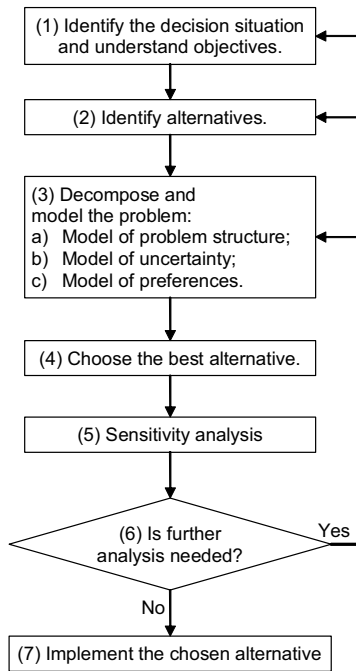
Fig. 7. A *Decision Analysis* process cycle (modified from Clemen 1996).

2.1 Identification of railway objectives and means

Clemen (1996) offers guidelines for the identification of <u>objectives</u> and <u>means</u> in *Decision Analysis*. This portion of the decision modelling process is often referred as 'brainstorming". Figure 8 describes the fundamental objectives hierarchy for the railway, for the context considered herein. The maximization of the railway system performance can be considered to be the most fundamental objective. Minimization of financial losses, injuries, loss of life, and the release of dangerous goods are objectives to be reached as part of the most fundamental objective. Finally, the objectives in the lower hierarchical places are the minimization of all types of geo-hazards. The hazard may be a mechanical, geotechnical, or a human action problem. The widely used global *factor of safety* concept will be used to quantify embankment stability hazard levels. Debris flows, rock falls, and volume change problems may require different hazard quantification parameters.

The identification of the means available to deal with geo-hazards is less straightforward. Figure 9 presents the *means-objectives* network for the railway system. The <u>means</u> to maximize the railway system performance are numerous, and only a few are presented in the figure in order to keep the context of the problem from becoming excessive. Two distinct types of <u>means</u> can be identified;

namely, reactive and proactive means. As geo-hazard assessment techniques were not available in the past, the rail industry needed to invest most of its resources on reactive methodologies. As our knowledge and understanding of geo-hazards develops, new proactive methodologies become an option. Figure 9 presents the most important means towards the implementation of proactive methodologies.

2.2   Identification of railway alternatives

The decision at hand has two possible alternatives; namely, to take action or not take action. The question of whether or not action needs to be taken is of paramount importance in the management of a railway system. The ability to identify high-level hazards along the railway would render considerable savings. By taking precautionary measures, loss of equipment can be prevented and the safety of the railway workers increases, reducing the number of injuries and the chance of fatalities. A major concern to the railway companies is the frequent delays caused by accidents along the track, and in this case delays could be reduced.
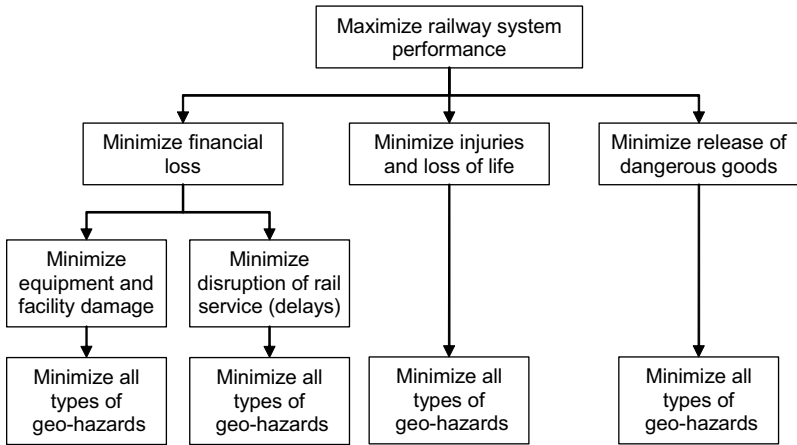

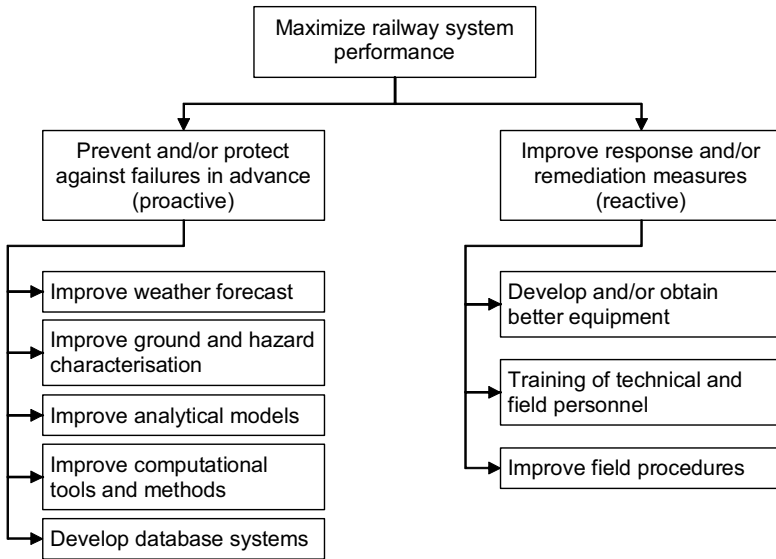**Fig. 8.** A Fundamental objectives hierarchy of the W-GHA model.

Fig. 9. Means-objectives network of the W-GHA model.

The two generic alternatives (i.e., to <u>take action</u> or <u>not take action</u>) are considered herein. However, different hazard levels and conditions would require different actions. Stronger actions must be taken for greater risks and different actions must be taken for different hazard characteristics. Details regarding the railway system management and the consideration of types of actions to be taken are issues that must be addressed by the *Decision Makers*. Specific alternatives can be considered using the proposed framework.

3   Model for the problem structure

The deterministic modelling of railway embankment stability problems represents the most complex part of developing the W-GHA model. A traditional geotechnical engineering approach is used in the sense that the stability of railway embankments is idealized as a function of the stress state (i.e., total stresses and pore-water pressure) and the shear strength along a critical slip surface within the earth mass. The *Factor of Safety*, F_s, is determined using an optimization technique.

The W-GHA model is based on a series of partial differential equations governing the thermo-hydro-mechanical behaviour of the saturated/unsaturated soil system. Appropriate boundary conditions to account for evaporation, precipitation, and runoff are given. The manner in which the pore-water pressures and total stress distributions are used to determine stability is explained later.

3.1   W-GHA model components

Figure 10 illustrates the environmental factors affecting the stability of an embankment. Changes in the stress state distribution and shear strength within the soil mass take place in response to moisture fluxes at the soil-atmosphere boundary. In order to determine the moisture flux and changes in pore-water pressure in the soil, partial differential equations (PDE's) governing the flow of water must be combined with appropriate boundary conditions and solved for the period of time under consideration. The PDE governing the flow of heat must also be solved since the amount of liquid water and water vapour flow depends on the temperature, which in turn, changes in response to the energy available at ground surface. Special procedures to determine the amount of run-off and actual evaporation are also required. The total stress distribution and the shear stress acting along a particular slip surface are obtained by solving the PDE's governing static equilibrium of forces.

The W-GHA model incorporates the influence of soil-atmosphere moisture fluxes on the stability of an embankment according to the flowchart presented in Figure 11. An essential component of the model is the *Dynamic Programming* algorithm associated with the slope stability analysis. The algorithm is used to determine critical conditions and the corresponding factors of safety F_s at any time, t. In order to determine critical conditions, the net stress distribution at $t = t_i$ and the corresponding pore-water pressure distribution, u_w, at $t = t_i$ are required. The pore-water pressure distribution is determined by solving two-dimensional, partial differential equations governing transient moisture and heat flow. The initial pore-water pressure distribution, u_{w0}, is also required. Realistic functions for the amount of precipitation and evaporation are combined with the moisture and heat flow analysis to determine the transient soil-atmosphere boundary flux.
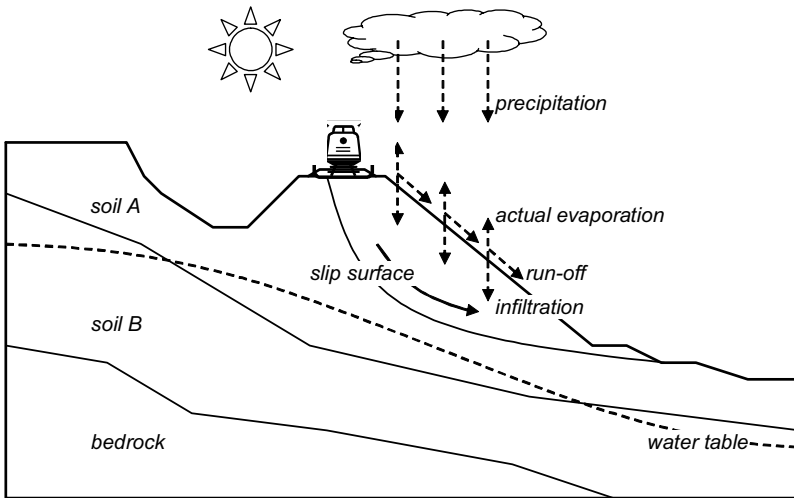

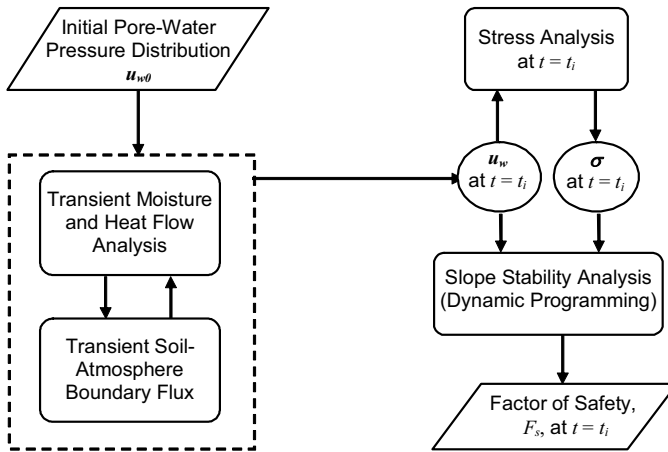**Fig. 10.** Factors affecting the stability of an embankment.

Fig. 11. W-GHA model flowchart.

In order to determine embankment stability, the pore-water pressure distribution is sampled at several pre-determined times, $t = t_i$. The degree of saturation (or water content) within the soil mass and the soil unit weight distribution are computed as functions of the pore-water pressure distribution (i.e., the SWCC). For each of the chosen sampling times, the partial differential equations governing static equilibrium are solved using the soil unit weight distribution and external loads. Finally, the *Dynamic Programming* optimization algorithm uses the net total stresses and pore-water pressure distributions to determine the location and shape of the critical slip surface and the corresponding factor of safety.

The W-GHA model considers uncertainties related to soil properties and weather conditions through an appropriate frequency or probabilistic analysis. The probabilistic model consists of sampling the frequency distribution of the variables considered as uncertain. This is done a number of times and the deterministic model is run using each set of sampled values. The organization of several scenarios obtained from the discrete frequency distributions is presented in the format of a *Decision Tree*. The probability of the embankment becoming unstable is assessed based on the outcomes from the *Decision Tree*.

3.2   Partial differential equations governing soil behaviour

The hydro-thermo-mechanical behaviour of the soil comprising a railway embankment can be represented by a system of partial differential equations (PDE's). These equations are obtained using a traditional continuum mechanics approach and appropriate state variables. The broadly accepted stress state variables; namely, net total stress (σ-u_a) and matric suction (u_a-u_w), are used. The displacement state variables are the horizontal and vertical displacements, u and v, and the change in volume of water and air in a referential volume. The PDE's governing

static force equilibrium, flow of moisture, and flow of heat are obtained from basic continuity and equilibrium laws, combined with constitutive laws that describe soil behaviour.

Moisture moves through soils driven by gradients of total head and/or partial pressures for each of the moisture phases (i.e., both liquid water and water vapour). The ratio between the flow of liquid water and water vapour depends mainly on the temperature and degree of saturation of the soil. Consequently, the transient temperature distribution needs to be taken into account when simulating the flow of moisture. Appropriate equations for the soil-atmosphere flux boundary conditions are required. The two-dimensional PDE's used in this study are an extension of the one-dimensional formulations presented by Philip and de Vries (1957) and Wilson et al. (1994).

3.2.1   *Conservation and flow of moisture*

A series of assumptions form the backdrop for the equations accounting for the flow of liquid water and water vapour in soils. Some of the assumptions are as follows; namely, (i) the soil phases are individually continuous and therefore can be described using a continuum mechanics approach; (ii) the air phase is in permanent contact with the atmosphere; (iii) the flow of air due to thermal gradients has not been considered; (iv) osmotic pressure gradients are negligible; (v) local thermodynamic equilibrium between the liquid water and water vapour phases exists at all times at any point in the soil; (vi) temperature within the soil remains below the boiling point and above the freezing point of water at all times; (vii) dissolution of air into the liquid water phase is not considered; (viii) interphase water vapour flux caused by changes in partial vapour pressure and/or air phase volume is neglected; and (ix) hysteretic behaviour of the soil-water characteristic curve can be approximated by taking the average between the main drying and main wetting curves.

The conservation of mass equation for the water phase can be derived by taking the rate of flux of water mass in and out of a representative elemental volume (REV) and equating the difference to the rate of change of water mass within the element with time (Fig. 12). The x- and y-directions are considered for two-dimensional flow. Three types of water mass flow are considered; namely, mass flux of liquid water by advection (q^w); mass flux of water vapour by diffusion (q^{dv}); mass flux of water vapour carried by bulk air by diffusion (q^{av}). The mass flux of liquid water in unsaturated soils can be described by using Darcy's law. The mass flux of water vapour can occur by diffusion and can be described using Fick's law (Philip and de Vries 1957 and Dakshanamurthy and Fredlund 1981). Only the gradient in the partial water vapour pressure component of the total pressure gradient in air is considered (i.e., partial pressure of the dry air is considered constant and equal to the atmospheric pressure). The volume of water within the REV can be expressed in terms of the stress state variables. The coefficient of water volume change, m_2^w, can be written as the derivative of the soil-water characteristic curve. Combining the conservation of mass equation, the constitutive laws

for water and air flow, and the derivative of the soil-water characteristic curve, the following PDE is obtained:

$$\frac{\partial}{\partial x}\left[k^w \frac{\partial(u_w/\gamma_w)}{\partial x} + \frac{\bar{u}_a + p_v}{\bar{u}_a} \frac{D^v}{\rho_w} \frac{\partial p_v}{\partial x} \right]$$

$$+ \frac{\partial}{\partial y}\left[k^w \frac{\partial(u_w/\gamma_w + y)}{\partial y} + \frac{\bar{u}_a + p_v}{\bar{u}_a} \frac{D^v}{\rho_w} \frac{\partial p_v}{\partial y} \right] = -m_2^w \frac{\partial u_w}{\partial t} \quad (1)$$

where k^w is the hydraulic conductivity ($k^w = f(u_a\text{-}u_w)$, m/s); u_a is the pore-air pressure, kPa; u_w is the pore-water pressure, kPa; γ_w is the unit weight of water, ≈ 9.81 kN/m^3; y is the elevation, m; $\bar{u}_a$ is the total pressure in the bulk air phase, $u_{atm}+u_a$, kPa; p_v is the partial pressure of water vapour, kPa; D^v is the diffusion coefficient of the water vapour through the soil, (kg.m)/(kN.s); ρ_w is the density of water, ≈ 981.0 kg/m^3; m_2^w is the coefficient of water volume change with respect to matric suction, $m_2^w = (e/(1+e))(dS/d(u_a - u_w))$, 1/kPa; and e is the void ratio.

A relationship between the partial pressure of water vapour and the total potential of the liquid pore-water (or total suction) can be obtained based on the thermodynamic theory of soil moisture (Edlefsen and Anderson 1943). Assuming local thermodynamic equilibrium, neglecting the effects of the osmotic suction, and assuming that the air pressure is equal to the atmospheric pressure, the following relationship applies:

$$p_v = p_{vsat}\, \exp\left[\frac{u_w g W_v}{\gamma_w RT} \right] \quad (2)$$

where p_{vsat} is the saturation vapour pressure of the soil water at temperature T, kPa; g is the acceleration of gravity, 9.81 m/s^2; W_v is the molecular weight of water, 0.018016 kg/mol; R is the universal gas constant, 8.314 J/(mol.K); and T is the temperature, K.

According to Eq. 2, any of the three variables, u_w, p_v, and T, can be determined by the value of the other two variables. Therefore, the gradient of any of the three state variables is also determined by the gradient of the other two variables, as follows:

$$\nabla p_v = \frac{gW_v p_v}{\gamma_w RT}\left(\nabla u_w - \frac{u_w}{T}\nabla T \right) \quad (3)$$

Expressing the gradients of partial vapour pressure in Eq. 1 in terms of the gradients of pore-water pressure and temperature by using Eq. 3, the following PDE is obtained:

$$\frac{\partial}{\partial x}\left[\left(\frac{k^w}{\gamma_w}+D^{v*}\right)\frac{\partial u_w}{\partial x}-D^{v*}\frac{u_w}{T}\frac{\partial T}{\partial x}\right]$$ (4)

$$+\frac{\partial}{\partial y}\left[\left(\frac{k^w}{\gamma_w}+D^{v*}\right)\frac{\partial u_w}{\partial y}+k^w-D^{v*}\frac{u_w}{T}\frac{\partial T}{\partial y}\right]=-m_2^w\frac{\partial u_w}{\partial t}$$

where $D^{v*}=\left(\left(\overline{u}_a+p_v\right)p_v/\left(\rho_w\overline{u}_a\right)\right)\left(W_v/\left(\rho_w RT\right)\right)D^v$. Equation 4 is the final PDE governing the flow of moisture by liquid water and water vapour flow. Temperature gradients required to render this equation solvable can be obtained by solving the PDE satisfying conservation of thermal energy. Three unsaturated soil property functions can be identified in Eq. 4; namely: the hydraulic conductivity, the vapour diffusion coefficient, and the coefficient of water volume change. These soil properties functions vary with soil suction, and therefore the PDE is non-linear.
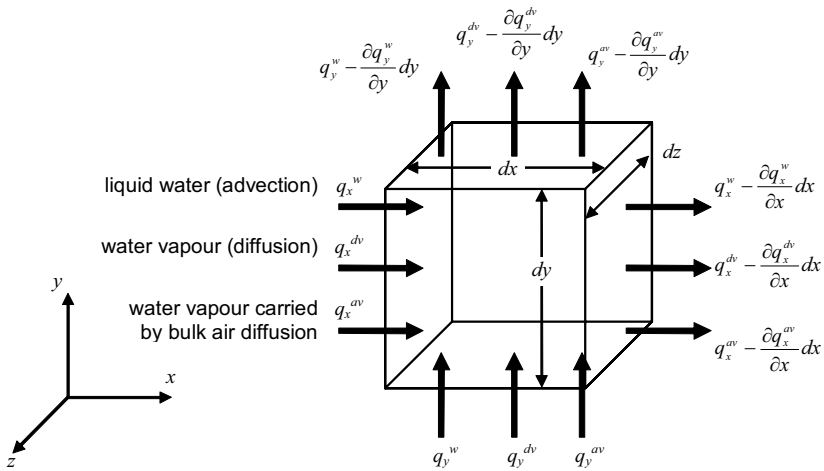
Fig. 12. Soil representative elemental volume and water mass fluxes.

3.2.2   *Conservation and flow of heat*

Heat transfer in soils occurs by three mechanisms, namely: conduction; convection; and latent heat due to phase change. Heat transfer by convection of the pore-fluid in soils is considerably smaller than conductive heat transfer (Milly 1984) and therefore can be neglected for the problem at hand. Vaporization is the only phase change presently of concern. Considering these conditions, the conductive and latent heat transfer in soils can be modelled using the Fourier equation (Dakshanamurthy and Fredlund 1981), as follows:

$$L_V \frac{\bar{u}_a + p_v}{\bar{u}_a} \frac{\partial}{\partial x}\left(D^v \frac{\partial p_v}{\partial x}\right) + L_V \frac{\bar{u}_a + p_v}{\bar{u}_a} \frac{\partial}{\partial y}\left(D^v \frac{\partial p_v}{\partial y}\right) \tag{5}$$

$$+ \frac{\partial}{\partial x}\left(\lambda \frac{\partial T}{\partial x}\right) + \frac{\partial}{\partial y}\left(\lambda \frac{\partial T}{\partial y}\right) = \zeta \frac{\partial T}{\partial t}$$

where L_V is the latent heat of vaporization, $4.187 \times 10^3 (591 - 0.51T)$, J/kg; T is the temperature, °C; λ is the thermal conductivity, $\lambda = f(u_a - u_w)$, W/(m °C); and ζ is the volumetric specific heat of soil, $\zeta = f(u_a - u_w)$, J/(m³ °C).

The first two terms in the left-hand side of Eq. 5 correspond to the heat energy released when there is a transfer of water between the vapour and liquid water phases (i.e., latent heat transfer by vaporization). Expressing the gradients of partial vapour pressure in Eq. 5 in terms of gradients of pore-water pressure and temperature by using Eq. 3, the following PDE is obtained:

$$\frac{\partial}{\partial x}\left[L_V D^{v*} \rho_w \frac{\partial u_w}{\partial x} + \left(\lambda - L_V D^{v*} \rho_w \frac{u_w}{T}\right)\frac{\partial T}{\partial x}\right] \tag{6}$$

$$+ \frac{\partial}{\partial y}\left[L_V D^{v*} \rho_w \frac{\partial u_w}{\partial y} + \left(\lambda - L_V D^{v*} \rho_w \frac{u_w}{T}\right)\frac{\partial T}{\partial y}\right] = \zeta \frac{\partial T}{\partial t}$$

The PDE for the flow of heat shown in Eq. 6 must be solved in a coupled manner along with Eq. 4. The primary variables are u_w and T. Two unsaturated soil property functions can be identified in Eq. 6; namely: the thermal conductivity function and the volumetric specific heat. These soil properties functions also vary with soil suction, rendering the PDE non-linear. All of the above-mentioned unsaturated soil property functions bear a relationship to the SWCC.

3.2.3   Static equilibrium of forces and stress-strain relationship

The PDE's governing the static equilibrium of forces can be obtained by considering the equilibrium of forces acting upon a REV of soil. For the two-dimensional case, equilibrium in the x- and y-directions must be considered. The forces are expressed in terms of stresses and infinitesimal areas. Combining the equilibrium equations with Hooke's generalised stress-strain law, and expressing the strain in terms of small displacements, the following PDE's are obtained for the x- and y-directions:

$$\frac{\partial}{\partial x}\left[D_{11}\frac{\partial u}{\partial x} + D_{12}\frac{\partial v}{\partial y}\right] + \frac{\partial}{\partial y}\left[D_{44}\left(\frac{\partial u}{\partial y} + \frac{\partial v}{\partial x}\right)\right] = 0 \tag{7}$$

$$\frac{\partial}{\partial x}\left[D_{44}\left(\frac{\partial u}{\partial y} + \frac{\partial v}{\partial x}\right)\right] + \frac{\partial}{\partial y}\left[D_{12}\frac{\partial u}{\partial x} + D_{11}\frac{\partial v}{\partial y}\right] + \gamma = 0 \tag{8}$$

where u and v are the displacement in the x- and y-directions respectively, m; $D_{11} = E(1-\mu)/[(1+\mu)(1-2\mu)]$; ; $D_{12} = E\mu/[(1+\mu)(1-2\mu)]$; ; $D_{44} = E/[2(1+\mu)]$; E is the Young modulus, kPa; μ is the Poisson ratio; $\gamma = (G_s + Se)\gamma_w/(1+e)$ is the unit weight of the soil, kN/m^3; and G_s is the specific unit weight of soil particles.

Overall volume changes in the soil due to changes in pore-water pressure are neglected in Eqs. 7 and 8. If the volume changes due to changes in pore-water pressure are to be considered, constitutive relationships between volume change and pore-water pressure would have to be considered and Eqs. 7 and 8 would have to be solved in a coupled manner with Eqs. 4 and 6. The primary variable of interest in the W-GHA model is the change in pore-water pressure and net total stresses in response to the atmospheric boundary conditions. Therefore, the stress equilibrium-moisture flow coupling would not appear to be essential.

The system formed by Eqs. 4, 6, 7, and 8 represents a thermal-hydromechanical model appropriate for the application at hand. In order to solve these equations, the W-GHA model has made use of a multi-purpose partial differential equation solver, FlexPDE (PDE solutions 2003). FlexPDE uses the Finite Element (FE) and the Finite Difference (FD) methods combined with Newton-type methods of solution of non-linear coupled systems. The friendly input and output features combined with automatic mesh generation, time-step control, and choice of non-linear approaches makes FlexPDE a powerful part of a complete *problem solving environment* (PSE) (Gallopoulos et al. 1994). SoilVision Systems (2003) is another example of a PSE developed specifically for geotechnical engineering problems.

3.3   Weather-related boundary conditions

The partial differential equations based on the conservation of moisture and heat require boundary conditions related to atmospheric forcing conditions. The net soil-atmosphere moisture flux is a function of some of the key components of the hydrological cycle; namely, precipitation, actual evaporation, and run-off. Other components, such as depression storage, interception, and plant transpiration, are not considered herein, but could also be included in the formulation. The heat flow at the soil-atmosphere boundary is a function of the net radiation available at ground surface and the latent heat of evaporation. Appropriate equations to represent these boundary conditions are presented in the following sections.

3.3.1   Net soil-atmosphere moisture flux

The combination of precipitation, actual evaporation, and runoff can produce a net soil-atmosphere boundary flux designated either as infiltration (positive flux) or exfiltration (negative flux). The amount of net soil-atmosphere moisture flux must satisfy the following water balance equation:

$$NF = P - AE - R \tag{9}$$

where *NF* is the net moisture flux, m/s; *P* is the precipitation, m/s; *AE* is the actual evaporation, m/s; and *R* is the runoff, m/s. The net moisture flux must be applied as the component of the vertical vector of magnitude *NF*, normal to the ground surface and as a natural boundary condition to Eq. 4. The amount of precipitation, *P*, will be a known input based upon weather data. The amount of actual evaporation, *AE*, and runoff, *R*, are a function of both weather and soil conditions. More specifically, *AE* and *R* are a function of the soil suction at the soil-atmosphere boundary. As a result, the net moisture flux is an unknown that must be computed by simultaneously solving the net soil-atmosphere moisture flux boundary condition and the PDE's governing the movement of water and heat.

The amount of actual evaporation is a function of *potential evaporation*, *PE* (i.e., the amount of evaporation from a water surface under specific atmospheric conditions), and the soil surface conditions. The flow of moisture towards the soil surface for wet conditions occurs primarily as liquid water movement. As the soil dries, water begins to move in the form of vapour. A decrease in water content at the soil surface corresponds to an increase in soil suction. As soil suction increases, a larger amount of energy is required to remove water from the soil surface. Wilson et al. (1997) demonstrated that the actual evaporation from a soil surface can be determined by using a measure of potential evaporation combined with a limiting function. This limiting function reflects the decrease in actual evaporation as soil suction at the boundary is increased:

$$AE = PE\left[\frac{RH - \left(p_{vsat}^{air}/p_{vsat}\right)RH_{air}}{1 - \left(p_{vsat}^{air}/p_{vsat}\right)RH_{air}}\right] \tag{10}$$

where $RH = p_v/p_{vsat}$ is the relative humidity at the soil surface, given by Eq. 2; p_{vsat}^{air} is the saturation vapour pressure of the air, kPa; and RH_{air} is the relative humidity of the air near the ground surface. According to Eq. 2, as soil suction increases, *RH* decreases until it eventually approaches zero for a value of suction approximately equal to 1×10^{-6} kPa. Likewise, Eq. 10 shows that as the relative humidity decreases, *AE* decreases until it approaches zero when the relative humidity approaches zero. If a direct measure of potential evaporation is not available, it is possible to use one of the several equations proposed in the literature to calculate *PE* based on weather data.

The net moisture flux at the soil-atmosphere boundary (Eq. 9) can be determined once the amount of precipitation is known and the parameters of the *AE* equation are obtained. The third component in Eq. 9 is runoff and it can be computed in an interactive way. If the embankment being analysed has an effective drainage system, any runoff water will be removed from the ground surface. In this case, the amount of net moisture flux, *NF*, should not produce pore-water pressures at ground surface higher than zero. Therefore, the following set of conditions is used:

$$NF = \begin{cases} P - AE & : \text{if } P - AE > 0 \text{ and } u_{ws} < 0 \\ EF(0 - u_{ws}) & : \text{if } P - AE > 0 \text{ and } u_{ws} \geq 0 \\ P - AE & : \text{if } P - AE \leq 0 \end{cases} \tag{11}$$

where u_{ws} is the pore-water pressure at the surface, kPa; and EF is simply a large number, such as 1×10^4. If the multiplier EF tends to infinity, the area flux boundary condition $NF = EF(0 - u_{ws})$ becomes mathematically equivalent to the boundary node value pore-water pressure, $u_w = 0$. Therefore, the boundary condition using the flux $[EF(0 - u_{ws})]$ is used as an alternative to switching the category of boundary condition when the pore-water pressure at the soil surface reaches zero. Equation 11 has been implemented in FlexPDE using conditional functions built into the software. Runoff can occur when the potential infiltration is sufficiently large and the hydraulic conductivity is small relative to the water available for infiltration. The amount of runoff corresponds to the difference between the water available (i.e., $P - AE$), minus the amount of net flux computed in the interactive manner from Eq. 11.

3.3.2   Heat flow

The heat flow at the ground surface must be in accordance with the following energy balance equation:

$$H = Q_n - AE \tag{12}$$

where H is the heat flux at the soil surface, W/m^2; Q_n is the net radiation available at the soil surface, W/m^2; and AE is the actual evaporation, W/m^2. The heat flux H must be applied as a natural (flux) boundary condition, to Eq. 6.

3.4   Stability analysis using Dynamic Programming

The *Dynamic Programming Method* (DPM) is a general method of maximization and minimization of linear (additive) functionals (Bellman 1957). Baker (1980) applied the DPM to slope stability problems, while retaining the Spencer (1967) assumption regarding interslice forces. Yamagami and Ueta (1988) extended the DPM approach and replaced the Spencer limit equilibrium method with stresses computed from a Finite Element stress analysis. The result of DPM studies have also been presented by Zou et al. (1995), Pham et al. (2001), and Pham (2002).

Conventional limit equilibrium methods are usually combined with an assumption regarding the shape of the critical slip surface. The DPM represents an important breakthrough in that the slip surface shape restrictions are significantly relaxed. The combined use of Finite Element stress fields further enhances the analysis by providing a means of incorporating into the slope stability analysis more realistic boundary conditions, soil stress-strain properties, and stress history. Little human interference in the analysis process is required once the problem geometry, boundary conditions, material properties, and search grid are established.

The input requirements for the DPM combined with Finite Element stress fields are quite similar to those of conventional limit equilibrium methods. The stress-strain constitutive parameters and the boundary conditions are the only additional parameters that must be designated. The use of a problem solving environment, such as FlexPDE, can make stress-strain analyses as easy as traditional limit equilibrium procedures since only approximate values of the elasticity parameters are required (Pham 2002). If a linear constitutive law is adopted in the stress analysis, the computational time can be similar to, or shorter than that of conventional limit equilibrium codes (Pham et al. 2001). The characteristics of the DPM combined with Finite Element stress fields are particularly desirable for the W-GHA model because all analyses are reduced to the solution of a series of partial differential equations.

3.4.1   Optimization procedure

Figure 13 presents the analytical scheme for stability analysis using the *Dynamic Programming* Method, DPM (Yamagami and Ueta 1988 and Pham et al. 2001). The procedure used in the W-GHA model is based on the assumption that the critical slip surface can be defined using "*n*" linear segments. Each linear segment connects two *state points* located at two successive *stages*. The *search grid* consists of a collection of *state points* lying on "*n+1*" *stages*. A relatively coarse search grid is superimposed on the geometry shown in Figure 13. The dynamic programming procedure is used to determine a continuous assemblage of segments that corresponds to a minimum overall factor of safety. In order to quantify the overall stability, a *factor of safety*, F_s, along a slip surface is defined in its discrete form as:

$$F_s = \sum_{i=1}^{n} R_i \bigg/ \sum_{i=1}^{n} S_i = \sum_{i=1}^{n} \tau_{f_i} \Delta L_i \bigg/ \sum_{i=1}^{n} \tau_i \Delta L_i \qquad (13)$$

where n is the total number of segments; R_i is the resisting force of the soil along the ith segment, kN/m; S_i is the shear force acting along the ith segment, kN/m; τ_{fi} is the shear strength of the soil along the ith segment, kPa; ΔL_i is the length of the ith segment, m; and τ_i is the shear stress along the ith segment, kPa. This definition of factor of safety (i.e., considering the state of overall limit equilibrium of forces), puts the DPM within a similar class to the limit equilibrium methods. The unique characteristic of the DPM lies in the manner by which the shape and position of the critical slip surface, along with the corresponding minimum F_s, is obtained.

In order to minimize the <u>non-additive</u> F_s functional the following <u>additive</u> functional is introduced (Baker, 1980):

$$G = \sum_{i=1}^{n} (\tau_{f_i} \Delta L_i - F_s \tau_i \Delta L) \qquad (14)$$

In order to minimise G, the *optimal function*, H, is used. $H_{i+1}(j)$ is defined as the minimum of G between any *state point* at the initial *stage* and any posterior *state point* $[i, j]$. According to the principle of optimality (Bellman 1957), the optimal function at a posterior *stage*, $H_{i+1}(j)$, is a function of the optimal function at the prior *stage*, $H_i(k)$, as follows:

$$H_{i+1}(j) = \min\left[H_i(k) + DG_{i+1}(j,k)\right] \tag{15}$$

where $i = 1, n$; $j = 1, NP(i+1)$; $k = 1, NP(i)$; $NP(i)$ is the number of *state points* on *stage i*; and $DG_{i+1}(j,k) = \tau_{f_i}\Delta L_i - F_s\tau_i\Delta L$. The term $DG_{i+1}(j, k)$ corresponds to the 'cost' of passing between the *state points* $[i+1, j]$ and $[i, k]$, and is termed the *return function*. The principle of optimality establishes that the optimal function at each *state point* of a posterior *stage* corresponds to the minimum value amongst all the sums of the optimal functions at each *state point* of the prior *stage* and the 'costs' of passing between the *state points* $[i+1, j]$ and $[i, k]$. The optimal path that defines the critical slip surface is found by connecting the optimal *state points*, traced back from the final *stage* to the initial *stage*. The value of F_s is given an assumed value for the first slip surface computation and replaced by the newly obtained F_s. This process must be repeated until the F_s converges to a unique value while respecting an error tolerance.
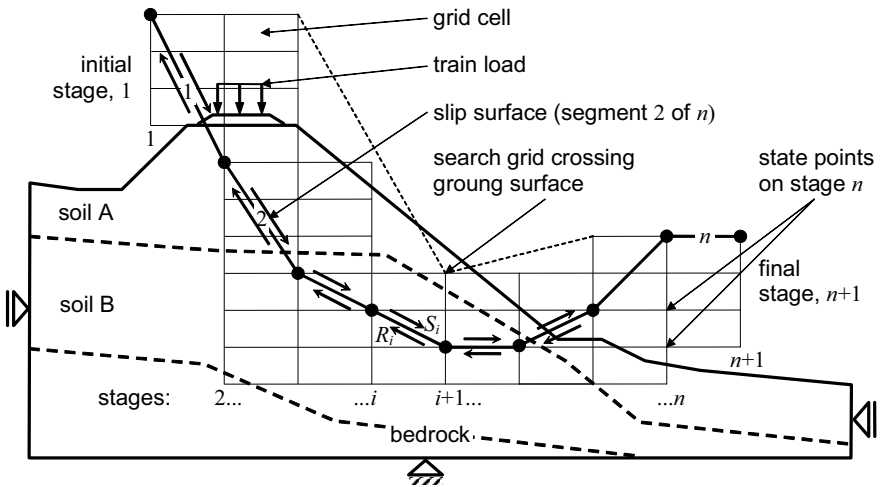

Fig. 13. Analytical scheme for stability analysis using Dynamic Programming Method.

3.4.2   *Shear strength and stresses within the DPM search grid*

The shear strength, normal stress, and acting shear stress at all *state points* must be determined in order to solve Eqs. 14 and 15. These variables can be calculated

based on the finite element stress field, pore-water pressure field, shear strength parameters, and orientation angle of each slip surface segment. The stress field is obtained by solving the PDE's governing static equilibrium (i.e., Eqs. 7 and 8). The pore-water pressure field is determined by solving the PDE's governing water (and heat) movement along with appropriate soil-atmospheric boundary conditions (Eqs. 4, 6, and 12).

The shear strength, τ_{fi}, can be determined by using the shear strength envelope for a saturated/unsaturated soil (Fredlund and Rahardjo 1993). The shear strength with respect to soil suction can be based on a prediction technique dependent upon the SWCC. The normal stress, σ_{ni}, and shear stress, τ_i, acting on a plane inclined at an angle θ can be computed from the stress state defined by σ_x, σ_y, and τ_{xy}:

$$\sigma_{n_i} = \sigma_x \sin^2 \theta + \sigma_y \cos^2 \theta - \tau_{xy} \sin 2\theta \tag{16}$$

$$\tau_i = [(\sigma_x - \sigma_y)/2]\sin 2\theta - \tau_{xy} \cos 2\theta \tag{17}$$

where σ_x and σ_y are the total normal stresses acting on the *x*- and *y*-directions, respectively; and τ_{xy} is the total shear stress acting on the *x*-plane and *y*-direction. The normal stress, σ_{ni}, (Eq. 16) is later used in the calculation of shear strength. The actuating shear stress, τ_i, (Eq. 17) is required in the factor of safety equation. A computer model called SAFE-DP (Stability Analysis using Finite Element stress fields and Dynamic Programming) was written and integrated with Flex-PDE. SAFE-DP performs the DPM analysis based on a finite element stress analysis, along with the pore-water pressure fields. The model can accommodate complex geometries and stratigraphy.

4   UNSATURATED SOIL PROPERTIES ASSESSMENT

Table 1 presents a summary of the soil properties required by the W-GHA model. The soil properties are found in the PDE's governing the hydro-thermo-mechanical behaviour of the soil comprising a railway embankment (Eqs. 4, 6, 7, and 8). The shear strength properties required by the *Dynamic Programming* optimization are also listed. A large number of soil properties are required in order to access weather-related embankment hazards. The properties associated with unsaturated soil behaviour are particularly difficult to measure. Figure 14 presents the approaches that can be taken for the assessment of unsaturated soil properties. A variety of direct (laboratory and field) and indirect (prediction) methods can be used. Laboratory and field approaches are usually complex, costly, and time consuming. It is not feasible to implement the W-GHA model if demanding test procedures are required for the assessment of unsaturated soil properties.

The second main branch of Fig. 14 presents two estimation approaches that can be used. These approximate methods rely on soil data that is simpler, and easier to obtain. The use of estimation methods results in additional uncertainty to the

embankment stability measure. However, the uncertainties can be rationally assessed and taken into account in the analyses using probabilistic approaches.

Unsaturated soil properties are primarily a function of the amount of water stored in the soil, amongst other secondary factors. Therefore, the estimation of unsaturated soil properties relies on the physical significance of the soil-water characteristic curve. Most unsaturated property functions can be shown to be a function of the saturated soil properties and the soil-water characteristic curve, as shown in Figure 15. Thermal properties could also be listed in Fig 15 as being dependent on the SWCC. The next sections present some estimation techniques for obtaining unsaturated soil property functions using the SWCC. A method of prediction of the SWCC based on the grain-size distribution can be found in Fredlund (1999).

Table 1. Material parameters required by the W-GHA model.

	Property	Parameters	(*)
Moisture flow	m_2^w	ψ_b, ψ_{res}, S_{res}, a, m_v, e.	1
	k^w	ψ_b, ψ_{res}, S_{res}, a, k^w_{sat}, η.	2
	D^v	ψ_b, ψ_{res}, S_{res}, a, e, D^{vap}.	1
Heat flow	L_V	L_V.	1
	λ	ψ_b, ψ_{res}, S_{res}, a, λ_s, λ_w, λ_{a1}, λ_{a2}.	4
	ζ	ψ_b, ψ_{res}, S_{res}, a, e, C_s, C_w.	2
Stress and stability	D_{ij}	E, μ.	2
	γ_y	ψ_b, ψ_{res}, S_{res}, a, e, G_s.	1
	τ_f	ψ_b, ψ_{res}, S_{res}, a, c', ϕ', κ.	3

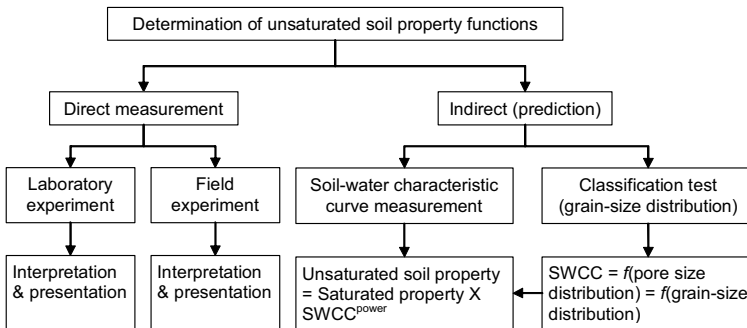(*) – Number of exclusive properties.

Fig. 14. Approaches to determine the unsaturated soil property functions.

An estimation of an appropriate SWCC for any particular soil can be obtained from a database such as that available through SoilVision (1996). Either a description of the soil or a grain-size distribution curve can be used to proceed with 'mining' or 'querying' the database for appropriate SWCC information. The SoilVision computer software also can be used to compute all the corresponding unsaturated soil property functions.

4.1 Hydraulic conductivity

The methods of assessing the hydraulic conductivity function can be classified as empirical equations, mechanistic models, and statistical models. Huang et al. (1998) presents a summary of the available methods. There is a clear relationship between the SWCC and the mechanistic and statistical models. Mechanistic models are based on the application of the capillary theory to the soil pores. The soil-water characteristic curve is used to indicate the size of the water-filled pores.
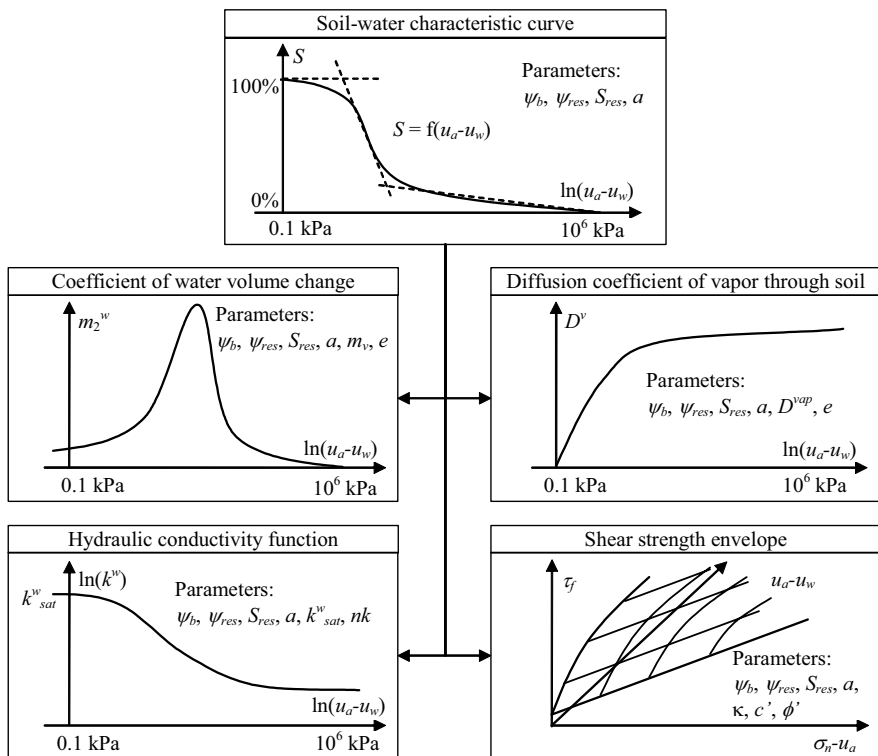

Fig. 15. Soil properties required by the W-GHA model.

Brooks and Corey (1964) developed the following equation using the mechanistic approach:

$$k = k_{sat}^w \text{ for } \psi < \psi_b \tag{18}$$

$$k = k_{sat}^w [\psi_b / \psi]^\eta \text{ for } \psi \geq \psi_b$$

where k_{sat}^w is the saturated hydraulic conductivity; $\eta = 2 + 3\lambda$; $\lambda = \Delta\log S_e / \Delta\log\psi$; and $S_e = [(S-S_{res})/(1- S_{res})]$. The portion of the SWCC past the air entry value is assumed to follow a straight line when plotted in the diagram $\log S_e$ vs. $\log \psi$. The mechanistic equations have a theoretical basis and have been repeatedly tested against experimental data (Mualem 1976). The mechanistic equations are also easy to use.

Statistical models are based on a random variation of pore sizes. The SWCC is again used to access the size of the pores based on the soil suction. Childs and Collis-George (1950) present one of the well known methods. Fredlund et al. (1994) proposed a permeability function that uses a similar approach, but applies the Fredlund and Xing (1994) SWCC equation. There are limitations associated with applying these equations to clayey soils.

4.2   Diffusion coefficient of vapour through soil

The diffusion coefficient of water vapour through soil, D^v, can be predicted using the following equation:

$$D^v = \alpha\beta D^{vap} W_v / RT \tag{19}$$

where a is the tortuosity factor of the soil, $\alpha = \beta^{2/3}$; β is the cross-sectional area of soil available for vapour flow per total area, $\beta = (1 - S)n$; $S = V_w/V_v$; n is the soil porosity; D^{vap} is the molecular diffusivity of water vapour in air, $D^{vap} = 0.229 \times 10^{-4}(1+T/273.15)^{1.75}$, m^2/s; W_v is the molecular weight of water, 18.016 kg/kmol; R is the universal gas constant, 8.314 J/(mol.K); an T is the temperature, K. Equation 19 shows that D^v is a function of S and n, which in turn are functions of soil suction (i.e., the SWCC).

4.3   Thermal properties

The volumetric heat capacity and the thermal conductivity of the soil can be calculated by proportioning air, water, and soils by volume and using the thermal properties of each phase (de Vries 1963). The equation for the heat capacity of the soil, neglecting the heat capacity of the air phase, is as follows:

$$\zeta = \zeta_s \frac{V_s}{V} + \zeta_w \frac{V_w}{V} = \zeta_s(1-n) + \zeta_w nS \tag{20}$$

where ζ_s is the volumetric specific heat of solids, 2.235x10^6, J/(m^3 °C); and ζ_w is the volumetric specific heat of water, 4.154x10^6 at 35°C, J/(m^3 °C).

The equation for the assessment of the thermal conductivity function proposed by de Vries (1963) is as follows:

$$\lambda = \left(F_s \lambda_s \frac{V_s}{V} + F_w \lambda_w \frac{V_w}{V} + F_a \lambda_a \frac{V_a}{V} \right) \Big/ \left(F_s \frac{V_s}{V} + F_w \frac{V_w}{V} + F_a \frac{V_a}{V} \right) \qquad (21)$$

where λ_s is the thermal conductivity of solids, typically around $\lambda_s = 6.0$, W/(m °C); λ_w is the thermal conductivity of water, typically around $\lambda_s = 0.57$, W/(m °C); $\lambda_a = \lambda_{da} + \lambda_{va}$; λ_{da} is the thermal conductivity of dry air, typically around $\lambda_{da} = 0.025$, W/(m °C); λ_{va} is the thermal conductivity of water vapour, assumed as $\lambda_{va} = (0.0736)S$, W/(m °C); $F_{a,s} = 1/3 \sum_{i=1}^{3} \left[1 + \left(\lambda_{a,s}/\lambda_w - 1 \right) g_i \right]^{-1}$; $F_w = 1.0$ (water assumed as the continuum medium) ; $g_{1,2} = 0.015 + (0.333 - 0.015)S$ (assuming spherical particles) ; and $g_3 = 1 - g_1 - g_2$.

4.4   Shear strength

The shear strength envelope for an unsaturated soil can be predicted using the soil-water characteristic curve and the saturated shear strength parameters, c' and ϕ'. Theoretical models supported by experimental evidence show that the slope of the plot of shear strength versus soil suction, ϕ^b, begins to deviate from the effective angle of internal friction as the soil desaturates. The reduced slope is associated with a reduction in the effective wetted area of contact past the air-entry value (Fredlund et al. 1996 and Vanapalli et al. 1996):

$$\tau_{f_i} = c' + (\sigma_{n_i} - u_a) \tan \phi' + (u_a - u_w) \Theta^\kappa \tan \phi' \qquad (22)$$

where $\Theta = S$; and κ is a fitting parameter to account for any non-linearity between the area and volume representation of the amount of water contributing to the shear strength. Vanapalli et al. (1996) presents a second procedure, defining $\Theta = \Theta_e = (S - S_{res})/(1 - S_{res})$ and not requiring κ. This second procedure renders the envelope potentially less flexible once the fitting parameter κ is not used. However, the use of Θ_e may be interpreted as a direct method for accounting for the same non-linearity that κ accounts for. The use of Θ set equal to S seems appropriate for the W-GHA model since shear strength at failure can be applied along the entire soil suction range.

5   FREQUENCY AND SENSITIVITY ANALYSIS

The assessment of weather-related geo-hazards is done in terms of the frequency distribution of a measure of stability (i.e., the *Factor of Safety*). The choice of variables that must be modelled as uncertainties (i.e., probabilistically modelled) is based on sensitivity analyses. The *Decision Analysis* framework adopted by the W-GHA model provides an efficient and systematic environment for frequency and sensitivity analyses.

5.1   Frequency (probabilistic) analysis

Frequency analyses correspond to step 4 of the *Decision Analysis* cycle (see Fig. 7). In order to perform frequency analyses, the relationships, dependences (correlations), and frequency distributions of the involved parameters must be established. The relationships between variables correspond to the previously presented model of the problem. These relationships can be illustrated using an *Influence Diagram* for the W-GHA model (Fig. 16). The variables presented inside the round boxes are the uncertain variables. The variables presented inside the square boxes are certain (fixed) values. These values are included for clarity and informative purposes, and could be included in the deterministic equations without being explicitly shown on the *Influence Diagram*. The arrows indicate the relationships between the parameters and variables. The *Factor of Safety* box is the final outcome, or the direct and indirect recipient of all arrows. The decision as to which variables must be modelled as uncertainties and which correlations must be taken into account depends on the sensitivity of each variable in the computation of the stability of the railway embankment. The uncertainties indicated in Fig. 16 are preliminary and form an illustrative *Influence Diagram* for the W-GHA model since the study is still underway.

A discrete stochastic analysis has been applied to the embankment hazard problem. According to this efficient approach, the frequency distributions of the uncertain variables can be represented by a few sampling points. The reduced numbers of sampling points produces lower computational effort while not significantly compromising the results (Clemen 1996). Discrete frequency distributions must be represented using complementary scenarios (i.e., scenarios whose sum of probabilities is "1"). For example, the air-entry value of the soil comprising a railway embankment may be modelled as an uncertain variable using a normal distribution with a determined mean and standard deviation. The entire continuous distribution can be presented using three scenarios; namely, a low, a mean (or nominal), and a high air-entry value. The value and probability of each scenario is assigned based on the given standard deviation, while adding up to "1".

The presence of several uncertain variables produces a combination of different scenarios. The presentation of several scenarios is called the *Decision Tree*. Figure 17 presents the *Decision Tree* corresponding to the *Influence Diagram* shown in Fig. 16. Three branches are used for each variable. The notation used here to

present the *Decision Tree* is from the popular *Decision Programming* language called DPL (Applied Decision Analysis LLC 1998). In the notation of Fig. 17 the branches are suppressed, improving the clarity of the *Decision Tree* and allowing the presentation of more information in less space. Ultimately, 729 scenarios (3^6) can be obtained from the 6 uncertain variables represented by three branches.
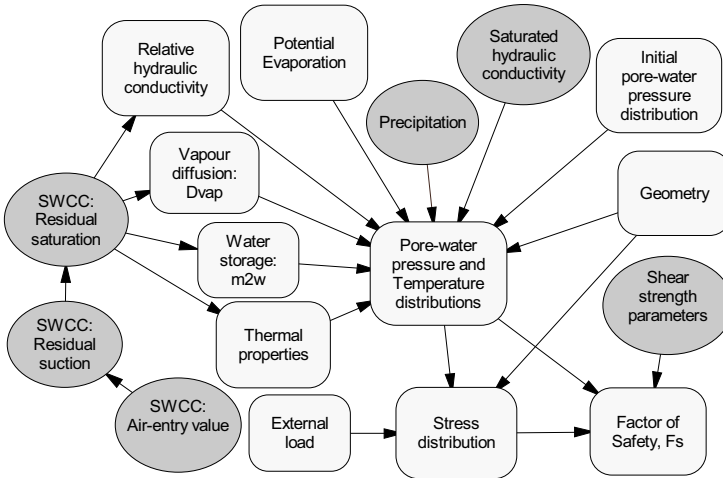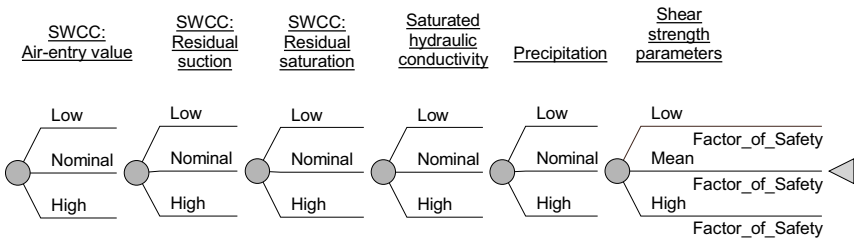

Fig. 16. An influence diagram for the W-GHA model.

Fig. 17. A decision tree for the W-GHA model.

Informative results have been obtained thus far in the study; however, some limitations of the model became apparent. Hazard assessment problems of extremely low failure frequency are difficult to solve. The solution becomes quite sensitive to the number points sampled and to the frequency distribution equations adopted. On the other hand, the accuracy of the computation of extremely low failure frequencies is less critical because this type of condition is usually within acceptable hazard levels for the problem at hand.

5.2   Sensitivity analysis

The determination of those variables that are of reduced importance is paramount to the success of the W-GHA model. For example, if the residual degree of saturation in Fig. 16 is found to have a relatively lower sensitivity to the *Factor of Safety*, it could be modelled as a known, fixed value, reducing the number of scenarios to 343 (i.e., 3^5). Tools and techniques common to *Decision Analysis* have been used to determine the variables that are most sensitive within the analysis. Rainbow diagrams, expected value tornado diagrams, and event tornado diagrams have been constructed for some cases. A type of "*Value of Information*" analysis is also being used to allow researchers and CP Rail officials to focus investigations on the parameters that have the greatest effect on the stability of an embankment. Such information allows an optimized allocation of funds for investigation, research, and monitoring.

   Preliminary analyses indicate that precipitation is the most sensitive variable in most regions, and therefore the assessment of precipitation distributions becomes a priority. However, there may be some regions with different climates where potential evaporation is as important as precipitation, and both must be assigned the same level of priority. The sensitivity analyses are being conducted using hypothetical cases. The cases embrace a range of typical cross-sections along the Canadian railway system.

6   FINAL REMARKS

A model for the assessment of weather-related geo-hazards (W-GHA model) has been presented. The W-GHA model consists of a slope stability analysis on a two-dimensional embankment combined with the analysis of the effects of weather conditions on the pore-water pressures. A discrete stochastic approach has been implemented within the proposed framework. Unsaturated soil mechanics has been taken from the soil property assessment level using techniques based on the soil-water characteristic curve (SWCC), to the assessment of weather-related geo-hazards.

   A series of partial differential equations governing the thermo-hydro-mechanical behaviour of saturated/unsaturated soils has been presented, along with appropriate soil-atmosphere boundary conditions. Robust problem solving environments, such as FlexPDE, make the solution of the rigorous series of PDE's relatively simple and quick. A slope stability algorithm called SAFE-DP using the *Dynamic Programming* method has been developed and incorporated into the W-GHA model. Stability conditions can be computed using SAFE-DP, the stress distribution, and the pore-water pressure distribution that reflect the weather conditions.

   The unsaturated soil property functions required as input to the W-GHA model have been presented along with a relatively simple prediction methodology. The prediction methods are based on the relationship between unsaturated soil behav-

iour and the SWCC. As a result, a reduced number of soil properties are required for the implementation of the W-GHA model into engineering practice. The paper illustrates the feasibility of quantitatively assessing embankment stability based on weather conditions.

ACKNOWLEDGMENTS

REFERENCES

Applied Decision Analysis LLC. (1998). "DPL 4.0 – Professional Decision Analysis Software – Academic Edition." Price WaterHouse Coopers. Pacific Grove, USA.. 682 pp.

Baker, R. (1980). "Determination of the critical slip surface in slope stability computation." International Journal for Numerical and Analytical Methods in Geomechanics, 4, 333-359.

Bellman, R. (1957). "Dynamic programming." Princeton University Press, Princeton, N.J.

Brooks, R.H. and Corey, A.T. (1964). "Hydraulic properties of porous media." *Colorado State University Hydrology Paper*. No 3., 27 pp.

Bunn, D. (1984). "Decision Analysis with Multiple Conflicting Objectives." John Wiley and Sons, New York.

Childs, E.C. and Collins-George, N. (1950). "The permeability of porous materials." *Proceedings Royal Society.* vol. 201A, 392-405.

Clemen, R.T. (1996). "Making Hard Decisions." Duxbury Press, U.S.. 664 pp.

Dakshanamurthy, V. and Fredlund, D.G. (1981). "A mathematical model for predicting moisture flow in an unsaturated soil under hydraulic and temperature gradients." *Water Resources Journal*, 17(3): 714-722.

de Vries, D.A. (1963). "Thermal properties of soils." *in The Physics of Plant Environment*, W.R. Van Wijk, Ed. 382 pp.

Einstein, H.H. (1997). "Landslide risk – Systematic approaches to assessment and management." Proceedings of the International Workshop on Landslide Risk Assessment, Feb. 19-21. Honolulu, USA. 25-50.

Einstein, H.H., Labreche, D.A., Markow, M.J., and Baecher, G.B. (1978). "Decision analysis applied to rock tunnel exploration." Engineering Geology. 12, 143-161.

Edlefsen, N.E. & Anderson, A.B.C. (1943). "Thermodynamics of soil moisture." Hilgardia 15: 2: 31-298.

Fell, R. (1994). "Landslide risk assessment and acceptable risk." Canadian Geotechnical Journal. 31, 261-272.

Fredlund, D.G. & Rahardjo, H. (1993). "Soil Mechanics for Unsaturated Soil." John Wiley & Sons, New York, United States of America, 517 p.

Fredlund, D.G. and Xing, A. (1994). "Equations for the soil-water characteristic curve." Canadian Geotechnical Journal, Ottawa, 31: 521-532.

Fredlund, D.G., Xing, A. & Fredlund, M.D. (1996). "The relationship of the unsaturated shear strength to the soil-water characteristic curve." Canadian Geotechnical Journal, 33(3): 440-448.

Fredlund, D.G., Xing, A. & Huang, S. (1994). "Predicting the permeability function for unsaturated soil using the soil-water characteristic curve." Canadian Geotechnical Journal, 31(4): 533-546.

Fredlund, M.D. (1999). "*The Role of Unsaturated Soil Property Functions in the Practice of Unsaturated Soil Mechanics.*" Ph.D. Thesis. University of Saskatchewan, Saskatoon, Canada. 292 p.

Gallopoulos, E., Houstis, E., and Rice, J.R. (1994). "Computer as thinker/doer: problem-solving environments for computational science." *IEEE Computational Science & Engineering*, 1(2): 11-23

Gitirana Jr, G.F.N and Fredlund, D.G. (2003). "Soil-water characteristic curve equation with independent properties." *Journal of Geotechnical and Geoenvironmental Engineering, ASCE*. (submitted).

Huang, S., Barbour, S.L. & Fredlund, D.G. (1998). "Development and verification of a coefficient of permeability function for a deformable unsaturated soil." Canadian Geotechnical Journal, 35: 411-425.

Keeney, R.L. and Raiffa, H. (1976). "Decision Analysis with Multiple Conflicting Objectives." John Wiley and Sons, New York.

Mackay, C.H. (1997). "Management of rock slopes on the Canadian Pacific Railway." Proceedings of the International Workshop on Landslide Risk Assessment, Feb. 19-21. Honolulu, USA. p. 271-275.

Milly, P.C.D. (1984). "A linear analysis of thermal effects on evaporation from soil." Water Resources Research, 20(8): 1075-1085.

Morgenstern, N.R. (1995). "Managing risk in geotechnical engineering." Proceedings of the 10th Pan American Conference on Soil Mechanics and Foundation Engineering, Guadalajara, Mexico.

Morgenstern, N.R. (1997). "Toward landslide risk assessment in practice." Proceedings of the International Workshop on Landslide Risk Assessment, Feb. 19-21. Honolulu, USA. 15-23.

Mualen, Y. (1976). "A new model for predicting the hydraulic conductivity of unsaturated porous media." Water Resources Research, 12: 513-522.

Office of Critical Infrastructure Protection and Emergency Preparedness. (2001). "Natural Hazards of Canada: Landslides and Snow Avalanches Map." Government of Canada.

PDE Solutions Inc. (2003). "FlexPDE 3.10 - Reference Manual." Antioch, CA, USA.

Pham, H.T.V. (2002). "*Slope stability analysis using dynamic programming combined with finite element stress analysis.*" M.Sc. Thesis. University of Saskatchewan, Saskatoon, SK, Canada, 200 pp..

Pham, H.T.V., Fredlund, D.G., and Gitirana Jr, G.F.N. (2001). "Slope stability analysis using dynamic programming combined with finite element stress analysis." *In International Conference on Management of the Land and Water Resources – MLWR*. Hanoi, Vietnam. v. 1, 107-114.

Philip, J.R. and de Vries, D.A. (1957). "Moisture movement in porous materials under temperature gradients." *Transactions, American Geophysical Union*, 38(2): 222-232.

Spencer, E. (1967). "A method for analysis of the stability of embankments assuming parallel interslice forces". *Geotechnique*, 17(1), 11-26.

SoilVision Systems Ltd. (1996). "SoilVision User's Guide – a Knowledge-based System for Geotechnical Engineers. Version 1.0." Saskatoon, SK, Canada.

SoilVision Systems Ltd. (2003). "SVFlux User's Manual." Saskatoon, SK, Canada.

Transportation Safety Board of Canada (1994). "A Special Study of Main Track Derailments." Transportation Safety Board Press, Ottawa, Canada.

Transportation Safety Board of Canada (2001). "Annual statistics – 2001." Transportation Safety Board Press, Ottawa, Canada.

Vanapalli, S.K., Fredlund, D.G., Pufahl, D.E. and Clifton, A.W. (1996). "Model for the prediction of shear strength with respect to soil suction." Can. Geotech. J., Ottawa, 33: 379-392.

Whitman, R.V. (1984). "Evaluating calculated risk in geotechnical engineering." Journal of Geotechnical Engineering

Wilson, G.W., Barbour, S.L., & Fredlund, D.G. (1997). "The effect of soil suction on evaporative fluxes from soil surfaces." Canadian Geotechnical Journal, 34(1): 145-155.

Wilson, G.W., Fredlund, D.G., & Barbour, S.L. (1994). "Coupled soil-atmosphere modeling for soil evaporation." Canadian Geotechnical Journal, 31(2): 151-161.

Yamagami, T., and Ueta, Y. (1988). "Search for critical slip lines in finite element stress field by dynamic programming." *In Proceedings of the 6th International Conference on Numerical Methods in Geomechanics*, Innsbruck, 1347-1352.

Zou, J. Z., Williams, D. J., and Xiong, W. L. (1995). "Search for critical slip surfaces based on finite element method." *Canadian Geotechnical Journal*, 32, 233-246.

Large scale hill creep in cohesive sediments: A field and model study

Erwin Zehe[1], Falk Lindenmaier[2], and Jürgen Ihringer[2]

(1) Institute of Hydraulic Engineering, University of Stuttgart; zehe@iws.uni-stuttgart.de
(2) Institute for Water Resources Management and Rural Engineering,
University of Karlsruhe; lindenmaier@iwk.uka.de

Abstract: A fine-grained slope that exhibits slow movement rates was investigated to understand the mechanisms which lead to a consecutive development of mass movements in the Vorarlberg Alps (Austria). For that purpose intensive hydro-meteorological, hydrogeological and geotechnical observations as well as survey of surface movement rates were conducted from 1998 -2001. Subsurface water dynamics at the creeping slope turned out to be dominated by a 3 dimensional pressure system. The pressure reaction is triggered by fast infiltration of surface water and subsequent lateral water flow in the south west part of the hillslope. The related pressure signal was shown to propagate further downhill, causing fast reactions of the piezometric head in 5.5 m depth on a daily time scale. The observed pressure reactions might belong to a temporary hillslope water body that extends further downhill. The related buoyancy forces could be one of the driving forces for the mass movement. A physically based hydrological model was adopted to model simultaneously surface and subsurface water dynamics including evapotranspiration and runoff production. It was possible to reproduce subsurface pressure reactions and observed runoff in principle. However, as soil hydraulic functions were only estimated on pedotransfer functions a quantitative comparison between observed and simulated subsurface dynamics is not feasible. Nevertheless, the results suggest that similar methods of coupling surface and subsurface processes should be employed in coupled models for large mass movement and that it is possible to reconstruct important spatial structures based on sparse observations in the field.

Introduction

The development of large hillslopes up to their failure is determined by non linear interactions of surface- and subsurface processes across a range of temporal and spatial scales. Fast processes as extreme rainfall, infiltration of surface water and subsurface stormflow trigger the subsurface water and pressure dynamics which in turn may lead to deformations of the porous medium (Tsaparas et al. 2002). The spatial variability of these process interactions, which is determined by

the spatial pattern of dominating heterogeneities, such as preferential pathways, fractures and strata in the hillslope body, is crucial for the spatio-temporal development of subsurface pressure heads (Reid 1997; Hicks & Samy 2002) and therefore for the development of possible shear zones. Within the prediction of large scale mass movement therefore three major problems may be identified:

- **Development of fully coupled models** that may numerically treat all relevant processes that determine large scale mass movements with characteristic time scales ranging from minutes (surface processes), over days (sub surface fluid dynamics) to months (elastic deformation).
- **Experimental identification of the governing processes** that trigger mass movement and to understand their local interactions across time scales (Bogaard et al. 2000; Bogaard 2001; Eberhardt 2001).
- **Identification of spatial structures** such as heterogeneities or layers that determine the spatio-temporal pattern of process interactions on the scale of large hillslopes and the **representation** of these structures within coupled models.

Addressing the first and the last problem, our investigation focused on a fine-grained slope with slow movement rates in the Vorarlberg Alps (Austria). Our experimental objectives were: a) To identify mechanisms which cause a consecutive development of the mass movement in this typical hydro-meteorological and geological environment. And b) to identify critical rainfall input (Chowdhury & Flentje 2002) or critical states of the hillslope that favor mass movements.

The theoretical objective of this study addresses problem number two by presenting a coupled hydrological model for simulating processes at the soil surface and the unsaturated zone. In particular we want to explore whether the governing subsurface heterogeneity might be identified and represented in the model such that the observed surface and subsurface dynamics may be reproduced simultaneously. We do not address the interaction between fluid and pore space. Nevertheless, we consider this as valuable contribution. Because future coupled models for simulating mass movements in the field have also to account for the coupling between atmosphere and sub surface. In section 2 we characterise the study area and the setup to observe data on hydro-meteorology, subsurface water dynamics and mass movement. Section 3 gives a brief outline of the hydrological model, followed by a synopsis of important experimental results in section 4. Section 5 gives an outline of simulation results followed by discussion and conclusions in section 6.

Field observations and study area

The investigated Heumoes Slope is located in the eastern Voralberg Alps, 20 km east of Dornbirn at the village of Ebnit (**Fig. 1**). The slope belongs to the head of a very steep, mountainous catchment which is drained by the Ebnit and Dornbirn rivers. The extension of the slope is 1800 m in east-west and about 500 m in north-south direction, the elevation ranges from 940 m to 1350 m. It is

drained by three deeply cut creeks that contribute to the Ebnit river. The slope is partly forested, used as pastures or meadows in summer or for skiing in winter.
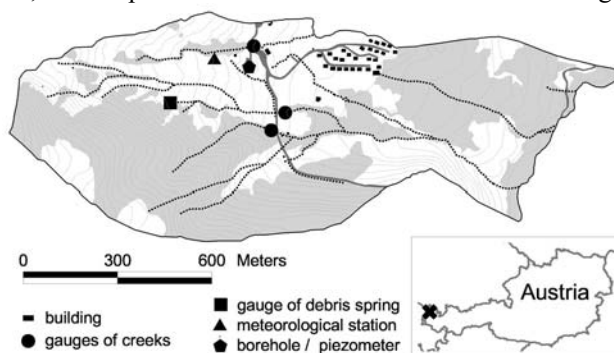

Fig. 1. Location of the Heumoes slope and measurement setup

Measurement network and field observations

Hydrogeology and geology: One borehole (KB 3) on the Heumoes slope (**Fig. 1**) and three boreholes in adjacent slopes were instrumented with inclinometers and piezometer heads (Schneider 1999) to observe groundwater pressure dynamics and the development of a possible shear zones. In 2001 geoelectrical and geomagnetical profiles were taken to shed light on the subsurface structure and the depth of the slope body (Van den Ham & Czurda 2002).

Soils and vegetation: The assessment of the spatial distribution of soils, preferential pathways and vegetation is crucial for understanding the water dynamics especially the exchange processes at the slope. The hillslope scale soil pattern and the soil moisture regime of typical soils were determined using transects of a total of 49 drilling logs and a mapping of indicator plants. Furthermore, 33 undisturbed 100 cm^3 soil cores were extracted from 4 soil profiles and analysed for their hydraulic conductivity and porosity.

Hydro-meteorological observations: Precipitation data with a 10 min resolution are available for 2 rain gauges, nearby the village (since January 1998) and at the meteorological station (since August 2001) at the Heumoes slope (**Fig. 1**). The station also samples temperature, windspeed and -direction, air moisture and temperature. A soil profile was equipped with TDR-rods (Time Domaine Reflectrometry) to determine the evolution of soil-moisture at the meteorological station. Discharge at three gauges as well as a debris spring below the southern slope has been observed continuously since September 1998. A major problem of obtaining continuous and reliable discharge are possible changes in the discharge curve due to high sediment loads, which are transported in the creeks. Digital discharge data for the Dornbirn river, which drains about 50 km², is available for the years 2000 and 2001.

Surveying of surface movement: Surface movement has been measured with GPS (Global Positioning System) and terrestrial survey from 1998 to 2001 with usually three measurements per year, due in May, August and October (Depenthal 2003). Furthermore, a digital elevation model was derived from GPS observations carried out in 2001.

Characteristics of the Heumoes slope

Geology and Hydrogeology

The surrounding bedrock and also the top area of the Heumoes slope consist of upper cretaceous sediments, mainly marls and limy marls (**Fig. 2**). These layers belong to the Amden, Wang and Leimern groups and have a low to very low hydraulic conductivity (Oberhauser 1980; Schneider 1999). The limy marls are assumed to have hydraulic relevant fissures zones, which cannot be quantified more precisely, though. The hillslope body consists of subglacial till, which is dated to the Würm glacial maximum (Sibinga-Lokker 1965), followed by scree and weathered scree (**Fig. 2**), material properties are given in **Table 1**. As can be seen in the geological profile of borehole KB 3 (**Fig. 3**) the srcee material is heterogeneous due to debris flow, rock fall and weathering processes. The foot of the hillslope has been eroded by the Ebnit river down to bedrock. Groundwater related discharge is generally low due to the low baseflow of the Ebnit and Dornbirn rivers.
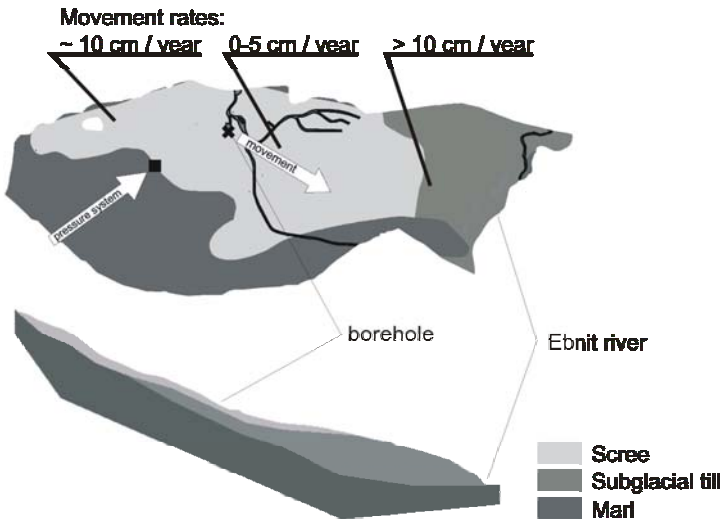

Fig. 2. Geological overview and cross sections of Heumoes slope, areas of similar surface movement rates, and principle sketch of pressure system and subsurface movement.

Table 1. Material properties of the different geological formations in the Heumoes slope

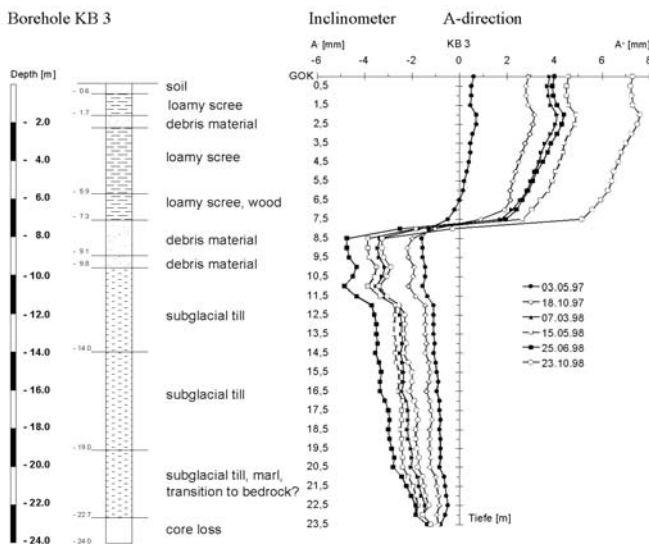| geology	material	hydr. cond. [m/s]	consistency
loamy scree	silty – clayey	$\sim 10^{-7}$	soft – very soft
coarse scree	rocks, silt	$> 10^{-7}$	(soft – very soft)
subglacial till	sandy- clayey	$< 10^{-7}$	stiff – soft
marl	bedrock	impervious	-

Fig. 3. Geological profile observed in borehole KB 3 as well as the development of a possible zone in the debris material in 8.5 m depth observed with the inclinometer. As the bedrock is in app. 60 m depth, it was impossible to fix the inclinometer there. The measurement yields therefore relative movements.

Soils, vegetation and soil water regime

In general gley and stagno gley soils (silty clay to silty loams according to the US Soil Taxonomy) with low hydraulic conductivity (10^{-7} m/s) may be found at the Heumoes slope. The presence of macropores, mainly roots and wormholes (forest) but also cracks in some parts, may enhance the infiltration capacity up to 10^{-4} m/s. Due to their high silt content the soils have a high field capacity. The soil profiles show a weak soil development and due to the marly source rocks the soil texture is similar in all profiles. Nevertheless, there is variability in terms of the amount of roots, skeleton and the thickness of different soil horizons and the soil cover in general. Based on the analysis of soils, topography and slope as well as indicator plants, four hydrotopes, i.e. areas with similar soil moisture regime could be identified (**Fig. 4**).
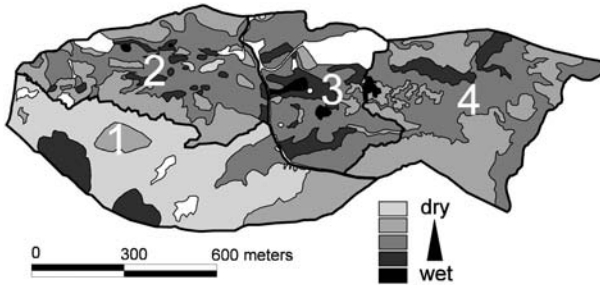
Fig. 4. Areas of similar soil water regime that were determined by joined analysis of soils, topography and indicator plants: Fast infiltration of precipitation and subsequent lateral water movement dominates in area #1, which is also marked by the fast discharge reactions at spring 1 (compare **Fig. 1** and **Table 2**). In case of rainfall, surface runoff production is the dominating process at the rest of the hillslope

- The south-western part of the hill (area #1) which is very steep, exhibits thin debris or residual soils on top (< 1 m), quickly followed by bedrock in 1-2 m depth. The area is predominantly covered with fir trees. The infiltration capacity in this area is considerably higher than at the rest of the slope. Fast preferential infiltration and lateral subsurface stormflow are the dominating processes (compare discharge time series of the spring in section 4.2).
- The northwestern part of the slope (area #2) is dominated by pastures and shows a highly variable relief, with small scale features that may be attributed to soilcreep (bulging and plane areas). As shown by different indicator plants bulging areas are drier and plane areas are usually very moist to wet. Soil profiles are not developed thoroughly. They show significant stagnic properties, indicating low infiltration capacities. Thus surface runoff generation should dominate in this area in case of rainfall.
- The central area (area #3) offers very wet soil moisture conditions, besides fir and alder islands there are meadows. Infiltration is low into the highly stagnic soils, thus saturation excess runoff generation dominates in this part in case of rainfall.
- The eastern, lower part of the slope (area #4), adjacent to area #3 shows a gradual change of steepness towards the Ebnit river. An additional small scale relief is found due to small scale landslides and soilcreep. The area has been used as meadows until the turn of the century and has changed to a forest with fur and alders trees. Infiltration here is low again, runoff production is related to the small scale relief and also exfiltration of near surface water may be observed.

Climate, precipitation and runoff

Precipitation and climate conditions are determined by the westward opening mountain range, which may lead to strong precipitation events in case of a dominant eastward wind direction. Average annual precipitation is about 2000 mm.

Storm events dominate in summer (April to September) where rainfall intensity is high with peaks up to 140 mm/h, but with usually short duration.

Outline of the hydrological model

CATFLOW is a physically based hydrological model to simulate the water balance of small catchments. In the 2 dimensional hillslope module Evapo-Transpiration is represented using an advanced SVAT (soil, vegetation, atmosphere transfer) model based on the Penman-Monteith approach, that accounts for plant growth as well as soil albedo as a function of soil moisture. Soil water dynamics modeled solving 2 d Richards Equation (Eq. 1) in the pressure based form on a 2 dimensional curvilinear finite difference grid adopting an implicit mass conservative "picard iteration" scheme (Celia & Bouloutas 1990). The simulation time step is dynamically adjusted to achieve an optimal change of the simulated soil moisture per time step, which assures fast convergence of the iteration. Soil hydraulic functions are parameterized after van Genuchten (1980) and Mualem (1976).

$$C\frac{\partial h}{\partial t} = \nabla\big(k\nabla(h+z)\big); \quad C = \begin{cases} \dfrac{\partial \theta}{\partial h} & \theta < \theta_s \\ S_e & \theta = \theta_s \end{cases} \tag{1}$$

To simulate soil water dynamics under temporary saturated conditions, we use the specific storage capacity (S_e) of the porous medium from theory of shallow aquifers (see e.g. Kinzelbach, 1987) as the water capacity (C) tends to zero in case of saturation. In case of surface runoff production, runoff is routed downhill by means of 1 d shallow water equation. Several hillslope may be interconnected by a river channel network, runoff which is fed into the river net is routed downstream.

CATFLOW provides advanced physically approaches for describing the exchange of water and energy between the unsaturated zone and the atmosphere, i.e. infiltration, runoff and evapotranspiration, which is an important step towards building fully coupled models for mass movements. For further details on the model physics and successful model applications at different scales the reader may refer to (Zehe et al, 2001a, Zehe et al, 2001b; Zehe and Blöschl, 2001).

Synopsis of experimental results

Geology and hillslope creep

Geoelectrical profiles show a total depth of subglacial till and scree material on top of the marls of more than 60 m. The inclinometer measurements at the borehole KB 3 indicate possible deformation zone in 7.5 m to 8.5 m depth, which is

the transition between subglacial till and overlying scree (**Fig. 3**). Inclinometer measurements in an adjacent hillslope in the Ebnit village with a almost the same geological build-up, show higher movement rates in summer and lower movement rates in winter.

Based on GPS observations and terrestrial survey, three zones with different surface velocities were identified (**Fig. 2**) The upper (western) and the lower part exhibit surface movements larger than 0.1 m per year, the central part is slower with up to 0.05 m per year (Depenthal 2003). The surface movement did not show any correlation to slowly varying hydrological signals such as variation of base-flow in the Ebnit and Dornbirn river. Thus, we may conclude that a temporal increment of 2 to 3 months is too large to resolve time scale of the mass movement.

Rainfall-runoff and subsurface water dynamics

Due to the low hydraulic conductivity in most areas of the hillslope, surface runoff response is in general very fast, exhibiting high runoff coefficients and also a fast relaxation of the hydrographs to base flow conditions (**Table 2**).

This is exemplified by two events in May 11-15th 1999 and Sept 2000 (**Fig. 5**). In May 1999 two large events brought twice as much rainfall as the long year monthly average (430 mm compared to 200 mm). The response time at the outlet of Heumoes slope (drainage area 0.05 km2) and downstream at the Dornbirn river (drainage area 50 km^2) are almost the same. Discharge at the debris spring which is located in the south-east, shows a similar fast reaction as the rivers, but a more prolonged tailing. However, this similar fast reactions of the river discharge and the debris spring is caused by different mechanisms.

Table 2. Precipitation sum (N), Runoff coefficients and time to peak (t_{peak}), for the Heumoes creek and for the spring observed during selected rainfall events

	Events	10.05. 1999	20.05. 1999	14.06. 2000	20.09. 2000	01.10. 2000	21.06. 2000	23.06. 2000
	N [mm]	200	214	61	95	53	25	16
	duration [h]	93	120	9.7	21	40	13.3	15
H. Creek	**runoff coeff.**	0.9	0.971	0.3	0.8	0.7	0.08	0.5
(0.05 km^2)	**t_{peak} [h]**	3		0.4	1.3		2	15
Spring	**runoff coeff.**	0.36	0.28	1.0	0.9	1.1	0.734	1.14
(4 10^{-4} km^2)	**t_{peak} [h]**	31.7*	0.1	1.5	0.1	63.2*	2.8	22.5*

*here, high t_{peak} values are due to long duration of precipitation events

Due to the high infiltration capacity of the surface in area #1 the fast reaction of the spring is caused by fast preferential infiltration of surface water that triggers a lateral water movement on the impervious bedrock in approximately 1 m depth.

The corresponding runoff coefficients in **Table 2** indicate that area #1 behaves completely different from the rest of the hillslope. Nearly all precipitation infiltrates into the subsurface which leads to a pressure signal that may propagate further downhill in case of a continuous hillslope water body.
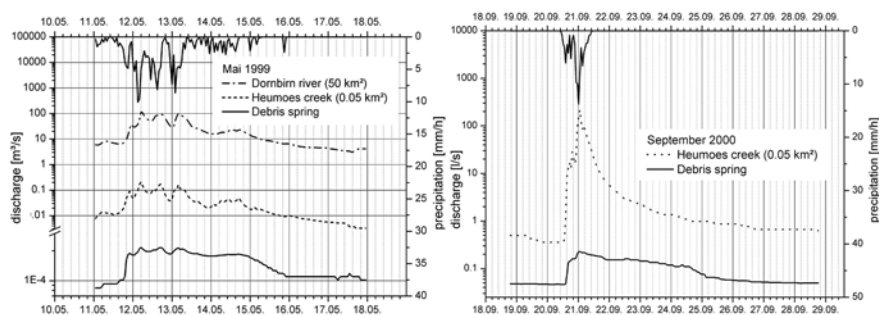
Fig. 5. Rainfall runoff events in May 1999 and September 2000 at the Dornbirn River (drainage area 50 km², the Heumoes Creek (drainage area 0.05 km²) and debris spring (drainage area 400 m²)

The subsoil water content near the climate station is close to saturation throughout the whole year. Topsoil moisture in the upper 0.2 m is also high but exhibits small fluctuations due to transpiration and slow matrix infiltration. The variation of pore water pressure observed in borehole KB 3 is generally low during the winter period (**Fig. 6a**). But in summer time the pressure head in 5.5 m depth may show fast increases up to 1 m on the daily time scale as response to extreme rainfall events (**Fig. 6a** and **b**).
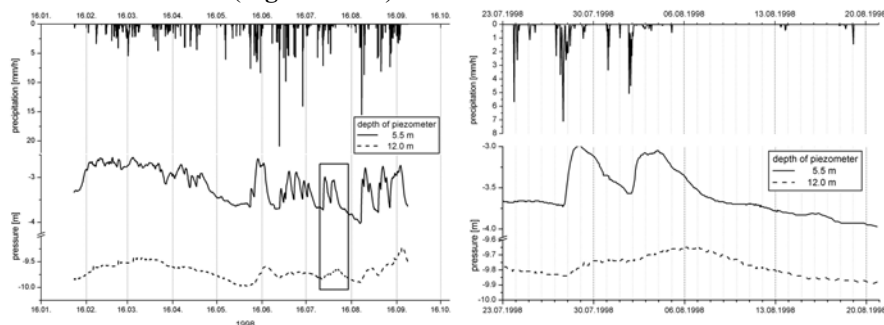
Fig. 6. a, b) Piezometric heads observed at borehole KB 3 in 1998

Due to the low hydraulic conductivity of 10^{-7} m/s (1 cm/d) of the gley soil in this central part of the slope (area #3), this reaction in 5.5 m depth cannot be triggered by vertically infiltrating surface water, as the response time would be of order 1 year. We state the hypothesis that these fast reactions are due to the propagation of the pressure signal that originates from the subsurface lateral water movement in area #1, as sketched in **Fig. 2**.

Simulation of subsurface water dynamics and runoff

To explore whether the observed development of a subsurface pressure system in area #1 may in principle be simulated, we used a hillslope model of 280 m length, 120 m elevation difference and 8 m thickness. Based on the available texture information we estimated the soil hydraulic properties using the pedotransfer function of Carsel and Parrish (1988). The debris layer in the upper 1 m of the subsurface was represented by a sandy clay loam, followed by a silty clay of low conductivity representing the marl (**Fig. 7, Table 3**). In the lower part of the hill the sandy clay extends over the whole depth of the slope and is followed by a lens of less conductive silty clay loam, that represents the loamy scree.

Table 3. Van Genuchten-Mualem parameters of the three soil types estimated based on available texture information after Carsel and Parrish (1988), S_e specific storage coefficient, k_s saturated hydraulic conductivity, θ_s/θ_r residual soil water content, a air entry value, n width of pore size distribution.

	S_e[1/m]	k_s [m/s]	θ_s [-]	θ_r [-]	α [1/m]	n [-]
silty clay loam (SICL)	0.02	$1.36\ 10^{-7}$	0.60	0.10	1.00	1.23
sandy clay loam (SCL)	0.03	$8.10\ 10^{-6}$	0.38	0.07	2.70	1.23
sandy loam (SL)	0.09	$1.00\ 10^{-5}$	0.41	0.07	7.50	1.89
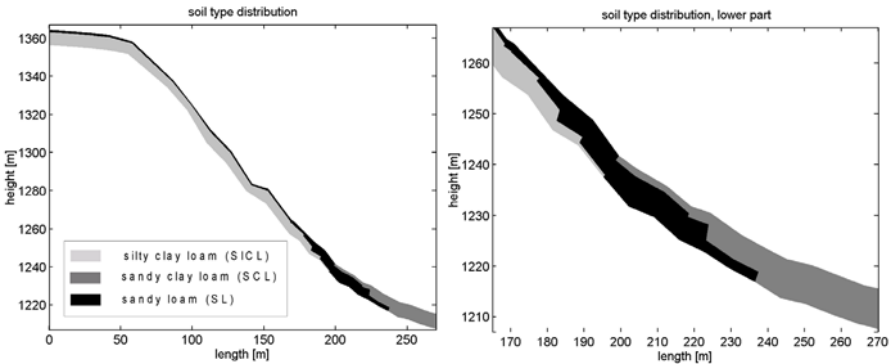
Fig. 7. Distribution of soil types in the idealised slope. Darker shading indicates a higher hydraulic conductivity in addition to soil type distribution.

The lower boundary condition was no flux to account for impervious bedrock in that depth. At the left and right boundary a seepage boundary condition allowed exfiltration of water from the hill slope body, in case of saturation. The upper boundary condition was of the cauchy type to represent infiltration/runoff in case of rainfall and as well as evaporation losses. Simultaneously we adopted CATFLOW in the "catchment" mode, using soil hydraulic functions given in **Table 3**. The intention was to check, whether the model is able to reproduce observed runoff dynamics based on these estimated parameters

Using the observed precipitation and meteorological data as input, the water cycle at the hillslope in area #1 and the water cycle in the sub catchment drained by the Heumoese slope were simulated for the period of January 1998 to December 2000.
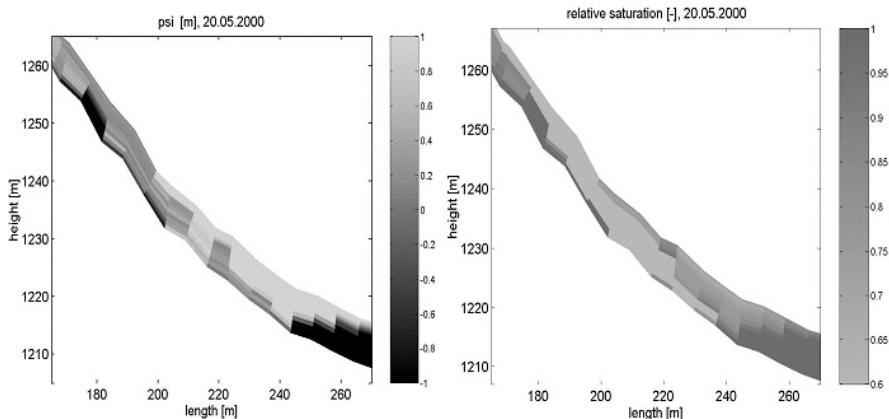

Fig. 8. The relative saturation and matric potential head in May 2000 are given in the lower diagrams, negative values indicate water pressures higher than atmospheric pressure.
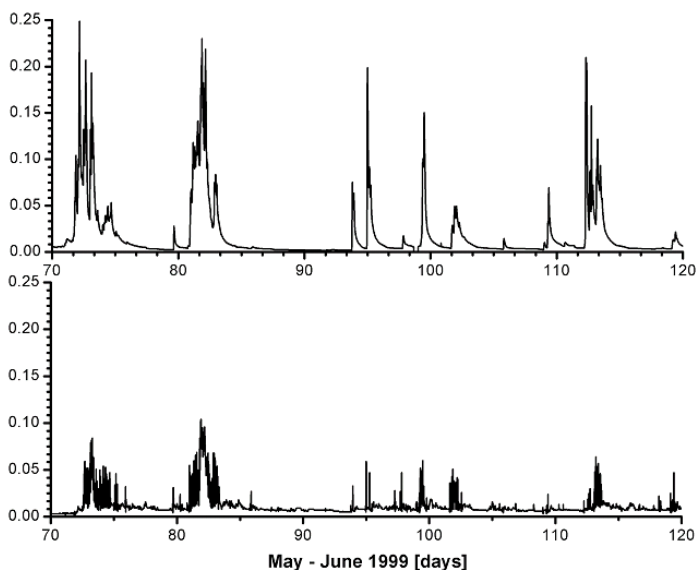

Fig. 9. Predicted and observed discharge at the Heumoes creek. Although the magnitude of the peaks is underestimated, the timing is perfect. As the discharge data are quite uncertain, we did not further tune the soil hydraulic conductivity to yield a better fit.

A snapshot of the distribution of relative saturation and pressure head is given in **Fig. 8**. As expected, a temporary ground water body developed above the less conductive silty clay loam lens in the lower part of the hill, with up to 5 m pressure head, which is of the same magnitude as observed at KB 3 (compare **Fig. 6a** and **b**). However, as soil hydraulic functions were only estimated on pedotransfer functions a quantitative comparison between observed and simulated subsurface dynamics is not feasible.

The simulation yielded also a reasonable discharge time series (**Fig. 9 lower panel**) for the Heumoes creek compared to the observations (**Fig. 9 upper panel**). The systematic underestimation of the flood peaks, indicates that the estimated saturated hydraulic conductivity based on the pedotransfer function are a too high. Decreasing the k_s values within the uncertainty range of the pedotransfer functitons would certainly yield a better fit. However, the discharge observation are error prone, because the accumulation of sediments before the weir causes changes in the rating curve (that relates water levels to discharge).

Discussion and Conclusions

The presented experimental evidence suggests that subsurface water dynamics at the Heumoes slope is dominated by a 3 dimensional pressure system, which is triggered by fast infiltration of surface water in the south west part, subsequent lateral water flow and a related pressure. This signal seems to propagate further downhill to the piezometer in borehole KB 3. The results hint that the fast pressure reactions at KB 3 belong to a temporary continuous water body, which could further extends downhill. Related buoyancy forces, could be a driving force for a further development of the possible shear zone in about 8 m depth. Higher movement rates that were observed at the inclinometer stations in summer time, may be explained by the higher frequency of extreme precipitation events in the summer period, that lead more frequently to these critical pressure states in the hillslope body. The relaxation time of the pressure signals is approximately 4 days, which is in our opinion short compared to the time scales where elastic and plastic or the porous medium develop. If this is true, a sequence of these critical pressures states caused by a sequence of serious rainfall events is necessary to have an impact on the stability of the porous medium. Further investigation to underpin this hypothesis should include higher resolved GPS observations to resolve the time scale of the hill creep and install and additional piezometer.

We could show furthermore that the physically based hydrological model CATFLOW is able to simulate the important exchange processes of water at the soil-atmosphere-plant interface and water dynamics in the unsaturated zone. Based on a simplified representation of the main subsurface layers it was possible to simulate subsurface pressure reactions in the infiltration dominated area #1 which are of same magnitude as observed in borehole KB 3. Using the same estimated hydraulic properties it was possible to reproduce the behaviour of the surface runoff dominated subcatchment that is drained by the Heumoes creek. This suggests

that methods to couple unsaturated zone and surface processes used implemented in CATFLOW could also be employed when building coupled models for predicting mass movements. Future research activities should concentrate on a) implementing these descriptions of exchange surface processes (evapotranspiration, infiltration, runoff) into advanced models for unsaturated/saturated multi phase fluid dynamics in the underground based such as MUFTE UG (Helmig et al. 1998), and b) on coupling these models with models for mechanics in soil continua such as PANDAS (Ehlers and Ellsiepen, 1998).

Acknowledgements.

References

Boogard, T.A., Antoine, P., Desvarreux, P., Giraud, A., van Asch, Th.W.J. (2000): The slope movements within the Mondorès graben (Drôme, France); the interaction between geology, hydrology, typology. In: Engineering geology 55, p. 297-.312.

Bogaard, T.A. (2001): Analysis of hydrological processes in unstable clayey slopes, Ph. D Thesis, Netherlands Geographical Studies 287, Knag/Faculteit Ruimetlijke Westeenschappen Universiteit Utrecht, ISBN 90-6809-321-5, 192 p.

Carsel, R., F. and Parrish, R,. S. (1988): Development of joint probability distributions of soil water retention characteristics. In: Water Resour. Res. 24 (5): 755 – 769.

Celia, M. A. and Bouloutas, E. T. (1990): A general mass-conservative numerical solution for the unsaturated flow equation. Water Resour. Res. 26 (7): 1483 – 1496.

Cho, S.E., Lee, S.R. (2001): Instability of unsaturated soil slopes due to infiltration. Computers and Geotechnics 28, 2001 p. 185-208.

Chowdhury, R., Flentje, P. (2002): Uncertainties in rainfall-induced landslide hazard. Quarterly Journal of Engineering Geology and Hydrogeology, 35, p. 61-70.

Depenthal, C. (2003): Monitoring of a landslide in Vorarlberg/Austria. 11th International Symposium on Deformation Measurements, 25-28 May 2003, submitted

Eberhardt, E., Willenberg, H., Loew, S., Mauerer, H. (2001): Active Rockslides in Switzerland - Understanding mechanisms and processes, In: Proceedings of Landslides-Causes, Impacts and Countermeasures, Meeting June 2001

Ehlers. W., Ellsiepen P. (1998): PANDAS: Ein FE-System zur Simulation von Sonderproblemen der Bodenmechanik. In P. Wriggers, U. Meißner, E. Stein, W. Wunderlich (eds.): Finite Elemente in der Baupraxis - FEM '98, Ernst & Sohn, Berlin, 391-400.

Helmig, R., Bastian, P., Class, H., Ewing, J., Hinkelmann, R., Huber, R.U., Jakobs, H. und H. Sheta: Architecture of the Modular Program System MUFTE-UG for Simulating Multiphase Flow and Transport Processes in Heterogeneous Porous Media. Mathematische Geologie, Berlin, 1998. - Vol.: 2 - Seiten: 123-131

Hicks, M.A. & Samy, K. (2002): Influence of heterogeneity on undrained clay slope stability. Quarterly Journal of Engineering Geology an Hydrology, 35, p. 41-49

Kinzelbach, W. (1987): Groundwater modelling : an introduction with sample programs in BASIC. Amsterdam : Elsevier: 333 p.

Mualem, Y. (1976): A new model for predicting the hydraulic conductivity of unsaturated porous media. Water Resources Res. 12: 513 –522.

Oberhauser, R. (1991): Erläuterungen zu Blatt 110 St. Gallen Süd und 111 Dornbirn Süd. Geologische Bundesanstalt, Wien.

Rahardjo, H., Leong, E.C., Rezaur, R.B. (2002): Unsaturated soil mechanics for the study of rainfall-induced slope failures, Proceedingss of 4th Workshop on Unsaturated Soils, Bauhaus Universtiät Weimar

Reid, M.E. (1997): Slope instability caused by small variations in hydraulic conductivity. Journal of Geotechnical and Geoenvironmental Engineering, 123/8, p. 717-725.

Sibinga-Lokker, C. S. (1965): Beiträge zur Geomorphologie und Glaziologie des Einzugsgebiets der Dornbirner Ache (Vorarlberg, Österreich). Dissertation, Rijksuniversiteit te Leiden, 123 S.

Schneider, U. (1999): Untersuchungen zur Kinematik von Massenbewegungen im Modellgebiet Ebnit (Vorarlberger Helvetikum). Dissertation, Schriftenreihe Angewandte Geologie Karlsruhe, Universität Karlsruhe (TH), 57: 149 p.

Tsaparas, I., Rahadjo, H., Toll, D.G., Leong, E.C. (2002): Controlling Parameters for rainfall-induced landslides. Computers and Geotechnics 29: 1-27 p.

Van Genuchten, M. T. (1980): A closed-form equation for predicting the hydraulic conductivity of unsaturated soils. Soil Sci. Soc. Am. Jour. 44: 892 – 898.

Van den Ham, G., Czurda, K. (2002): Numerical modelling of a slowly deforming slope in the Vorarlbergian Alps, Austria. Geophysical Research Abstracts, European Geophysical Society 27th General Assembly, Volume 4, 2002.

Zehe, E., Maurer, T., Ihringer, J., Plate, E. (2001a): Modelling water flow and mass transport in a Loess catchment. Physics & Chemistry of the Earth, Part B, Vol. 26 (7-8): 487-507 .

Zehe, E., Becker, R., Bardossy, A. (2001b): The influence of spatial variability of soil moisture and precipitation on runoff production. Presentation at the International Workshop on Catchment scale Hydrologic Modelling and Data Assimilation, Sept. 3-5 2001, Wageningen, Book of Abstracts: 57-58.

Zehe, E. And Blöschl, G. (2001): Implications of non-linearity and data uncertainty for hydrological modelling. Presentation at the International Workshop on Catchment scale Hydrologic Modelling and Data Assimilation, Sept. 3-5 2001, Wageningen, Book of Abstracts: 54-56.

The effect of soil suction in stability of partially submerged slopes

I. Bellezza[1] and E. Fratalocchi[2]

[1] Dipartimento di Ingegneria Civile, Università di Trieste, piazzale Europa 1, 34127 - Trieste, Italy, bellezza@dic.univ.trieste.it

[2] Dipartimento di Fisica e Ingegneria Materiali, Università Politecnica delle Marche, via Brecce Bianche, 60131 Ancona, Italy, fratalocchi@univpm.it

Abstract: The paper deals with the stability of slopes under drawdown conditions taking into account the effect of negative pore-water pressures, usually neglected in routine analyses. A simplified unsaturated soil profile above the water table was assumed and soil suction was estimated using a Brooks and Corey type soil-water characteristic curve. A parametric study was carried out to evaluate the influence of geometrical, physical and mechanical parameters of a simple slope. The results for complete and rapid drawdown conditions show that the factor of safety varies less than 10% for dams or reservoirs with initial drawdown ratios less than 0.3. Soil suction becomes more significant (safety factor variation up to 50%) for railway or road embankments with the water level at the base of the slope.

INTRODUCTION

A typical example of unsaturated soils is represented by compacted soils that are widely used in the construction of earth structures. These structures have initially a degree of saturation depending on compaction water content and compaction effort; even in working conditions it is rare for an earth dam to be fully submerged and it is reasonable to suppose that an upper zone remains unsaturated. Even so, earth dams or embankments are usually designed neglecting the effect of soil suction (Morgestern, 1963; Desai, 1977, Lane and Griffiths, 2000). In stability analysis this approach is conservative, but in post-failure studies the exclusion of suction effects can result in an overestimate of the back-calculated saturated shear strength. The aim of this paper is to quantify the effect of negative pore-water pressures in simple slopes and to evaluate the influence of the geometrical, physical and mechanical parameters needed to model the problem. For a fine-grained soil, two limiting conditions are usually considered, called slow and rapid drawdown (Lane and Griffiths, 2000). In the slow drawdown problem the water level within the slope is supposed to equalise the reservoir level at any time (Griffiths and Lane, 1999). In case of rapid drawdown, which is the most critical condition, it is assumed that the pore-water pressures within the embankment continue to reflect the original water level (Morgestern, 1963).

METHOD

Slope geometry

A simple slope is examined, with a height H and an inclination β to the horizontal (Fig. 1). It is supposed that a firm layer exists at a depth DH from the top of the slope and that the slip surface cannot pass into this stratum. The soil is assumed to be homogeneous, with respect to saturated and unsaturated strength parameters.

The water table is supposed to be horizontal at a depth L below the crest; for rapid drawdown analysis the external water level is considered at a depth L_f below the crest. For a complete drawdown, $L_f = H$. Above the phreatic surface a saturated zone is considered (capillary fringe, Fig. 1); the height of this zone, h_{sat}, is numerically related to the air-entry value (Bouwer, 1978):

$$h_{sat} = \frac{\psi_b}{\gamma_w}$$

(1)

where ψ_b is the air-entry value or bubbling pressure and γ_w is the unit weight of the water. The bubbling pressure can be determined by the construction of soil-water characteristic curve (e.g. Fredlund and Xing, 1994). Its value (and hence the height of the capillary fringe), depends on the pore size of the soil and it generally increases with the soil plasticity. However, for a given soil, laboratory tests indicate that the air-entry value can be strongly influenced by other factors, such as void ratio, dry density and preparation technique (Khalili and Khabbaz, 2001).

Above the capillary fringe, the degree of saturation is assumed to linearly decrease, reaching an assigned constant value, S_{R0}, at the slope surface (Fig. 1):

$$S_R = 1 - (1 - S_{R0})\frac{x}{h_{uns}}$$

(2)

where x is the distance between the top of the capillary fringe and the point; h_{uns} is the distance between the top of the capillary fringe and the slope surface.
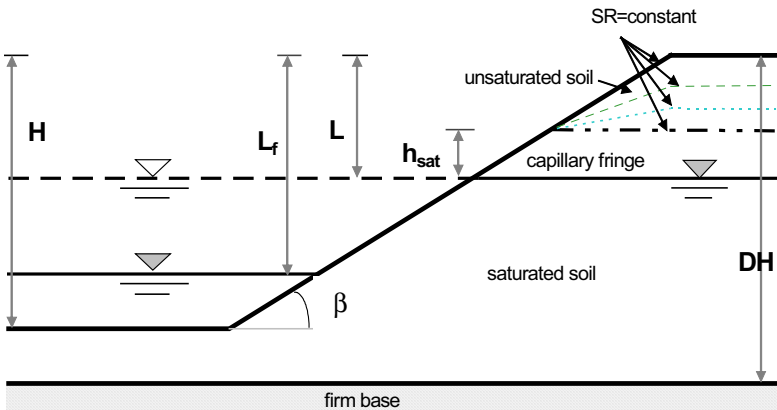
Fig. 1. Slope geometry

Calculation of negative pore-water pressures

Above the water table the pore-water pressures is negative. In the capillary fringe (Fig. 2) water is supposed to be in hydrostatic conditions and therefore the negative pore-water pressure (u_w) at a given point is assumed to be proportional to the height, h_w, of that point above the water table:

$$- u_w = \gamma_w \, h_w \tag{3}$$

In the unsaturated zone, the soil suction can be calculated by the soil-water characteristic curve. In the literature different equations have been proposed to represent sorption or desorption curves (e.g. Fredlund and Xing, 1994). In this study the soil suction is calculated according to the Brooks and Corey (BC) function, one of the most used in practice (Brooks and Corey, 1964; Russo, 1988; Chiu and Shackelford, 1998). Assuming the pore-air pressure to be atmospheric (i.e., $u_a=0$), soil suction is given by the following equation:

$$-u_w = \psi_b \left(\frac{1 - S_{RES}}{S_R - S_{RES}} \right)^{1/\lambda} \tag{4}$$

where S_R is the degree of saturation; S_{RES} is the residual degree of saturation and λ is the pore-size distribution index. The parameters of the BC function may be determined by either graphical or automatic numerical procedures (e.g. Milly, 1987). Statistical analysis of the BC parameters across USDA soil textures classes are given by Mc Cuen et al. (1981) and Sillers and Fredlund (2001).

It can be noted that (4) is valid for suction values greater than the air-entry value and for degrees of saturation greater than the residual degree of saturation. In addition, the use of the Brooks and Corey function implies a cusp point at the top of the capillary fringe (Fig. 2).
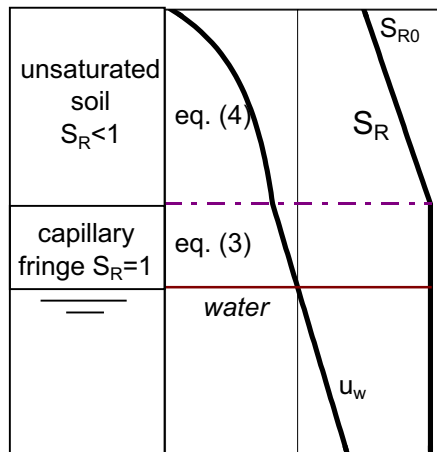
Fig. 2. Assumed trend of the degree of saturation with depth and correspondent pore-water pressures.

Shear strength of unsaturated soil

Shear strength of unsaturated soils is usually evaluated by two main approaches available in the literature, proposed by Bishop (1959) and Fredlund et al. (1978) and described by the following expressions, respectively:

$$\tau = c' + \left[(\sigma - u_a) + \chi(u_a - u_w) \right] \tan \phi' \qquad (5)$$

$$\tau = c' + (\sigma - u_a) \tan \phi' + (u_a - u_w) \tan \phi^b \qquad (6)$$

where c' is the effective cohesion of saturated soil; ϕ' is the effective angle of shear resistance of saturated soil; σ is the total normal stress; χ is a numerical co-efficient ranging from 0 to 1, ϕ^b is the friction angle for changes in matric suction. The previous approaches can be considered equivalent, provided that:

$$\tan \phi^b = \chi \tan \phi' \qquad (7)$$

In this study χ is calculated according to Khalili and Khabbaz (1998): at suction values below the air-entry value, the soil is saturated and $\chi=1$, otherwise the following correlation is used:

$$\chi = \left[\frac{\psi_b}{u_a - u_w} \right]^{0.55} \qquad (8)$$

Considering that for a suction range of 0-500 kPa the saturated friction angle ϕ' can be assumed constant (e.g. Vanapalli et al., 1996; Karube, 1988), equations (7) and (8) show that as the suction increases, the χ coefficient and therefore ϕ^b decreases, according to observed experimental behaviour (e.g. Gan et al., 1988; Escario and Juca, 1989; Mahalinga-Iyer and Williams, 1995; Nishimura and Fredlund, 2001). The combined use of (7) and (8) allows to predict the shear strength of unsaturated soil without performing elaborate and time consuming laboratory tests to measure ϕ^b; it is sufficient only the measurement of the air-entry value, easily determinable in any physics laboratory.

Combining (4) and (8), the contribution of soil suction to the shear strength can be expressed as:

$$\chi(u_a - u_w) = \Psi_b \left(\frac{1 - S_{RES}}{S_R - S_{RES}} \right)^{0.45/\lambda} \qquad (9)$$

Dimensionless parameters

Table 1 lists the parameters which can affect the factors of safety of a partly submerged slope. Suction effects are considered by the air-entry value (ψ_b), the pore-size distribution index (λ) and the residual degree of saturation (S_{RES}) defined by the BC equation. The base value of λ is assumed equal to 0.33, which represents an average value over all texture classes of the U.S. Department of Agriculture texture triangle (Mc Cuen et al., 1981).

In this study both saturated and dry unit weight are maintained constant; in particular, the dimensionless factors γ_{sat}/γ_w and $\gamma_{dry}/\gamma_{sat}$ are assumed equal to 2.0 and 0.8, respectively (i.e. porosity, $n = 0.4$ and specific gravity of soil, $G_s = 2.67$). Rapid and complete drawdown conditions are investigated ($L_f/H = 1$).

Slope analysis method

The effect of soil suction on the slope stability is expressed by a dimensionless parameter R defined as the ratio of the factor of safety calculated considering soil suction (F_{SUC}) to the factor of safety neglecting soil suction and assuming a constant unit weight below and above the water table (F_{SAT}):

$$R = \frac{F_{SUC}}{F_{SAT}} \tag{10}$$

Both factors of safety are calculated by the Bishop's simplified method (Bishop, 1955). The search for the critical failure surface is performed by an automatic search routine implemented in the computer code AUTOJB (Bellezza, 2000).

Table 1. Parameters influencing slope stability of partly submerged slope.

Parameter	symbol	dimension	dimensionless factor	default value
slope angle	β	[-]	$\cot\beta$	2
initial water level below slope crest	L	[L]	L/H	variable
water level after rapid drawdown	L_f	[L]	L_f/H	1
depth of the firm base	DH	[L]	D	1
frictional strength	ϕ'	[-]	ϕ'	20°
cohesive strength	c'	[FL^{-2}]	$c'/\gamma_{sat}H$	0.05
saturated unit weight	γ_{sat}	[FL^{-3}]	γ_{sat}/γ_w	2
dry unit weight	γ_d	[FL^{-3}]	γ_d/γ_{sat}	0.8
degree of saturation at the slope surface	S_{R0}	[-]	S_{R0}	0.5
air-entry value	ψ_b	[FL^{-2}]	$\psi_b/\gamma_{sat}H$	0.05
pore-size distribution index	λ	[-]	λ	0.33
residual degree of saturation	S_{RES}	[-]	S_{RES}	0.1

RESULTS OF THE PARAMETRIC STUDY

Drawdown ratio

Figure 3 shows the calculated values of F_{suc}, F_{sat} and R versus the initial water level ratio (L/H). The trend of F_{sat} is in good agreement with those found by Lane and Griffiths with Finite Element Method. The R value starts from 1 when L/H=0, (i.e the slope before drawdown is completely submerged and no soil suction exists) and then it increases with L/H until about 1.17 for L/H=1. This can be explained considering that the soil mass subjected to negative pore-water pressures increases with L/H.

From a practical point of view, assuming a safety factor, Fs = 1.2 as a minimum required for rapid drawdown, soil suction allow to start a complete drawdown from L/H equal to 0.6, instead of 0.7
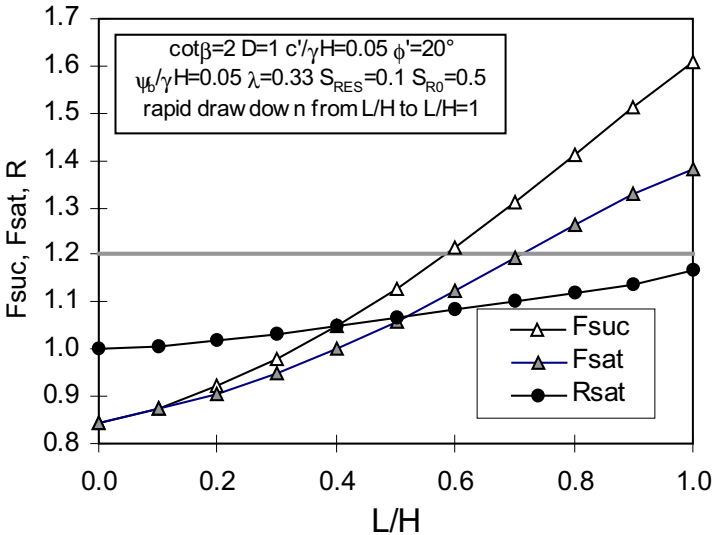
Fig. 2. Factors of safety and factors of safety ratio versus drawdown ratio

Slope inclination

In Figure 4 the calculated values of R are plotted against the inclination of slope for three different values of the initial water level. In the investigated range (cotβ = 2-5), the effect of the inclination on R is small, particularly for low L/H values. It is important to point out that the maximum variations are achieved for the maximum inclination investigated (cotβ = 2), i.e. when the safety factor assumes the lowest value.
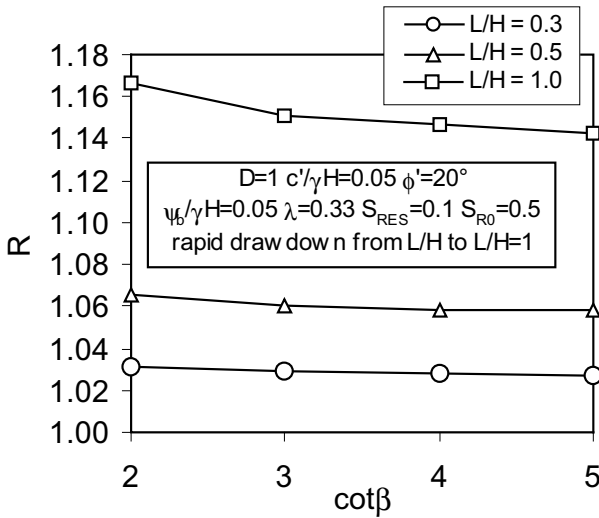
Fig. 4. Effect of the slope inclination on the ratio of safety factors, R

Depth factor

Figure 5 shows the calculated values of R versus the depth factor for slopes with different inclinations for three different values of the drawdown ratio. The maximum value of R, R_{max}, is achieved for $D = 1$; R_{max} depends on the initial water level, ranging from about 1.03, 1.07 and 1.17 for L/H =0.3, 0.5 and 1.0, respectively. Of course, increasing D both factors of safety F_{SAT} and F_{SUC} decrease (or remain constant), but the reduction of F_{SAT} is smaller and the coefficient R decreases. For a slope with a given inclination, a value of the depth factor exists beyond which the factor R is constant, because the critical slip surfaces (for both F_{SAT} and F_{SUC}) remain the same. This threshold value of D ranges from 1.25 and 2 and it tends to increase with decreasing inclination

Saturated shear strength parameters

To investigate the influence of the saturated shear strength parameters (c' and ϕ') on R, the dimensionless factor $\lambda_{c\phi} = \gamma H tan\phi'/c'$ is used. This parameter was introduced by Janbu (1954) and later used by many others (e.g., Cousins, 1978) to develop stability charts for cohesive-frictional slopes. It is easy to construct stability charts in terms of the stability number $N_F=\gamma HF/c'$ against the dimensionless parameter $\lambda_{c\phi}$ both considering (N_{FSUC}) and neglecting (N_{FSAT}) the soil suction. Taking into account that the ratio of the above stability numbers (N_{FSUC} and N_{FSAT}) coincides with the ratio between F_{SUC} and F_{SAT} (i.e., R), Figure 6 presents the effect

of the Janbu's dimensionless parameter on R for slopes with two different initial water levels. The results indicate that R reaches a maximum when $\lambda_{c\phi}$ is approximately equal to 13-15. The maximum value of R increases with increasing the initial water level (1.04 and 1.07 for L/H=0.3 and 0.5, respectively). For $\lambda_{c\phi}$ tending to 0, R decreases because the cohesive strength becomes prevalent respect to the strength due to soil suction. Once the maximum is overcome, the coefficient R decreases with increasing $\lambda_{c\phi}$ and it tends to the unity. This is because for high values of $\lambda_{c\phi}$ the cohesive strength tends to 0 and the critical slip surfaces become shallower and tend to be located in a zone of the slope that is not subjected to negative pore-water pressures.
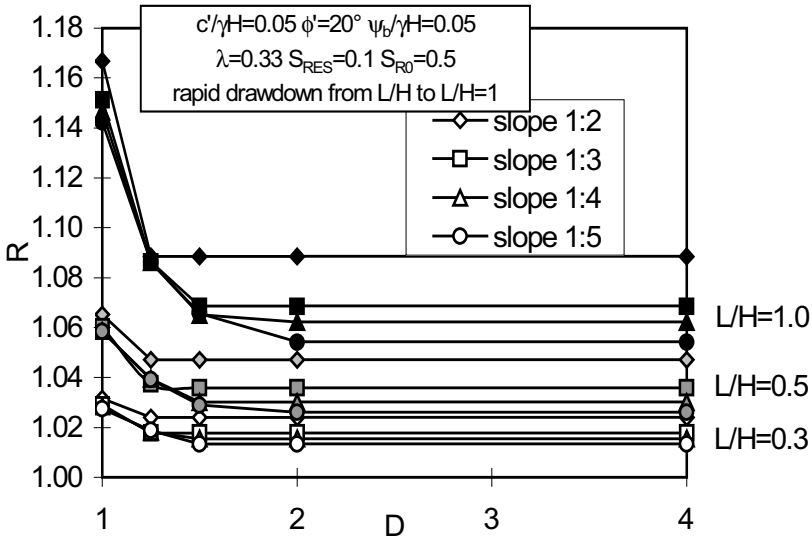
Fig. 5. Effect of the slope inclination on the ratio of safety factors, R
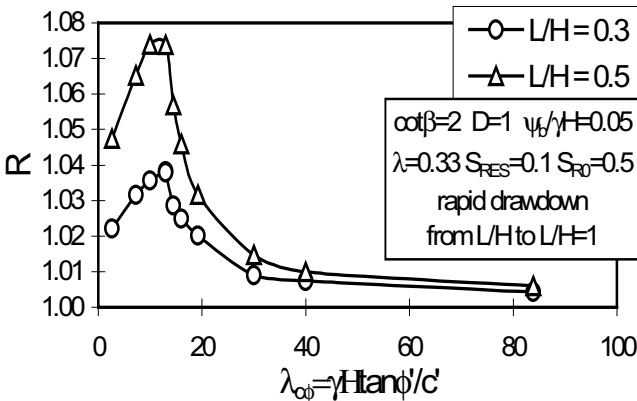
Fig. 6. Effect of the Janbu's dimensionless parameter on the factor of safety ratio

Air-entry value

Figure 7 shows the influence of the normalised air-entry value on the coefficient R for three different initial water levels. The critical slip surfaces always pass trough the crest of the slope and their location is found to be poorly influenced by the normalised air-entry value. All the curves of Figure 7 have a similar trend with a maximum value of R reached at a normalised air-entry value, which increases with increasing L/H. The maximum values of R are found to be 1.03, 1.09 and 1.39 for L/H=0.3, 0.5 and 1.0, respectively. The observed trends are mainly due to the soil shear strength above the water table. As the air-entry value increases, an increased zone in the failure mass tends to pass from an unsaturated state to the capillary fringe. In the first part of the curves, the factor of safety F_{SUC} (and consequently R) rises because the suction rates in the capillary fringe are greater than those calculated by (9). In addition, in the unsaturated zone the increased air-entry value has a greater stabilizing effect than the increased degree of saturation (see [9]). At higher air-entry values, the factor of safety slightly falls because the suction rates calculated by (9) become greater than those in the capillary fringe. Moreover, the increased weight of the soil in the upper zone of the failure mass starts to have a destabilizing influence on slope stability.

Finally, it should be noted that for a given initial water level L/H, if the normalised air-entry value exceeds the value $L\gamma_w/H\gamma_{sat}$ (i.e. 0.5L/H), the coefficient R remains unchanged and independent of Brooks and Corey parameters (λ and S_{RES}) since all the soil above the water level is saturated and all negative pore-water-pressures are calculated by (3).
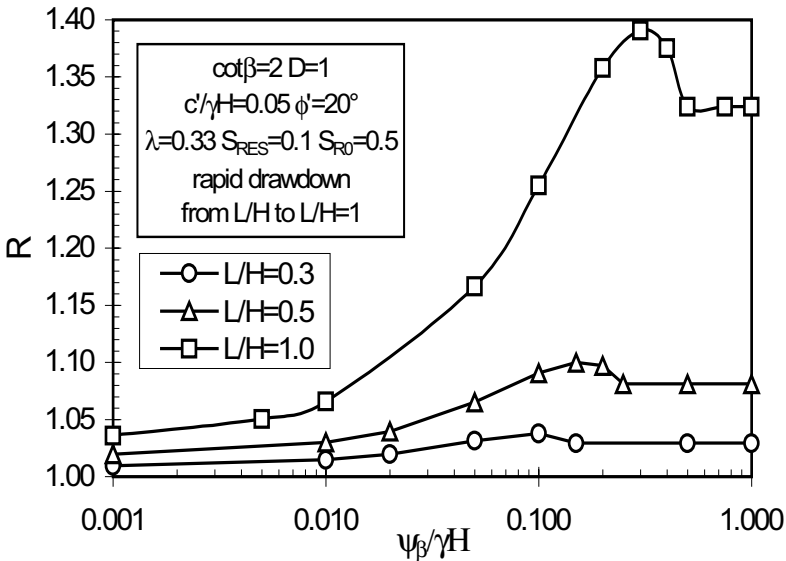
Fig. 7. Effect of the normalised air-entry value on the factor of safety ratio

λ papameter of the BC function

Figure 8 plots the values of R by varying the pore-size distribution index of the BC function for three different value of the initial water level. As expected, the influence of soil suction in slope stability increases with decreasing λ. For $\lambda < 0.2$, R strongly depends on λ and the effect of soil suction becomes significant.
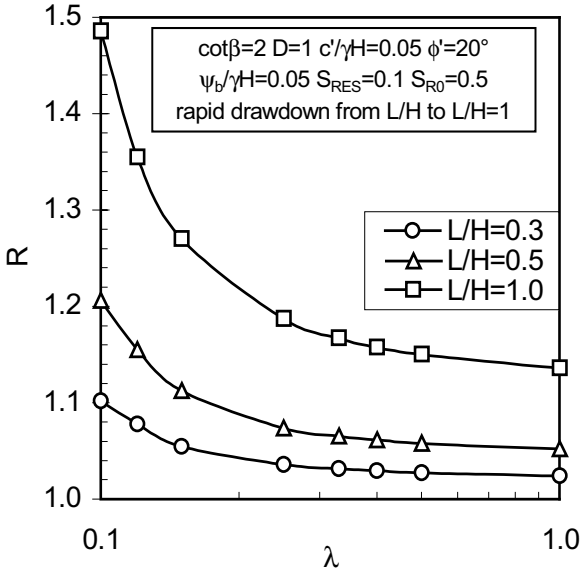

Fig. 8. Effect of the pore-size distribution index on the factor of safety ratio

Residual degree of saturation

Figure 9 shows the values of R versus the residual degree of saturation of the soil for three different values of the initial water level. It can be observed that, all other factors being equal, soil suction effects are practically independent of S_{RES}.

Degree of saturation at the slope surface

Figure 10 shows the values of R versus the degree of saturation at the slope surface for three different values of the initial water level. As expected, R increases with decreasing S_{R0}. This is because the soil suction is inversely proportional to the degree of saturation of the soil. For $S_{R0} > 0$ the relationship between R and S_{R0} is approximately linear.
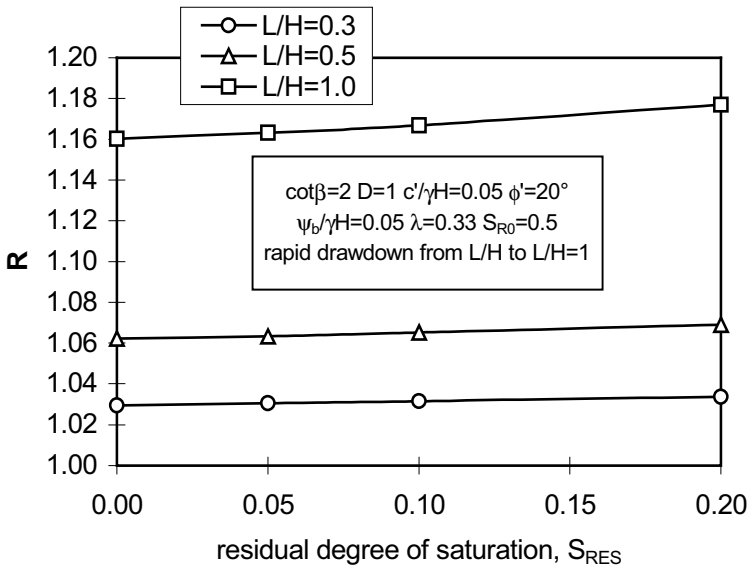
Fig. 9. Effect of residual degree of saturation on the factor of safety ratio
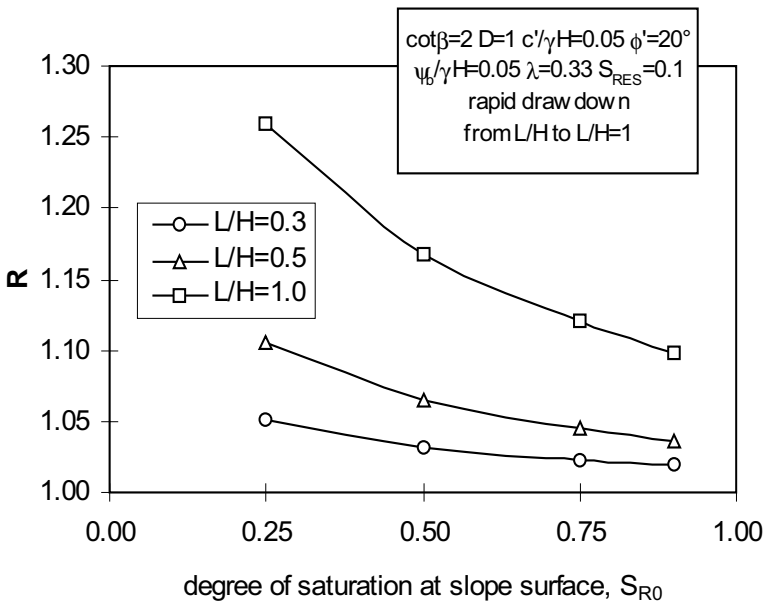
Fig. 10. Effect of the degree of saturation at the slope surface on the factor of safety ratio

CONCLUSIONS

This study was directed to compare slope stability analysis including soil suction effects with the results obtained neglecting it.

Suction values were calculated by the characteristic curve of Brooks and Corey (1964), with the assumption of a linear unsaturated soil profile. The unsaturated shear strength was calculated according to the correlation of Khalili and Khabbaz (1998).

A parametric analysis has been carried out on a simple slope subjected to rapid and complete drawdown conditions. The following main conclusions can be drawn from the results presented in this paper.

- Errors resulting from neglecting soil suction slightly increase with the inclination of the slope and they reach the maximum value when the firm stratum is at the base of the embankment (D=1).
- The effect of the saturated shear strength parameters, evaluated by the Janbu's dimensionless coefficient $\lambda_{c\phi}$, were found to be small, especially for $\lambda_{c\phi} > 25$.
- The slope stability is found to be strongly sensitive to variation of the pore-size distribution index λ. The influence of the residual degree of saturation seems to be negligible.

From a practical point of view if the initial water level ratio (L/H) is less than 0.3 the factor of safety variations are less than 10% and then comparable with the uncertainties associated with material heterogeneity, sampling and testing.

The effect of suction can be significant for road or railway embankments with the water level at the base of the slope (L/H=1). For example, in the cases here presented, the ratio F_{SUC}/F_{SAT} ranges from 5% to 50%.

REFERENCES

Bellezza, I. 2000. Limit equilibrium methods for stability analysis in landfills. Proc. I Int. Conf. on Geotechnical Engineering and Training. Sinaia Romania, 265-270.

Bishop, A.W. 1955. The use of the slip circle in the stability analysis of slopes. Geotechnique, 5(1), 7-17.

Bishop, A.W. 1959. The principle of effective stress. Teknisk Ukeblad, 106 (39), 859-863.

Bouwer, H. 1978. Groundwater hydrology. McGraw-Hill Book Co. New York.

Brooks, R.H. and Corey, A.T. 1964. Hydraulic properties of porous media. Hydrology Vol.27 No.3. Colorado State University, Fort Collins.

Chiu, T.F. and Shackelford, C.D. 1998. Unsaturated Hydraulic Conductivity of Compacted Sand-Kaolin Mixtures. Journal of Geotechnical and Geoenvironmental Engineering, ASCE, 124 (2), 160-170.

Cousins, B.F. 1978. Stability charts for simple earth slopes. Journal of Geotechnical Engineering Division, ASCE, 104(2), 267-279.

Desai, C. S. 1977. Drawdown analysis of slopes by numerical method. Journal of Geotechnical Engineering Division, ASCE, 103 (7), 667-676.

Escario, V. and Juca, J. 1989. Strength and deformation of partly saturated soils. Proc. XII Int. Conf. Soil Mechanics and Foundation Engineering, Rio de Janeiro, Vol.3, 43-46.

Fredlund, D.G., and Xing, A. 1994. Equations for the soil-water characteristic curve. Canadian Geotechnical Journal, 31, 521-532.

Fredlund, D.G., Morgestern, N.R., and Widger, R.A. 1978. The shear strength of unsaturated soils. Canadian Geotechnical Journal, 15, 315-321.

Gan, J.K.M., Fredlund, D.G., and Rahardjo, H. 1988. Determination of the shear strength parameters of an unsaturated soils using the direct shear tests. Canadian Geotechnical Journal, 25 (3), 500-510.

Griffiths D.V. and Lane, P.A. 1999. Slope stability analysis by finite elements. Geotechnique, 49(3), 387-403.

Janbu, N. 1954. Stability analysis of slopes with dimensionless parameters. Harward Soil mechanics series, No.46.

Karube, D. 1988. New concept of effective stress in unsaturated soil and its proving test. In Advanced triaxial testing of soil and rock. ASTM SPT No. 977, 539-552.

Khalili, N. and Khabbaz, M.H. 1998. A unique relationship for the determination of the shear strength of unsaturated soils. Geotechnique, 48(5), 681-687.

Lane, P.A. and Griffiths D.V. 2000. Assessment of stability of slopes under drawdown conditions. Journal of Geotechnical and Geoenvironmental Engineering, ASCE, 126(5), 443-450.

Mahalinga-Iyer, U. and Williams, D.J. 1995. Unsaturated strength behaviour of compacted lateritic soils. Geotechnique, 45(2), 317-320.

Mc Cuen R.H., Rawls, W.J., and Brakensiek D. L. 1981. Statistical analysis of the Brooks-Corey and the Green-Ampt parameters across soil textures. Water Resources Research, 17(4) 1005-1013.

Milly, P.C.D. 1987. Estimation of the Brooks-Corey parameters from water-retention data. Water Resources Research, 23(6), 1085-1089.

Morgestern, N. R. 1963. Stability charts for earth slopes during rapid drawdown. Geotechnique, 13(1), 121-131.

Nishimura T., and Fredlund, D.G. 2001. Failure envelope of a desiccated unsaturated silty soil. Proc. XV Int. Conf. Soil Mechanics and Geotechnical Engineering, Istanbul, Vol. 3, 615-618.

Russo, D. 1988. Determining soil hydraulic properties by parameter estimation: on the selection of a model for the hydraulic properties. Water Resources Research, 24(3) 453-459.

Siller, W.J., and Fredlund, D.G. 2001. Statistical assessment of soil-water characteristic curve models for geotechnical engineering. Canadian Geotechnical Journal, 38(6), 1297-1313.

Vanapalli, S.K., Fredlund, D.G., Pufahl, D.E. and Clifton, A,W. 1996. Model for the prediction of shear strength with respect to soil suction. Canadian Geotechnical Journal, 31(3), 379-392.

Effects of unsaturation on the stability of a moraine slope

L. Simeoni[1], A. Tarantino[2], and L. Mongiovì[3]

[1] Dipartimento di Ingegneria Meccanica e Strutturale, Università degli Studi di Trento, Italy, via Mesiano 77, 38050 Trento, Italy, lucia.simeoni@ing.unitn.it

[2] Dipartimento di Ingegneria Meccanica e Strutturale, Università degli Studi di Trento, Italy, via Mesiano 77, 38050 Trento, Italy, tarantin@ing.unitn.it

[3] Dipartimento di Ingegneria Meccanica e Strutturale, Università degli Studi di Trento, Italy, via Mesiano 77, 38050 Trento, Italy, mongiovi@ing.unitn.it

Abstract: The papers presents a numerical analysis of the stability of a moraine slope that reactivated after two heavy rainfall events in November 2000. To analyse the pore water pressure distribution within the slope, rainfall and evapotranspiration were applied to the slope over a period of four years that preceded the main landslide reactivation. Because of the uncertainty about the saturated hydraulic conductivities of the landslide soils, different combinations of these coefficients were analysed. The factor of safety of the slope was then calculated at the time where the slope moved, as recorded by the inclinometer measurements. This made it possible to verify which combinations of saturated hydraulic conductivities were compatible with the slope movements.

Keywords: case study, evapotranspiration, numerical analysis, slope stability, unsaturated flow.

1 Introduction

Glacial soils are widespread in the Trentino-Alto Adige region in northern Italy and form the slopes of many valleys in the region. The *Val di Non* valley, renowned for its apple cultivation, is one of the largest valleys of glacial origin and is covered by a glacial deposit having thickness up to 40 m. The *Val di Non* is cut by the *Noce* River, whose tributaries have eroded narrow incisions making slopes as steep as 30° and making the area prone to landsliding.

A very intense and prolonged rainfall in November 2000 triggered new landslides and reactivated many pre-existing ones in the *Val di Non* region. One of these landslides reactivated on the hill where *Castel Valer* stands, threatening to carry away the castle.

The landslide has been investigated since 1996, when ground investigations were carried out by means of 5 boreholes (Fig. 1). Three boreholes (P2, P3, and P5) were then equipped with open-standpipe piezometers to monitor water table level, and two boreholes (I1 and I4) were equipped with inclinometer casings to monitor deep movements by means of inclinometer probes. In 2001, three other boreholes were drilled (C9, C10 and C11) and were equipped with Casagrande piezometers.
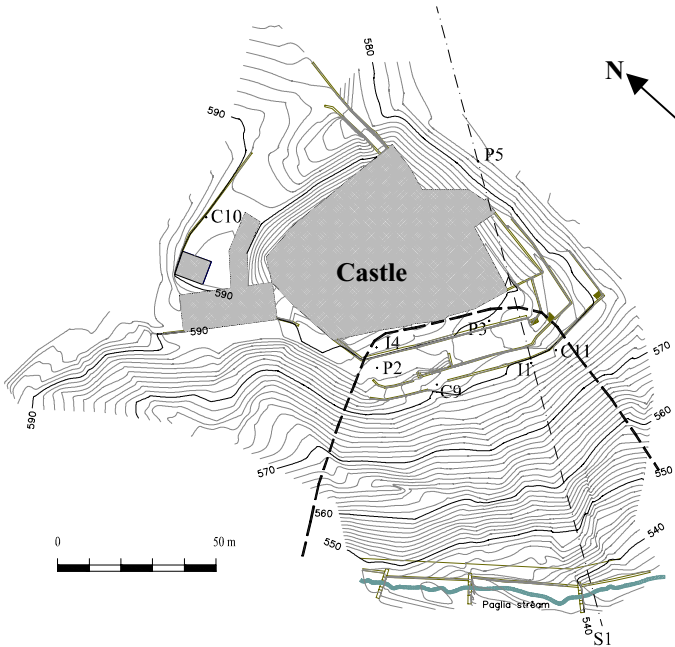

Fig. 1. Location map and borehole positions. P1, P3 and P5: open-standpipe piezometers (1996); C9, C10 and C11: piezometric cells of Casagrande type (2001); I1 and I4: inclinometer casings (1996).

In November 2000, two heavy rainfall events occurred for a total of 490 mm in 27 days: 183 mm of rain fell from 30 October to 10 November and 307 mm fell from 13 to 25 November. Following these two events, a displacement along the sliding surface of 30 mm was calculated at the inclinometer I1, and a displacement of 5 mm was calculated at the inclinometer I4.

Since November 2000, a study has been underway to investigate the causes of reactivation and to design landslide countermeasures. As a part of this study, the effect of rainfall on slope stability was investigated by taking into account the un-saturated nature of the soils forming the slope. The paper presents some of the numerical simulations carried out to investigate the interplay between slope insta-bility and climatic conditions. The problem of defining suitable initial and bound-ary conditions is first addressed. Then, the main features of the finite element modelling are illustrated.

Finally, the results from preliminary numerical simulations are presented. These were aimed at back-calculating the permeability of the soils forming the slope. Results from laboratory and field testing gave saturated hydraulic conductivities differing four orders of magnitude. To investigate the permeability characteristics of the landslide soils, stability analyses were performed by selecting different values of saturated hydraulic conductivities. The factors of safety obtained from these analyses were then compared to the landslide movements recorded by the inclinometers over a period of four years.

2 Landslide description

The landslide is situated on a south-facing slope between 537 and 594 m above sea level, with inclinations between 26° and 31°. The *Paglia* stream flows at the toe of this slope and it is likely that stream downcutting caused the original slope failure in the eighteen century, when a section of the castle is reported to have collapsed. The sliding mass has a width of approximately 75 m. The soil profile consists of a glacial deposit lying on a bedrock of grey to blue marl. The marl bedrock interface is roughly horizontal and is located at a medium altitude of 554 m above sea level. As a result, the marl outcrops at the toe of the slope. At the contact with the overlying glacial deposit, the marl changes to a brown colour and consists of a soft matrix with widespread stiff flakes included in it.
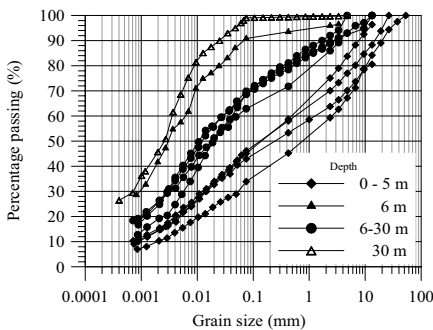
Fig. 2. Grain size distribution of samples collected at different depths.

The glacial deposit is up to 40 m thick and the soil is very well graded, including gravel, sand, silt and clay particles. Thin layers of fine-grained materials (clayey silt) were locally recognised within the deposit, and a layer of coarser material of 4 to 6 m thick is located at its top. Fig. 2 shows the grain size distributions of samples taken at different depths from the glacial deposit. The soil may be classified as clayey and sandy silt with a variable content of gravel. The liquid limit of the soil from the glacial deposit was found to range from 0,15 to 0,21 and the plastic limit from 0,27 to 0,43. The shear strength of the soil in saturated state was investigated by means of direct shear tests. The glacial soil was found to have a re-

sidual shear strength characterised by an effective cohesion ranging from 4 to 10 kPa and an effective angle of shearing resistance from 26° to 30°. The weathered marl was found to have residual shear strength characterised by an effective cohesion of 0 kPa and an effective angle of shearing resistance of 26°.

Inclinometer measurements revealed that the slide moved downslope along the direction of maximum slope. Movements were often associated with heavy rainfall. Piezometric levels in the open standpipe piezometers P2 and P3 varied from 4 to 30 m from the ground surface over a period of 4 years, while the level in the piezometer P5 varied from 0 to 3 m. The piezometer measurements were doubtful because of the high response time of this type of piezometer, the way the standpipes were installed, and inconsistency in the response of the three piezometers.

As a result, one of the main problems in the back-analysis of the landslide reactivation was to simulate the pore water pressure changes within the slope in absence of field measurements. The approach followed in this paper was to calculate the pore water pressure distributions associated with a given climatic history and then comparing the factor of safety of the slope with the landslide displacements as measured by the inclinometers.

3 Numerical analysis

The analysis of the infiltration/exfiltration flow in the unsaturated soil was performed using a two-dimensional finite element code (SEEP/W, GeoSlope International Ltd. 1997). Stability of the landslide was investigated by using a program based on the limit equilibrium method (SLOPE/W, GeoSlope International Ltd. 1999). The Bishop's simplified method was used in this study.

3.1 Geometry

The cross-section S1 of the landslide analyzed in this paper is illustrated in Fig. 3. It intersects with the inclinometer I1 and is oriented along the direction of landslide displacement as recorded by this inclinometer. The inclination of the slope along this cross-section is 27°. This inclination is not truly representative of slope inclination that can reach 31° at the northern part of the landslide. Higher factors of safety than the actual ones should be then expected for slope stability analysis, but the use of a two-dimensional model neglects the side-effects and likely reduces this overestimate.

The deposit was divided in three layers: the coarser upper glacial soil, the lower glacial soil and the weathered marl.

The mesh used for the seepage analyses comprised 3602 nodes and 3614 triangular or quadrilateral elements. Slope stability analyses were performed for the same sliding surface that intersects the inclinometer I1 where local displacements were measured. This surface was defined as a polygonal surface so as to approximated a circular shape.
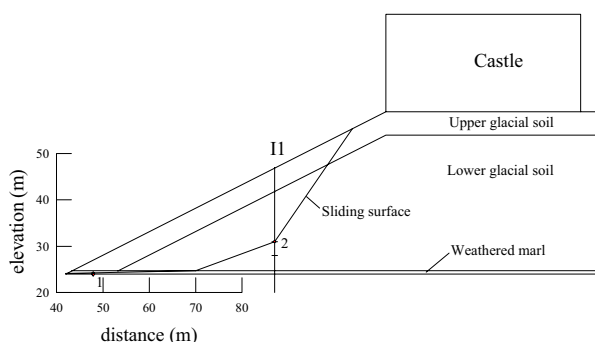
Fig. 3. Cross-section S1 used in the analyses.

3.2 Boundary conditions

The boundary conditions were given as total head or unit flux. A constant total head was specified at the right boundary corresponding to a water level of 2 m below the ground surface. This value corresponds to the average value measured in the piezometer P5. A condition of zero flux was specified at the bottom of the slope. Along the slope surface, two flux conditions were applied: daily rainfall (water inflow) to the ground surface, and evapotranspiration (water outflow) to 50 cm below the ground surface to account for the uptake of water by roots.

3.2.1 Rainfall

Rainfall data were obtained from the closest station (Cles, 5 km far from Castel Valer and 60 m higher in elevation). Daily rainfalls (Fig. 4) from 1 January 1997 to 31 December 2000 were applied to the slope. It was assumed that ponding on the surface could not occur. Accordingly, a pore-water pressure greater than zero was not allowed on the slope surface by switching the boundary condition from unit flux to zero pore water pressure.

3.2.2 Evapotranspiration

Evapotranspiration was calculated using the FAO Penman-Monteith equation according to the method recommended by the FAO for computing water requirements (Allen et al. 1998). The method provides the reference evapotranspiration ET_0 calculated for the hypothetical reference crop having height of 0,12 m, surface resistance of 70 s m^{-1} and albedo of 0,23, which closely resembles to the evaporation of an extension surface of green grass of uniform height, actively growing and adequately watered.

ET_0 was derived from the original Penman-Montheith equation (Monteith 1965):

$$\lambda ET = \frac{\Delta (R_n - G) + \rho_a c_p \dfrac{(e_s - e_a)}{r_a}}{\Delta + \gamma \left(1 + \dfrac{r_s}{r_a}\right)} \qquad (1)$$

where λ=latent heat of vaporisation of water [J kg^{-1}], ET=evapotranspiration [mm day^{-1}], R_n=net radiation at the crop surface [MJ m^{-2} day $^{-1}$], G=soil heat flux density [MJ m^{-2} day $^{-1}$], ρ_a = mean air density at constant pressure [Kg m^{-3}], c_p=specific heat at constant pressure [MJ kg^{-1} °C^{-1}], e_s-e_a=saturation vapour pressure deficit [kPa], r_a=aerodynamic resistance [s m^{-1}], r_s= bulk surface resistance [s m^{-1}], Δ=slope vapour pressure curve [kPa °C^{-1}], γ=psychrometric constant [kPa °C^{-1}]. Assuming the aerodynamic resistance as:

$$r_a = \frac{208}{u_2} \qquad (2)$$

where u$_2$ is the wind speed [m s^{-1}] at 2 m, the surface resistance r_s equal to 70 s m^{-1}, and the latent heat of vaporisation of water λ equal 2,45 J kg^{-1}, ET_0 becomes:

$$ET_0 = \frac{0{,}408\Delta (R_n - G) + \gamma \dfrac{900}{T + 273} u_2 (e_s - e_a)}{\Delta + \gamma (1 + 0{,}34 u_2)} \qquad (3)$$

The psychrometric constant γ depends on the atmospheric pressure. However it can be assumed constant for each location as it is slightly affected by atmospheric pressure fluctuations. γ is equal to 0,063 kPa °C^{-1} for Castel Valer, whose elevation is about 600 m above sea level. Evapotranspiration ET_0 was calculated by using the climatic data from the station of Cles.

The actual evapotranspiration ET_c from other crops can be calculated by multiplying ET_0 by the crop coefficient Kc, which is related to the type of vegetation. The crop coefficient Kc account for the differences in evaporation and transpiration due to the ground cover features (standard conditions refer to crops in large fields under excellent agronomic and soil water conditions), canopy properties and aerodynamic resistance.

Most of the effects of the various weather conditions are incorporated into the ET_0 estimate. ET_0 therefore represents an index of climatic demand, whereas Kc varies predominately with the specific crop characteristics and only to a limited extent with climate. This enables the use of standard values for Kc (Allen et al. 1998) for different locations and climates.

Kc represents an integration of the effects of four primary characteristics that distinguish the crop from the reference grass. These characteristics are: crop height, albedo, canopy resistance and evaporation from soil. As a consequence, the crop coefficient Kc may vary during the growing period of the crop. For the ground of the Castel Valer landslide Kc was assumed with reference to apple trees, and its values are reported in table 1. ET_c values are shown in Fig. 4.

Table 1. Values of crop coefficient Kc assumed for Castel Valer

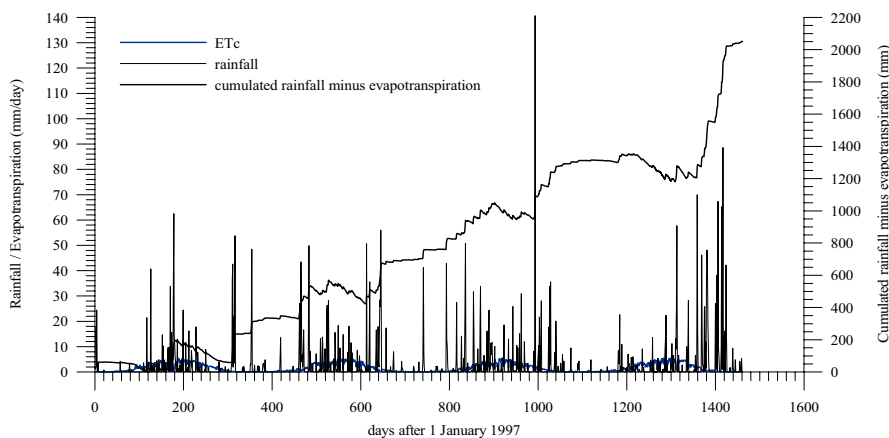| Month	J	F	M	A	M	J	J	A	S	O	N	D
Kc	0,30	0,30	0,30	0,60	0,90	0,90	1,10	1,10	0,95	0,85	0,50	0,30

Fig. 4. Daily rainfall and evapotranspiration and cumulated rainfall minus evapotranspiration.

3.3 Unsaturated soil properties

The soil-moisture characteristics of the lower glacial soil was assessed in the laboratory using Trento tensiometers (direct measurements of matric suction) and transistor psychrometers (indirect measurements of total suction). The soil-moisture characteristics for the upper glacial soil was estimated by using a pedo-transfer function (PTF) based on the grain size distribution (Saxton et al. 1986). The relative unsaturated hydraulic conductivities were then estimated from the water retention curves (Fig. 5) using the equation proposed by Van Genuchten (1980). Two values of saturated hydraulic conductivity were assumed for the lower glacial soil: $k_s = 10^{-7}$ m/s according to one field measurement, and $k_s = 10^{-9}$ m/s, two orders of magnitude greater than the value of 10^{-11} m/s measured in the laboratory on a small sample.

Saturated hydraulic conductivity of the upper glacial soil was assumed to be one order of magnitude greater than the value of the lower glacial soil accordingly to the larger diameter corresponding to the 10% of passing.

Seepage analyses were therefore performed with these two couples of saturated hydraulic conductivity: $k_s = 10^{-6}$-10^{-7} m/s and $k_s = 10^{-8}$-10^{-9} m/s.

For slope stability analyses the Mohr-Coulomb criterion was adopting with c'=0 kPa and $\Phi' = \Phi'_b = 30°$. The high air entry values of the glacial soils may justifies the assumption $\Phi' = \Phi'_b$.
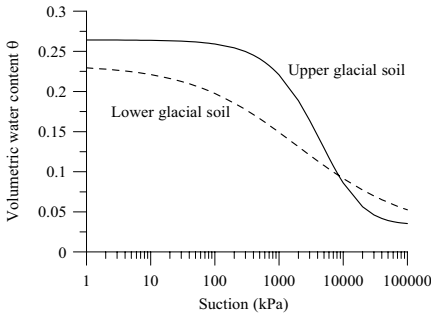
Fig. 5. Soil-moisture characteristics of the two glacial soils.

3.4 Initial conditions

Steady state condition corresponding to the water level of 2 m below the ground surface at the right boundary and a zero influx to the slope surface was assumed as initial condition. This initial condition is arbitrary but its effects on pore-water pressure distributions were cancelled by applying a climatic history for a sufficiently long period (four years) preceding the last landslide reactivation.

4 Results and discussion

In the following, the analysis with $k_s=10^{-6}-10^{-7}$ m/s will be identified with H (higher hydraulic conductivities), whereas the analysis with $k_s=10^{-8}-10^{-9}$ m/s will be identified with L (lower hydraulic conductivities). Results of seepage analyses are reported for time intervals of 10 days. Figures 6 and 7 show the pressure variations calculated at point 1 and 2 on the sliding surface for both cases H and L. Point 1 (Fig. 3) is located at the toe of the slide 3 m below the ground surface and within the upper glacial soil; point 2 was chosen 15 m below the ground surface on the inclinometer vertical and within the lower glacial soil.

Pore-water pressures at point 1 show approximately similar cyclic behaviors for both cases H and L. It can be seen that pore-water pressure values are in phase with the effective rainfall (rainfall minus evapotranspiration) reported in Fig. 4: pore-water pressure is minimum when the effective rainfall is negative (months of August and September). This is because point 1 is located at small distance from the ground surface and pore-water pressures are directly affected by the climatic conditions. Although cyclic behaviours are similar, pore-water pressure values from the two analyses considerably differ. Pore-water pressures from the analysis H are always positive, whereas values from the analysis L are generally negative and greater in magnitude.
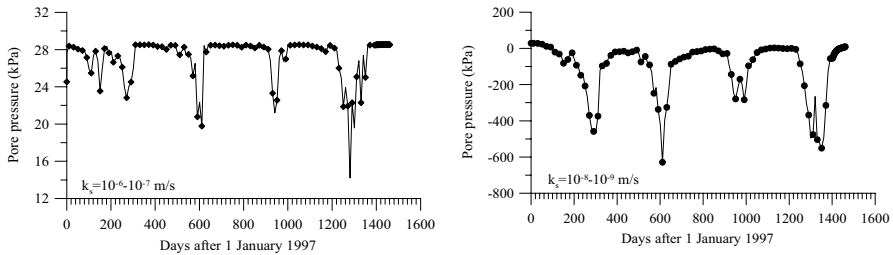
Fig. 6. Pore-water pressures at point 1 from analysis H (left) and analysis L (right).

At point 2 pore-water pressures always remained positive for case H, whereas pore-water pressures ranged from negative to positive values for the case L. It is worth noting that pore-water pressures at point 2 for the case L is out of phase with respect to the effective rainfall. This is due to the lower saturated hydraulic conductivities and the greater depth of point 2 from the ground surface.
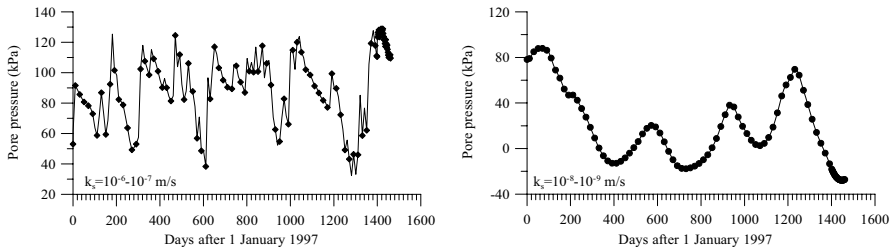

Fig. 7. Pore-water pressures at point 2 from analysis H (left) and analysis L (right).

In Fig. 8 the pore-water pressure contours from analyses H and L are compared at day 611 (dry period where the difference between rainfall and evapotranspiration is negative) and day 1421 (rainfall event of November 2000 where effective rainfall is positive).

When evapotranspiration predominates (day 611), pore-water pressures are negative below the slope surface. In the analysis L the hydraulic conductivity is lower and, as a result, pressure gradients are higher and pressures are more negative. In the analysis H, hydraulic conductivity is higher, pressure gradients are lower and the pore-water pressure distribution above the water table is quasi-hydrostatic.

When infiltration is predominant (day 1421) a sharp infiltration front forms below the ground surface for the analysis L. In contrast, for the analysis H, the infiltrating rainwater rapidly reaches the water table which raises up to the slope surface. This different behaviour can again be explained by the different hydraulic conductivities.

It is also interesting to compare the pore pressure contours at day 611 to day 1421 for the cases H and L. For the case H it can be noted that the water table is directly affected by climatic conditions, as it rises during wet periods and lowers during dry periods. For the case L, the water table at day 1421 is deeper than at

Analysis L: $k_s = 10^{-8} - 10^{-9}$ m/s

Analysis L: $k_s = 10^{-8} - 10^{-9}$ m/s
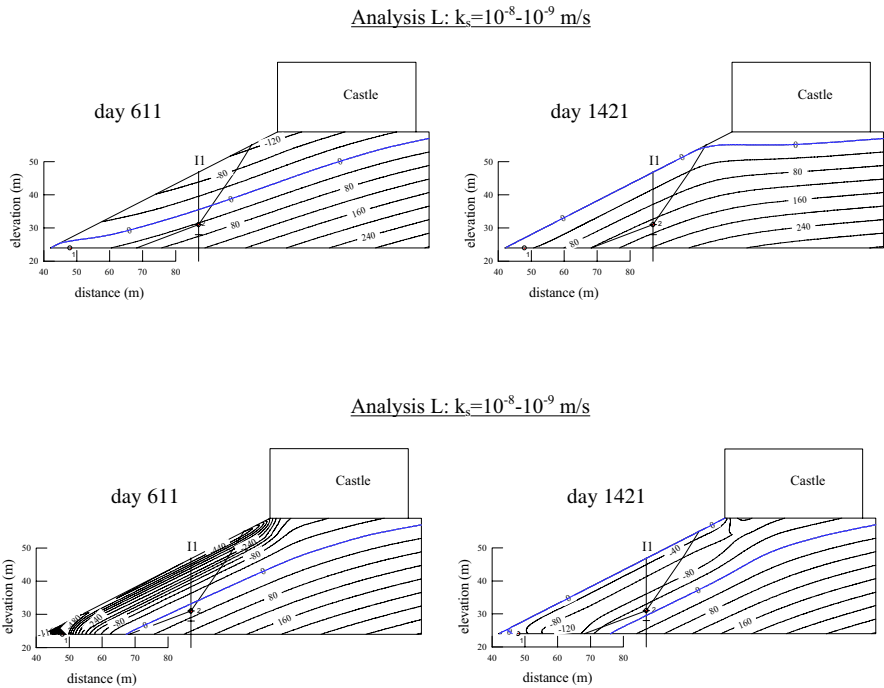
Fig. 8. Pore-water pressures contours from analysis H (top) and analysis L (bottom) during a dry period (day 611) and a wet period (day 1421).

day 611 because of the time lag in the response of the slope. Besides, at day 1421, pore-water pressures increase in a relative thin zone below the ground surface, and positive pore-water pressures develops only at the toe of the slope.

The different response of the slopes H and L to rainfall can be explained by the different ratios of rainfall intensity to saturated hydraulic conductivity (Tarantino and Bosco 2000). For the case H this ratio is small ($\leq 1,63\ k_s$) and pore-water pressure changes propagates down to the water table. For the case L the ratio is 100 times higher and, as a result, pore-water pressure changes take place in a zone close to the ground surface.

The two cases L and H provided significantly different pore-water pressure patterns in the slope, but neither of them could be corroborated by field measures as water level measurements were not reliable. The most realistic case was then assessed by determining the factor of safety at the dates where displacements were observed in the field. Although this approach is not rigorous because displacements cannot be directly related to the factor of safety, it was expected that factors of safety calculated when no displacements occurred had to be greater than those obtained when the landslide moved. With reference to the displacements measured at the inclinometer I1 (Fig. 9) three different day-intervals where displacements of higher mean velocities occurred (intervals 175-206; 485-525 and 1282-1437) and

two day-intervals where no displacements occurred (intervals 577-637 and 1246-1282) were taken into account.

For seepage analysis H, the minimum factor of safety calculated when no displacements occurred is equal to 0,91. The factors of safety calculated when displacements occurred were always less than 0,91 with a minimum of 0,72. It may be surprising that a factor of safety of 0.91 (<1) was obtained for the case where no movements were recorded. However, it should be noted that different positions of the failure surface and different values of effective cohesion could have been assumed.

For analysis L, the minimum factor of safety calculated when no displacements occurred is equal to 1,49. Some factors of safety calculated when displacements occurred were greater than 1,49.

It can be therefore inferred that the only case H provides factors of safety consistent with the landslide movements. Accordingly, saturated hydraulic conductivities of 10^{-6} m/s and of 10^{-7} m/s for the upper and lower glacial soil respectively are likely to reproduce correctly the pore-water pressure distributions within the slope.
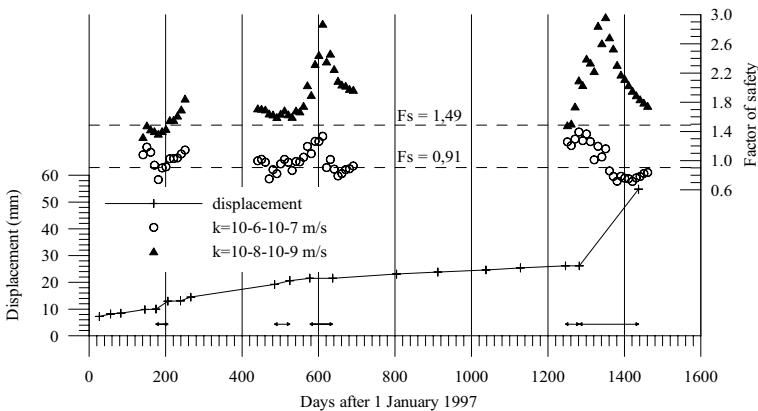
Fig. 9. Inclinometer displacements and factors of safety during landslide movements.

5 Conclusions

An analysis of seepage in a moraine slope was performed to back calculate the actual hydraulic conductivities of the two soils forming the glacial deposit. This analysis was required to achieve a realistic simulation of pore water pressure distribution within the slope and, hence, effectively design remedial measures.

Seepage analysis was performed taking into account the unsaturated state of the two glacial soils forming the slope. Two couples of saturated hydraulic conductivities were used: 10^{-6} -10^{-7} m/s (analysis H) and 10^{-8}-10^{-9} m/s (analysis L).

The soil-moisture characteristics of the lower soil were measured in the laboratory and the soil-moisture characteristics of the upper soil were estimated using a pedo-transfer function. The relative unsaturated hydraulic conductivities were calculated by adopting the equation proposed by Van Genuchten (1980). A four years climatic history was applied to the slope.

Two flux conditions were considered: daily rainfall applied to the ground surface (water inflow), and evapotranspiration 50 cm below the ground surface (water outflow) to account for the uptake of water by roots.

For analysis H, pore-water pressure changes at the ground surface rapidly propagated down to the water table and pore-water pressures along the sliding surface were generally positive during the rainfall events. In contrast, for analysis L, pore-water pressure changes during rainfall events occurred near the ground surface and the sliding surface was only partially subject to positive pore-water pressures.

Slope stability analyses were then performed by considering the pore-water pressure distributions at the dates where the slide moved and at dates where the slide did not move. Factors of safety calculated in the former case are expected to be greater than those calculated in the latter. Only simulation H achieved this condition. Accordingly, the saturated hydraulic conductivities of 10^{-6} and 10^{-7} m/s for the upper and lower glacial soil respectively appear to produce the most realistic pore-water pressure distributions.

References

Allan RG, Pereira LS, Raes D, Smith M (1998) FAO Irrigation and Drainage Paper No. 56: Crop Evapotranspiration (guidelines for computing crop water requirements). ISBN 92-5-104219-5.

Geoslope International Ltd (1997) Seep/W User's Guide for finite element Analysis, Version 4.05, Geoslope International Ltd., Calgary, Alberta, Canada.

Geoslope International Ltd (1999) Slope/W User's Guide for finite element Analysis, Version 4.22, Geoslope International Ltd., Calgary, Alberta, Canada.

Montheith JL (1965) Evaporation and environment. The State and Movement of Water in Living Organism. Proc. 19th Symp. Soc. Exp. Biol., Cambridge University Press, pp. 205-233.

Saxton KE, Rawls WJ, Romberger JS, Papendick RI (1986) Estimating generalized soil-water characteristics from texture. Soil Science Society of American Journal, 50, pp. 1031-1036.

Tarantino A, Bosco G (2000) Role of soil suction in understanding the triggering mechanisms of flow slides associated with rainfall. In G.F. Wieczorek N.D. Naeser (eds.), Second International Conference on debris-flow hazards mitigation, Taipei, Taiwan, Rotterdam: A. A. Balkema, pp. 81-88.

van Genuchten, M.T. (1980). A closed form equation for predicting the hydraulic conductivity of unsaturated soils. Soil Science Society of American Journal, 44, pp. 892-898.

A large physical Mock-Up model for investigating engineered barriers

Jaroslav Pacovský

Centre of Experimental Geotechnics, Faculty of Civil Engineering,
Czech Technical University, Prague, Czech Republic

Abstract. Research on a bentonite-based engineered barrier for use in the safe underground disposal of high-level radioactive waste is a special multidisciplinary issue. In order to obtain findings enabling the design of such a construction, it is necessary to employ all the available experimental tools and procedures. With respect to the extremely long-term time requirements for the rheological stability and safety of the system as a whole, the results of long-term research have fully justified the use of physical modelling. The most relevant model types applied have been found to be those made at a scale of 1:1, referred to as Mock-Up models. A vertical model of a bench-scale buffer mass test of Czech smectitic clay in the KBS-3 modification (Swedish system) has been built at the Centre of Experimental Geotechnics, CTU, Prague. The model is fully instrumented, providing the continual multiparametrical measurement of all the relevant parameters. The whole experiment including the development of all the parameters measured can be seen on free-access dynamic web-sites (http://ceg.fsv.cvut.cz).

1 Introduction

The Centre of Experimental Geotechnics, CTU, Prague is involved in solving those problems connected with underground radioactive waste repositories. Radioactive waste has to be safely isolated from the biosphere in the long-term, in the order of 100 thousand years.

The principle of waste isolation is based on a multi-barrier system. The whole system is composed of two basic components – namely engineered and natural barriers. Apart from the waste container itself, the engineered barrier consists of a multi-layered barrier the basis of which is bentonite.

Bentonite has been chosen as the result of various studies of natural analogues since it displays, when compared to other materials (such as concrete or cement), the most stable rheological properties – i.e. its behaviour and properties remain unchanged for thousands of years [1],[2]. Bentonites may be subdivided into highly swelling Na-bentonites (of the Wyoming type) and less swelling potassium, calcium and magnesium bentonites. In the Czech Republic, the bentonites extracted and treated by activation are magnesium–calcium bentonites or calcium-magnesium bentonites. Natural sodium bentonites are not found in this country.

The extent of the research into bentonites is due to the unique requirements arising from their specialised application. Bentonite, or a bentonite-based material, will form an engineered barrier in the deep underground repository preventing a potential leakage of radionuclides from the high-level nuclear waste container into the natural barrier and beyond into the biosphere. Such an engineered barrier must retain this capacity for a period of hundreds of thousands of years. Bentonite will fulfil the functions of filling and sealing as well as acting as a buffer within the engineered barrier. Consequently, the geotechnical requirements for such a barrier include low permeability, swelling capacity, high plasticity, good thermal conductivity and rheological stability [3],[4].

The requirement for rheological stability constitutes the most difficult part of the research assignment. It is, however, clear that the implementation of this research requires a multi-disciplinary approach employing all available methods. These methods include experimental investigation, physical and mathematical modelling and the investigation of natural analogues. Rheological research cannot be conducted without physical modelling. Various model sizes are used. Small models serve for the determination of local phenomena, such as cyclic wetting and drying of joints, while larger models at a scale of 1:1 (Mock-Up) study the problem in its complexity.

2 Design and construction of MOCK-UP CZ

As part of the research on engineered barriers being carried out in the Czech Republic, a large physical model of the behaviour of a vertical container mounted in large-size boreholes (KBS System) resembling the Mock-Up type is presently being studied at the Centre of Experimental Geotechnics, CTU's laboratories in Prague. The construction of the Mock-Up-CZ model commenced at the beginning of 2000, and the experiment itself was launched on 7th May, 2002.

2.1 Basic description

The model is placed in an underground test silo with dimensions of 3000 x 3000 x 3000 mm. The Mock-Up-CZ model itself consists of a steel tank (an oven) with a cylinder diameter d = 800 mm, a height of 2230 mm and a wall

thickness of 8 mm. The bottom and top cover are made of steel of 50 mm thickness. These individual parts are connected using 16 bolts, d = 24 mm. The system was designed to withstand an internal pressure of up to 5 MPa (Fig. 1.).

Fig. 1. MOCK-UP CZ

The vessel containing highly radioactive waste is simulated using a heater which has been placed in an experimental bin. The heater consists of a steel cylinder with an outside diameter of 320 mm and a height of 1300 mm. The wall thickness is 25 mm. Flat steel flanges with a thickness of 40 mm have been welded onto the bottom and top parts of the cylinder. Two thermal radiators have been installed inside the cylinder, each of 1000 W maximum output. The content of the model container, the heating medium, is oil. Its capacity is approx. 70 l, the total weight of the heater being 320 kg. The heater's heating mode is fully automated using ZEPAX 01 regulators. The temperature range may be set at between 20 °C and 300 °C.

2.2 Buffer material

Based on an evaluation of the Czech bentonite research achievements, the most appropriate material for the buffer was found to be a mixture of treated bentonite (from the "Rokle" locality), silica sand ("Provodin" locality) and graphite (from the conditioning plant at "Netolice"). Sand is added so that the swelling abilities of bentonite can be controlled. While loose bentonite is able to produce a swelling pressure of up to 500 kPa, highly compacted bentonite with a dry density of $\rho_d = 1700$ kg/m^3 produces pressures of up to 8 -10 MPa. Such high pressure, however, is not desirable within the engineered barrier, therefore by adding sand the pressure is reduced to 3 - 5 MPa. Graphite is added to the mixture to increase its thermal conductivity so that the heat produced by the container is more easily redistributed towards the natural barrier [5].

The basic mixture contains 85 % RMN bentonite, 10 % silica sand and 5 % graphite. This mixture can be found in Mock-Up-CZ in two different forms. The lining of the container is made up of individual blocks assembled into an annulus. The space between the barrier blocks and the walls of the experimental bin is filled with a loose, hand-compacted mixture of the same composition as the blocks.

2.3 Hydration system

The potential inflow of granitic water from the natural barrier (it is expected that the Czech underground repository will be constructed in granitic rock) will be simulated by using a flooding system installed on the inner side of the bin featuring two concentric filters, the one closer to the bin being coarse-meshed and the other having voids of less than 100 μm. The inside diameter of the filters measures approximately 790 mm. Water is let in through four vertical perforated tubes. A hydration system which allows an increase in hydration pressure of up to 1 MPa is placed outside the experimental silo. Synthetic granitic water is used for saturation. The amount of water and saturation speed are continually recorded.

2.4 Model instrumentation

The Mock-Up physical model is equipped with 52 thermometers, 50 hydraulic pressure cells, 37 humidity sensors of varying construction and 20 resistive tensiometers (see http://ceg.fsv.cvut.cz).

The construction of the model allows the taking of core samples of the buffer barrier from 8 different positions at any time during the progress of the experiment. Special filters installed in the Mock-Up serve for the testing of the buffer's gas permeability. When the buffer becomes saturated, an inert gas will be injected through the filters attached to the heater. It will be possible to increase the gas pressure incrementally according to a program to be worked out later.

2.5 Range of recording parameters

Temperature, swelling pressure and hydration measurements are taken continuously inside the bentonite barrier throughout the entire duration of the experiment. These checks are carried out at six measurement profiles located from the top of the vertical model to the bottom (Fig. 2.).

In addition, there are checks for heater position changes as well as those for tightness along the outside surface of the bin and the construction rods. Measurements of energy consumption and the amount of saturation water are also taken. Samples of metals will be placed inside the barrier for corrosion research.

All core samples allow the precise determination of the range and degree of buffer clay saturation, potential changes in swelling ability (swelling pressure), permeability (permeability coefficient) and the thermal properties (conductivity) of the buffer.

The places used for core sampling will be immediately sealed by means of plugs made of a highly compacted bentonite mixture, and/or will be used for new instrumentation.

The whole system of registration, evaluation and transfer of data is based on the use of 3 small portable AD-SYS data loggers connected to a CEG server. All the data recorded is available on the web site. The experiment is monitored with the use of 4 web-cameras operating 24 hours a day.
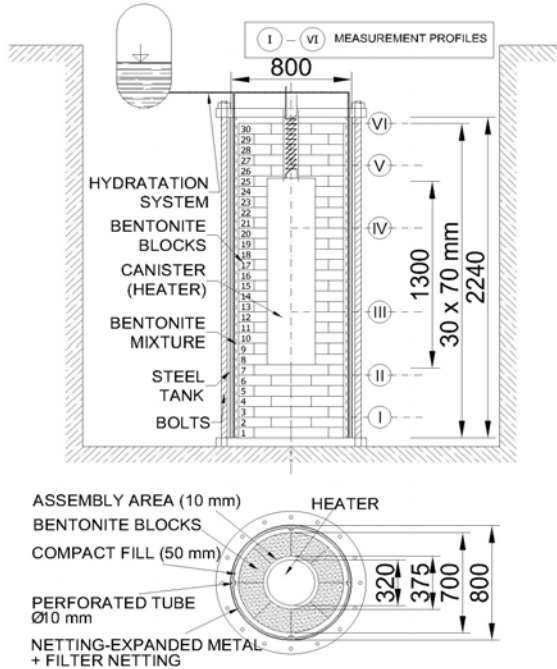
Fig. 2. Vertical and horizontal scheme of MOCK-UP CZ

3 Experimental procedures

It is assumed that the duration of the Mock-Up-CZ experiment will not be shorter than 4 years (phase 1, 2 and 3). Then, after a cooling period, the experiment will be dismantled and all the available results will be collected and evaluated.

3.1 Phase 1

The filter is kept dry and the power is switched on to reach a maximum temperature in the bentonite of 90 °C. Temperature, swelling pressure and hydration recordings are taken continuously for 6 months. The buffer evolution in Phase 1 involves:

- Redistribution of initial porewater generated by the thermal gradient across the buffer
- Homogenisation and subsequent consolidation of the mixture fill under the swelling pressure exerted by the hydrating and expanding dense blocks.

A core sample of the buffer will be analysed for the possibility of defining porewater redistribution.

3.2 Phase 2

The power is maintained at a constant level and the filter is filled with synthetic granitic water by connecting two of the perforated pipes to a water reservoir and using the other two for letting out air; these are then connected to the water source. Temperature, swelling pressure and hydration recordings are then taken continuously for 3 - 4 years, whereupon the buffer is presumed to reach a state of full saturation. The buffer evolution involves:

- Saturation of the buffer is associated with a change in temperature.
- There are some C-effects although they are not supposed to be of great importance. The wetting has a C-effect since minerals with reversed solubility, such as sulphates and carbonates, will be precipitated at the wetting front, which will be moving towards the heater.

During the whole of phase 2, core samples will be taken at pre-set intervals in order to determine the stage of the saturation process and the effect of processes underway on the permeability and swelling capacity of the bentonite mixture. Before the conclusion of Phase 2, gas permeability tests will be carried out.

3.3 Phase 3

Saturation and temperature loading of the buffer by the heater will be stopped during this phase. When the heater is switched off, the cooling phase will commence lasting approximately 2 weeks.

3.4 Dismantling and post-mortem analyses

The dismantling process will be conducted according to a detailed project which will include the following:

- Scientific program (tests and analyses foreseen on samples)
- Sampling plan (location and specific requirements of each sample)
- Scenario (guidelines and procedures for dismantling and sampling operations, work organisation and records & documents)

Detailed tests will focus on backfill material, corrosion and instrumentation. What is expected upon dismantling:

- To verify certain hypotheses or assumptions made on the basis of observations made during the test.
- To characterize the Mock-Up components and to better understand the phenomena occurring during the operational phases
- To provide advice for the next research programme

4 Results from running the experiment up to the present (December 2002)

4.1 Phase 1 (7.5.02 – 4.11.02)

The Mock-Up experiment began o n 7th May 2002 when the heater was switched on. The temperature was increased step by step to reach a maximum temperature in the bentonite of about 90 °C. With respect to the high thermal conductivity of the bentonite mixture, the maximum temperature of the oil in the heater had to be increased to 120 °C. The high thermal conductivity of the buffer (easy heat removal) also caused a greater difference between the temperature of the oil in the upper and lower parts of the heater (the difference being about 25 °C).

The required equilibrium temperature was reached after 2.5 months. A maximum temperature in the bentonite of 93 °C was measured close to the upper surface of the heater (Fig. 3.).

The process of moisture redistribution was much slower. Moisture content transported to places located further away from the heater caused local increases

in swelling pressure, mainly in the area of the 50 mm filling. This pressure, in turn, affected the spatial redistribution of the bentonite blocks, which locally caused increases in the radial pressures measured by means of pressure cells.

Before the end of Phase 1 (2.10.02) a core sample was taken from half way up the bin. The sample taken contained completely undisturbed core (Fig. 4.).
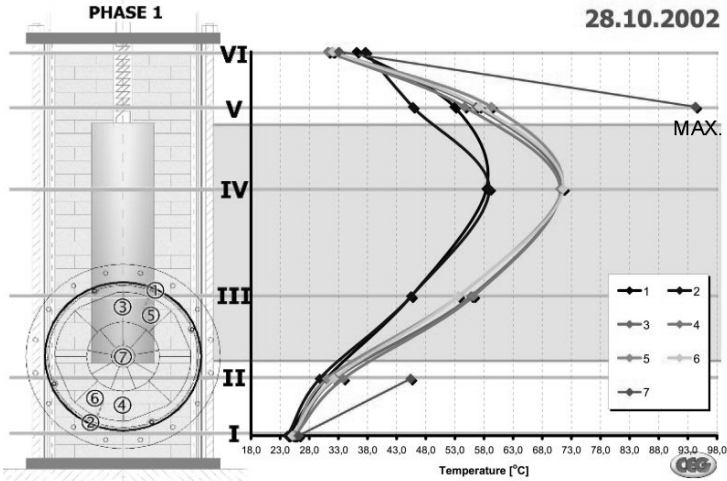
Fig. 3. Maximum temperature in bentonite (Phase 1)
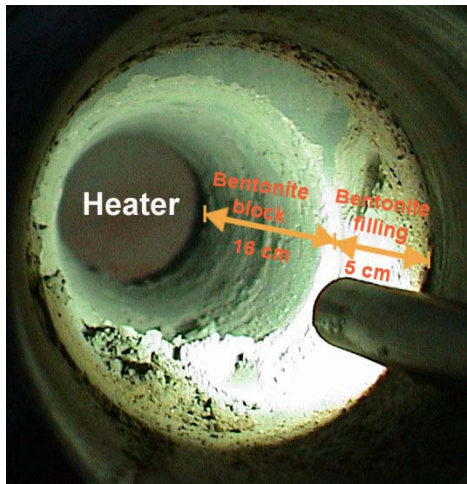
Fig. 4. Sight inside finished drill

By means of a water content test the following moisture distribution was de-termined. Highly compacted bentonite block material close to the heater w = 2 %, bentonite block material in contact with the filling w = 5 %, 50 mm filling be-tween the blocks and hydration filter w = 20 %.

At the same time, the sample was used to determine permeability and swelling pressure. The results of these tests did not exhibit significant differences to the initial parameters.

Before saturation commenced, a gas sample was taken from the bin and ex-posed to analysis with the following result: 87.5% N_2, 15% O_2, 5% CO_2.

4.2 Phase 2 (4.11.02 – up to the present)

The saturation process commenced on 4th November by filling the hydration sys-tem with synthetic granitic water. 78 l of water was required to fill the whole sys-tem.

The water caused a shock drop in buffer temperature. A new equilibrium tem-perature was established approximately 15 days later.

At the same time, swelling pressure started to increase significantly (Fig.5.). Should no problems occur, the project will continue as planned.
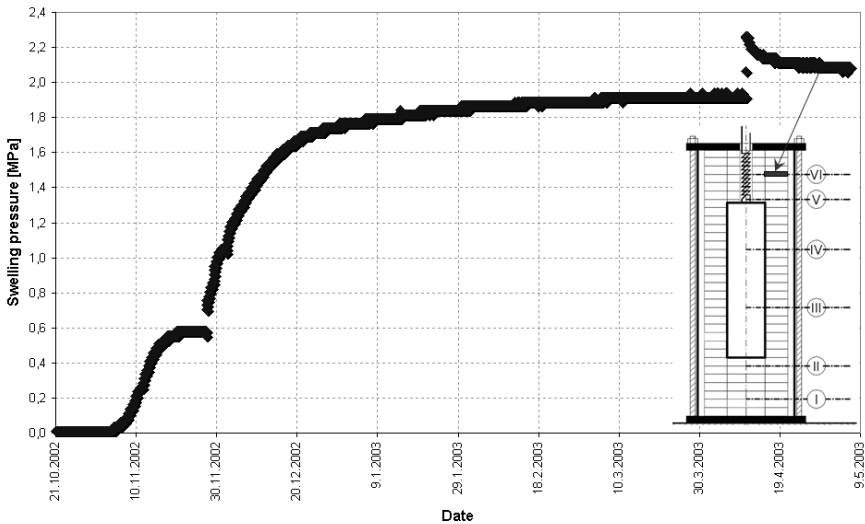
Fig. 5. Swelling pressure measurement (Phase 2)

5 Conclusion

An underground repository is an engineering construction with an extremely long service life requirement. To obtain the findings enabling the design of such a construction, all the experimental tools and procedures at our disposal must be employed. Physical modelling of the problems is undoubtedly one such tool. However, the methods and procedures selected must allow the extrapolation of short-term experimental results (obtained after several years) for long-term validity (speeding up of processes, their accumulation and cycling).

Such experiments include the use of Mock-Up type models, with an operation period of usually between 3 and 10 years. Mock-Up-CZ is one such experiment. The period of operation should last as long as possible and will be a determining factor in the accuracy of the findings regarding research into engineered barriers. A very important (if not the most important) stage in these experiments is the dismantling stage. The model is dismantled after the termination of the experiment and each part is subjected to a detailed rheological examination. In this way it is possible to determine what kind of influence the application of selected processes has had over the years on the rheological stability of materials and the construction as a whole.

Acknowledgement

References

[1] F. HUERTAS et al., Full-Scale Engineered Barriers Experiment for a Deep Geological Repository for High-Level Radioactive Waste in Crystalline Host Rock (FEBEX Project),   European Commission, 362 p., ISSN 1134-380, (2000).

[2] J. PACOVSKÝ, The Impact of Thermal Loading on the Plasticity of the Engineered Barrier's Material, Proceedings of International Conference on Radioactive Waste Disposal, Berlin, pp. 418 – 421, ISBN3-9806415-3-8 (2000).

[3] KUDRNÁČOVÁ et al., Laboratory Research of Component Structural Materials of the Barrier, CTU Reports, Proceeding of Workshop 2000, Volume 4, 581 pp., ISBN 80-01-02229-3 (2000).

[4] E. HYNKOVÁ, Thermal Loading of Bentonite". International Symposium on Soft Solution Processing, Tokyo, pp. 78. SSP (2000).

[5] J. PACOVSKÝ et al., Research on Bentonite Barriers in Underground Repository of Nuclear Waste". Proceedings of the International Symposium on Problematic Soils, Sendai, pp. 615 – 618, ISBN 90 5410998 (Oct. 1998).

Experimental testing and modelling of a Design for HLW Disposal through a Large Scale Mock-Up

Jan Verstricht, Xiang Ling Li, and Frédéric Bernier

EIG EURIDICE c/o SCK•CEN, Mol, Belgium

Abstract

Since 1974, Belgium investigates the design for disposal of its High Level Radio-active Waste (HLW) in a deep clay formation, the "Boom Clay". Although the clay formation is the main (natural) barrier against the transport of the radionuclides towards the biosphere, the design also involves several engineered barriers (multi-barrier principle). In the design developed in the late 1980's, a non-saturated bentonite based material was chosen as part of this barrier system. Prior to demonstrating this design in *in-situ* conditions, a surface mock-up test has been operated between 1997 and 2002. This test served as a preliminary test on the performance of several components of the system, such as bentonite based backfill blocks and instrumentation. With clearly defined heating and hydration conditions, it gave us the opportunity to perform a large scale simulation of the hydration/saturation of the backfill at controlled conditions. After describing the general disposal design and the experimental set-up, this paper will detail the measurements and observations obtained during operating and dismantling the mock-up. To support the interpretation of these measurements and observations, a modelling of the experimental set-up is being performed. We further detail the characterisation programme carried out to obtain the input data for the modelling. Finally, lessons learned for the development of the design for the HLW disposal will be drawn.

Introduction

Some 60% of the total electricity production in Belgium originates from nuclear power plants. For the scheduled nuclear programme, about 5000 tonnes of uranium heavy metal are required. At present contracts for the reprocessing of only 630 tU have been concluded, and this will result in 420 canisters of 0.15 m³ vitrified high-level waste. A complete reprocessing of all spent fuel will result in 3915 canisters. Research on the disposal of vitrified high level radioactive waste (HLW) in Belgium is being performed since 1974. The reference site for these studies is the Boom Clay layer at the Mol site (NE of Belgium). This formation is a marine sediment of tertiary, Rupelian age. It is a plastic, organic-rich clay, with a very low hydraulic conductivity. Another clay layer (Ypresian clay) is being considered as an alternative.

The repository concept that has been developed in the late 1980's is based on a horizontal network of galleries, located in the middle of the clay layer as shown in Figure 1. The HLW disposal galleries have an inner diameter of approximately 2 m. After a cooling time (50 to 60 years) to reduce the thermal output from each canister from about 2000 W to around 500 W, the 0.43 m diameter canisters are placed in an overpack (2 to 3 cm thick), with a design lifetime of approximately 1000 years during which it should remain intact. This prevents contact from the clay water with the waste glass matrix when temperatures are significantly above the initial value. The canister with overpack is placed in a disposal tube. The annular space between this tube and the gallery lining is backfilled with bentonite based, pre-compacted blocks. These blocks will slow water movement, and sorb radionuclides and retard radionuclide transport when the packages eventually fail. All the engineered barriers should prevent contact between the waste matrix and the clay water for a period during which the temperature is significantly higher than the original temperature (up to 500 years for HLW canisters, up to a few thousand years for direct disposal of spent fuel).
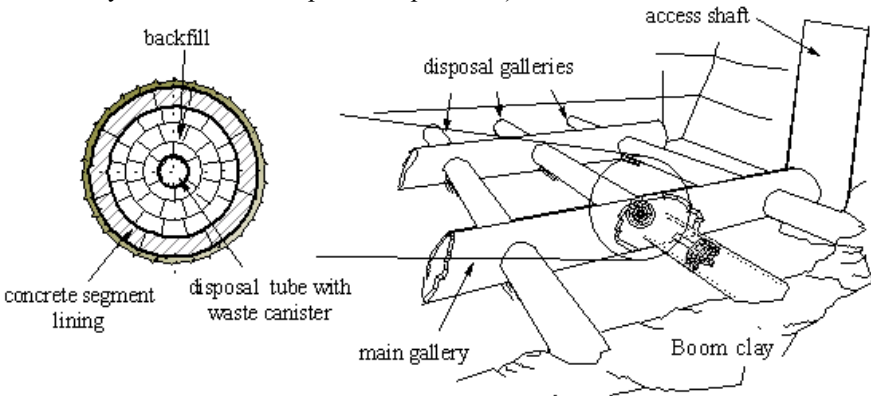
Fig. 1. Concept consists of horizontal gallery network with multiple engineered barriers

The nature of the issue of HLW disposal makes a demonstration phase essential. We plan to perform this by constructing and operating a dummy (i.e. non radioactive) but otherwise representative section of a disposal gallery of some 30 m long. This demonstration gallery will be excavated from the newly constructed connecting gallery, around which the Boom Clay is in a largely undisturbed state, and will be the core of the planned in situ test, where both the engineered barriers, as well as their interaction with the Boom Clay will be investigated through the different experimental phases (from construction up to dismantling).

Mock-up experimental design

Before performing the actual demonstration test in the underground facility, we decided to build a surface mock-up as several technical aspects of this in-situ test were not detailed yet. The main objective was to review the chosen options for the design and in-situ testing of the disposal system such as the backfill material (specifications, manufacturing, installation, hydration), the disposal tube and the monitoring devices. The mock-up also allowed a large-scale investigation of the thermo-hydro-mechanical behaviour of the clay-based backfill material.

General set-up

Basically, the mock-up has been conceived as a horizontal steel cylinder of 2 m inner diameter and 5 m long, simulating a section of a disposal gallery. A central tube (0.5 m diameter) contains the heating elements, which simulate the heat dissipation of the waste forms. The annular gap between the central tube and the outer lining is backfilled with pre-compacted blocks of clay-based material. A small concrete segmented ring has been installed to investigate the behaviour of concrete in this environment as the concrete segment lining of an actual waste gallery has been substituted by the steel liner to limit the size of the set-up.

Hydration of the backfill blocks to a saturated state is essential to arrive at their sealing function. Swelling and the subsequent closure of the joints and voids is indeed essential to limit water circulation around the rock. In the host rock, hydration would occur by the saturated clay environment (although very slowly). In the experimental set-up, we simulated and accelerated this by 16 hydration tubes at the outside of the backfill assembly, through which we could supply water at a pressure up to 1 MPa. The water composition was based on the in situ clay water.

Heating of the mock-up was performed at a constant linear power of 450 W/m. This rating was higher than the actual heat release from the waste forms. However, a high power during a shorter period was suggested for the in situ test, to obtain temperatures in the host clay that would be representative for the actual disposal site over longer time spans. An external temperature control system was further added to the confining structure to apply the thermal boundary conditions. Figure 2 shows the mock-up structure, partially filled (left) with backfill blocks

during construction. The hydration tubes and instrumentation cables can be observed clearly as well. The concrete segmented ring (right) was installed in the final part of the mock-up and replaced the middle ring of backfill blocks; to simulate the mechanical conditions of a gallery lining (external pressure) the inner ring was filled with sand, while the outer ring consisted of backfill blocks with an increased amount of bentonite clay.
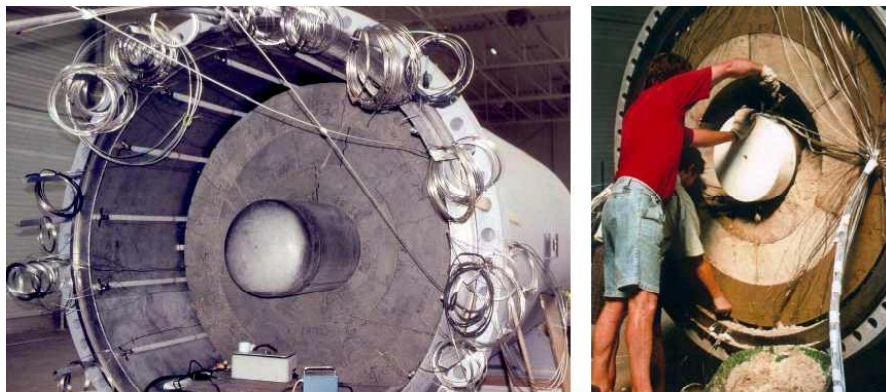

Fig. 2. View of the mock-up during construction

Development of backfill material

The specifications for the development of the backfill material depend on the repository concept, and deal with operational issues, short-term and long-term characteristics and performance. Operational aspects include the manufacturing, handling and installation; a typical example is the mechanical strength of clay-based blocks, as they have to remain intact from the manufacturing up to the on-site installation. Short-term issues include the initial thermal, hydraulic and mechanical behaviour of the material, such as the ability to fill all voids by swelling (hydration of smectite clay), as well as the speed and homogeneity of hydration – optionally combined with a thermal gradient. Long-term behaviour may include the maintaining of low permeability or the retardation of radionuclides, which is usually required with a granitic host rock.

Within the Belgian concept, the backfill material is applied to obtain an environment with low permeability and high thermal conductivity in the near-field of the central tube of the disposal gallery. The thermal loading can be dealt with by adding graphite to obtain an elevated thermal conductivity. Although the overall temperature in the clay formation will not be influenced as the heat generation is unchanged, local gradients, and hence the maximal temperature in the waste canisters can be limited. The low hydraulic permeability limits the water flow around the central tube, reducing possible corrosion risks. Mechanically, the backfill should provide a smooth pressure on the central tube, to prevent local stress gradi-

ents, while its swelling pressure must not be much larger than the in situ stress conditions, which led to the addition of sand as an inert material. The final composition was fixed at 60 % FoCa smectite clay, 35 % sand, and 5 % graphite.

The horizontal nature of the concept led to a backfill in the form of precompacted blocks (60 MPa uniaxial compaction) to be installed on the spot. They were limited in weight (convenient manual handling), robust and with precise dimensions to minimise the voids between the blocks, and between the central tube and block assembly (Gatabin and Rodriguez 1999; Verstricht et al. 2001).

Instrumentation

The internals of the mock-up were instrumented with some 150 sensors, mainly thermocouples to monitor the temperature field. The swelling pressure was monitored by strain gauges on the central tube and total pressure sensors in the backfill. The hydration of the backfill was observed through humidity sensors and water pressure sensors. The concrete segment ring was also equipped with sensors to measure pressure on, and loads between the segments.

Mock-up operation and main test results

After the assembly and closure of the mock-up experiment, we first hydrated the set-up (end 1997), followed by a heating phase of 4 years (mid 1998 – mid 2002), after which we let cool down the set-up before dismantling it (Oct 2002).

After connection of the water supply (2 Dec 1997), the void volume of about 1.55 m³ was filled in a short time (less than 1 hour). Over the next weeks, we gradually increased the pressure up to 1 MPa. The flow rate decreased rather quickly during the next months, and the last two years of the experiment, the water in- and outflow seemed mainly to be related to temperature variations. During the cooling period, an important amount of water had to be injected again to compensate for the thermal contraction of the water.

The heating elements in the central tube were switched on mid 1998. Later on, the external temperature control system was switched on to increase the overall temperature and to obtain a stable and uniform outer temperature.

Prior to the dismantling of the mock-up, we switched off the heating elements, and in about four weeks it cooled down to ambient temperature.

After switching on the heating elements in the central tube (June 1998), we obtained a maximum temperature of 105 °C on the central tube. When we switched on the external temperature control system, the temperatures increased further to reach maximum temperatures (June 2000) of some 137 °C on the central tube and 117 °C at the outer boundary of the backfill. These temperatures were maintained for two more years. The temperature gradient observed indicated a high (apparent) thermal conductivity, which is higher than can be expected for a porous material. A probable explanation is the non-radial thermal transport, which modelling might

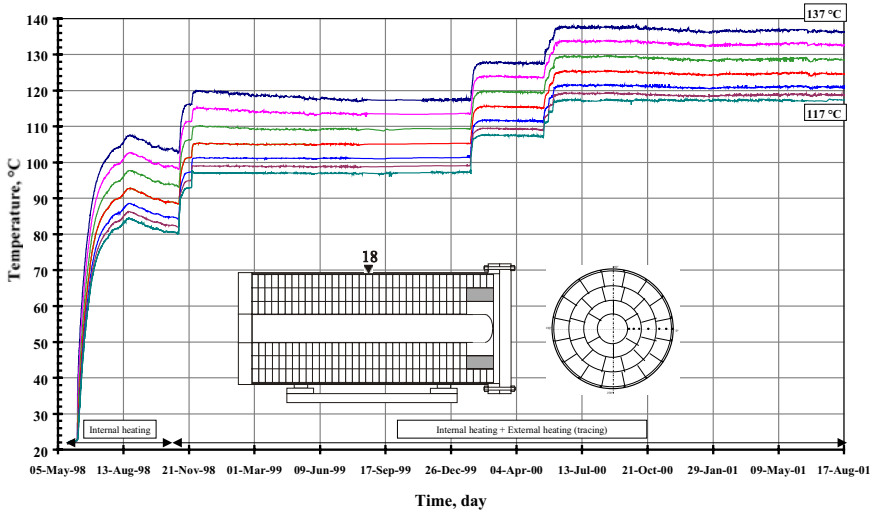confirm. Figure 3 shows the temperature evolution in a radial profile in the middle of the mock-up.

Fig. 3. Evolution in the temperature of a radial profile in the middle of the mock-up

The main pressure variations in the mock-up (Fig. 4) are caused by the hydration and heating systems. Initially, the pressure at the outside of the backfill follows the injection pressure. More towards the central tube, some pressure sensors show the pressure increase with a certain delay, indicating the gradual hydration/saturation of the backfill material. Near the central tube, no significant pressure variation is visible after several months, indicating a slow progress of the hydration front. Large pressure peaks then occurred due to the temperature increases, especially when the water supply had been switched off (for test purposes). More surprisingly, we could hardly observe high swelling pressures. Moreover, this swelling tended to decrease (collapse?) with time at elevated temperatures. Additional lab tests (suction controlled tests) will give more insight in the phenomena that are likely to occur in these conditions.

Physico-chemical phenomena within the backfill material were also observed. The strain gauges on the central tube appeared to be prone to corrosion, as water leaked out through several sensor cables. This water indicated a high content of solutes (up to 1000 ppm of Cl⁻), probably close to the central tube, showing evidence for transport mechanism that require further characterisation. Sulphides, detected in the hydration water when water was expulsed from the mock-up after a temperature increase, probably indicate the presence of sulphate reducing mechanisms.
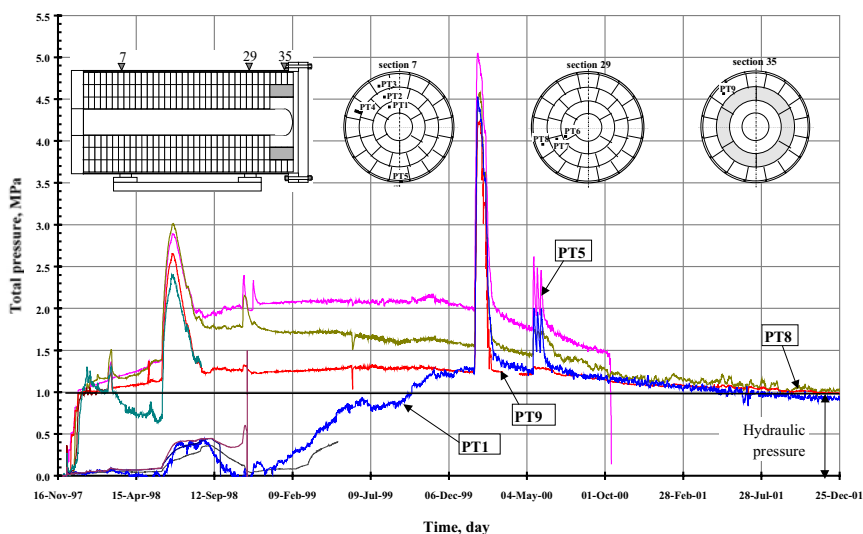
Fig. 4. The total pressure inside the backfill is highly sensitive to temperature transients, but the swelling pressure has decreased to low values

The operational stages of the mock-up already highlighted the importance of the chemical processes occurring in the backfill, as they could have a detrimental effect on the performance of the backfill material, and on the integrity of the metallic barriers.

Modelling of the mock-up experiment

The modelling of the experiment will provide a good support to understand the physical phenomena that take place in the system. A basic laboratory Thermal-Hydro-Mechanical characterisation programme has been launched on the original (i.e. not exposed to the mock-up conditions) material to provide the input data for the modelling. It comprises the following aspects:

- thermal characteristics: thermal conductivity and specific heat capacity at different temperatures;
- hydraulic properties: water retention curves and saturated permeability at different temperature, relative permeability in function of the suction;
- hydro-mechanical behaviour: saturated oedometer and triaxial tests, suction and temperature controlled oedometer and triaxial tests.

Most tests are still running, the hydro-mechanical tests in particular take more time than expected due to the very low hydraulic permeability. This delays the representative modelling due to the lack of input data. Indeed, the preliminary modelling showed a high sensitivity to the hydro-mechanical parameters which are yet to be determined. We will present here only the basic hydro-mechanical

characteristics obtained up to now. The modelling results are too preliminary to be presented yet.

The FoCa clay is a French clay and contains 50% of calcic smectite, which gives the clay its swelling properties, and 50% of kaolinite. The principal role of the sand in the backfill is to regulate the swelling pressure. The graphite is added to increase the thermal conductivity. Table 1 gives the main physical and thermal hydraulic characteristics of backfill blocks. The saturated permeability increases with temperature as shown in Table 2.

Table 1. The main physical and thermal hydraulic characteristics at initial state

Dry density [g/cm^3]	Water content [%]	Saturated Permeability [m/s]	Thermal conductivity [W/m.K]
1.9	7.7	1.8e-13	2.86

Table 2. Variation of the saturated permeability with temperature

T [°C]	22	40	80	120	150
K$_w$ [m/s]	$1.8 *10^{-13}$	$3.3 *10^{-13}$	$7.8 *10^{-13}$	$3.9 *10^{-12}$	$1.0 *10^{-11}$

The water retention curves upon wetting–drying paths at ambient temperature have been determined by means of controlled relative humidity (equilibrium with different saturated saline solutions). The water relative permeability was obtained with the help of an analytical solution based on the sorption-desorption kinetics on the tested samples (Fig. 5 a and b) (Olchitzky 2002). All measurements are performed under unconstraint condition. We can remark that the hysteresis is very weak in this condition. In addition, due to the high swelling properties, it was difficult to saturate the samples (figure 5 c and d). Taking into account the on site condition of the mock-up, the determination of the water retention curves under constraint condition is necessary for the sake of modeling.

a) relative permeability-suction

b) water content – suction relation

c) void ratio –suction relation

d) saturation – suction relation
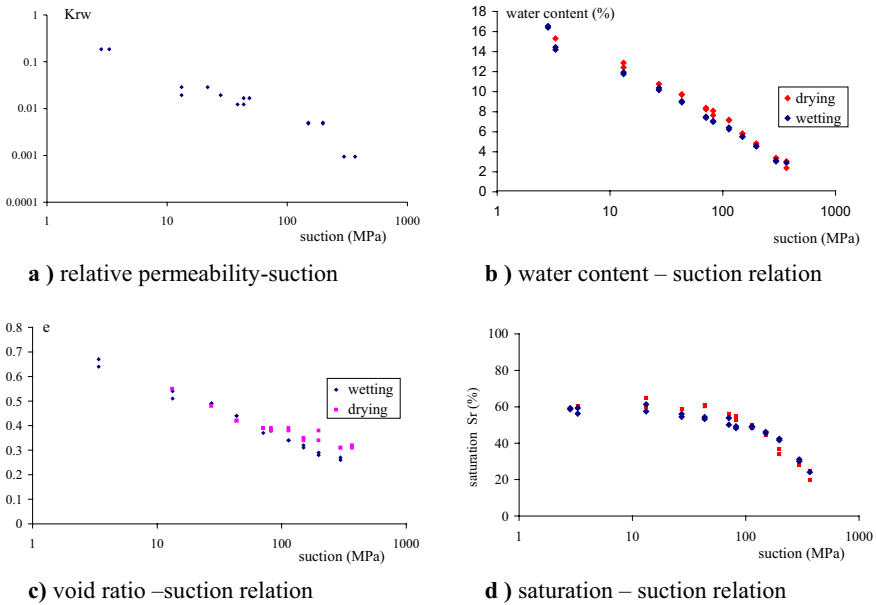
Fig. 5. Water retention curves and relative permeability

The saturated oedometer tests were realised on both compacted block and initial backfill mixture. The compressibility obtained by the two tests remains rather consistent (Fig. 6).
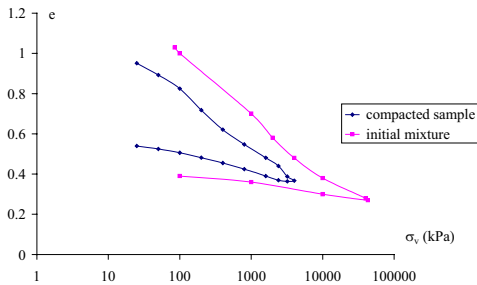
Fig. 6. Oedometer tests results

Mock-up dismantling and sampling

A thorough characterisation and understanding of the phenomena occurred during the hydration and heating of the set-up was the main objective for the dismantling.

The measurements and other observations during the experiment had pointed the attention to some unexpected phenomena, such as the high apparent thermal conductivity of the backfill, the low and decreasing swelling pressure, high salt (Cl^-) concentration in the backfill, and the corrosion of some sensors. The dismantling should provide us with a unique "hands-on" experience by visualising the backfill and other materials exposed to the experimental conditions. Together with the analysis of the samples obtained, it should help us to better understand the mock-up measurements and to improve the modelling by providing more accurate input data. Recalibration of functional sensors, and the diagnosis of sensors that failed, would allow us to improve the specifications for future long-term monitoring in disposal sites. Also characterisation of chemical and micro-biological processes, as well as the assessment of corrosion susceptibility of metallic components, would benefit from the dismantling. The dismantling would further deliver valuable input for the optimisation of the in situ demonstration test from both a scientific (e.g. which processes to monitor), and technical point of view (e.g. which sensors are most reliable). Also the review of the design of the HLW disposal architecture would benefit greatly from the dismantling.

Methodology and operation

The dismantling programme was based on key phenomena defined by a multi-disciplinary team of scientists and engineers. These phenomena were:
- backfill: hydration process and thermal transfer;
- geochemical and microbiological processes linked with corrosion;
- hydro-mechanical properties of the backfill;
- sensor performance.

For each phenomenon, we defined tests and analyses to be performed on the samples. This was structured in a sampling plan, with sample locations and test procedures. Apart from the backfill, we also sampled the concrete segment ring and the steel structure; also many sensors were to be retrieved.

Before the actual dismantling, the set-up was cooled down by switching off the heating elements. A large amount of water (70 l) had to be injected to keep the water at a pressure of 1 MPa. It was clear however that in the backfill itself, pressures must have dropped very low due to the low permeability. To avoid a modification of the prevailing anaerobic conditions inside the mock-up, only de-aired water was supplied. The dismantling was further preceded by a cored sampling of the backfill through the 55 mm thick outer steel lining - our first contact with the backfill. We observed an immediate swelling of the backfill, and could verify that this backfill had completely filled all the voids. The large cover was finally removed on 2 October 2002, and from then on, dismantling and sampling progressed uninterrupted during 10 days and nights in two shifts.

Observations

The main observation was the expansion of the backfill blocks, and closure of all voids. With the largest voids at the outside of the backfill, it was evident that the outer blocks showed the largest expansion. The beige colour at these places confirmed the swelling of the clay platelets. There was also a good contact with the central tube. The joints between the blocks were still clearly visible, but there was a significant mechanical bond, with only a slight preferential behaviour along these joints – mainly between subsequent sections. The hydraulic behaviour of these joints still has to be assessed. Overall, one can state that the backfill blocks behaved as expected, but the saturation seems to be a very slow process. The hydration state, showing swelling that mainly occurred at the outside, was also confirmed by the on site determination of water content, dry density and saturation degree as a function of radial distance.

The corrosion inside the mock-up was limited to a few very specific cases. All steel parts in contact with the backfill were made from stainless steel (AISI 304L or equivalent). One hydration tube showed a green-blue colour (spreading up to a few cm in the backfill), due to the (galvanic) corrosion of a humidity sensor. All sensors of this type were severely damaged by galvanic corrosion (copper – stainless steel), and the power supply of these sensors probably made this corrosion even worse. On some other hydration tubes, a grey coating was observed, which might be due to pyrite recrystallisation. Also some corrosion was visible on the central tube where it was in contact with the sand. In general, the sand had allowed some circulation of the water, which proved to be detrimental. Avoiding any significant water flow is essential to obtain stable chemical conditions.

A lot of useful feedback came from the sensors. Some types, such as thermocouples and piezometers, were well designed for their task. Other sensor types suffered from corrosion, such as the internal strain gauges. To monitor deformation of the central tube, we had selected a hermetically sealed type, specially designed for underwater applications. However, it turned out that the solder used at the cable connection with the sensor body had completely disappeared. Other sensors seemed not to comply with their temperature specifications.

Microbiological analyses are also still going on. The main activity seemed to be related to the hydration circuit, where the water temperature ranged from above 100 °C to ambient temperature. With the circulation in some tubes due to thermoconvection, it is not surprising that high concentrations of different species were detected. We were interested in sulfato-reducing bacteria, thio-sulfato-reducing bacteria and methane forming bacteria, and all were detected in high numbers (> 140 000 / ml). The results in the backfill are less clear. In principle, bacteria can hardly survive at high temperatures and with limited possibility to move (small pore size), but the possible contamination by the injection of hydration water during the cooling phase troubles the current interpretation.

Analysis programme and first results

The backfill analyses are still running, but the first results on the concrete have been obtained yet. Samples were taken from the concrete ring to check if the mechanical strength had deteriorated when compared with a non-exposed segment. In contrast to what we had expected, compression and tensile strength of the exposed concrete appeared to have improved considerably, due maybe to the saturated environment at elevated temperatures.

Conclusions

The results of this experiment have spurred the re-evaluation of the disposal design. Aspects are the reliability of one long central tube (the current option considers rather short sections), the maximum temperature in the backfill (100 °C), and also the type of backfill (one alternative design does not rely anymore on backfill).

The experiment has also provided us with very valuable experience on the long-term behaviour of sensors. Apart from its evident use for the demonstration tests, such knowledge will be indispensable when discussing the operational or post-closure monitoring at disposal sites.

References

Gatabin C, Rodrigues S (1999) Projet Praclay, maquette Ophélie, Données complémentaires concernant la barrière ouvragée. CEA Technical Note N.T. SESD 99-56.

Verstricht J, Demarche M, Gatabin C (2001) Development of a backfill material within the Belgian concept for geological disposal of high-level radioactive waste: an example of successful international co-operation. In: Proc. Int. Symp. Waste Management '01, Tucson (AZ).

Olchitzky E (2002) Couplage hydromécanique et perméabilité d'une argile gonflante non saturée sous sollicitations hydriques et thermiques, courbe de sorption et perméabilité à l'eau. Ph. D. thesis, Ecole Nationale des Ponts et Chaussées, Paris.

SPRINGER PROCEEDINGS IN PHYSICS